# Geochemistry and Nd isotope study of Ultramafic-Mafic rocks from Southern Bundelkhand Craton, Central India: Implications for Archean Mantle Evolution, Crustal growth and PGE mineralization

A thesis submitted to the University of Hyderabad in partial fulfillment of the award of a Ph.D. degree in Earth and Space Sciences

By

Niranjan Mohanty 14ESPE05

Under the supervision of

Prof. M Jayananda Dr. M Satyanarayanan



Centre for Earth, Ocean and Atmospheric Sciences

**School of Physics** 

University of Hyderabad (P.O.) Central University, Gachibowli

Hyderabad-500 046

Telangana, India

January 2023

# **DECLARATION**

I, Niranjan Mohanty, hereby declare that this thesis entitled "Geochemistry and Nd isotope study of Ultramafic-Mafic rocks from Southern Bundelkhand Craton, Central India: Implications for Archean Mantle Evolution, Crustal growth and PGE mineralization"Submitted by me under the guidance and supervision of Prof M Jayananda, Center for Earth, Ocean and Atmospheric science, School of Physics, University of Hyderabad, and Dr. M Satyanarayanan, CSIR-National Geophysical Research Institute, Hyderabad Is a bonafide research work.

I also declare that it has not been submitted previously in part or in full tothis University or any other University or Institution for the award of any degree or diploma.

Date: 31/01/2023
Place: Hydenasad

Name: AIRANJAN MOHANTY

Signature of the Student: Alivantan Molonty

Regd. No. 14ESPEOS



This is to certify that the thesis entitled "Geochemistry and Nd isotope study of Ultramafic-Mafic rocks from Southern Bundelkhand Craton, Central India: Implications for Archean Mantle Evolution, Crustal growth and PGE mineralization" submitted by Niranjan Mohanty bearing Registration Number 14ESPE05 in partial fulfillment of the requirements for the award of Doctor of Philosophy in Earth and Space Sciences is a bonafide work carried out by him/her under my supervision and guidance.

This thesis is free from Plagiarism and has not been submitted previously in part or infull to this or another University or Institution for the award of any degree or diploma.

Further, the student has the following publication(s) before submission of the thesis/monograph for adjudication and has produced evidence for the same in the form of an acceptance letter or the reprint in the relevant area of his research: (Note: At least one publication in referred journal is required)

- Mohanty, N., Singh, S. P., Satyanarayanan, M., Jayananda, M., Korakoppa, M. M., & Hiloidari, S. (2019). Chromian spinel compositions from Madawara ultramafics, Bundelkhand Craton: Implications on petrogenesis and tectonic evolution of the southern part of Bundelkhand Craton, Central India. Geological Journal, 54: 2099–2123. https://doi.org/10.1002/gj.3286.
  - This publication appears in chapter IV of the dissertation.
- Satyanarayanan M, Singh SP, Balaram V and Mohanty N (2015). Geochemistry of Madawara Igneous Complex, Bundelkhand Craton, Central India: Implications for PGE Metallogeny. Open Geosciences, 7 (1), 836-853. https://doi.org/10.1515/geo-2015-0016.
   This publication appears in chapter VI of the dissertation and has made the following presentation at the conference,
  - Niranjan Mohanty, M. Satyanarayanan, S. P. Singh, 2016., Mineral chemistry of Chromian-spinel from Madawara Ultramafic intrusion, Bundelkhand Craton, Central India" Abstract published in the National Conference on "Precambrians of India" at the Department of Geology, Bundelkhand University, Jhansi (Uttar Pradesh), 2016.
  - 2. N Mohanty, M Satyanarayanan, S P Singh, M Jayananda, M M Korakappa, S

Hiloidari. 2017, Genesis of ultramafic-mafic complex from southern Bundelkhand Craton, Central India: Insights from chrome spinel chemistry. Abstract published in Nation symposium on Emerging trend in Geoscience, conducted by ISAG, 2017.

3. Niranjan Mohanty, S. P. Singh, M. Satyanarayanan 2017. Chrome-spinel geochemistry of Madawara Igneous Complex, Bundelkhand Craton, Central India". Abstract published in National Seminar on recent advances and challenges in geochemistry, environmental and sedimentary geology conducted by Aligarh Muslim University, 2017.

Further, the student has passed the following courses towards fulfilment of coursework requirement for Ph.D. / was exempted from doing coursework (recommended by Doctoral Committee) on the basis of the following courses passed during his PhD program.

Course Code	Name	Credits	Pass/Fail
1. ES-801	Earth System Sciences	4	Pass
2. ES-805	Research Methodology	3	Pass
3. ES-806	Mathematics for Earth Sciences	4	Pass
4. ES-807	Interdisciplinary course	3	Exempted
830	Special Paper on Specified Research Topic	2	Pass

ee. Prof. M Jayananda

(Supervisor) or. M. Jayananda, FASc, FNASc, FNA Professor Centre for Earth, Ocean and Atmospheric Sciences University of Hyderabad Hyderabad-500 046, Telangana, India

M. Su

Dr. M Satyanarayanan

(CONSTRAYANAN ठाँ. एम. सत्यनारायणन वरिष्ठ प्रधान वैज्ञानिक Senior Principal Scientist

वे औ. अ.प. - राष्ट्रीय भूभौतिकीय अनुसंधान संस्थान CSIR- National Geophysical Research Institute (विज्ञान एव प्रोद्योगिकी मंत्रालय, भारत सरकार) (Ministry of Science and Technology, Govt. of India) उप्पत मार्ग Uppai Road, हैदराबाद Hyderabad - 500007 Head (CEOAS) ad Atmospheric Sciences University of Hyderabad Hyderabad-500 046, INDIA

Dean of School

School of Physics

DEAN 31/1/2023

School of Physics University of Hyderabad HYDERABAD - 500 046



This is to certify that the thesis entitled "Geochemistry and Nd isotope study of Ultramafic-Mafic rocks from Southern Bundelkhand Craton, Central India: Implications for Archean Mantle Evolution, Crustal growth and PGE mineralization" submitted by Niranjan Mohanty bearing Registration Number 14ESPE05 in partial fulfillment of the requirements for the award of Doctor of Philosophy in Earth and Space Sciences is a bonafide work carried out by him/her under my supervision and guidance.

This thesis is free from Plagiarism and has not been submitted previously in part or in full to this or any other University or Institution for the award of any degree or diploma.

Prof. M Jayananda (Supervisor)

Dr. M. Jayananda, FASc, FNASc, FNA Professor Centre for Earth, Ocean and Atmospheric Sciences University of Hyderabad Hyderabad-500 046, Telangana, India

Head Head

CEOAS Earth, Ocean &
CEOAS Earth, Ocean &
University of Hyderabad
Hyderabad-500 046, INDIA

Dr. M Satyanarayanan

Dr. M Satyanarayanan (Co-Supervisor)

Dr. M. SATHYANARAYANAN डॉ. एम. सत्यनारायणन

वरिष्ठ प्रधान वैज्ञानिक Senior Principal Scientist वै. ओ. अ. प. - राष्ट्रीय भूभौतिकीय अनुसंधान संस्थान CSIR- National Geophysical Research Institute (विज्ञान एवं प्रौद्योगिकी मंत्रालय, भारत सरकार) (Ministry of Science and Technology, Govt. of India) उप्पल मार्ग Uppal Road, हैबराबाद Hyderabad - 500007

Dean 31/1/2023 (School of Physics)

DEAN
School of Physics
University of Hyderabad
HYDERABAD - 500 046

### ACKNOWLEDGEMENTS

First and foremost, I would like to acknowledge my supervisor **Prof. M. Jayananda** for making me complete my thesis and enriching my life with beautiful lessons. I am very lucky to have him as my guide and extremely benefited from his valuable knowledge and constant support. His continuous effort and endless encouragement throughout my journey imbued me to understand science which pulled me closer to this subject.

I owe my deep sense of gratitude and heartfelt thanks to my co-supervisor **Dr. M. Satyanarayanan,** who always have been very close to my heart and consistently guiding me with a ray of hope through his valuable guidance to travel all the way in this wonderful journey. His love, affection and care to me are inexpressible in words. It is because of him I could see a shimmering light in the environs of darkness. Thank you, to come in my life.

I show my gratitude to **Prof. S P Singh** from Department of Geology, Bundelkhand University who provided enormous guidance during my field trip in the Bundelkhand Craton and shared his valuable experience which developed my keen interest regarding my field area.

I am much obliged to Ex-Director, **Dr. V M Tiwari**, and present Director, **Dr. Prakash Kumar** CSIR-NGRI for providing necessary infrastructures and facilities to pursue my research.

I sincerely thank **Prof. K.S. Krishna**, the present head of the University of Hyderabad, for supporting me and allowing me to work in the department of the university. I am also thankful to all the faculties, especially my DRC members, **Prof. V. Chakravarthi** and **Dr. Sri Lakshmi**, for their endless support and encouragement to complete my thesis.

I would like to thank the colleagues Elango, Ajay, Abhirami, Arjit, Dhan Kumar, Rajnikant Khelen, Barnita, Puja, Soumya and Sikha from CSIR-NGRI, Geochemistry division for their support throughout my research. I would like to thanks to my senior com brothers **Dr. Rajiv, Dr. Sunil**, **Dr. Radheshyam**, **Dr. Prakash**, **Dr. Satrughna** and **Mr Umasankar**. Special thanks to all my Odia friends at CSIR-NGRI e.g., Santosh, Chinmoy, Soumendra, Biswajit, Sivasis, Ramakant, Abhijeet, Rupali, Nihar, Aurobinda, Sarbajit, Sumanata and many more at the Research Scholar's Hostel-I and II. Kindly forgive me if I have missed anyone.

My special acknowledgment goes to my lab seniors at University of Hyderabad: **Dr. K.R. Adhisesan** and **Dr. Sucharita Pal** for their endless effort to complete my thesis. I want to thank my lab juniors Aindrila Mukherjee, Balaji Rao, Tarun Thomas, and Tarun Kumar from

the University of Hyderabad. Special thanks to Ranjit, Abhay, Debasis, Dr. Gorachandra

for all time effort for helping me in all corners at University of Hyderabad.

I show my humble thanks to Dr. Ritesh Purohit, the head of the department of Geology at

Mohanlal Sukhadia University (MLSU), for permitting me to take leave my workplace. I am

also thankful to all my colleagues who supported me throughout and I am very fortunate that I

get to work with them. I am indebted to my juniors of MLSU, Gopal, Pratap and Jitu who

supported me during my research.

I am also thankful to my very close friends **Deba**, **Biswajit**, **Mahesh**, **Manu**, **Bishu**, **Sangram**,

**Binod** and **Rabi** for always being supportive since my college days.

I cannot express my indebtness to my beloved Maa, Late Bapa and two elder sisters

Nirupama, and Niharika through words for their profound love, affection and sacrifices at

every stage of my thesis.

Last but not least, I would like to express my thanks to my beloved wife **Archana** (**Kakun**)

for showering her unconditional love, support and encouragement throughout my PhD journey

and beyond.

Finally, it gives me immense pleasure to express my heartfelt gratitude to everyone who has

made this research journey possible. My sincere thanks to the Almighty to fulfil my dream into

reality.

Thank you all!!!!

Niranjan Mohanty

Ш

### **List of Publications**

- Mohanty, N., Singh, S. P., Satyanarayanan, M., Jayananda, M., Korakoppa, M. M., & Hiloidari, S. (2019). Chromian spinel compositions from Madawara ultramafics, Bundelkhand Craton: Implications on petrogenesis and tectonic evolution of the southern part of Bundelkhand Craton, Central India. Geological Journal, 54: 2099–2123. https://doi.org/10.1002/gj.3286.
   This publication appears in chapter IV of the dissertation.
- 2. Satyanarayanan M, Singh SP, Balaram V and Mohanty N (2015). Geochemistry of Madawara Igneous Complex, Bundelkhand Craton, Central India: Implications for PGE Metallogeny. Open Geosciences, 7 (1), 836-853. https://doi.org/10.1515/geo-2015-0016.

  This publication appears in chapter VI of the dissertation.

#### **List of Abstracts**

- 1. Niranjan Mohanty, M. Satyanarayanan, S. P. Singh, 2016., Mineral chemistry of Chromian-spinel from Madawara Ultramafic intrusion, Bundelkhand Craton, Central India" Abstract published in the National Conference on "Precambrians of India" at the Department of Geology, Bundelkhand University, Jhansi (Uttar Pradesh), 2016.
- N Mohanty, M Satyanarayanan, S P Singh, M Jayananda, M M Korakappa, S Hiloidari. 2017, Genesis of ultramafic-mafic complex from southern Bundelkhand Craton, Central India: Insights from chrome spinel chemistry. Abstract published in Nation symposium on Emerging trend in Geoscience, conducted by ISAG, 2017.
- 3. Niranjan Mohanty, S. P. Singh, M. Satyanarayanan 2017. Chrome-spinel geochemistry of Madawara Igneous Complex, Bundelkhand Craton, Central India". Abstract published in National Seminar on recent advances and challenges in geochemistry, environmental and sedimentary geology conducted by Aligarh Muslim University, 2017.

### List of abbreviations

**BIF- Banded Iron Formation** 

BnGC- Bundelkhand Gneissic Complex

BTZ- Bundelkhand Tectonic Zone

CBC-Central Bundelkhand Craton

CBGB-Central Bundelkhand Greenstone belt

CITZ-Central India Tectonic Zone

Ga- Giga annum (Billions of Years)

HDEHP-2- ethyl hexyl hydrogen phosphate

HFSE- High Field Strength Element

HREE- Heavy Rare Earth Element

ICP-MS- Inductively Coupled Plasma Mass Spectrometer

LILE- Large Ion Lithophile Elements

LREE- Light Rare Earth Elements

Ma- Mega Annum (Million Years)

MB-Migraineur belt

MSWD-Mean Square of Weighted Deviates

MUC-Madawara ultramafic complex

NBC- Northern Bundelkhand Craton

N-MORB- Normal-Mid Atlantic Ridge Basalt

OIB- Ocean Island Basalt

PM- Primitive Mantle

ppm- parts per millions

QPC- Quartz Pebble Conglomerate

SBC- Southern Bundelkhand Craton

SBC-Southern Bundelkhand Craton

SBGB-Southern Bundelkhand Greenstone belt

TIMS- Thermal Ionization Mass Spectrometers

TTG- Tonalite Trondhjemite Gneiss

USGS- United States Geological Survey

XRF- X-Ray Fluorescence

## **CONTENTS**

Acknowledgements	II
List of Publications	III
Conferences and workshop proceeding	IV
List of Abbreviations	V
List of Figures	VII
List of Tables	XVI
Abstract	XVII
1. Introduction	1 - 32
1.1. Unique features of the Archean Earth	3
1.1.1. High Heat production and hotter mantle	3
1.1.2. Tonalite -Trondhjemite-Granodiorite (TTG) type granitoids	5
1.1.3. Greenstone belts with komatiites	7
1.1.4. Late calc-alkaline to K-rich granites and sanukitoids	9
1.1.5. Absence of HP-LT metamorphism	11
1.1.6. Structural patterns	12
1.1.7. Major period of continental growth	14
1.1.8. Geodynamic models	15
1.2. Geological framework of the Bundelkhand Craton	18
1.3. Previous work	18
1.4. Major scientific issues to be addressed	22
1.5. Objectives	23
1.6. Methodology	24
1.7. Analytical procedures	24
1.7.1. Loss of Ignition (LOI)	24
1.7.2. X-ray Fluorescence analysis (XRF)	25
1.7.3. Inductively Coupled Plasma-Mass Spectrometry (ICP-MS)	26
1.7.4. Laser Ablation-Inductively Coupled Plasma-Mass	28
Spectrometry (LA-ICP-MS)	

1.7.5. Multi Collector-Inductively Coupled Plasma-Mass	29
Spectrometry (MC-ICP-MS) (Nd-Sr isotope analysis)	
1.7.6. Electron Probe Micro Analyses (EPMA)	31
1.7.7. Scanning Electron Microscope-Energy Dispersive	32
Spectrophotometer (SEM-EDS)	
1.8. Location and Accessibility	32
2. Geological settings	35- 52
2.1. Regional geology and tectonic framework of the Bundelkhand Craton	
2.1.1. Lithologies	37
2.1.1.1. Granitoids of TTG affinity	37
2.1.1.2. Volcano sedimentary Greenstone sequence	38
2.1.1.3. High K-granitoids (Sanukitoids and anatectic granites)	42
2.1.1.4. Mafic dykes and Quartz reefs	43
2.2. Madawara Ultramafic-mafic Complex (MUC)	44
2.2.1. Madawara region	47
2.2.2. Ikauna region	47
2.2.3. Hanumathgarh region	51
3. Petrography and SEM study	53-66
3.1. Ultramafic-mafic of Madawara region	53
3.2. Ultramafic-mafic- intermediate of Ikauna region	57
3.3. Ultramafic-mafic of Hanumathgarh region	60
3.4. SEM-EDX study	62
3.4.1 Opaque mineralogy	62
3.5. Summary	65
4. Mineral Chemistry	67 -105
4.1. Silicates	67
4.1.1. Olivines	67

4.	.1.2. Amphiboles	69
4.	.1.3. Plagioclase	71
4.	.1.4. Serpentines	71
4.	.1.5. Chlorites	72
4.2. No	on-silicates	73
4.2	2.1. Chrome spinel	73
4.7	2.2. Fe-Ti oxides	75
4.3. O	exygen fugacity	76
4.4. P	arental melt composition	77
4.5. A	lteration and formation of zoned chromite	79
4.6. N	Iantle source using chrome spinel chemistry	82
4.7. N	lagmatism and geodynamics	88
4.8. L	A-HR-ICP-MS study of chrome spinel	90
5. Geoch	emistry and Radiogenic isotopes	106 - 139
5.1. M	Iadawara section	106
5.2. Ik	cauna section	115
5.3. H	anumathgarh section	120
5.4. W	Whole rock Sr-Nd Isotopes	121
5.5. P	GE Geochemistry	125
5.:	5.1 PGE in Madawara region	126
5.:	5.2. PGE in Ikauna region	128
5	5.3. PGE in Hanumathgarh region	131
6. Petro	ogenesis and sources	141- 172
6.1. E	Effect of secondary processes on elemental mobility	141

6.2. Crustal contamination	145
6.3. Fractional crystallization	151
6.4. Composition of sources and melting processes	153
6.4.1. Depth of magma generation and temperature of eruption	154
6.4.1.1. Constraints from trace elements	156
6.5. Origin of Madawara ultramafic-mafic rocks	161
6.6. Origin of Ikauna ultramafic-mafic rocks	164
6.7. Origin of Hanumathgarh ultramafic rocks	165
6.8. Implication for PGE mineralization	166
7. Discussion and conclusion	173-184
7.1. Time relationship of ultramafic mafic magmatism with	173
an adjoining basement	
7.2. Implications for mantle evolution and crustal growth	176
7.3. Tectonic context of ultramafic-mafic magmatism	179
7.4. Conclusions	183
7.5. Future scopes	183
References	184-195
Similarity index	196-197
Appendix	198-199

# **List of Figures**

Figure 1.1	The distribution of Archean cratons around the globe (1) Slave, (2) Wyoming, (3) Superior, (4) Greenland, (5) Fennoscandian, (6) Siberian, (7): North China, (8) west Australian, (9) Indian, (10) Tarim, (11) Tanzanian, (12) South African (Kaapvaal) (13) Congo, (14) west African, (15) Amazonia and (16) Colorado Plateau. (Reference: Lee et al., 2011). Map of Precambrian (>540 Mya) and Phanerozoic (<540 Mya) crustal basements are shown here. Archean cratons are shown in regal red in colour.	2
Figure 1.2	A selection of crustal growth models. Models shown here adopted from Fyre 1978, Reymer & Schubert 1984, Armstrong 1981, Hurley 1968, Hurley & Rand 1969, Veizer & Jansen 1979 and Taylor & McLellan 1982.	4
Figure 1.3	Metamorphic thermal gradient (T/P) for 456 localities grouped as high dT/dP in red, intermediate dT/dP in green and low dT/dP in blue, and plotted against age (Brown, 2018). (b) A crustal growth model based on Hf isotope ratios in zircons (Dhuime 2012) and a shift in the composition of juvenile crust from mafic to more intermediate compositions accompanied by an inferred increase in crustal thickness (Dhuime 2015).	11
Figure. 1.4	Schematic representation of proposed structural models for the dynamics of Archean crust (Stern et al., 2018).	13
Figure 1.5	(a) Schematic temporal evolution of the lithosphere associated with decreasing mantle temperature. Schematic model detailing the proposed temporal evolution of the Earth with decreasing mantle temperature; Cawood et al. (2018). (b) Early Earth, pre-plate tectonic (>3.2 Ga) involves a non-plate tectonic regime, with magmatism characterized by a bimodal association of TTG (tonalites, trondhjemites and granodiorites) and greenstone belts. Mantle plumes are the major source of mafic magmatism. Recycling occurs through delamination and mantle convection is of a relatively small wavelength. Subduction, where present, is transitory. Plate tectonics (<2.5 Ga) is associated with large aspect ratio mantle convection. Between these two tectonic regimes is a transition phase (3.2-2.5 Ga) in which the lithosphere is stabilized and differentiates into oceanic and continental types, with the latter undergoing thickening, enabling its emergence and erosion.	16
Figure 1.6	Simplified diagram depicting the different types of tectonic settings for the ultramafic mafic complex	17

Figure 1.7.	Map of India showing the relative position of the Bundelkhand	19
	craton with respect to various cratons of the Indian shield (modified after Pradhan et al. 2009).	
Figure 1.8.	Geological map of the Bundelkhand craton (reproduced after	20
	Basu 1986). The various magmatism ages reported by various	
	authors are displayed on the map (Mondal et al. 2002; Kaur et al.	
	2014, 2016; Joshi et al. 2016, Singh et.al. 2018, Sikha et.al. 2021)	
Figure 2.1.	Geological map of the study area showing the distribution of	45
	ultramafic-mafic complexes along with other lithological units and	
	their relationship. The various magmatism ages reported by	
	various authors are displayed on the map (	
Figure 2.2.	(a) Field photograph showing nearly E-W trend of ultramafic	48
	outcrops intruding into Bundelkhand gneissic complex (BnGC)	
	near Madawara village. (b) Field photograph of peridotite	
	showing a large number of embedded Cr-spinel crystals in the	
	peridotite at Madawara village (c) Field photograph of peridotite	
	showing solution channel weathering in the Madawara village. (d)	
	The old TTG shows banding about 4 km north of Madawara town.	
	(e) Field photograph of E-W trending shear zone occurred north	
	of the ultramafic outcrop near Madawara village. (f) Field	
	photograph showing the highly deformed intrusive relationship of	
	ultramafic-mafic rocks with older granitoids.	
Figure 2.3.	(g) Field photograph showing nearly E-W trending ultramafic	49
	outcrop intruded into Bundelkhand granitoids near Ikauna. (h)	
	Field photograph of nearly E-W trending gabbro occurred outward	
	to the peridotite in Dangli village (i) Field photograph of Gabbroic	
	diorite and diorite in the outer rim of ultramafic near Ikauna and	
	Bighai village. (j) Field photograph showing the intrusive between	
	ultramafic and older granitoid near Hanumathgarh village. (k)	
	Filed photograph showing the granitic gneisses in the Ganeshpura	
	area. (1) Field photograph of dispersed lensoidal ultramafic	
	outcrops near Hanumathgarh.	
Figure 2.4	(m) Banded iron ore formation of the Girar belt in the southern	50
	Bundelkhand craton. (n) field photograph of meta basalt near to	
	Badawar village of the southern Bundelkhand craton (0 & p) field	
	photograph of large, nearly unstretched pillows near the Dhasan river of southern Bundelkhand craton. (o) oligomictic	
	river of southern Bundelkhand craton. (o) oligomictic conglomeratic outcrops of the southern greenstone belt. (p) Nearly	
	NW-SE trending mafic dykes exposed near Girar of the southern	
	Bundelkhand craton	

Figure 3.1.	(a) Microphotograph of peridotite showing cumulate texture sieved by inclusions of euhedral to subhedral chromite grains in the olivine pseudomorph and its grain boundary. (b) Poikilitic texture in olivine pyroxenites showing rounded crystals of olivine and euhedral spinel. (c) Cumulate pyroxenite with the inclusion of chromite grains and serpentine, particularly in the left bottom corner (d) Cumulate hornblende pyroxenite showing variable altered to tremolite and actinolite variety. (e) Gabbro with zoned plagioclase feldspar and clino- pyroxenes showing cumulate texture (f) Gabbro showing the presence of feldspar, pyroxene, and hornblende which are variably altered to actinolite variety. (g) Photomicrograph of ultramafic showing mineral assemblages of serpentine-tremolite-carbonate. (h) photomicrograph showing hornblende mantled by tremolite with chlorite in hornblende-pyroxene-rich ultramafic rocks.	54
Figure 3.2.	(a) Microphotograph of peridotite showing cumulate texture with relict olivine as cumulus and intercumulus space filled by pyroxenes in Ikauna village (b) Relict olivine showing highly fractured with filed by opaque minerals. (c) Photomicrograph of ultramafic showing the different mineral assemblages of serpentine-tremolite-chlorite sieved with chrome spinel (d) photomicrograph of Gabbroic rocks showing the mineral assemblages of plagioclase and pyroxene. (e) Gabbroic diorite shows the mineral assemblages hornblende, plagioclase, and a few quartzes. (f) Diorite shows large crystals of hornblende and plagioclase, in which plagioclase shows a cloudy appearance due to saussuritization. (g) Microphotograph showing the presence of pentlandite with few millerites occurred in the intercumulus spaces of olivine in the ultramafics of Ikauna.(h)Microphotograph showing the presence of pentlandite (creamish yellow colour) in the ultramafics of Ikauna.	59
Figure 3.3	(a) Microphotograph showing the mineral assemblages of serpentine-tremolite-chrome spinels in the ultramafics of Hanumathgarh. (b) Microphotograph showing the mineral assemblages serpentine-tremolite-chlorite along with chrome spinels. (c) Microphotograph showing the included chrome spinel with clinochlore. (d) Microphotograph showing the mineral assemblages of serpentine-tremolite-clinopyroxene. (e) Microphotograph showing the mineral assemblages of tremolite-actinolite-hornblende in hornblende-rich peridotite (f)	61

	Microphotograph showing the mineral assemblages of serpentine-	
	hornblende-tremolite-actinolite in hornblende rich peridotite. (g)	
	Reflected light microphotographs of pentlandite (light yellow) with	
	millerite (dark yellow) along with surrounding late phases	
	magnetite. (h) Reflected microphotographs of included chromite	
	within olivine with intercumulus space filled by pentlandite and	
	millerite.	
Figure 3.4	(a) SEM-EDX study of ultramafic rocks of MUC (a-b)	63
	Backscattered electron (BSE) images showing the presence (Ni, Fe)	
	S and NiS phases such as pentlandite and millerite in the	
	intercumulus spaces of olivine (c-d) BSE images showing the	
	presence of early (Ni, Fe) S phases within the chromite.	
Figure 3.4	SEM-EDX study of ultramafic rocks of MUC (e-f) Backscattered electron (BSE) images showing the presence (Ni, Fe) S and NiS phases such as pentlandite and millerite in the intercumulus spaces of olivine (g) BSE images showing the presence of (Ni, Fe) S phases with the clinopyroxenes (h) PGE mineralisation along the boundary of silicates.	64
Figure 4.1	Forsterite (Fo) versus NiO and MnO (wt.%) contents for olivine in the ultramafic of MUC. (c) Plot of CaO versus forsterite (Fo) contents in olivine (after Li et al., 2012).	68
Figure 4.2	(a) Amphibole classification after Leake et al. (1997) (b) TiO <sub>2</sub> (wt.%) versus SiO <sub>2</sub> (wt.%) plot (after Rock 1991) suggesting the secondary nature of amphiboles in the peridotite of the MUC. (c) Na + K versus the Si content in the amphibole highlights the Alaskan-type ultramafic complex. The data for the Alaskan-type complex in the middle Tianshan massif, China, is from Su et al. (2012), Quetico type from Pettigrew and Hattori (2006); Gabbro Akarem from Helmy and El Mahallawi (2003); arc-cumulate field (Beard and Barker 1989). The trends for the arc-cumulate field (1990).	70
Figure 4.3	(a) Plot of chlorite analyses from the present study on a chlorite classification diagram of Hey (1954). MUC chlorite analyses display a compositional range and plot in fields of penninite and clinochlore. (b) Plot of Ab-Or-An contents in plagioclase of MUC display compositional ranges and plot in the field from bytownite to andesine (after Li et al.,2012).(c-d) Plots of SiO2 (wt.%) versus MgO (wt.%) and MgO (wt.%) versus FeO (wt.%) of serpentine minerals under study. Most MUC serpentine samples can be classified as chrysotile and antigorite varieties.	72

Figure 4.4.	(a) Spinel prism for the multi-component systems of spinels for	74
	representation (After Deer et al., 1992). (b) Triangular	
	classification diagram of spinel group of minerals (Field of	
	"spinel gap" is from Barnes & Roeder, 2001)	
Figure 4.5	Cr spinel-melt bivariate diagram for (a) $Al_2O_3$ and (b) $TiO_2$ . The	78
	estimated composition of parental melt that is in equilibrium with	
	Cr-spinel from peridotite and olivine pyroxenite was calculated	
	from EPMA data (in wt.%). Please see the text for more details.	
	The regression lines are derived from the experimental study of	
	Maurel &Maurel (1982) and Cr spinel-melt inclusion studies in	
	MORB, OIB, LIP, and ARC from Kamenetsky 2001. Only Al-	
	chromite data has been used for the calculation of the parental	
	melt.	
Figure 4.6	Back-scattered electron (BSE) images of chrome spinels along with	81
	silicates from ultramafics of Madawara showing different textures	
	and structures during the alteration showing (a) cumulate	
	peridotite with large grain olivine pseudomorph altered to	
	serpentine and intercumulus phase containing clinopyroxene	
	altered to tremolite and in some part to chlorite (b) homogeneous	
	Cr-spinel (low Al-chromite) in serpentinised peridotite (c) Zoned	
	chrome spinels with Al-chromite core rimmed by Fe-chromite (e)	
	Partly altered euhedral zoned chromite crystals present as	
	inclusions in the pyroxene with a very thin rim of ferrite chromite	
	in the olivine pyroxenite (f) Euhedral zoned chromite in peridotite	
	with core-rim compositional variation and presence of magnetite	
	and ilmenite in the intercumulus space (f) Zoned chromite in	
	amphibole rich peridotite (g) Homogeneous Fe-chromite present in	
	the matrix of olivine in peridotite rock (h) Alteration of chrome	
	magnetite and magnetite in peridotite. Notes: Al-chr: Al-chromite,	
	Fe-chr: ferrian chromite, Cr-mag: chrome magnetite, mag:	
	Magnetite, Ol: Olivine, Ser: Serpentine, Amp: Amphibole, Chl:	
	Chlorite.	
Figure 4.7	Variation diagram between Cr <sub>2</sub> O <sub>3</sub> and Fe <sub>2</sub> O <sub>3</sub> showing a strong	84
	negative correlation of Al chromite from Madawara ultramafic	
	complex (MUC)	
Figure 4.8	(a) The Cr-Al-Fe <sup>3+</sup> variation diagram of Al-Chromite and Fe-	86
-	Chromite of the MUC shows an iron enrichment trend. The	
	defined fields are from Barnes and Roeder (2001) and Wang et al.,	
	2010. (b) $TiO_2$ (Wt.%) versus $Fe^{3+}/(Cr+Al+Fe^{3+})$ plot for primary	
	Al-Chromite in peridotite and olivine pyroxenite. The demarcated	

	fields are from Angi (1002) Parmas & Dander (2001) (a) The	
	fields are from Arai (1992), Barnes & Roeder (2001). (c) The	
	bivariant diagram of 100 *Cr# versus 100 * Mg# of Al-Chromite	
	shows a distinct linear trend. Fields of stratiform complexes	
	(Irvine, 1967, 1974), Worldwide Alaskan-type intrusions (Barnes	
	& Roeder 2001, Helmy and El Mahallawi, 2003, Farath & Helmy,	
	2006), island-arc intrusions (Spandler et al., 2003), abyssal	
	peridotites (Dick and Bullen, 1984) are shown here for	
	comparison. Most of the chrome spinel (Al-chromite) follows the	
	trend of the Alaskan-type complex. (d) Bivariant plot of 100	
	$*^{Y}Fe^{+3}$ versus 100 $*Mg\#$ of Al-Chromite. Field of Alaskan type	
	intrusions are obtained from (Himmelberg and Loney 1995,	
	Batanova et.al.2005,) island-arc intrusions (Spandler et al., 2003),	
	stratiform complexes (Irvine, 1967, 1974), mid-oceanic Ridge	
	basalt (MORB) (Barnes and Roeder, 2001), are shown here in the	
	diagram for comparison.	
Figure 4.9	(a) Plot of 100 *Cr/ (Cr+Al) versus TiO <sub>2</sub> (wt.%) of Al-Chromite	87
	from the study area. Spinels from abyssal (Dick 1989, Dick and	
	Bullen, 1984) and fore arc (Ishii et al., 1992) peridotites, MORB,	
	boninites (Arai, 1992, Barnes and Roeder, 2001), Aleutian xenoliths	
	(Conrad and Kay, 1984, Debari et al., 1987) and Alaskan-type	
	ultramafic intrusions (Himmelberg and Loney, 1995) are shown	
	here for comparison. (b) Plot between $Al_2O_3$ versus $TiO_2$ in wt.% of	
	Al chromite. Fields of LIP (large igneous province basalts), OIB	
	(ocean-island basalts), MORB (mid-ocean ridge basalts), ARC,	
	MOR (mid-ocean ridge) peridotites are after Kamenetsky et al.	
	(2001), and Alaskan-type complexes from Alaska were obtained	
	from (Himmelberg and Loney 1995). (c) Bivariate plot of Al <sub>2</sub> O <sub>3</sub> vs.	
	$Cr_2O_3$ (wt.%) from Franz & Wirth (2000), modified after Seo et al.	
	(2013), showing near to Arc cumulate setting. (d) Variation	
	diagram for $\Delta \log fO_2$ (FMQ) versus Cr# of Al-Chromite from the	
	study area. The field of Arc cumulates (Ballhaus 1993) and Abyssal	
	peridotites (Bryndzia & wood 1990) are shown here for	
	comparison.	
Figure 4.10	Olivine (Fo) chemistry of peridotite and olivine pyroxenite from	89
1 18410 7.10	the study area and its comparison with olivine (Fo) content from	37
	worldwide Alaskan-type intrusions.	
Figure 4.11	The chondrite normalized REE of chrome spinel (sun and	90
rigure 4.11	McDonogh, 1989)	<del>20</del>
Figure 5 1		100
Figure 5.1	(a) $(Gd/Yb)_N$ versus $Al_2O_3/TiO_2$ (after Arndt 2003) indicates	109
	residual garnet's role in most studied samples. (b) $(Gd/Yb)_N$ versus	

	$CaO/Al_2O_3$ (after Jahn et.al., 2003) shows the role in most studied samples.	
Figure 5.2	(a) AFM diagrams after (Irvine and Baragar, 1971) (a) CaO-MgO-Al <sub>2</sub> O <sub>3</sub> diagram after Jenson (1976), Modified by Viljoen et al., (1982). (b) Al <sub>2</sub> O <sub>3</sub> -(Fe <sub>2</sub> O <sub>3</sub> +TiO <sub>2</sub> )-MgO triangular diagram (Jenson, 1976; modified by Viljoen et al., (1982). (c) (Na <sub>2</sub> O+K <sub>2</sub> O)-FeO <sub>t</sub> -MgO discrimination ternary diagram for the ultramafic-mafic rocks of MUC. Fields of both cumulate and non-cumulate rocks are from Beard (1986).	110
Figure 5.3	Harker's binary plot for major oxides against MgO of ultramafic-mafic of the Madawara ultramafic complex.	112
Figure 5.4	Harker's binary plot for trace elements against MgO of ultramafic- mafic of the Madawara ultramafic complex	113
Figure 5.5	(a-h) Chondrite-normalized REE patterns and primitive normalized multi-element spider diagrams of the ultramafic-mafic of the Madawara region	114
Figure 5.6	(a-h) Chondrite-normalized REE patterns and primitive normalized multi-element spider diagrams of the ultramafic-mafic of the Ikauna region.	117
Figure 5.7	(a-b) Chondrite-normalized REE patterns and primitive normalized multi-element spider diagrams of the ultramafic-mafic of the Hanumathgarh region.	119
Figure 5.8	(a) Sm-Nd whole rock isochron for the ultramafic-mafic of Madawara ultramafic complex. (b) $\varepsilon$ Nd versus time evolution diagram showing the involvement of depleted to slightly enriched mantle source.	121
Figure 5.9	(a-b) Plot of Nb/La and $\varepsilon$ Nd(t) versus MgO (c-d) Plots of La/Sm and $\varepsilon$ Nd(t) versus Nb/La (e) Ti/Y versus $\varepsilon$ Nd(t) diagram after shellnutt et al., (2015) (f) $I_{sr}$ versus $\varepsilon$ Nd(t) diagram to examine the fractionation crystallization (FC) and assimilation fractionation crystallization (AFC) processes.	123
Figure 5.10	(a-h) Chondrite and primitive mantle normalized PGE patterns of ultramafics of the MUC	129
Figure 6.1	Bivariant diagrams of Yb versus selected trace elements of the ultramafic-mafic of MUC.	143
Figure 6.2	(a-c) Correlation diagrams of trace elemental ratios of MUC in the southern Bundelkhand craton. (Th/Yb) <sub>PM</sub> , (Nb/Th) <sub>PM</sub> are the primitive mantle normalized values. Data sources of the primitive mantle (PM), Normal mid-oceanic ridge basalt (N-MORB), Enriched mid-oceanic ridge basalt (E-MORB), Oceanic Island	146

	basalt (OIB), Lower crust and Upper crust values are from Sun and McDonough (1989).	
Figure 6.3	SiO <sub>2</sub> versus Th/La indicating fractional crystallization of the ultramafic mafic of the MUC.	151
Figure 6.4	(a) (La/Sm) <sub>CN</sub> vs (Gd/Yb) <sub>CN</sub> diagram as a proxy for lithospheric contribution and/or degree of partial melting vs depth of melting. The diagram shows that the melt has generated in both spinel and garnet stability zones with a considerable crustal input. The garnet-spinel stability fields are taken from 'Alvaro et al. (2014). CN, chondrite normalized; PM, primitive mantle; OIB, ocean island basalt (McDonough & Sun, 1989); UC, upper crust; BCC, bulk continental crust (Rudnick & Gao, 2003). (b) MgO (wt.%) versus FeO (wt.%). Fields of partial melts and residue (after Hanson and Langmuir, 1978) of MUC, Bundelkhand Craton.	154
Figure 6.5	(a) Nb/U versus Nb/Th plot (after Saunders et al., 1988) shows primitive mantle reservoirs with minor crustal contamination for the ultramafic-mafic of MUC. (b) Nb/Y versus Zr/Y (Condie, 2003) plot indicating depleted to primitive mantle source reservoirs for the ultramafic-mafic rocks of MUC.	157
Figure 6.6	(a) (Ta/La) <sub>PM</sub> versus (Hf/Sm) <sub>PM</sub> (after Laflèche et al., 1998) (b) Th/Zr and Nb/Zr plot for the ultramafic-mafic of MUC.	158
Figure 6.7	(a) Th/Yb versus Nb/Yb binary plot (Pearce, 2008) indicating depleted mantle with arc source reservoirs for the ultramaficmafic rocks. (b) Zr/Nb versus Nb/Th plot (Condie, 2003) showing arc to the primitive mantle for the ultramafic-mafic rocks of MUC. Abbreviations used: subduction (SUB); PM, primitive mantle; DM, depleted mantle; ARC, arc-related sources; N-MORB, normal ocean ridge basalt; OIB, oceanic island basalt; DEP, deep depleted mantle; EN, enriched component. (c) Plot Nb/U versus Nb showing arc affinity for the ultramafic-mafic of MUC. Data for the primitive mantle and normal mid-oceanic ridge basalt (N-MORB) are from Sun and McDonough (1989); oceanic island basalt (OIB) and island arc basalt (IAB) are from Niu and O'Hara (2003).	159
Figure 6.8	(a) Pt/Pt* [Pt <sub>N</sub> /(Rh <sub>N</sub> *Pd <sub>N</sub> )1/2] versus Pd/Ir of the studied samples showing the role of fractional crystallization. Fractionation and partial melting trends are from Garuti et al. (1997). (b) Cu versus Pd plot indicating sulphur under-saturated nature of the studied samples (after Hoatson & Keays, 1989); (c) Pd/Ir versus Ni/Cu diagram (after Barnes, 1990) in which the studied samples	166

occupying the field of near komatiitic field indicating moderate to
high degree of partial melting. (d) Cu/Ir vs. Ni/Pd variation
diagram in which the ultramafics showing the olivine and sulphide
fractionation trend (after Barnes et al.,1985).

Table	Table caption	Page No.
Table 1.1	Instrumental parameter setting for the trace elemental analysis in HR-ICP-MS	33
Table 1.2	Standard deviation and relative standard deviations for the standards to recheck the instrumental analysis	34
Table 4.1	Representative electron microprobe (EPMA) analysis of amphiboles from the MUC.	92-94
Table 4.2	Representative electron microprobe (EPMA) analysis of olivine from the ultramafic rocks of Madawara ultramafic complex (MUC).	95-96
Table 4.3	Representative electron microprobe (EPMA) analysis of serpentines and chlorite from the MUC.	97
Table 4.4	Representative electron microprobe (EPMA) analysis of plagioclase from the ultramafic rocks of the MUC.	98-99
Table 4.5	Representative electron microprobe (EPMA) analysis of chrome spinels (chromites) from the ultramafic rocks of MUC.	100-102
Table 4.6	Representative LA-ICP-MS data of chrome spinels from the ultramafic of the MUC.	103
Table 4.7	Estimated maximum, minimum, and average value of Al2O3, FeO/MgO and TiO2 of parental melts in ultramafic rocks from the study area in comparison with parental melt of different tectonic setting. Temperature and oxygen fugacity values wherever available are also given in the table.	104
Table 4.8	Comparison between worldwide Alaskan type intrusion and Madawara ultramafic complex.	105
Table 5.1	Major and trace elements data for ultramafic mafic and intermediate rocks of the MUC.	132-136
Table 5.2	Platinum group element (PGEs) data for the ultramafic-mafic of the MUC.	137-139
Table 5.3	Sm-Nd and Rb-Sr isotopic data of ultramafic mafic and intermediate rocks of the MUC	140

#### ABSTRACT

The Bundelkhand craton in Northcentral India preserves a composite mosaic of semi-circular Archean continental nuclei, that occupies about ~26,000 sq. km. The craton has a very complex geological, metamorphic and tectonic history from ca. 3.8-2.5 Ga. Multidisciplinary research studies involving detailed field, petrological, geophysical, geochronologic, elemental and isotope over three decades immensely contributed to our understanding of the fundamental architecture as well as crust formation in the Bundelkhand craton. Recent studies suggest that the Bundelkhand craton can be divided into three crustal blocks: the northern, central, and southern blocks. These blocks can be distinguished by their distinctive geological signatures, like basement TTG-type granitoids, greenstone assemblages, various granitoids, and ultramafic mafic intrusive rocks, deformation, metamorphic events, and the degree of melting of the older crustal fragments. The Bundelkhand craton essentially consists of three major lithological associations including a vast area of Paleoarchean to Mesoarchean polyphase granitoids of TTG affinity (3555-3270 Ma), Mesoarchean to Neoarchean volcano-sedimentary greenstone sequences (2800-2500 Ma) and voluminous Neoarchean (2583-2536 Ma) high K- granitoids including sanukitoids and anatectic granites.

The present study is focused mainly on the Madawara ultramafic-mafic complex (MUC) with an aim to understand the petrogenetic process and geodynamic context of ultramafic mafic magmatism of the southern part of the Bundelkhand craton. The southern part of the Bundelkhand craton preserves high-grade basement rocks of TTG affinity such as granitic gneisses, gneisses, migmatite, amphibolites, and hornblende-biotite gneisses. These rocks are exposed around Rajola and north of Madawara. The low-grade volcano-sedimentary rocks such as banded hematite-magnetite quartzite, quartzite, mica-schists, and amphibolites are exposed around Girar, Baraitha, and Badwar villages called as southern greenstone belt of the Bundelkhand craton (SGBC). The MUC lies north of the SBGB in the form of lensoidal bodies

marked by intrusive relation with the Bundelkhand granitoids. This lensoidal ultramafic-mafic intrusive unit comprises peridotite, pyroxenite, olivine pyroxenite, hornblendite, gabbro, gabbroic diorite and diorite exposed at mainly around Madawara, Ikauna, Pindar and Hanumathgarh. The largest ultramafic body is exposed at the SE part of Madawara village and is in the form of a low-lying asymmetric ridge that is ~400 m wide and extends laterally up to 5 km. These ultramafic—mafic bodies are nearly subparallel and are confined between the Madawara—Karitoran shear zone in the north and Sonrai—Girar shear zone in the south. Both the MUC and older granitoids have been affected by shearing and fluid flow, demonstrating a fluid-induced alteration of the ultramafic rocks into serpentine-tale-chlorite schists and talc tremolite-actinolite schists. These ultramafic units are further traversed by Bundelkhand granitoids and NE—SW trending quartz reefs. At Madawara, the intrusion is asymmetric with ultramafic rocks in the centre comprising peridotite, olivine pyroxenite, pyroxenite, and hornblende-rich peridotite with grading towards gabbro in the rim part. On the other hand, the Ikauna ultramafic rocks show peridotitic nature occurring in the core while gabbro and diorites occur towards the rim part.

The petrographic studies of the ultramafic-mafic of the MUC (Madawara, Ikauna, and Hanumathagrh) show significant differences in terms of mineralogy, textures, and alteration patterns. The petrographic characteristics of the majority of the ultramafic rocks of MUC do not show any preserved primary mineralogy, however, the presence of relict olivine is observed in the few ultramafic rock samples of the Madawara region showing cumulate to poikilitic textures. The observed mineralogy developed due to fluid-induced hydrothermal alteration processes associated with shearing along the margin of the intrusions. The presence of tiny carbonate veins in a few of the sections indicates CO<sub>2</sub> rich fluid-induced alteration process. On the other hand, the mafic rock of the MUC has not been altered and preserved its primary mineralogy showing ophitic to sub-ophitic textures. The presence of channelised flow filled

with iron oxides in the ultramafic indicates the area is affected by the alteration process. The preserved mineral assemblages and textures in the Madawara ultramafic complex (MUC) indicate the area is subjected to alteration with mild deformation and metamorphism. The sulphides are the least opaque mineral in the ultramafic-mafic rocks of the MUC. The reflected microscopic studies show the presence of sulphide phases mainly pentlandite ((Fe, Ni)<sub>9</sub>S<sub>8</sub>) and millerite (NiS) in the intercumulus spaces of olivines. The SEM-EDX studies show the rare occurrences of PGM in the form of alloys occurred as disseminated grains in the interspace of olivine as well as the cleavage planes of pyroxenes. The sulphide phases are more in the ultramafic of the Madawara sector compared to the ultramafic of the Ikauna sectors while the oxide phases are more in the Ikauna in comparison to the oxide phases of the Madawara.

The EPMA studies of Cr-spinel (chromite) from the Madawara ultramafic complex can be classified mainly into three types on the basis of textural and mineral chemistry. Type I chromite shows homogeneous Al-chromite in composition which is more likely primary in nature. Type II chromites are zoned in nature showing core-rim compositional variation. Type III chromite shows homogeneous Fe-chromite in the composition is more likely modified in nature and is formed either by the involvement of fluid in the subsequent stages of magmatic evolution or by alteration in the serpentinization process. The primary type-I Cr-spinel is characterized by low Al<sub>2</sub>O<sub>3</sub> (10.63–21.87 wt.%), TiO<sub>2</sub> (0.2–0.6 wt.%), and Mg# (9.30–26.22) and high Cr# (55.12–76.48) and Fe# (73.78–90.70). Parental melt calculation of type I Cr-spinel shows that low Al<sub>2</sub>O<sub>3</sub> (9.22 to 14.30 wt.%) and high oxygen fugacity (+0.26 to +2.14) could be related to magma generation in oxidizing environments of arc setting. The plot of type- I Cr-spinel in various discrimination diagrams suggests that MUC is formed in an arc environment, which is very similar to Alaskan-type magmatism.

The studied ultramafic rocks show low to intermediate values of (Gd/Yb) N (0.9-2.0), Al<sub>2</sub>O<sub>3</sub>/TiO<sub>2</sub> (12.12-19.46) coupled with low to high values CaO/Al<sub>2</sub>O<sub>3</sub>

(0.52-2.47) implying that the variable involvement of garnet in the residues. This indicates their derivation from a relatively deeper mantle with the presence of minor garnet or absence of garnet in the source residue. This is substantiated by to flat to slightly fractionated HREE patterns [ $(Gd/Yb)_N = 0.9\text{-}2.0$ ] in the chondrite normalized diagrams indicate presence of minor residual garnet or without garnet influence in the mantle source residue. The samples with lower  $CaO/Al_2O_3$  despite lower  $Al_2O_3/TiO_2$  could be related to the mobility of CaO and its removal by  $CO_2$ -rich fluid phases probable during the hydrothermal alteration process and deposited as tiny carbonate microscopic veins.

The ultramafic rocks of the MUC show a total REE content ranging from sub-chondritic (6.67) to 9.89 ppm) to chondritic (10.84 to 15.81 ppm) except a few rock samples show slightly higher total REE (18 to 24 ppm) suggesting their derivation from heterogeneous mantle source reservoirs ranging in composition from highly depleted to primitive mantle reservoirs. On the other hand, the mafic rocks from this study show a wide range of total REE contents (16.47 to 127.44 ppm), which also implies heterogeneous shallower mantle sources. The studied ultramafic samples of the MUC show variable (negative or insignificant) Zr-Hf anomalies implying origin of magmas at different depths (200-250 km) whilst the mafic samples show negative Nb-Ta with positive Y anomalies, and variable Zr-Hf anomalies precluding the involvement of garnet in the residue suggesting either melt generated at shallower mantle in arc environments. The elemental ratios of Nb/U, Nb/Th, Zr/Nb, Nb/Th, Nb/Y and Zr/Y of the MUC reveal their origin from heterogeneous relatively deeper to shallower involving primitive mantle to depleted mantle sources. The existence of a depleted mantle at 2.67 Ga indicates an earlier episode of mantle differentiation and continental growth probable ca. 3.2-3.4 Ga. The ultramafic rocks show moderate to high content of Platinum Group of Elements (PGE) content while the mafic rocks have low PGE content. The low Pd/Ir ratio with (PPGE/IPGE<1) Ikauna ultramafic suggests a higher degree of parental melting and the presence of PGE in the form of alloys within the olivine or chromite. However, the ultramafic of the Madawara shows a relatively higher Pd/Ir ratio with (PPGE/IPGE>1) in comparison to Ikuana ultramafic suggests they are attributed to lower degree partial melting with PPGE enrichment in the melt phase. This is indicated by the presence of interstitial sulphides (pentlandite and millerite) in the SEM-EDX studies which are also supported by the petrographic studies.

Based on the detailed study of their field relationships, elemental geochemistry, and Nd-isotopic data it can be inferred that the Madawara ultramafic-mafic complex reveals "long-term depletion of mantle reservoirs" suggesting large-scale differentiation of mantle and continental growth during ca. 3.5-2.7 Ga in the Bundelkhand craton. The ultramafic-mafic magma generation in the deeper mantle is probably related to slab breakoff and fluid input. Alternatively, these ultramafic-mafic magmas may be related to tectonically abducted mantle material through back thrusting in an oceanic arc setting wherein upward moving mantle could be melted through decompression leading to the origin of ultramafic-mafic magmas at different levels.

### **CHAPTER-I**

In this chapter, an attempt has been made to present an overview of lithological assemblages, tectonic framework, thermal records, crustal accretion patterns, rates of crustal growth and geodynamic models of the early Earth. Further, an overview of the regional geological and tectonic framework of the Bundelkhand craton is presented, outlining previous work and major scientific issues to be addressed, the defined objectives of the thesis, and the methodology adopted.

### 1. Introduction

The dynamics of the evolving early earth including the coupled evolution of the "crust-mantle" system," continental growth, and craton development, are the principal areas of research in the Earth system sciences. Understanding early earth dynamics is crucial to comprehend the thermal and mechanical process of crust formation and associated mineral resources. In the past four decades, several studies carried out on the Archean cratons that immensely contributed knowledge base on the fundamental structure of the lithosphere and crust-mantle evolution system of the early earth. More recent research on the Archean cratons around the globe has improved our knowledge of the "geological, tectonic and biological processes that transformed our planet into sustainable planet earth." ("Smithies et al., 2018; Bedard et al., 2018; Wyman et al., 2018; Jayananda et al., 2018, 2020, 2023"). Throughout the history of the planet, the evolution of continents-from their formation through their fragmentation and eventual distribution had a significant impact on biological evolution and climate variability ("Condie 2005"). The "Archean Eon," which spans a time period of 1500 Ma, has seen significant evolutions in the geologic and tectonic processes, as well as the origin of life on earth, oxygenated habitats, and mettallogeny. In spite of years of research on magmatism, metamorphism and the tectonic process of early earth still it is a topic of much discussion and debate. A multi-disciplinary approach of work involving field, geochemistry

and isotope tracers is essential to reconstruct the early earth's history. The target rocks include greenstone volcanic assembles, ultramafic-mafic intrusions, and associated TTG-type granitoids from the Archean cratons offer an excellent opportunity to address the evolution of crust-mantle systems through time. The major Archean cratons are distributed around the world. (See figure 1.1)

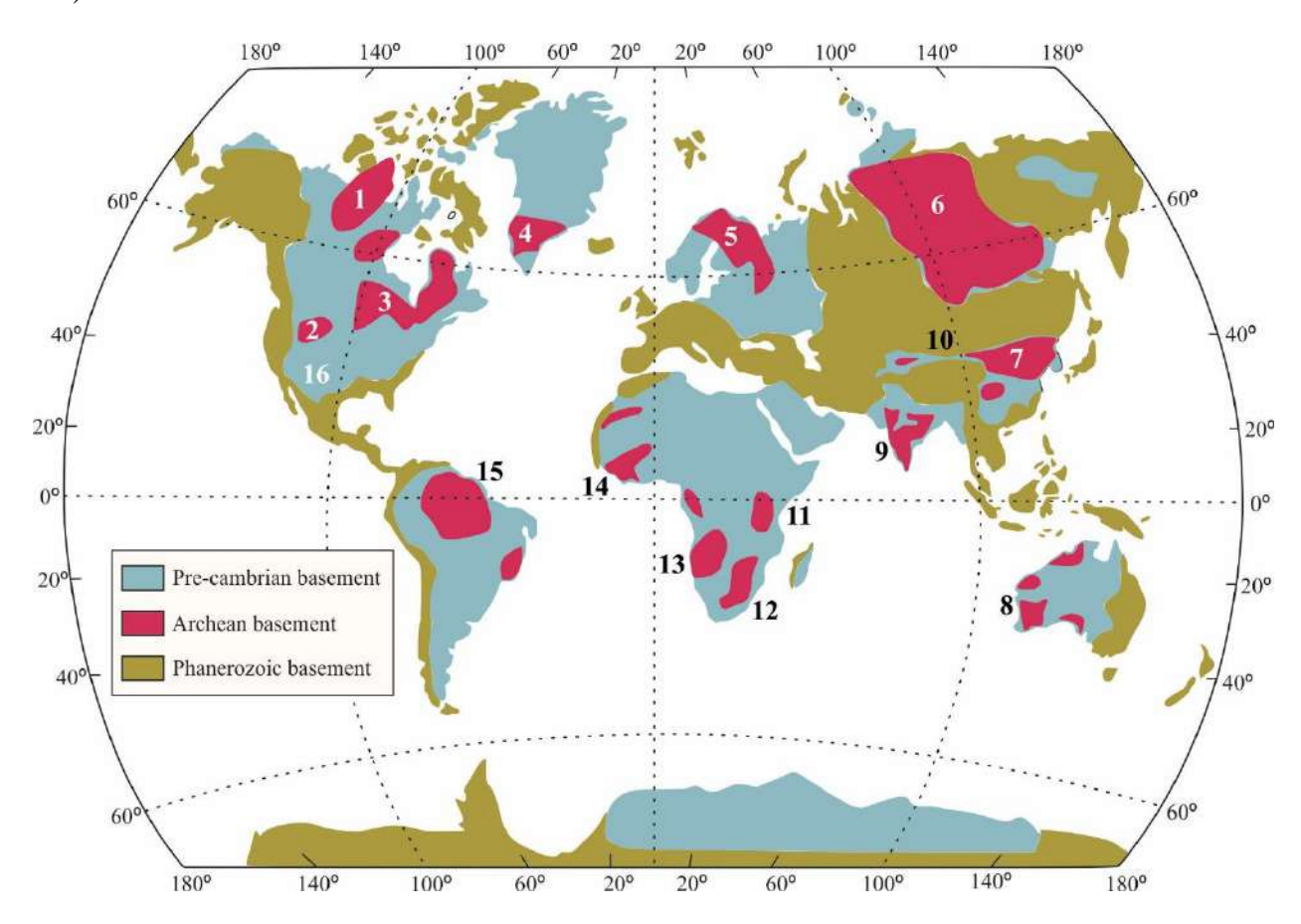


Figure 1.1 The distribution of Archean cratons around the globe (1) Slave, (2) Wyoming, (3) Superior, (4) Greenland, (5) Fennoscandian, (6) Siberian, (7): North China, (8) west Australian, (9) Indian, (10) Tarim, (11) Tanzanian, (12) South African (Kaapvaal) (13) Congo, (14) west African, (15) Amazonia and (16) Colorado Plateau. (Reference: Lee et al., 2011). Map of Precambrian (>540 Mya) and Phanerozoic (<540 Mya) crustal basements are shown here. Archean cratons are shown in regal red in colour.

### 1.1. Unique features of the Archean Earth

The planet earth preserves 1/3 of Archean history. Although 60-70 % of the crust has been generated and stabilized into cratonic land mass, still this period is subject of debate and discussion in the context of geodynamic evolution. The Archean period is characterized by distinct lithological assemblages, structural patterns, geothermal records, and rate of continental growth. This period marks the complex geological process in terms of magmatism, crust formation and reworking of old crust, metamorphism and associated mineralization ("Nutman et al., 2001; Zhai et al., 2014; Groves et al., 2021").

- 1.1.1. High heat production and hotter mantle
- 1.1.2. Tonalite-Trondhjemite-Granodiorite (TTG) type granitoids
- 1.1.3. Greenstones with komatiites
- 1.1.4. Late calc-alkaline to K-rich granites and sanukitoids
- 1.1.5. Absence of HP-LT metamorphism

### 1.1.1 High heat production and hotter mantle

Earth's heat production during the Archean period is much higher compared to the present day ("Fyfe, 1978; Nisbet et al., 1993 Abbott et al, 1994"). The Precambrian terrains observed heat flow data indicate that heat flow on the continents diminishes with increasing tectonic age ("Kraskovski, 1961; Nyblade and Pollack, 1993 and reference therein") (see figure 1.2). This heat is produced during the early stages of the "Earth's accretion" as well as latent heat from the decay of radioactive elements with a short half-life such as <sup>26</sup>Al and <sup>129</sup>I stored in mantle and core or long-lived radiogenic isotopes such as <sup>40</sup>K, <sup>235</sup>U, <sup>238</sup>U and <sup>232</sup>Th contributed to high heat flow of the early Earth. ("Wasserburg et al., 1964; Mc Kenzie and Weiss, 1975; Lambert, 1976"). The tectonic processes operated at the time of mantle melting or accretion may largely be controlled by the

thermal structure and convection patterns. Numerous workers have addressed the extraction of the juvenile crust from the mantle and the extensive reworking of the continental crust between ca 4.0-2.5 Ga in the Archean cratons. This period represents the largest global thermo-tectonic processes and major crustal growth in the history of the earth, driven by high heat flow linked to large-scale instabilities in the mantle convection regimes. ("Stein and Hofmann, 1994; Condie, 1993").

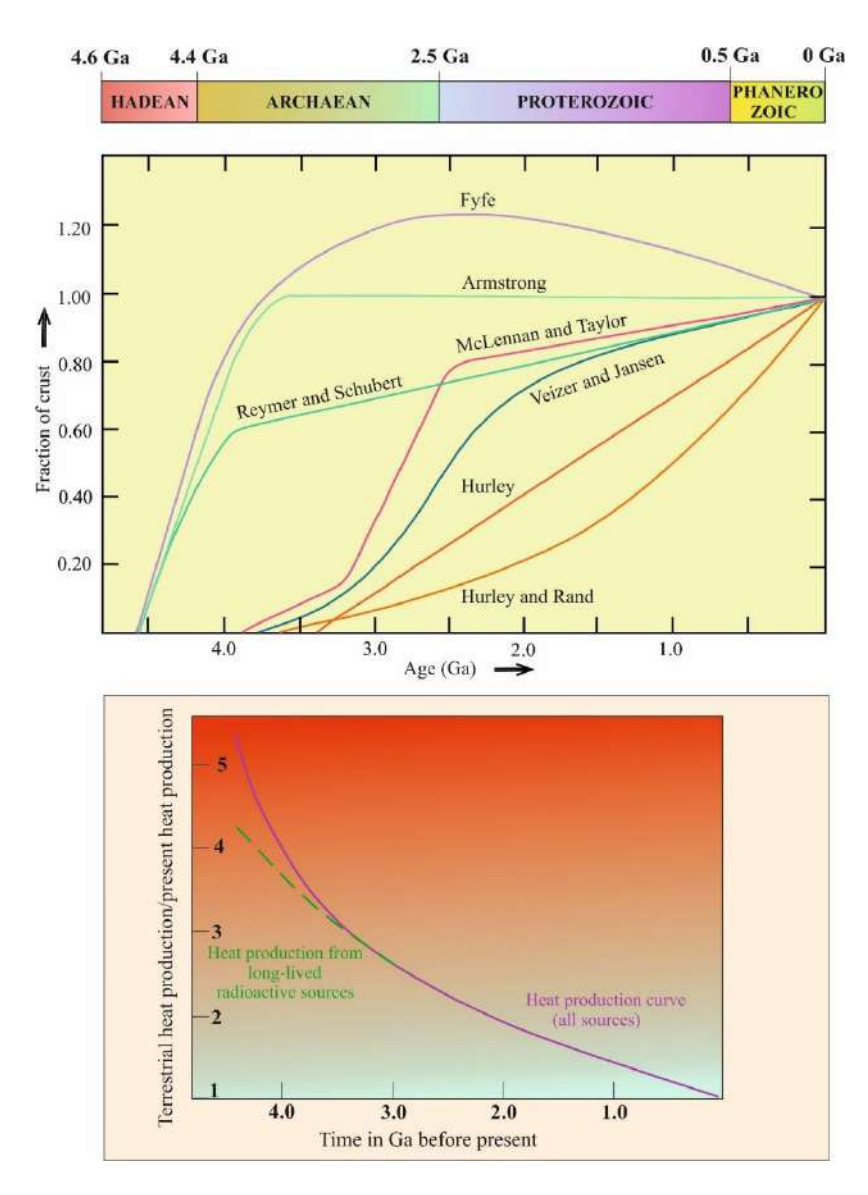


**Figure 1.2** A selection of crustal growth models. Models shown here adopted from Fyre 1978, Reymer & Schubert 1984, Armstrong 1981, Hurley 1968, Hurley & Rand 1969, Veizer & Jansen 1979 and Taylor & McLellan 1982.

The internal heat of the earth is dissipated by transforming thermal energy into kinetic energy through convection processes at ridge axes, hot spots, and marginal basins. The Archaean earth is thought to have formed through a more chaotic convection regime that resulted in the production of more hot spots and thicker oceanic crust while some researchers have postulated very different convection regimes for the "early earth." ("Sleep, 1979, Richter, 1985, 1988").

### 1.1.2 Tonalite-Trondhjemite-Granodiorite (TTG) type granitoids

Granitoids are dominated by variable proportions of "tonalite, trondhjemite, and granodiorite" and some of which correspond to the oldest preserved continental nuclei. ("Barker, 1979"). The TTG suites are the Earth's oldest preserved crust and are the major constituent of the exposed Archaean continental crust. ("Condie, 1981"). The oldest dated TTG suites across the World include 4.0 Ga Acasta gneiss from Archaean Slave province, Canada ("Bowring et al., 1989"), 3.9 Ga in Greenland ("Kinny, 1986"), 3.65 Ga in southern Africa ("Compston and Kroner, 1988"), 3.45 Ga in west Africa ("Potrel et al., 1994"), Antarctica ("Black et al., 1986"), 3.6 Ga in Siberian craton ("Bibikova, 1984") and 3.8-3.4 Ga in India ("Meen et al., 1992; Peucat et al., 1993, 2012; Guitreau et al., 2017; Jayananda et al., 2015,2023; Ranjan et al., 2020; Mondal et 1998, 2002; Kaur et al., 2014, 2016; Chaudhuri et al., 2018"). TTGs are typically thought to be produced by the "partial melting" of mafic protoliths at different depths in the crust, arc crust, or mantle ("Arth and Hanson, 1975; Glikson, 1979; Jahn et al., 1981; Jahn and Zhang, 1984; Martin, 1986, 1994; Martin & Moyen, 2002; Evans & Hanson, 1992; Polat et al., 2012"). However, other scholars have suggested that the origin of these early felsic crusts may be formed by the fractional crystallisation of a hydrated basaltic magma. ("Barker, 1979; Arth et al., 1978; Kramers, 1988").

The composition of these TTG suites is comparable from craton to craton during the Archean period. They are typically "quartzo-feldspathic gneisses," rich in sodic-plagioclase with

containing biotite and hornblende. Geochemical analysis of the TTG series reveals a high concentration of silica, sodium content, and low content of ferromagnesian elements. Notwithstanding their mode of formation, they were thought to have originated in an environment with a high heat flux regime that is closely associated with mafic magmatism. ("Choukroune et al., 1997"). Subsequently, several other workers ("Smithies, 2000; Adams et al; 2012; Polat et al., 2012; Martin et al., 2014; Jayananda et al. 2023") proposed melting of the base of thickened oceanic plateaus or melting of the mafic crust of a thicken island arc episodically throughout the earth histories. ("Huang et al., 2012; Polat et al., 2012; Jayananda et al., 2015"). The model of TTG shows its origin by partial melting of the hydrous oceanic crust in subduction tectonic settings ("Martin, 1994; Foley et al., 2002; Rappe et al., 2003"). The mineralogical and chemical composition of the TTG also depends upon the angle of subduction and depth of melting attributed to the time-dependent secular cooling of the planet earth. (Martin and Moyen, 2002).

Recent studies, however, demonstrate that melting of oceanic crust formed at oceanic spreading centres impoverished in incompatible elements and melting of which cannot yield the large incompatible element contents reported in TTGs ("Martin et al., 2014; Jayananda et al., 2015, 2023"). The reworking of TTG crust in the Neoarchean led to the generation of high potassic granites.

TTG-type granitoids form abundant lithological associations in the Bundelkhand craton. Magmatic protoliths of TTGs in Bundelkhand craton formed in four major events during the Paleoarchean time period viz. 3.55 Ga, 3.44 Ga, 3.30 Ga and 3.20 Ga ("Mondal et al., 2002; Kaur et al., 2014, 2016; Saha et al., 2016 and Joshi et al., 2022"). The younger phase of granodioritic gneiss formation ca. 2.71-2.67 Ga has been documented by. (Verma et al., 2016).

#### 1.1.3. Greenstone belts with komatiites

Archean greenstone belts provide important constraints for our understanding Archean mantle, crustal growth, and geodynamics evolution of early Earth ("Windley, 1995, Polat et al., 1998; Polat and Kerrich, 1999; Chavagnac et al., 2004; Jayananda et al., 2008, 2016; Mole et al., 2015; Jayananda et al., 2023 and references therein"). They are widespread throughout the Archean cratons, and their ages are typically between "3.5 Ga to 2.7 Ga." ("Condie, 1981; 1994"). "Archean greenstone" volcanic assemblages are stratigraphically comparable from one craton to the next and are dominated by komatiite-basalt associations with modest intermediate to felsic volcanics and sedimentary sequences. They typically consist of basal sequences, which are usually mafic-ultramafic volcanics from the tholeite-komatiite series that transition into felsic volcanics at higher stratigraphic levels and exhibit calc-alkaline lineage. The sedimentary rocks are made up of conglomerate, siliciclastic rocks, turbidites, or sediments linked to faulting (Mueller et al., 1994). Some of these tectonic components in the greenstone belts have been compared to preserved oceanic crust or modern ophiolitic complexes (Jayananda et al., 2023, de Witt et al., 1987).

Komatiites are the Mg-rich ultramafic lava lavas which are first reported from the Archean Barberton greenstone belt by (Viljoen and Viljoen, 1969). Subsequently, komatiites are documented in other cratons. Komatiite lavas are found in the majority of the Archean cratons (South Africa, Australia, India, Brazil, Finland, etc.). The Komatiite lava flows exhibit pillow structures and spinifex texture. The spinifex texture is characterized by skeletal crystals of olivine and pyroxene set in random orientation and has the appearance of spinifex grass of Western Australia. They contain primary mineralogy of olivine, pyroxene, and glass with at least 18% of MgO content (Arndt and Nisbet, 1982). Their low level of incompatible trace elements coupled with high MgO contents reveals the high degree of mantle melting and their estimated temperature

of eruption is approximately ~1600-1700°C (Arndt and Nisbet, 1982; Nisbet et.al., 1993). Komatiites exhibit large degrees of partial melting in the hot ambient upper mantle (Nisbet, 1982). Archean greenstone belt formation and tectonic development continue to be the subject of much discussion and debate, especially in relation to the significance of subduction, plume magmatism, rifting, the connection to diapirism, and autochthonous versus allochthonous settings ("Choukroune et al., 1997; Chardon et al., 1998; de Wit, 1998; Chadwick et al., 2000, 2007; Hamilton, 2003; Chavagnac, 2004; Jayananda et al., 2008, 2016 2023; Tushipokla and Jayananda, 2013").

Bundelkhand craton preserves volcanic-sedimentary greenstone successions ("Singh and Slabunov, 2015, 2016; Singh et.al, 2018"). The volcano-sedimentary sequences in the Bundelkhand craton have been subdivided into two groups named as "Central Bundelkhand Greenstone Component (CBGC) and the Southern Bundelkhand Greenstone Component (SBGC)." ("Singh and Slabunov 2015, 2016"). The CBGC is characterized by ultramafic-mafic, intermediate to felsic rock assemblages along with sedimentary sequences like greywackes, phyllite, banded hematite magnetite quartzite, and quartzites. The whole rock Sm-Nd dating of ultramafic-mafic reveals an age of 3435±161 Ma (Singh et al., 2019) and high-Mg basalts reveal a U-Pb zircon age of 2687±11 Ma (Slabunov and Singh, 2015). The felsic volcanics from this greenstone reveal two different ages 2810±13 Ma and 2557±33 Ma (Slabunov and Singh, 2015). On the other hand, the SBGC is s characterized by metavolcanics, banded iron formations, oligomictic conglomerates, and quartzites. A recent study of metavolcanics from this greenstone reveals a whole-rock Sm-Nd age of 2986±190 Ma (Hiloidari et al., 2021) and quartzite's detrital zircon provides an older age of 3.4 Ga and a younger age of 3.25 Ga (Slabunov et al., 2017). The studied Madawara ultramafic-mafic rocks (MUC) occur within the gneisses and are found as

lensoidal bodies stretched in the E-W direction in the norther proximity of southern Bundelkhand greenstone belts. They are characterized by ultramafic-mafic to intermediate composition. The ages are not known for these ultramafic-mafic units.

### 1.1.4. Late calc-alkaline to K-rich granites and sanukitoids

Granitoids are abundant lithologies found in Archean cratons all over the world. They make up about 20% of the rocks exposed in Archean terrains and 30% of Archean granitoids, with the remaining 70% belonging to Na-rich TTG associations (Goodwin, 1991; Condie, 1993; Moyen et.al., 2011; Martin, 1994). The late granitoid intrusions are found as high-potassic granite plutons and calc-alkaline granitoids with affinities to sanukitoids (Stern et al., 1991; Martin and Moyen, 2002; Jayananda et al., 2000, 2006, 2018, 2020; Moyen et al., 2010). These granitoid generally intrude into the greenstone belts or greenstone-TTG interface. Their emplacement is spatially associated with the deformation and metamorphism of greenstones and surrounding basement TTG. These granitoid plutons mostly contain granite, granodiorite, quartz-monzonite, monzogranite, and monzodiorite, with minor amounts of tonalite. They are mantle and arc crust hybrid sources with varying amounts of ancient crust input (Laurent et al., 2014; Mondal et al., 2014; Singh et al., 2019; Jayananda et al., 2020; Singh et al., 2021, Joshi et al., 2022). The sources of most granitoids are from mantle-derived to crustal reworking and partial melting of older TTG are proposed for the origin of these granites and show a significant correlation with tectonic settings (Jayananda et al., 1995a, 2000, 2006, 2019, 2020; Laurent et al., 2014; Moyen et al., 2003a). According to (Barker and Arth, 1976), Archean potassic granites plot on the calc-alkaline differentiation trend on the Na-K-Ca diagram and follow the high-K calc-alkaline trend in the normative An-Ab-Or diagram (O'Connor, 1965; Barker and Arth, 1976). These rocks do not exhibit any affinity with the trondhjemitic trend that is typical of Archean TTGs.

Sanukitoids are a unique subclass of the Archean granitoid series with a high magnesium content. They were initially described by (Shirey and Hanson, 1984) from Canada. These sanukitoids have been documented over the last 20 years from Superior province, Canada (Shirey and Hanson, 1984; Stern and Hanson, 1991; Stevenson et al., 1999; Davis et al., 2005 and reference therein), Finland (Halla, 2005), Dharwar craton ("Balakrishnan and Rajamani, 1987; Jayananda et al., 1995a, 2000, 2018, 2020; Moyen et al., 2003b; Sarvothaman, 2001"), Pilbara craton (Smithies and Champion, 2000), southern Africa, ("Laurent et al., 2011"), North China craton ("Wang et al., 2009") and Amazonian craton, southern America (Althoff et al., 2000; Souza et al., 2001; Leite et al., 2004; Oliveira et al., 2009; Almeida, 2010), Zimbabwe craton (Bagai et al., 2002; Kampunzu et al., 2003) Greenland, (Steenfelt et al., 2005). Although the majority of known sanukitoids were originated during the Neoarchean (2.7–2.5 Ga) and spatially associated with arc-related greenstone volcanism, the oldest sanukitoids (2.95 Ga) have been discovered in the granite-greenstone terrain of the Pilbara Craton, Western Australia (Smithies and Champion, 2000).

The Bundelkhand craton is occupied by a large volume of relatively undeformed high- K calc-alkaline granitoid intrusion comprised of "sanukitoids and anatectic granites." The sanukitoids are widely dispersed in the northern part of the "Bundelkhand craton" whilst the southern part of the "Bundelkhand craton" has relatively fewer occurrences. These granitoids are marked by intrusive into older TTG gneisses during ca 2.57-2.56 Ga (Joshi et al., 2017; Singh et al., 2019). The anatectic granites are widespread though out the craton and intruded into both TTG and greenstone belts with a time period of 2.57-2.52 Ga ("Kaur et al., 2016; Joshi et al., 2016, 2022; Singh et al., 2019"). The field relationship shows both anatectic granite and sanukitoids are contemporaneous in nature ("Joshi et al., 2017; Singh et al., 2019b").

### 1.1.5. Absence of HP-LT metamorphism

The Archean cratons are mostly devoid of high pressure (HP) and low temperature (LT) litho-assemblages whilst Phanerozoic orogenic belts contain "high -P and low-T assemblages like blueschist and eclogite facies," ("Windley and Bridge water 1971, Choukroune et.al. 1997, Chardon et.al, 2009"). The Archean cratons have witnessed uniformly low-P and high-T metamorphism. ("Brown 2014, 2018"). This metamorphic assemblage gives evidence that the tectonic process of the earth during Archean is different from modern/phanerozoic orogens (See figure 1.3). The Archean cratons preserve low pressure (3-8 kbar) and medium to high temperature (450-900°C) metamorphic assemblages in the form of granulite-gneiss-greenstone components.

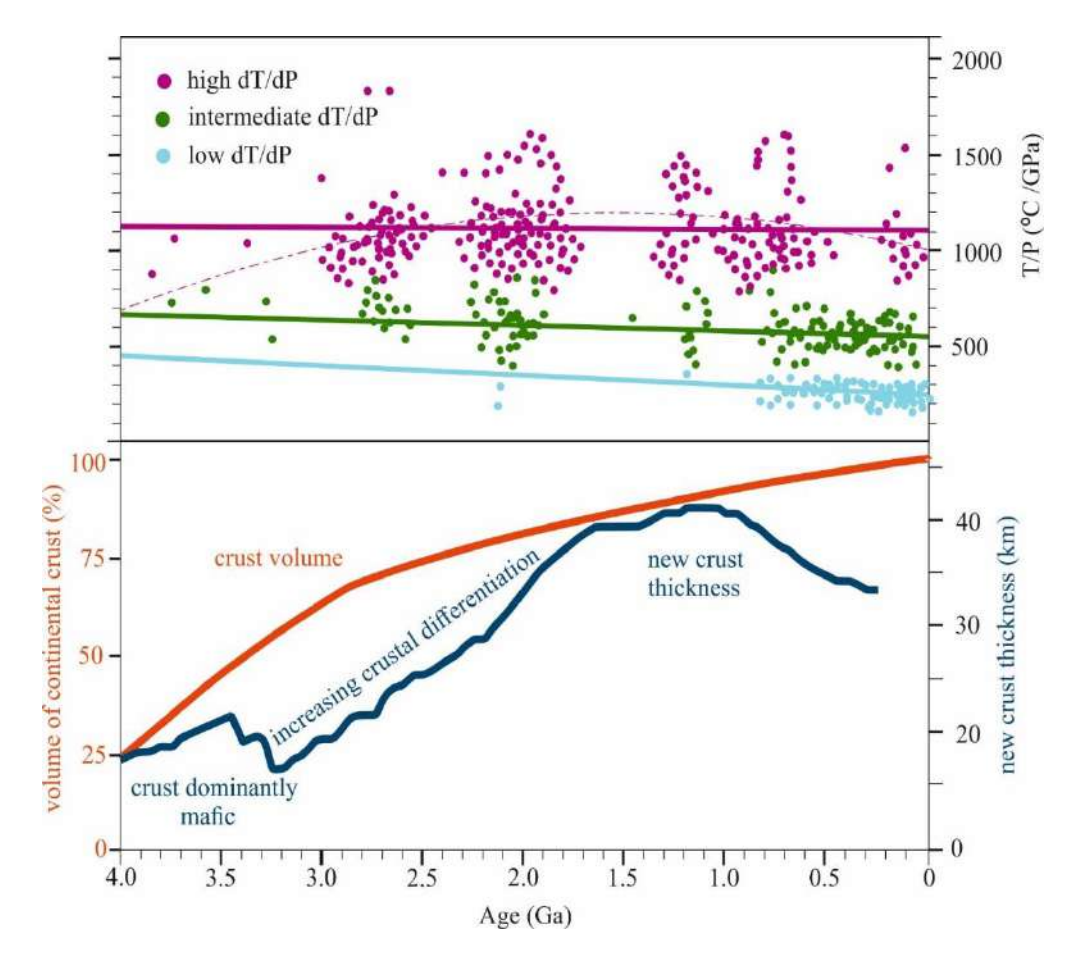


Figure 1.3 (a) Metamorphic thermal gradient (T/P) for 456 localities grouped as high dT/dP in red, intermediate dT/dP in green and low dT/dP in blue, and plotted against age (Brown, 2018).

(b) A crustal growth model based on Hf isotope ratios in zircons (Dhuime 2012) and a shift in the composition of juvenile crust from mafic to more intermediate compositions accompanied by an inferred increase in crustal thickness (Dhuime 2015).

These "low-pressure, high-temperature" metamorphic assemblages show evidence that the Archean tectonic environment was devoid of "phanerozoic-style" tectonic settings. Earlier researchers believed that the Bundelkhand Craton (BC) was metamorphosed under greenschist to amphibolite facies. According to (Saha et al. 2011) and (Slabunov et al. (2019, 2021), several cratonic regions have been investigated and accounted for polyphase metamorphism. It has also been established that the Bundelkhand craton exhibits three stages of the metamorphic event and deformation that took place both in TTG and ultramafic-mafic rocks. The presence of ca. 2.78 Ga high-pressure eclogite facies (11 kbar) was documented in the central Bundelkhand craton, indicating that Neoarchean collisional orogenesis took place in a similar manner to today (Saha et al., 2011).

### 1.1.6. Structural patterns

"Archean cratons are marked by widespread dome and basin structure patterns with different dimensions. ("Bouhallier et al., 1993, 1995; Chardon et al., 2002, Choukroune et al., 1997"). This "dome and basin pattern" is not recorded in modern orogenic belts. The typical dome and basin structure is well known in various Archean greenstone belts of different parts of the world as well as in India, e.g., Kaapval craton, Zimbabwe cratons, Pilbara craton (Western Australia), Dharwar Craton (Southern India). The "dome and basin" structures are developed due to interference of folds and reheating of the crust associated with gravitational instabilities. Thrust-imbricated structures associated with asymmetric folding are mostly found in the late Archean cratons (Southwest Greenland, Southern Africa, Yilgarn) consistent with the horizontal movement of

tectonic plates. The "dome and keel structures" of the oldest Archean cratonic cores represent the vertical motions acting at the interior of the matured crust while duplex structures are mostly found in the plate margin setting of Neoarchean crust, which emerged as a result to the lateral accretion process of juvenile arc magmas along the cratons margin ("Kimura et al., 1993; Chadwick et al., 2000") (See figure 1.4). A 2D computational model in conjunction with thermo-mechanical and petrological evidence suggests that the "P-T-t paths" of metamorphism and associated dome and keel structures could be the result of both horizontal and vertical tectonic linked to mantle upwelling in Eoarchean and Mesoarchean crust (Jayananda et al., 2023).

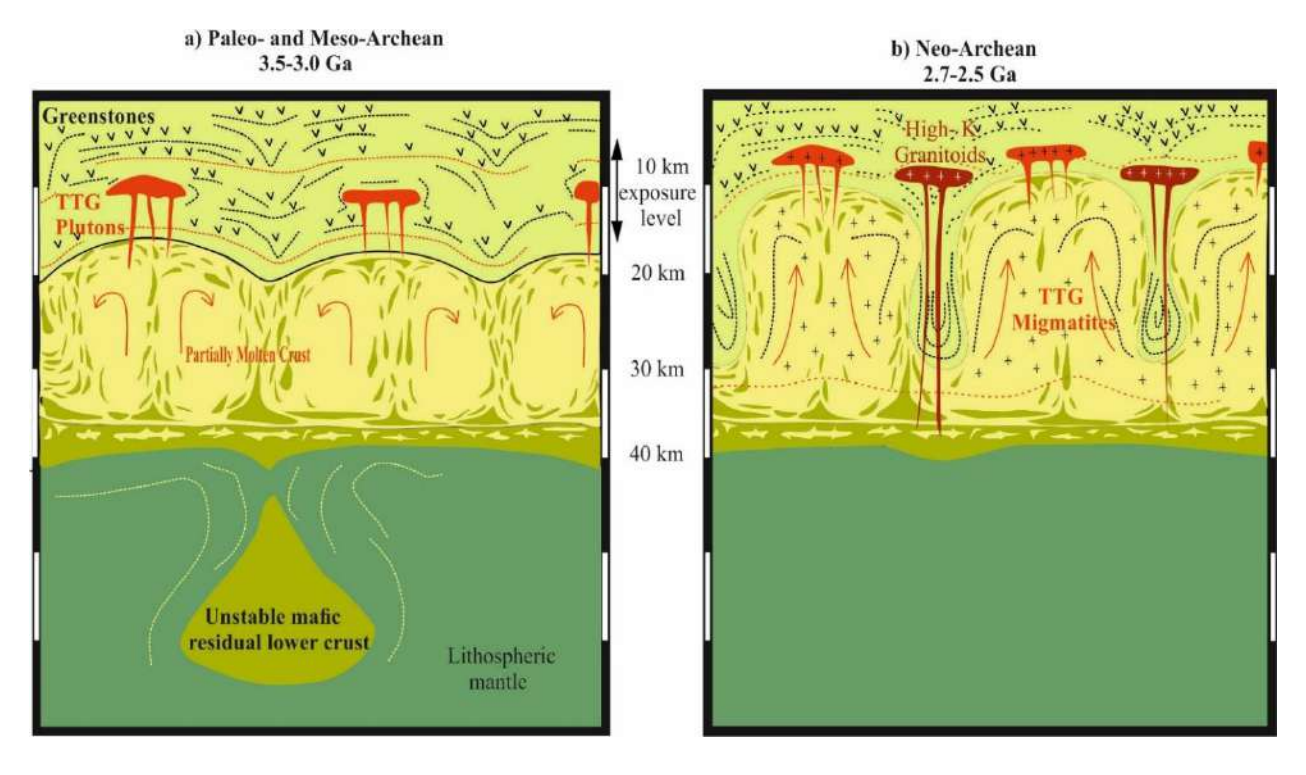


*Figure. 1.4* Schematic representation of proposed structural models for the dynamics of Archean crust (Stern et al., 2018).

The Bundelkhand craton has not shown any preserved dome and basin structures, however, it is dominated by magmatic and mylonitic foliation associated with progressive sinistral shears in different phases (Deb et al., 2022). Bundelkhand craton documented four phases of deformation. The first two phases of deformation marked the folding of TTG basement along with

metasedimentary rocks of green stone sequence during ca 3.4-3.2 Ga. The third phase deformation was marked by the intrusion of granites along the fractures during ca. 2.56-2.44 Ga. The fourth phase of deformation is marked by three different phases of a single stress field implying "E-W, NE-SW, N-S, NW-SE, NNE-SSW, and ENE-WSW" trending shear zones with fractures which are manifested by mafic dykes and quartz reefs after Neoarchean. (Bhatt et al., 2011; Deb et al., 2022).

### 1.1.7 Major period of continental growth

In the last few decades, several combined geochronologic and isotope (Nd-Hf) studies discussed the rates of continental growth. Earlier it was defined that crustal growth is the net gain in the volume or mass of the continental crust per unit of time. Creation of oceanic crust along the accretionary plate boundaries is essentially balanced by the loss of this material along converging plate margin, (Reymer and Schubert, 1984). Two schools of thought have been proposed, one model proposes that during the Archean period, continental crust formed extremely early in the history of the earth. After that, it recycled, with the volume of the crust remaining essentially unchanged. (Armstrong, 1981, 1991; Amelin et al., 2000; Harrison et al., 2005 Dhuime et al., 2012). Several workers documented continents grew progressively through time with the addition of mantle-derived juvenile crust (Hurley and Rand, 1969; Taylor and McLennan, 1985; McCulloch and Bennett, 1994 Arculus, 1999), with no records of continental crust older than 4 Ga. According to, (Moorbath and Taylor, 1981), crustal growth is progressive with the possibility of episodic growth and a limited degree of crustal recycling. Other models (Stern and Hanson, 1991; Condie, 1994, 1998), predict episodic growth with the volume of the depleted mantle gradually rising over time with recording significant episodic pulses of juvenile magmatism (Cawood et al., 2009; Rollinson, 2006) (See figure 1.2). Zircon age distributions show major peaks at 2.7 and 1.9 Ga,

which is consistent with episodic continental growth and superplume events (Condie, 1998; Rino et al., 2004), with the generation of significant amounts of juvenile crust. According to, (Condie & Aster, 2010), the episodic pattern of crustal growth points to significant episodes of rapid continental growth at around 2.9, 2.7, 2.1, 1.9, 1.8, 1.2, 0.9, and 0.8 Ga. The Archean may be characterised by periods of plate tectonics that alternate with mantle overturn events, according to, (Davies, 1995 & Isozaki et al. 2010), also postulated the growth of SW Japan by severe shrinking caused by the sinking of the arc crust. According to (Stein and Hofmann, 1994 & Condie 1998), periodic crustal growth is likely related to the activity of mantle plumes, implying that magmatic arcs may be the locations of continental growth. Crustal growth was more active and vigorous in the Archean as compared to the present day (Condie, 1998, 2004; Hawkesworth and Kemp, 2006; Kemp et al., 2006), due to the higher mantle temperature during the Archean period. About 60-70 % of the present-day continental crust is believed to be formed during the Archean (Taylor and McLennan, 1995). (Albarede, 1998), pointed out that assumptions like (i) an increase in crustal volume through time in spite of continental material erosion and subduction back to the mantle, (ii) faster crustal growth rate in the Archean as compared to recent, and (iii) clustering of crust formations in a small number of orogenic periods, are now almost widely perceived. It is now generally accepted that continents grew through a combined process of the addition of mantlederived (juvenile) material by subduction and amalgamations of pre-existing older terranes. (de Wit et al., 1992).

#### 1.1.8 Geodynamic models

The geodynamic context of komatiite-dominated ultramafic-mafic magmatism and associated TTG-type granitoids formation during Archean is still a lot of argument and discussion. In several studies from the last couple of decades, various models have been proposed, including the

uniformitarian model ("Gerya, 2014; Cawood et al., 2018; Wyman, 2018"), which involves the lateral accretion of arcs; the non-uniformitarian model (Bedard, 2018; Hamilton, 1998; Choukroune et al., 1995; Johnson et al., 2018), which involves the vertical growth of crust in hot spot tectonic settings and a combination of both (Puchtel et al., 1997; Jayananda et al., 2008, 2016), involving the formation of komatiite volcanic as oceanic plateaus and subduction of intervening oceanic crust in the arc settings generate mafic to felsic magmas (See figure 1.5-1.6).

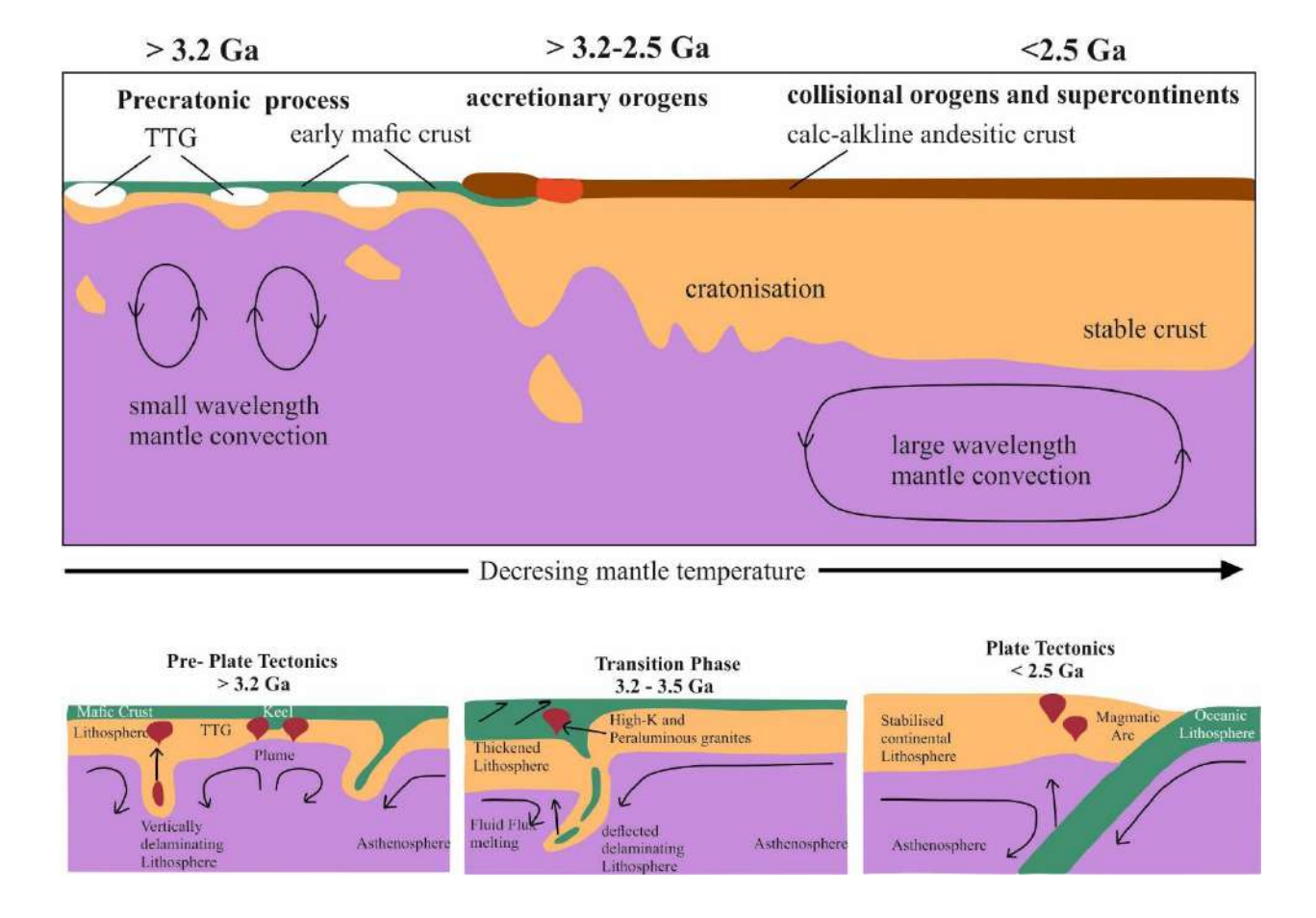


Figure 1.5 (a) Schematic temporal evolution of the lithosphere associated with decreasing mantle temperature. Schematic model detailing the proposed temporal evolution of the Earth with decreasing mantle temperature; Cawood et al. (2018). (b) Early Earth, pre-plate tectonic (>3.2 Ga) involves a non-plate tectonic regime, with magmatism characterized by a bimodal association of TTG (tonalites, trondhjemites and granodiorites) and greenstone belts. Mantle plumes are the major source of mafic magmatism. Recycling occurs through delamination and mantle convection is of a relatively small wavelength. Subduction, where present, is transitory. Plate tectonics (<2.5

Ga) is associated with large aspect ratio mantle convection. Between these two tectonic regimes is a transition phase (3.2-2.5 Ga) in which the lithosphere is stabilized and differentiates into oceanic and continental types, with the latter undergoing thickening, enabling its emergence and erosion.

Several workers have worked on the Bundelkhand craton to address the tectonic process operated for the building of crust during Archean based on geochemical and isotopic, including geophysical studies. The study proposed a uniformitarian model based on the Wilson cycle model involving subduction tectonic for the formation of TTG during paleo Archean and a recent study suggests the non-uniformitarian model based on vertical accretion of juvenile crust in plume settings related to hot spot environments ("Chauhan et al., 2018; Singh et al., 2021"). "The initiation of the subduction process is marked by the Neoarchean TTG." ("Joshi et al. 2022").

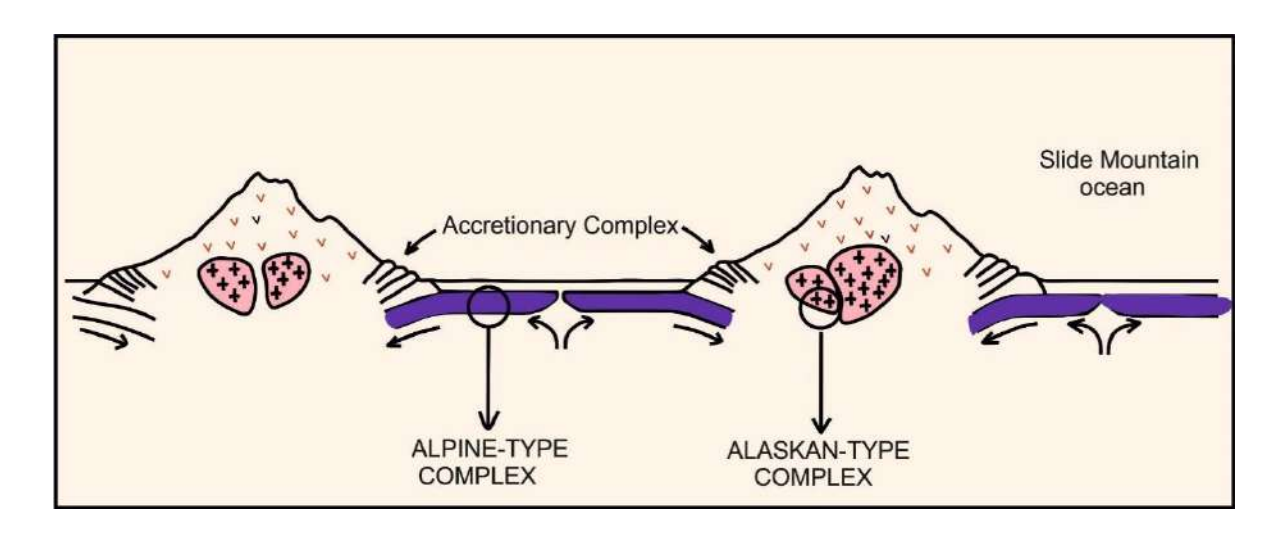


Figure 1.6 Simplified diagram depicting the different types of tectonic settings for the ultramafic mafic complex

Few workers suggested the combined plume arc theory for the formation of greenstone volcanism contemporaneous with the surrounding TTG of the Central Bundelkhand craton, whilst the greenstone volcanism of Southern Bundelkhand explains the horizontal plate tectonic association

with subduction tectonic settings (Singh et al., 2017; Hiloidari et al., 2021). Even after numerous research on the Bundelkhand Craton, the tectonics of the Bundelkhand Craton during the Archean Period is still hotly debated and discussed. Consequently, to address this, a multidisciplinary approach including field, petrography, elemental chemistry, geochemistry, and isotope studies of ultramafic mafic magmatism of the Southern Bundelkhand craton has been taken into account. The selected study area contains distinct ultramafic mafic-intermediate lithological assemblages which will provide the geodynamics process operated in the Southern Bundelkhand craton.

### 1.2 Geological framework of the Bundelkhand Craton

The Bundelkhand craton is located in Northcentral India in the form of composite semi-circular crustal nuclei, which cover an area of 26000 sq. km (Basu 1986, Singh et al., 2007; Ramakrishnan and Vaidyanathan 2010, Satyanarayanan et al., 2015). This craton is covered by the Indo-Gangetic alluvial plain in its north and bounded by the "Central India tectonic zone (CITZ) in its south." The craton is covered by the Proterozoic Vindhyan basin in the southeast, south, and west called as Bijawar, Sonrai, and Gwalior basins respectively ("Basu, 1986, Sharma, 1998; Ramakrishnan and Vaidyanathan 2010").

The Bundelkhand contains a significant component of Archean basement rocks which includes "TTG-type gneisses, volcano-sedimentary greenstone sequences, and high K granitoids." ("Mondal et al., 2002, Kaur et al., 2014, 2016; Singh and Slabunov 2015, Joshi et al., 2017; Singh et al., 2019"). The post-Archean period is marked by NW-SE trending mafic dykes and NE-SW trending quartz reefs. (Rao et al., 2005; Pati et al., 2007) (See figure 1.7-1.8).

#### 1.3. Previous work

Archean ultramafic-mafic rocks are abundant and are mainly found as lava flows in the greenstone sequences and also occur as layered intrusions or accreted oceanic fragments. studied

(Ishiwatari et al., 2004; Yan et al., 2019; Mathew et al., 2022 Villares et al., 2022). In this context, the ultramafic mafic rocks from the "Southern Bundelkhand Craton (SBC)" are relevant and significant.

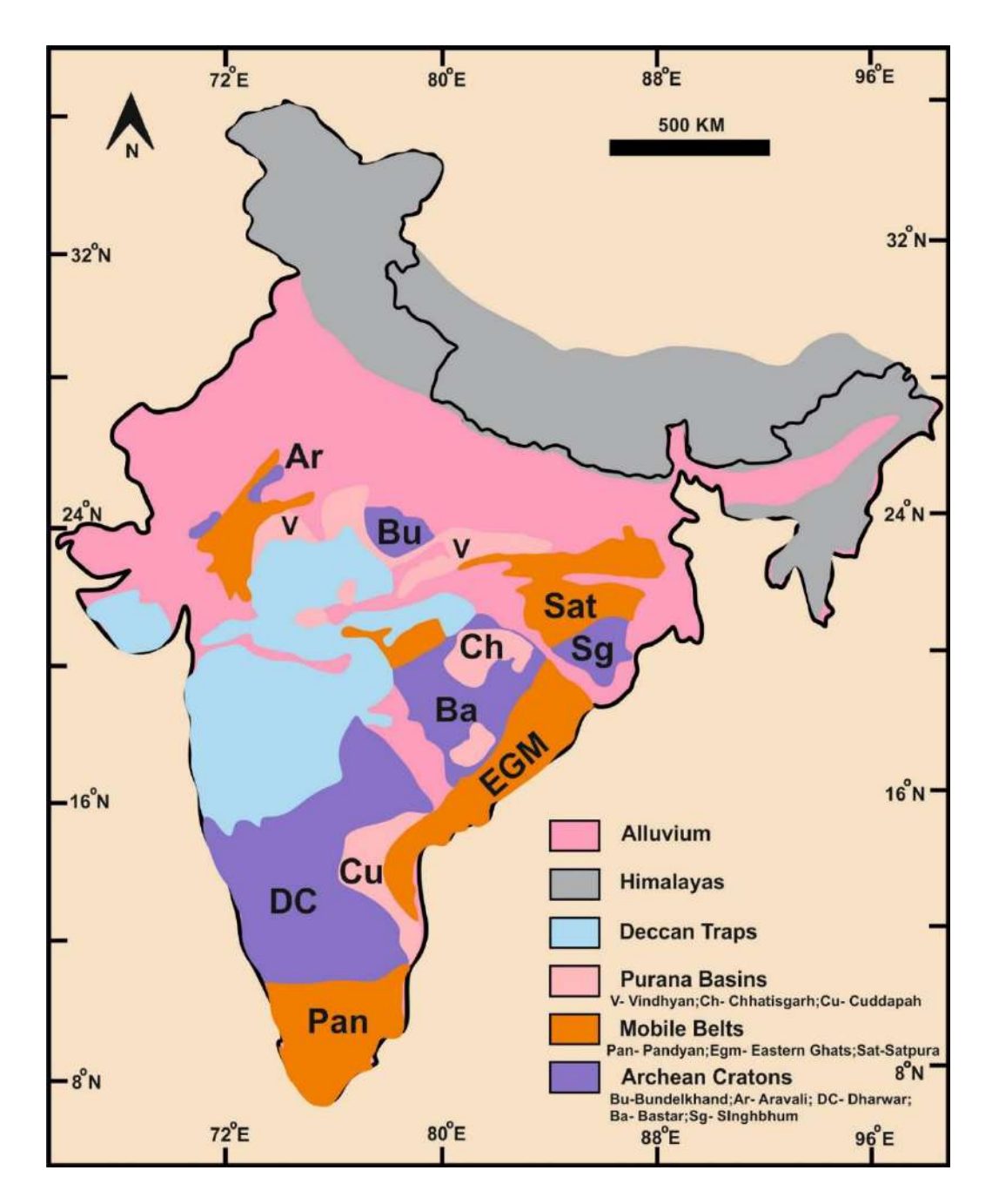


Figure 1.7. Map of India showing the relative position of the Bundelkhand craton with respect to various cratons of the Indian shield (modified after Pradhan et al. 2009).

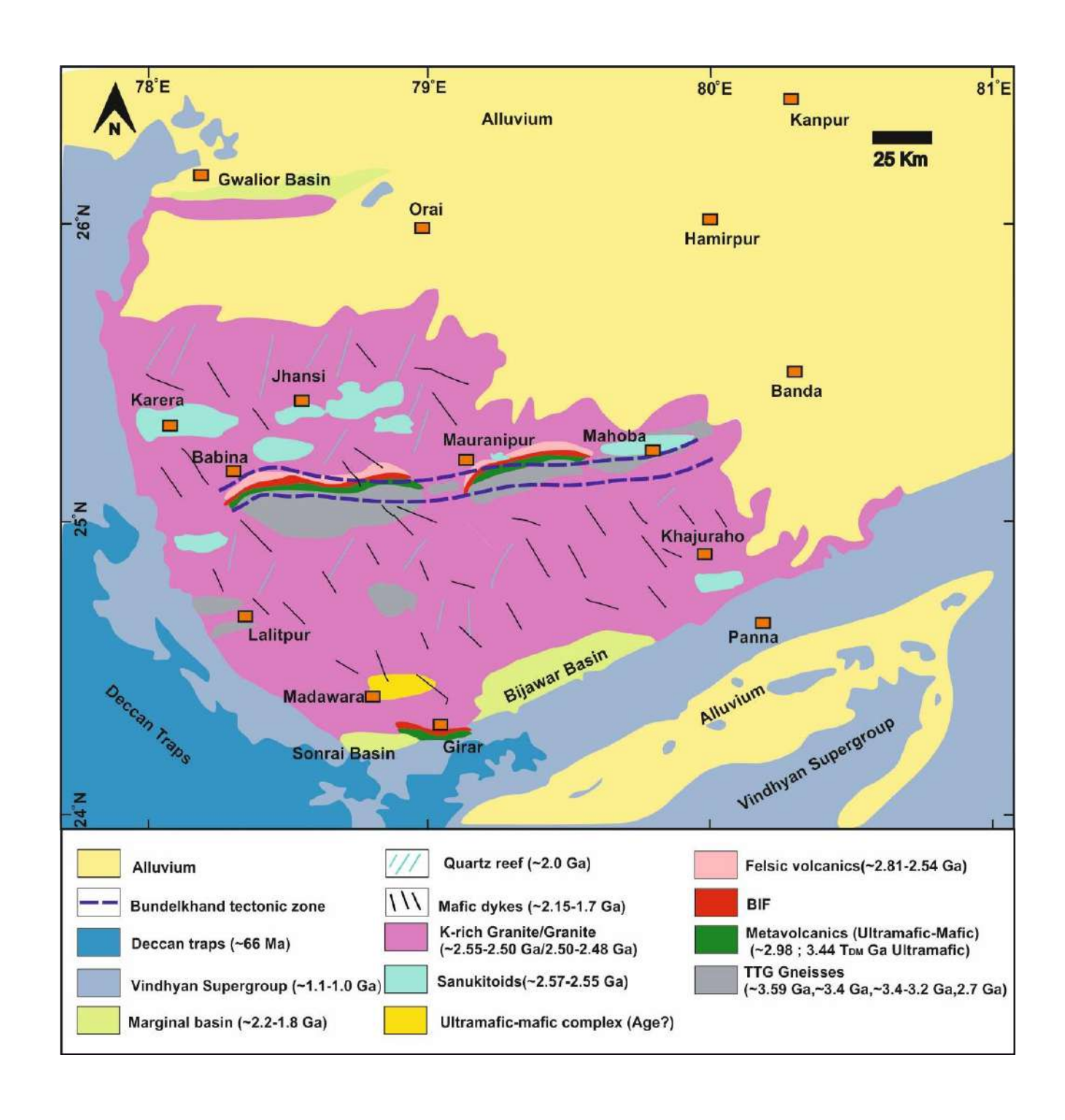


Figure 1.8. Geological map of the Bundelkhand craton (reproduced after Basu 1986). The various magmatism ages reported by various authors are displayed on the map (Mondal et al. 2002; Kaur et al. 2014, 2016; Joshi et al. 2016, Singh et.al. 2018, Sikha et.al. 2021)

Ultramafic-mafic lava flows from the greenstone sequences are subjected to numerous studies (Smithis et al., 1980; Wilson et al., 2003; Jayananda et al., 2016; 2023), whilst ultramafic-mafic complexes found as accreted intrusive complexes or tectonically abducted slices are less

In the past several decades, geoscientists from all over the world have become more interested in the Bundelkhand Craton (BC), which has experienced multi-stage crustal formation during the Paleoarchean to Neoarchean age. ("Basu, 1986; Mondal et al., 2002; Malviya et al., 2006; Kaur et al., 2014, 2016; Singh and Slabunov, 2015, 2016; Saha et al., 2016; Verma et al., 2016; Joshi et al., 2017; Slabunov et al., 2017; Singh et al., 2018; Singh et al., 2019a"). However, there has been debate regarding the Bundelkhand craton's mantle evolution and mechanisms for continental growth. ("Mondal et al., 2002; Kaur et al., 2014, 2016; Singh and Slabunov, 2015, 2016; Saha et al., 2016; Verma et al., 2016; Joshi et al., 2017; Slabunov et al., 2017; Slabunov and Singh, 2019; Singh et al., 2019a, b"). "The Bundelkhand craton is generally described by the southern and northern block separated by an east-west ~200 km long brittle-ductile shear zone known as the Bundelkhand Tectonic Zone (BTZ)." ("Kaur et al., 2016"). The Bundelkhand craton preserves two volcano-sedimentary greenstone components, called the Central Bundelkhand Greenstone Complex (CBGC) and the Southern Bundelkhand Greenstone Complex (SBGC). The CBGC, which is located in the Bundelkhand craton's centre, is predominantly composed of greenstone sequences, TTG suites, and numerous high-K granite intrusions. In contrast, the SBGC is found at the southern fringe of the Bundelkhand craton called as Girar greenstone belt and is made up primarily of quartzites, BIFs, TTG suites, and high K-granite, with evidences of dolomitic marble and chlorite schist lenses at the interface between quartzite and BIF rocks (Pascoe, 1950; Slabunov et al., 2017a). The formation of CBGC which is in between the northern and southern Bundelkhand block is thought to be originated during the Mesoarchean Island arc setting by the geochemical

data of ultrabasic and felsic (rhyolite, dacite) volcanic rocks dated at ca ~2.8 Ga (Slabunov and Singh, 2019). In addition, the Banded iron formation (BIF) rocks of the CBGB likely to be deposited in a forearc or back-arc basin associated with this island-arc system (Slabunov and Singh, 2019). The formation of SBGC in the southern Bundelkhand, which has been recently studied named as Khurrat-Badwar-Girar greenstone belt formed in an intra-oceanic subductionrelated back-arc rift environment by the geochemical data of mafic volcanic rocks dated at ca. 2.98 Ga (Hiloidari et al., 2021). However, few studies have focused on the geodynamics of the ultramafic-mafic intrusion of the southern Bundelkhand block, which is located to the north of the SBGC. To address, the Archean geodynamic processes, mantle evolution, and crustal growth the present Ph.D. thesis focus on the ultramafic-mafic rocks of the southern Bundelkhand craton. The ultramafic-mafic rock is occurred as lensoidal and discontinuous bands within dominantly granitoid (TTG gneisses and granites). Their elemental and isotopic studies have not yet been examined, and their link to nearby granitoids is also unclear. Recent studies on ultramafic rocks of the southern Bundelkhand craton reveals potential PGE mineralization (Farooqi and Singh 2010, Singh et al., 2011; Satyanarayanan et.al 2015, Mohanty et.al.2019 and references therein). Consequently, "the ultramafic-mafic rocks of southern Bundelkhand" are key to our understanding of Archean mantle evolution, crustal growth, geodynamic processes, and PGE mineralization. In this context, it is important to focus on a multi-disciplinary study involving detailed field, petrology, mineralogy, geochemistry, and Nd isotope tracers to understand the ultramafic-mafic magmatism of the southern Bundelkhand craton.

## 1.4. Major scientific issues to be addressed

Recent studies reveal that Bundelkhand has distinct three cratonic blocks separated by E-W trending Bundelkhand tectonic zone (BTZ). (Gokarn et al., 2013; Nandakumar et al., 2018). The

three cratonic blocks have independent geological signatures. This signature also corroborated with geophysical studies (Gokarn et al, 2013). Extensive geological studies have been carried out in the central and northern domains; however, the southern block has been less studied in terms of mantle evolution and crustal growth. The Archean ultramafic mafic magmatism is the ideal target to unravel the early earth "thermal and geodynamic evolution". In this context, the ultramafic mafic magmatism of the southern Bundelkhand craton has been selected for a detailed integrated study.

### 1.5. Objectives

The ultramafic-mafic rocks of southern Bundelkhand are ideal targets to address magmatism, Archean mantle evolution, crustal growth, geodynamic processes, and PGE mineralization. In this context, the focus of the present study is to present a multi-disciplinary study involving field, petrology, mineralogy, geochemistry, and Nd isotope traces to understand the ultramafic mafic magmatism of the southern Bundelkhand craton formation. The main objectives of the thesis are

- To understand the petrogenesis of ultramafic/mafic rocks including magmatic evolution, composition of potential mantle reservoirs, and degree and depth of melting.
- To decipher the chemical and thermal evolution of mantle during Archean, and its spatial link to crustal growth.
- To investigate the geodynamic context of ultramafic-mafic magmatism and their link to the accretion of adjoining granitoid basement.
- To enumerate the Archean crustal evolution and craton building processes in Bundelkhand craton.
- To characterize potential PGE mineralization in ultramafic-mafic rocks.

# 1.6. Methodology

To achieve the above-mentioned objectives, systematic field work carried out for study the field relationships and sampling of the lensoidal ultramafic mafic bodies and spatially associated granitoids (TTGs and potassic granites) found along the southern fringe of the Bundelkhand craton. Altogether 86 samples were collected for the detailed petrographic analysis. After careful study of petrographic analysis, a total 56 samples had selected for the whole rock geochemistry and 32 samples for the PGE analysis. A total of 16 samples also selected for the Rb-Sr and Sm-Nd isotopic analysis. For the mineral characterization as the total of 10 sample had chosen for the SEM-EDS and EPMA analysis. One sample also selected for the trace element mineral chemistry through the LA-ICP-MS study.

Samples of ultramafic-mafic intrusive rocks have been processed at the CSIR-National Geophysical Research Institute for thin section, grinding, crushing, and major and trace element analysis. The samples are studied carefully to characterize the mineralogy and secondary alteration process. These samples are powdered at CSIR-NGRI using a jaw crusher to obtain approximately -60 to -80 mesh size and then samples are transformed to a laboratory disc mill to reduce the powder to approximately -200 mesh size which is very ideal for most of the analytical techniques.

# 1.7. Analytical procedures:

# 1.7.1. Loss on Ignition (LOI)

The loss on ignition was measured to provide information about the alteration effect and presence of volatile phases in the rock. The loss on ignition was estimated by weighing about 1g of the sample powder in a pre-weighed silica crucible followed by their heating in a muffle furnace preheated to about 650°C for 30 minutes. A muffle furnace (M/s. Krishna Enterprises, Secunderabad, India) constructed with silicon carbide tiles and Kanthal heating elements held in

ceramic tubes with digital temperature controller (maximum temperature up to 1150°C) was used for heating. The crucibles were then transferred carefully to a desiccator, tightly covered and allowed to cool to room temperature. The weight of silica crucible along with heated sample was noted and finally the loss on ignition was calculated accordingly. Duplicate samples were processed along with each batch for LOI and the precision of the measurement was found to be within permissible error. The LOI is calculated by using the formula:

$$LOI = \frac{(W_3 - W_2)}{(W_2 - W_1)} X100$$

W<sub>1</sub>= weight of the empty crucible

W<sub>2</sub>= (weight of the crucible+ sample weight) before ignition

W<sub>3</sub>= (weight of the crucible+ sample weight) after ignition

# 1.7.2. X-ray Fluorescence analysis (XRF)

The whole rock samples were analysed for major elements by using X-ray fluorescence spectrometry. It is employed for the bulk chemical analysis of rocks, soils and sediments. It is non-destructive and several elements can be determined rapidly without different sample preparation for each element. A Philips MagiX PRO, Model PW 2440 (Philips, Eindhoven, The Netherlands), sequential wavelength dispersive X-ray fluorescence spectrometer, coupled with an automatic sample changer PW 2540 and provided with suitable software SUPER Q 3.0, was used for this study. The MagiX PRO is a sequential instrument with a single goniometer-based measuring channel covering the complete elemental measurement range from F to U of the order of 1.0 ppm or mg/kg to % level. The instrument is "microprocessor controlled for maximum flexibility and consists of an end window X-ray tube with an Rh anode and a maximum voltage/current of 60 kV/125mA at a maximum power level of 4 kW. (Krishna et al., 2016). Measurement conditions

were optimized to ensure best signal-to-background ratio and minimum line overlap. Two grams of the fine powdered sample was weighed using an analytical balance with a precision as low as 0.0001 g. The fine powder samples were prepared as pressed pellets by using collapsible aluminium cups (Krishna et al., 2007). These cups are filled at the bottom with ~2.5 g of boric acid (A-R grade) as a bonder and sub stratum, and the 2 g of the fine powdered sample is placed on the top. The sample powder was evenly sprinkled and then pressed under a hydraulic pressure of 25 tons to obtain the pellet of each sample. US Geological Survey standards (BHVO-1, BCR-1, BIR-1), French standards (UB-N), Geological Survey of Japan (JB-1, JB-1a, JB-2, JB-3, JP-1) and Chinese reference material (GSR-3) were used to prepare the calibration curves for major and trace elements, and to check the accuracy of analytical data. The precision obtained for most of the major oxides were less than 2% RSD.

## 1.7.3. Inductively Coupled Plasma Mass Spectrometry analysis (ICP-MS)

The trace elements were analysed by using HR-ICP-MS at National Geophysical Research Institute. The trace elements including rare earth element (REE) and high field strength elements (HFSE) were determined from solutions prepared from homogenized sample powder which dissolved in reagent grade HF:HNO3 acid mixture in Savillex® screw top vessels. About 0.05 g of powered sample was taken in 25 ml Savillex Teflon pressure decomposition vessels. To each sample about, 10 ml of an acid mixture (containing 7:3 HF-HNO3) was added. Subsequently, 5 ml of 1 ng/ml <sup>103</sup>Rh solution was added as an internal standard to each Savillex vessel. After thorough swirling, the vessels were tightly closed and kept on a hot plate at ~140°C for 48 h. Following this, the vessels were opened and the contents were evaporated at 200°C to near dryness with a few drops of HClO4 to ensure complete removal of HF from the mixture. It was further dissolved by adding 10 ml of 1:1 HNO3 for about an hour at 80°C. Then the volume was made to

250 ml by adding of another 10 ml 1:1 HNO<sup>3</sup>, 5ml of ng/ml <sup>103</sup>Rh solution and then the rest of the volume is filled with, and the solution was stored finally in HDPE bottles. 5 ml of each sample is taken in a 50 ml volumetric flask and the volume is made by adding Milli Q® de-ionized water (18  $M\Omega$ ) and finally stored in Eppendorf® tubes for analysis using HR-ICP-MS. The Matrix matching certified reference materials BHVO-1, BCR-1 (USGS), JB-2, JP-1 (Japan), UB-N (ANRT, France), NIM-P (South Africa) along with "couple of procedural blanks were also prepared with the sample batch by adopting the same protocol described above to negate errors due to reagent and handling. In the present investigation, very clear solutions were obtained for all the samples and calibration standards. Solutions were analysed at CSIR-NGRI, Hyderabad, by high resolution inductively coupled mass spectrometer (HR-ICP-MS) (Nu Instruments Attom®, UK) in jumpwiggle mode at moderate resolution of 300 which permits all the analytes of interest to be measured accurately. The sample introduction consisted of a standard Meinhard® nebulizer with a cyclonic spray chamber housed in Peltier cooling system. All quantitative measurements were performed using the instrument software (Attolab v.2.6.0), while the data processing was done using Nu Quant®, which uses knowledge-driven routines in combination with numerical calculations (quantitative analysis) to perform an automated/manual interpretation of the spectrum of interest." Instrumental parameters are given in table 2.2. The instrument was optimized using 1ppb tuning solution and the sensitivity of 114In was about 1 million cps. Oxide and oxy-hydroxide ratios were low (< 0.2%) and the double charges ions ratio was < 3%. Mass bias fractionation and several well-known isobaric interferences were addressed by using certified geochemical reference materials. Precision and accuracy are better than RSD 3% for the majority of trace elements.

# 1.7.4. Laser Ablation-Inductively Coupled Plasma Mass Spectrometer (LA-ICP-MS)

REEs were determined on polished moulds containing chrome spinels from Madawara Complex to understand about their origin. For this, chrome spinels were separated from bulk rock mechanically through mild crushing and sieving, while taking care that the matrix of the spinel are not disturbed. Representative chrome spinel picked after checking through ore microscope, and was mounted in epoxy resin for in-situ analysis. Exposed zones of the polished mould were subjected to laser ablation analysis. "REE data were collected using a New Wave Research (NWR 213) Laser Ablation system coupled to a Nu Instruments AttoM® single-collector high resolution inductively coupled plasma mass spectrometer (HR-ICP-MS). A large-format New Wave Research cell was used-a two volume design featuring a moveable cup that decreases the ablation volume and washout time to <0.5 s. Optimal signal strengths were attained using the following ablation parameters: 40 um spot diameter; 5 Hz; 1.9–2.5 J/cm2; 10 s wait between ablations to ensure sample washout and a 30 s ablation time. Oxide production was minimised by tuning the gas flows such that ThO <0.4%, and UO <0.1%. Before each analysis, the grain surface was cleaned by rostering the laser beam over the target area (~700 um2), at a low fluence. The energy profile of the beam was stabilised by firing the laser for 10 s behind the shutter prior to each ablation. On ablation, sample aerosols were transported using a He carrier gas; Ar was introduced into the sample line via a T-piece midway between the cell and torch to form a ~50:50 Ar-He mix. The detection system in the NGRI Nu AttoM comprises a single Mass Com secondary electron multiplier. The AttoM was operated in peak-jumping mode which permits measurement of <sup>44</sup>Ca, <sup>139</sup>La, <sup>140</sup>Ce, <sup>141</sup>Pr, <sup>146</sup>Nd, <sup>147</sup>Sm, <sup>153</sup>Eu, <sup>157</sup>Gd, <sup>159</sup>Tb, <sup>163</sup>Dy, <sup>165</sup>Ho, <sup>166</sup>Er, <sup>169</sup>Tm, <sup>172</sup>Yb, <sup>175</sup>Lu, <sup>232</sup>Th and <sup>238</sup>U during a single scan of the electrostatic analyser, whilst the magnet current is held static.

Each data integration records 100 sweeps of the measured masses, which roughly equates to 0.18 s". "Mass bias fractionation is inherent to ICPMS and likely originates from mass- and charge-dependent processes operating during sample ablation and introduction of sample aerosol into the plasma. (e.g., Tanner et al., 1994). Correction for instrumental drift and laser-induced elemental fractionation was addressed via analysis of (i) NIST 610, 611, 612 and 614 and (ii) BCR-2g, using a standard-sample-bracketing routine. Reduction of REE data was performed off-line reduction scheme IOLITE (version 3.64) with 44Ca as internal standard (Woodhead et al., 2007; Hellstrom et al., 2008; Paton et al., 2011). External certified reference materials used included (i) NIST 610, 611, 612 and 614 and (ii) BCR-2g, and the drift corrections was applied using the baseline reduction scheme IOLITE (version 3.64) with 44Ca as internal standard. The accuracy and precision were better than 10% (RSD) for ppm level concentrations while the detection limits were in the range of 1-10 ppb.

# 1.7.5. Multi Collector-Inductively Coupled Plasma Mass Spectrometer (MC-ICP-MS) (Nd-Sr isotope analysis)

High precision analyses of radiogenic <sup>87</sup>Sr/<sup>86</sup>Sr, <sup>143</sup>Nd/<sup>144</sup>Nd isotopes for selected granites were performed on an in-house National Facility Nu Plasma High-Resolution Multi-Collector Inductively coupled Plasma-Mass Spectrometry (Nu Plasma HR- MC-ICP-MS) at National Geophysical Research Institute, Hyderabad. Sample dissolution, column chemistry and mass spectrometry procedures follow the established routine procedures (Sukumaran et al., 2009). Chemical processing of samples (digestions and chromatographic separations and purifications) was carried out in over pressurized HEPA filtered laminar flow hoods in the clean laboratory using high purity mineral acids and thoroughly cleaned lab wares.

Approximately 50-100mg of whole rock powders depending upon the elemental abundance were weighed into 15ml Savillex<sup>TM</sup> (PFA) vials and dissolved in a 3:1 ratio of doubledistilled concentrated HF: HNO<sub>3</sub>. The acid mixture was heated to 120°C on a hotplate with the vials being capped for at least two days. During this initial drying, the sample solution turned white in colour and dissolution appeared complete. Samples were then evaporated to dryness at 120°C to drive silica off as SiF<sub>4</sub> gas, nitrated twice with each addition of 1ml con HNO<sub>3</sub> and subsequently converted to chlorides using 6M HCl. Samples were then dried and re-dissolved in 2ml of 2.5N HCl and this solution virtually free of any precipitates was preserved for the determination of Sr and Nd isotopic compositions. Chemical separation of Sr and Rare Earth Elements (for Nd) generally follows the conventional ion-exchange chromatography using Savillex<sup>TM</sup> Teflon columns (Bio-Rad® AG50W-X8 (200-400 mesh size). Sr was eluted with 2.5M HCl and REE's with 6N HCl. Separation of Nd from other REE's was performed in quartz columns containing Teflon powder coated with HDEHP [di (2-ethylhexyl) ortho phosphoric acid with 0.25N HCl. Isotopic ratios were measured using a Nu Plasma MC-ICPMS (Nu Instruments, UK) in static multi-collection mode. Analyses used 'On Peak Zeros' correction routine for the background blank and memory. Nd was measured in dry plasma mode using a Nu DSN 100 desolvating system and Sr analysis employed wet plasma mode. Sample solutions of Sr, and Nd were prepared in 2% (v/v) optima HNO<sub>3</sub>. Sr and Nd isotope ratios were corrected for "mass fractionation using <sup>86</sup>Sr/<sup>88</sup>Sr = 0.1194 and  $^{146}$ Nd/ $^{144}$ Nd = 0.7219. The average values for NIST SRM987 and JNdi-1 during the course of analysis are  ${}^{87}\text{Sr}/{}^{86}\text{Sr} = 0.710253 \pm 25 \text{ (36ppm, n=5)}$  and  ${}^{143}\text{Nd}/{}^{144}\text{Nd} = 0.512076 \pm 15$ (30ppm/0.30epsilon units, n=5) at the  $2\sigma$  level of uncertainty (where  $\sigma$  is the standard deviation calculated on the mean of individual analyses)." The in-run precision quantified by twice the standard error (2SE) was on an average smaller (18ppm for Sr and 31ppm for Nd) than the 2 $\sigma$ 

external reproducibility. Measured ratios were normalized to the accepted ratio of 0.710245 for NIST SRM987 87Sr/86Sr and 0.512115 for the JNdi-1  $^{143}$ Nd/ $^{144}$ Nd. (Tanaka et al., 2000). USGS Basalt standard BCR-2 was used as an external standard and processed through the same procedure as samples to evaluate the accuracy of the analyses. Its measured value for  $^{87}$ Sr/ $^{86}$ Sr = 0.704944  $\pm$  17 (24ppm,  $1\sigma$ ) and  $^{143}$ Nd/ $^{144}$ Nd=0.512633  $\pm$  6 (12ppm,  $1\sigma$ ), are within errors of the published values of this standard (Weis et al., 2006; Raczek et al., 2001). The total procedural blanks were <150pg for Sr, and ~35pg for Nd insignificant compared to the size of the samples analysed.

### 1.7.6. Electron Probe Micro Analyzer (EPMA)

The Samples were studied by both transmitted and reflected ore microscopy as well as by scanning electron microscopy (SEM-EDS) at CSIR-NGRI, Hyderabad, under back-scattered electron (BSE) mode prior to EPMA analysis. Some parts of the analysis of Cr-spinel and associated silicate minerals were carried out quantitatively using the CAMECA SX-100 instrument at the Geological Survey of India (GSI), Bangalore. The analytical conditions for silicate and oxide phases were set up using 15 kV acceleration voltage and 15 nA beam current with 1 µm beam size. The counting time for peak measurement was 10 s and with half of the peak measurement time allotted for background measurement. A few analyses were also obtained using the CAMECA SX-5 instrument at Banaras Hindu University (BHU), Varanasi. The corresponding analytical conditions were kept at 15 keV accelerating voltage, 10 nA probe current with a beam size of 1 µm. The precisions of all analysed elements were better than 1%. Natural minerals and synthetic oxides were used as standards, and a program based on the ZAF online procedure was used for data correction. The amount of Fe<sup>2+</sup> and Fe<sup>3+</sup> in the Cr-spinels was calculated assuming spinel stoichiometry. (AB<sub>2</sub>O<sub>4</sub>; Droop, 1987).

# 1.7.7. Scanning Electron Microscope-Energy Dispersive Spectrophotometer (SEM-EDS)

A scanning electron microscope (SEM) is a type of electron microscope that produces images of a sample by scanning it with a focused beam of electrons. Fast moving negatively charged ions interact with the atoms in the sample, generating an image that contain information about the sample's surface topography. An energy dispersive spectrometer (EDS) attached with the SEM is used to deduce mineralogical information. Mineralogical data from representative samples were acquired at CSIR-National Geophysical Research Institute using Scanning Electron Microscope (Hitachi®) equipped with an Energy Dispersive Spectrometer (SEM-EDS) for semi-quantitative chemical analysis. The minerals were investigated using both reflected light and scanning electron microscopy. Chemical compositions were determined using the Oxford Inca® energy dispersive analytical system (EDS), operating at accelerating voltage of 15 kV, beam current of 2.9 nA and measurement time 60 second. Atomic ratios were calculated with the ZAF-4® program, which performs the necessary corrections for the overlapping peaks of different elements.

# 1.8. Location & Accessibility

The present study area lies in the Southern part of the Bundelkhand craton covering-Madawara, Ikauna, Pindar, and Hanumathgarh regions falling in the Survey of India (SOI) Toposheet no. 54L/14 & 54L/15. This study area is situated 25 km from Mehroni Tehsil of Lalitpur district, 61 km from Lalitpur town and 145 km from Jhansi, Uttara Pradesh. The area has good accessibility with well-connected road network.

Table 1.1: Instrument operating conditions of HR-ICP-MS (Nu Attom®).

# Plasma control parameters

Coolant gas flow (L/min)	13.0
Auxillary gas flow (L/min)	0.95
Nebulizer gas flow (psi)	34.0
Forward RF Power (W)	1300
Peristaltic rate (RPM)	15.0
Peltier cooling temperature (°C)	5.0

Spray chamber Glass-Cyclonic

Sample uptake (ml/min) 0.2

Detector Ion counter and faraday Sensitivity  $1 \times 10^6$  counts for  $^{115}$ In  $2 \times 10^6$  counts for  $^{238}$ U

Scan type Magnet jumping with electric scan over a

small mass range

Ion lens setting Optimized for sensitivity and resolution

peaks

## **Data acquisition parameters**

Dwell time per peak (ms)	3
Switch delay per peak (µs)	200
Number of sweeps	100
Number of cycles	3
Instrument resolution	300
Internal standard	$^{103}$ Rh

Analyte	Mass No.	UB-N				BHVO-1				BCR-1				JB-2			
		A	В	SD	%RSD	A	В	SD	%RSD	A	В	SD	%RSD	A	В	SD	%RSD
Sc	45	12.768	13.000	0.017	0.14	32.602	31.800	1.359	4.167	33.513	32.600	0.186	0.56	52.428	54.400	2.914	5.558
V	51	74.365	75.000	0.260	0.35	314.326	317.000	3.815	1.214	411.989	407.000	1.966	0.48	558.696	578.000	27.123	4.855
Cr	53	2267.455	2300.000	2.285	0.10	285.859	289.000	3.371	1.179	15.103	16.000	1.682	11.14	26.679	27.400	1.527	5.723
Co	59	98.903	100.000	0.392	0.40	44.742	45.000	0.372	0.832	37.114	37.000	0.030	0.08	37.259	39.800	2.542	6.823
Ni	60	1983.022	2000.000	9.447	0.48	120.453	121.000	0.731	0.607	12.381	13.000	0.874	7.06	15.259	14.200	0.456	2.990
Cu	63	27.710	28.000	0.104	0.38	134.996	136.000	0.542	0.401	20.567	19.000	0.295	1.43	222.530	227.000	5.312	2.387
Zn	66	85.471	85.000	1.272	1.49	104.702	105.000	0.209	0.199	123.448	129.500	5.362	4.34	116.269	110.000	6.261	5.385
Ga	71	2.956	3.000	0.038	1.27	21.420	21.000	0.916	4.276	21.520	22.000	0.153	0.71	16.600	17.000	0.662	3.987
Rb	85	3.973	4.000	0.009	0.24	11.000	11.000	0.025	0.228	49.623	47.200	3.622	7.30	6.787	6.200	0.532	7.832
Sr	88	8.997	9.000	0.030	0.33	402.484	403.000	1.912	0.475	348.127	330.000	1.754	0.50	177.685	178.000	9.686	5.451
Y	89	2.471	2.500	0.019	0.77	27.538	27.600	0.056	0.205	37.961	38.000	0.053	0.14	23.823	24.900	1.270	5.332
Zr	90	3.634	4.000	0.087	2.40	178.639	179.000	0.200	0.112	196.329	190.000	1.012	0.52	49.350	51.400	1.784	3.614
Nb	93	0.048	0.050	0.001	1.30	18.990	19.000	0.073	0.386	12.947	14.000	0.075	0.58	0.819	0.800	0.072	8.802
Cs	133	9.852	10.000	0.002	0.02	0.130	0.130	0.008	5.778	0.880	0.960	0.054	6.16	0.822	0.900	0.047	5.725
Ba	137	28.155	27.000	1.354	4.81	141.664	139.000	4.215	2.975	674.488	681.000	9.485	1.41	206.500	208.000	5.185	2.511
La	139	0.346	0.350	0.003	0.85	15.972	15.800	0.409	2.564	26.602	24.900	0.335	1.26	2.285	2.370	0.091	3.966
Ce	140	0.791	0.800	0.003	0.41	39.419	39.000	0.792	2.009	56.109	53.700	0.780	1.39	6.669	6.770	0.200	2.999
Pr	141	0.117	0.120	0.001	1.23	5.748	5.700	0.100	1.738	7.424	6.800	0.128	1.73	1.030	0.960	0.014	1.367
Nd	146	0.586	0.600	0.016	2.73	25.077	25.200	0.108	0.429	30.002	28.800	0.287	0.96	6.292	6.700	0.512	8.139
Sm	147	0.180	0.200	0.002	0.94	6.193	6.200	0.035	0.560	6.859	6.590	0.013	0.19	2.193	2.250	0.133	6.086
Eu	153	0.080	0.080	0.001	1.43	2.043	2.060	0.031	1.499	1.992	1.950	0.006	0.32	0.797	0.860	0.036	4.565
Gd	157	0.295	0.300	0.003	1.09	6.427	6.400	0.011	0.175	7.061	6.680	0.021	0.30	3.096	3.280	0.189	6.097
Tb	159	0.058	0.060	0.001	1.80	0.945	0.960	0.005	0.520	1.104	1.050	0.015	1.39	0.564	0.620	0.038	6.731
Dy	163	0.392	0.380	0.010	2.49	5.207	5.200	0.049	0.933	6.354	6.340	0.052	0.81	3.702	3.660	0.168	4.544
Но	165	0.092	0.090	0.001	1.09	0.976	0.990	0.004	0.407	1.323	1.260	0.000	0.01	0.831	0.810	0.036	4.382
Er	166	0.283	0.280	0.006	1.96	2.417	2.400	0.010	0.407	3.521	3.630	0.014	0.40	2.550	2.630	0.145	5.681
Tm	169	0.042	0.045	0.001	2.67	0.326	0.330	0.002	0.570	0.525	0.560	0.008	1.49	0.436	0.450	0.002	0.491
Yb	172	0.277	0.280	0.003	1.25	2.050	2.020	0.024	1.164	3.437	3.380	0.017	0.48	2.481	2.510	0.065	2.619
Lu	175	0.047	0.045	0.001	2.44	0.291	0.291	0.004	1.212	0.529	0.510	0.005	0.97	0.391	0.390	0.012	3.155
Hf	178	0.093	0.100	0.001	0.85	4.406	4.380	0.046	1.038	4.957	4.950	0.041	0.83	1.517	1.420	0.067	4.407
Ta	181	0.019	0.020	0.001	4.13	1.226	1.230	0.012	0.943	0.863	0.810	0.084	9.71	0.216	0.200	0.015	6.963
Pb	208	13.125	13.000	0.579	4.41	2.641	2.600	0.110	4.170	13.843	13.600	0.605	4.37	4.950	5.400	0.287	5.798
Th	232	0.064	0.070	0.004	5.74	1.078	1.080	0.008	0.734	5.557	5.980	0.480	8.64	0.326	0.330	0.022	6.776
U	238	0.070	0.070	0.001	0.72	0.424	0.420	0.008	1.831	1.597	1.750	0.067	4.18	0.156	0.160	0.006	3.781

A – values from HR-ICP-MS (average of 6 values) B – values from Govindaraju (1994) and GEOREM (georem.mpch-mainz.gwdg.de)

## **CHAPTER-II**

# **Geological Setting**

The aim of this chapter is to present details of the regional geology and tectonic framework of the Bundelkhand craton with special emphasis on the field, stratigraphy, and structural relationship of the Madawara ultramafic-mafic complex (MUC) and its surrounding TTG type granitoids from west to east covering Madawara-Ikauna-Hanumathgarh sectors.

### 2.1. Regional geology and tectonic framework of the Bundelkhand Craton

The "Bundelkhand craton in Northcentral India" preserves a composite mosaic of semi-circular Archean continental nuclei, that occupies about ~26,000 sq. km. (Basu 1986, Singh et al., 2007, Mondal et.al., 2002, Satyanarayanan et al., 2015, Joshi et.al., 2016). The craton has a very complex geological, metamorphic and tectonic history from ca. 3.8-2.5 Ga (Kaur et.al., 2014, 2016; Singh and Slabunov et al., 2015; Joshi et al., 2017; Singh et al., 2019). The Bundelkhand craton primarily consists of major lithological assemblages including a large area of Paleoarchean to Mesoarchean polyphase granitoids of TTG affinity (3555-3270 Ma), Mesoarchean to Neoarchean volcanosedimentary greenstone sequences (2800-2500 Ma) and voluminous Neoarchean (2583-2536 Ma) high K- granitoids including sanukitoids and anatectic granites (see figure 1.8) ("Mondal et.al., 2002; Kaur et.al; 2014, 2016; Singh and Slabunov, 2015; Joshi et.al., 2017; Singh et.al., 2019"). Earlier, the Bundelkhand craton was considered a batholith like the Sierra Neveda batholith of the Western U.S.A and it is believed to have formed through the northward subduction of oceanic lithosphere (Singh and Slabunov et.al. 2019). Over the last couple of decades, several cutting-edge research groups have carried out Multidisciplinary research studies involving detailed field,

petrological, geophysical, geochronologic, and elemental and isotope over "three decades immensely contributed to our understanding of the fundamental architecture as well as crust formation in the Bundelkhand cratons". According to recent studies, the Bundelkhand craton can be divided into three crustal blocks: the northern, central, and southern blocks. These blocks can be distinguished by their distinctive geological signatures, which reveal basement TTGtype granitoids, greenstone assemblages, various granitoids, and ultramafic mafic intrusive rocks as well as deformation, metamorphic events, and the degree of melting of the older crustal fragments ("Kaur et.al., 2014, 2016; Singh and Slabunov, 2015; Verma et.al, 2016; Joshi et.al; 2017"). The field and petrographic characteristics coupled with geophysical data also in agreement with the existence of three blocks separated by Bundelkhand tectonic zones (Gokarn et.al, 2013; Mandal et al. 2020; Nandakumar and Kumar, 2018). The central block consists of Paleo-Neoarchean TTG-type granitoids, Meso-Neoarchean volcano-sedimentary sequences, and lesser Neoarchean K-rich granitoids. The crustal thickness of the central block is nearly about 60 km with moderate to high resistivity values (Gokarn et.al. 2013). The northern block is dominated by Neoarchean K-rich granites and sanukitoids whilst the TTG and ultramafic mafic rocks are very rare. The crust of the northern Bundelkhand block is nearly homogenous with high resistivity values and thickness is nearly 65-70 km. However, the *southern block* predominantly contains Neoarchean K-rich granites, Paleoarchean TTG-type granitoids, ultramafic-mafic intrusive, and sparse Neoarchean sanukitoids. The crustal thickness of the southern Bundelkhand is nearly 60 km (Gokarn et.al. 2013). On the basis of the gravity study, the Bundelkhand craton is divided into the southern Bundelkhand domain and northern Bundelkhand domain on either side of the Bundelkhand tectonic zone (BTZ) with gravity low and gravity high values respectively (Gokarn et.al. 2013). The depth of the Moho in the Bundelkhand craton also increases from south to north

(Singh et.al. 2017). The tectonic contact between the northern and southern Bundelkhand cratons is represented by this almost 200 km elongated Bundelkhand tectonic zone (BTZ), which forms E-W trending brittle-ductile shear zones. ("Malviya et.al., 2006; Gokarn et.al., 2013").

### 2.1.1. Lithologies:

Like other Archean crustal records, the Bundelkhand craton also contains three major lithological assemblages viz. (i) Granitoids of TTG- affinity (ii) Volcano-sedimentary greenstone sequences (iii) high K-granitoids.

## 2.1.1.1. Granitoids of TTG affinity

The "TTG-type granitoids (basement gneisses)" are the most abundant heterogeneous lithological associations spatially associated with volcano-sedimentary sequences exposed mostly in the centre and southern parts of the "Bundelkhand craton." The gneisses contain medium to coarse dark grey tonalite, coarse-grained grey granodiorite, and minor medium to fine-grained whitish grey trondhjemite. They also contain boudins, disrupted fragments, and thin layers of mafic rocks with very rare ultramafic xenoliths. The TTG gneisses show banding or weakly foliated migmatitic fabrics. The gneissic layer which consists of alternate light-coloured quartzo-feldspathic and dark-coloured mafic layers is also folded and intruded by late-phase anatectic granites. TTG gneisses are spatially associated with greenstone sequence and occur in the form of sporadic outcrops in and around Mauranipur, Baragaon, Babina, Mahoba, Kuraicha, Karitoran, Charkhari of the central Bundelkhand craton (See figure 1.8). These TTG gneisses metamorphosed under amphibolite facies conditions during Neoarchean and Paleoproterozoic periods (Singh and Slabunov 2019a). The Paleoarchean TTG-type gneiss (Ca.3.5-3.2 Ga) is more deformed with tonalite to trondhjemite in composition and shows classical-type gneiss (Banded to migmatitic in nature). In the high strain

zone of the central Bundelkhand block, the TTG-type gneiss also exhibits a tectonic interlayer of Ca. 3.34 Ga darker grey and Ca. 3.27 Ga whitish grey gneiss.

Most of the younger Neoarchean TTG-type gneisses (2.7-2.6 Ga) are confined to the Bundelkhand craton's central block. They were found as sporadic low-lying outcrops in form of dispersed plutons adjoining the greenstone sequences of the Babina belt. They are grey to dark grey gneisses displaying banded to weakly migmatitic fabrics (Verma et al., 2016). The Neoarchean TTG-type gneiss is granodioritic in composition, is largely undeformed, and exhibits a transitional nature (banded) as described in many places of the world. (Jayananda et.al., 2018, Dey et.al., Laurent et al., 2014). The Neoarchean gneisses devoid of xenocrystic zircon ages reveal the juvenile origin of magma. Pink granite and mafic dykes of varied ages have severely encroached onto them. The Neoarchean TTG-type gneiss is less evolved in comparison to the Paleoarchean TTG with the dominance of the mafic mineral.

On the other hand, the southern Bundelkhand craton has preserved a relatively lower age of (ca. 3.44-3.28 Ga) TTG gneisses in the form of patchy to sporadic outcrops of basement gneiss (TTG) near the Rungaon area. TTG-type granitoids are associated with the ultramafic-mafics unit of the southern Bundelkhand craton and are distributed around Rungaon, Madawara, and Ganeshpura regions. However, the northern Bundelkhand craton is dominated by patchy occurrences of sanukitoids in association with K-rich granitoids and older TTG-type gneisses.

### 2.1.1.2. Volcano sedimentary Greenstone sequence

The volcano-sedimentary greenstone sequences have been exposed along the Mauranipur, Babina of the central block and Girar, Badwar of the southern block of the Bundelkhand Craton. ("Singh

& Slabunov 2015a, 2015b, 2016; Slabunov et al. 2017a; Slabunov & Singh 2019a, Singh et al., 2018, Hiloidari et al., 2021"). They are mainly comprised of "ultramafic-mafic-felsic volcanic and metasedimentary (BIFs)" rocks which are associated with highly deformed TTG-type gneissic basement rocks. (Mondal et.al, 2002, Kaur et al., 2014, Saha et al., 2016, Singh et al., 2019b). The Babina-Mauranipur belt, a 200 km wide E-W trending belt that connects Babina to Mahoba through Mauranipur, is spread along the central Bundelkhand craton and forms a significant structural element of the craton (see figure 1.8) (Mondal et al. 2002; Malviya et al. 2006; Singh & Slabunov 2015a; Kaur et al. 2016; Saha et al. 2016; Singh et al. 2019a; Slabunov & Singh 2019a; Singh & Singh 2019). The SBGB, forms a sporadic outcrop dispersed from Girar to Badwar called as Girar-Badwar belt (Hiloidari et al., 2021).

The "Mauranipur belt of the CBGC" comprises three different litho assemblages, namely early Paleoarchean ultramafic mafic volcanics (Basalts and Basaltic komatiites), Mesoarchean felsic volcanics with metasedimentary (BIF) and late Neoarchean felsic volcanic rocks. This area contains well-preserved outcrops at Baragaon, Kuraicha, and Roni areas of the central block of the Bundelkhand craton, which is nearly 4-6 km long and 1-2 km wide. ("Malviya et al., 2006, Singh and Slabunov 2015, Singh et al., 2017 Singh and Slabunov 2019"). The ultramafic mafic volcanic are usually dark grey colours and have sheared/faulted contact with the sedimentary rocks. These litho assemblages metamorphosed under greenschist to amphibolite facies of metamorphism. In Mauranipur, the early ultramafic volcanic is dark green to grey in colour extremely serpentinized and characterized by basaltic komatiite affinity (Malviya et al. 2006). The meta basalt is the most common volcanic of the Mauranipur belt and metamorphosed to amphibolite facies and shows occasional pillow structure. The metasediments (BIFs) are intercalated with metamorphosed pillow basalts. The Mauranipur greenstone belt's metamorphism

is thought to have occurred at 2687±11 Ma, (metamorphic age) according to the zircon ages of basalts. The Metasediments in particular to BIF probably formed after the early ultramafic mafic volcanism of the Mauranipur-Babina belt and could be related to the Mesoarchean event (Singh and Slabunov, 2013, 2015). The "felsic volcanic rock of the earlier and late assemblage yielded a U-Pb zircon age of 2810±13 Ma, and 2557±33 Ma, respectively suggesting Mesoarchean to Neoarchean age" (Singh and Slabunov 2016). The elemental and isotopic data reveal that the ultramafic mafic formed through a magmatic differentiation process with negligible crustal contamination formed in a subduction-related tectonic environment (Malviya et al., 2006, Singh and Slabunov 2015, 2016, 2019). On the contrary, (Singh et al., 2018), propose "plume-arc accretionary tectonics for the Central Bundelkhand Greenstone Belt."

The "Babina greenstone component" is also part of the CBGB and exposed in the form of an E-W trending belt linear belt 30-40 km long and up to 4-5 km in width. This greenstone belt also comprises ultramafic-mafic-felsic volcanic and metasedimentary rocks (Sing and Slabunov et al., 2015). The early ultramafic mafic volcanic component comprises komatiite, basaltic komatiites, and tholeiitic basalt to basaltic andesite, which are variably metamorphosed to greenschist and amphibolite facies. ("Malviya et al., 2006, Singh and Slabunov, 2015, Singh et al., 2018, Singh et al., 2019a"). It makes up nearly 5–10% of the greenstone belt's overall outcrop. The Babina belt has BIFs that are 1–10 cm thick and almost 10-200 m wide in the metasedimentary unit ("Singh and Slabunov, 2015; Alfimova et al., 2019"). These BIFs are presumably to be deposited at ca~2.8 Ga, indicating a Mesoarchean event ("Singh and Slabunov 2013, 2015"). The felsic volcanic rock in the late assemblage of this belt yielded a U-Pb zircon age of 2542±17 Ma, indicating Neoarchean age. The felsic volcanism is synchronous with abundant anatectic granite. So, the litho assemblages of both the Mauranipur and Babiana belts evolved through the same time

frame. The Local positive gravity anomalies in the Central Bundelkhand block are correlated with the mafic-ultramafic rocks surrounded by K–rich granitoids. (Gokaran et al. 2013).

The SBGB comprises a small section of the greenstone belt coupled with most voluminous Neoarchean high-K calc-alkaline granitoids (Singh & Slabunov 2016; Slabunov et al. 2017a, 2018; Joshi et al. 2017; Mohanty et.al. 2019; Singh & Slabunov, 2019). The greenstone component in the SBGB is exposed in the form of small dispersed outcrops named as Rungaon-Girar greenstone belts (Slabunov et al., 2017). A recent study reported the presence of greenstone components exposed near Badwar, Khurrat, and Girar and named as Badwar-Girar greenstone belt (Hiloidari et al 2021). This greenstone component is unconformably overlain by the Paleoproterozoic Bijawar group of rocks. The metasedimentary rocks of the SBGB are mostly dominated by BIFs and quartzites. The quartzites and BIFs are considered part of the "Berwar formation" of the Mehroni group (Pasco, 1950). The quartzites are mainly fuchsite quartzite and hematite-magnetitebearing quartz arenite with laminae of meta-argillite. The BIFs show a nearly E-W trend with a tight folding structure (Singh & Slabunov et al., 2015). These BIFs appear to have originated far from terrigenous source areas in a basin with significant hydrothermal activity. The traces of carbonates are found along the contact between quartzite and BIF rocks (Singh and Slabunov 2015). The detrital zircon suggests that the existence of a possible older TTG-type granitoid (3.4-3.2 Ga) source occurs in the SBGB. The metavolcanic of the SBGB yielded a Mesoarchean age (ca. 2.98 Ga) (Hiloidari et al., 2021). All the litho assemblages are invaded by Neoarchean high K-granitoids along with Paleoproterozoic mafic dykes and quartz reefs. (Kaur et al., 2016, Joshi et.al. 2017).

### 2.1.1.3. "High K-Granitoids (Sanukitoids, and anatectic granites)"

The Bundelkhand granitoid complex covers volumetrically nearly 80% of the total area of the Bundelkhand Craton ("Joshi et al., 2016"). The high-K calc alkaline granitoids emplaced into the older deformed TTG basement rocks. The diversified high-K calc alkaline granitoid comprises sanukitoids, and anatectic granites (Joshi et al., 2022). The Northern Bundelkhand block comprises sanukitoids in association with anatectic granites consisting of TTG enclaves (Slabunov & Singh 2019b Joshi et al. 2017; Singh et al. 2019b; Joshi & Slabunov 2019). However, in the southern block of Bundelkhand, sanukitoids are relatively rare with E-W trending batholiths invaded by high-K anatectic granites. Sanukitoids are mesocratic rocks that are medium to coarse in texture, moderately to coarsely foliated, and include localised aggregation of mafic minerals, including amphiboles and biotite. They do not show any deformation except minor shearing with late intrusive of pegmatite and quartz veins. Sanukitoids that occurred in the northern part of the craton yielded U-Pb ages between ca. 2560, (Joshi et al. 2017) 2577 Ma (Singh et al. 2019b). The sanukitoids exposures from this terrane in the field show a subvolcanic character. In the northern part of the Nivari-Sakrar region, fine-grained sanukitoids exposures also occur in E-W shear zones. They exhibit a lineation of mineral movement along the E-W trend. Throughout the Bundelkhand Craton, anatectic granites were present. In addition, the presence of xenocryst zircons from sanukitoids of older dates ("2914±8 Ma, 2842±3 Ma, 2644±25, and 2619±24 Ma") indicates that ancient crustal material played a role in their formation ("Joshi et al., 2017; Singh et al., 2019b, c"). According to "Condie and Aster (2010) and Jayananda et al. (2018)," there was a similar Neoarchean sanukitoids intrusion in the BC in various cratons in India and around the world. The field relationships of sanukitoids and anatectic granites magmatism are concurrent with the age of about 2.55 Ga (Mondal et al., 2002; Kaur et al., 2016; Joshi et al., 2017; Singh et al., 2019b, c).

### 2.1.1.4. Mafic dykes and Quartz reefs

The Paleoproterozoic mafic dyke swarms mark the last phase of regional tectonic activity in the Bundelkhand craton. The dykes are mostly dolerite with subordinate pyroxenite dykes in nature (Rao et al., 2004, 2005). Dolerite dykes are found as linear ridges and are frequently identified by sharp contacts with host granites that have chilled margins. Most of the dykes have a NW-SE orientation, and a small number also show NE-SW to ENE-WSW direction, suggesting at least two separate phases occur in the Bundelkhand craton. (Rao et al., 2005, Pradhan et al., 2012). The dykes show a cross-cut relationship with both TTG gneisses and granitoids ("Pradhan et al. 2012"). The Bundelkhand craton shows the cross-cutting relationship between the dykes indicates that the NW-SE dykes are the oldest, flowed by NE-SW dykes, and ENE-WSW dykes are marked by the youngest phase. According to (Radhakrishnan et al., 2020 and Pati et.al., 2008) the U-Pb zircon ages demonstrate that the NW-SE mafic dykes were deposited between 2.2 and 1.8 Ga, with only a few showing emplacements at 1.98 Ga. However, NE-SW mafic dyke emplaced at about ~2.00 Ga according to Ar-Ar dating (Rao et al., 2005). According to (Pradhan et al. 2012), the mafic dykes in the Mahoba emplaced at around ~1.11 Ga and were trending ENE-WSW. In summary, the mafic dykes are plume generated and emplaced along the tectonic extensional area (Pati et al., 2020). The Bundelkhand has giant quartz reefs with emplacement occurs at ~2.1 Ga, ~1.9 Ga, and ~1.8 Ga. Most of the quartz reefs were emplaced in the NE-SW direction with few oriented in N-S, E-W, and NNE-SSW orientations. Most of the reef is 1 km long, with only a few reefs showing minor offshoots that cross one another. They display brittle-ductile deformation and range in colour from milky white to light pink (Pati et al., 2007, Bhattacharya and Singh 2013). This reef's origin is still up for debate. The widely accepted view is that they were created by late-stage hydrothermal activity along tectonically weaker planes.

### 2.2. Madawara Ultramafic-Mafic Complex (MUC)

Madawara ultramafic complex (MUC) comprises a series of E-W trending ultramafic-mafic outcrops dispersed in the form of the lenticular body spread over the "Madawara, Ikauna, Pindar, Hanumathgarh, Bhikampura, Ramgarh, Hansra and Girar of the southern block of Bundelkhand Craton," (See figure 2.2). ("Satyanarayanan et al., 2010,2015; Singh et al., 2017; Mohanty et.al., 2018"). These lensoidal bodies intrusive into the TTG type granitoids with varying in size stretched over nearly 30 km from east of Madawara to Dhasan river. The ultramafic mafic plutonic rocks are relatively undeformed with variables affected by alteration. ("Malviya et al. 2006"), reported that it is an intrusive body comprising peridotites, pyroxenites, and gabbros which are closely associated with metabasic rocks and BIFs in the southern fringe of the Bundelkhand craton. The largest ultramafic body is exposed at the SE part of Madawara village and is in the form of lowlying lensoid outcrops with ~400 m wide and extends laterally nearly E-W direction up to 5 km. At Madawara the intrusion is an asymmetric ring-like intrusion with ultramafic rocks comprising of peridotite, olivine pyroxenite, pyroxenite, and hornblende pyroxenite, occurs in the core part and mafic to intermediate rocks such as gabbro and diorite occurs towards the rim part. These "ultramafic-mafic" bodies are nearly subparallel to the other ultramafic mafic bodies of MUC and confined between the "Madawara-Karitoran shear zone in the north and Sonrai-Girar shear zone in the south." The contact between the TTG-type granitoids and MUC has been marked by sheared and weathered which are wrapped by serpentine-talc-chlorite schist and talc-tremolite-actinolite schist. The Madawara ultramafic-mafic rocks are further traversed by Bundelkhand granitoids, NE-SW trending quartz reefs, and NW-SE mafic dykes. Although a few studies have been attempted regarding the tectonic context of ultramafic mafic magmatism of MUC, still it is very conjectural and there are no detailed elemental geochemistry and isotope studies of ultramaficmafic units from MUC have not been reported, however, the lot of work has been done on strategic PGE mineralization hosted by this ultramafic unit.

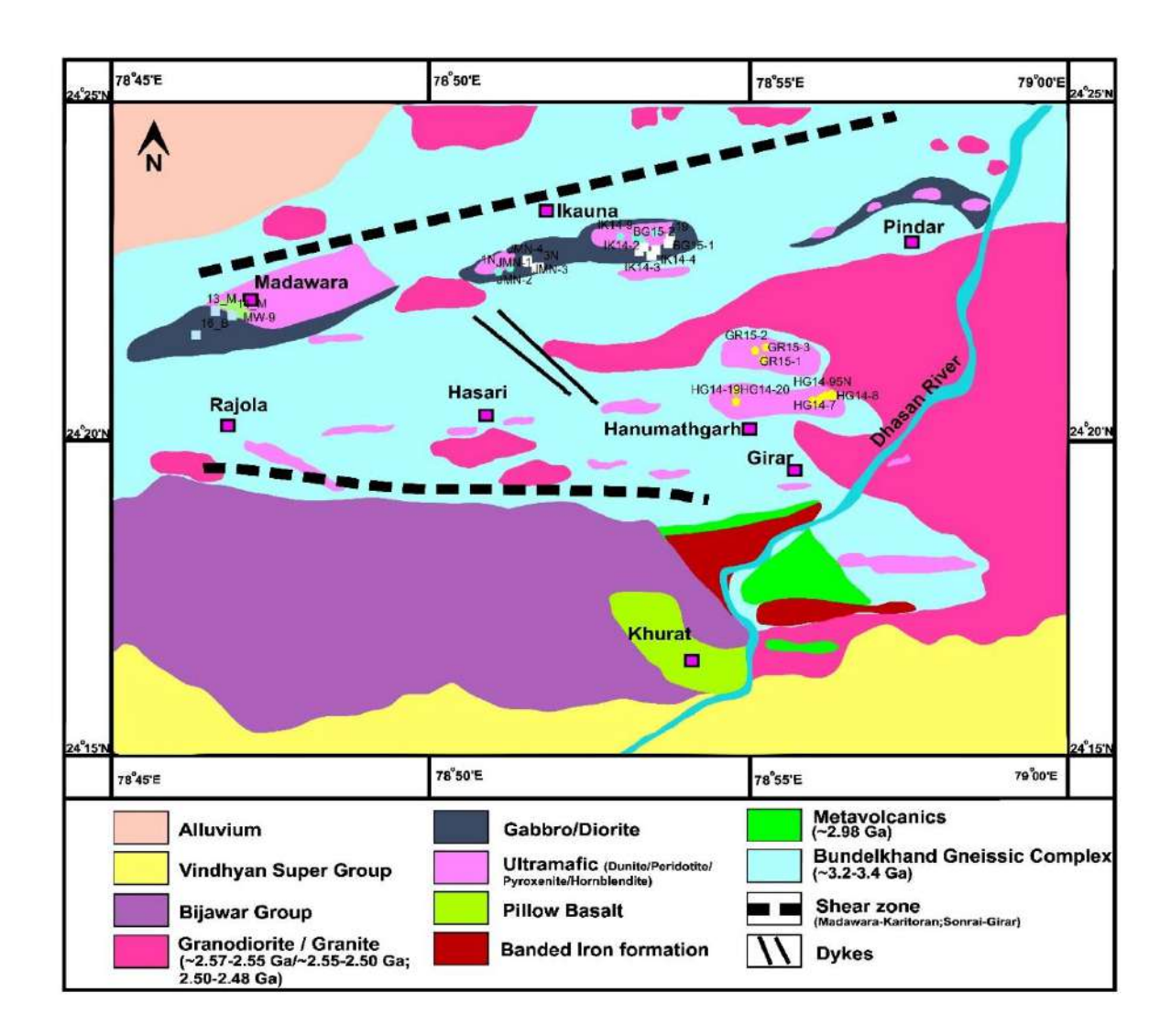


Figure 2.1. Geological map of the study area showing the distribution of ultramafic-mafic complexes along with other lithological units and their relationship. The various magmatism ages reported by various authors are displayed on the map (Mondal et al., 2002; Singh et. al., 2011; Kaur et al., 2014, 2016; Joshi et al., 2016, Singh et.al, 2019b, Sikha et.al. 2021).

This explains a lot of ambiguity about the ages and hence it creates ambiguity in understanding the tectonic settings of this ultramafic-mafic complex. Based on field relationship, MUC is "older than high-K calc-alkaline granitoids and younger than TTG-type granitoids." (See figure. 2.1) ("Farooqui and Singh, 2006; Balaram et al., 2013; Satyanarayanan et al., 2015; Singh and Slabunov, 2016; Slabunov et al., 2017; Mohanty et al., 2018; Ramiz et al., 2018"). ("Mondal et.al.,1996"), suggested that the presence of thickened continental crust in the north and the predominance of greenstone components along with Madawara ultramafic mafic suite (Gravity high) in the southern margin of the Bundelkhand massif could be marked as the oceanic remnants in the form of ophiolites. ("Slabunov et al., 2018") suggested that these ultramafic-mafics are represented as layered intrusions and show similarities to the layered intrusions of the peridotitegabbronorite complex of the Karelian Craton, which could be formed due to mantle-plume activity in the late Archaean and cross-cut by K-rich granitoids (ca. 2.5 Ga). ("Ramiz et al., 2018") suggested that the MUC comprises two litho assemblages "deformed low-grade metamorphosed high-Mg ultramafic rocks comprising serpentinites and spinel-bearing schistose and "undeformed ultramafic mafic rocks comprising of gabbro, harzburgite, lherzolite, and olivine websterite." However, ("Ramiz et al. 2018"), suggest a "continental arc setting characterized by northward subduction of the oceanic crust below a 3.5-3.2 Ga TTG-dominated continental crust". It is revealed that the "deformed high Mg-ultrabasic rocks are the result of shallow partial melting of the metasomatized mantle." The ultramafic-mafic plutonic rocks, on the other hand, "were created as a result of asthenosphere upwelling from a deeper depth which induced the lithosphere to melt". The MUC has large lensoidal outcrops that mainly occur at the Madawara, Ikauna, Girar, and Hanumathgarh regions with nearly E-W trending having varied ultramafic lithology. The present thesis mainly focuses on the detailed aforementioned ultramafic mafic assemblages that occur between Madawara-Karitoran and Sonrai-Girar shear zone.

### 2.2.1. Madawara region

The Madawara section is one of the largest lensoidal outcrops of the MUC exposed at the SE of Madawara village. It is in the form of low-lying lensoidal outcrops with ~400 m wide and extends laterally in an E-W direction up to 5 km (see figure 2.1). It shows an asymmetric ring-like structure with ultramafic rocks in the centre comprising peridotite, olivine pyroxenite, pyroxenite, and mafic rocks occur towards the rim part comprising hornblende gabbro and gabbro. However, the Madawara section is dominated by ultramafic rocks, which covers s nearly 80% of the total exposure in the Madawara region. The ultramafic rocks are is coarse-grained with light greenishblack to light yellow in colour. They are nearly undeformed, subparallel, and are confined between the Madawara-Karitoran shear zone in the north and Sonrai-Girar shear zone in the south (See figure 2.1). The north part of the Madawara block was affected by major shear deformation revealed by very closely spaced foliation planes with the adjoining granitoids. The ultramafic rocks have been affected by shearing and fluid flow, demonstrating a fluid-induced alteration of the ultramafic rocks into serpentine-talc-chlorite schists and talc-tremolite- actinolite schists however mafic rocks are less altered and preserve the primary mineralogy. The diorites are absent in this section. These ultramafic units are further traversed by Bundelkhand granitoid and NE-SW trending quartz reefs.

### 2.2.2. Ikauna region

The ultramafic and mafic rocks of Ikauna occurred at the eastern extension of Madawara ultramafic-mafic and lie about 10 km east of Madawara town. The Ikauna ultramafic-mafic is a nearly 3.5 km E-W trending linear belt with a width varying from 90-180 m width. The chrome spinel-bearing ultramafic rock is traced to more than 1 km along the strike length.



Figure 2.2. (a) Field photograph showing nearly E-W trend of ultramafic outcrops intruding into Bundelkhand gneissic complex (BnGC) near Madawara village. (b) Field photograph of peridotite showing a large number of embedded Cr-spinel crystals in the peridotite at Madawara village (c) Field photograph of peridotite showing solution channel weathering in the Madawara village. (d) The old TTG shows banding about 4 km north of Madawara town. (e) Field photograph of E-W trending shear zone occurred north of the ultramafic outcrop near Madawara village. (f) Field

photograph showing the highly deformed intrusive relationship of ultramafic-mafic rocks with older granitoids.



**Figure 2.3.** (g) Field photograph showing nearly E-W trending ultramafic outcrop intruded into Bundelkhand granitoids near Ikauna. (h) Field photograph of nearly E-W trending gabbro occurred outward to the peridotite in Dangli village (i) Field photograph of Gabbroic diorite and

diorite in the outer rim of ultramafic near Ikauna and Bighai village. (j) Field photograph showing the intrusive between ultramafic and older granitoid near Hanumathgarh village. (k) Filed photograph showing the granitic gneisses in the Ganeshpura area. (l) Field photograph of dispersed lensoidal ultramafic outcrops near Hanumathgarh.

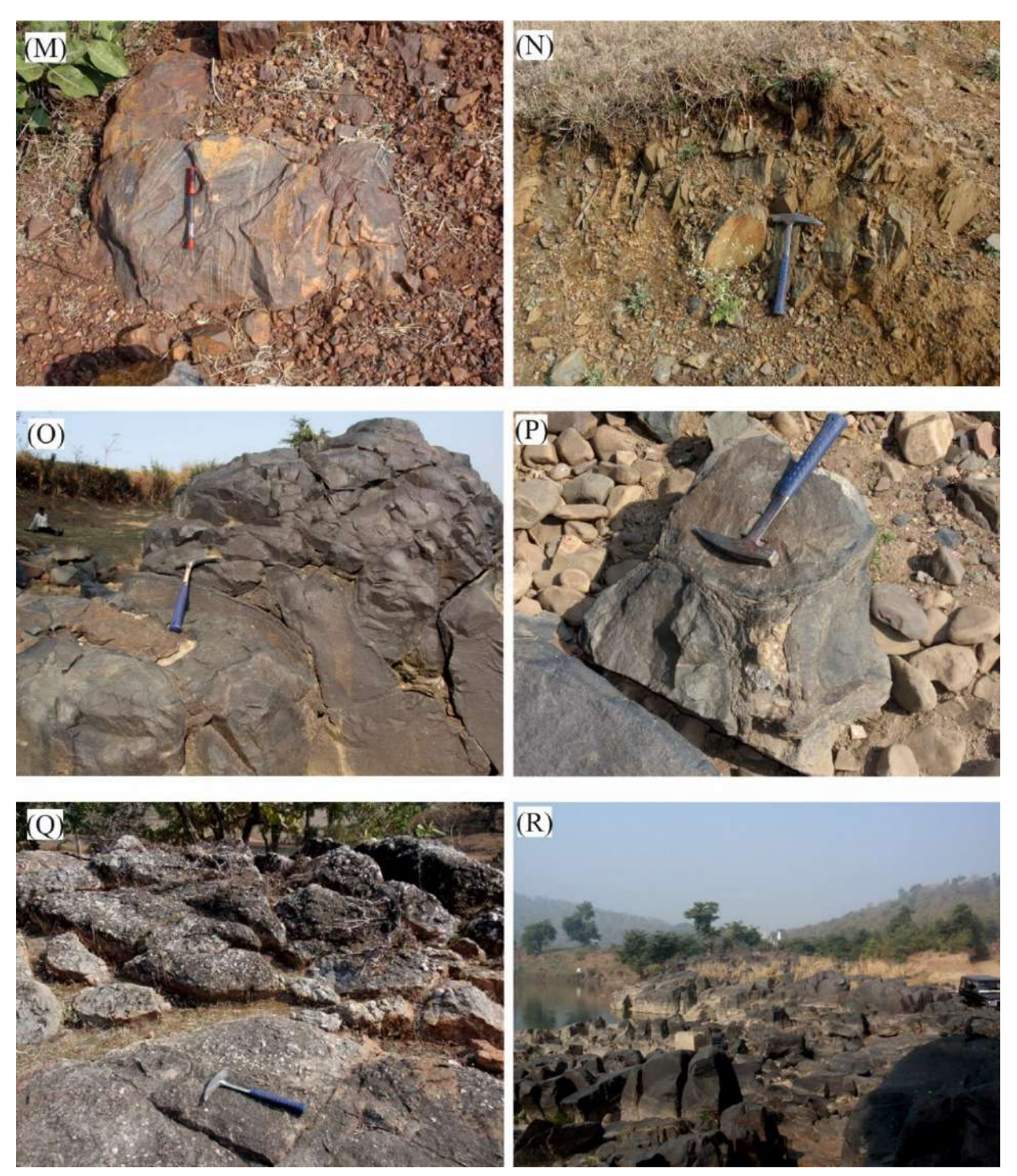


*Figure 2.4* (m) Banded iron ore formation of the Girar belt in the southern Bundelkhand craton.

(n) field photograph of meta basalt near to Badawar village of the southern Bundelkhand craton (0 & p) field photograph of large, nearly unstretched pillows near the Dhasan river of southern Bundelkhand craton. (o) oligomictic conglomeratic outcrops of the southern greenstone belt. (p) Nearly NW-SE trending mafic dykes exposed near Girar of the southern Bundelkhand craton.

At Ikauna these intrusions are nearly symmetric ring-like intrusions with ultramafic rocks in the centre comprising of peridotite occur in the core part while mafic rocks such as pegmatitic gabbro, gabbro, gabbroic diorite and diorite rocks grading towards the rim part (see figure 2.3 h & i). At Ikauna the gabbro ultramafic is the dominant lithology which covers nearly 60% of the total exposure in the Ikauna region while intermediate rocks nearly cover 40% of the total exposure. The gabbro mostly occurs in the northern part of the Ikauna sector, whereas pegmatitic gabbro and diorite mostly occur southern part of the Ikauna sector. The lensoidal dark-colored peridotite is highly altered and the margin is altered to talc chlorite and talc chlorite actinolite schist. The contact between Ikauna ultramafic mafic with the TTG type granitoids is marked sheared and mylotinised. The metagabbro is cross-cut by high K-granitoids at the southern Bundelkhand craton. The contact is partially enveloped by mylonitised chlorite (± talc) actinolite schist. The Ikauna ultramafic body is also dissected by NW- SE mafic dykes at several places.

### 2.2.3. Hanumathgarh Sector

The Hanumathgarh ultramafic mafic is a nearly E-W to ENE-WSW trend linear belt with a length of 1 km width that varies from 90-180m. The ultramafic rocks of Hanumathgarh form the southeastern extension of Madawara ultramafic-mafic and lie about 15 km southeast of Madawara town. At Hanumathgarh the intrusion is mostly dominated by ultramafic rocks comprising peridotite and amphibole-rich peridotite, however, this sector is devoid of gabbro and diorite. The lensoidal dark-colored peridotite is highly altered and has sheared contact with granitic gneiss (See figure 2.3 1).

The contact is partially enveloped by mylonitised chlorite ( $\pm$  talc) actinolite schist. The Hanumathgarh ultramafic body is also dissected by NW- SE trending faults at several places.

## **CHAPTER-III**

# Petrography and SEM study

In this chapter, an attempt has been made to present the petrographic description of ultramafic-mafic-intermediate rocks of the Madawara, Ikauna and Hanumathgarh sectors. The main objective of the petrographic analysis is to identify the texture and mineralogy of ultramafic, mafic, and intermediate rocks and to establish the effect of alteration and metamorphism on minerals which in turn affect the chemical composition. A total of about 73 ultramafic-intermediate samples were selected and studied extensively for this purpose.

## 3.1 Ultramafic-mafic of Madawara region

The "ultramafic-mafic" rocks of the Madawara region shows variation in terms of mineralogy, texture, and grain size. The Madawara sector is dominantly ultramafic with subordinate mafic rocks. The studied ultramafic rock show very coarse-grained cumulate textures while the mafic rock exhibits coarse-grained ophitic to occasionally medium-grained textures. The petrographic characteristics of the Madawara sector are as follows-

The ultramafic rocks show the following common mineral assemblages:

Serpentine-tremolite-chlorite-spinels (figure 3.1 a)

Olivine-serpentine-clinopyroxene (figure 3.1 b)

Clinopyroxene-serpentine-tremolite- (figure 3.1 c)

Pyroxène-Amphibole-tremolite-chlorite (figure 3.1 d)

Plagioclase-pyroxene-hornblende-actinolite (figure 3.1 e & f)

Serpentine-carbonate-tremolite (figure 3.1 g) and Talc-carbonate-chlorite (figure 3.1 h)

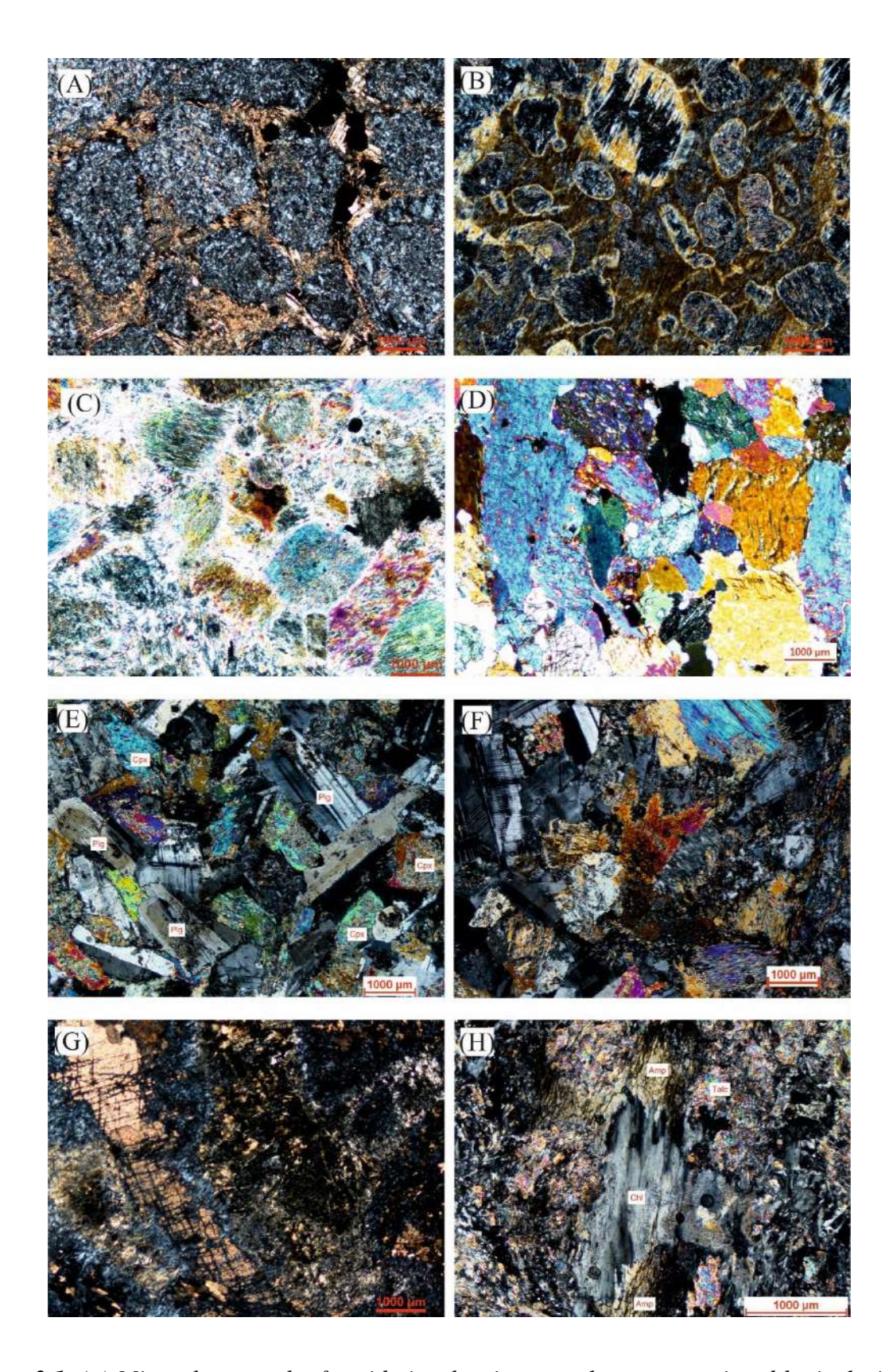


Figure 3.1. (a) Microphotograph of peridotite showing cumulate texture sieved by inclusions of euhedral to subhedral chromite grains in the olivine pseudomorph and its grain boundary. (b)

Poikilitic texture in olivine pyroxenites showing rounded crystals of olivine and euhedral spinel. (c) Cumulate pyroxenite with the inclusion of chromite grains and serpentine, particularly in the left bottom corner (d) Cumulate hornblende pyroxenite showing variable altered to tremolite and actinolite variety. (e) Gabbro with zoned plagioclase feldspar and clino- pyroxenes showing cumulate texture (f) Gabbro showing the presence of feldspar, pyroxene, and hornblende which are variably altered to actinolite variety. (g) Photomicrograph of ultramafic showing mineral assemblages of serpentine-tremolite-carbonate. (h) photomicrograph showing hornblende mantled by tremolite with chlorite in hornblende-pyroxene-rich ultramafic rocks.

The ultramafic unit mainly comprises peridotite, pyroxenite, and hornblende pyroxenite, which show serpentine-tremolite-chlorite-spinels, serpentinite-tremolite-carbonates, olivine-serpentine-tremolite-chlorite, olivine-pyroxene-tremolite-chlorite and pyroxene-amphibole-chlorite assemblages. The primary mineralogy of the most of samples are completely altered during the hydrothermal alteration processes.

The peridotites contain mainly relict olivine (~70-80 vol.%) and altered pyroxene (~0-15 vol.%) with few amounts of opaque minerals (0-5 vol.%) which show a very coarse-grained cumulate texture. Relict olivines are the major abundant cumulus phases whereas the pyroxene and spinel occur as subordinate to minor phases at the intercumulus spaces. Olivine occurs as big rounded grains, highly cracked and shows colourless in plane-polarized light with higher order interference colour under crossed Nicols. The serpentine grains occur as fine-grained aggregates and show colourless in plane polarised light and shows light grey to dark grey to whitish colour in crossed polarised light. The primary olivine is observed in olivine pyroxenite and rarely in peridotite. pyroxene occurs as intercumulus phases and dispersed grains and is variably altered to tremolite and chlorite. Tremolite occurs as subhedral to anhedral in shape with colourless in plane polarised light and shows light grey in colour in crossed Nicol. The carbonate minerals are rarely found and occur both in the form of veins and small tiny aggregates of grain with dusty pink in colour under

cross-polarized light. Chlorites are found in the intercumulus spaces and show green in colour with low-order interference colour. The opaque mineral is mainly chrome spinels occur as euhedral to subhedral grains and are partially or totally included by silicate minerals indicating primary magmatic origins occurring in the form of intercumulus phases. Fe-Ti oxide phases such as ilmenite occur as small grains as well as thin lamellae enclosed in the cleavage plane of pyroxene. The other opaque phases are pentlandite and millerite under reflected microscopy.

The olivine pyroxenite mainly consists of clinopyroxene (~70-80 vol.%) and olivine (5-10 vol.%) with less than 5 vol.% amphiboles and other opaque minerals. It shows coarse to medium-grained texture. The rock shows poikilitic textures characterized by occurrences of multiple small rounded olivine inclusions in pyroxene where the pyroxene acts as oikocryst and olivine as chadacryst. The pyroxene grains are occasionally altered to both tremolite and chlorite varieties. In some cases, the hornblende is altered to chlorite.

The pyroxenite and hornblende pyroxenite is coarse-grained consisting essentially of cumulus clinopyroxene (~80-90 vol.%) with interstitial amphibole which has been occasionally altered to chlorite. They are mostly colourless prismatic crystals and show second-order blue-orange interference colour. Olivine occurs as euhedral crystals, highly cracked, sometimes filled with both spinels and Fe-Ti oxides. Amphibole occurs as green platy or prismatic crystals which are rarely replaced by chlorite. Orthopyroxene is also present as anhedral to subhedral small prismatic crystals with first-order yellow interference colour. In the case of pyroxene hornblendite, the mineral phases are hornblende and plagioclase subordinate amount of pyroxene with Fe-Ti oxides phases (magnetite and ilmenite). The mafic rocks show the following mineral assemblages:

Plagioclase-pyroxene-hornblende-actinolite (Figure 3.1 e)

Plagioclase-pyroxene-hornblende (Figure 3.1 f)

The mafic rocks are mainly Plagioclase-pyroxene-hornblende-actinolite and Plagioclase-pyroxene-hornblende assemblages. The rocks are medium to coarse-grained and composed of plagioclase, and clinopyroxene, with subordinate amphibole and Fe-Ti oxides phases. The plagioclase occurs as euhedral to subhedral with moderate to well-developed twinning. They also show zoning with a darker core and whitish rim at places. The pyroxenes are euhedral to subhedral in shape and are colourless under plane polarized light with second-order blue and orange interference colour. The hornblendes occur in subordinate amounts with euhedral to subhedral in shape and are characterised by moderate to well-developed cleavages.

### 3.2. Ultramafic-mafic-intermediate of Ikauna region

The Ikauna sector is dominated by ultramafic and mafic rocks with subordinate gabbroic diorite and diorite rocks. They show coarse to medium-grained texture. The primary mineralogy of the ultramafic rocks is variably altered by the hydrothermal alteration process.

The ultramafic rock shows cumulate textures where the relict olivine occurs as large rounded grains, fractured and variably altered to serpentine. Serpentine occurs as fine-grained aggregates and is colourless under plane-polarized light and shows greyish to dark in colour in crossed polar. Tremolite occurs as colourless with grey to greyish white colour in crossed polar on the other hand, the pale green actinolite shows elongated with high order interference colour. Chlorites are found in the intercumulus space as elongated grains and occur in patches with light green and low-order interference colours. Common accessory minerals include opaques and a few carbonate minerals. The euhedral to subhedral opaque minerals occur as inclusions both in serpentine and tremolite. The thin lamellae opaque minerals show light grey in colour in the reflected light identified as ilmenite which is crystallised along the cleavage planes of pyroxene. Pentaldite and millerite phases are light yellows to dark yellow in colour and occur at the intercumulus phases of olivine.

The main mineral assemblages observed in these rocks are

Olivine-serpentine-spinel (figure 3.2 a)

Serpentine-talc-tremolite (figure 3.2 b)

Serpentine-chlorite-talc-spinel (Figure 3.2 c)

The mafic rocks show mainly plagioclase-pyroxene-hornblende-actinolite assemblage, while the intermediate rocks show plagioclase-hornblende-quartz assemblages. The plagioclase and pyroxene occur as euhedral to subhedral in shape. Plagioclase show well-developed twinning and display crude zonation with a darker core and whitish rim. The pyroxenes are elongated in habit with colourless in plane-polarized light and show second order blue orange interference colour. The gabbroic diorite and diorite occur as the subordinate amount in comparison to the ultramafic and mafic rocks of the Ikauna region. In gabbroic diorite, hornblende is the most abundant phase followed by plagioclase, while in the diorite the plagioclase and amphibole occur as equal in proportions. Hornblende is the major abundant phase in gabbroic diorite and plagioclase occurs as the second most abundant phase which occurs as subhedral grains and shows well-developed parallel twining. It is colourless in plane polarized light and shows grey under crossed Nicol. Hornblende shows well-developed cleavages and strongly pleochroic greenish-yellow to green. It occurs as both prismatic and diamond-shaped crystals. Generally, hornblende is stable and occasionally alters to chlorite in gabbroic diorite. Few occurrences of quartz show colourless anhedral grains with characteristics of undulose extinction.

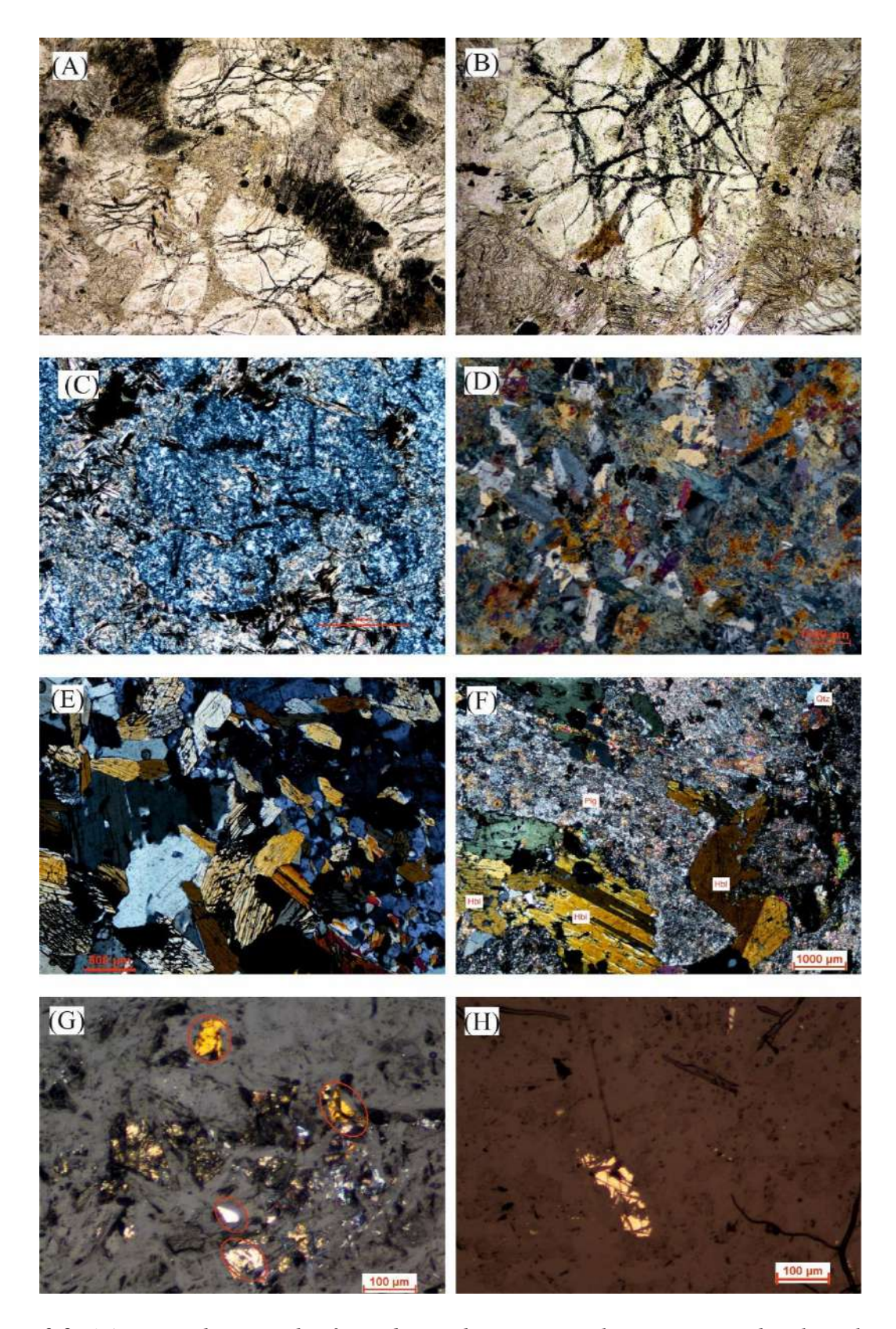


Figure 3.2. (a) Microphotograph of peridotite showing cumulate texture with relict olivine as cumulus and intercumulus space filled by pyroxenes in Ikauna village (b) Relict olivine showing

highly fractured with filed by opaque minerals. (c) Photomicrograph of ultramafic showing the different mineral assemblages of serpentine-tremolite-chlorite sieved with chrome spinel (d) photomicrograph of Gabbroic rocks showing the mineral assemblages of plagioclase and pyroxene. (e) Gabbroic diorite shows the mineral assemblages hornblende, plagioclase, and a few quartzes. (f) Diorite shows large crystals of hornblende and plagioclase, in which plagioclase shows a cloudy appearance due to saussuritization. (g) Microphotograph showing the presence of pentlandite with few millerites occurred in the intercumulus spaces of olivine in the ultramafics of Ikauna. (h)Microphotograph showing the presence of pentlandite (creamish yellow colour) in the ultramafics of Ikauna.

Plagioclase-pyroxene-opaque (figure 3.2 d)

Plagioclase-hornblende-actinolite±quartz (figure 3.2e)

Plagioclase-hornblende-quartz (Figure 3.2 f)

Pentaldite-millerite (figure 3.2 g and figure 3.2 h)

In diorite, the hornblende and plagioclase are in equal proportion along with a subordinate amount of quartz. Plagioclase occurs as large subhedral grains with well-developed multiple twinning. Hornblende shows well-developed cleavages with strong pleochroism from light yellow to dark yellow to green. Quartz is a minor phase and occurs as anhedral grains associated with hornblende. Quartz shows typical characteristics of being colourless and first-order grey in colour with undulose extinction.

### 3.3. Ultramafic-mafic of Hanumathgarh region

The ultramafics are widely distributed throughout this area followed by gabbro. The diorites are almost absent in this region. Serpentine occurs as colourless tiny aggregates which show light grey to dark grey in colour in hand specimen. Talc is colourless and occurs as an aggregate of flakes due to the alteration of tremolite. Chlorites occur as elongated patches, shows light green with a low order interference colour. The following mineral assemblages are commonly observed

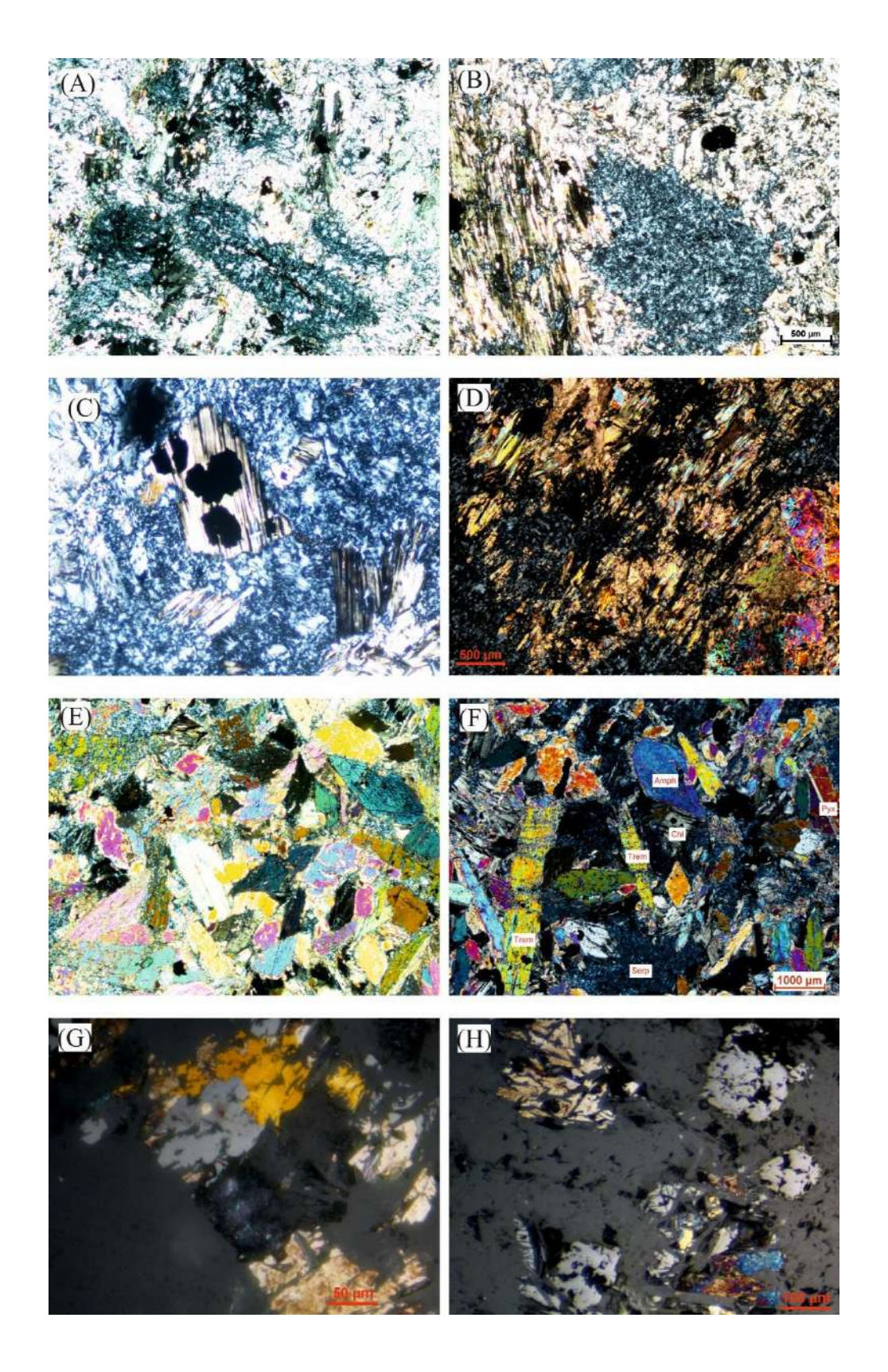


Figure 3.3 (a) Microphotograph showing the mineral assemblages of serpentine-tremolite-chrome spinels in the ultramafics of Hanumathgarh. (b) Microphotograph showing the mineral

assemblages serpentine-tremolite-chlorite along with chrome spinels. (c) Microphotograph showing the included chrome spinel with clinochlore. (d) Microphotograph showing the mineral assemblages of serpentine-tremolite-clinopyroxene. (e) Microphotograph showing the mineral assemblages of tremolite-actinolite-hornblende in hornblende-rich peridotite (f) Microphotograph showing the mineral assemblages of serpentine-hornblende-tremolite-actinolite in hornblende rich peridotite. (g) Reflected light microphotographs of pentlandite (light yellow) with millerite (dark yellow) along with surrounding late phases magnetite. (h) Reflected microphotographs of included chromite within olivine with intercumulus space filled by pentlandite and millerite.

Serpentine-tremolite-chlorite (figure 3.3a)

Serpentine-talc-tremolite-chlorite (figure 3.3b)

Serpentine-chlorite-spinels (figure 3.3 c) & Serpentine-tremolite-chlorite (figure 3.3 d)

Tremolite-actinolite-hornblende (figure 3.3 e)

Tremolite-actinolite-serpentine (figure 3.3 f)

Pentaldite-millerite-magnetite (figure 3.3 g) & pentlandite-chrome-spinel (figure 3.3 h)

The pale green to blue actinolite shows higher-order interference colour with an elongated habit, on the other hand, tremolite is colourless to pale grey in colour with high relief. Tremolite occurs as both elongated as well as aggregate of grains. Hornblende occurs as subordinate phases and occurs as a subhedral prismatic shape with well-developed cleavages. Occasionally, the actinolite shows kinking and fractures which could be formed due to shearing.

### 3.4 SEM-EDS study

## 3.4.1. Opaque mineralogy

The texture and qualitative chemical composition of both oxide and sulphide phases of 10 selected ultramafic samples were studied using SEM/EDS. The results indicate that the oxide phases are mostly chromite, chrome magnetite and magnetite while the sulphide phases are pentlandite and millerite. Majority of the chromite occurs as euhedral to subhedral grains with isotropic homogeneous in nature, whereas few of the crystals show well-developed zoned textures with

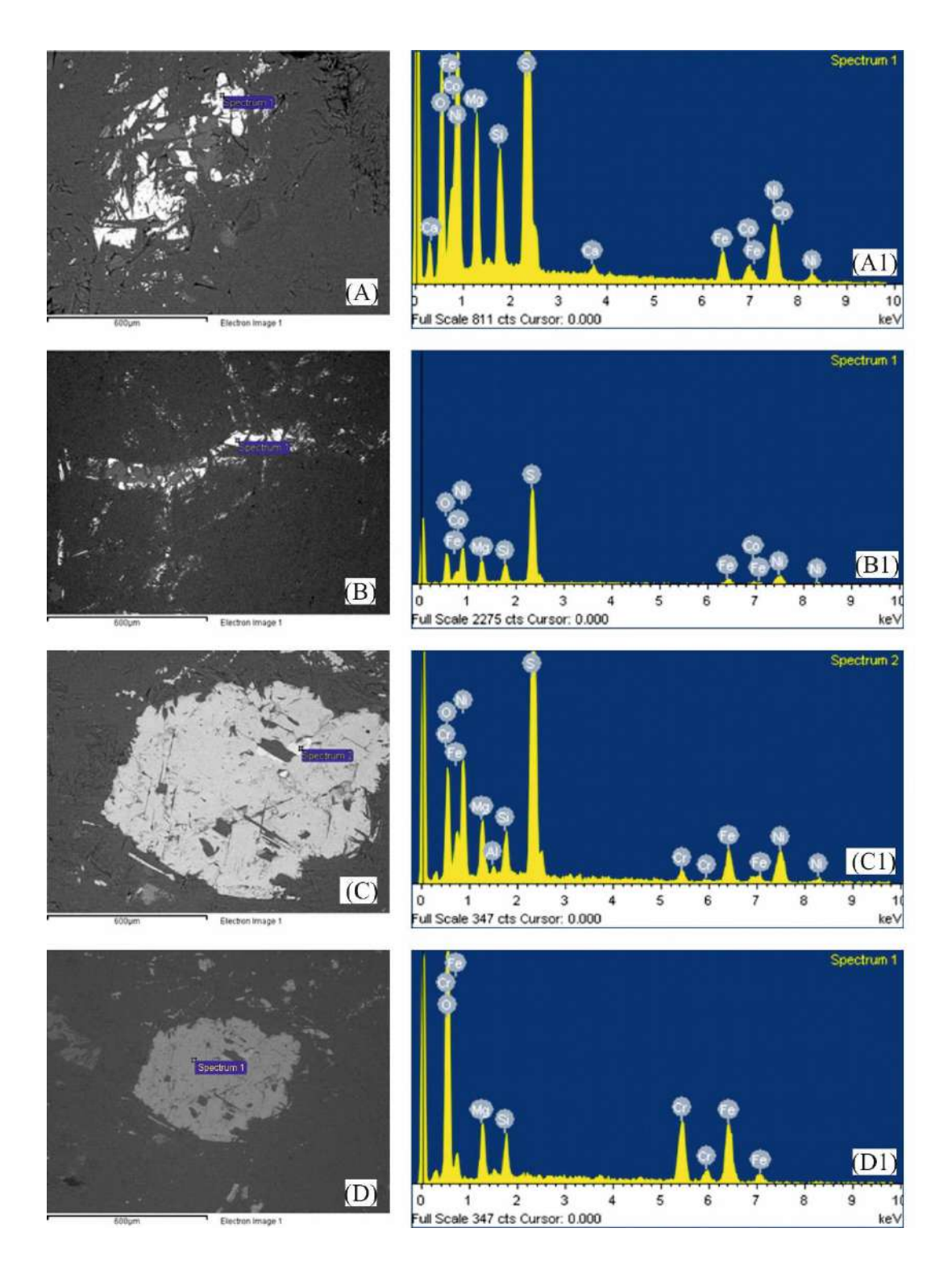


**Figure 3.4(a)** SEM-EDX study of ultramafic rocks of MUC (a-b) Backscattered electron (BSE) images showing the presence (Ni, Fe) S and NiS phases such as pentlandite and millerite in the intercumulus spaces of olivine (c-d) BSE images showing the presence of early (Ni, Fe) S phases within the chromite.

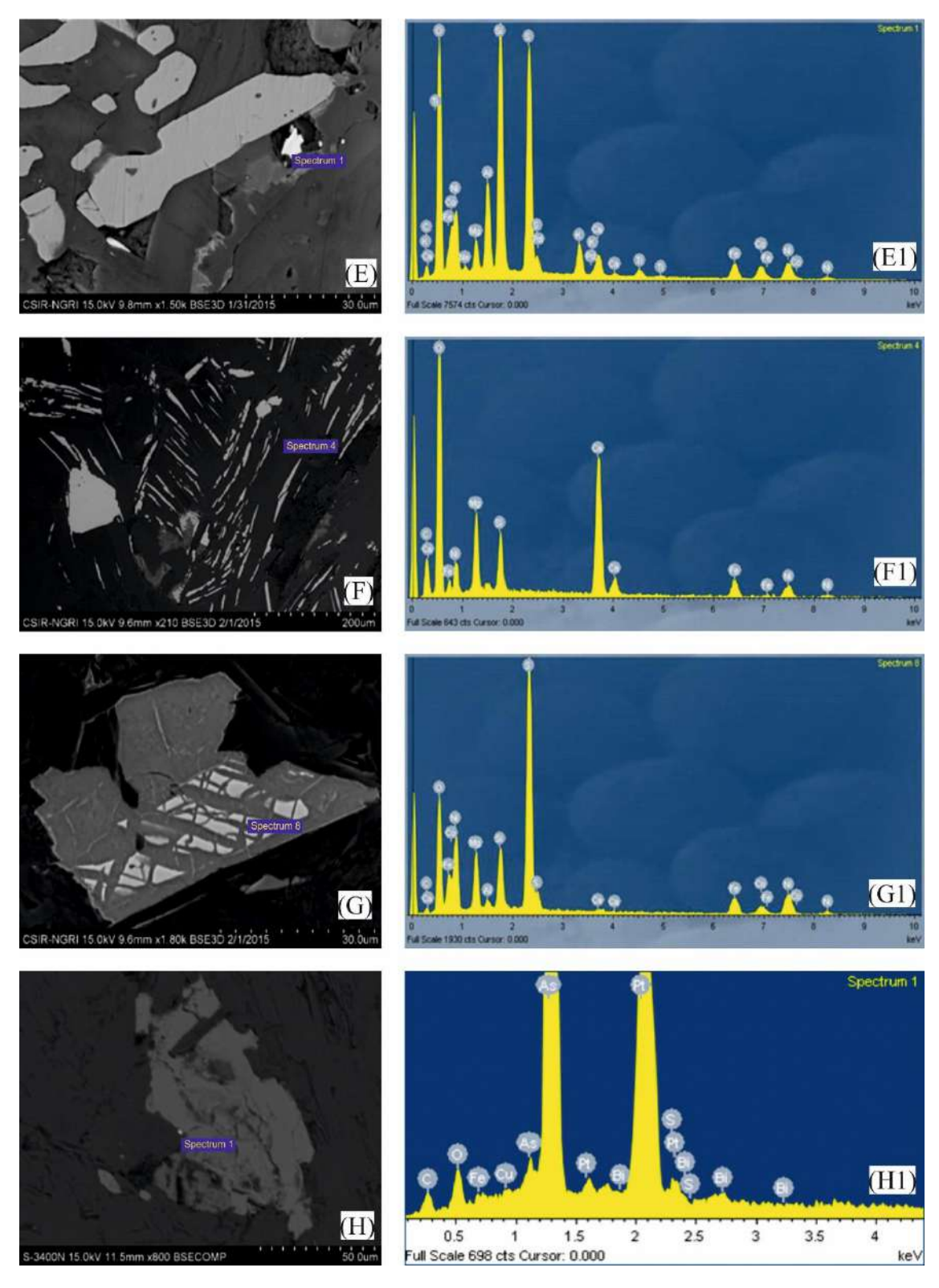


Figure 3.4(b) SEM-EDX study of ultramafic rocks of MUC (e-f) Backscattered electron (BSE) images showing the presence (Ni, Fe) S and NiS phases such as pentlandite and millerite in the

intercumulus spaces of olivine (g) BSE images showing the presence of (Ni, Fe) S phases with the clinopyroxenes (h) PGE mineralisation along the boundary of silicates.

different shades of grey. The inner core of the zoned chromite is dark grey rich in Cr, Al while the outer rim is light grey rich in Fe and identified as chrome magnetite. The core is identified as a remnant of unaltered chromite. The contact between them is usually very sharp. The magnetite is homogeneous and isotropic in nature. Both magnetite and titanium magnetite exhibit higher reflectance in comparison to chromite. The chrome and titanomagnetite are mostly distributed either in the intercumulus phases or along the cleavage planes. The Sulphide phases are more present in the Madawara region while they are very less abundant in Ikauna and Hanumathgarh regions. The total amount of opaque mineral phases ranges from 3-5 vol% in the total volume of the rock. The sulphides are the least opaque mineral in the ultramafic-mafic rocks of the MUC. The sulphides are mainly pentlandite ((Fe, Ni)<sub>9</sub>S<sub>8</sub>) and millerite (NiS). The SEM-BSE images show the presence of pentlandite, millerite, and chalcopyrite along with inclusions of spinel and rare occurrences of PGM in the form of alloys occurred as disseminated grains in the interspace of olivine as well as the cleavage planes of pyroxenes. In summary, the presence of sulphides is more in the ultramafics of the Madawara ultramafic-mafic tract compared to the ultramafics of the Ikauna tract while the oxide phases are more in the Ikauna in comparison to the oxide phases of the Madawara.

### **3.5. Summary**

Most of the ultramafic rocks in the Madawara, Ikauna, and Hanumathgarh areas shows lack of any retained primary mineralogy as evidenced by their petrographic features. The observed mineralogy formed as a result of hydrothermal alteration procedures linked to shearing along the intrusions' border. The presence of tiny carbonate veins in a few of the sections indicates CO<sub>2</sub> rich fluid-induced alteration process. The mafic and intermediate rock of the above three sectors has not been

extensively altered and their primary mineralogy is well preserved. The presence of channelised flow filled with iron oxides indicates the area is affected by the alteration process. The preserved mineral assemblages in the Madawara ultramafic complex (MUC) indicate the area is subjected to alteration with feeble affected by deformation and metamorphism.

## **CHAPTER-IV**

## MINERAL CHEMISTRY

In this chapter, an attempt has been made to present the mineral chemistry of both silicate and non-silicate minerals (olivine, amphibole, plagioclase, and chrome spinel) together with trace elements of chrome-spinel by LA-HR-ICP-MS covering the ultramafic-mafic rocks of the Madawara, Ikauna, Girar and Hanumathgarh region. The mineral chemistry and trace element data of chrome spinel is used to address alteration, magmatic process, parental melt composition, and the geodynamic setting of the ultramafic mafic magmatism and its comparison with various types of ultramafic mafic complex. A total of 10 samples have been selected, out of which 6 ultramafic samples from Madawara, Ikauna, and Hanumathgarh, 2 mafic samples from Madawara, and 2 intermediate samples from the Ikauna have been analysed for both major and trace elements present in table 4.1 to 4.6

#### 4.1. Silicates

#### **4.1.1.** Olivine

Olivine grains are observed in peridotite, olivine pyroxenite, and pyroxenite of the Madawara, Ikauna and Hanumathgarh regions. Most of the olivine grains are altered to serpentine in the case of peridotite. However, olivine grains are well preserved in olivine pyroxenite and rarely in pyroxenite rocks. The chemical composition of olivine is presented in the table (see table 4.2). The olivine grains are nearly homogenous in composition in pyroxenite and olivine pyroxenite, however, olivine grains in peridotite are inhomogeneous due to alteration. The olivine shows very high MgO contents (38.4-40.4 wt.%), low SiO<sub>2</sub>(35.9-39.5 wt.%), low MnO (0.20-0.35 wt.%), low NiO (0.00-0.28 wt.%) contents and very low CaO contents (<0.04 wt.%). The olivine shows lower

NiO content (<0.4 wt.%) in comparison to the olivine from mantle restite ("Sato et.al., 1977") signifies its crystallization through magmatic differentiation process.

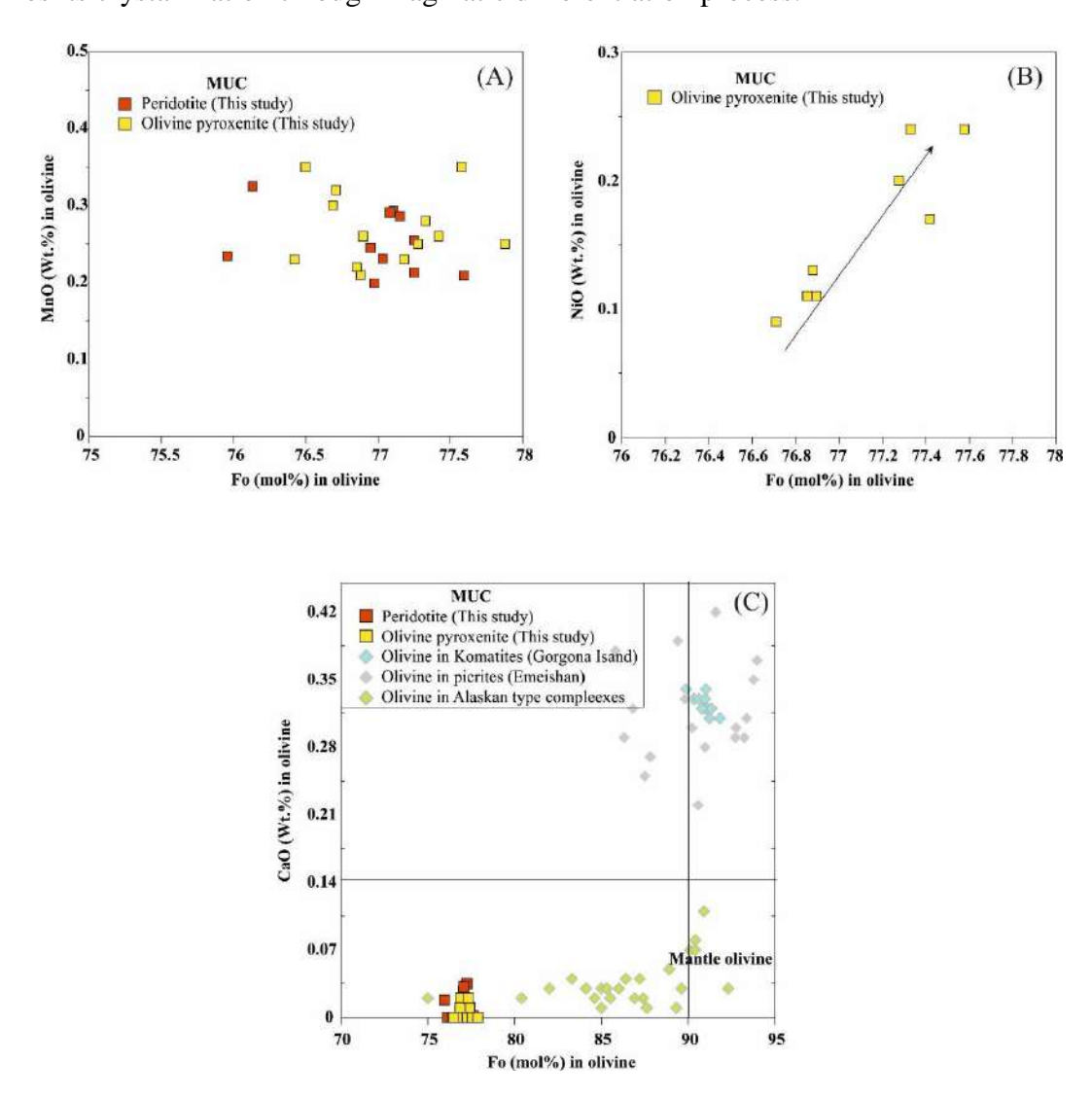


**Figure 4.1** (a) Forsterite (Fo) versus NiO and MnO (wt.%) contents for olivine in the ultramafic of MUC. (c) Plot of CaO versus forsterite (Fo) contents in olivine (after Li et al.,2012).

The olivine displays a narrow range of forsterite (Fo) values ranging between 75.9 to 77.8 wt. % with low CaO contents in comparison to the olivine from komatiite and picrite and shows very comparable to the olivine from Alaskan-type complexes (see figure 4.1a) ("Irvine, 1974, Kamenetsky et al. 2010, Li et al. 2012b; Krause et al. 2007").

### 4.1.2. Amphiboles

The amphiboles of MUC have a wide range of Mg#  $[=Mg/(Mg + Fe^{2+})]$  varying from 0.62 to 0.98 with the lowest values recorded in the diorite. Both primary and secondary amphiboles occur in the studied ultramafic-mafic rocks. The amphiboles in the ultramafic rock show high SiO<sub>2</sub> contents (51.36-58.44 wt. %), low to moderate FeO contents (0.02-12.38 wt. %), and low Al<sub>2</sub>O<sub>3</sub> (0.04-5.55 wt. %) (See table 4.1). It shows (Ca +  $Al^{iv}$ ) < 2.5, suggest an altered in nature and could be formed through the secondary process of replacing clinopyroxene. These secondary amphiboles show rich in MgO, poor in alkalis (Na+K < 0.5 wt.%), and attributed to tremolite variety while few amphiboles in peridotite show Ca+Aliv> 2.5, and low Si (<7.50 apfu) contents suggest primary in nature with pargasite, and magnesio-hastingsite hornblende variety ("Leake et.al., 1997"). Amphiboles in the peridotite and olivine pyroxenite inherit precursory compositions of clinopyroxenes and occur as magnesio-hornblende and tremolite in composition. The amphiboles in gabbro show a compositional variation in SiO<sub>2</sub> (51.71-54.15 wt. %), Al<sub>2</sub>O<sub>3</sub> (2.52-5.39 wt. %), and FeO (6.59-9.35 wt. %) and having affinity toward the secondary amphibole actinolite variety, whereas the primary amphiboles in the gabbros are mainly magnesio-hornblende with relatively homogeneous composition. On the other hand, the investigated amphibole of leucogabbro/gabbroic diorite and diorite have (Ca+Aliv)>2.5 reflecting magmatic origin ("Giret et al., 1980"). They are characterized by low Si contents (mostly < 7.50 apfu) and the high Al<sup>IV</sup>/Al<sup>VI</sup> ratios (>2) further support the igneous origin. ("Leake, 1971, Fleet and Barnett, 1978, Leake et al., 1997"). They are calcic in composition ranging mainly from magnesio hornblende to magnesio tschermakite (i.e., Al<sup>VI</sup> < Fe<sup>3+</sup>). ("Leake et al., 1997") (see figure 4. 2 a & b). The primary hornblende from the leuco-gabbro/gabbroic diorite and diorite shows sub-alkalic affinity (A<sub>Na</sub> + A<sub>K</sub> less than 0.5) and are classified as "magnesio-hornblende and tschermakitic-hornblende."

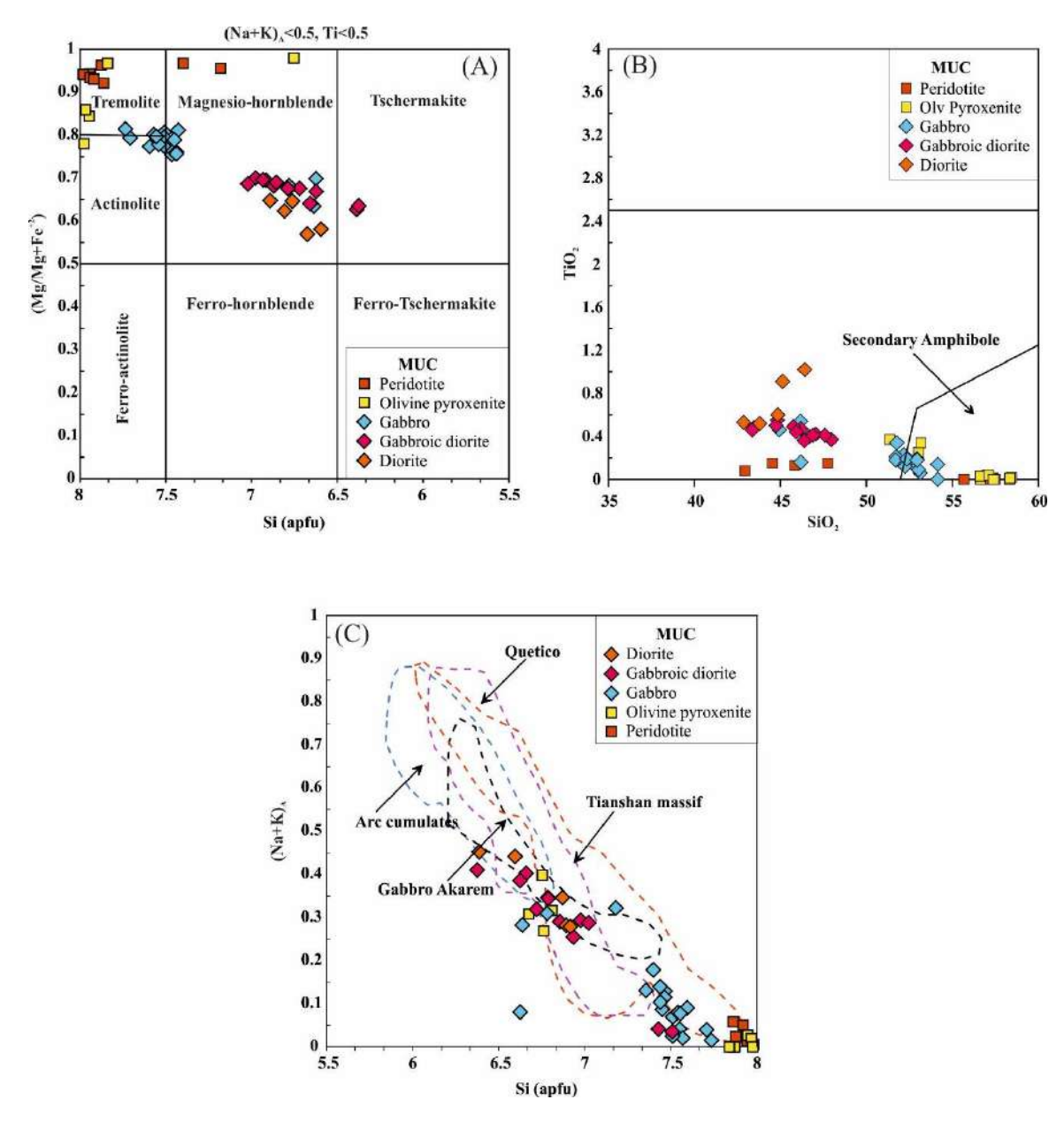


Figure 4.2 (a) Amphibole classification after Leake et al. (1997) (b) TiO<sub>2</sub> (wt.%) versus SiO<sub>2</sub> (wt.%) plot (after Rock 1991) suggesting the secondary nature of amphiboles in the peridotite of the MUC. (c) Na + K versus the Si content in the amphibole highlights the Alaskan-type ultramafic complex. The data for the Alaskan-type complex in the middle Tianshan massif, China, is from Su et al. (2012), Quetico type from Pettigrew and Hattori (2006); Gabbro Akarem from Helmy and El Mahallawi (2003); arc-cumulate field (Beard and Barker 1989). The trends for the arc-cumulate field (1990).

All the amphiboles in the MUC exhibit negative correlations between Si and Na + K, consistent with the variations observed in typical Alaskan-type complexes (See figure 4. 2c). The investigated primary hornblende displays a greater range of major oxides and is characterized by low alkali contents, and high Mg contents and shows affinity towards Alaskan-type complex (Helmy and El Mahallawi, 2003, Himmelberg and Loney, 1995, Eyuboglu et al., 2010) with significant arc affinities.

### 4.1.3. Plagioclase:

Plagioclase grains are completely absent in peridotite, olivine pyroxenite, and pyroxenite however, they are present in gabbros, leuco- gabbro/gabbroic diorite, and diorites with less affected by alteration. The plagioclase is mainly anorthite (An90-100) in composition (See table 4.4). The plagioclase in gabbro and gabbroic diorite/leuco-gabbro show bytownite to labradorite in composition whilst the diorite shows labradorite to andesine in composition. The Na<sub>2</sub>O content increases with a decrease in CaO suggesting a magmatic fractionation trend. Most plagioclase have anorthite content (An37-An73) consistent with those from mafic-ultramafic of Alaskan-type complexes (see figure 4.3b). (Irvine, 1974; Himmelberg and Loney, 1995; Eyuboglu et al., 2010)

### 4.1.4. Serpentine

Serpentine show compositional variation in peridotite with SiO<sub>2</sub> content ranges between (39.59-43.39 wt.%), MgO varies from 32.54-36.65 wt.% and Al<sub>2</sub>O<sub>3</sub> varies from 0.56 to 2.79 wt.%. They show low to moderate Fe<sub>2</sub>O<sub>3</sub> (1.91–6.53wt.%), and low content of Al<sub>2</sub>O<sub>3</sub>, TiO<sub>2</sub>, Cr<sub>2</sub>O<sub>3</sub>, NiO, CaO, Na<sub>2</sub>O, and K<sub>2</sub>O (see table 4. 3a). In the binary diagram of MgO versus SiO<sub>2</sub> and FeO, the analyzed minerals in the peridotite display mainly antigorite variety, while those containing very less amount of serpentine in olivine pyroxenite are mainly showing higher FeO with trending towards antigorite variety (See figure 4.3 c &d).

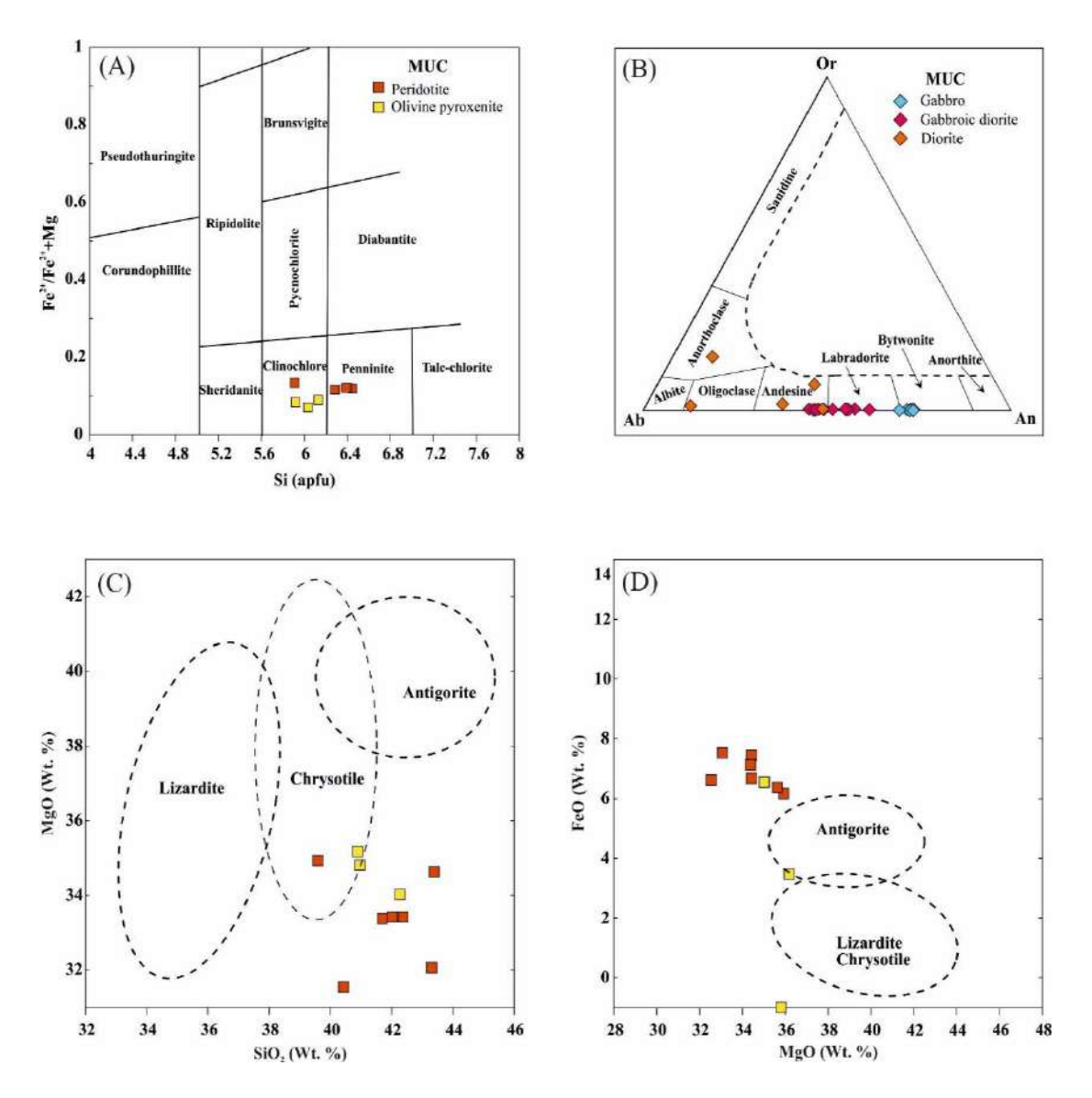


Figure 4.3 (a) Plot of chlorite analyses from the present study on a chlorite classification diagram of Hey (1954). MUC chlorite analyses display a compositional range and plot in fields of penninite and clinochlore. (b) Plot of Ab-Or-An contents in plagioclase of MUC display compositional ranges and plot in the field from bytownite to andesine (after Li et al.,2012).(c-d) Plots of SiO2 (wt.%) versus MgO (wt.%) and MgO (wt.%) versus FeO (wt.%) of serpentine minerals under study. Most MUC serpentine samples can be classified as chrysotile and antigorite varieties.

### 4.1.5. Chlorites

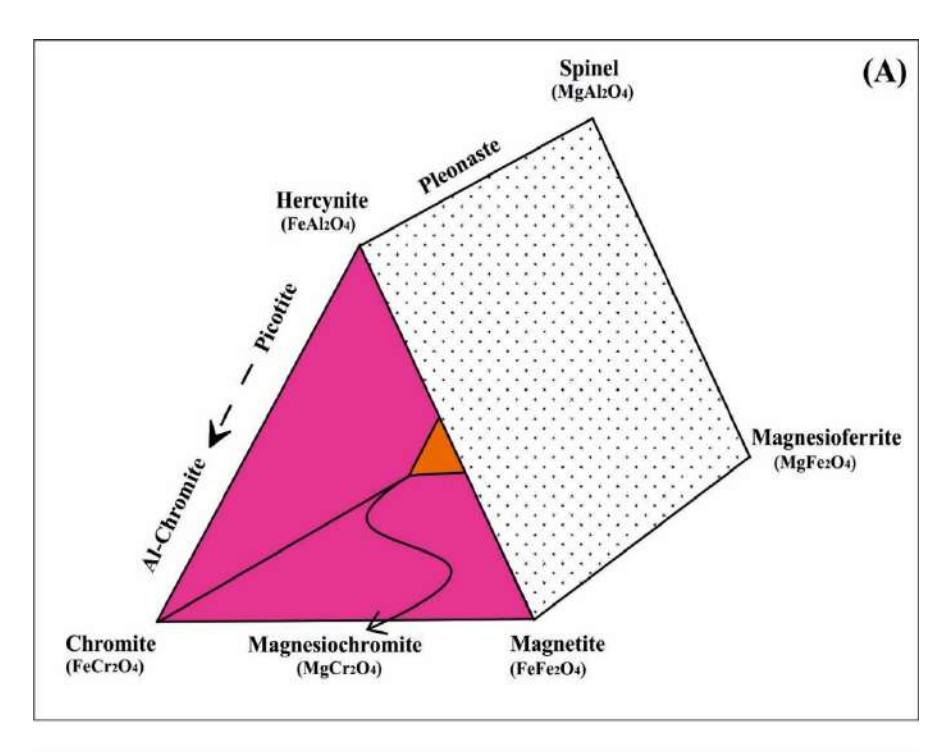
The chlorite grains are mostly observed in the peridotite and olivine pyroxenite of the MUC. It shows high Cr<sub>2</sub>O<sub>3</sub> (0.32-2.43 wt. %), high MgO (29.17-31.62 wt.%) low Al<sub>2</sub>O<sub>3</sub> (12.42-17.81wt.

%) and low FeO (3.68-7.97 wt. %) with very low content of TiO<sub>2</sub>, MnO, and NiO trending towards Mg-Cr-rich chlorite (see table 4.3b). The chlorite shows high-Si content varying from 5.91 to 6.45 and (Fe<sup>+2</sup>/ Fe<sup>+2</sup>+Mg) ratios ranging from 0.07 to 0.13 (see figure.4.3 a). ("Hey et.al, 1954"). The chlorite aureole mostly found around altered spinel are generally rich in Cr<sub>2</sub>O<sub>3</sub> whereas matrix chlorite is impoverished in Cr<sub>2</sub>O<sub>3</sub>. The formation of chloritic aureole around mainly ferrit-chromite can be attributed to the dissolution of chrome spinels giving rise to ferric chromite rims. The ferrit-chromite retains Cr and Fe, whereas Al and Mg are released to coexisting silicate minerals. Excess Al reacts with serpentine minerals to produce chloritic aureoles. On compositional fields for all the aureole chlorites plot within the pennite, clinochlore fields (Hey et.al, 1954).

#### 4.2. Non-silicates:

## **4.2.1.** Chrome-Spinel (Cr-spinel)

Chrome spinel from six representative samples comprising of peridotite and olivine pyroxenite were analysed for major element analysis through EPMA and are given in table 4.2. In the Cr-Al-Fe<sup>+3</sup> ternary diagram, the samples fall in the field of aluminium chromite, ferrous chromite, ferrian chromite, chrome magnetite and magnetite showing a Fe-enrichment trend. As the rocks have undergone a variety of alterations, it is necessary to analyse the unmodified chromite grain cores in order to explain their petrogenesis in terms of primary magmatic processes in the mantle. The EPMA data on the core of the homogeneous, unzoned Cr-spinel (*Type-I*) shows low Al<sub>2</sub>O<sub>3</sub> (10.63-21.87 wt. %), low MgO (1.71-4.92 wt. %) contents, and moderate to high Cr<sub>2</sub>O<sub>3</sub> (38.16-51.5 wt. %) with a wide range of Fe<sub>2</sub>O<sub>3</sub> (3.2-14.51wt. %) contents indicating their primary magmatic nature.



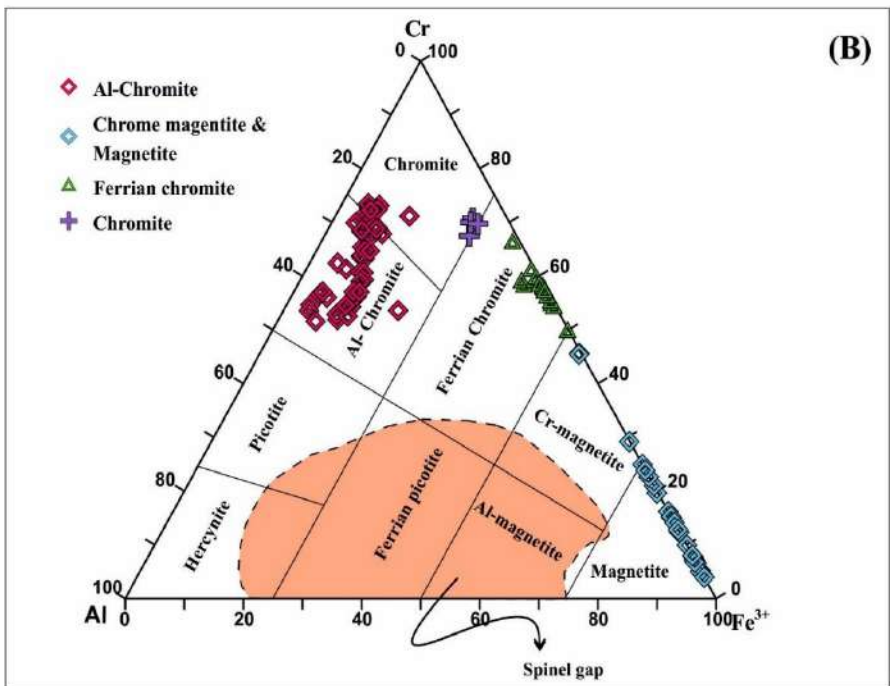


**Figure 4.4.** (a) Spinel prism for the multi-component systems of spinels for representation (After Deer et al., 1992). (b) Triangular classification diagram of spinel group of minerals (Field of "spinel gap" is from Barnes & Roeder, 2001)

They are aluminous-chromite in composition and are characterized by low Mg# number [100Mg/(Mg+Fe<sup>2+</sup>)] ranging from 9.30 to 26.22 and moderate to high Cr# number [100Cr/(Cr+Al)] ranging from 55.12 to 76.48. Their Fe<sup>3+</sup>#[100Fe<sup>3+</sup>/(Cr+Al+Fe<sup>3+</sup>)] ratios range between 8 to 19 while the homogenous ferrous chromites (Type II) characterized by very low Al<sub>2</sub>O<sub>3</sub> (2.60-3.52 wt.%), Mg# (3.08-4.21), and high Cr# (89.40-91.37) and Fe<sub>2</sub>O<sub>3</sub>(16.22-20.86) wt.%) compared to type I chromite. The composition of the homogeneous ferrian chromites (Type-III) are relatively low in  $Al_2O_3$  (0.06-1.53wt.%),  $Cr_2O_3$ (19.56-37.90 wt.%), and MgO (0.15-0.80 wt. %) and very high Fe<sub>2</sub>O<sub>3</sub> (25.54-47.60 wt. %). They are characterized by low Mg# (0.90-4.43), high Cr# (94.27 to 99.54) and Fe<sup>3+</sup># (38 to 70). Ferrous chromite is coarse-grained and homogeneous in nature. In some cases, the core of ferrous chromite is however classified as Alchromite due to the presence of  $Al_2O_3$  and MgO components and low  $Fe^{3+}\# [Fe^{3+}/(Fe^{3+}+Fe^{2+})]$ (0.33-0.39). The homogeneous ferrian chromite contains much higher ratios of Fe<sup>3+</sup># (0.38-0.70)signifying changes in chemical composition from Al-chromite to ferrian chromite. (See table 4.5) However, in the case of zoned Cr-spinel, the rim part of Cr-spinel is usually characterized by chrome magnetite (*Type-IV*). It shows very low Al<sub>2</sub>O<sub>3</sub> (<0.1 wt.%), Cr<sub>2</sub>O<sub>3</sub> (10.23-16.0wt.%), TiO<sub>2</sub> (0.28-0.37 wt.%), and MgO (0.03-0.93 wt.%). The MnO is low 0.01- 0.68 wt.%) and their Fe<sub>2</sub>O<sub>3</sub> is high (50.1-58.7 wt.%), while the magnetite and titano-magnetite (Type-V) are medium to coarsegrained, homogenous in nature and occur as disseminated grains. They are associated with chromemagnetite in the partly altered Cr-spinels. The magnetite in the type-V group contains the highest Fe<sub>2</sub>O<sub>3</sub> (57.58 to 64.87 wt. %) and FeO (29.5 to 30.5 wt. %) and low TiO<sub>2</sub> (0.03 to 0.24 wt. %), very low Cr<sub>2</sub>O<sub>3</sub> (2.55 to 9.66 wt. %), while Al<sub>2</sub>O<sub>3</sub> is completely absent.

## 4.2.2. Fe-Ti Oxides:

Fe-Ti oxides are found in peridotite, olivine pyroxenite, and pyroxenite from MUC are mainly "magnetite with minor ilmenite." Magnetite has high FeO (82.67-93.68 wt.%) and low TiO<sub>2</sub> (0.01-4.38 wt.%), MgO (0.0-0.48 wt.%), MnO (0.0-0.37 wt.%) and Al<sub>2</sub>O<sub>3</sub> (0.0-3.25 wt.%) (See table 4.5), while ilmenite has high TiO<sub>2</sub> (50.42 - 51.40 wt.%) and FeO (44.6 - 45.5 wt.%).

## 4.3. Oxygen fugacity

The oxygen fugacity (fO<sub>2</sub>) is an important parameter for physical and chemical processes that occur in the upper mantle and during the cooling, which provides an idea of the evolution of the magmatic systems controlled by different buffers and determines the crystallization of the mineral assemblages during the process of fractional crystallization. The partitioning of Al<sub>2</sub>O<sub>3</sub> between forsterite and chrome spinel is temperature dependent and experimentally calibrated is discussed in detail in (Wan et.al. 2008.) The temperature estimates based on the equilibrium between olivine-spinel using the thermometry of show between 929°C to 1095°C.

$$T(o_C) = \left(\frac{10^4}{0.512 + 0.873Y_{Cr} - 0.91\ln(K_d)}\right) - 273$$

Where  $Y_{Cr}$ =Cr/(Cr+Al) in spinel in atomic proportion and  $K_d$ =Al<sub>2</sub>O<sub>3</sub>Ol/Al<sub>2</sub>O<sub>3</sub>spl in wt.%. The textural evidence indicates the presence of magnetite, ulvospinel, ilmenite, and titanomagnetite phases in the peridotites that occur in the interstitial spaces of Cr-spinel, olivine, and pyroxene minerals. Since these phases are very much sensitive to oxidation, their empirical calibration of oxygen fugacity estimates on the above phases would reflect the fluid behaviour during crystallization. The empirical calibrations from coexisting olivine and Cr-spinel in the peridotite and olivine pyroxenite point out that the oxygen fugacity for ultramafics of MUC is between two important buffers namely quartz-magnetite-fayalite (QFM) and hematite-magnetite (HM) buffers. The quantitative estimates of -log fO<sub>2</sub> range from 14 to 17 (thermodynamic data

from (Holland and Powell, 2000). Thus, the oxidation state was much closer to the QFM and much above the wustite-magnetite (WM) as well as graphite buffers. The oxygen fugacity obtained from the peridotite and olivine pyroxenite of MUC is also calculated based on the method proposed by (Ballhaus et al., 1990, 1991; Dare et al., 2009). The results also lie above the FMQ buffer line and the fugacity ( $\Delta$  log fO<sub>2</sub>) ranges from +0.26 to +2.14 (see figure 4.2a.). The prevalence of high fugacity at the late cooling stage is also evident from the common presence of spinel coexisting with magnetite, titano-magnetite, rutile, and ilmenite.

## **4.4 Parental Melt Composition**

The chemistry of Cr-spinel and olivine minerals are very sensitive to bulk composition of the melt and the reaction between Cr- spinel or olivine with silicate liquid is elucidated to estimate the parental melt composition and the state of oxidation fugacity during the cooling of magma ("Uysal et al. 2009; González-Jiménez et al. 2011 Barnes and Roeder, 2001; Dick and Bullen, 1984; Kamenetsky et al.2001"). The Fe-Mg exchange mineral chemistry and textures of the study area point out that the core of Cr-spinel retains mostly the initial composition in Al chromite and the rim is altered to Cr-magnetite. In case of more olivine and amphibole rich ultramafic rocks, most of the homogeneous Cr-spinels are changed/altered to Fe-chromite, Cr-magnetite and magnetite could be formed due to subsequent reactions with intercumulus liquid or sub solidus reequilibrations. The olivine in the olivine pyroxenite is less affected by post-magmatic alteration and represents the early crystallization phases from the parental melt before its progressive fractionation. The melt composition involved in the formation of such Cr- spinel, their Al<sub>2</sub>O<sub>3</sub> and TiO<sub>2</sub> content and the FeO/MgO ratio of olivine phases are used to estimate the parental melt calculation.

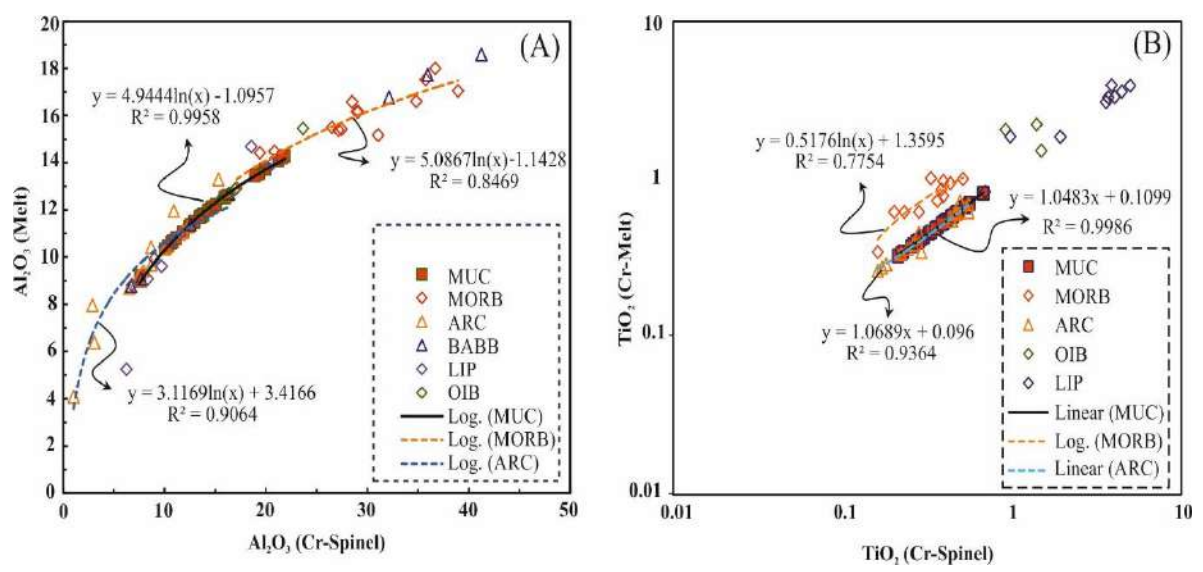


Figure 4.5 Cr spinel-melt bivariate diagram for (a) Al<sub>2</sub>O<sub>3</sub> and (b) TiO<sub>2</sub>. The estimated composition of parental melt that is in equilibrium with Cr-spinel from peridotite and olivine pyroxenite was calculated from EPMA data (in wt.%). Please see the text for more details. The regression lines are derived from the experimental study of Maurel &Maurel (1982) and Cr spinel-melt inclusion studies in MORB, OIB, LIP, and ARC from Kamenetsky 2001. Only Al-chromite data has been used for the calculation of the parental melt.

The  $Al_2O_3$  content of the parental melt equilibrium with Cr spinel is calculated based on an experimentally calculated formula with the assumption that the  $Al_2O_3$  content in spinel is the only function of  $Al_2O_3$  content in the melt (Maurel and Maurel 1982, Kamenetsky et al.2001) and is as follows,

$$Al_2O_3_{(Sp)} = 0.035 \times (Al_2O_3)_{Liq}^{2.42} (Al_2O_3)inwt.\%$$

The Al<sub>2</sub>O<sub>3</sub> content of the parental melt equilibrated with Cr spinels ranges from 9.22 to 14.22 wt.% (11.74 wt.% on average) and 11.49 to 14.30 wt.% (12.53 wt.% in average) in peridotite and olivine pyroxenite respectively. The TiO<sub>2</sub> content of the parental melt ranges from 0.32 to 0.69 wt. % (0.49 wt. % in average) and 0.34 to 0.80 wt. % (0.56 wt. % on average) in peridotite and olivine pyroxenite respectively.

The (FeO/MgO) ratio of the parental melt is also calculated using olivine composition in the olivine pyroxenite by using the equation of (Roeder and Emslie, 1970)

$$K_D = \frac{(\text{FeO/MgO})_{Olv}}{(\text{FeO/MgO})_{Liq}}$$
 where the coefficient  $K_D = 0.3$  for olivine

On the other hand, the FeO/MgO ratio of the parental melt from which olivine crystallised range from 1.72 to 1.92 wt. % (1.78 wt. % in average).

#### 4.5 Alteration and formation of zoned chromite

The alteration of Chromian spinel has been the subject of intense debate and it is suggested that during alteration Cr-spinel leads to the formation of ferrian chromite, chrome magnetite, magnetite etc. which exhibits zoning in the Cr-spinel (Gervilla et al. 2012; Barra et al., 2014; Ruan et al. 2017) The Cr-spinels from ultramafic rocks of Madawara showing zoned texture and distinct variation in mineral compositions during the alteration and physiochemical changes (see figure 4.6). A detailed investigation of minerals was carried out under SEM-EDS at CSIR-NGRI Hyderabad. The BSE images show that most of Cr -spinels developed zoning due to subsequent metasomatic and alteration where the core of the Cr-spinel still preserve their original composition (see figure 4.3b). These crystals were crystallized along with olivine and some early formed sulphides. In few crystals the appearance of thin rim of Fe rich chromites developed around Alchromites (See figure.4.6 c) is an indication of the beginning of physiochemical changes and replacement of Mg<sup>2+</sup> and Al<sup>3+</sup> from Cr-spinel with Fe<sup>2+</sup> and minor amount of Fe<sup>3+</sup>. Also, in some crystals Fe-chromite and chrome magnetite grew at the rim of partly altered Al-chromites (See figure 4.6 c & d). Such textural evidence indicates that ferrian chromite rim was firstly involved in the incorporation of Fe<sup>3+</sup> from silicates followed by the formation of Cr- magnetite. The SEM textural studies and EPMA data point out that ferrous chromite and ferrian chromite were formed successively at the rim part of Al-chromite with varying  $Fe^{3+}/(Fe^{3+}+Fe^{2+})$  ratios during the advance stage of physiochemical changes. (Gervilla et al. 2012), suggested that degree of oxidation state is a major factor for their stability. The ferrous chromites appear where  $Fe^{3+}/(Fe^{3+}+Fe^{2+})$  ratios are less than 0.4 (40%), while ferrian chromite formation begins with values greater than 0.4 (Gervilla et al. 2012). The core of some homogenous chromite shows high  $Fe^{3+}/(Fe^{3+}+Fe^{2+})$  ratio (0.46-0.66) signifying ferrian chromite in nature.

The EPMA data of the core of the primary magmatic Cr-spinel in the Cr-Al-Fe<sup>3+</sup> ternary diagram falls in field of Al-chromite and few in the ferrian chromite region (See figure.4.4b). The rim composition of Cr-spinel lies towards the Fe<sup>3+</sup> enrichment and plots in the field of chrome magnetite (Cr-mag) and magnetite (mgt.). The changes in chemical composition of core of the zoned Cr-spinels vary from Al-chromite to Fe-rich chromite indicating a Fe<sub>2</sub>O<sub>3</sub>-enrichment trend (See figure 4.4b). The EPMA data of zoned crystals also suggest that Mg and Al decreased, whereas Fe increased significantly from aluminous to the ferrous core and ferrian chromite to chrome magnetite rim.). The alteration is marked by the abundant presence of chlorite and magnetite minerals related to hydrothermal activities. Chlorite association with the ferrian chromite and magnetite rims are usually Cr-enriched (2.2-2.4 wt. %) and favours the formation from the alteration of Cr- spinels under the hydrous conditions (Mellini et al. 2005; Merlini et al. 2009; Grieco & Merlini 2012; Gervilla et al. 2012). The high-Mg and Cr content in chlorite may be due to the preferred partition from ferrian chromite.

The primary Cr-spinel (Al-chromite) and olivine were crystallized from melts at high-temperature and during their cooling, they preserve several signatures which can be used to find out the of involvement of fluid activities, alteration and metasomatism. The FeO-rich intercumulus magma reacted with Cr-spinel with gradual decrease in temperature leads to subsequent release of Fe<sup>2+</sup>

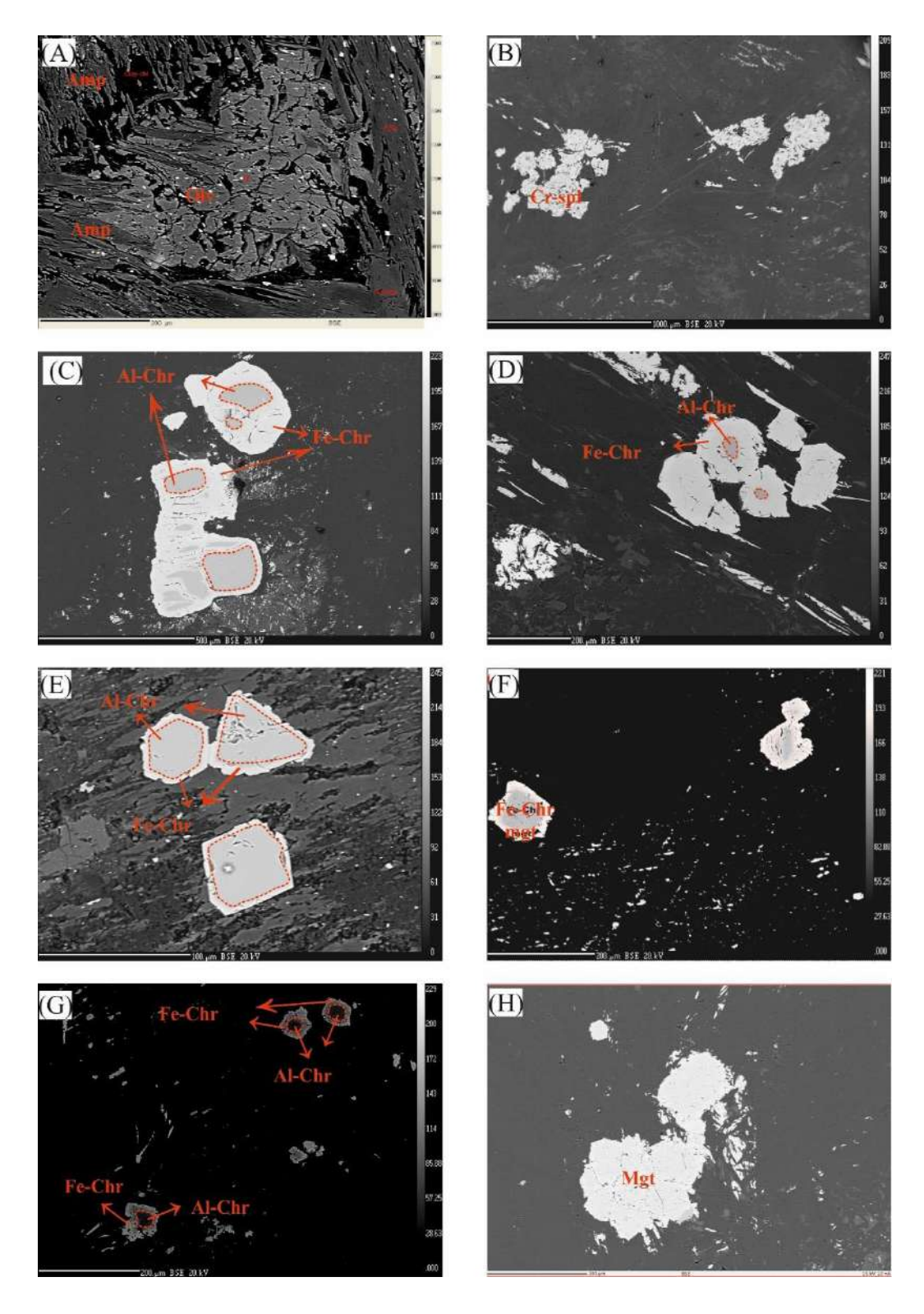


Figure 4.6 Back-scattered electron (BSE) images of chrome spinels along with silicates from ultramafics of Madawara showing different textures and structures during the alteration showing (a) cumulate peridotite with large grain olivine pseudomorph altered to serpentine and intercumulus phase containing clinopyroxene altered to tremolite and in some part to chlorite (b)

homogeneous Cr-spinel (low Al-chromite) in serpentinised peridotite (c) Zoned chrome spinels with Al-chromite core rimmed by Fe-chromite (e) Partly altered euhedral zoned chromite crystals present as inclusions in the pyroxene with a very thin rim of ferrite chromite in the olivine pyroxenite (f) Euhedral zoned chromite in peridotite with core-rim compositional variation and presence of magnetite and ilmenite in the intercumulus space (f) Zoned chromite in amphibole rich peridotite (g) Homogeneous Fe-chromite present in the matrix of olivine in peridotite rock (h) Alteration of chrome magnetite and magnetite in peridotite. Notes: Al-chr: Al-chromite, Fe-chr: ferrian chromite, Cr-mag: chrome magnetite, mag: Magnetite, Ol: Olivine, Ser: Serpentine, Amp: Amphibole, Chl: Chlorite.

from olivine that gets incorporated into the primary Al- chromite to form ferrous chromite (See figure 4. 6). The alteration of olivine and chromite under high H<sub>2</sub>O-saturated conditions with high silica activities (i.e., high fluid/rock ratios) promoted the formation of Fe-chromite and chlorite that has been envisaged by several workers ("Mellini et al. 2005; Gervilla et al. 2012; Barra et al. 2014") has been explained by the following reaction.

(Gervilla et al., 2012) opined that ferrian chromites were formed under oxidizing and hydrothermal conditions with decrease in temperature and increase in  $fO_2$ . If the chromite/silicate and fluid/rock ratio is relatively high, then such conditions favour migration of  $Mg^{2+}$  and  $Al^{3+}$ , thereby leading to the formation of chrome magnetite, magnetite and Mg-Cr-chlorite minerals. This also indicated by the presence of serpentinisation and high activity of hydrothermal fluids ( See figure 4.6).

# 4.6. Mantle source using Cr-spinel mineral chemistry

In petrogenesis of ultramafic rocks only core of the primary chrome spinels or chromite has been considered as they preserved primary magmatic characteristics. The plot between Cr<sub>2</sub>O<sub>3</sub> vs. Fe<sub>2</sub>O<sub>3</sub> of primary Cr-spinel shows strong negative correlation and display Fe-enrichment trend (see figure 4.7). In the Cr-Al-Fe<sup>3+</sup> triangular diagram, most of the chrome spinel falls near to the field of Alaskan-type intrusion of island arc environment with few of them showing Fe enrichment trend

(See figure 4.8 a). Such Fe- enrichment trend in the Cr- spinel is mainly due to the replacement of Cr<sup>3+</sup> by Fe<sup>3+</sup>. It is formed either by the reaction of spinel with intercumulus fluid over a considerable temperature or it may be sub-solidus equilibration with olivine. The Al-enrichment trend is very common in the case of layered intrusion due to the reaction of Cr-spinels with intercumulus liquid rich in plagioclase component which is not the case in our present investigation. The chromite from the ophiolitic complex is characterized by constant Fe<sup>3+</sup> and substitutions of Cr<sup>3+</sup> by Al<sup>3+</sup> in the octahedral site of the chromite. This is also not the case with our analysed Cr-spinel ("Snoke et.al.1981; Nixon et.al.1990; Bell & Claydon, 1992; Barnes & Roeder, 2001; Helmy & Mahallawi 2003; Krause et al. 2007"). The changes in the composition from Al-chromite to Fe-chromite are related to intercumulus fluid activities at the arc source and much close to Alaskan-type magmatism as has been recorded from elsewhere also (Dönmez et. al 2014, Arai & Miura et.al., 2016, Arai et. al., 2011). The bivariate diagram between TiO<sub>2</sub> and <sup>Y</sup>Fe<sup>3+</sup># [Fe<sup>3+</sup>/ (Fe<sup>3+</sup> +Cr+ Al)] (see figure 4.8b) shows a linear relationship and most of the investigated Cr-spinels plot in the field of Alaskan type complex (Barnes and Roeder, 2001). The high -TiO<sub>2</sub> content from the core of Cr-spinels (0.22-0.67 wt. %) are similar to those from Alaskan type ultramafic mafic rocks at deeper level of island arc intrusion. (Jan and Windley, 1990) suggested that TiO<sub>2</sub> wt. % level (0.3 wt. %) is the limiting factor between ophiolitic rocks from layered or stratiform complexes and in the Alaskan-type complex.

The spinels are characterized by low Mg# (9.30-26.22), moderately high Cr# (55.15-81.35) and very high Fe# [100Fe<sup>2+</sup>/Fe<sup>2+</sup>+Mg] (73.78-88.93) indicating a distinct linear trend similar to worldwide Alaskan type intrusions (see figure 4.8c). In figure 4.8d Mg# vs. YFe<sup>3+</sup>the compositions of Cr-spinels of the MUC are outside the designated field, but very close to the trend of the Alaskan type field.

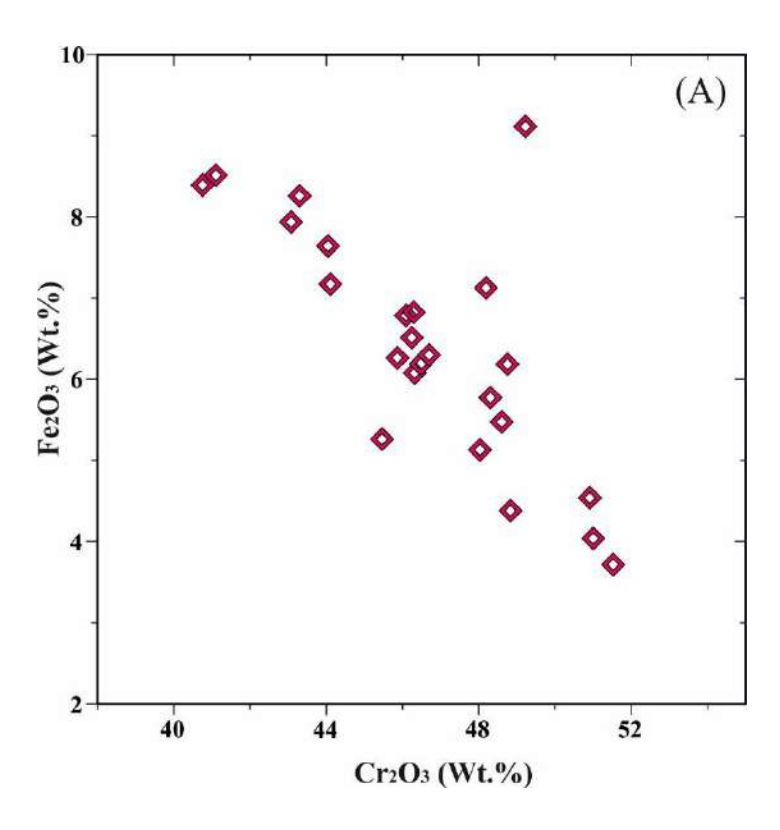


**Figure 4.7.** Variation diagram between  $Cr_2O_3$  and  $Fe_2O_3$  showing a strong negative correlation of Al chromite from Madawara ultramafic complex (MUC)

The bivariate diagram between the Cr ratio and TiO<sub>2</sub> of the Cr spinel plot in the field of Alaskan type intrusions (see figure 4.2p). The plots of spinel composition in the TiO<sub>2</sub> vs. Al<sub>2</sub>O<sub>3</sub> diagram ("Arai et.al. 2011") is used to distinguish between the different tectonic settings such as midoceanic ridge, island arc including Alaskan type environment and oceanic hotspot. The core compositions of most of the Cr- spinels are in the range of Al<sub>2</sub>O<sub>3</sub> (10.63-21.87 wt. %) and TiO<sub>2</sub> (0.22-0.67 wt. %) and lie in the field of island arc cumulates of Alaskan type complex to back-arc basin basalt (BABB) regions (see figure 4.2q). This mixed source of both island arc and BABB signifies that the subduction-related geodynamic setting with a local extension due to the upwelling of anomalous high-temperature convecting mantle, which is very similar to the origin of Alaskan type ultramafic complex (Tistle 1994., Ripley, 2009; Chen et al., 2009; Su et al., 2013). This may create rifting and vertical upliftment of the Alaskan-type complex. Similarly, the plots of Cr<sub>2</sub>O<sub>3</sub>

vs. Al<sub>2</sub>O<sub>3</sub> for the core composition lie towards the Arc-cumulate type tectonic setting for the Crspinels of Madawara (See figure 4.9c). The parental melt calculated form the composition of primary chrome spinel (chromite) to address the composition of the melt involved in the formation of such chromite. The calculated Al<sub>2</sub>O<sub>3</sub>, FeO/MgO and TiO<sub>2</sub> ratios of the melts forming the chromite grains in Madawara ultramafics are shown in table 4.7. The calculated parental melt composition with Al<sub>2</sub>O<sub>3</sub>, TiO<sub>2</sub> contents and FeO/MgO ratio of the parental melt is also compared with parental melt composition estimates in different tectonic settings, namely, Taftafan Alaskan type complex of the western Arabian shield (Habtoor et.al., 2016), layered intrusions of Bushveld complex ("Mondal et al., 2006"), average BABB magma (Kamenetsky et al., 2001; Pearce et al., 2000) average worldwide boninites and MORB magmas (Wilson, 1989). Based on the regression analyses of the estimated melt composition compared with that of the melt composition from other tectonic settings, the melt composition equilibrium with the Madawara ultramafic complex is similar to arc type, which is similar to the magma involved in the formation of Alaskan type complex. The bivariant diagram of fO<sub>2</sub> and Cr# of spinel (see figure.4.9 d) distinguishes the oxidation state of peridotites crystallized from different tectonic settings (Dare et. al. 2009; Ballhaus et al. 1991, Elburg and Kamenetsky., 2007). The oxygen fugacity is also considered an index function of different tectonic environments (Ahmed and Habtoor 2016). Cr spinel peridotites from arc magma are more oxidized than those from MORB magma. The spinels formed from the hydrous arc magma are more oxidized in nature than the anhydrous conditions. Similarly, the Crspinel crystallized from hydrous magma poses higher fO<sub>2</sub> values in comparison to the Cr- spinel formed in MORB setting ("Habtoor et. al. 2016., Ballhaus et al. 1991., Dare et al. 2009., Parkinson & Pearce 1998, Pearce et al., 2000").

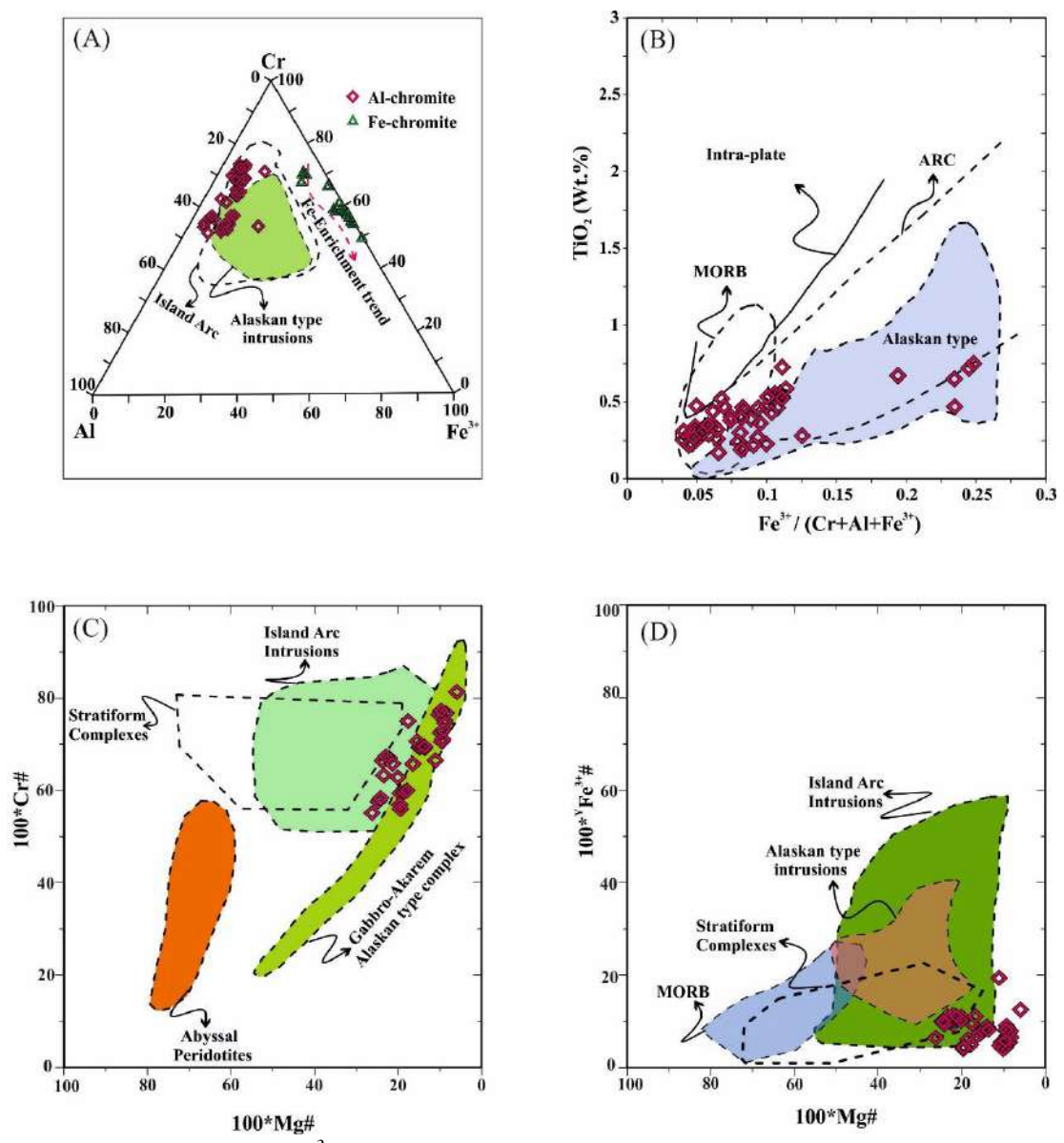


Figure 4.8 (a) The Cr-Al- $Fe^{3+}$  variation diagram of Al-Chromite and Fe-Chromite of the MUC shows an iron enrichment trend. The defined fields are from Barnes and Roeder (2001) and Wang et al., 2010. (b) TiO<sub>2</sub> (Wt.%) versus  $Fe^{3+}/(Cr+Al+Fe^{3+})$  plot for primary Al-Chromite in peridotite and olivine pyroxenite. The demarcated fields are from Arai (1992), Barnes & Roeder (2001). (c) The bivariant diagram of 100 \*Cr# versus 100 \*Mg# of Al-Chromite shows a distinct linear trend. Fields of stratiform complexes (Irvine, 1967, 1974), Worldwide Alaskan-type intrusions (Barnes & Roeder 2001, Helmy and El Mahallawi, 2003, Farath & Helmy, 2006), island-arc intrusions (Spandler et al., 2003), abyssal peridotites (Dick and Bullen, 1984) are shown here for comparison. Most of the chrome spinel (Al-chromite) follows the trend of the Alaskan-type complex. (d) Bivariant plot of  $100 *^YFe^{+3}$  versus 100 \*Mg# of Al-Chromite. Field of Alaskan type intrusions are obtained from (Himmelberg and Loney 1995, Batanova et.al.2005,) island-arc intrusions (Spandler et al., 2003), stratiform complexes (Irvine, 1967, 1974), mid-oceanic Ridge basalt (MORB) (Barnes and Roeder, 2001), are shown here in the diagram for comparison.

The spinel from peridotite and pyroxenite from MUC plot in the arc peridotite region and show as increasing (fO<sub>2</sub>) oxidized conditions trend with fractional crystallization. Based on the comparison, the parental melt estimation with the different tectonic settings of the world wide, the melt composition of MUC resembles an arc environment and is similar to the Alaskan type complex.

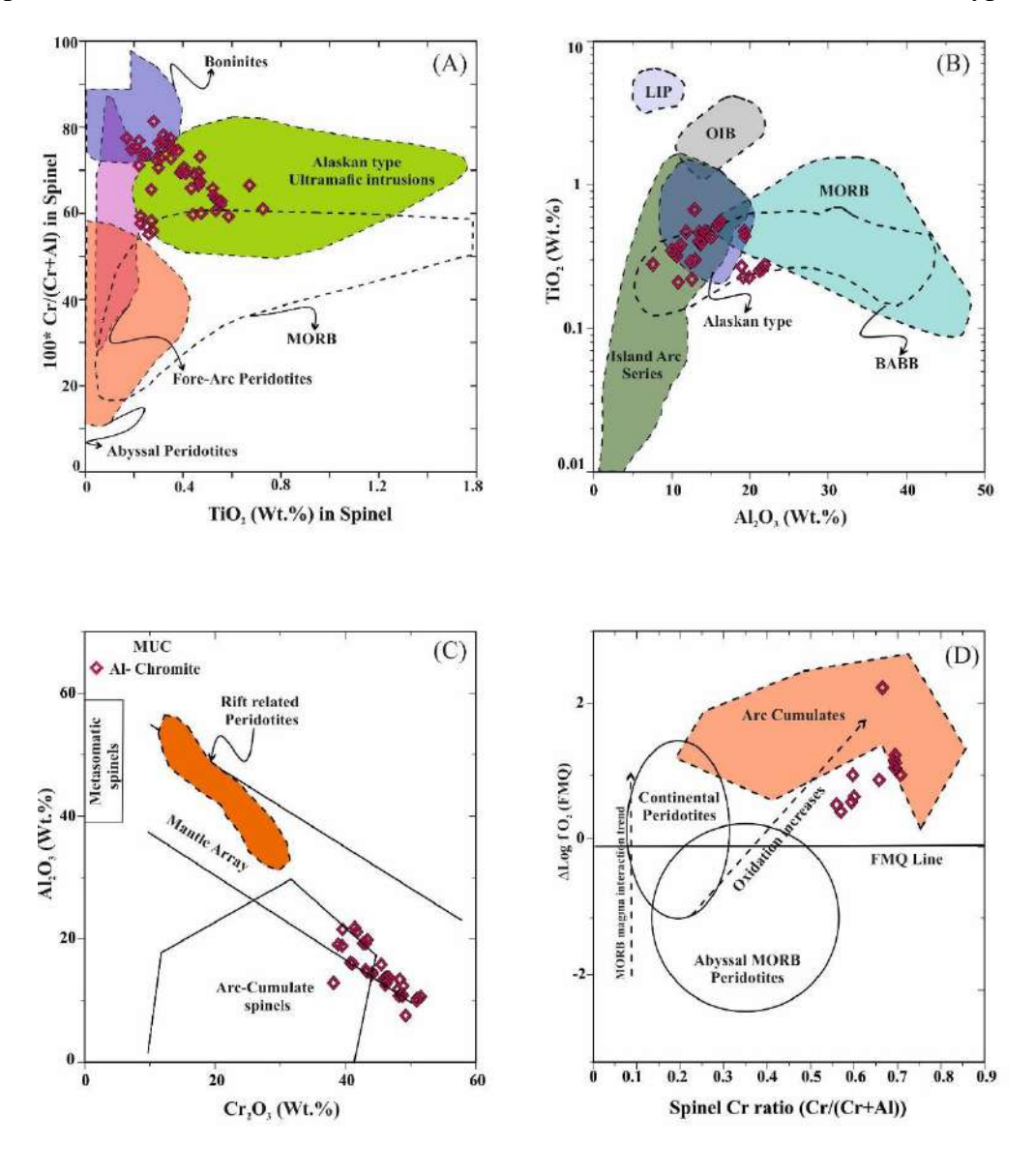
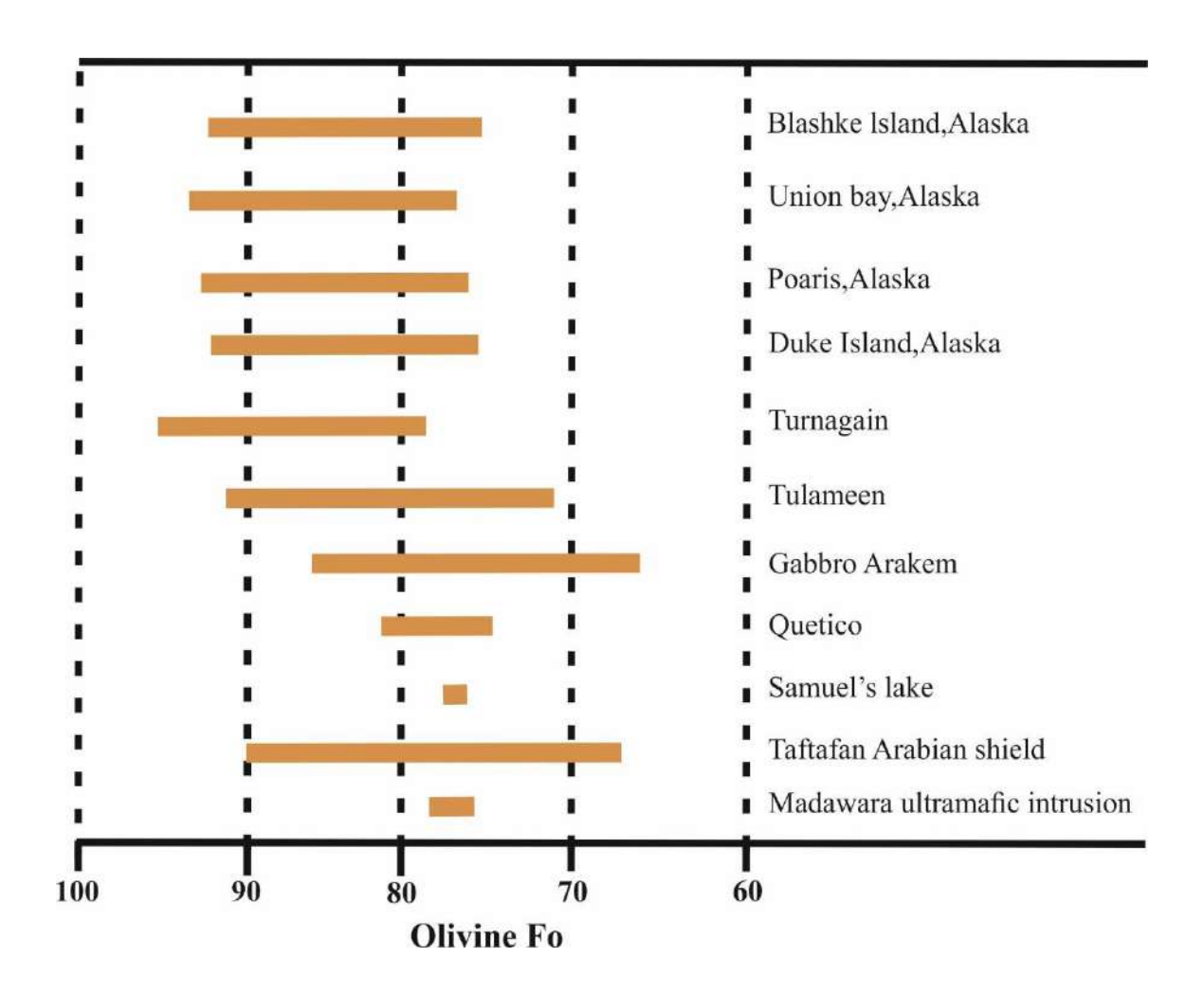


Figure 4.9 (a) Plot of 100 \*Cr/(Cr+Al) versus TiO<sub>2</sub> (wt.%) of Al-Chromite from the study area. Spinels from abyssal (Dick 1989, Dick, and Bullen, 1984) and fore arc (Ishii et al., 1992) peridotites, MORB, boninites (Arai, 1992, Barnes and Roeder, 2001), Aleutian xenoliths (Conrad and Kay, 1984, Debari et al., 1987) and Alaskan-type ultramafic intrusions (Himmelberg and Loney, 1995) are shown here for comparison. (b) Plot between Al<sub>2</sub>O<sub>3</sub> versus TiO<sub>2</sub> in wt.% of Al

chromite. Fields of LIP (large igneous province basalts), OIB (ocean-island basalts), MORB (midocean ridge basalts), ARC, MOR (mid-ocean ridge) peridotites are after Kamenetsky et al. (2001), and Alaskan-type complexes from Alaska were obtained from (Himmelberg and Loney 1995). (c) Bivariate plot of  $Al_2O_3vs$ .  $Cr_2O_3$  (wt.%) from Franz & Wirth (2000), modified after Seo et al. (2013), showing near to Arc cumulate setting. (d) Variation diagram for  $\Delta log fO_2$  (FMQ) versus Cr# of Al-Chromite from the study area. The field of Arc cumulates (Ballhaus 1993) and Abyssal peridotites (Bryndzia & wood 1990) are shown here for comparison.

### 4.7. Magmatism and geodynamics:

The mineral chemistry of Cr-spinel discussed in the preceding section provides significant information about conditions in the mantle during the emplacement ultramafic magmas in the "Southern part of the Bundelkhand craton." Thus, present information invariably indicates that the E-W trending series of lensoidal mafic and ultramafic intrusions from MUC in an area of around 400km<sup>2</sup> could be a part of Archean orogeny. The peridotite and associated rock assemblages in the orogenic belts are usually classified as either Alpine-type (including ophiolite assemblages) or Alaskan-type intrusions (Irvine, 1974). The Alaskan type ultramafic- mafic complex is thought to be island arc magmatism or shallow crustal level intrusion into the continental basement ("Irvine, 1974; Johan., 2002; Pettigrew & Hattori., 2006; Thakurta et al., 2008; Ripley, 2009; Su et al., 2013, Dong et al 2017"). The origin of Alaskan-type complexes has been well documented and are formed in the subduction zones representing arc magmas or arc root complexes (Irvine., 1974; Debari & Coleman., 1989; Helmy et al., 2014, 2015; Chen et al., 2009; Tistl et al., 1994). The mineral chemistry of Cr- spinels in the Madawara ultramafic intrusion are characterized by low Mg# (9.30-26.22), variable Fe<sup>3+</sup># (4-19 wt.%), and moderately high Cr# (55.12-76.48) and very high Fe# (73.78-88.93) relative to both stratiform and ophiolitic complexes (See figure 4.8).



**Figure 4.10** Olivine (Fo) chemistry of peridotite and olivine pyroxenite from the study area and its comparison with olivine (Fo) content from worldwide Alaskan-type intrusions.

The Cr-spinels plotted in different discrimination diagrams demarcate a distinct subduction type geodynamics which is similar to the Alaskan type tectonic model. The Cr-spinel from MUC is distinguished by its comparatively low Mg# and TiO<sub>2</sub> concentrations and high Fe# values. The Cr-Spinels from Madawara ultramafics display a distinct negative correlation between Fe<sub>2</sub>O<sub>3</sub> and Cr<sub>2</sub>O<sub>3</sub> and positive correlation between TiO<sub>2</sub> and Fe<sup>+3</sup>#. Moreover, the olivine of the MUC shows forsterite contents in the range of 75.96 -77.59. It overlaps with the forsterite range of the typical worldwide Alaskan-type complexes (See figure 4.10) . The Cr-spinel and olivine mineral chemistry plot displayed in different discriminate diagrams suggest a subduction-related tectonic

setting prevailed at the southern part of Bundelkhand Craton which resembles more towards Alaskan type magmatism.

## 4.8. LA-HR-ICP-MS study of chrome spinel

Chromian spinel is an accessory phase in many ultramafic—mafic rocks and their chemistry is sensitive to melt-rock interaction processes, oxygen fugacity and pressure—temperature conditions.

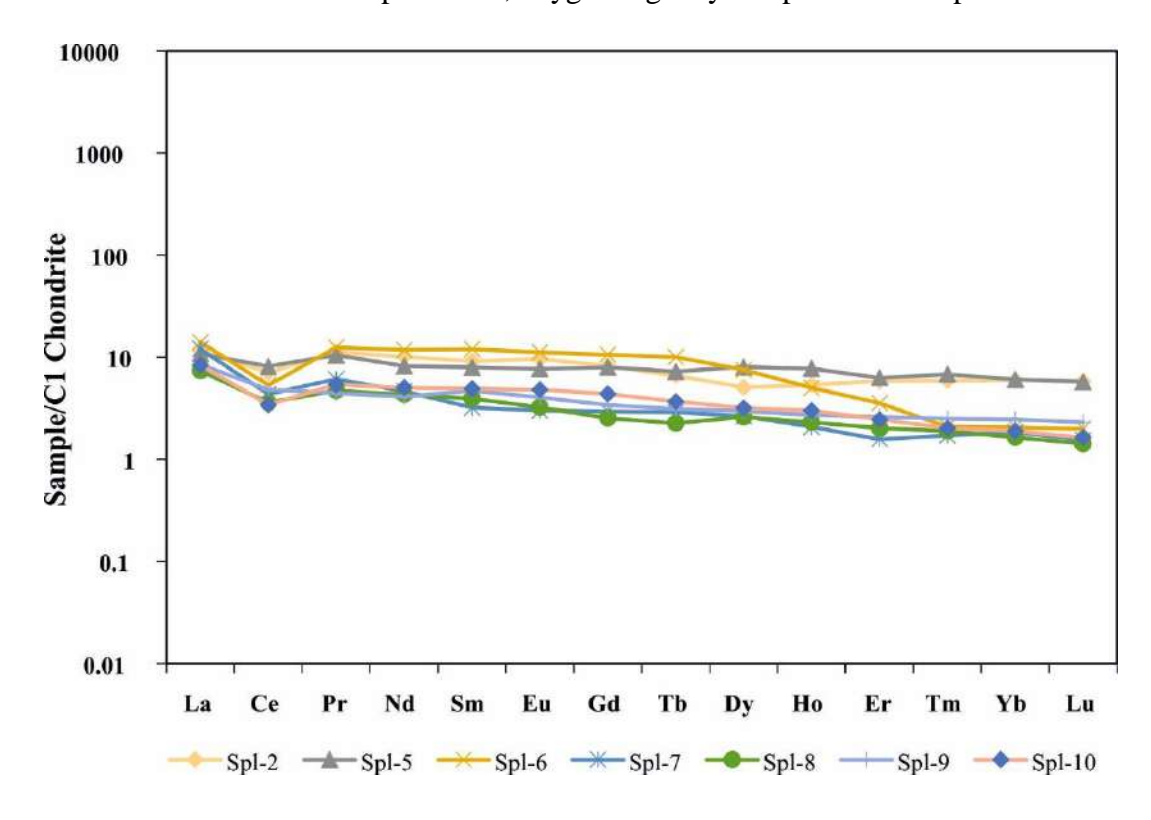


Figure 4.11 The chondrite normalized REE of chrome spinel (sun and McDonogh, 1989)

It is one of the earliest minerals to crystallize from ultramafic—mafic magmas and is resistant to post-magmatic processes, and therefore is reliable for petrogenetic as well as in provenance studies. Spinels are little examined with respect to the distribution of lithophile trace elements particularly the REE contained in them due to their relatively low concentrations ("Lesnov, 2013") nevertheless, they provide immense information. An attempt is made here to determine REE in chromian spinels from Madawara ultramafic complex using laser ablation high-resolution inductively coupled plasma mass spectrometry (LA-HR-ICP-MS). The total REE of the Cr-spinel

varied from 3.8 to 20.8 ppm with the LREE/HREE ratio ranging from 3.1 to 6.2. The REE pattern shows a flat trend with prominent Ce anomaly ( $Ce/Ce^* = 0.40$  to 0.78) indicating initial crystallization of Cr-spinel under reducing conditions (see figure 4.11). The flat HREE with low total REE content suggest the chrome spinel formed at a high degree of partial melting of depleted mantle sources.

Sample No.	IK-13/P	IK-13/P	IK-13/P	IK-13/P	IK-13/P	IK-13/P	IK-13/P	IK-13/P	IK-13/P	IK-13/P
Mineral	magnesio-	magnesio-	magnesio-	Tremolite	Tremolite	Tremolite	Tremolite	Tremolite	Tremolite	Tremolite
Ref. Point	hornblende 1	hornblende 2	hornblende 3	4	5	6	7	8	9	10
iO <sub>2</sub>	53.05	53.17	51.36	56.64	57.47	56.62	58.44	57.12	58.34	57.38
$iO_2$ $iO_2$	0.25	0.34	0.37	0.00	0.00	0.03	0.02	0.04	0.01	0.00
$I_2O_3$	3.81	3.81	5.55	0.53	0.10	0.22	0.02	0.04	0.01	0.00
										0.28
r <sub>2</sub> O <sub>3</sub>	0.55	0.77	0.64	0.00	0.00	0.03	0.00	0.00	0.06	0.03
e <sub>2</sub> O <sub>3</sub>	4.03	5.30	3.55		0.00	1.71	1.02	0.00	0.35	
'eO	1.25	0.02	1.67	3.43	2.49	1.55	2.51	2.84	2.95	2.98
InO	0.22	0.16	0.05	0.07	0.02	0.12	0.06	0.10	0.07	0.10
/IgO	20.62	20.99	20.11	22.42	22.82	22.56	22.63	22.68	22.30	22.46
liO	0.07	0.02	0.27	0.02	0.11	0.26	0.04	0.07	0.12	0.08
aO	12.47	12.35	12.56	13.91	14.02	13.41	13.36	13.75	13.22	13.57
$Ia_2O$	1.08	1.04	1.56	0.11	0.05	0.06	0.03	0.02	0.07	0.09
$C_2O$	0.13	0.12	0.10	0.16	0.06	0.05	0.03	0.05	0.00	0.15
aO	0.00	0.00	0.00	0.00	0.00	0.00	0.00	0.00	0.00	0.02
I <sub>2</sub> O*	2.15	2.17	2.14	2.16	2.17	2.16	2.20	2.16	2.18	2.17
'otal	99.67	100.26	99.93	99.45	99.31	98.78	100.39	98.83	99.75	99.75
ations.	23(O)	23(O)	23(O)	Cations.	23(O)	23(O)	23(O)	23(O)	23(O)	23(O)
i	7.40	7.36	7.18	7.86	7.94	7.88	7.98	7.94	8.02	7.92
l iv	0.60	0.62	0.82	0.09	0.02	0.04	0.01	0.00	0.00	0.05
l <sup>vi</sup>	0.02	0.00	0.09	0.00	0.00	0.00	0.00	0.00	0.01	0.00
i	0.02	0.04	0.04	0.00	0.00	0.00	0.00	0.00	0.00	0.00
r	0.06	0.08	0.07	0.00	0.00	0.00	0.00	0.00	0.00	0.00
e <sup>3+</sup>	0.42	0.55	0.07	0.00	0.00	0.00	0.00	0.00	0.01	0.04
e <sup>2+</sup>	0.42	0.00	0.20	0.40	0.00	0.18	0.11	0.00	0.04	0.04
Ín Ia	0.03	0.02	0.01	0.01	0.00	0.01	0.01	0.01	0.01	0.01
lg	4.29	4.33	4.19	4.64	4.70	4.68	4.61	4.70	4.57	4.62
i	0.01	0.00	0.03	0.00	0.01	0.03	0.00	0.01	0.01	0.01
a	1.86	1.83	1.88	2.07	2.08	2.00	1.95	2.05	1.95	2.01
a	0.29	0.28	0.42	0.03	0.01	0.02	0.01	0.01	0.02	0.02
	0.02	0.02	0.02	0.03	0.01	0.01	0.01	0.01	0.00	0.03
a	0.00	0.00	0.00	0.00	0.00	0.00	0.00	0.00	0.00	0.00
H*	2.00	2.00	2.00	2.00	2.00	2.00	2.00	2.00	2.00	2.00
otal	17.18	17.13	17.32	17.12	17.06	17.02	16.97	17.06	16.96	17.06
Na+K) (A)	0.18	0.13	0.32	0.06	0.02	0.02	0.01	0.01	0.00	0.05
Ig/(Mg+Fe <sup>+2</sup> )	0.97	1.00	0.96	0.92	0.94	0.96	0.94	0.93	0.93	0.93
a+Al IV	2.46	2.45	2.70	2.16	2.09	2.03	1.96	2.05	1.95	2.05
i	7.40	7.36	7.18	7.86	7.94	7.88	7.98	7.94	8.02	7.92
ample No.	16 OP/14 /1	16 OP/15 /1	16 OP/16/ 1	16 OP/19/1	16 OP/20 / 1	16 OP/21 /1	16 OP/22 /1	16 OP/28 / 1	16 OP/29 /1	16 OP/23
_			subcalcic		calcian-		calcian-			magnesio
Ineral	anthophyllite	tremolite	tremolite	anthophyllite	anthophyllite	anthophyllite	anthophyllite	anthophyllite	tremolite	hornblend
ef. Point	16 OP/14 /1	16 OP/15 /1	16 OP/16/ 1	16 OP/19/1	16 OP/20 / 1	16 OP/21 /1	16 OP/22 /1	16 OP/28 / 1	16 OP/29 /1	16 OP/23
$iO_2$	58.32	57.16	56.99	57.24	56.88	57.36	57.03	56.86	55.67	47.76
$iO_2$	0.00	0.00	0.03	0.01	0.03	0.01	0.04	0.00	0.00	0.15
$l_2O_3$	0.04	0.44	0.16	0.05	0.32	0.10	0.21	0.07	0.12	10.51
$r_2O_3$	0.02	0.08	0.01	0.00	0.04	0.08	0.01	0.04	0.04	0.02
$e_2O_3$	0.00	4.48	6.43	0.00	0.16	0.00	0.00	0.30	5.73	4.98
eO	11.34	0.00	0.00	10.82	8.01	11.31	7.09	12.83	1.26	0.68
InO	0.33	0.40	0.18	0.32	0.32	0.38	0.19	0.34	0.28	0.16
IgO	26.99	22.73	23.49	24.95	24.33	25.55	24.25	25.56	20.71	18.25
iO	0.00	0.00	0.00	0.00	0.00	0.00	0.00	0.00	0.00	0.00
aO	0.10	11.67	9.05	3.06	6.25	1.11	7.24	0.57	12.20	11.74
aO a₂O	0.10	0.17	0.09	0.03	0.10	0.05	0.10	0.57	0.03	2.20
a₂O ₂O										
	0.00	0.00	0.00	0.00	0.00	0.00	0.00	0.00	0.00	0.09
aO O#	0.00	0.03	0.00	0.02	0.00	0.00	0.08	0.00	0.00	0.00
2O*	2.18	2.18	2.17	2.14	2.15	2.14	2.15	2.14	2.13	2.12
otal	99.35	99.34	98.61	98.64	98.59	98.09	98.39	98.71	98.16	98.66
ations.	23(O)	23(O)	23(O)	23(O)	23(O)	23(O)	23(O)	Cations.	23(O)	23(O)
i .	8.04	7.87	7.87	8.01	7.95	8.04	7.97	7.98	7.84	6.75
l iv	0.00	0.07	0.03	0.00	0.05	0.00	0.03	0.01	0.02	1.25
l <sup>vi</sup>	0.01	0.00	0.00	0.01	0.00	0.02	0.00	0.00	0.00	0.51
	0.00	0.00	0.00	0.00	0.00	0.00	0.00	0.00	0.00	0.02
r	0.00	0.01	0.00	0.00	0.00	0.01	0.00	0.00	0.00	0.00
3+	0.00	0.46	0.67	0.00	0.02	0.00	0.00	0.03	0.61	0.53
2+	1.31	0.00	0.00	1.27	0.94	1.33	0.83	1.50	0.15	0.08
in	0.04	0.05	0.02	0.04	0.04	0.05	0.02	0.04	0.03	0.02
g	5.55	4.66	4.84	5.20	5.07	5.34	5.05	5.35	4.35	3.85
i	0.00	0.00	0.00	0.00	0.00	0.00	0.00	0.00	0.00	0.00
a	0.01	1.72	1.34	0.46	0.94	0.17	1.08	0.09	1.84	1.78
	0.01	0.05	0.02	0.40	0.94	0.17	0.03	0.09	0.01	0.60
a										
	0.00	0.00	0.00	0.00	0.00	0.00	0.00	0.00	0.00	0.02
a	0.00	0.00	0.00	0.00	0.00	0.00	0.00	0.00	0.00	0.00
H*	2.00	2.00	2.00	2.00	2.00	2.00	2.00	2.00	2.00	2.00
otal	16.96	16.89	16.79	16.99	17.03	16.95	17.02	17.00	16.85	17.40
Na+K) (A)	0.00	0.00	0.00	0.00	0.03	0.00	0.02	0.00	0.00	0.40
		4.00	1.00	0.90	0.84	0.90	0.86	0.78	0.97	0.98
Ig/(Mg+Fe <sup>+2</sup> )	0.81	1.00	1.00	0.80		0.80	0.80	0.78	0.97	
Ig/(Mg+Fe <sup>+2</sup> ) a+Al IV	0.81 0.01	1.00	1.37	0.46	0.84	0.80	1.12	0.10	1.86	3.03

Table 4.1 continues......

Sample No. Mineral	BGD/1 / 1	BGD/3 /1								
Mineral			BGD/8 /1	BGD/9 /1	HD/2 /1	HD/3 / 1	HD/4 / 1	HD/8 / 1	HD/9 / 1	HD/10 / 1
	magnesio- hornblende	Ferrian- magnesio-	magnesio- hornblende	magnesio- hornblende	magnesio- hornblende	tschermakitic hornblende	magnesio- hornblende	magnesio- hornblende	magnesio- hornblende	magnesio- hornblende
Ref. Point	BGD/1 / 1	BGD/3 /1	BGD/8 /1	BGD/9 /1	HD/2 /1	HD/3 / 1	HD/4 / 1	HD/8 / 1	HD/9 / 1	HD/10 / 1
SiO <sub>2</sub>	45.13	44.85	43.80	46.42	47.06	43.46	46.69	46.19	44.82	46.39
TiO <sub>2</sub>	0.91	0.60	0.52	1.02	0.42	0.48	0.40	0.47	0.55	0.36
_	7.73	7.87	9.26	6.91	9.21	13.43	9.37	10.12	11.30	9.52
$Al_2O_3$										
$Cr_2O_3$	0.00	0.01	0.00	0.00	0.00	0.02	0.00	0.00	0.01	0.00
$Fe_2O_3$	4.67	6.91	5.67	4.99	2.47	3.85	2.01	2.32	1.93	2.74
FeO	12.31	10.99	13.14	11.86	10.25	11.42	10.93	10.90	11.73	10.32
MnO	0.48	0.53	0.48	0.38	0.22	0.36	0.06	0.27	0.22	0.24
MgO	11.43	11.27	9.75	12.23	13.15	10.76	13.15	12.70	11.73	12.88
NiO	0.00	0.00	0.00	0.00	0.00	0.00	0.00	0.00	0.00	0.00
CaO	12.11	11.69	11.69	12.19	12.24	12.15	12.51	12.48	12.30	12.36
Na <sub>2</sub> O	0.74	0.84	0.83	0.73	1.01	1.55	1.08	1.06	1.26	0.92
$K_2O$	0.74	0.70	0.79	0.70	0.34	0.52	0.35	0.43	0.43	0.37
BaO	0.00	0.00	0.00	0.00	0.00	0.00	0.03	0.04	0.02	0.00
$H_2O*$	1.99	1.99	1.97	2.02	2.04	2.04	2.04	2.04	2.02	2.03
Total	98.24	98.25	97.90	99.45	98.42	100.04	98.62	99.01	98.32	98.12
Cations.	23(O)	23(O)	23(O)	23(O)	23(O)	23(O)	23(O)	Cations.	23(O)	23(O)
Si	6.81	6.76	6.68	6.89	6.92	6.39	6.87	6.79	6.66	6.86
Al iv	1.19	1.24	1.32	1.11	1.08	1.61	1.13	1.21	1.34	1.14
Al vi	0.18	0.16	0.34	0.10	0.51	0.71	0.50	0.54	0.64	0.51
Ti	0.10	0.07	0.06	0.11	0.05	0.05	0.04	0.05	0.06	0.04
Cr	0.00	0.00	0.00	0.00	0.00	0.00	0.00	0.00	0.00	0.00
Fe <sup>3+</sup>	0.53	0.78	0.65	0.56	0.27	0.43	0.22	0.26	0.22	0.30
Fe <sup>2+</sup>	1.55	1.39	1.67	1.47	1.26	1.40	1.34	1.34	1.46	1.27
Mn	0.06	0.07	0.06	0.05	0.03	0.04	0.01	0.03	0.03	0.03
	2.57			2.71			2.88			2.84
Mg		2.53	2.22		2.88	2.36		2.78	2.60	
Ni	0.00	0.00	0.00	0.00	0.00	0.00	0.00	0.00	0.00	0.00
Ca	1.96	1.89	1.91	1.94	1.93	1.91	1.97	1.96	1.96	1.96
Na	0.22	0.25	0.25	0.21	0.29	0.44	0.31	0.30	0.36	0.26
K	0.14	0.13	0.15	0.13	0.06	0.10	0.07	0.08	0.08	0.07
Ba	0.00	0.00	0.00	0.00	0.00	0.00	0.00	0.00	0.00	0.00
OH*	2.00	2.00	2.00	2.00	2.00	2.00	2.00	2.00	2.00	2.00
Total	17.32	17.27	17.31	17.28	17.28	17.45	17.35	17.35	17.40	17.29
		0.27	0.31	0.28	0.28	0.45	0.35	0.35	0.40	0.29
(Na+K) (A)	0.32			0.65	0.70	0.63	0.68	0.68	0.64	0.69
Mg/(Mg+Fe <sup>+2</sup> )	0.62	0.65	0.57	0.65	0.70					
		0.65 3.13	0.57 3.23	3.05	3.01	3.53	3.10	3.18	3.30	3.10
Mg/(Mg+Fe <sup>+2</sup> )	0.62									
Mg/(Mg+Fe <sup>+2</sup> ) Ca+Al <sup>IV</sup> Si	0.62 3.15 6.81	3.13 6.76	3.23 6.68	3.05 6.89	3.01 6.92	3.53 6.39	3.10 6.87	3.18 6.79	3.30 6.66	3.10 6.86
Mg/(Mg+Fe <sup>+2</sup> ) Ca+Al <sup>IV</sup> Si Sample No.	0.62 3.15 6.81 HD/11 / 1	3.13 6.76 HD/14 / 1	3.23 6.68 HD/17 / 1	3.05 6.89 HD/19 / 1	3.01 6.92 HD/20 / 1	3.53 6.39 MDG/3 /1	3.10 6.87 MDG/7 /1	3.18 6.79 MDG27/10 /1	3.30 6.66 MDG/1 /1	3.10 6.86 MDG27/2 /1
Mg/(Mg+Fe <sup>+2</sup> ) Ca+Al <sup>IV</sup> Si	0.62 3.15 6.81 HD/11 / 1 magnesio-	3.13 6.76 HD/14 / 1 magnesio-	3.23 6.68 HD/17 / 1 magnesio-	3.05 6.89 HD/19 / 1 magnesio-	3.01 6.92 HD/20 / 1 tschermakitic	3.53 6.39	3.10 6.87 MDG/7 /1 actinolitic	3.18 6.79 MDG27/10 /1 actinolitic	3.30 6.66	3.10 6.86 MDG27/2 /1 actinolitic
Mg/(Mg+Fe <sup>+2</sup> ) Ca+Al <sup>IV</sup> Si Sample No. Mineral	0.62 3.15 6.81 HD/11 / 1 magnesio- hornblende	3.13 6.76 HD/14 / 1 magnesio- hornblende	3.23 6.68 HD/17 / 1 magnesio- hornblende	3.05 6.89 HD/19 / 1 magnesio- hornblende	3.01 6.92 HD/20 / 1 tschermakitic hornblende	3.53 6.39 MDG/3 /1 actinolite	3.10 6.87 MDG/7 /1 actinolitic hornblende	3.18 6.79 MDG27/10 /1 actinolitic hornblende	3.30 6.66 MDG/1 /1 actinolite	3.10 6.86 MDG27/2 /1 actinolitic hornblende
Mg/(Mg+Fe <sup>+2</sup> ) Ca+Al <sup>IV</sup> Si Sample No. Mineral Ref. Point	0.62 3.15 6.81 HD/11 / 1 magnesio- hornblende HD/11 / 1	3.13 6.76 HD/14 / 1 magnesio- hornblende HD/14 / 1	3.23 6.68 HD/17 / 1 magnesio- hornblende HD/17 / 1	3.05 6.89 HD/19 / 1 magnesio- hornblende HD/19 / 1	3.01 6.92 HD/20 / 1 tschermakitic hornblende HD/20 / 1	3.53 6.39 MDG/3 /1 actinolite MDG/3 /1	3.10 6.87 MDG/7 /1 actinolitic hornblende MDG/7 /1	3.18 6.79 MDG27/10 /1 actinolitic hornblende MDG27/10 /1	3.30 6.66 MDG/1 /1 actinolite MDG/1 /1	3.10 6.86 MDG27/2 /1 actinolitic hornblende MDG27/2 /1
$Mg/(Mg+Fe^{+2})$ $Ca+Al^{IV}$ $Si$ Sample No.  Mineral  Ref. Point $SiO_2$	0.62 3.15 6.81 HD/11 / 1 magnesio- hornblende HD/11 / 1 45.76	3.13 6.76 HD/14 / 1 magnesio- hornblende HD/14 / 1 47.97	3.23 6.68 HD/17 / 1 magnesio- hornblende HD/17 / 1 44.75	3.05 6.89 HD/19 / 1 magnesio- hornblende HD/19 / 1 45.92	3.01 6.92 HD/20 / 1 tschermakitic hornblende HD/20 / 1 43.36	3.53 6.39 MDG/3 /1 actinolite MDG/3 /1 52.38	3.10 6.87 MDG/7 /1 actinolitic hornblende MDG/7 /1 52.16	3.18 6.79 MDG27/10 /1 actinolitic hornblende MDG27/10 /1 51.92	3.30 6.66 MDG/1 /1 actinolite MDG/1 /1 53.13	3.10 6.86 MDG27/2 /1 actinolitic hornblende MDG27/2 /1 51.73
Mg/(Mg+Fe <sup>+2</sup> ) Ca+Al <sup>IV</sup> Si Sample No. Mineral Ref. Point SiO <sub>2</sub> TiO <sub>2</sub>	0.62 3.15 6.81 HD/11 / 1 magnesio- hornblende HD/11 / 1 45.76 0.49	3.13 6.76 HD/14 / 1 magnesio- hornblende HD/14 / 1 47.97 0.37	3.23 6.68 HD/17 / 1 magnesio- hornblende HD/17 / 1 44.75 0.50	3.05 6.89 HD/19 / 1 magnesio- hornblende HD/19 / 1 45.92 0.44	3.01 6.92 HD/20 / 1 tschermakitic hornblende HD/20 / 1 43.36 0.46	3.53 6.39 MDG/3 /1 actinolite MDG/3 /1 52.38 0.16	3.10 6.87 MDG/7 /1 actinolitic hornblende MDG/7 /1 52.16 0.23	3.18 6.79 MDG27/10 /1 actinolitic hornblende MDG27/10 /1 51.92 0.17	3.30 6.66 MDG/1/1 actinolite MDG/1/1 53.13 0.06	3.10 6.86 MDG27/2 /1 actinolitic hornblende MDG27/2 /1 51.73 0.21
Mg/(Mg+Fe <sup>+2</sup> ) Ca+Al <sup>IV</sup> Si Sample No. Mineral Ref. Point SiO <sub>2</sub> TiO <sub>2</sub> Al <sub>2</sub> O <sub>3</sub>	0.62 3.15 6.81 HD/11 / 1 magnesio- hornblende HD/11 / 1 45.76 0.49 10.73	3.13 6.76 HD/14 / 1 magnesio- hornblende HD/14 / 1 47.97 0.37 8.91	3.23 6.68 HD/17 / 1 magnesio- hornblende HD/17 / 1 44.75 0.50 11.13	3.05 6.89 HD/19 / 1 magnesio- hornblende HD/19 / 1 45.92 0.44 9.89	3.01 6.92 HD/20 / 1 tschermakitic hornblende HD/20 / 1 43.36 0.46 13.32	3.53 6.39 MDG/3 /1 actinolite MDG/3 /1 52.38 0.16 4.00	3.10 6.87 MDG/7 /1 actinolitic hornblende MDG/7 /1 52.16 0.23 4.58	3.18 6.79 MDG27/10 /1 actinolitic hornblende MDG27/10 /1 51.92 0.17 4.69	3.30 6.66 MDG/1/1 actinolite MDG/1/1 53.13 0.06 4.26	3.10 6.86 MDG27/2 /1 actinolitic hornblende MDG27/2 /1 51.73 0.21 5.07
Mg/(Mg+Fe <sup>+2</sup> ) Ca+Al <sup>IV</sup> Si Sample No. Mineral Ref. Point SiO <sub>2</sub> TiO <sub>2</sub>	0.62 3.15 6.81 HD/11 / 1 magnesio- hornblende HD/11 / 1 45.76 0.49	3.13 6.76 HD/14 / 1 magnesio- hornblende HD/14 / 1 47.97 0.37	3.23 6.68 HD/17 / 1 magnesio- hornblende HD/17 / 1 44.75 0.50	3.05 6.89 HD/19 / 1 magnesio- hornblende HD/19 / 1 45.92 0.44	3.01 6.92 HD/20 / 1 tschermakitic hornblende HD/20 / 1 43.36 0.46	3.53 6.39 MDG/3 /1 actinolite MDG/3 /1 52.38 0.16	3.10 6.87 MDG/7 /1 actinolitic hornblende MDG/7 /1 52.16 0.23	3.18 6.79 MDG27/10 /1 actinolitic hornblende MDG27/10 /1 51.92 0.17	3.30 6.66 MDG/1/1 actinolite MDG/1/1 53.13 0.06	3.10 6.86 MDG27/2 /1 actinolitic hornblende MDG27/2 /1 51.73 0.21
Mg/(Mg+Fe <sup>+2</sup> ) Ca+Al <sup>IV</sup> Si Sample No. Mineral Ref. Point SiO <sub>2</sub> TiO <sub>2</sub> Al <sub>2</sub> O <sub>3</sub>	0.62 3.15 6.81 HD/11 / 1 magnesio- hornblende HD/11 / 1 45.76 0.49 10.73	3.13 6.76 HD/14 / 1 magnesio- hornblende HD/14 / 1 47.97 0.37 8.91	3.23 6.68 HD/17 / 1 magnesio- hornblende HD/17 / 1 44.75 0.50 11.13	3.05 6.89 HD/19 / 1 magnesio- hornblende HD/19 / 1 45.92 0.44 9.89	3.01 6.92 HD/20 / 1 tschermakitic hornblende HD/20 / 1 43.36 0.46 13.32	3.53 6.39 MDG/3 /1 actinolite MDG/3 /1 52.38 0.16 4.00	3.10 6.87 MDG/7 /1 actinolitic hornblende MDG/7 /1 52.16 0.23 4.58	3.18 6.79 MDG27/10 /1 actinolitic hornblende MDG27/10 /1 51.92 0.17 4.69	3.30 6.66 MDG/1/1 actinolite MDG/1/1 53.13 0.06 4.26	3.10 6.86 MDG27/2 /1 actinolitic hornblende MDG27/2 /1 51.73 0.21 5.07
Mg/(Mg+Fe <sup>2</sup> ) Ca+Al <sup>IV</sup> Si Sample No.  Mineral  Ref. Point SiO <sub>2</sub> TiO <sub>2</sub> Al <sub>2</sub> O <sub>3</sub> Cr <sub>2</sub> O <sub>3</sub>	0.62 3.15 6.81 HD/11 / 1 magnesio- hornblende HD/11 / 1 45.76 0.49 10.73 0.02	3.13 6.76 HD/14 / 1 magnesio- hornblende HD/14 / 1 47.97 0.37 8.91 0.00	3.23 6.68 HD/17 / 1 magnesio- hornblende HD/17 / 1 44.75 0.50 11.13 0.00	3.05 6.89 HD/19 / 1 magnesio- hornblende HD/19 / 1 45.92 0.44 9.89 0.00	3.01 6.92 HD/20 / 1 tschermakitic hornblende HD/20 / 1 43.36 0.46 13.32 0.01	3.53 6.39 MDG/3 /1 actinolite MDG/3 /1 52.38 0.16 4.00 0.24	3.10 6.87 MDG/7 /1 actinolitic hornblende MDG/7 /1 52.16 0.23 4.58 0.27	3.18 6.79 MDG27/10 /1 actinolitic hornblende MDG27/10 /1 51.92 0.17 4.69 0.30	3.30 6.66 MDG/1/1 actinolite MDG/1/1 53.13 0.06 4.26 0.17	3.10 6.86 MDG27/2 /1 actinolitic hornblende MDG27/2 /1 51.73 0.21 5.07 0.08
Mg/(Mg+Fe <sup>2</sup> ) Ca+AI <sup>N</sup> Si Sample No. Mineral Ref. Point SiO <sub>2</sub> TiO <sub>2</sub> Al <sub>2</sub> O <sub>3</sub> Cr <sub>2</sub> O <sub>3</sub> Fe <sub>2</sub> O <sub>3</sub> FeO	0.62 3.15 6.81 HD/11/1 magnesio- hornblende HD/11/1 45.76 0.49 10.73 0.02 3.18 10.53	3.13 6.76 HD/14/1 magnesio- hornblende HD/14/1 47.97 0.37 8.91 0.00 1.65 10.46	3.23 6.68 HD/17/1 magnesio- hornblende HD/17/1 44.75 0.50 11.13 0.00 3.23 10.64	3.05 6.89 HD/19 / 1 magnesio- hornblende HD/19 / 1 45.92 0.44 9.89 0.00 2.68 10.80	3.01 6.92 HD/20 / 1 tschermakitic hornblende HD/20 / 1 43.36 0.46 13.32 0.01 4.43 11.10	3.53 6.39 MDG/3 /1 actinolite MDG/3 /1 52.38 0.16 4.00 0.24 2.69 7.18	3.10 6.87 MDG/7/1 actinolitic hornblende MDG/7/1 52.16 0.23 4.58 0.27 3.02 6.95	3.18 6.79 MDG27/10 /1 actinolitic hornblende MDG27/10 /1 51.92 0.17 4.69 0.30 0.75 9.35	3.30 6.66 MDG/1 /1 actinolite MDG/1 /1 53.13 0.06 4.26 0.17 1.70 7.73	3.10 6.86 MDG27/2 /1 actinolitic hornblende MDG27/2 /1 51.73 0.21 5.07 0.08 0.72 8.80
Mg/(Mg+Fe <sup>12</sup> ) Ca+Al <sup>IV</sup> Si Sample No. Mineral Ref. Point SiO <sub>2</sub> TiO <sub>2</sub> Al <sub>2</sub> O <sub>3</sub> Cr <sub>2</sub> O <sub>3</sub> FeO MnO	0.62 3.15 6.81 HD/11/1 magnesio- hornblende HD/11/1 45.76 0.49 10.73 0.02 3.18 10.53 0.18	3.13 6.76 HD/14 / 1 magnesio- hornblende HD/14 / 1 47.97 0.37 8.91 0.00 1.65 10.46 0.26	3.23 6.68 HD/17 / 1 magnesio- hornblende HD/17 / 1 44.75 0.50 11.13 0.00 3.23 10.64 0.32	3.05 6.89 HD/19 / 1 magnesio- hornblende HD/19 / 1 45.92 0.44 9.89 0.00 2.68 10.80 0.17	3.01 6.92 HD/20 / 1 tschermakitic hornblende HD/20 / 1 43.36 0.46 13.32 0.01 4.43 11.10 0.25	3.53 6.39 MDG/3/1 actinolite MDG/3/1 52.38 0.16 4.00 0.24 2.69 7.18 0.22	3.10 6.87 MDG/7 /1 actinolitic hornblende MDG/7 /1 52.16 0.23 4.58 0.27 3.02 6.95 0.27	3.18 6.79 MDG27/10 /1 actinolitic hornblende MDG27/10 /1 51.92 0.17 4.69 0.30 0.75 9.35 0.18	3.30 6.66 MDG/1 /1 actinolite MDG/1 /1 53.13 0.06 4.26 0.17 1.70 7.73 0.22	3.10 6.86 MDG27/2 /1 actinolitic hormblende MDG27/2 /1 51.73 0.21 5.07 0.08 0.72 8.80 0.18
Mg/(Mg+Fe <sup>2</sup> ) Ca+Al <sup>N</sup> Si Sample No. Mineral Ref. Point SiO <sub>2</sub> TiO <sub>2</sub> Al <sub>2</sub> O <sub>3</sub> Cr <sub>2</sub> O <sub>3</sub> Fe <sub>2</sub> O <sub>3</sub> FeO MnO MgO	0.62 3.15 6.81 HD/11/1 magnesio- hornblende HD/11/1 45.76 0.49 10.73 0.02 3.18 10.53 0.18 12.33	3.13 6.76 HD/14 / 1 magnesio- homblende HD/14 / 1 47.97 0.37 8.91 0.00 1.65 10.46 0.26 13.71	3.23 6.68 HD/17 / 1 magnesio- homblende HD/17 / 1 44.75 0.50 11.13 0.00 3.23 10.64 0.32 12.06	3.05 6.89 HD/19 / 1 magnesio- homblende HD/19 / 1 45.92 0.44 9.89 0.00 2.68 10.80 0.17 12.64	3.01 6.92 HD/20 / 1 tschermakitic hornblende HD/20 / 1 43.36 0.46 13.32 0.01 4.43 11.10 0.25 10.85	3.53 6.39 MDG/3 /1 actinolite MDG/3 /1 52.38 0.16 4.00 0.24 2.69 7.18 0.22 16.82	3.10 6.87 MDG/7 /1 actinolitic hornblende MDG/7 /1 52.16 0.23 4.58 0.27 3.02 6.95 0.27 16.79	3.18 6.79 MDG27/10 /1 actinolitic hornblende MDG27/10 /1 51.92 0.17 4.69 0.30 0.75 9.35 0.18 16.15	3.30 6.66 MDG/1 /1 actinolite MDG/1 /1 53.13 0.06 4.26 0.17 1.70 7.73 0.22 16.91	3.10 6.86 MDG27/2 /1 actinolitic hornblende MDG27/2 /1 51.73 0.21 5.07 0.08 0.72 8.80 0.18 16.18
Mg/(Mg+Fe <sup>2</sup> ) Ca+Al <sup>IV</sup> Si Sample No. Mineral Ref. Point SiO <sub>2</sub> TiO <sub>2</sub> Al <sub>2</sub> O <sub>3</sub> Cr <sub>2</sub> O <sub>3</sub> Fe <sub>2</sub> O <sub>3</sub> FeO MnO MgO NiO	0.62 3.15 6.81 HD/11/1 magnesio-hornblende HD/11/1 45.76 0.49 10.73 0.02 3.18 10.53 0.18 12.33 0.00	3.13 6.76 HD/14 / 1 magnesio- hornblende HD/14 / 1 47.97 0.37 8.91 0.00 1.65 10.46 0.26 13.71 0.00	3.23 6.68 HD/17 / 1 magnesio- hornblende HD/17 / 1 44.75 0.50 11.13 0.00 3.23 10.64 0.32 12.06 0.00	3.05 6.89 HD/19 / 1 magnesio- hornblende HD/19 / 1 45.92 0.44 9.89 0.00 2.68 10.80 0.17 12.64 0.00	3.01 6.92 HD/20 / 1 tschermakitic hornblende HD/20 / 1 43.36 0.46 13.32 0.01 4.43 11.10 0.25 10.85 0.00	3.53 6.39 MDG/3 /1 actinolite MDG/3 /1 52.38 0.16 4.00 0.24 2.69 7.18 0.22 16.82 0.00	3.10 6.87 MDG/7/1 actinolitic hornblende MDG/7/1 52.16 0.23 4.58 0.27 3.02 6.95 0.27 16.79 0.00	3.18 6.79 MDG27/10 /1 actinolitic hornblende MDG27/10 /1 51.92 0.17 4.69 0.30 0.75 9.35 0.18 16.15 0.00	3.30 6.66 MDG/1 /1 actinolite MDG/1 /1 53.13 0.06 4.26 0.17 1.70 7.73 0.22 16.91 0.00	3.10 6.86 MDG27/2 /1 actinolitic hornblende MDG27/2 /1 51.73 0.21 5.07 0.08 0.72 8.80 0.18 16.18 0.00
Mg/(Mg+Fe <sup>2</sup> ) Ca+Al <sup>IV</sup> Si Sample No. Mineral Ref. Point SiO <sub>2</sub> TiO <sub>2</sub> Al <sub>2</sub> O <sub>3</sub> Cr <sub>2</sub> O <sub>3</sub> FeO MnO MgO NiO CaO	0.62 3.15 6.81 HD/11/1 magnesio-hornblende HD/11/1 45.76 0.49 10.73 0.02 3.18 10.53 0.18 12.33 0.00 12.18	3.13 6.76 HD/14 / 1 magnesio- hornblende HD/14 / 1 47.97 0.37 8.91 0.00 1.65 10.46 0.26 13.71 0.00 12.59	3.23 6.68 HD/17 / 1 magnesio- hornblende HD/17 / 1 44.75 0.50 11.13 0.00 3.23 10.64 0.32 12.06 0.00 12.25	3.05 6.89 HD/19 / 1 magnesio- hornblende HD/19 / 1 45.92 0.44 9.89 0.00 2.68 10.80 0.17 12.64 0.00	3.01 6.92 HD/20 / 1 tschermakitic hornblende HD/20 / 1 43.36 0.46 13.32 0.01 4.43 11.10 0.25 10.85 0.00	3.53 6.39 MDG/3/1 actinolite MDG/3/1 52.38 0.16 4.00 0.24 2.69 7.18 0.22 16.82 0.00 12.51	3.10 6.87 MDG/7/1 actinolitic hornblende MDG/7/1 52.16 0.23 4.58 0.27 3.02 6.95 0.27 16.79 0.00 12.59	3.18 6.79 MDG27/10 /1 actinolitic hornblende MDG27/10 /1 51.92 0.17 4.69 0.30 0.75 9.35 0.18 16.15 0.00 12.95	3.30 6.66 MDG/1/1 actinolite MDG/1/1 53.13 0.06 4.26 0.17 1.70 7.73 0.22 16.91 0.00 12.67	3.10 6.86 MDG27/2 /1 actinolitic hornblende MDG27/2 /1 51.73 0.21 5.07 0.08 0.72 8.80 0.18 16.18 0.00
Mg/(Mg+Fe <sup>2</sup> ) Ca+Al <sup>W</sup> Si Sample No. Mineral Ref. Point SiO <sub>2</sub> TiO <sub>2</sub> Al <sub>2</sub> O <sub>3</sub> Cr <sub>2</sub> O <sub>3</sub> Fe <sub>2</sub> O MnO MgO NiO CaO Na <sub>2</sub> O	0.62 3.15 6.81 HD/11/1 magnesio- hornblende HD/11/1 45.76 0.49 10.73 0.02 3.18 10.53 0.18 12.33 0.00 12.18 1.13	3.13 6.76 HD/14 / 1 magnesio- hornblende HD/14 / 1 47.97 0.37 8.91 0.00 1.65 10.46 0.26 13.71 0.00 12.59 0.96	3.23 6.68 HD/17/1 magnesio- hornblende HD/17/1 44.75 0.50 11.13 0.00 3.23 10.64 0.32 12.06 0.00 12.25 1.26	3.05 6.89 HD/19 / 1 magnesio- hornblende HD/19 / 1 45.92 0.44 9.89 0.00 2.68 10.80 0.17 12.64 0.00 12.38 1.08	3.01 6.92 HD/20 / 1 tschermakitic hornblende HD/20 / 1 43.36 0.46 13.32 0.01 4.43 11.10 0.25 10.85 0.00 12.29 1.38	3.53 6.39 MDG/3 /1 actinolite MDG/3 /1 52.38 0.16 4.00 0.24 2.69 7.18 0.22 16.82 0.00 12.51 0.35	3.10 6.87 MDG/7/1 actinolitic hornblende MDG/7 /1 52.16 0.23 4.58 0.27 3.02 6.95 0.27 16.79 0.00 12.59 0.35	3.18 6.79 MDG27/10 /1 actinolitic hornblende MDG27/10 /1 51.92 0.17 4.69 0.30 0.75 9.35 0.18 16.15 0.00 12.95 0.41	3.30 6.66 MDG/1/1 actinolite MDG/1/1 53.13 0.06 4.26 0.17 1.70 7.73 0.22 16.91 0.00 12.67 0.36	3.10 6.86 MDG27/2 /1 actinolitic hornblende MDG27/2 /1 51.73 0.21 5.07 0.08 0.72 8.80 0.18 16.18 0.00 12.70 0.43
Mg/(Mg+Fe <sup>2</sup> ) Ca+Al <sup>W</sup> Si Sample No. Mineral Ref. Point SiO <sub>2</sub> TiO <sub>2</sub> Al <sub>2</sub> O <sub>3</sub> Cr <sub>2</sub> O <sub>3</sub> Fe <sub>2</sub> O MnO MgO NiO CaO Na <sub>2</sub> O K <sub>2</sub> O	0.62 3.15 6.81 HD/11/1 magnesio- hornblende HD/11/1 45.76 0.49 10.73 0.02 3.18 10.53 0.18 12.33 0.00 12.18 1.13	3.13 6.76 HD/14 / 1 magnesio- hornblende HD/14 / 1 47.97 0.37 8.91 0.00 1.65 10.46 0.26 13.71 0.00 12.59 0.96	3.23 6.68 HD/17/1 magnesio- hornblende HD/17/1 44.75 0.50 11.13 0.00 3.23 10.64 0.32 12.06 0.00 12.25 1.26	3.05 6.89 HD/19 / 1 magnesio- hornblende HD/19 / 1 45.92 0.44 9.89 0.00 2.68 10.80 0.17 12.64 0.00 12.38 1.08	3.01 6.92 HD/20 / 1 tschermakitic hornblende HD/20 / 1 43.36 0.46 13.32 0.01 4.43 11.10 0.25 10.85 0.00 12.29 1.38	3.53 6.39 MDG/3 /1 actinolite MDG/3 /1 52.38 0.16 4.00 0.24 2.69 7.18 0.22 16.82 0.00 12.51 0.35	3.10 6.87 MDG/7 /1 actinolitic hornblende MDG/7 /1 52.16 0.23 4.58 0.27 3.02 6.95 0.27 16.79 0.00 12.59 0.35 0.13	3.18 6.79 MDG27/10 /1 actinolitic hornblende MDG27/10 /1 51.92 0.17 4.69 0.30 0.75 9.35 0.18 16.15 0.00 12.95 0.41	3.30 6.66 MDG/1 /1 actinolite MDG/1 /1 53.13 0.06 4.26 0.17 1.70 7.73 0.22 16.91 0.00 12.67 0.36	3.10 6.86 MDG27/2 /1 actinolitic hormblende MDG27/2 /1 51.73 0.21 5.07 0.08 0.72 8.80 0.18 16.18 0.00 12.70 0.43
Mg/(Mg+Fe <sup>2</sup> ) Ca+Al <sup>IV</sup> Si Sample No. Mineral Ref. Point SiO <sub>2</sub> TiO <sub>2</sub> Al <sub>2</sub> O <sub>3</sub> Cr <sub>2</sub> O <sub>3</sub> Fe <sub>2</sub> O MnO MgO NiO CaO Na <sub>2</sub> O	0.62 3.15 6.81 HD/11/1 magnesio- hornblende HD/11/1 45.76 0.49 10.73 0.02 3.18 10.53 0.18 12.33 0.00 12.18 1.13	3.13 6.76 HD/14 / 1 magnesio- hornblende HD/14 / 1 47.97 0.37 8.91 0.00 1.65 10.46 0.26 13.71 0.00 12.59 0.96	3.23 6.68 HD/17/1 magnesio- hornblende HD/17/1 44.75 0.50 11.13 0.00 3.23 10.64 0.32 12.06 0.00 12.25 1.26	3.05 6.89 HD/19 / 1 magnesio- hornblende HD/19 / 1 45.92 0.44 9.89 0.00 2.68 10.80 0.17 12.64 0.00 12.38 1.08	3.01 6.92 HD/20 / 1 tschermakitic hornblende HD/20 / 1 43.36 0.46 13.32 0.01 4.43 11.10 0.25 10.85 0.00 12.29 1.38	3.53 6.39 MDG/3 /1 actinolite MDG/3 /1 52.38 0.16 4.00 0.24 2.69 7.18 0.22 16.82 0.00 12.51 0.35	3.10 6.87 MDG/7/1 actinolitic hornblende MDG/7 /1 52.16 0.23 4.58 0.27 3.02 6.95 0.27 16.79 0.00 12.59 0.35	3.18 6.79 MDG27/10 /1 actinolitic hornblende MDG27/10 /1 51.92 0.17 4.69 0.30 0.75 9.35 0.18 16.15 0.00 12.95 0.41	3.30 6.66 MDG/1/1 actinolite MDG/1/1 53.13 0.06 4.26 0.17 1.70 7.73 0.22 16.91 0.00 12.67 0.36	3.10 6.86 MDG27/2 /1 actinolitic hornblende MDG27/2 /1 51.73 0.21 5.07 0.08 0.72 8.80 0.18 16.18 0.00 12.70 0.43
Mg/(Mg+Fe <sup>2</sup> ) Ca+Al <sup>IV</sup> Si Sample No. Mineral Ref. Point SiO <sub>2</sub> TiO <sub>2</sub> Al <sub>2</sub> O <sub>3</sub> Cr <sub>2</sub> O <sub>3</sub> Fe <sub>2</sub> O MnO MgO NiO CaO Na <sub>2</sub> O K <sub>2</sub> O	0.62 3.15 6.81 HD/11/1 magnesio- hornblende HD/11/1 45.76 0.49 10.73 0.02 3.18 10.53 0.18 12.33 0.00 12.18 1.13	3.13 6.76 HD/14 / 1 magnesio- hornblende HD/14 / 1 47.97 0.37 8.91 0.00 1.65 10.46 0.26 13.71 0.00 12.59 0.96	3.23 6.68 HD/17/1 magnesio- hornblende HD/17/1 44.75 0.50 11.13 0.00 3.23 10.64 0.32 12.06 0.00 12.25 1.26	3.05 6.89 HD/19 / 1 magnesio- hornblende HD/19 / 1 45.92 0.44 9.89 0.00 2.68 10.80 0.17 12.64 0.00 12.38 1.08	3.01 6.92 HD/20 / 1 tschermakitic hornblende HD/20 / 1 43.36 0.46 13.32 0.01 4.43 11.10 0.25 10.85 0.00 12.29 1.38	3.53 6.39 MDG/3 /1 actinolite MDG/3 /1 52.38 0.16 4.00 0.24 2.69 7.18 0.22 16.82 0.00 12.51 0.35	3.10 6.87 MDG/7 /1 actinolitic hornblende MDG/7 /1 52.16 0.23 4.58 0.27 3.02 6.95 0.27 16.79 0.00 12.59 0.35 0.13	3.18 6.79 MDG27/10 /1 actinolitic hornblende MDG27/10 /1 51.92 0.17 4.69 0.30 0.75 9.35 0.18 16.15 0.00 12.95 0.41	3.30 6.66 MDG/1 /1 actinolite MDG/1 /1 53.13 0.06 4.26 0.17 1.70 7.73 0.22 16.91 0.00 12.67 0.36	3.10 6.86 MDG27/2 /1 actinolitic hornblende MDG27/2 /1 51.73 0.21 5.07 0.08 0.72 8.80 0.18 16.18 0.00 12.70 0.43
Mg/(Mg+Fe <sup>2</sup> ) Ca+Al <sup>IV</sup> Si Sample No. Mineral Ref. Point SiO <sub>2</sub> TiO <sub>2</sub> Al <sub>2</sub> O <sub>3</sub> Cr <sub>2</sub> O <sub>3</sub> Fe <sub>2</sub> O <sub>3</sub> FeO MnO MgO NiO CaO Na <sub>2</sub> O K <sub>2</sub> O BaO H <sub>2</sub> O*	0.62 3.15 6.81 HD/11/1 magnesio-hornblende HD/11/1 45.76 0.49 10.73 0.02 3.18 10.53 0.18 12.33 0.00 12.18 1.13 0.43 0.05 2.04	3.13 6.76 HD/14 / 1 magnesio- hornblende HD/14 / 1 47.97 0.37 8.91 0.00 1.65 10.46 0.26 13.71 0.00 12.59 0.96 0.33 0.04	3.23 6.68 HD/17 / 1 magnesio- hornblende HD/17 / 1 44.75 0.50 11.13 0.00 3.23 10.64 0.32 12.06 0.00 12.25 1.26 0.43 0.09 2.03	3.05 6.89 HD/19 / 1 magnesio- hornblende HD/19 / 1 45.92 0.44 9.89 0.00 2.68 10.80 0.17 12.64 0.00 12.38 1.08 0.39 0.00	3.01 6.92 HD/20 / 1 tschermakitic hornblende HD/20 / 1 43.36 0.46 13.32 0.01 4.43 11.10 0.25 10.85 0.00 12.29 1.38 0.43 0.02 2.04	3.53 6.39 MDG/3 /1 actinolite MDG/3 /1 52.38 0.16 4.00 0.24 2.69 7.18 0.22 16.82 0.00 12.51 0.35 0.09	3.10 6.87 MDG/7/1 actinolitic hornblende MDG/7/1 52.16 0.23 4.58 0.27 3.02 6.95 0.27 16.79 0.00 12.59 0.35 0.13 0.09 2.11	3.18 6.79  MDG27/10 /1 actinolitic hornblende  MDG27/10 /1  51.92 0.17 4.69 0.30 0.75 9.35 0.18 16.15 0.00 12.95 0.41 0.11 0.00 2.09	3.30 6.66 MDG/1 /1 actinolite MDG/1 /1 53.13 0.06 4.26 0.17 1.70 7.73 0.22 16.91 0.00 12.67 0.36 0.07	3.10 6.86 MDG27/2 /1 actinolitic hornblende MDG27/2 /1 51.73 0.21 5.07 0.08 0.72 8.80 0.18 16.18 0.00 12.70 0.43 0.17 0.04
Mg/(Mg+Fe <sup>2</sup> ) Ca+Al <sup>IV</sup> Si Si Sample No.  Mineral  Ref. Point SiO <sub>2</sub> TiO <sub>2</sub> Al <sub>2</sub> O <sub>3</sub> Fe <sub>2</sub> O <sub>3</sub> Fe <sub>2</sub> O MnO MgO NiO CaO Na <sub>2</sub> O K <sub>2</sub> O BaO H <sub>2</sub> O* Total	0.62 3.15 6.81 HD/11/1 magnesio-hornblende HD/11/1 45.76 0.49 10.73 0.02 3.18 10.53 0.18 12.33 0.00 12.18 1.13 0.43 0.05 2.04 99.05	3.13 6.76 HD/14 / 1 magnesio- hornblende HD/14 / 1 47.97 0.37 8.91 0.00 1.65 10.46 0.26 13.71 0.00 12.59 0.96 0.33 0.04 2.06 99.31	3.23 6.68 HD/17/1 magnesio- hornblende HD/17/1 44.75 0.50 11.13 0.00 3.23 10.64 0.32 12.06 0.00 12.25 1.26 0.43 0.09 2.03 98.69	3.05 6.89 HD/19 / 1 magnesio- hornblende HD/19 / 1 45.92 0.44 9.89 0.00 2.68 10.80 0.17 12.64 0.00 12.38 1.08 0.39 0.00	3.01 6.92 HD/20 / 1 tschermakitic hornblende HD/20 / 1 43.36 0.46 13.32 0.01 4.43 11.10 0.25 10.85 0.00 12.29 1.38 0.43 0.02 2.04	3.53 6.39 MDG/3/1 actinolite MDG/3/1 52.38 0.16 4.00 0.24 2.69 7.18 0.22 16.82 0.00 12.51 0.35 0.09 0.00 2.09 98.73	3.10 6.87 MDG/7/1 actinolitic hornblende MDG/7/1 52.16 0.23 4.58 0.27 3.02 6.95 0.27 16.79 0.00 12.59 0.35 0.13 0.09 2.11	3.18 6.79 MDG27/10 /1 actinolitic hornblende MDG27/10 /1 51.92 0.17 4.69 0.30 0.75 9.35 0.18 16.15 0.00 12.95 0.41 0.11 0.00 2.09 99.06	3.30 6.66 MDG/1/1 actinolite MDG/1/1 53.13 0.06 4.26 0.17 1.70 7.73 0.22 16.91 0.00 12.67 0.36 0.07 0.00 2.11	3.10 6.86 MDG27/2 /1 actinolitic hornblende MDG27/2 /1 51.73 0.21 5.07 0.08 0.72 8.80 0.18 16.18 0.00 12.70 0.43 0.17 0.00 2.08 98.35
Mg/(Mg+Fe <sup>2</sup> ) Ca+Al <sup>IV</sup> Si Sample No. Mineral Ref. Point SiO <sub>2</sub> TiO <sub>2</sub> Al <sub>2</sub> O <sub>3</sub> Cr <sub>2</sub> O <sub>3</sub> FeO MnO MgO NiO CaO Na <sub>2</sub> O K <sub>2</sub> O BaO H <sub>2</sub> O* Total Cations.	0.62 3.15 6.81 HD/11/1 magnesio- hornblende HD/11/1 45.76 0.49 10.73 0.02 3.18 10.53 0.18 12.33 0.00 12.18 1.13 0.43 0.05 2.04 99.05	3.13 6.76 HD/14/1 magnesio- hornblende HD/14/1 47.97 0.37 8.91 0.00 1.65 10.46 0.26 13.71 0.00 12.59 0.96 0.33 0.04 2.06 99.31	3.23 6.68 HD/17/1 magnesio- hornblende HD/17/1 44.75 0.50 11.13 0.00 3.23 10.64 0.32 12.06 0.00 12.25 1.26 0.43 0.09 2.03 98.69	3.05 6.89 HD/19 / 1 magnesio- homblende HD/19 / 1 45.92 0.44 9.89 0.00 2.68 10.80 0.17 12.64 0.00 12.38 1.08 0.39 0.00 2.03 98.42	3.01 6.92 HD/20 / 1 tschermaktiic hornblende HD/20 / 1 43.36 0.46 13.32 0.01 4.43 11.10 0.25 10.85 0.00 12.29 1.38 0.43 0.02 2.04 99.94 23(O)	3.53 6.39 MDG/3 /1 actinolite MDG/3 /1 52.38 0.16 4.00 0.24 2.69 7.18 0.22 16.82 0.00 12.51 0.35 0.09 0.00 2.09 98.73	3.10 6.87  MDG/7 /1 actinolitic hornblende MDG/7 /1 52.16 0.23 4.58 0.27 3.02 6.95 0.27 16.79 0.00 12.59 0.35 0.13 0.09 2.11 99.54 Cations.	3.18 6.79  MDG27/10 /1 actinolitic hornblende  MDG27/10 /1 51.92 0.17 4.69 0.30 0.75 9.35 0.18 16.15 0.00 12.95 0.41 0.11 0.00 2.09 99.06 23(O)	3.30 6.66 MDG/1/1 actinolite MDG/1/1 53.13 0.06 4.26 0.17 1.70 7.73 0.22 16.91 0.00 12.67 0.36 0.07 0.00 2.11 99.39	3.10 6.86 MDG27/2 /1 actinolitic hornblende MDG27/2 /1 51.73 0.21 5.07 0.08 0.72 8.80 0.18 16.18 0.00 12.70 0.43 0.17 0.00 2.08 98.35
Mg/(Mg+Fe <sup>2</sup> ) Ca+Al <sup>IV</sup> Si Sample No. Mineral Ref. Point SiO <sub>2</sub> TiO <sub>2</sub> Al <sub>2</sub> O <sub>3</sub> Cr <sub>2</sub> O <sub>3</sub> FeO MnO MgO NiO CaO Na <sub>2</sub> O K <sub>2</sub> O BaO H <sub>2</sub> O* Total Cations. Si	0.62 3.15 6.81 HD/11/1 magnesio-hornblende HD/11/1 45.76 0.49 10.73 0.02 3.18 10.53 0.18 12.33 0.00 12.18 1.13 0.43 0.05 2.04 99.05 23(0) 6.72	3.13 6.76 HD/14 / 1 magnesio- homblende HD/14 / 1 47.97 0.37 8.91 0.00 1.65 10.46 0.26 13.71 0.00 12.59 0.33 0.04 2.06 9.31 2.3(0) 6.98	3.23 6.68 HD/17 / 1 magnesio- hornblende HD/17 / 1 44.75 0.50 11.13 0.00 3.23 10.64 0.32 12.06 0.00 12.25 1.26 0.43 0.09 2.03 98.69 23(0) 6.62	3.05 6.89 HD/19 / 1 magnesio- hornblende HD/19 / 1 45.92 0.44 9.89 0.00 2.68 10.80 0.17 12.64 0.00 12.38 1.08 0.39 0.00 2.03 98.42 23(O) 6.79	3.01 6.92 HD/20 / 1 tschermakitic hornblende HD/20 / 1 43.36 0.46 13.32 0.01 4.43 11.10 0.25 10.85 0.00 12.29 1.38 0.43 0.02 2.04 99.94 23(O) 6.38	3.53 6.39 MDG/3 /1 actinolite MDG/3 /1 52.38 0.16 4.00 0.24 2.69 7.18 0.22 16.82 0.00 12.51 0.35 0.09 0.00 2.09 9.8.73 23(O) 7.51	3.10 6.87  MDG/7 /1 actinolitic hornblende MDG/7 /1 52.16 0.23 4.58 0.27 3.02 6.95 0.27 16.79 0.00 12.59 0.35 0.13 0.09 2.11 99.54 Cations. 7.43	3.18 6.79  MDG27/10 /1 actinolitic hornblende  MDG27/10 /1 51.92 0.17 4.69 0.30 0.75 9.35 0.18 16.15 0.00 12.95 0.41 0.11 0.00 2.09 99.06 23(0) 7.46	3.30 6.66 MDG/1/1 actinolite MDG/1/1 53.13 0.06 4.26 0.17 1.70 7.73 0.22 16.91 0.00 12.67 0.36 0.07 0.00 2.11 99.39 23(O) 7.55	3.10 6.86 MDG27/2 /1 actinolitic hormblende MDG27/2 /1 51.73 0.21 5.07 0.08 0.72 8.80 0.18 16.18 0.00 12.70 0.43 0.17 0.00 2.08 98.35 23(0) 7.46
Mg/(Mg+Fe <sup>2</sup> ) Ca+Al <sup>W</sup> Si Sample No. Mineral Ref. Point SiO <sub>2</sub> TiO <sub>2</sub> Al <sub>2</sub> O <sub>3</sub> Cr <sub>2</sub> O <sub>3</sub> FeO MnO MgO NiO CaO Na <sub>2</sub> O K <sub>2</sub> O BaO H <sub>2</sub> O* Total Cations. Si Al <sup>W</sup>	0.62 3.15 6.81 HD/11/1 magnesio-hornblende HD/11/1 45.76 0.49 10.73 0.02 3.18 10.53 0.18 12.33 0.00 12.18 1.13 0.43 0.05 2.04 99.05 2.3(O) 6.72 1.28	3.13 6.76 HD/14 / 1 magnesio- hornblende HD/14 / 1 47.97 0.37 8.91 0.00 1.65 10.46 0.26 13.71 0.00 12.59 0.96 0.33 0.04 2.06 99.31 23(O) 6.98 1.02	3.23 6.68 HD/17 / 1 magnesio-hornblende HD/17 / 1 44.75 0.50 11.13 0.00 3.23 10.64 0.32 12.06 0.00 12.25 1.26 0.43 0.09 2.03 98.69 23(O) 6.62 1.38	3.05 6.89 HD/19 / 1 magnesio-hornblende HD/19 / 1 45.92 0.44 9.89 0.00 2.68 10.80 0.17 12.64 0.00 12.38 1.08 0.39 0.00 2.03 98.42 23(O) 6.79 1.21	3.01 6.92 HD/20 / 1 tschermakitic hornblende HD/20 / 1 43.36 0.46 13.32 0.01 4.43 11.10 0.25 10.85 0.00 12.29 1.38 0.43 0.02 2.04 99.94 23(O) 6.38 1.62	3.53 6.39 MDG/3 /1 actinolite MDG/3 /1 52.38 0.16 4.00 0.24 2.69 7.18 0.22 16.82 0.00 12.51 0.35 0.09 0.00 2.09 98.73 23(O) 7.51	3.10 6.87 MDG/7 /1 actinolitic hornblende MDG/7 /1 52.16 0.23 4.58 0.27 3.02 6.95 0.27 16.79 0.00 12.59 0.35 0.13 0.09 2.11 99.54 Cations. 7.43 0.57	3.18 6.79  MDG27/10 /1 actinolitic hornblende  MDG27/10 /1  51.92 0.17 4.69 0.30 0.75 9.35 0.18 16.15 0.00 12.95 0.41 0.11 0.00 2.09 99.06 23(O) 7.46 0.54	3.30 6.66 MDG/1/1 actinolite MDG/1/1 53.13 0.06 4.26 0.17 1.70 7.73 0.22 16.91 0.00 12.67 0.36 0.07 0.00 2.11 99.39 23(O) 7.55 0.45	3.10 6.86  MDG27/2 /1 actinolitic hormblende MDG27/2 /1 51.73 0.21 5.07 0.08 0.72 8.80 0.18 16.18 0.00 12.70 0.43 0.17 0.00 2.08 98.35 23(O) 7.46 0.54
Mg/(Mg+Fe <sup>2</sup> ) Ca+Al <sup>N</sup> Si Sample No. Mineral Ref. Point SiO <sub>2</sub> TiO <sub>2</sub> Al <sub>2</sub> O <sub>3</sub> Fe <sub>2</sub> O <sub>3</sub> Fe <sub>2</sub> O <sub>3</sub> Fe <sub>2</sub> O <sub>3</sub> FeO MnO MgO NiO CaO Na <sub>2</sub> O K <sub>2</sub> O BaO H <sub>3</sub> O* Total Cations. Si Al <sup>N</sup>	0.62 3.15 6.81 HD/11/1 magnesio-hornblende HD/11/1 45.76 0.49 10.73 0.02 3.18 10.53 0.18 12.33 0.00 12.18 1.13 0.43 0.05 2.04 99.05 23(0) 6.72	3.13 6.76 HD/14 / 1 magnesio- homblende HD/14 / 1 47.97 0.37 8.91 0.00 1.65 10.46 0.26 13.71 0.00 12.59 0.33 0.04 2.06 9.31 2.3(0) 6.98	3.23 6.68 HD/17 / 1 magnesio- hornblende HD/17 / 1 44.75 0.50 11.13 0.00 3.23 10.64 0.32 12.06 0.00 12.25 1.26 0.43 0.09 2.03 98.69 23(0) 6.62	3.05 6.89 HD/19 / 1 magnesio- hornblende HD/19 / 1 45.92 0.44 9.89 0.00 2.68 10.80 0.17 12.64 0.00 12.38 1.08 0.39 0.00 2.03 98.42 23(O) 6.79	3.01 6.92 HD/20 / 1 tschermakitic hornblende HD/20 / 1 43.36 0.46 13.32 0.01 4.43 11.10 0.25 10.85 0.00 12.29 1.38 0.43 0.02 2.04 99.94 23(O) 6.38	3.53 6.39 MDG/3 /1 actinolite MDG/3 /1 52.38 0.16 4.00 0.24 2.69 7.18 0.22 16.82 0.00 12.51 0.35 0.09 0.00 2.09 9.8.73 23(O) 7.51	3.10 6.87  MDG/7 /1 actinolitic hornblende MDG/7 /1 52.16 0.23 4.58 0.27 3.02 6.95 0.27 16.79 0.00 12.59 0.35 0.13 0.09 2.11 99.54 Cations. 7.43	3.18 6.79  MDG27/10 /1 actinolitic hornblende  MDG27/10 /1 51.92 0.17 4.69 0.30 0.75 9.35 0.18 16.15 0.00 12.95 0.41 0.11 0.00 2.09 99.06 23(0) 7.46	3.30 6.66 MDG/1/1 actinolite MDG/1/1 53.13 0.06 4.26 0.17 1.70 7.73 0.22 16.91 0.00 12.67 0.36 0.07 0.00 2.11 99.39 23(O) 7.55	3.10 6.86 MDG27/2 /1 actinolitic hormblende MDG27/2 /1 51.73 0.21 5.07 0.08 0.72 8.80 0.18 16.18 0.00 12.70 0.43 0.17 0.00 2.08 9.835 23(O) 7.46
Mg/(Mg+Fe <sup>2</sup> ) Ca+Al <sup>N</sup> Si Sample No. Mineral Ref. Point SiO <sub>2</sub> TiO <sub>2</sub> Al <sub>2</sub> O <sub>3</sub> Cr <sub>2</sub> O <sub>3</sub> FeO MnO MgO NiO CaO Na <sub>2</sub> O BaO H <sub>2</sub> O* Total Cations. Si	0.62 3.15 6.81 HD/11/1 magnesio-hornblende HD/11/1 45.76 0.49 10.73 0.02 3.18 10.53 0.18 12.33 0.00 12.18 1.13 0.43 0.05 2.04 99.05 2.3(O) 6.72 1.28	3.13 6.76 HD/14 / 1 magnesio- hornblende HD/14 / 1 47.97 0.37 8.91 0.00 1.65 10.46 0.26 13.71 0.00 12.59 0.96 0.33 0.04 2.06 99.31 23(O) 6.98 1.02	3.23 6.68 HD/17 / 1 magnesio-hornblende HD/17 / 1 44.75 0.50 11.13 0.00 3.23 10.64 0.32 12.06 0.00 12.25 1.26 0.43 0.09 2.03 98.69 23(O) 6.62 1.38	3.05 6.89 HD/19 / 1 magnesio-hornblende HD/19 / 1 45.92 0.44 9.89 0.00 2.68 10.80 0.17 12.64 0.00 12.38 1.08 0.39 0.00 2.03 98.42 23(O) 6.79 1.21	3.01 6.92 HD/20 / 1 tschermakitic hornblende HD/20 / 1 43.36 0.46 13.32 0.01 4.43 11.10 0.25 10.85 0.00 12.29 1.38 0.43 0.02 2.04 99.94 23(O) 6.38 1.62	3.53 6.39 MDG/3 /1 actinolite MDG/3 /1 52.38 0.16 4.00 0.24 2.69 7.18 0.22 16.82 0.00 12.51 0.35 0.09 0.00 2.09 98.73 23(O) 7.51	3.10 6.87 MDG/7 /1 actinolitic hornblende MDG/7 /1 52.16 0.23 4.58 0.27 3.02 6.95 0.27 16.79 0.00 12.59 0.35 0.13 0.09 2.11 99.54 Cations. 7.43 0.57	3.18 6.79  MDG27/10 /1 actinolitic hornblende  MDG27/10 /1  51.92 0.17 4.69 0.30 0.75 9.35 0.18 16.15 0.00 12.95 0.41 0.11 0.00 2.09 99.06 23(O) 7.46 0.54	3.30 6.66 MDG/1/1 actinolite MDG/1/1 53.13 0.06 4.26 0.17 1.70 7.73 0.22 16.91 0.00 12.67 0.36 0.07 0.00 2.11 99.39 23(O) 7.55 0.45	3.10 6.86  MDG27/2 /1 actinolitic hornblende  MDG27/2 /1 51.73 0.21 5.07 0.08 0.72 8.80 0.18 16.18 0.00 12.70 0.43 0.17 0.00 2.08 98.35 23(O) 7.46 0.54
Mg/(Mg+Fe <sup>2</sup> ) Ca+Al <sup>IV</sup> Si Sample No. Mineral Ref. Point SiO <sub>2</sub> TiO <sub>2</sub> Al <sub>2</sub> O <sub>3</sub> Fe <sub>2</sub> O <sub>3</sub> Fe <sub>2</sub> O <sub>3</sub> Fe <sub>2</sub> O MnO MgO NiO CaO Na <sub>2</sub> O K <sub>2</sub> O BaO Cations. Si Al <sup>IV</sup> Al <sup>Vi</sup> Ti	0.62 3.15 6.81 HD/11/1 magnesio-hornblende HD/11/1 45.76 0.49 10.73 0.02 3.18 10.53 0.18 12.33 0.00 12.18 1.13 0.43 0.05 2.04 99.05 23(O) 6.72 1.28 0.58	3.13 6.76 HD/14/1 magnesio- hornblende HD/14/1 47.97 0.37 8.91 0.00 1.65 10.46 0.26 13.71 0.00 12.59 0.96 0.33 0.04 2.06 99.31 23(O) 6.98 1.02 0.50 0.04	3.23 6.68 HD/17/1 magnesio- hornblende HD/17/1 44.75 0.50 11.13 0.00 3.23 10.64 0.32 12.06 0.00 12.25 1.26 0.43 0.09 2.03 98.69 23(O) 6.62 1.38 0.57 0.06	3.05 6.89 HD/19 / 1 magnesio- hornblende HB/19 / 1 45.92 0.44 9.89 0.00 2.68 10.80 0.17 12.64 0.00 12.38 1.08 0.39 0.00 2.03 98.42 23(O) 6.79 1.21 0.51	3.01 6.92 HD/20 / 1 tschermakitic hornblende HD/20 / 1 43.36 0.46 13.32 0.01 4.43 11.10 0.25 10.85 0.00 12.29 1.38 0.43 0.02 2.04 99.94 23(O) 6.38 1.62 0.68 0.05	3.53 6.39 MDG/3 /1 actinolite MDG/3 /1 52.38 0.16 4.00 0.24 2.69 7.18 0.22 16.82 0.00 12.51 0.35 0.09 0.00 2.09 98.73 23(O) 7.51 0.49 0.18 0.02	3.10 6.87  MDG/7 /1 actinolitic hornblende MDG/7 /1 52.16 0.23 4.58 0.27 3.02 6.95 0.27 16.79 0.00 12.59 0.35 0.13 0.09 2.11 99.54 Cations. 7.43 0.57 0.20 0.02	3.18 6.79  MDG27/10 /1 actinolitic hornblende  MDG27/10 /1 51.92 0.17 4.69 0.30 0.75 9.35 0.18 16.15 0.00 12.95 0.41 0.11 0.00 2.09 99.06 23(O) 7.46 0.54 0.26 0.02	3.30 6.66  MDG/1/1  actinolite  MDG/1/1  53.13 0.06 4.26 0.17 1.70 7.73 0.22 16.91 0.00 12.67 0.36 0.07 0.00 2.11 99.39 23(O) 7.55 0.45 0.26 0.01	3.10 6.86 MDG27/2/1 actinolitic hormblende MDG27/2/1 51.73 0.21 5.07 0.08 0.72 8.80 0.18 16.18 0.00 12.70 0.43 0.17 0.00 2.08 98.35 23(O) 7.46 0.54 0.33 0.02
Mg/(Mg+Fe <sup>12</sup> ) Ca+Al <sup>IV</sup> Si Sample No. Mineral Ref. Point SiO <sub>2</sub> TiO <sub>2</sub> Al <sub>2</sub> O <sub>3</sub> Cr <sub>2</sub> O <sub>3</sub> Fe <sub>2</sub> O <sub>3</sub> Fe <sub>2</sub> O MnO MgO NiO CaO Na <sub>2</sub> O BaO H <sub>2</sub> O* Total Cations. Si Al <sup>IV</sup> Al <sup>Vi</sup> Ti Cr	0.62 3.15 6.81 HD/11/1 magnesio-hornblende HD/11/1 45.76 0.49 10.73 0.02 3.18 10.53 0.18 12.33 0.00 12.18 1.13 0.43 0.05 2.04 99.05 23(O) 6.72 1.28 0.58 0.05 0.00	3.13 6.76 HD/14 / 1 magnesio- homblende HD/14 / 1 47.97 0.37 8.91 0.00 1.65 10.46 0.26 13.71 0.00 12.59 0.96 0.33 0.04 2.06 99.31 23(O) 6.98 1.02 0.50 0.04	3.23 6.68 HD/17/1 magnesio- hornblende HD/17/1 44.75 0.50 11.13 0.00 3.23 10.64 0.32 12.06 0.00 12.25 1.26 0.43 0.09 2.03 98.69 23(O) 6.62 1.38 0.57 0.06	3.05 6.89 HD/19 / 1 magnesio- hornblende HD/19 / 1 45.92 0.44 9.89 0.00 2.68 10.80 0.17 12.64 0.00 12.38 1.08 0.39 0.00 2.03 98.42 23(O) 6.79 1.21 0.51 0.05	3.01 6.92 HD/20 / 1 tschermakitic hornblende HD/20 / 1 43.36 0.46 13.32 0.01 4.43 11.10 0.25 10.85 0.00 12.29 1.38 0.43 0.02 2.04 99.94 23(O) 6.38 1.62 0.68 0.05 0.00	3.53 6.39 MDG/3 /1 actinolite MDG/3 /1 52.38 0.16 4.00 0.24 2.69 7.18 0.22 16.82 0.00 12.51 0.35 0.09 0.00 2.09 98.73 23(O) 7.51 0.49 0.18 0.02 0.03	3.10 6.87  MDG/7 /1 actinolitic hornblende MDG/7 /1 52.16 0.23 4.58 0.27 3.02 6.95 0.27 16.79 0.00 12.59 0.35 0.13 0.09 2.11 99.54 Cations. 7.43 0.57 0.20 0.02	3.18 6.79  MDG27/10 /1 actinolitic hornblende  MDG27/10 /1  51.92 0.17 4.69 0.30 0.75 9.35 0.18 16.15 0.00 12.95 0.41 0.11 0.00 2.09 99.06 23(O) 7.46 0.54 0.26 0.02 0.03	3.30 6.66  MDG/1/1  actinolite  MDG/1/1  53.13 0.06 4.26 0.17 1.70 7.73 0.22 16.91 0.00 12.67 0.36 0.07 0.00 2.11 99.39 23(O) 7.55 0.45 0.26 0.01 0.02	3.10 6.86  MDG27/2 /1 actinolitic hormblende  MDG27/2 /1 51.73 0.21 5.07 0.08 0.72 8.80 0.18 16.18 0.00 12.70 0.43 0.17 0.00 2.08 98.35 23(O) 7.46 0.54 0.33 0.02 0.01
Mg/(Mg+Fe <sup>2</sup> ) Ca+Al <sup>W</sup> Si Sample No. Mineral Ref. Point SiO <sub>2</sub> TiO <sub>2</sub> Al <sub>2</sub> O <sub>3</sub> Cr <sub>2</sub> O <sub>3</sub> FeO MnO MgO NiO CaO Na <sub>2</sub> O BaO H <sub>2</sub> O* Total Cations. Si Al <sup>W</sup> Al <sup>W</sup> Ti Cr Fe <sup>3+</sup>	0.62 3.15 6.81 HD/11/1 magnesio-hornblende HD/11/1 45.76 0.49 10.73 0.02 3.18 10.53 0.18 12.33 0.00 12.18 1.13 0.43 0.05 2.04 99.05 2.3(0) 6.72 1.28 0.58 0.05 0.00 0.35	3.13 6.76 HD/14/1 magnesio-homblende HD/14/1 47.97 0.37 8.91 0.00 1.65 10.46 0.26 13.71 0.00 12.59 0.96 0.33 0.04 2.06 99.31 23(0) 6.98 1.02 0.50 0.04	3.23 6.68 HD/17 / 1 magnesio-homblende HD/17 / 1 44.75 0.50 11.13 0.00 3.23 10.64 0.32 12.06 0.00 12.25 1.26 0.43 0.09 2.03 98.69 2.3(0) 6.62 1.38 0.57 0.06 0.00 0.36	3.05 6.89 HD/19 / 1 magnesio-homblende HD/19 / 1 45.92 0.44 9.89 0.00 2.68 10.80 0.17 12.64 0.00 12.38 1.08 0.39 0.00 2.03 98.42 23(0) 6.79 1.21 0.51 0.05 0.00 0.30	3.01 6.92 HD/20 / 1 tschermakitic hornblende HD/20 / 1 43.36 0.46 13.32 0.01 4.43 11.10 0.25 10.85 0.00 12.29 1.38 0.43 0.02 2.04 99.94 23(0) 6.38 1.62 0.68 0.05 0.00 0.49	3.53 6.39 MDG/3 /1 actinolite MDG/3 /1 52.38 0.16 4.00 0.24 2.69 7.18 0.22 16.82 0.00 12.51 0.35 0.09 0.00 2.09 98.73 23(O) 7.51 0.49 0.18 0.02 0.03 0.29	3.10 6.87  MDG/7 /1 actinolitic hornblende  MDG/7 /1 52.16 0.23 4.58 0.27 3.02 6.95 0.27 16.79 0.00 12.59 0.35 0.13 0.09 2.11 99.54 Cations. 7.43 0.57 0.20 0.02 0.03 0.32	3.18 6.79  MDG27/10 /1 actinolitic hornblende  MDG27/10 /1  51.92 0.17 4.69 0.30 0.75 9.35 0.18 16.15 0.00 12.95 0.41 0.11 0.00 2.09 99.06 23(0) 7.46 0.54 0.26 0.02 0.03 0.08	3.30 6.66  MDG/1/1  actinolite  MDG/1/1  53.13 0.06 4.26 0.17 1.70 7.73 0.22 16.91 0.00 12.67 0.36 0.07 0.00 2.11 99.39 23(O) 7.55 0.45 0.26 0.01 0.02 0.18	3.10 6.86  MDG27/2 /1 actinolitic hormblende  MDG27/2 /1  51.73 0.21 5.07 0.08 0.72 8.80 0.18 16.18 0.00 12.70 0.043 0.17 0.00 2.08 98.35 23(O) 7.46 0.54 0.33 0.02 0.01 0.08
Mg/(Mg+Fe <sup>2</sup> ) Ca+Al N Si Sample No. Mineral Ref. Point SiO <sub>2</sub> TiO <sub>2</sub> Al <sub>2</sub> O <sub>3</sub> Fe <sub>2</sub> O <sub>3</sub> Fe <sub>2</sub> O <sub>3</sub> FeO MnO MgO NiO CaO Na <sub>2</sub> O K <sub>2</sub> O BaO H <sub>3</sub> O* Total Cations. Si Al N Ti Cr Fe <sup>3+</sup> Fe <sup>2+</sup>	0.62 3.15 6.81 HD/11/1 magnesio-hornblende HD/11/1 45.76 0.49 10.73 0.02 3.18 10.53 0.18 12.33 0.00 12.18 1.13 0.43 0.05 2.04 99.05 23(O) 6.72 1.28 0.58 0.05 0.05 0.00 0.35 1.29	3.13 6.76 HD/14 / 1 magnesio-homblende HD/14 / 1 47.97 0.37 8.91 0.00 1.65 10.46 0.26 13.71 0.00 12.59 0.96 0.33 0.04 2.06 99.31 23(O) 6.98 1.02 0.50 0.04 0.00 0.18	3.23 6.68 HD/17 / 1 magnesio-homblende HD/17 / 1 44.75 0.50 11.13 0.00 3.23 10.64 0.32 12.06 0.00 12.25 1.26 0.43 0.09 2.03 98.69 23(O) 6.62 1.38 0.57 0.06 0.00 0.36 1.32	3.05 6.89 HD/19 / 1 magnesio-hornblende HD/19 / 1 45.92 0.44 9.89 0.00 2.68 10.80 0.17 12.64 0.00 12.38 1.08 0.39 0.00 2.03 98.42 23(O) 6.79 1.21 0.51 0.05 0.00 0.30 1.33	3.01 6.92 HD/20 / 1 tschermakitic hornblende HD/20 / 1 43.36 0.46 13.32 0.01 4.43 11.10 0.25 10.85 0.00 12.29 1.38 0.43 0.02 2.04 99.94 23(O) 6.38 1.62 0.68 0.05 0.00 0.49 1.37	3.53 6.39 MDG/3 /1 actinolite MDG/3 /1 52.38 0.16 4.00 0.24 2.69 7.18 0.22 16.82 0.00 12.51 0.35 0.09 0.00 2.09 98.73 23(O) 7.51 0.49 0.18 0.02 0.03 0.29 0.86	3.10 6.87 MDG/7/1 actinolitic hornblende MDG/7/1 52.16 0.23 4.58 0.27 3.02 6.95 0.27 16.79 0.00 12.59 0.35 0.13 0.09 2.11 99.54 Cations. 7.43 0.57 0.20 0.02 0.03 0.32 0.83	3.18 6.79  MDG27/10 /1 actinolitic hornblende  MDG27/10 /1  51.92 0.17 4.69 0.30 0.75 9.35 0.18 16.15 0.00 12.95 0.41 0.11 0.00 2.09 99.06 23(O) 7.46 0.54 0.26 0.02 0.03 0.08 1.12	3.30 6.66  MDG/1/1 actinolite  MDG/1/1 53.13 0.06 4.26 0.17 1.70 7.73 0.22 16.91 0.00 12.67 0.36 0.07 0.00 2.11 99.39 23(O) 7.555 0.45 0.26 0.01 0.02 0.18 0.92	3.10 6.86  MDG27/2 /1 actinolitic homblende MDG27/2 /1 51.73 0.21 5.07 0.08 0.72 8.80 0.18 16.18 0.00 12.70 0.43 0.17 0.00 2.08 98.35 23(O) 7.46 0.54 0.33 0.02 0.01 0.08 1.06
Mg/(Mg+Fe <sup>2</sup> ) Ca+AI <sup>N</sup> Si Sample No. Mineral Ref. Point SiO <sub>2</sub> TiO <sub>2</sub> Al <sub>2</sub> O <sub>3</sub> Fe <sub>2</sub> O <sub>3</sub> Fe <sub>2</sub> O <sub>3</sub> Fe <sub>2</sub> O <sub>3</sub> Fe <sub>2</sub> O MnO MgO NiO CaO Na <sub>2</sub> O K <sub>2</sub> O BaO Caions. Si Al <sup>N</sup> Ti Cr Fe <sup>3+</sup> Fe <sup>2+</sup> Mn	0.62 3.15 6.81 HD/11/1 magnesio-hornblende HD/11/1 45.76 0.49 10.73 0.02 3.18 10.53 0.18 12.33 0.00 12.18 1.13 0.43 0.05 2.04 99.05 23(O) 6.72 1.28 0.58 0.05 0.00 0.35 1.29 0.02	3.13 6.76 HD/14 / 1 magnesio-hornblende HD/14 / 1 47.97 0.37 8.91 0.00 1.65 10.46 0.26 13.71 0.00 12.59 0.96 0.33 0.04 2.06 99.31 23(O) 6.98 1.02 0.50 0.04 0.00 0.18 1.27 0.03	3.23 6.68 HD/17 / 1 magnesio-hornblende HD/17 / 1 44.75 0.50 11.13 0.00 3.23 10.64 0.32 12.06 0.00 12.25 1.26 0.43 0.09 2.03 98.69 23(O) 6.62 1.38 0.57 0.06 0.00 0.36 1.32 0.04	3.05 6.89 HD/19 / 1 magnesio-hornblende HD/19 / 1 45.92 0.44 9.89 0.00 2.68 10.80 0.17 12.64 0.00 12.38 1.08 0.39 0.00 2.03 98.42 23(O) 6.79 1.21 0.51 0.05 0.00 0.30 1.33	3.01 6.92 HD/20 / 1 tschermakitic hornblende HD/20 / 1 43.36 0.46 13.32 0.01 4.43 11.10 0.25 10.85 0.00 12.29 1.38 0.43 0.02 2.04 99.94 23(O) 6.38 1.62 0.68 0.05 0.00 0.49 1.37 0.03	3.53 6.39 MDG/3 /1 actinolite MDG/3 /1 52.38 0.16 4.00 0.24 2.69 7.18 0.22 16.82 0.00 12.51 0.35 0.09 0.00 2.09 98.73 23(O) 7.51 0.49 0.18 0.02 0.03 0.29 0.86 0.03	3.10 6.87 MDG/7/1 actinolitic hornblende MDG/7/1 52.16 0.23 4.58 0.27 3.02 6.95 0.27 16.79 0.00 12.59 0.35 0.13 0.09 2.11 99.54 Cations. 7.43 0.57 0.20 0.02 0.03 0.32 0.83 0.03	3.18 6.79  MDG27/10 /1 actinolitic hornblende  MDG27/10 /1  51.92 0.17 4.69 0.30 0.75 9.35 0.18 16.15 0.00 12.95 0.41 0.11 0.00 2.09 99.06 23(O) 7.46 0.54 0.26 0.02 0.03 0.08 1.12 0.02	3.30 6.66  MDG/1 /1 actinolite  MDG/1 /1  53.13 0.06 4.26 0.17 1.70 7.73 0.22 16.91 0.00 12.67 0.36 0.07 0.00 2.11 99.39 23(O) 7.55 0.45 0.26 0.01 0.02 0.18 0.92 0.03	3.10 6.86  MDG27/2 /1 actinolitic hornblende MDG27/2 /1 51.73 0.21 5.07 0.08 0.72 8.80 0.18 16.18 0.00 12.70 0.43 0.17 0.00 2.08 98.35 23(O) 7.46 0.54 0.33 0.02 0.01 0.08 1.06 0.02
Mg/(Mg+Fe <sup>2</sup> ) Ca+Al <sup>IV</sup> Si Sample No. Mineral Ref. Point SiO <sub>2</sub> TiO <sub>2</sub> Al <sub>2</sub> O <sub>3</sub> Cr <sub>2</sub> O <sub>3</sub> Fe <sub>2</sub> O <sub>3</sub> Fe <sub>2</sub> O MnO MgO NiO CaO Na <sub>2</sub> O K <sub>2</sub> O BaO Cations. Si Al <sup>IV</sup> Total Cr Fe <sup>2+</sup> Fe <sup>2+</sup> Mn Mg	0.62 3.15 6.81 HD/11/1 magnesio- hornblende HD/11/1 45.76 0.49 10.73 0.02 3.18 10.53 0.18 12.33 0.00 12.18 1.13 0.43 0.05 2.04 99.05 23(O) 6.72 1.28 0.58 0.05 0.00 0.35 1.29 0.02 2.70	3.13 6.76 HD/14 / 1 magnesio- hornblende HD/14 / 1 47.97 0.37 8.91 0.00 1.65 10.46 0.26 13.71 0.00 12.59 0.96 0.33 0.04 2.06 99.31 23(O) 6.98 1.02 0.50 0.04 0.00 0.18 1.27 0.00	3.23 6.68 HD/17/1 magnesio-hornblende HD/17/1 44.75 0.50 11.13 0.00 3.23 10.64 0.32 12.06 0.00 12.25 1.26 0.43 0.09 2.03 98.69 23(O) 6.62 1.38 0.57 0.06 0.00 0.36 1.32 0.04 2.66	3.05 6.89 HD/19 / 1 magnesio- hornblende HD/19 / 1 45.92 0.44 9.89 0.00 2.68 10.80 0.17 12.64 0.00 12.38 1.08 0.39 0.00 2.03 98.42 23(O) 6.79 1.21 0.51 0.05 0.00 0.30 1.33 0.02 2.79	3.01 6.92 HD/20 / 1 tschermakitic hornblende HD/20 / 1 43.36 0.46 13.32 0.01 4.43 11.10 0.25 10.85 0.00 12.29 1.38 0.43 0.02 2.04 99.94 23(O) 6.38 1.62 0.68 0.05 0.00 0.49 1.37 0.03 2.38	3.53 6.39 MDG/3 /1 actinolite MDG/3 /1 52.38 0.16 4.00 0.24 2.69 7.18 0.22 16.82 0.00 12.51 0.35 0.09 0.00 2.09 98.73 23(O) 7.51 0.49 0.18 0.02 0.03 0.29 0.86 0.03 3.59	3.10 6.87  MDG/7 /1 actinolitic homblende MDG/7 /1 52.16 0.23 4.58 0.27 3.02 6.95 0.27 16.79 0.00 12.59 0.35 0.13 0.09 2.11 99.54  Cations. 7.43 0.57 0.20 0.02 0.03 0.32 0.83 0.03 3.56	3.18 6.79  MDG27/10 /1 actinolitic hornblende  MDG27/10 /1  51.92 0.17 4.69 0.30 0.75 9.35 0.18 16.15 0.00 12.95 0.41 0.11 0.00 2.09 99.06 23(O) 7.46 0.54 0.26 0.02 0.03 0.08 1.12 0.02 3.46	3.30 6.66  MDG/1 /1  actinolite  MDG/1 /1  53.13 0.06 4.26 0.17 1.70 7.73 0.22 16.91 0.00 12.67 0.36 0.07 0.00 2.11 99.39 23(O) 7.55 0.45 0.26 0.01 0.02 0.18 0.92 0.03 3.58	3.10 6.86  MDG27/2 /1 actinolitic hormblende MDG27/2 /1 51.73 0.21 5.07 0.08 0.72 8.80 0.18 16.18 0.00 12.70 0.43 0.17 0.00 2.08 98.35 23(O) 7.46 0.54 0.54 0.33 0.02 0.01 0.08 1.06 0.02 3.48
Mg/(Mg+Fe <sup>2</sup> ) Ca+Al <sup>W</sup> Si Sample No. Mineral Ref. Point SiO <sub>2</sub> TiO <sub>2</sub> Al <sub>2</sub> O <sub>3</sub> Cr <sub>2</sub> O <sub>3</sub> Fe <sub>2</sub> O <sub>3</sub> Fe <sub>2</sub> O <sub>3</sub> Fe <sub>2</sub> O MnO MgO NiO CaO Na <sub>2</sub> O K <sub>2</sub> O BaO Cations. Si Al <sup>W</sup> Ti Cr Fe <sup>3+</sup> Fe <sup>2+</sup> Mn	0.62 3.15 6.81 HD/11/1 magnesio-hornblende HD/11/1 45.76 0.49 10.73 0.02 3.18 10.53 0.18 12.33 0.00 12.18 1.13 0.43 0.05 2.04 99.05 23(O) 6.72 1.28 0.58 0.05 0.00 0.35 1.29 0.02	3.13 6.76 HD/14 / 1 magnesio-hornblende HD/14 / 1 47.97 0.37 8.91 0.00 1.65 10.46 0.26 13.71 0.00 12.59 0.96 0.33 0.04 2.06 99.31 23(O) 6.98 1.02 0.50 0.04 0.00 0.18 1.27 0.03	3.23 6.68 HD/17 / 1 magnesio-hornblende HD/17 / 1 44.75 0.50 11.13 0.00 3.23 10.64 0.32 12.06 0.00 12.25 1.26 0.43 0.09 2.03 98.69 23(O) 6.62 1.38 0.57 0.06 0.00 0.36 1.32 0.04	3.05 6.89 HD/19 / 1 magnesio-hornblende HD/19 / 1 45.92 0.44 9.89 0.00 2.68 10.80 0.17 12.64 0.00 12.38 1.08 0.39 0.00 2.03 98.42 23(O) 6.79 1.21 0.51 0.05 0.00 0.30 1.33	3.01 6.92 HD/20 / 1 tschermakitic hornblende HD/20 / 1 43.36 0.46 13.32 0.01 4.43 11.10 0.25 10.85 0.00 12.29 1.38 0.43 0.02 2.04 99.94 23(O) 6.38 1.62 0.68 0.05 0.00 0.49 1.37 0.03	3.53 6.39 MDG/3 /1 actinolite MDG/3 /1 52.38 0.16 4.00 0.24 2.69 7.18 0.22 16.82 0.00 12.51 0.35 0.09 0.00 2.09 98.73 23(O) 7.51 0.49 0.18 0.02 0.03 0.29 0.86 0.03	3.10 6.87 MDG/7/1 actinolitic hornblende MDG/7/1 52.16 0.23 4.58 0.27 3.02 6.95 0.27 16.79 0.00 12.59 0.35 0.13 0.09 2.11 99.54 Cations. 7.43 0.57 0.20 0.02 0.03 0.32 0.83 0.03	3.18 6.79  MDG27/10 /1 actinolitic hornblende  MDG27/10 /1  51.92 0.17 4.69 0.30 0.75 9.35 0.18 16.15 0.00 12.95 0.41 0.11 0.00 2.09 99.06 23(O) 7.46 0.54 0.26 0.02 0.03 0.08 1.12 0.02	3.30 6.66  MDG/1 /1 actinolite  MDG/1 /1  53.13 0.06 4.26 0.17 1.70 7.73 0.22 16.91 0.00 12.67 0.36 0.07 0.00 2.11 99.39 23(O) 7.55 0.45 0.26 0.01 0.02 0.18 0.92 0.03	3.10 6.86  MDG27/2 /1 actinolitic hornblende MDG27/2 /1 51.73 0.21 5.07 0.08 0.72 8.80 0.18 16.18 0.00 12.70 0.43 0.17 0.00 2.08 98.35 23(O) 7.46 0.54 0.33 0.02 0.01 0.08 1.06 0.02
Mg/(Mg+Fe <sup>2</sup> ) Ca+Al W Si Sample No. Mineral Ref. Point SiO <sub>2</sub> TiO <sub>2</sub> Al <sub>2</sub> O <sub>3</sub> Cr <sub>2</sub> O <sub>3</sub> Fe <sub>2</sub> O <sub>3</sub> Fe <sub>2</sub> O MnO MgO NiO CaO Na <sub>2</sub> O K <sub>2</sub> O BaO Ctions. Si Al <sup>10</sup> Ti Cr Fe <sup>2+</sup> Fe <sup>2+</sup> Mn Mg	0.62 3.15 6.81 HD/11/1 magnesio- hornblende HD/11/1 45.76 0.49 10.73 0.02 3.18 10.53 0.18 12.33 0.00 12.18 1.13 0.43 0.05 2.04 99.05 23(O) 6.72 1.28 0.58 0.05 0.00 0.35 1.29 0.02 2.70	3.13 6.76 HD/14 / 1 magnesio- hornblende HD/14 / 1 47.97 0.37 8.91 0.00 1.65 10.46 0.26 13.71 0.00 12.59 0.96 0.33 0.04 2.06 99.31 23(O) 6.98 1.02 0.50 0.04 0.00 0.18 1.27 0.00	3.23 6.68 HD/17/1 magnesio-hornblende HD/17/1 44.75 0.50 11.13 0.00 3.23 10.64 0.32 12.06 0.00 12.25 1.26 0.43 0.09 2.03 98.69 23(O) 6.62 1.38 0.57 0.06 0.00 0.36 1.32 0.04 2.66	3.05 6.89 HD/19 / 1 magnesio- hornblende HD/19 / 1 45.92 0.44 9.89 0.00 2.68 10.80 0.17 12.64 0.00 12.38 1.08 0.39 0.00 2.03 98.42 23(0) 6.79 1.21 0.51 0.05 0.00 0.30 1.33 0.00 2.79 0.00	3.01 6.92 HD/20 / 1 tschermakitic hornblende HD/20 / 1 43.36 0.46 13.32 0.01 4.43 11.10 0.25 10.85 0.00 12.29 1.38 0.43 0.02 2.04 99.94 23(O) 6.38 1.62 0.68 0.05 0.00 0.49 1.37 0.03 2.38	3.53 6.39 MDG/3 /1 actinolite MDG/3 /1 52.38 0.16 4.00 0.24 2.69 7.18 0.22 16.82 0.00 12.51 0.35 0.09 0.00 2.09 98.73 23(O) 7.51 0.49 0.18 0.02 0.03 0.29 0.86 0.03 3.59	3.10 6.87  MDG/7 /1 actinolitic hornblende MDG/7 /1 52.16 0.23 4.58 0.27 3.02 6.95 0.27 16.79 0.00 12.59 0.35 0.13 0.09 2.11 99.54  Cations. 7.43 0.57 0.20 0.02 0.03 0.32 0.83 0.03 3.56	3.18 6.79  MDG27/10 /1 actinolitic hornblende  MDG27/10 /1  51.92 0.17 4.69 0.30 0.75 9.35 0.18 16.15 0.00 12.95 0.41 0.11 0.00 2.09 99.06 23(0) 7.46 0.54 0.26 0.02 0.03 0.08 1.12 0.02 3.46 0.00	3.30 6.66  MDG/1 /1  actinolite  MDG/1 /1  53.13 0.06 4.26 0.17 1.70 7.73 0.22 16.91 0.00 12.67 0.36 0.07 0.00 2.11 99.39 23(O) 7.55 0.45 0.26 0.01 0.02 0.18 0.92 0.03 3.58	3.10 6.86  MDG27/2 /1 actinolitic hormblende MDG27/2 /1 51.73 0.21 5.07 0.08 0.72 8.80 0.18 16.18 0.00 12.70 0.043 0.17 0.00 2.08 98.35 23(O) 7.46 0.54 0.33 0.02 0.01 0.08 1.06 0.02 3.48
Mg/(Mg+Fe <sup>2</sup> ) Ca+Al <sup>IV</sup> Si Sample No. Mineral Ref. Point SiO <sub>2</sub> TiO <sub>2</sub> Al <sub>2</sub> O <sub>3</sub> Cr <sub>2</sub> O <sub>3</sub> FeO MnO MgO NiO CaO Na <sub>2</sub> O BaO H <sub>2</sub> O <sup>8</sup> Total Cations. Si Al <sup>IV</sup> Al <sup>Vi</sup> Ti Cr Fe <sup>3+</sup> Fe <sup>2+</sup> Mn Mg Ni Ca	0.62 3.15 6.81 HD/11/1 magnesio-hornblende HD/11/1/1 45.76 0.49 10.73 0.02 3.18 10.53 0.18 12.33 0.00 12.18 1.13 0.43 0.05 2.04 99.05 23(O) 6.72 1.28 0.58 0.05 0.00 0.35 1.29 0.02 2.70 0.00 1.92	3.13 6.76  HD/14 / 1  magnesio-homblende  HD/14 / 1  47.97 0.37 8.91 0.00 1.65 10.46 0.26 13.71 0.00 12.59 0.96 0.33 0.04 2.06 99.31 23(O) 6.98 1.02 0.50 0.04 0.00 0.18 1.27 0.03 2.97 0.00 1.96	3.23 6.68 HD/17 / 1 magnesio-homblende HD/17 / 1 44.75 0.50 11.13 0.00 3.23 10.64 0.32 12.06 0.00 12.25 1.26 0.43 0.09 2.03 98.69 23(0) 6.62 1.38 0.57 0.06 0.00 0.36 1.32 0.04 2.66 0.00 1.94	3.05 6.89 HD/19 / 1 magnesio-hornblende HD/19 / 1 45.92 0.44 9.89 0.00 2.68 10.80 0.17 12.64 0.00 12.38 1.08 0.39 0.00 2.03 98.42 23(O) 6.79 1.21 0.51 0.05 0.00 0.30 1.33 0.02 2.79 0.00 1.96	3.01 6.92 HD/20 / 1 tschermakitic hornblende HD/20 / 1 43.36 0.46 13.32 0.01 4.43 11.10 0.25 10.85 0.00 12.29 1.38 0.43 0.02 2.04 99.94 23(O) 6.38 1.62 0.68 0.05 0.00 0.49 1.37 0.03 2.38 0.00 1.94	3.53 6.39 MDG/3 /1 actinolite MDG/3 /1 52.38 0.16 4.00 0.24 2.69 7.18 0.22 16.82 0.00 12.51 0.35 0.09 0.00 2.09 98.73 23(O) 7.51 0.49 0.18 0.02 0.03 0.29 0.86 0.03 3.59 0.00 1.92	3.10 6.87  MDG/7 /1 actinolitic homblende MDG/7 /1 52.16 0.23 4.58 0.27 3.02 6.95 0.27 16.79 0.00 12.59 0.35 0.13 0.09 2.11 99.54 Cations. 7.43 0.57 0.20 0.02 0.03 0.32 0.83 0.03 3.56 0.00 1.92	3.18 6.79  MDG27/10 /1 actinolitic hornblende  MDG27/10 /1  51.92 0.17 4.69 0.30 0.75 9.35 0.18 16.15 0.00 12.95 0.41 0.11 0.00 2.09 99.06 23(0) 7.46 0.54 0.26 0.02 0.03 0.08 1.12 0.02 3.46 0.00 1.99	3.30 6.66  MDG/1/1 actinolite  MDG/1/1  53.13 0.06 4.26 0.17 1.70 7.73 0.22 16.91 0.00 12.67 0.36 0.07 0.00 2.11 99.39 23(O) 7.55 0.45 0.26 0.01 0.02 0.18 0.92 0.03 3.58 0.00 1.93	3.10 6.86  MDG27/2 /1 actinolitic hornblende  MDG27/2 /1 51.73 0.21 5.07 0.08 0.72 8.80 0.18 16.18 0.00 12.70 0.43 0.17 0.00 2.08 98.35 23(O) 7.46 0.54 0.33 0.02 0.01 0.08 1.06 0.02 3.48 0.00 1.96
Mg/(Mg+Fe <sup>2</sup> ) Ca+AI <sup>N</sup> Si Sample No. Mineral Ref. Point SiO <sub>2</sub> TiO <sub>2</sub> Al <sub>2</sub> O <sub>3</sub> Fe <sub>2</sub> O <sub>3</sub> Fe <sub>2</sub> O <sub>3</sub> Fe <sub>2</sub> O <sub>3</sub> Fe <sub>2</sub> O <sub>4</sub> MnO MgO NiO CaO Na <sub>2</sub> O K <sub>2</sub> O BaO Cations. Si Al <sup>N</sup> Ti Cr Fe <sup>2+</sup> Fe <sup>2+</sup> Mn Mg Ni Ca Na Na	0.62 3.15 6.81 HD/11/1 magnesio-hornblende HD/11/1 45.76 0.49 10.73 0.02 3.18 10.53 0.18 12.33 0.00 12.18 1.13 0.43 0.05 2.04 99.05 23(O) 6.72 1.28 0.58 0.05 0.00 0.35 1.29 0.02 2.70 0.00 1.92 0.32	3.13 6.76  HD/14 / 1  magnesio- hornblende  HD/14 / 1  47.97 0.37 8.91 0.00 1.65 10.46 0.26 13.71 0.00 12.59 0.96 0.33 0.04 2.06 99.31 23(O) 6.98 1.02 0.50 0.04 0.00 0.18 1.27 0.03 2.97 0.00 1.96 0.27	3.23 6.68 HD/17 / 1 magnesio-hornblende HD/17 / 1 44.75 0.50 11.13 0.00 3.23 10.64 0.32 12.06 0.00 12.25 1.26 0.43 0.09 2.03 98.69 23(O) 6.62 1.38 0.57 0.06 0.00 0.36 1.32 0.04 2.66 0.00 1.94 0.36	3.05 6.89 HD/19 / 1 magnesio-hornblende HD/19 / 1 45.92 0.44 9.89 0.00 2.68 10.80 0.17 12.64 0.00 12.38 1.08 0.39 0.00 2.03 98.42 23(O) 6.79 1.21 0.51 0.05 0.00 0.30 1.33 0.02 2.79 0.00 1.96 0.31	3.01 6.92 HD/20 / 1 tschermakitic hornblende HD/20 / 1 43.36 0.46 13.32 0.01 4.43 11.10 0.25 10.85 0.00 12.29 1.38 0.43 0.02 2.04 99.94 23(O) 6.38 1.62 0.68 0.05 0.00 0.49 1.37 0.03 2.38 0.00 1.94 0.39	3.53 6.39 MDG/3 /1 actinolite MDG/3 /1 52.38 0.16 4.00 0.24 2.69 7.18 0.22 16.82 0.00 12.51 0.35 0.09 0.00 2.09 98.73 23(O) 7.51 0.49 0.18 0.02 0.03 0.29 0.86 0.03 3.59 0.00 1.92 0.10	3.10 6.87  MDG/7 /1 actinolitic hornblende MDG/7 /1 52.16 0.23 4.58 0.27 3.02 6.95 0.27 16.79 0.00 12.59 0.35 0.13 0.09 2.11 99.54 Cations. 7.43 0.57 0.20 0.02 0.03 0.32 0.83 0.03 3.56 0.00 1.92 0.10	3.18 6.79  MDG27/10 /1 actinolitic hornblende  MDG27/10 /1  51.92 0.17 4.69 0.30 0.75 9.35 0.18 16.15 0.00 12.95 0.41 0.11 0.00 2.09 99.06 23(O) 7.46 0.54 0.26 0.02 0.03 0.08 1.12 0.02 3.46 0.00 1.99 0.11	3.30 6.66  MDG/1 /1 actinolite  MDG/1 /1  53.13 0.06 4.26 0.17 1.70 7.73 0.22 16.91 0.00 12.67 0.36 0.07 0.00 2.11 99.39 23(O) 7.55 0.45 0.26 0.01 0.02 0.18 0.92 0.03 3.58 0.00 1.93 0.10	3.10 6.86  MDG27/2 /1 actinolitic hornblende  MDG27/2 /1 51.73 0.21 5.07 0.08 0.72 8.80 0.18 16.18 0.00 12.70 0.43 0.17 0.00 2.08 98.35 23(O) 7.46 0.54 0.33 0.02 0.01 0.08 1.06 0.02 3.48 0.00 1.96 0.12
Mg/(Mg+Fe²²) Ca+Al N Si Sample No. Mineral Ref. Point SiO2 TiO2 Al2O3 Fe2O3 Fe2O3 Fe2O MnO MgO NiO CaO Na2O K2O BaO H2O* Total Cations. Si Al 1'i Al v'i Ti Cr Fe³²² Fe²² Mn Mg Ni Ca Na Mg Ni Ca Na Mg Ni Ca Na Mg Ni Ca Na	0.62 3.15 6.81 HD/11/1 magnesio-hornblende HD/11/1 45.76 0.49 10.73 0.02 3.18 10.53 0.18 12.33 0.00 12.18 1.13 0.43 0.05 2.04 99.05 23(O) 6.72 1.28 0.58 0.05 0.00 0.35 1.29 0.02 2.70 0.00 1.92 0.32 0.08	3.13 6.76 HD/14/1 magnesio-hornblende HD/14/1 47.97 0.37 8.91 0.00 1.65 10.46 0.26 13.71 0.00 12.59 0.96 0.33 0.04 2.06 99.31 23(O) 6.98 1.02 0.50 0.04 0.00 0.18 1.27 0.03 2.97 0.00 1.96 0.27 0.06	3.23 6.68 HD/17/1 magnesio-hornblende HD/17/1 44.75 0.50 11.13 0.00 3.23 10.64 0.32 12.06 0.00 12.25 1.26 0.43 0.09 2.03 98.69 23(O) 6.62 1.38 0.57 0.06 0.00 0.36 1.32 0.04 2.66 0.00 1.94 0.36 0.08	3.05 6.89 HD/19 / 1 magnesio- hornblende HD/19 / 1 45.92 0.44 9.89 0.00 2.68 10.80 0.17 12.64 0.00 12.38 1.08 0.39 0.00 2.03 98.42 23(O) 6.79 1.21 0.51 0.05 0.00 0.30 1.33 0.02 2.79 0.00 1.96 0.31 0.07	3.01 6.92 HD/20 / 1 tschermaktiic hornblende HD/20 / 1 43.36 0.46 13.32 0.01 4.43 11.10 0.25 10.85 0.00 12.29 1.38 0.43 0.02 2.04 99.94 23(O) 6.38 1.62 0.68 0.05 0.00 0.49 1.37 0.03 2.38 0.00 1.94 0.39 0.08	3.53 6.39 MDG/3 /1 actinolite MDG/3 /1 52.38 0.16 4.00 0.24 2.69 7.18 0.22 16.82 0.00 12.51 0.35 0.09 0.00 2.09 98.73 23(O) 7.51 0.49 0.18 0.02 0.03 0.29 0.86 0.03 3.59 0.00 1.92 0.10 0.02	3.10 6.87  MDG/7 /1 actinolitic hornblende MDG/7 /1 52.16 0.23 4.58 0.27 3.02 6.95 0.27 16.79 0.00 12.59 0.35 0.13 0.09 2.11 99.54 Cations. 7.43 0.57 0.20 0.02 0.03 0.32 0.83 0.03 3.56 0.00 1.92 0.10 0.02	3.18 6.79  MDG27/10 /1 actinolitic hormblende  MDG27/10 /1 51.92 0.17 4.69 0.30 0.75 9.35 0.18 16.15 0.00 12.95 0.41 0.11 0.00 2.09 99.06 23(O) 7.46 0.54 0.26 0.02 0.03 0.08 1.12 0.02 3.46 0.00 1.99 0.11 0.02	3.30 6.66  MDG/1 /1 actinolite  MDG/1 /1 53.13 0.06 4.26 0.17 1.70 7.73 0.22 16.91 0.00 12.67 0.36 0.07 0.00 2.111 99.39 23(O) 7.55 0.45 0.26 0.01 0.02 0.18 0.92 0.03 3.58 0.00 1.93 0.10 0.01	3.10 6.86  MDG27/2 /1 actinolitic hormblende MDG27/2 /1 51.73 0.21 5.07 0.08 0.72 8.80 0.18 16.18 0.00 12.70 0.43 0.17 0.00 2.08 98.35 23(O) 7.46 0.54 0.33 0.02 0.01 0.08 1.06 0.02 3.48 0.00 1.96 0.12 0.03
Mg/(Mg+Fe²²) Ca+A1 N Si Sample No. Mineral Ref. Point SiO <sub>2</sub> TiO <sub>2</sub> Al <sub>2</sub> O <sub>3</sub> Cr <sub>2</sub> O <sub>3</sub> FeO MnO MgO NiO CaO Ma <sub>2</sub> O BaO H <sub>2</sub> O* Total Cations. Si Al iv Al vi Ti Cr Fe²²² Mn Mg Ni Ca Nag Ni Ca	0.62 3.15 6.81 HD/11/1 magnesio-hornblende HD/11/1 45.76 0.49 10.73 0.02 3.18 10.53 0.18 12.33 0.00 12.18 1.13 0.43 0.05 2.04 99.05 23(O) 6.72 1.28 0.58 0.05 0.00 0.35 1.29 0.02 2.70 0.00 1.92 0.32 0.08 0.00	3.13 6.76  HD/14 / 1 magnesio- hornblende  HD/14 / 1  47.97 0.37 8.91 0.00 1.65 10.46 0.26 13.71 0.00 12.59 0.96 0.33 0.04 2.06 99.31 23(O) 6.98 1.02 0.50 0.04 0.00 0.18 1.27 0.03 2.97 0.00 1.96 0.27 0.06 0.00	3.23 6.68 HD/17 / 1 magnesio- hornblende HD/17 / 1 44.75 0.50 11.13 0.00 3.23 10.64 0.32 12.06 0.00 12.25 1.26 0.43 0.09 2.03 98.69 23(O) 6.62 1.38 0.57 0.06 0.00 0.36 1.32 0.04 2.66 0.00 1.94 0.36 0.08 0.01	3.05 6.89 HD/19 / 1 magnesio- hornblende HD/19 / 1 45.92 0.44 9.89 0.00 2.68 10.80 0.17 12.64 0.00 12.38 1.08 0.39 0.00 2.03 98.42 23(O) 6.79 1.21 0.51 0.05 0.00 0.30 1.33 0.02 2.79 0.00 1.96 0.31 0.07 0.00	3.01 6.92 HD/20 / 1 tschermakitic hornblende HD/20 / 1 43.36 0.46 13.32 0.01 4.43 11.10 0.25 10.85 0.00 12.29 1.38 0.43 0.02 2.04 99.94 23(O) 6.38 1.62 0.68 0.05 0.00 0.49 1.37 0.03 2.38 0.00 1.94 0.39 0.08 0.00	3.53 6.39 MDG/3 /1 actinolite MDG/3 /1 52.38 0.16 4.00 0.24 2.69 7.18 0.22 16.82 0.00 12.51 0.35 0.09 0.00 2.09 98.73 23(O) 7.51 0.49 0.118 0.02 0.03 0.29 0.86 0.03 3.59 0.00 1.92 0.10 0.02 0.00	3.10 6.87  MDG/7 /1 actinolitic hornblende MDG/7 /1 52.16 0.23 4.58 0.27 3.02 6.95 0.27 16.79 0.00 12.59 0.35 0.13 0.09 2.11 99.54 Cations. 7.43 0.57 0.20 0.02 0.03 0.32 0.83 0.03 3.56 0.00 1.92 0.10 0.02 0.01	3.18 6.79  MDG27/10 /1 actinolitic hornblende  MDG27/10 /1  51.92 0.17 4.69 0.30 0.75 9.35 0.18 16.15 0.00 12.95 0.41 0.11 0.00 2.09 99.06 23(O) 7.46 0.54 0.26 0.02 0.03 0.08 1.12 0.02 3.46 0.00 1.99 0.11 0.02 0.00	3.30 6.66  MDG/1/1  actinolite  MDG/1/1  53.13 0.06 4.26 0.17 1.70 7.73 0.22 16.91 0.00 12.67 0.36 0.07 0.00 2.11 99.39 23(O) 7.55 0.45 0.26 0.01 0.02 0.18 0.92 0.03 3.58 0.00 1.93 0.10 0.01 0.00	3.10 6.86  MDG27/2 /1 actinolitic hormblende MDG27/2 /1 51.73 0.21 5.07 0.08 0.72 8.80 0.18 16.18 0.00 12.70 0.043 0.17 0.00 2.08 98.35 23(O) 7.46 0.54 0.33 0.02 0.01 0.08 1.06 0.02 3.48 0.00 1.96 0.12 0.03 0.00
Mg/(Mg+Fe <sup>2</sup> ) Ca+Al <sup>W</sup> Si Sample No. Mineral Ref. Point SiO <sub>2</sub> TiO <sub>2</sub> Al <sub>2</sub> O <sub>3</sub> Cr <sub>2</sub> O <sub>3</sub> Fe <sub>2</sub> O <sub>3</sub> Fe <sub>2</sub> O MnO MgO NiO CaO Na <sub>2</sub> O BaO H <sub>2</sub> O* Total Cations. Si Al <sup>W</sup> Ti Cr Fe <sup>3+</sup> Fe <sup>2+</sup> Mn Mg Ni Ca Na K Ba OH*	0.62 3.15 6.81 HD/11/1 magnesio-hornblende HD/11/1 45.76 0.49 10.73 0.02 3.18 10.53 0.18 12.33 0.00 12.18 1.13 0.43 0.05 2.04 99.05 23(O) 6.72 1.28 0.58 0.05 0.00 0.35 1.29 0.02 2.70 0.00 1.92 0.32 0.08 0.00 2.00	3.13 6.76  HD/14 / 1  magnesio-homblende  HD/14 / 1  47.97 0.37 8.91 0.00 1.65 10.46 0.26 13.71 0.00 12.59 0.96 0.33 0.04 2.06 99.31 23(O) 6.98 1.02 0.50 0.04 0.00 0.18 1.27 0.03 2.97 0.00 1.96 0.27 0.06 0.00 2.00	3.23 6.68 HD/17 / 1 magnesio-homblende HD/17 / 1 44.75 0.50 11.13 0.00 3.23 10.64 0.32 12.06 0.00 12.25 1.26 0.43 0.09 2.03 98.69 23(0) 6.62 1.38 0.57 0.06 0.00 0.36 1.32 0.04 2.66 0.00 1.94 0.36 0.00 1.94 0.36 0.08 0.01 2.00	3.05 6.89 HD/19 / 1 magnesio-homblende HD/19 / 1 45.92 0.44 9.89 0.00 2.68 10.80 0.17 12.64 0.00 12.38 1.08 0.39 0.00 2.03 98.42 23(0) 6.79 1.21 0.51 0.05 0.00 0.30 1.33 0.02 2.79 0.00 1.96 0.31 0.07 0.00 2.00	3.01 6.92 HD/20 / 1 tschermakitic hornblende HD/20 / 1 43.36 0.46 13.32 0.01 4.43 11.10 0.25 10.85 0.00 12.29 1.38 0.43 0.02 2.04 23(0) 6.38 1.62 0.68 0.05 0.00 0.49 1.37 0.03 2.38 0.00 1.94 0.39 0.08 0.00 2.00	3.53 6.39 MDG/3 /1 actinolite MDG/3 /1 52.38 0.16 4.00 0.24 2.69 7.18 0.22 16.82 0.00 12.51 0.35 0.09 0.00 2.09 98.73 23(O) 7.51 0.49 0.18 0.02 0.03 0.29 0.86 0.03 3.59 0.00 1.92 0.10 0.02 0.00 2.00	3.10 6.87  MDG/7 /1 actinolitic hornblende  MDG/7 /1 52.16 0.23 4.58 0.27 3.02 6.95 0.27 16.79 0.00 12.59 0.35 0.13 0.09 2.11 99.54 Cations. 7.43 0.57 0.20 0.03 0.32 0.83 0.03 3.56 0.00 1.92 0.10 0.02 0.01 2.00	3.18 6.79  MDG27/10 /1 actinolitic hornblende  MDG27/10 /1  51.92 0.17 4.69 0.30 0.75 9.35 0.18 16.15 0.00 12.95 0.41 0.11 0.00 2.09 99.06 23(0) 7.46 0.54 0.26 0.02 0.03 0.08 1.12 0.02 3.46 0.00 1.99 0.11 0.02 0.00 2.00	3.30 6.66  MDG/1/1  actinolite  MDG/1/1  53.13 0.06 4.26 0.17 1.70 7.73 0.22 16.91 0.00 12.67 0.36 0.07 0.00 2.11 99.39 23(O) 7.55 0.45 0.26 0.01 0.02 0.18 0.92 0.03 3.58 0.00 1.93 0.10 0.00 2.00	3.10 6.86  MDG27/2 /1 actinolitic hormblende MDG37/2 /1 51.73 0.21 5.07 0.08 0.72 8.80 0.18 16.18 0.00 12.70 0.43 0.17 0.00 2.08 9.35 23(O) 7.46 0.54 0.33 0.02 0.01 0.08 1.06 0.02 3.48 0.00 1.96 0.12 0.03 0.00 2.00
Mg/(Mg+Fe <sup>2</sup> ) Ca+Al <sup>W</sup> Si Sample No. Mineral Ref. Point SiO <sub>2</sub> TiO <sub>2</sub> Al <sub>2</sub> O <sub>3</sub> Cr <sub>2</sub> O <sub>3</sub> FeO MnO MgO NiO CaO Na <sub>2</sub> O K <sub>2</sub> O BaO H <sub>2</sub> O* Total Cations. Si Al <sup>W</sup> Ti Cr Fe <sup>2+</sup> Mn Mg Ni Ca Na	0.62 3.15 6.81 HD/11/1 magnesio-hornblende HD/11/1 45.76 0.49 10.73 0.02 3.18 10.53 0.18 12.33 0.00 12.18 1.13 0.43 0.05 2.04 99.05 23(O) 6.72 1.28 0.58 0.05 0.00 0.35 1.29 0.02 2.70 0.00 1.92 0.32 0.08 0.00	3.13 6.76  HD/14 / 1 magnesio- hornblende  HD/14 / 1  47.97 0.37 8.91 0.00 1.65 10.46 0.26 13.71 0.00 12.59 0.96 0.33 0.04 2.06 99.31 23(O) 6.98 1.02 0.50 0.04 0.00 0.18 1.27 0.03 2.97 0.00 1.96 0.27 0.06 0.00	3.23 6.68 HD/17 / 1 magnesio- hornblende HD/17 / 1 44.75 0.50 11.13 0.00 3.23 10.64 0.32 12.06 0.00 12.25 1.26 0.43 0.09 2.03 98.69 23(O) 6.62 1.38 0.57 0.06 0.00 0.36 1.32 0.04 2.66 0.00 1.94 0.36 0.08 0.01	3.05 6.89 HD/19 / 1 magnesio- hornblende HD/19 / 1 45.92 0.44 9.89 0.00 2.68 10.80 0.17 12.64 0.00 12.38 1.08 0.39 0.00 2.03 98.42 23(O) 6.79 1.21 0.51 0.05 0.00 0.30 1.33 0.02 2.79 0.00 1.96 0.31 0.07 0.00	3.01 6.92 HD/20 / 1 tschermakitic hornblende HD/20 / 1 43.36 0.46 13.32 0.01 4.43 11.10 0.25 10.85 0.00 12.29 1.38 0.43 0.02 2.04 99.94 23(O) 6.38 1.62 0.68 0.05 0.00 0.49 1.37 0.03 2.38 0.00 1.94 0.39 0.08 0.00	3.53 6.39 MDG/3 /1 actinolite MDG/3 /1 52.38 0.16 4.00 0.24 2.69 7.18 0.22 16.82 0.00 12.51 0.35 0.09 0.00 2.09 98.73 23(O) 7.51 0.49 0.118 0.02 0.03 0.29 0.86 0.03 3.59 0.00 1.92 0.10 0.02 0.00	3.10 6.87  MDG/7 /1 actinolitic hornblende MDG/7 /1 52.16 0.23 4.58 0.27 3.02 6.95 0.27 16.79 0.00 12.59 0.35 0.13 0.09 2.11 99.54 Cations. 7.43 0.57 0.20 0.02 0.03 0.32 0.83 0.03 3.56 0.00 1.92 0.10 0.02 0.01	3.18 6.79  MDG27/10 /1 actinolitic hornblende  MDG27/10 /1  51.92 0.17 4.69 0.30 0.75 9.35 0.18 16.15 0.00 12.95 0.41 0.11 0.00 2.09 99.06 23(O) 7.46 0.54 0.26 0.02 0.03 0.08 1.12 0.02 3.46 0.00 1.99 0.11 0.02 0.00	3.30 6.66  MDG/1/1  actinolite  MDG/1/1  53.13 0.06 4.26 0.17 1.70 7.73 0.22 16.91 0.00 12.67 0.36 0.07 0.00 2.11 99.39 23(O) 7.55 0.45 0.26 0.01 0.02 0.18 0.92 0.03 3.58 0.00 1.93 0.10 0.01 0.00	3.10 6.86  MDG27/2 /1 actinolitic hornblende MDG27/2 /1 51.73 0.21 5.07 0.08 0.72 8.80 0.18 16.18 0.00 12.70 0.043 0.17 0.00 2.08 98.35 23(O) 7.46 0.54 0.33 0.02 0.01 0.08 1.06 0.02 3.48 0.00 1.96 0.12 0.03 0.00
Mg/(Mg+Fe <sup>2</sup> ) Ca+Al <sup>W</sup> Si Sample No. Mineral Ref. Point SiO <sub>2</sub> TiO <sub>2</sub> Al <sub>2</sub> O <sub>3</sub> Cr <sub>2</sub> O <sub>3</sub> Fe <sub>2</sub> O <sub>3</sub> Fe <sub>2</sub> O MnO MgO NiO CaO Na <sub>2</sub> O BaO H <sub>2</sub> O* Total Cations. Si Al <sup>W</sup> Ti Cr Fe <sup>2+</sup> Mn Mg Ni Ca Na K Ba OH*	0.62 3.15 6.81 HD/11/1 magnesio-hornblende HD/11/1 45.76 0.49 10.73 0.02 3.18 10.53 0.18 12.33 0.00 12.18 1.13 0.43 0.05 2.04 99.05 23(O) 6.72 1.28 0.58 0.05 0.00 0.35 1.29 0.02 2.70 0.00 1.92 0.32 0.08 0.00 2.00	3.13 6.76  HD/14 / 1  magnesio-homblende  HD/14 / 1  47.97 0.37 8.91 0.00 1.65 10.46 0.26 13.71 0.00 12.59 0.96 0.33 0.04 2.06 99.31 23(O) 6.98 1.02 0.50 0.04 0.00 0.18 1.27 0.03 2.97 0.00 1.96 0.27 0.06 0.00 2.00	3.23 6.68 HD/17 / 1 magnesio-homblende HD/17 / 1 44.75 0.50 11.13 0.00 3.23 10.64 0.32 12.06 0.00 12.25 1.26 0.43 0.09 2.03 98.69 23(0) 6.62 1.38 0.57 0.06 0.00 0.36 1.32 0.04 2.66 0.00 1.94 0.36 0.00 1.94 0.36 0.08 0.01 2.00	3.05 6.89 HD/19 / 1 magnesio-homblende HD/19 / 1 45.92 0.44 9.89 0.00 2.68 10.80 0.17 12.64 0.00 12.38 1.08 0.39 0.00 2.03 98.42 23(0) 6.79 1.21 0.51 0.05 0.00 0.30 1.33 0.02 2.79 0.00 1.96 0.31 0.07 0.00 2.00	3.01 6.92 HD/20 / 1 tschermakitic hornblende HD/20 / 1 43.36 0.46 13.32 0.01 4.43 11.10 0.25 10.85 0.00 12.29 1.38 0.43 0.02 2.04 23(0) 6.38 1.62 0.68 0.05 0.00 0.49 1.37 0.03 2.38 0.00 1.94 0.39 0.08 0.00 2.00	3.53 6.39 MDG/3 /1 actinolite MDG/3 /1 52.38 0.16 4.00 0.24 2.69 7.18 0.22 16.82 0.00 12.51 0.35 0.09 0.00 2.09 98.73 23(O) 7.51 0.49 0.18 0.02 0.03 0.29 0.86 0.03 3.59 0.00 1.92 0.10 0.02 0.00 2.00	3.10 6.87  MDG/7 /1 actinolitic hornblende  MDG/7 /1 52.16 0.23 4.58 0.27 3.02 6.95 0.27 16.79 0.00 12.59 0.35 0.13 0.09 2.11 99.54 Cations. 7.43 0.57 0.20 0.03 0.32 0.83 0.03 3.56 0.00 1.92 0.10 0.02 0.01 2.00	3.18 6.79  MDG27/10 /1 actinolitic hornblende  MDG27/10 /1  51.92 0.17 4.69 0.30 0.75 9.35 0.18 16.15 0.00 12.95 0.41 0.11 0.00 2.09 99.06 23(0) 7.46 0.54 0.26 0.02 0.03 0.08 1.12 0.02 3.46 0.00 1.99 0.11 0.02 0.00 2.00	3.30 6.66  MDG/1/1  actinolite  MDG/1/1  53.13 0.06 4.26 0.17 1.70 7.73 0.22 16.91 0.00 12.67 0.36 0.07 0.00 2.11 99.39 23(O) 7.55 0.45 0.26 0.01 0.02 0.18 0.92 0.03 3.58 0.00 1.93 0.10 0.00 2.00	3.10 6.86  MDG27/2/1 actinolitic hornblende MDG27/2/1 51.73 0.21 5.07 0.08 0.72 8.80 0.18 16.18 0.00 12.70 0.43 0.17 0.00 2.08 9.35 23(O) 7.46 0.54 0.33 0.02 0.01 0.08 1.06 0.02 3.48 0.00 1.96 0.12 0.03 0.00 2.00
Mg/(Mg+Fe <sup>2</sup> ) Ca+Al <sup>W</sup> Si Sample No. Mineral Ref. Point SiO <sub>2</sub> TiO <sub>2</sub> Al <sub>2</sub> O <sub>3</sub> Fe <sub>2</sub> O <sub>3</sub> Fe <sub>2</sub> O <sub>3</sub> Fe <sub>2</sub> O <sub>3</sub> Fe <sub>2</sub> O MnO MgO NiO CaO Na <sub>2</sub> O K <sub>2</sub> O BaO H <sub>2</sub> O* Total Cations. Si Al <sup>10</sup> Al <sup>11</sup> Ti Cr Fe <sup>3+</sup> Fe <sup>2+</sup> Mn Mg Ni Ca Na Na Na Na Na K Ba OH* Total (Na+K) (A)	0.62 3.15 6.81 HD/11/1 magnesio-hornblende HD/11/1 45.76 0.49 10.73 0.02 3.18 10.53 0.18 12.33 0.00 12.18 1.13 0.43 0.05 2.04 99.05 23(O) 6.72 1.28 0.58 0.05 0.00 0.35 1.29 0.02 2.70 0.00 1.92 0.32 0.08 0.00 0.00 0.32 0.32	3.13 6.76 HD/14/1 magnesio-hornblende HD/14/1 47.97 0.37 8.91 0.00 1.65 10.46 0.26 13.71 0.00 12.59 0.96 0.33 0.04 2.06 99.31 23(O) 6.98 1.02 0.50 0.04 0.00 0.18 1.27 0.03 2.97 0.00 1.96 0.27 0.06 0.00 2.00 17.30 0.29	3.23 6.68 HD/17/1 magnesio-hornblende HD/17/1 44.75 0.50 11.13 0.00 3.23 10.64 0.32 12.06 0.00 12.25 1.26 0.43 0.09 2.03 98.69 23(O) 6.62 1.38 0.57 0.06 0.00 0.36 1.32 0.04 2.66 0.00 1.94 0.36 0.08 0.01 2.00 17.39 0.39	3.05 6.89 HD/19 / 1 magnesio- hornblende HD/19 / 1 45.92 0.44 9.89 0.00 2.68 10.80 0.17 12.64 0.00 12.38 1.08 0.39 0.00 2.03 98.42 23(O) 6.79 1.21 0.51 0.05 0.00 0.30 1.33 0.02 2.79 0.00 1.96 0.31 0.07 0.00 2.00 17.34 0.34	3.01 6.92 HD/20 / 1 tschermakitic hornblende HD/20 / 1 43.36 0.46 13.32 0.01 4.43 11.10 0.25 10.85 0.00 12.29 1.38 0.43 0.02 2.04 99.94 23(O) 6.38 1.62 0.68 0.05 0.00 0.49 1.37 0.03 2.38 0.00 1.94 0.39 0.08 0.00 0.09 1.94 0.39 0.08 0.00 0.00 0.49 1.37	3.53 6.39 MDG/3 /1 actinolite MDG/3 /1 52.38 0.16 4.00 0.24 2.69 7.18 0.22 16.82 0.00 12.51 0.35 0.09 0.00 2.09 98.73 23(O) 7.51 0.49 0.18 0.02 0.03 0.29 0.86 0.03 3.59 0.00 1.92 0.10 0.02 0.00 1.92 0.10 0.02 0.00 2.00 1.703 0.03	3.10 6.87  MDG/7 /1 actinolitic hornblende MDG/7 /1 52.16 0.23 4.58 0.27 3.02 6.95 0.27 16.79 0.00 12.59 0.35 0.13 0.09 2.11 99.54 Cations. 7.43 0.57 0.20 0.02 0.03 0.32 0.83 0.03 3.56 0.00 1.92 0.10 0.02 0.01 2.00 1.92 0.01 0.02 0.01 2.00 17.05	3.18 6.79  MDG27/10 /1 actinolitic hormblende  MDG27/10 /1 51.92 0.17 4.69 0.30 0.75 9.35 0.18 16.15 0.00 12.95 0.41 0.11 0.00 2.09 99.06 23(O) 7.46 0.54 0.26 0.02 0.03 0.08 1.12 0.02 3.46 0.00 1.99 0.11 0.02 0.00 1.99 0.11 0.02 0.00 1.7.13 0.13	3.30 6.66  MDG/1/1 actinolite  MDG/1/1 53.13 0.06 4.26 0.17 1.70 7.73 0.22 16.91 0.00 12.67 0.36 0.07 0.00 2.11 99.39 23(O) 7.55 0.45 0.26 0.01 0.02 0.18 0.92 0.03 3.58 0.00 1.93 0.10 0.01 0.00 2.00 1.993 0.10 0.01 0.00 0.00 0.00 0.00 0.00 0.0	3.10 6.86  MDG27/2 /1 actinolitic hormblende MDG27/2 /1 51.73 0.21 5.07 0.08 0.72 8.80 0.18 16.18 0.00 12.70 0.43 0.17 0.00 2.08 98.35 23(O) 7.46 0.54 0.33 0.02 0.01 0.08 1.06 0.02 3.48 0.00 1.96 0.12 0.03 0.00 2.00 1.96
Mg/(Mg+Fe <sup>2</sup> ) Ca+Al <sup>W</sup> Si Sample No. Mineral Ref. Point SiO <sub>2</sub> TiO <sub>2</sub> Al <sub>2</sub> O <sub>3</sub> Fe <sub>2</sub> O <sub>3</sub> Fe <sub>2</sub> O <sub>3</sub> Fe <sub>2</sub> O <sub>3</sub> FeO MnO MgO NiO CaO Na <sub>2</sub> O K <sub>2</sub> O BaO Cations. Si Al <sup>W</sup> Ti Cr Fe <sup>2</sup> Mn Mg Ni Cr Fe <sup>2</sup> Mn Mg Ni Ca Na Na K Ba OH* Total	0.62 3.15 6.81 HD/11/1 magnesio-hornblende HD/11/1 45.76 0.49 10.73 0.02 3.18 10.53 0.18 12.33 0.00 12.18 1.13 0.43 0.05 2.04 99.05 23(O) 6.72 1.28 0.58 0.05 0.00 0.35 1.29 0.02 2.70 0.00 1.92 0.32 0.08 0.00 2.00 17.32	3.13 6.76  HD/14 / 1  magnesio-homblende  HD/14 / 1  47.97 0.37 8.91 0.00 1.65 10.46 0.26 13.71 0.00 12.59 0.96 0.33 0.04 2.06 99.31 23(O) 6.98 1.02 0.50 0.04 0.00 0.18 1.27 0.03 2.97 0.00 1.96 0.27 0.06 0.00 2.00 17.30	3.23 6.68 HD/17 / 1 magnesio-hornblende HD/17 / 1 44.75 0.50 11.13 0.00 3.23 10.64 0.32 12.06 0.00 12.25 1.26 0.43 0.09 2.03 98.69 23(O) 6.62 1.38 0.57 0.06 0.00 0.36 1.32 0.04 2.66 0.00 0.36 1.32 0.04 2.66 0.00 1.94 0.36 0.08 0.01 2.00 17.39	3.05 6.89 HD/19 / 1 magnesio-hornblende HD/19 / 1 45.92 0.44 9.89 0.00 2.68 10.80 0.17 12.64 0.00 12.38 1.08 0.39 0.00 2.03 98.42 23(O) 6.79 1.21 0.51 0.05 0.00 0.30 1.33 0.02 2.79 0.00 1.96 0.31 0.07 0.00 2.00 17.34	3.01 6.92 HD/20 / 1 tschermakitic hornblende HD/20 / 1 43.36 0.46 13.32 0.01 4.43 11.10 0.25 10.85 0.00 12.29 1.38 0.43 0.02 2.04 99.94 23(O) 6.38 1.62 0.68 0.05 0.00 0.49 1.37 0.03 2.38 0.00 1.94 0.39 0.08 0.00 1.94 0.39 0.08 0.00 2.00 17.41	3.53 6.39 MDG/3 /1 actinolite MDG/3 /1 52.38 0.16 4.00 0.24 2.69 7.18 0.22 16.82 0.00 12.51 0.35 0.09 0.00 2.09 98.73 23(O) 7.51 0.49 0.18 0.02 0.03 0.29 0.86 0.03 3.59 0.00 1.92 0.10 0.02 0.00 1.92 0.110 0.02 0.00 1.703	3.10 6.87  MDG/7 /1 actinolitic hornblende MDG/7 /1 52.16 0.23 4.58 0.27 3.02 6.95 0.27 16.79 0.00 12.59 0.35 0.13 0.09 2.11 99.54 Cations. 7.43 0.57 0.20 0.02 0.03 0.32 0.83 0.03 3.56 0.00 1.92 0.10 0.02 0.01 2.00 17.05	3.18 6.79  MDG27/10 /1 actinolitic hornblende  MDG27/10 /1  51.92 0.17 4.69 0.30 0.75 9.35 0.18 16.15 0.00 12.95 0.41 0.11 0.00 2.09 99.06 23(O) 7.46 0.54 0.26 0.02 0.03 0.08 1.12 0.02 3.46 0.00 1.99 0.11 0.00 2.09 0.11 0.00 2.00 1.99 0.11	3.30 6.66  MDG/1/1 actinolite  MDG/1/1 53.13 0.06 4.26 0.17 1.70 7.73 0.22 16.91 0.00 12.67 0.36 0.07 0.00 2.11 99.39 23(O) 7.55 0.45 0.26 0.01 0.02 0.18 0.92 0.03 3.58 0.00 1.93 0.10 0.01 0.01 0.01 0.00 2.00 17.04	3.10 6.86  MDG27/2/1 actinolitic hornblende MDG27/2/1 51.73 0.21 5.07 0.08 0.72 8.80 0.18 16.18 0.00 12.70 0.43 0.17 0.00 2.08 98.35 23(O) 7.46 0.54 0.33 0.02 0.01 0.08 1.06 0.02 3.48 0.00 1.96 0.12 0.03 0.00 1.96 0.12 0.03 0.00 1.96 0.12 0.03 0.00 1.96 0.12 0.03 0.00 1.96 0.12 0.03 0.00 1.96 0.12 0.03 0.00 1.96 0.12 0.03 0.00 1.96 0.12 0.03 0.00 1.96 0.12 0.03 0.00 1.96 0.11

Table 4.1 continues.....

Sample No.	MDG27/4 / 1	MDG27/5 /1	MDG27/6 /1	MDG27/8 / 1	MDG27/10 /1	MDG27/13 /1	MDG27/17 /1	MDG27/20 /1	MDG27/22 /1	MDG27/(27/1	MDG27/11 /1
Mineral	actinolitic hornblende	actinolite	actinolite	actinolite	actinolite	actinolite	actinolitic hornblende	actinolitic hornblende	actinolite	actinolite	Alumino- magnesio-
Ref. Point	MDG27/4 / 1	MDG27/5 /1	MDG27/6 /1	MDG27/8 / 1	MDG27/10 /1	MDG27/13 /1	MDG27/17 /1	MDG27/20 /1	MDG27/22 /1	MDG27/(27/1	MDG27/11 /1
SiO <sub>2</sub>	51.71	52.93	54.15	53.03	52.65	52.25	52.25	51.77	52.35	54.15	46.19
$TiO_2$	0.18	0.19	0.14	0.09	0.16	0.14	0.12	0.34	0.19	0.00	0.16
$Al_2O_3$	5.11	3.91	2.82	3.90	4.63	4.48	4.65	5.39	4.15	2.52	15.35
$Cr_2O_3$	0.18	0.16	0.10	0.13	0.28	0.25	0.18	0.01	0.14	0.01	0.04
$Fe_2O_3$	0.79	1.94	0.61	0.50	0.93	1.99	2.20	0.60	0.90	1.27	0.00
FeO	9.05	7.48	8.16	8.79	8.60	7.56	7.92	9.17	8.46	7.28	7.64
MnO	0.23	0.16	0.16	0.19	0.14	0.23	0.18	0.14	0.18	0.19	0.04
MgO	16.11	16.94	17.61	16.83	16.55	16.50	16.62	16.00	16.67	17.89	9.94
NiO	0.00	0.00	0.00	0.00	0.00	0.00	0.00	0.00	0.00	0.00	0.00
CaO	12.81	12.50	12.89	12.87	12.81	12.48	12.76	12.78	12.83	12.75	17.77
Na <sub>2</sub> O	0.52	0.32	0.24	0.37	0.35	0.33	0.45	0.41	0.29	0.19	0.25
$K_2O$	0.11	0.09	0.04	0.07	0.08	0.06	0.07	0.12	0.10	0.06	0.06
BaO	0.00	0.00	0.00	0.00	0.06	0.00	0.00	0.00	0.00	0.00	0.00
$H_2O*$	2.08	2.10	2.11	2.09	2.10	2.09	2.10	2.09	2.08	2.10	2.09
Total	98.88	98.71	99.03	98.86	99.33	98.36	99.50	98.82	98.34	98.41	99.53
Cations.	23(O)	23(O)	23(O)	23(O)	23(O)	Cations.	23(O)	23(O)	23(O)	23(O)	23(O)
Si	7.44	7.57	7.71	7.59	7.51	7.51	7.45	7.44	7.54	7.74	6.62
Al iv	0.56	0.43	0.29	0.41	0.49	0.49	0.55	0.56	0.46	0.26	1.38
Al vi	0.30	0.23	0.18	0.25	0.29	0.27	0.23	0.35	0.25	0.16	1.22
Ti	0.02	0.02	0.01	0.01	0.02	0.02	0.01	0.04	0.02	0.00	0.02
Cr	0.02	0.02	0.01	0.01	0.03	0.03	0.02	0.00	0.02	0.00	0.00
Fe <sup>3+</sup>	0.09	0.21	0.07	0.05	0.10	0.22	0.24	0.06	0.10	0.14	0.00
Fe <sup>2+</sup>	1.09	0.89	0.97	1.05	1.03	0.91	0.94	1.10	1.02	0.87	0.92
Mn	0.03	0.02	0.02	0.02	0.02	0.03	0.02	0.02	0.02	0.02	0.00
Mg	3.45	3.61	3.74	3.59	3.52	3.54	3.53	3.43	3.58	3.81	2.13
Ni	0.00	0.00	0.00	0.00	0.00	0.00	0.00	0.00	0.00	0.00	0.00
Ca	1.97	1.92	1.97	1.97	1.96	1.92	1.95	1.97	1.98	1.95	2.73
Na	0.15	0.09	0.07	0.10	0.10	0.09	0.12	0.11	0.08	0.05	0.07
K	0.02	0.02	0.01	0.01	0.01	0.01	0.01	0.02	0.02	0.01	0.01
Ba	0.00	0.00	0.00	0.00	0.00	0.00	0.00	0.00	0.00	0.00	0.00
OH*	2.00	2.00	2.00	2.00	2.00	2.00	2.00	2.00	2.00	2.00	2.00
Total	17.14	17.02	17.04	17.09	17.07	17.02	17.09	17.10	17.08	17.02	17.10
(Na+K) (A)	0.14	0.02	0.04	0.09	0.07	0.02	0.09	0.10	0.08	0.02	0.08
$Mg/(Mg+Fe^{+2})$	0.76	0.80	0.79	0.77	0.77	0.80	0.79	0.76	0.78	0.81	0.70
Ca+Al IV	2.54	2.35	2.26	2.38	2.45	2.41	2.50	2.53	2.44	2.22	4.11
Si	7.44	7.57	7.71	7.59	7.51	7.51	7.45	7.44	7.54	7.74	6.62

Sample No.	MDG27/12/1	MDG27/24 /1	HD/21 /1
Mineral	magnesio-	magnesio-	magnesio-
	hornblende	hornblende	hornblende
Ref. Point	MDG27/12/1	MDG27/24 /1	HD/21 /1
$SiO_2$	44.93	46.17	47.59
$TiO_2$	0.46	0.54	0.41
$Al_2O_3$	12.70	10.29	8.56
$Cr_2O_3$	0.22	0.41	0.01
$Fe_2O_3$	0.00	2.09	1.11
FeO	11.38	10.55	10.91
MnO	0.24	0.16	0.19
MgO	11.09	12.71	13.41
NiO	0.00	0.00	0.00
CaO	14.20	12.38	12.43
$Na_2O$	0.71	0.90	0.91
$K_2O$	0.42	0.56	0.33
BaO	0.00	0.00	0.00
$H_2O*$	2.03	2.04	2.03
Total	98.38	98.80	97.89
Cations.	23(O)	23(O)	23(O)
Si	6.64	6.78	7.02
Al iv	1.36	1.22	0.98
Al vi	0.85	0.56	0.51
Ti	0.05	0.06	0.05
Cr	0.03	0.05	0.00
Fe <sup>3+</sup>	0.00	0.23	0.12
Fe <sup>2+</sup>	1.41	1.30	1.35
Mn	0.03	0.02	0.02
Mg	2.44	2.78	2.95
Ni	0.00	0.00	0.00
Ca	2.25	1.95	1.96
Na	0.20	0.26	0.26
K	0.08	0.10	0.06
Ba	0.00	0.00	0.00
OH*	2.00	2.00	2.00
Total	17.33	17.31	17.29
(Na+K) (A)	0.28	0.31	0.29
$Mg/(Mg+Fe^{+2})$	0.63	0.68	0.69
Ca+Al IV	3.61	3.17	2.94
Si	6.64	6.78	7.02

Table 4.1. a. Representative electron microprobe (EPMA) analysis of olivine from the ultramafic rocks of Madawara ultramafic complex (MUC).

Table-4.2	Olivine composit							
Sample No.	MW/16/Ol pyr		17	MW/16/Ol pyr	MW/16/Ol pyr	17	MW/16/Ol pyr	MW/16/Ol pyr
Mineral	Olivine	Olivine	Olivine	Olivine	Olivine	Olivine	Olivine	Olivine
Ref.point	8/1.	9/1.	10 / 1 .	11 / 1 .	21 / 1 .	22 / 1 .	23 / 1 .	13 / 1 .
$SiO_2$	39.46	39.49	39.04	39.46	38.45	38.66	38.80	39.24
$TiO_2$	0.02	0.01	0.00	0.02	0.03	0.01	0.00	0.01
$Al_2O_3$	0.00	0.04	0.00	0.02	0.02	0.03	0.01	0.01
$Cr_2O_3$	0.02	0.17	0.00	0.00	0.70	0.07	0.08	0.12
$FeO_T$	21.39	21.50	21.09	21.19	22.05	20.96	21.78	21.40
MnO	0.29	0.25	0.26	0.21	0.23	0.29	0.20	0.23
MgO	40.41	40.26	40.17	40.37	39.08	39.55	40.06	40.26
CaO	0.00	0.00	0.00	0.04	0.02	0.03	0.02	0.03
Na <sub>2</sub> O	0.02	0.00	0.02	0.02	0.00	0.01	0.01	0.03
$K_2O$	0.02	0.01	0.00	0.01	0.01	0.00	0.00	0.00
NiO	0.00	0.00	0.00	0.00	0.00	0.00	0.00	0.00
Total	101.63	101.72	100.57	101.34	100.58	99.61	100.97	101.32
$Fe_2O_3$	0.00	0.00	0.00	0.00	0.00	0.00	0.46	0.00
FeO	21.39	21.50	21.09	21.19	22.05	20.96	21.36	21.40
Total	101.63	101.72	100.57	101.34	100.58	99.61	101.01	101.32
Cations:	4(O)	4(O)	4(O)	4(O)	4(O)	4(O)	4(O)	4(O)
Si	1.00	1.00	1.00	1.00	0.99	1.00	0.99	1.00
Ti	0.00	0.00	0.00	0.00	0.00	0.00	0.00	0.00
Al	0.00	0.00	0.00	0.00	0.00	0.00	0.00	0.00
Cr	0.00	0.00	0.00	0.00	0.01	0.00	0.00	0.00
Fe <sup>+3</sup>	0.00	0.00	0.00	0.00	0.00	0.00	0.01	0.00
Fe <sup>+2</sup>	0.45	0.46	0.45	0.45	0.48	0.45	0.46	0.46
Mn	0.01	0.01	0.01	0.00	0.01	0.01	0.00	0.00
Mg	1.53	1.52	1.54	1.53	1.51	1.53	1.53	1.53
Ca	0.00	0.00	0.00	0.00	0.00	0.00	0.00	0.00
Na	0.00	0.00	0.00	0.00	0.00	0.00	0.00	0.00
K	0.00	0.00	0.00	0.00	0.00	0.00	0.00	0.00
Ni	0.00	0.00	0.00	0.00	0.00	0.00	0.00	0.00
Total	3.00	2.99	3.00	3.00	3.00	3.00	3.00	3.00
Mol.per cent end	l-members :							
Forsterite (Fo)	77.11	76.95	77.25	77.25	75.96	77.08	76.97	77.03
Fayalite (Fa)	22.89	23.05	22.75	22.75	24.04	22.92	23.03	22.97
Total	100.00	100.00	100.00	100.00	100.00	100.00	100.00	100.00
Notes: $Fo = 100^\circ$	* (Mg/Mg+Fe), & 1	Fa = 100* (Fe/Fe-	⊦Mg)					
Sample No.	MW/16/Ol pyr	MW/16/Ol pyr	MW/16/Ol pyr	MW/16/Ol pyr	MW/16/Ol pyr	MW/16/Ol pyr	MW/16/Ol pyr	MW/16/Ol pyr
Mineral	Olivine	Olivine	Olivine	Olivine	Olivine	Olivine	Olivine	Olivine
Ref.point	24 / 1 .	25 / 1 .	11/1.	4/1.	5/1.	6/1.	7/1.	8/1.
SiO <sub>2</sub>	38.76	39.29	37.81	37.38	38.21	37.99	38.25	38.73

Sample No.	MW/16/Ol pyr	MW/16/Ol pyr	MW/16/Ol pyr	MW/16/OI pyr	MW/16/Ol pyr	MW/16/Ol pyr	MW/16/Ol pyr	MW/16/Ol pyr
Mineral	Olivine							
Ref.point	24 / 1 .	25 / 1 .	11/1.	4/1.	5 / 1 .	6/1.	7 / 1 .	8 / 1 .
SiO <sub>2</sub>	38.76	39.29	37.81	37.38	38.21	37.99	38.25	38.73
$TiO_2$	0.03	0.00	0.09	0.07	0.01	0.02	0.00	0.01
$Al_2O_3$	0.00	0.01	0.06	0.00	0.00	0.02	0.00	0.01
$Cr_2O_3$	0.00	0.00	1.29	0.55	0.02	0.01	0.04	0.00
$FeO_T$	21.61	20.61	22.13	21.34	21.39	20.79	21.20	20.74
MnO	0.29	0.21	0.33	0.23	0.32	0.26	0.21	0.26
MgO	40.02	40.03	38.87	38.38	39.16	38.82	39.33	39.89
CaO	0.00	0.00	0.00	0.00	0.00	0.00	0.02	0.01
Na <sub>2</sub> O	0.03	0.00	0.01	0.00	0.01	0.00	0.00	0.00
$K_2O$	0.01	0.01	0.01	0.00	0.01	0.03	0.00	0.00
NiO	0.00	0.00	0.00	0.15	0.09	0.11	0.13	0.17
Total	100.75	100.17	100.60	98.10	99.22	98.05	99.18	99.82
$Fe_2O_3$	0.54	0.00	0.45	0.26	0.22	0.00	0.13	0.00
FeO	21.13	20.61	21.72	21.11	21.19	20.79	21.08	20.74
Total	100.80	100.17	100.65	98.13	99.24	98.05	99.19	99.82
Cations:	4(O)							
Si	1.00	1.01	0.98	0.99	1.00	1.00	1.00	1.00
Ti	0.00	0.00	0.00	0.00	0.00	0.00	0.00	0.00
Al	0.00	0.00	0.00	0.00	0.00	0.00	0.00	0.00
Cr	0.00	0.00	0.03	0.01	0.00	0.00	0.00	0.00
Fe <sup>+3</sup>	0.01	0.00	0.01	0.01	0.00	0.00	0.00	0.00
Fe <sup>+2</sup>	0.45	0.44	0.47	0.47	0.46	0.46	0.46	0.45
Mn	0.01	0.00	0.01	0.01	0.01	0.01	0.00	0.01
Mg	1.53	1.53	1.50	1.52	1.52	1.53	1.53	1.54
Ca	0.00	0.00	0.00	0.00	0.00	0.00	0.00	0.00
Na	0.00	0.00	0.00	0.00	0.00	0.00	0.00	0.00
K	0.00	0.00	0.00	0.00	0.00	0.00	0.00	0.00
Ni	0.00	0.00	0.00	0.00	0.00	0.00	0.00	0.00
Total	3.00	2.99	3.00	3.00	3.00	3.00	3.00	3.00
Mol.per cent end	l-members :							
Forsterite (Fo)	77.15	77.59	76.13	76.42	76.71	76.90	76.88	77.42
Fayalite (Fa)	22.85	22.41	23.87	23.58	23.29	23.10	23.12	22.58
Total	100.00	100.00	100.00	100.00	100.00	100.00	100.00	100.00

Notes: Fo = 100\* (Mg/Mg+Fe), & Fa = 100\* (Fe/Fe+Mg)

Table 4.2 Continued.....

Sample No.	MW/16/Ol pyr							
Sample No. Mineral	Olivine							
Ref.point	9/1.	10 / 1 .	11 / 1 .	12 / 1 .	13 / 1 .	40 / 1 .	1/1.	2 / 1 .
SiO <sub>2</sub>	38.56	38.62	37.83	38.30	35.95	38.66	37.73	38.13
TiO <sub>2</sub>	0.01	0.00	0.00	0.03	0.25	0.00	0.06	0.04
Al <sub>2</sub> O <sub>3</sub>	0.00	0.00	0.00	0.00	0.04	0.00	0.07	0.00
$Cr_2O_3$	0.01	0.02	0.04	0.03	2.45	0.07	1.21	0.18
FeO <sub>T</sub>	20.81	20.69	21.14	21.24	23.17	21.21	21.69	21.17
MnO	0.25	0.23	0.22	0.30	0.35	0.28	0.35	0.25
MgO	39.70	39.26	38.92	39.13	38.59	39.96	38.86	39.93
CaO	0.00	0.00	0.01	0.00	0.00	0.02	0.00	0.00
Na <sub>2</sub> O	0.00	0.00	0.00	0.02	0.00	0.00	0.00	0.00
$K_2O$	0.00	0.00	0.00	0.01	0.00	0.00	0.01	0.02
NiO	0.20	0.04	0.11	0.28	0.24	0.24	0.23	0.10
Total	99.54	98.86	98.27	99.34	101.04	100.44	100.21	99.82
Fe <sub>2</sub> O <sub>3</sub>	0.00	0.00	0.27	0.04	3.65	0.36	0.45	1.06
FeO	20.81	20.69	20.89	21.20	19.88	20.88	21.28	20.22
Total	99.54	98.86	98.30	99.34	101.41	100.48	100.26	99.93
Cations:	4(O)							
Si	1.00	1.01	1.00	1.00	0.93	1.00	0.98	0.99
Ti	0.00	0.00	0.00	0.00	0.00	0.00	0.00	0.00
Al	0.00	0.00	0.00	0.00	0.00	0.00	0.00	0.00
Cr	0.00	0.00	0.00	0.00	0.05	0.00	0.02	0.00
Fe <sup>+3</sup>	0.00	0.00	0.01	0.00	0.07	0.01	0.01	0.02
Fe <sup>+2</sup>	0.45	0.45	0.46	0.46	0.43	0.45	0.46	0.44
Mn	0.01	0.01	0.00	0.01	0.01	0.01	0.01	0.01
Mg	1.54	1.53	1.53	1.52	1.49	1.53	1.51	1.54
Ca	0.00	0.00	0.00	0.00	0.00	0.00	0.00	0.00
Na	0.00	0.00	0.00	0.00	0.00	0.00	0.00	0.00
K	0.00	0.00	0.00	0.00	0.00	0.00	0.00	0.00
Ni	0.00	0.00	0.00	0.01	0.01	0.00	0.00	0.00
Total	3.00	2.99	3.00	3.00	3.00	3.00	3.00	3.00
Mol.per cent en								
Forsterite (Fo)	77.27	77.18	76.85	76.69	77.58	77.33	76.50	77.88
Fayalite (Fa)	22.73	22.82	23.15	23.31	22.42	22.67	23.50	22.12
Total	100.00	100.00	100.00	100.00	100.00	100.00	100.00	100.00

Notes: Fo = 100\* (Mg/Mg+Fe), & Fa = 100\* (Fe/Fe+Mg)

Table 4.3.a Representative electron microprobe (EPMA) analysis of serpentines from the MUC.

Table-4.3.a Serpentine composition of the ultramafic-mafic of MUC

Sample No.	MD/15/2	MD/15/2	MD/15/2	MD/15/2	MD/15/1	MD/15/1	MD/15/1	MD/15/1	MD/16	MD/16	MD/16
Mineral	Serp.	Serp.	Serp.	Serp.	Serp.	Serp.	Serp.	Serp.	Serp.	Serp.	Serp.
Ref.point	44 / 1 .	46 / 1 .	5/1.	7/1.	1/1.	9/1.	31 / 1 .	35 / 1 .	16/1-	20/1-	41/1-
$SiO_2$	43.31	39.59	42.02	42.38	40.43	41.69	43.39	42.27	40.89	40.96	41.35
$TiO_2$	0.05	0.00	0.01	0.03	0.09	0.01	0.00	0.00	0.03	0.03	0.03
$Al_2O_3$	2.37	0.96	2.38	1.74	2.62	2.45	0.56	1.42	1.56	2.54	2.79
$Cr_2O_3$	0.60	0.41	0.52	0.07	0.29	0.06	0.01	0.10	0.00	0.04	0.27
FeOT	8.53	8.19	8.45	7.68	7.62	8.13	7.37	7.55	4.48	4.31	4.59
MnO	0.07	0.10	0.15	0.06	0.09	0.07	0.07	0.11	0.07	0.10	0.18
MgO	33.06	35.93	34.42	34.42	32.54	34.38	35.63	35.02	36.18	35.81	36.65
CaO	0.03	0.02	0.03	0.06	0.04	0.02	0.00	0.00	0.00	0.02	0.03
Na2O	0.01	0.01	0.00	0.01	0.03	0.02	0.00	0.00	0.01	0.05	0.01
K2O	0.02	0.01	0.00	0.03	0.02	0.02	0.02	0.00	0.03	0.03	0.01
NiO	0.23	0.28	0.33	0.29	0.23	0.27	0.19	0.19			
Total	88.28	85.50	88.31	86.77	84.00	87.12	87.24	86.66	83.24	83.89	85.90
Fe2O3	0.00	1.13	0.00	0.00	0.00	0.00	0.00	0.00	0.00	4.31	0.00
FeO	8.53	7.17	8.45	7.68	7.62	8.13	7.37	7.55	4.48	0.00	4.59
Total	88.28	85.61	88.31	86.77	84.00	87.12	87.24	86.66	83.24	83.89	85.90
Cations:	7(O)	7(O)	7(O)	7(O)	7(O)	7(O)	7(O)	7(O)	7(O)	7(O)	7(O)
Si	2.04	1.94	1.99	2.03	2.00	2.00	2.06	2.03	2.01	1.70	1.97
Ti	0.00	0.00	0.00	0.00	0.00	0.00	0.00	0.00	0.00	0.00	0.00
Al	0.13	0.06	0.13	0.10	0.15	0.14	0.03	0.08	0.09	0.12	0.16
Cr	0.02	0.02	0.02	0.00	0.01	0.00	0.00	0.00	0.00	0.00	0.01
Fe+3	0.00	0.04	0.00	0.00	0.00	0.00	0.00	0.00	0.00	0.13	0.00
Fe+2	0.34	0.29	0.33	0.31	0.32	0.33	0.29	0.30	0.18	0.00	0.18
Mn	0.00	0.00	0.01	0.00	0.00	0.00	0.00	0.00	0.00	0.00	0.01
Mg	2.33	2.63	2.43	2.46	2.40	2.45	2.52	2.50	2.65	2.21	2.61
Ca	0.00	0.00	0.00	0.00	0.00	0.00	0.00	0.00	0.00	0.00	0.00
Na	0.00	0.00	0.00	0.00	0.00	0.00	0.00	0.00	0.00	0.00	0.00
K	0.00	0.00	0.00	0.00	0.00	0.00	0.00	0.00	0.00	0.00	0.00
Ni	0.01	0.01	0.01	0.01	0.01	0.01	0.01	0.01	0.00	0.00	0.00
Total	4.88	5.00	4.93	4.92	4.91	4.93	4.92	4.93	4.94	4.18	4.94

Note: Serp, Serpentine.
Table 4.3.b Chlorite composition of the ultramafic-mafic of MUC

Sample	Ik/13/P	Ik/13/P	Ik/13/P	Ik/13/P	Ik/13/P	Mw/16/Ol Pyr	Mw/16/Ol Pyr	MW/8/P
Mineral	Chl	Chl	Chl	Chl	Chl	Chl	Chl	Chl
Ref. Point	1	2	4/1-	4	15/1-	16-18/1	16-21/1	8-35/1
SiO <sub>2</sub>	29.93	33.13	32.20	31.86	32.42	31.61	31.32	29.75
$TiO_2$	0.07	0.05	0.07	0.07	0.06	0.03	0.04	0.06
$Al_2O_3$	17.56	13.68	13.38	12.42	12.87	17.81	16.01	16.79
$Cr_2O_3$	0.32	0.83	2.22	2.42	2.43	0.62	1.07	1.16
$Fe_2O_3$	0.00	0.65	0.00	0.55	0.52	0.68	0.42	0.00
FeO	7.97	6.79	7.29	6.79	6.86	3.68	5.04	4.91
MnO	0.01	0.01	0.00	0.06	0.09	0.00	0.05	0.10
MgO	29.17	30.53	30.96	29.48	30.00	31.62	30.77	30.67
NiO	0.19	0.33	0.29	0.35	0.20	0.25	0.02	0.06
CaO	0.03	0.04	0.10	0.10	0.13	0.02	0.02	0.02
Na <sub>2</sub> O	0.01	0.03	0.03	0.01	0.05	0.02	0.08	0.02
$K_2O$	0.01	0.04	0.03	0.01	0.05	0.02	0.02	0.01
BaO	0.00	0.02	0.00	0.00	0.00	0.00	0.02	0.00
H2O*	12.14	12.30	12.29	11.92	12.15	12.54	12.24	12.05
Total	97.41	98.42	98.86	96.05	97.84	98.89	97.10	95.59
Cations	28(O)	28(O)	28(O)	28(O)	28(O)	28(O)	28(O)	28(O)
Si	5.91	6.45	6.28	6.40	6.39	6.03	6.13	5.92
Al 1V	2.09	1.55	1.72	1.60	1.61	1.97	1.87	2.08
Al vi	2.00	1.59	1.36	1.35	1.38	2.05	1.83	1.86
Ti	0.01	0.01	0.01	0.01	0.01	0.00	0.01	0.01
Cr	0.05	0.13	0.34	0.38	0.38	0.09	0.17	0.18
Fe <sup>3+</sup>	0.00	0.09	0.00	0.08	0.08	0.10	0.06	0.00
Fe <sup>2+</sup>	1.33	1.11	1.19	1.14	1.13	0.59	0.82	0.83
Mn	0.00	0.00	0.00	0.01	0.02	0.00	0.01	0.02
Mg	8.58	8.86	9.01	8.83	8.81	8.99	8.98	9.10
Ni	0.03	0.05	0.05	0.06	0.03	0.03	0.00	0.01
Ca	0.01	0.01	0.02	0.02	0.03	0.00	0.00	0.00
Na	0.01	0.02	0.02	0.01	0.04	0.01	0.06	0.02
K	0.01	0.02	0.01	0.01	0.03	0.01	0.01	0.01
Ba	0.00	0.00	0.00	0.00	0.00	0.00	0.00	0.00
OH*	16.00	16.00	16.00	16.00	16.00	16.00	16.00	16.00
Total	36.02	35.89	36.02	35.90	35.92	35.88	35.95	36.03
Al total	4.09	3.14	3.08	2.95	2.99	4.01	3.70	3.94
Si	5.91	6.45	6.28	6.40	6.39	6.03	6.13	5.92
Fe/Fe+Mg	0.13	0.12	0.12	0.12	0.12	0.07	0.09	0.08

Note: Chl, Chlorite.

Table 4.4 Representative electron microprobe (EPMA) analysis of Plagioclase from the ultramafic rocks of Madawara ultramafic complex (MUC).

Table 4.4 Plagioclase composition of the mafic-intermediate rocks of the MUC

Table 4.4	Plagioclase con	iposition of the	mafic-intermedi	ate rocks of the	MUC				
Sample No.	MD/27	MD/27	MD/27	MD/27	MD/27	MD/27	MD/27	Ik/14/2	Ik/14/2
Ref.Point	1/1.	2/1.	4/1.	5 / 1 .	6/1.	8/1.	9/1.	1/1.	5 / 1 .
$SiO_2$	48.57	48.28	48.82	49.17	48.73	48.68	49.55	55.74	55.01
$TiO_2$	0.05	0.01	0.02	0.03	0.00	0.00	0.00	0.00	0.00
$Al_2O_3$	31.84	31.41	31.35	31.45	31.52	31.65	31.01	27.24	27.70
$Cr_2O_3$	0	0.01	0.00	0.00	0.00	0.00	0.00	0.00	0.00
$Fe_2O_3$	0	0.16	0.12	0.07	0.10	0.07	0.16	0.29	0.34
FeO	0	0.00	0.00	0.00	0.00	0.00	0.00	0.00	0.00
MnO	0	0.03	0.00	0.06	0.01	0.00	0.06	0.00	0.06
MgO	0.01	0.17	0.00	0.14	0.01	0.00	0.00	0.02	0.03
CaO	15.35	15.08	15.17	14.94	14.92	15.35	14.44	9.68	10.32
BaO	0	0.00	0.00	0.00	0.00	0.00	0.00	0.00	0.00
Na <sub>2</sub> O	3.04	3.07	3.31	3.12	3.13	3.07	3.47	6.13	5.89
$K_2O$	0.07	0.07	0.05	0.04	0.01	0.01	0.02	0.04	0.06
total	98.93	98.29	98.84	99.02	98.43	98.83	98.71	99.14	99.41
cations(apfu)	8 (O)	8 (O)	8 (O)	8 (O)	8 (O)	8 (O)	8 (O)	8 (O)	8 (O)
Si	2.24	2.24	2.25	2.26	2.26	2.24	2.28	2.52	2.49
Ti	0.00	0.00	0.00	0.00	0.00	0.00	0.00	0.00	0.00
Al	1.73	1.72	1.70	1.71	1.72	1.72	1.68	1.45	1.48
Cr Fe <sup>3+</sup>	0.00	0.00	0.00	0.00	0.00	0.00	0.00	0.00	0.00
Fe <sup>2+</sup>	0.00	0.01	0.00	0.00	0.00	0.00	0.01	0.01	0.01
He Mn	0.00 0.00	0.00 0.00	0.00 0.00	0.00 0.00	0.00 0.00	0.00 0.00	0.00 0.00	0.00 0.00	0.00 0.00
	0.00	0.00	0.00	0.00	0.00	0.00	0.00	0.00	0.00
Mg Ca	0.76	0.01	0.00	0.01	0.00	0.00	0.00	0.47	0.50
Ba	0.00	0.73	0.73	0.74	0.74	0.70	0.71	0.47	0.00
Na	0.27	0.28	0.30	0.28	0.28	0.27	0.31	0.54	0.52
K	0.00	0.00	0.00	0.00	0.00	0.00	0.00	0.00	0.00
tot. cat.	5.00	5.00	5.00	5.00	5.00	5.00	5.00	5.00	5.00
tot. oxy.	7.96	7.96	7.95	7.98	7.98	7.97	7.97	7.99	7.97
An	73.32	72.78	71.49	72.41	72.44	73.38	69.61	46.49	49.03
• •••	70.02								50.63
Ab	26.28	26.81	28.23	27.36	27.50	26.56	30.27	55.28	
Ab Or	26.28 0.40	26.81 0.40	28.23 0.28	27.36 0.23	27.50 0.06	26.56 0.06	30.27 0.11	53.28 0.23	
			28.23 0.28 Ik/14/2	27.36 0.23 Ik/14/2			30.27 0.11 Ik/14/2	0.23 Ik/14/2	0.34 Ik/14/2
Or	0.40	0.40	0.28	0.23	0.06	0.06	0.11	0.23	0.34
Or Sample No.	0.40 Ik/14/2	0.40 Ik/14/2	0.28 Ik/14/2	0.23 Ik/14/2	0.06 Ik/14/2	0.06 Ik/14/2	0.11 Ik/14/2	0.23 Ik/14/2	0.34 Ik/14/2
Or Sample No. Ref.Point SiO <sub>2</sub> TiO <sub>2</sub>	0.40 Ik/14/2 6 / 1 .	0.40 Ik/14/2 7 / 1 .	0.28 Ik/14/2 12 / 1 .	0.23 Ik/14/2 13 / 1 . 51.74 0.02	0.06 Ik/14/2 16 / 1 .	0.06 Ik/14/2 18 / 1 .	0.11 Ik/14/2 22 / 1 .	0.23 Ik/14/2 23 / 1 .	0.34 Ik/14/2 24 / 1 .
Or Sample No. Ref.Point SiO <sub>2</sub> TiO <sub>2</sub> Al <sub>2</sub> O <sub>3</sub>	0.40 Ik/14/2 6 / 1 . 52.82 0.02 29.34	0.40 Ik/14/2 7 / 1 . 56.19 0.03 27.18	0.28 Ik/14/2 12 / 1 . 55.60 0.03 27.69	0.23 Ik/14/2 13 / 1 . 51.74 0.02 29.88	0.06 Ik/14/2 16 / 1 . 53.95 0.05 27.89	0.06 Ik/14/2 18 / 1 . 53.70 0.00 28.62	0.11 Ik/14/2 22 / 1 . 53.43 0.00 28.62	0.23 Ik/14/2 23 / 1 . 55.33 0.00 27.75	0.34 Ik/14/2 24 / 1 . 55.67 0.01 27.63
Or Sample No. Ref.Point SiO <sub>2</sub> TiO <sub>2</sub> Al <sub>2</sub> O <sub>3</sub> Cr <sub>2</sub> O <sub>3</sub>	0.40 Ik/14/2 6 / 1 . 52.82 0.02 29.34 0.00	0.40 Ik/14/2 7 / 1 . 56.19 0.03 27.18 0.00	0.28 Ik/14/2 12 / 1 . 55.60 0.03 27.69 0.00	0.23 Ik/14/2 13 / 1 . 51.74 0.02 29.88 0.00	0.06 Ik/14/2 16 / 1 . 53.95 0.05 27.89 0.00	0.06 Ik/14/2 18 / 1 . 53.70 0.00 28.62 0.02	0.11 Ik/14/2 22 / 1 . 53.43 0.00	0.23 Ik/14/2 23 / 1 . 55.33 0.00 27.75 0.00	0.34 Ik/14/2 24 / 1 . 55.67 0.01 27.63 0.00
Or Sample No. Ref.Point SiO <sub>2</sub> TiO <sub>2</sub> Al <sub>2</sub> O <sub>3</sub> Cr <sub>2</sub> O <sub>3</sub> Fe <sub>2</sub> O <sub>3</sub>	0.40 Ik/14/2 6 / 1 . 52.82 0.02 29.34 0.00 0.12	0.40  Ik/14/2  7 / 1 .  56.19  0.03  27.18  0.00  0.25	0.28 Ik/14/2 12 / 1 . 55.60 0.03 27.69 0.00 0.29	0.23 Ik/14/2 13 / 1 . 51.74 0.02 29.88 0.00 0.30	0.06 Ik/14/2 16 / 1. 53.95 0.05 27.89 0.00 0.11	0.06 Ik/14/2 18 / 1. 53.70 0.00 28.62 0.02 0.22	0.11 Ik/14/2 22 / 1. 53.43 0.00 28.62 0.00 0.16	0.23 Ik/14/2 23 / 1 . 55.33 0.00 27.75 0.00 0.01	0.34 Ik/14/2 24 / 1 . 55.67 0.01 27.63 0.00 0.11
Or Sample No. Ref.Point SiO <sub>2</sub> TiO <sub>2</sub> Al <sub>2</sub> O <sub>3</sub> Cr <sub>2</sub> O <sub>3</sub> Fe <sub>2</sub> O <sub>3</sub> FeO	0.40  Ik/14/2  6 / 1 .  52.82  0.02  29.34  0.00  0.12  0.00	0.40 Ik/14/2 7/1. 56.19 0.03 27.18 0.00 0.25 0.00	0.28 Ik/14/2 12 / 1. 55.60 0.03 27.69 0.00 0.29 0.00	0.23 Ik/14/2 13 / 1 . 51.74 0.02 29.88 0.00 0.30 0.00	0.06 Ik/14/2 16 / 1. 53.95 0.05 27.89 0.00 0.11 0.00	0.06 Ik/14/2 18 / 1. 53.70 0.00 28.62 0.02 0.22 0.00	0.11 Ik/14/2 22 / 1. 53.43 0.00 28.62 0.00 0.16 0.00	0.23 Ik/14/2 23 / 1 . 55.33 0.00 27.75 0.00 0.01 0.00	0.34 Ik/14/2 24 / 1 . 55.67 0.01 27.63 0.00 0.11 0.00
Or Sample No. Ref.Point SiO <sub>2</sub> TiO <sub>2</sub> Al <sub>2</sub> O <sub>3</sub> Cr <sub>2</sub> O <sub>3</sub> Fe <sub>2</sub> O <sub>3</sub> FeO MnO	0.40  Ik/14/2  6 / 1 .  52.82  0.02  29.34  0.00  0.12  0.00  0.00	0.40  Ik/14/2  7 / 1 .  56.19  0.03  27.18  0.00  0.25  0.00  0.00	0.28 Ik/14/2 12 / 1 . 55.60 0.03 27.69 0.00 0.29 0.00 0.00	0.23 Ik/14/2 13 / 1 . 51.74 0.02 29.88 0.00 0.30 0.00 0.00	0.06 Ik/14/2 16 / 1. 53.95 0.05 27.89 0.00 0.11 0.00 0.01	0.06 Ik/14/2 18 / 1. 53.70 0.00 28.62 0.02 0.22 0.00 0.00	0.11 Ik/14/2 22 / 1. 53.43 0.00 28.62 0.00 0.16 0.00 0.05	0.23 Ik/14/2 23 / 1 . 55.33 0.00 27.75 0.00 0.01 0.00 0.02	0.34 Ik/14/2 24 / 1 . 55.67 0.01 27.63 0.00 0.11 0.00 0.02
Or Sample No. Ref.Point SiO <sub>2</sub> TiO <sub>2</sub> Al <sub>2</sub> O <sub>3</sub> Cr <sub>2</sub> O <sub>3</sub> Fe <sub>2</sub> O <sub>3</sub> FeO MnO MgO	0.40  Ik/14/2  6 / 1 .  52.82  0.02  29.34  0.00  0.12  0.00  0.00  0.00	0.40  Ik/14/2  7 / 1 .  56.19  0.03  27.18  0.00  0.25  0.00  0.00  0.00	0.28  Ik/14/2  12 / 1.  55.60 0.03 27.69 0.00 0.29 0.00 0.00 0.00 0.03	0.23 Ik/14/2 13 / 1 . 51.74 0.02 29.88 0.00 0.30 0.00 0.00 0.00	0.06  Ik/14/2  16 / 1.  53.95  0.05  27.89  0.00  0.11  0.00  0.01  0.00	0.06 Ik/14/2 18 / 1. 53.70 0.00 28.62 0.02 0.22 0.00 0.00 0.00	0.11 Ik/14/2 22 / 1. 53.43 0.00 28.62 0.00 0.16 0.00 0.05 0.00	0.23  Ik/14/2  23 / 1 .  55.33  0.00  27.75  0.00  0.01  0.00  0.02  0.00	0.34 Ik/14/2 24 / 1 . 55.67 0.01 27.63 0.00 0.11 0.00 0.02 0.00
Or Sample No. Ref.Point SiO <sub>2</sub> TiO <sub>2</sub> Al <sub>2</sub> O <sub>3</sub> Cr <sub>2</sub> O <sub>3</sub> Fe <sub>2</sub> O <sub>3</sub> FeO MnO MgO CaO	0.40  Ik/14/2  6 / 1 .  52.82  0.02  29.34  0.00  0.12  0.00  0.00  0.00  12.06	0.40  Ik/14/2  7 / 1 .  56.19  0.03  27.18  0.00  0.25  0.00  0.00  0.00  9.29	0.28  Ik/14/2  12 / 1.  55.60 0.03 27.69 0.00 0.29 0.00 0.00 0.00 9.64	0.23 Ik/14/2 13 / 1 . 51.74 0.02 29.88 0.00 0.30 0.00 0.00 0.01 12.84	0.06  Ik/14/2  16 / 1.  53.95  0.05  27.89  0.00  0.11  0.00  0.01  0.00  10.59	0.06  Ik/14/2  18 / 1.  53.70  0.00  28.62  0.02  0.22  0.00  0.00  0.00  11.53	0.11 Ik/14/2 22 / 1. 53.43 0.00 28.62 0.00 0.16 0.00 0.05 0.00 11.38	0.23  Ik/14/2  23 / 1 .  55.33  0.00  27.75  0.00  0.01  0.00  0.02  0.00  9.90	0.34 Ik/14/2 24 / 1 . 55.67 0.01 27.63 0.00 0.11 0.00 0.02 0.00 9.97
Or Sample No. Ref.Point SiO <sub>2</sub> TiO <sub>2</sub> Al <sub>2</sub> O <sub>3</sub> Cr <sub>2</sub> O <sub>3</sub> Fe <sub>2</sub> O <sub>3</sub> FeO MnO MgO CaO BaO	0.40  Ik/14/2  6 / 1 .  52.82  0.02  29.34  0.00  0.12  0.00  0.00  12.06  0.00	0.40  Ik/14/2  7/1.  56.19  0.03  27.18  0.00  0.25  0.00  0.00  9.29  0.00	0.28  Ik/14/2  12 / 1.  55.60 0.03 27.69 0.00 0.29 0.00 0.00 0.03 9.64 0.00	0.23  Ik/14/2  13 / 1.  51.74  0.02  29.88  0.00  0.30  0.00  0.00  0.01  12.84  0.00	0.06  Ik/14/2  16 / 1.  53.95  0.05  27.89  0.00  0.11  0.00  0.01  0.00  10.59  0.00	0.06  Ik/14/2  18 / 1.  53.70  0.00  28.62  0.02  0.22  0.00  0.00  11.53  0.00	0.11  Ik/14/2  22 / 1.  53.43  0.00  28.62  0.00  0.16  0.00  0.05  0.00  11.38  0.00	0.23  Ik/14/2  23 / 1 .  55.33  0.00  27.75  0.00  0.01  0.00  0.02  0.00  9.90  0.00	0.34  Ik/14/2  24 / 1 .  55.67  0.01  27.63  0.00  0.11  0.00  0.02  0.00  9.97  0.00
Or Sample No. Ref.Point SiO <sub>2</sub> TiO <sub>2</sub> Al <sub>2</sub> O <sub>3</sub> Cr <sub>2</sub> O <sub>3</sub> Fe <sub>2</sub> O <sub>3</sub> FeO MnO MgO CaO BaO Na <sub>2</sub> O	0.40  Ik/14/2  6 / 1.  52.82  0.02  29.34  0.00  0.12  0.00  0.00  0.00  12.06  0.00  4.91	0.40  Ik/14/2  7 / 1.  56.19  0.03  27.18  0.00  0.25  0.00  0.00  0.00  9.29  0.00  6.25	0.28  Ik/14/2  12 / 1.  55.60  0.03  27.69  0.00  0.29  0.00  0.00  0.03  9.64  0.00  6.20	0.23 Ik/14/2 13 / 1. 51.74 0.02 29.88 0.00 0.30 0.00 0.00 0.01 12.84 0.00 4.44	0.06  Ik/14/2  16 / 1.  53.95  0.05  27.89  0.00  0.11  0.00  0.01  0.00  10.59  0.00  5.51	0.06 Ik/14/2 18 / 1. 53.70 0.00 28.62 0.02 0.22 0.00 0.00 0.00 11.53 0.00 5.18	0.11  Ik/14/2  22 / 1.  53.43  0.00  28.62  0.00  0.16  0.00  0.05  0.00  11.38  0.00  5.06	0.23 Ik/14/2 23 / 1 . 55.33 0.00 27.75 0.00 0.01 0.00 0.02 0.00 9.90 0.00 5.99	0.34  Ik/14/2  24 / 1.  55.67  0.01  27.63  0.00  0.11  0.00  0.02  0.00  9.97  0.00  6.21
Or Sample No.  Ref.Point SiO <sub>2</sub> TiO <sub>2</sub> Al <sub>2</sub> O <sub>3</sub> Cr <sub>2</sub> O <sub>3</sub> Fe <sub>2</sub> O <sub>3</sub> FeO MnO MgO CaO BaO Na <sub>2</sub> O K <sub>2</sub> O	0.40  Ik/14/2  6 / 1.  52.82  0.02  29.34  0.00  0.12  0.00  0.00  12.06  0.00  4.91  0.09	0.40  Ik/14/2  7 / 1.  56.19  0.03  27.18  0.00  0.25  0.00  0.00  0.00  9.29  0.00  6.25  0.08	0.28  Ik/14/2  12 / 1.  55.60 0.03 27.69 0.00 0.29 0.00 0.00 0.03 9.64 0.00 6.20 0.04	0.23 Ik/14/2 13 / 1 . 51.74 0.02 29.88 0.00 0.30 0.00 0.00 0.01 12.84 0.00 4.44 0.05	0.06  Ik/14/2  16 / 1.  53.95  0.05  27.89  0.00  0.11  0.00  0.01  0.00  10.59  0.00  5.51  0.06	0.06  Ik/14/2  18 / 1.  53.70  0.00  28.62  0.02  0.22  0.00  0.00  0.00  11.53  0.00  5.18  0.05	0.11  Ik/14/2  22 / 1.  53.43  0.00  28.62  0.00  0.16  0.00  0.05  0.00  11.38  0.00  5.06  0.07	0.23  Ik/14/2  23 / 1 .  55.33  0.00  27.75  0.00  0.01  0.00  0.02  0.00  9.90  0.00  5.99  0.07	0.34  Ik/14/2  24 / 1.  55.67  0.01  27.63  0.00  0.11  0.00  0.02  0.00  9.97  0.00  6.21  0.05
Or Sample No. Ref.Point SiO <sub>2</sub> TiO <sub>2</sub> Al <sub>2</sub> O <sub>3</sub> Cr <sub>2</sub> O <sub>3</sub> Fe <sub>2</sub> O <sub>3</sub> FeO MnO MgO CaO BaO Na <sub>2</sub> O K <sub>2</sub> O total	0.40  Ik/14/2  6 / 1.  52.82  0.02  29.34  0.00  0.12  0.00  0.00  12.06  0.00  4.91  0.09  99.36	0.40 Ik/14/2 7 / 1 . 56.19 0.03 27.18 0.00 0.25 0.00 0.00 9.29 0.00 6.25 0.08 99.27	0.28  Ik/14/2  12 / 1.  55.60 0.03 27.69 0.00 0.29 0.00 0.00 0.03 9.64 0.00 6.20 0.04 99.52	0.23 Ik/14/2 13 / 1 . 51.74 0.02 29.88 0.00 0.30 0.00 0.00 0.01 12.84 0.00 4.44 0.05 99.28	0.06  Ik/14/2  16 / 1.  53.95  0.05  27.89  0.00  0.11  0.00  0.01  0.00  10.59  0.00  5.51  0.06  98.17	0.06  Ik/14/2  18 / 1.  53.70  0.00  28.62  0.02  0.22  0.00  0.00  11.53  0.00  5.18  0.05  99.32	0.11  Ik/14/2  22 / 1.  53.43  0.00  28.62  0.00  0.16  0.00  0.05  0.00  11.38  0.00  5.06  0.07  98.77	0.23  Ik/14/2  23 / 1 .  55.33  0.00  27.75  0.00  0.01  0.00  0.02  0.00  9.90  0.00  5.99  0.07  99.07	0.34  Ik/14/2  24 / 1.  55.67  0.01  27.63  0.00  0.11  0.00  0.02  0.00  9.97  0.00  6.21  0.05  99.67
Or Sample No. Ref.Point SiO <sub>2</sub> TiO <sub>2</sub> Al <sub>2</sub> O <sub>3</sub> Cr <sub>2</sub> O <sub>3</sub> Fe <sub>2</sub> O MnO MgO CaO BaO Na <sub>2</sub> O K <sub>2</sub> O total cations(apfu)	0.40  Ik/14/2  6 / 1.  52.82  0.02  29.34  0.00  0.12  0.00  0.00  12.06  0.00  4.91  0.09  99.36  8 (O)	0.40  Ik/14/2  7 / 1 .  56.19  0.03  27.18  0.00  0.25  0.00  0.00  0.00  9.29  0.00  6.25  0.08  99.27  8 (O)	0.28  Ik/14/2  12 / 1.  55.60 0.03 27.69 0.00 0.29 0.00 0.00 0.03 9.64 0.00 6.20 0.04 99.52 8 (O)	0.23  Ik/14/2  13 / 1 .  51.74  0.02  29.88  0.00  0.30  0.00  0.00  0.01  12.84  0.00  4.44  0.05  99.28  8 (O)	0.06  Ik/14/2  16 / 1.  53.95  0.05  27.89  0.00  0.11  0.00  10.59  0.00  5.51  0.06  98.17  8 (O)	0.06  Ik/14/2  18 / 1.  53.70  0.00  28.62  0.02  0.22  0.00  0.00  11.53  0.00  5.18  0.05  99.32  8 (O)	0.11  Ik/14/2  22 / 1.  53.43  0.00  28.62  0.00  0.16  0.00  0.05  0.00  11.38  0.00  5.06  0.07  98.77  8 (O)	0.23  Ik/14/2  23 / 1 .  55.33  0.00  27.75  0.00  0.01  0.00  0.02  0.00  9.90  0.00  5.99  0.07  99.07  8 (O)	0.34  Ik/14/2  24 / 1 .  55.67  0.01  27.63  0.00  0.11  0.00  0.02  0.00  9.97  0.00  6.21  0.05  99.67  8 (O)
Or Sample No. Ref.Point SiO <sub>2</sub> TiO <sub>2</sub> Al <sub>2</sub> O <sub>3</sub> Cr <sub>2</sub> O <sub>3</sub> Feo MnO MgO CaO BaO Na <sub>2</sub> O K <sub>2</sub> O total cations(apfu)	0.40  Ik/14/2  6 / 1.  52.82  0.02  29.34  0.00  0.12  0.00  0.00  12.06  0.00  4.91  0.09  99.36  8 (O)  2.40	0.40 Ik/14/2 7 / 1 . 56.19 0.03 27.18 0.00 0.25 0.00 0.00 9.29 0.00 6.25 0.08 99.27 8 (O) 2.54	0.28  Ik/14/2  12 / 1 .  55.60 0.03 27.69 0.00 0.29 0.00 0.00 0.03 9.64 0.00 6.20 0.04 99.52 8 (O) 2.51	0.23 Ik/14/2 13 / 1 . 51.74 0.02 29.88 0.00 0.30 0.00 0.01 12.84 0.00 4.44 0.05 99.28 8 (O) 2.36	0.06  Ik/14/2  16 / 1.  53.95  0.05  27.89  0.00  0.11  0.00  10.59  0.00  5.51  0.06  98.17  8 (O)  2.47	0.06  Ik/14/2  18 / 1.  53.70  0.00  28.62  0.02  0.22  0.00  0.00  11.53  0.00  5.18  0.05  99.32  8 (O)  2.44	0.11  Ik/14/2  22 / 1.  53.43  0.00  28.62  0.00  0.16  0.00  0.05  0.00  11.38  0.00  5.06  0.07  98.77  8 (O)  2.44	0.23  Ik/14/2  23 / 1 .  55.33  0.00  27.75  0.00  0.01  0.00  0.02  0.00  9.90  0.00  5.99  0.07  99.07  8 (O)  2.51	0.34  Ik/14/2  24 / 1 .  55.67  0.01  27.63  0.00  0.11  0.00  0.02  0.00  9.97  0.00  6.21  0.05  99.67  8 (O)  2.50
Or Sample No. Ref.Point SiO <sub>2</sub> TiO <sub>2</sub> Al <sub>2</sub> O <sub>3</sub> Cr <sub>2</sub> O <sub>3</sub> Fe <sub>2</sub> O <sub>3</sub> FeO MnO MgO CaO BaO Na <sub>2</sub> O K <sub>2</sub> O total cations(apfu) Si Ti	0.40  Ik/14/2  6 / 1 .  52.82  0.02  29.34  0.00  0.12  0.00  0.00  12.06  0.00  4.91  0.09  99.36  8 (O)  2.40  0.00	0.40  Ik/14/2  7 / 1 .  56.19  0.03  27.18  0.00  0.25  0.00  0.00  9.29  0.00  6.25  0.08  99.27  8 (O)  2.54  0.00	0.28  Ik/14/2  12 / 1 .  55.60 0.03 27.69 0.00 0.29 0.00 0.03 9.64 0.00 6.20 0.04 99.52 8 (O) 2.51 0.00	0.23  Ik/14/2  13 / 1 .  51.74  0.02  29.88  0.00  0.30  0.00  0.01  12.84  0.00  4.44  0.05  99.28  8 (O)  2.36  0.00	0.06  Ik/14/2  16 / 1.  53.95  0.05  27.89  0.00  0.11  0.00  10.59  0.00  5.51  0.06  98.17  8 (O)  2.47  0.00	0.06  Ik/14/2  18 / 1.  53.70  0.00  28.62  0.02  0.22  0.00  0.00  11.53  0.00  5.18  0.05  99.32  8 (O)  2.44  0.00	0.11  Ik/14/2  22 / 1.  53.43  0.00  28.62  0.00  0.16  0.00  0.05  0.00  11.38  0.00  5.06  0.07  98.77  8 (O)  2.44  0.00	0.23  Ik/14/2  23 / 1 .  55.33  0.00  27.75  0.00  0.01  0.00  0.02  0.00  9.90  0.00  5.99  0.07  99.07  8 (O)  2.51  0.00	0.34  Ik/14/2  24 / 1 .  55.67  0.01  27.63  0.00  0.11  0.00  0.02  0.00  9.97  0.00  6.21  0.05  99.67  8 (O)  2.50  0.00
Or Sample No. Ref.Point SiO <sub>2</sub> TiO <sub>2</sub> Al <sub>2</sub> O <sub>3</sub> Cr <sub>2</sub> O <sub>3</sub> Fe <sub>2</sub> O <sub>3</sub> FeO MnO MgO CaO BaO Na <sub>2</sub> O K <sub>2</sub> O total cations(apfu) Si Ti Al	0.40  Ik/14/2  6 / 1 .  52.82  0.02  29.34  0.00  0.12  0.00  0.00  12.06  0.00  4.91  0.09  99.36  8 (O)  2.40  0.00  1.57	0.40 Ik/14/2 7/1. 56.19 0.03 27.18 0.00 0.25 0.00 0.00 9.29 0.00 6.25 0.08 99.27 8 (O) 2.54 0.00 1.45	0.28  Ik/14/2  12 / 1 .  55.60 0.03 27.69 0.00 0.29 0.00 0.03 9.64 0.00 6.20 0.04 99.52 8 (O) 2.51 0.00 1.47	0.23  Ik/14/2  13 / 1 .  51.74  0.02  29.88  0.00  0.30  0.00  0.01  12.84  0.00  4.44  0.05  99.28  8 (O)  2.36  0.00  1.61	0.06  Ik/14/2  16 / 1.  53.95  0.05  27.89  0.00  0.11  0.00  10.59  0.00  5.51  0.06  98.17  8 (O)  2.47  0.00  1.51	0.06  Ik/14/2  18 / 1.  53.70  0.00  28.62  0.02  0.22  0.00  0.00  11.53  0.00  5.18  0.05  99.32  8 (O)  2.44  0.00  1.53	0.11  Ik/14/2  22 / 1.  53.43  0.00  28.62  0.00  0.16  0.00  0.05  0.00  11.38  0.00  5.06  0.07  98.77  8 (O)  2.44  0.00  1.54	0.23  Ik/14/2  23 / 1.  55.33  0.00  27.75  0.00  0.01  0.00  0.02  0.00  9.90  0.00  5.99  0.07  99.07  8 (O)  2.51  0.00  1.48	0.34  Ik/14/2  24 / 1 .  55.67  0.01  27.63  0.00  0.11  0.00  0.02  0.00  9.97  0.00  6.21  0.05  99.67  8 (O)  2.50  0.00  1.47
Or Sample No. Ref.Point SiO <sub>2</sub> TiO <sub>2</sub> Al <sub>2</sub> O <sub>3</sub> Cr <sub>2</sub> O <sub>3</sub> Fe <sub>2</sub> O <sub>3</sub> FeO MnO MgO CaO BaO Na <sub>2</sub> O K <sub>2</sub> O total cations(apfu) Si Ti Al Cr	0.40  Ik/14/2  6 / 1 .  52.82  0.02  29.34  0.00  0.12  0.00  0.00  12.06  0.00  4.91  0.09  99.36  8 (O)  2.40  0.00  1.57  0.00	0.40  Ik/14/2  7 / 1 .  56.19  0.03  27.18  0.00  0.25  0.00  0.00  9.29  0.00  6.25  0.08  99.27  8 (O)  2.54  0.00  1.45  0.00	0.28  Ik/14/2  12 / 1 .  55.60 0.03 27.69 0.00 0.29 0.00 0.03 9.64 0.00 6.20 0.04 99.52 8 (O) 2.51 0.00 1.47 0.00	0.23  Ik/14/2  13 / 1 .  51.74  0.02  29.88  0.00  0.30  0.00  0.01  12.84  0.00  4.44  0.05  99.28  8 (O)  2.36  0.00  1.61  0.00	0.06  Ik/14/2  16 / 1.  53.95  0.05  27.89  0.00  0.11  0.00  10.59  0.00  5.51  0.06  98.17  8 (O)  2.47  0.00  1.51  0.00	0.06  Ik/14/2  18 / 1.  53.70  0.00  28.62  0.02  0.22  0.00  0.00  11.53  0.00  5.18  0.05  99.32  8 (O)  2.44  0.00  1.53  0.00	0.11  Ik/14/2  22 / 1.  53.43  0.00  28.62  0.00  0.16  0.00  0.05  0.00  11.38  0.00  5.06  0.07  98.77  8 (O)  2.44  0.00  1.54  0.00	0.23  Ik/14/2  23 / 1.  55.33  0.00  27.75  0.00  0.01  0.00  0.02  0.00  9.90  0.00  5.99  0.07  99.07  8 (O)  2.51  0.00  1.48  0.00	0.34  Ik/14/2  24 / 1 .  55.67  0.01  27.63  0.00  0.11  0.00  0.02  0.00  9.97  0.00  6.21  0.05  99.67  8 (O)  2.50  0.00  1.47  0.00
Or Sample No. Ref.Point SiO <sub>2</sub> TiO <sub>2</sub> Al <sub>2</sub> O <sub>3</sub> Cr <sub>2</sub> O <sub>3</sub> Fe <sub>2</sub> O <sub>3</sub> FeO MnO MgO CaO BaO Na <sub>2</sub> O K <sub>2</sub> O total cations(apfu) Si Ti Al Cr Fe <sup>3+</sup>	0.40  Ik/14/2  6 / 1 .  52.82  0.02  29.34  0.00  0.12  0.00  0.00  12.06  0.00  4.91  0.09  99.36  8 (O)  2.40  0.00  1.57  0.00  0.00  0.00	0.40  Ik/14/2  7 / 1 .  56.19  0.03  27.18  0.00  0.25  0.00  0.00  9.29  0.00  6.25  0.08  99.27  8 (O)  2.54  0.00  1.45  0.00  0.01	0.28  Ik/14/2  12 / 1 .  55.60 0.03 27.69 0.00 0.29 0.00 0.03 9.64 0.00 6.20 0.04 99.52 8 (O) 2.51 0.00 1.47 0.00 0.01	0.23  Ik/14/2  13 / 1 .  51.74  0.02  29.88  0.00  0.30  0.00  0.01  12.84  0.00  4.44  0.05  99.28  8 (O)  2.36  0.00  1.61  0.00  0.01	0.06  Ik/14/2  16/1.  53.95  0.05  27.89  0.00  0.11  0.00  10.59  0.00  5.51  0.06  98.17  8 (O)  2.47  0.00  1.51  0.00  0.00	0.06  Ik/14/2  18 / 1.  53.70  0.00  28.62  0.02  0.22  0.00  0.00  11.53  0.00  5.18  0.05  99.32  8 (O)  2.44  0.00  1.53  0.00  0.01	0.11  Ik/14/2  22 / 1.  53.43  0.00  28.62  0.00  0.16  0.00  0.05  0.00  11.38  0.00  5.06  0.07  98.77  8 (O)  2.44  0.00  1.54  0.00  0.01	0.23  Ik/14/2  23 / 1.  55.33  0.00  27.75  0.00  0.01  0.00  0.02  0.00  9.90  0.00  5.99  0.07  99.07  8 (O)  2.51  0.00  1.48  0.00  0.00	0.34  Ik/14/2  24 / 1 .  55.67  0.01  27.63  0.00  0.11  0.00  0.02  0.00  9.97  0.00  6.21  0.05  99.67  8 (O)  2.50  0.00  1.47  0.00  0.00
Or Sample No. Ref.Point SiO <sub>2</sub> TiO <sub>2</sub> Al <sub>2</sub> O <sub>3</sub> Cr <sub>2</sub> O <sub>3</sub> Fe <sub>2</sub> O <sub>3</sub> FeO MnO MgO CaO BaO Na <sub>2</sub> O K <sub>2</sub> O total cations(apfu) Si Ti Al Cr Fe <sup>3+</sup> Fe <sup>2+</sup>	0.40  Ik/14/2  6 / 1 .  52.82  0.02  29.34  0.00  0.12  0.00  0.00  12.06  0.00  4.91  0.09  99.36  8 (O)  2.40  0.00  1.57  0.00  0.00  0.00  0.00  0.00  0.00  0.00	0.40  Ik/14/2  7 / 1 .  56.19  0.03  27.18  0.00  0.25  0.00  0.00  9.29  0.00  6.25  0.08  99.27  8 (O)  2.54  0.00  1.45  0.00  0.01  0.00	0.28  Ik/14/2  12 / 1.  55.60 0.03 27.69 0.00 0.29 0.00 0.03 9.64 0.00 6.20 0.04 99.52 8 (O) 2.51 0.00 1.47 0.00 0.01 0.00	0.23  Ik/14/2  13 / 1 .  51.74  0.02  29.88  0.00  0.30  0.00  0.01  12.84  0.00  4.44  0.05  99.28  8 (O)  2.36  0.00  1.61  0.00  0.01  0.00	0.06  Ik/14/2  16/1.  53.95  0.05  27.89  0.00  0.11  0.00  10.59  0.00  5.51  0.06  98.17  8 (O)  2.47  0.00  1.51  0.00  0.00  0.00  0.00  0.00	0.06  Ik/14/2  18 / 1 .  53.70  0.00  28.62  0.02  0.22  0.00  0.00  11.53  0.00  5.18  0.05  99.32  8 (O)  2.44  0.00  1.53  0.00  0.01  0.00	0.11  Ik/14/2  22 / 1.  53.43  0.00  28.62  0.00  0.16  0.00  0.05  0.00  11.38  0.00  5.06  0.07  98.77  8 (O)  2.44  0.00  1.54  0.00  0.01  0.00	0.23  Ik/14/2  23 / 1.  55.33  0.00  27.75  0.00  0.01  0.00  0.02  0.00  9.90  0.00  5.99  0.07  99.07  8 (O)  2.51  0.00  1.48  0.00  0.00  0.00  0.00	0.34  Ik/14/2  24 / 1 .  55.67  0.01  27.63  0.00  0.11  0.00  0.02  0.00  9.97  0.00  6.21  0.05  99.67  8 (O)  2.50  0.00  1.47  0.00  0.00  0.00  0.00  0.00  0.00
Or Sample No. Ref.Point SiO2 TiO2 Al2O3 Cr2O3 Fe2O3 FeO MnO MgO CaO BaO Na2O K2O total cations(apfu) Si Ti Al Cr Fe3+ Fe2+ Mn	0.40  Ik/14/2  6 / 1 .  52.82  0.02  29.34  0.00  0.12  0.00  0.00  12.06  0.00  4.91  0.09  99.36  8 (O)  2.40  0.00  1.57  0.00  0.00  0.00  0.00  0.00  0.00  0.00  0.00  0.00  0.00  0.00  0.00  0.00  0.00	0.40  Ik/14/2  7 / 1 .  56.19  0.03  27.18  0.00  0.25  0.00  0.00  9.29  0.00  6.25  0.08  99.27  8 (O)  2.54  0.00  1.45  0.00  0.01  0.00  0.00  0.00	0.28  Ik/14/2  12 / 1.  55.60 0.03 27.69 0.00 0.29 0.00 0.03 9.64 0.00 6.20 0.04 99.52 8 (O) 2.51 0.00 1.47 0.00 0.01 0.00 0.00	0.23  Ik/14/2  13 / 1 .  51.74  0.02  29.88  0.00  0.30  0.00  0.01  12.84  0.00  4.44  0.05  99.28  8 (O)  2.36  0.00  1.61  0.00  0.01  0.00  0.01  0.00  0.01	0.06  Ik/14/2  16/1.  53.95 0.05 27.89 0.00 0.11 0.00 0.01 0.00 10.59 0.00 5.51 0.06 98.17 8 (O) 2.47 0.00 1.51 0.00 0.00 0.00 0.00 0.00	0.06  Ik/14/2  18 / 1 .  53.70  0.00  28.62  0.02  0.22  0.00  0.00  11.53  0.00  5.18  0.05  99.32  8 (O)  2.44  0.00  1.53  0.00  0.01  0.00  0.00  0.00	0.11  Ik/14/2  22 / 1.  53.43  0.00  28.62  0.00  0.16  0.00  0.05  0.00  11.38  0.00  5.06  0.07  98.77  8 (O)  2.44  0.00  1.54  0.00  0.01  0.00  0.00	0.23  Ik/14/2  23 / 1.  55.33  0.00  27.75  0.00  0.01  0.00  0.02  0.00  9.90  0.00  5.99  0.07  99.07  8 (O)  2.51  0.00  1.48  0.00  0.00  0.00  0.00  0.00  0.00  0.00	0.34  Ik/14/2  24 / 1 .  55.67  0.01  27.63  0.00  0.11  0.00  0.02  0.00  9.97  0.00  6.21  0.05  99.67  8 (O)  2.50  0.00  1.47  0.00  0.00  0.00  0.00  0.00  0.00  0.00  0.00  0.00
Or Sample No. Ref.Point SiO <sub>2</sub> TiO <sub>2</sub> Al <sub>2</sub> O <sub>3</sub> Cr <sub>2</sub> O <sub>3</sub> Fe <sub>2</sub> O <sub>3</sub> FeO MnO MgO CaO BaO Na <sub>2</sub> O K <sub>2</sub> O total cations(apfu) Si Ti Al Cr Fe <sup>3+</sup> Fe <sup>2+</sup> Mn Mg	0.40  Ik/14/2  6 / 1 .  52.82  0.02  29.34  0.00  0.12  0.00  0.00  12.06  0.00  4.91  0.09  99.36  8 (O)  2.40  0.00  1.57  0.00  0.00  0.00  0.00  0.00  0.00  0.00  0.00  0.00  0.00  0.00  0.00  0.00  0.00  0.00  0.00	0.40  Ik/14/2  7 / 1 .  56.19  0.03  27.18  0.00  0.25  0.00  0.00  9.29  0.00  6.25  0.08  99.27  8 (O)  2.54  0.00  1.45  0.00  0.01  0.00  0.00  0.00  0.00  0.00  0.00  0.00	0.28  Ik/14/2  12 / 1.  55.60 0.03 27.69 0.00 0.29 0.00 0.03 9.64 0.00 6.20 0.04 99.52 8 (O) 2.51 0.00 1.47 0.00 0.01 0.00 0.00 0.00 0.00 0.00	0.23  Ik/14/2  13 / 1 .  51.74  0.02  29.88  0.00  0.30  0.00  0.01  12.84  0.00  4.44  0.05  99.28  8 (O)  2.36  0.00  1.61  0.00  0.01  0.00  0.01  0.00  0.01  0.00  0.00  0.00	0.06  Ik/14/2  16/1.  53.95 0.05 27.89 0.00 0.11 0.00 0.01 0.00 10.59 0.00 5.51 0.06 98.17 8 (O) 2.47 0.00 1.51 0.00 0.00 0.00 0.00 0.00 0.00	0.06  Ik/14/2  18 / 1 .  53.70 0.00 28.62 0.02 0.22 0.00 0.00 0.00 11.53 0.00 5.18 0.05 99.32 8 (O) 2.44 0.00 1.53 0.00 0.01 0.00 0.00 0.00 0.00	0.11  Ik/14/2  22 / 1.  53.43  0.00  28.62  0.00  0.16  0.00  0.05  0.00  11.38  0.00  5.06  0.07  98.77  8 (O)  2.44  0.00  1.54  0.00  0.01  0.00  0.00  0.00  0.00	0.23  Ik/14/2  23 / 1.  55.33  0.00  27.75  0.00  0.01  0.00  0.02  0.00  9.90  0.00  5.99  0.07  99.07  8 (O)  2.51  0.00  1.48  0.00  0.00  0.00  0.00  0.00  0.00  0.00  0.00  0.00  0.00	0.34  Ik/14/2  24 / 1 .  55.67  0.01  27.63  0.00  0.11  0.00  0.02  0.00  9.97  0.00  6.21  0.05  99.67  8 (O)  2.50  0.00  1.47  0.00  0.00  0.00  0.00  0.00  0.00  0.00  0.00  0.00  0.00  0.00
Or Sample No. Ref.Point SiO <sub>2</sub> TiO <sub>2</sub> Al <sub>2</sub> O <sub>3</sub> Cr <sub>2</sub> O <sub>3</sub> Fe <sub>2</sub> O <sub>3</sub> FeO MnO MgO CaO BaO Na <sub>2</sub> O K <sub>2</sub> O total cations(apfu) Si Ti Al Cr Fe <sup>3+</sup> Fe <sup>2+</sup> Mn Mg Ca	0.40  Ik/14/2  6 / 1.  52.82  0.02  29.34  0.00  0.12  0.00  0.00  12.06  0.00  4.91  0.09  99.36  8 (O)  2.40  0.00  1.57  0.00  0.00  0.00  0.00  0.00  0.00  0.00  0.00  0.00  0.00  0.00  0.00  0.59	0.40  Ik/14/2  7 / 1.  56.19  0.03  27.18  0.00  0.25  0.00  0.00  0.00  9.29  0.00  6.25  0.08  99.27  8 (O)  2.54  0.00  1.45  0.00  0.01  0.00  0.00  0.00  0.00  0.00  0.00  0.00  0.00  0.00  0.00  0.45	0.28  Ik/14/2  12 / 1.  55.60 0.03 27.69 0.00 0.29 0.00 0.03 9.64 0.00 6.20 0.04 99.52 8 (O) 2.51 0.00 1.47 0.00 0.01 0.00 0.00 0.00 0.00 0.00 0.0	0.23  Ik/14/2  13 / 1.  51.74  0.02  29.88  0.00  0.30  0.00  0.01  12.84  0.00  4.44  0.05  99.28  8 (O)  2.36  0.00  1.61  0.00  0.01  0.00  0.00  0.00  0.00  0.00  0.00  0.00  0.00  0.00  0.00  0.00  0.00  0.00  0.00  0.00  0.63	0.06  Ik/14/2  16 / 1.  53.95  0.05  27.89  0.00  0.11  0.00  10.59  0.00  5.51  0.06  98.17  8 (O)  2.47  0.00  1.51  0.00  0.00  0.00  0.00  0.00  0.00  0.00  0.00  0.00  0.00  0.52	0.06  Ik/14/2  18 / 1.  53.70  0.00  28.62  0.02  0.22  0.00  0.00  11.53  0.00  5.18  0.05  99.32  8 (O)  2.44  0.00  1.53  0.00  0.01  0.00  0.00  0.00  0.00  0.00  0.00  0.00  0.00  0.00  0.00  0.00  0.00  0.56	0.11  Ik/14/2  22 / 1.  53.43  0.00  28.62  0.00  0.16  0.00  0.05  0.00  11.38  0.00  5.06  0.07  98.77  8 (O)  2.44  0.00  1.54  0.00  0.01  0.00  0.00  0.00  0.00  0.00  0.00  0.00  0.56	0.23  Ik/14/2  23 / 1 .  55.33  0.00  27.75  0.00  0.01  0.00  0.02  0.00  9.90  0.00  5.99  0.07  99.07  8 (O)  2.51  0.00  1.48  0.00  0.00  0.00  0.00  0.00  0.00  0.00  0.00  0.00  0.48	0.34  Ik/14/2  24 / 1.  55.67  0.01  27.63  0.00  0.11  0.00  0.02  0.00  9.97  0.00  6.21  0.05  99.67  8 (O)  2.50  0.00  1.47  0.00  0.00  0.00  0.00  0.00  0.00  0.00  0.00  0.00  0.48
Or Sample No. Ref.Point SiO <sub>2</sub> TiO <sub>2</sub> Al <sub>2</sub> O <sub>3</sub> Cr <sub>2</sub> O <sub>3</sub> Fe <sub>2</sub> O <sub>3</sub> FeO MnO MgO CaO BaO Na <sub>2</sub> O K <sub>2</sub> O total cations(apfu) Si Ti Al Cr Fe <sup>3+</sup> Fe <sup>2+</sup> Mn Mg Ca Ba Ca Ba Ca Ba	0.40  Ik/14/2  6 / 1.  52.82  0.02  29.34  0.00  0.12  0.00  0.00  12.06  0.00  4.91  0.09  99.36  8 (O)  2.40  0.00  1.57  0.00  0.00  0.00  0.00  0.00  0.00  0.00  0.00  0.00  0.00  0.00  0.00  0.00  0.59  0.00	0.40  Ik/14/2  7 / 1.  56.19  0.03  27.18  0.00  0.25  0.00  0.00  0.00  6.25  0.08  99.27  8 (O)  2.54  0.00  1.45  0.00  0.01  0.00  0.00  0.00  0.00  0.00  0.00  0.00  0.00  0.00  0.00  0.00  0.00  0.00  0.00  0.00  0.45  0.00	0.28  Ik/14/2  12 / 1.  55.60 0.03 27.69 0.00 0.29 0.00 0.03 9.64 0.00 6.20 0.04 99.52 8 (O) 2.51 0.00 1.47 0.00 0.01 0.00 0.00 0.00 0.00 0.00 0.0	0.23  Ik/14/2  13 / 1.  51.74  0.02  29.88  0.00  0.30  0.00  0.01  12.84  0.00  4.44  0.05  99.28  8 (O)  2.36  0.00  1.61  0.00  0.01  0.00  0.00  0.00  0.00  0.00  0.00  0.00  0.00  0.00  0.00  0.00  0.00  0.00  0.00  0.00  0.00	0.06  Ik/14/2  16 / 1.  53.95  0.05  27.89  0.00  0.11  0.00  10.59  0.00  5.51  0.06  98.17  8 (O)  2.47  0.00  1.51  0.00  0.00  0.00  0.00  0.00  0.00  0.00  0.00  0.00  0.00  0.00  0.00  0.52  0.00	0.06  Ik/14/2  18 / 1.  53.70  0.00  28.62  0.02  0.22  0.00  0.00  11.53  0.00  5.18  0.05  99.32  8 (O)  2.44  0.00  1.53  0.00  0.01  0.00  0.00  0.00  0.00  0.00  0.00  0.00  0.00  0.00  0.00  0.00  0.00  0.00  0.56  0.00	0.11  Ik/14/2  22 / 1.  53.43  0.00  28.62  0.00  0.16  0.00  0.05  0.00  11.38  0.00  5.06  0.07  98.77  8 (O)  2.44  0.00  1.54  0.00  0.01  0.00  0.00  0.00  0.00  0.00  0.00  0.00  0.00  0.56  0.00	0.23  Ik/14/2  23 / 1.  55.33  0.00  27.75  0.00  0.01  0.00  0.02  0.00  9.90  0.00  5.99  0.07  99.07  8 (O)  2.51  0.00  1.48  0.00  0.00  0.00  0.00  0.00  0.00  0.00  0.00  0.00  0.00  0.48  0.00	0.34  Ik/14/2  24 / 1.  55.67  0.01  27.63  0.00  0.11  0.00  0.02  0.00  9.97  0.00  6.21  0.05  99.67  8 (O)  2.50  0.00  1.47  0.00  0.00  0.00  0.00  0.00  0.00  0.00  0.00  0.48  0.00
Or Sample No. Ref.Point SiO <sub>2</sub> TiO <sub>2</sub> Al <sub>2</sub> O <sub>3</sub> Cr <sub>2</sub> O <sub>3</sub> FeO MnO MgO CaO BaO Na <sub>2</sub> O K <sub>2</sub> O total cations(apfu) Si Ti Al Cr Fe <sup>3+</sup> Fe <sup>2+</sup> Mn Mg Ca Ba Na Na	0.40  Ik/14/2  6 / 1.  52.82  0.02  29.34  0.00  0.12  0.00  0.00  12.06  0.00  4.91  0.09  99.36  8 (O)  2.40  0.00  1.57  0.00  0.00  0.00  0.00  0.00  0.00  0.00  0.00  0.00  0.00  0.00  0.00  0.59	0.40  Ik/14/2  7 / 1.  56.19  0.03  27.18  0.00  0.25  0.00  0.00  0.00  9.29  0.00  6.25  0.08  99.27  8 (O)  2.54  0.00  1.45  0.00  0.01  0.00  0.00  0.00  0.00  0.00  0.00  0.00  0.00  0.00  0.00  0.45	0.28  Ik/14/2  12 / 1.  55.60 0.03 27.69 0.00 0.29 0.00 0.03 9.64 0.00 6.20 0.04 99.52 8 (O) 2.51 0.00 1.47 0.00 0.01 0.00 0.00 0.00 0.00 0.00 0.0	0.23  Ik/14/2  13 / 1.  51.74  0.02  29.88  0.00  0.30  0.00  0.01  12.84  0.00  4.44  0.05  99.28  8 (O)  2.36  0.00  1.61  0.00  0.01  0.00  0.00  0.00  0.00  0.00  0.00  0.00  0.00  0.00  0.00  0.00  0.00  0.00  0.00  0.00  0.63	0.06  Ik/14/2  16 / 1.  53.95  0.05  27.89  0.00  0.11  0.00  10.59  0.00  5.51  0.06  98.17  8 (O)  2.47  0.00  1.51  0.00  0.00  0.00  0.00  0.00  0.00  0.00  0.00  0.00  0.00  0.52	0.06  Ik/14/2  18 / 1.  53.70  0.00  28.62  0.02  0.22  0.00  0.00  11.53  0.00  5.18  0.05  99.32  8 (O)  2.44  0.00  1.53  0.00  0.01  0.00  0.00  0.00  0.00  0.00  0.00  0.00  0.00  0.00  0.00  0.00  0.00  0.56	0.11  Ik/14/2  22 / 1.  53.43  0.00  28.62  0.00  0.16  0.00  0.05  0.00  11.38  0.00  5.06  0.07  98.77  8 (O)  2.44  0.00  1.54  0.00  0.01  0.00  0.00  0.00  0.00  0.00  0.00  0.00  0.56	0.23  Ik/14/2  23 / 1 .  55.33  0.00  27.75  0.00  0.01  0.00  0.02  0.00  9.90  0.00  5.99  0.07  99.07  8 (O)  2.51  0.00  1.48  0.00  0.00  0.00  0.00  0.00  0.00  0.00  0.00  0.00  0.48	0.34  Ik/14/2  24 / 1.  55.67  0.01  27.63  0.00  0.11  0.00  0.02  0.00  9.97  0.00  6.21  0.05  99.67  8 (O)  2.50  0.00  1.47  0.00  0.00  0.00  0.00  0.00  0.00  0.00  0.00  0.00  0.48
Or Sample No. Ref.Point SiO <sub>2</sub> TiO <sub>2</sub> Al <sub>2</sub> O <sub>3</sub> Cr <sub>2</sub> O <sub>3</sub> Fe <sub>2</sub> O <sub>3</sub> FeO MnO MgO CaO BaO Na <sub>2</sub> O K <sub>2</sub> O total cations(apfu) Si Ti Al Cr Fe <sup>3+</sup> Fe <sup>2+</sup> Mn Mg Ca Ba Na K	0.40  Ik/14/2  6 / 1.  52.82  0.02  29.34  0.00  0.12  0.00  0.00  12.06  0.00  4.91  0.09  99.36  8 (O)  2.40  0.00  1.57  0.00  0.00  0.00  0.00  0.00  0.00  0.00  0.00  0.00  0.00  0.00  0.00  0.59  0.00  0.43	0.40  Ik/14/2  7 / 1.  56.19  0.03  27.18  0.00  0.25  0.00  0.00  0.00  9.29  0.00  6.25  0.08  99.27  8 (O)  2.54  0.00  1.45  0.00  0.01  0.00  0.00  0.00  0.00  0.00  0.00  0.00  0.00  0.00  0.00  0.55	0.28  Ik/14/2  12 / 1.  55.60 0.03 27.69 0.00 0.29 0.00 0.03 9.64 0.00 6.20 0.04 99.52 8 (O) 2.51 0.00 1.47 0.00 0.01 0.00 0.00 0.00 0.00 0.00 0.0	0.23  Ik/14/2  13 / 1.  51.74  0.02  29.88  0.00  0.30  0.00  0.01  12.84  0.00  4.44  0.05  99.28  8 (O)  2.36  0.00  1.61  0.00  0.01  0.00  0.01  0.00  0.01  0.00  0.01  0.00  0.01  0.00  0.01  0.00  0.01  0.00  0.00  0.00  0.00  0.00  0.00  0.39	0.06  Ik/14/2  16 / 1.  53.95  0.05  27.89  0.00  0.11  0.00  10.59  0.00  5.51  0.06  98.17  8 (O)  2.47  0.00  1.51  0.00  0.00  0.00  0.00  0.00  0.00  0.00  0.00  0.00  0.00  0.49	0.06  Ik/14/2  18 / 1.  53.70  0.00  28.62  0.02  0.22  0.00  0.00  11.53  0.00  5.18  0.05  99.32  8 (O)  2.44  0.00  1.53  0.00  0.01  0.00  0.00  0.00  0.00  0.00  0.00  0.00  0.00  0.00  0.00  0.00  0.46	0.11  Ik/14/2  22 / 1.  53.43  0.00  28.62  0.00  0.16  0.00  0.05  0.00  11.38  0.00  5.06  0.07  98.77  8 (O)  2.44  0.00  1.54  0.00  0.01  0.00  0.01  0.00  0.00  0.00  0.00  0.56  0.00  0.45	0.23  Ik/14/2  23 / 1 .  55.33  0.00  27.75  0.00  0.01  0.00  0.02  0.00  9.90  0.00  5.99  0.07  99.07  8 (O)  2.51  0.00  1.48  0.00  0.00  0.00  0.00  0.00  0.00  0.00  0.00  0.00  0.00  0.48  0.00  0.53	0.34  Ik/14/2  24 / 1.  55.67  0.01  27.63  0.00  0.11  0.00  0.02  0.00  9.97  0.00  6.21  0.05  99.67  8 (O)  2.50  0.00  1.47  0.00  0.00  0.00  0.00  0.00  0.00  0.00  0.48  0.00  0.54
Or Sample No. Ref.Point SiO <sub>2</sub> TiO <sub>2</sub> Al <sub>2</sub> O <sub>3</sub> Cr <sub>2</sub> O <sub>3</sub> Fe <sub>2</sub> O <sub>3</sub> FeO MnO MgO CaO BaO Na <sub>2</sub> O K <sub>2</sub> O total cations(apfu) Si Ti Al Cr Fe <sup>3+</sup> Fe <sup>2+</sup> Mn Mg Ca Ba Na	0.40  Ik/14/2  6 / 1.  52.82  0.02  29.34  0.00  0.12  0.00  0.00  12.06  0.00  4.91  0.09  99.36  8 (O)  2.40  0.00  1.57  0.00  0.00  0.00  0.00  0.00  0.00  0.00  0.00  0.00  0.00  0.00  0.00  0.00  0.59  0.00  0.43  0.01	0.40  Ik/14/2  7 / 1.  56.19  0.03  27.18  0.00  0.25  0.00  0.00  9.29  0.00  6.25  0.08  99.27  8 (O)  2.54  0.00  1.45  0.00  0.01  0.00  0.00  0.00  0.00  0.00  0.00  0.00  0.00  0.00  0.00  0.00  0.00  0.05  0.00	0.28  Ik/14/2  12 / 1.  55.60 0.03 27.69 0.00 0.29 0.00 0.03 9.64 0.00 6.20 0.04 99.52 8 (O) 2.51 0.00 1.47 0.00 0.01 0.00 0.00 0.00 0.00 0.00 0.0	0.23  Ik/14/2  13 / 1.  51.74  0.02  29.88  0.00  0.30  0.00  0.01  12.84  0.00  4.44  0.05  99.28  8 (O)  2.36  0.00  1.61  0.00  0.01  0.00  0.01  0.00  0.01  0.00  0.01  0.00  0.01  0.00  0.01  0.00  0.01  0.00  0.01	0.06  Ik/14/2  16 / 1.  53.95  0.05  27.89  0.00  0.11  0.00  10.59  0.00  5.51  0.06  98.17  8 (O)  2.47  0.00  1.51  0.00  0.00  0.00  0.00  0.00  0.00  0.00  0.00  0.00  0.00  0.00  0.49  0.00	0.06  Ik/14/2  18 / 1.  53.70  0.00  28.62  0.02  0.22  0.00  0.00  11.53  0.00  5.18  0.05  99.32  8 (O)  2.44  0.00  1.53  0.00  0.01  0.00  0.00  0.00  0.00  0.00  0.00  0.00  0.00  0.00  0.00  0.00  0.00  0.46  0.00	0.11  Ik/14/2  22 / 1.  53.43  0.00  28.62  0.00  0.16  0.00  0.05  0.00  11.38  0.00  5.06  0.07  98.77  8 (O)  2.44  0.00  1.54  0.00  0.01  0.00  0.01  0.00  0.00  0.00  0.00  0.00  0.56  0.00  0.45  0.00	0.23  Ik/14/2  23 / 1 .  55.33  0.00  27.75  0.00  0.01  0.00  0.02  0.00  9.90  0.00  5.99  0.07  99.07  8 (O)  2.51  0.00  1.48  0.00  0.00  0.00  0.00  0.00  0.00  0.00  0.00  0.00  0.00  0.00  0.00  0.53  0.00  5.00	0.34  Ik/14/2  24 / 1.  55.67  0.01  27.63  0.00  0.11  0.00  0.02  0.00  9.97  0.00  6.21  0.05  99.67  8 (O)  2.50  0.00  1.47  0.00  0.00  0.00  0.00  0.00  0.00  0.00  0.00  0.00  0.48  0.00  0.54  0.00
Or Sample No. Ref.Point SiO <sub>2</sub> TiO <sub>2</sub> Al <sub>2</sub> O <sub>3</sub> Cr <sub>2</sub> O <sub>3</sub> Fe <sub>2</sub> O <sub>3</sub> FeO MnO MgO CaO BaO Na <sub>2</sub> O total cations(apfu) Si Ti Al Cr Fe <sup>3+</sup> Fe <sup>2+</sup> Mn Mg Ca Ba Na K tot. cat.	0.40  Ik/14/2  6 / 1.  52.82  0.02  29.34  0.00  0.12  0.00  0.00  12.06  0.00  4.91  0.09  99.36  8 (O)  2.40  0.00  1.57  0.00  0.00  0.00  0.00  0.00  0.00  0.00  0.00  0.00  0.00  0.00  0.00  0.00  0.59  0.00  0.43  0.01  5.00	0.40  Ik/14/2  7 / 1.  56.19  0.03  27.18  0.00  0.25  0.00  0.00  9.29  0.00  6.25  0.08  99.27  8 (O)  2.54  0.00  1.45  0.00  0.01  0.00  0.00  0.00  0.00  0.00  0.00  0.00  0.00  5.00	0.28  Ik/14/2  12 / 1.  55.60 0.03 27.69 0.00 0.29 0.00 0.00 0.03 9.64 0.00 6.20 0.04 99.52 8 (O) 2.51 0.00 1.47 0.00 0.01 0.00 0.00 0.00 0.00 0.00 0.0	0.23  Ik/14/2  13 / 1.  51.74  0.02  29.88  0.00  0.30  0.00  0.01  12.84  0.00  4.44  0.05  99.28  8 (O)  2.36  0.00  1.61  0.00  0.01  0.00  0.01  0.00  0.01  0.00  0.01  0.00  0.01  0.00  0.01  0.00  0.00  0.00  0.00  0.00  0.00  0.00  0.39  0.00  5.00	0.06  Ik/14/2  16 / 1.  53.95  0.05  27.89  0.00  0.11  0.00  10.59  0.00  5.51  0.06  98.17  8 (O)  2.47  0.00  1.51  0.00  0.00  0.00  0.00  0.00  0.00  0.00  0.00  0.00  0.00  0.52  0.00  0.49  0.00  5.00	0.06  Ik/14/2  18 / 1.  53.70  0.00  28.62  0.02  0.22  0.00  0.00  11.53  0.00  5.18  0.05  99.32  8 (O)  2.44  0.00  1.53  0.00  0.01  0.00  0.00  0.00  0.00  0.00  0.00  0.00  0.00  0.00  0.00  0.00  0.00  0.56  0.00  0.46  0.00  5.00	0.11  Ik/14/2  22 / 1.  53.43  0.00  28.62  0.00  0.16  0.00  0.05  0.00  11.38  0.00  5.06  0.07  98.77  8 (O)  2.44  0.00  1.54  0.00  0.01  0.00  0.00  0.00  0.00  0.00  0.00  0.00  0.56  0.00  0.45  0.00  5.00	0.23  Ik/14/2  23 / 1 .  55.33  0.00  27.75  0.00  0.01  0.00  0.02  0.00  9.90  0.00  5.99  0.07  99.07  8 (O)  2.51  0.00  1.48  0.00  0.00  0.00  0.00  0.00  0.00  0.00  0.00  0.00  0.00  0.00  0.00  0.00  0.05  0.00  0.53  0.00	0.34  Ik/14/2  24 / 1.  55.67  0.01  27.63  0.00  0.11  0.00  0.02  0.00  9.97  0.00  6.21  0.05  99.67  8 (O)  2.50  0.00  1.47  0.00  0.00  0.00  0.00  0.00  0.00  0.00  0.00  0.00  0.48  0.00  0.54  0.00  5.00
Or Sample No. Ref.Point SiO <sub>2</sub> TiO <sub>2</sub> Al <sub>2</sub> O <sub>3</sub> Cr <sub>2</sub> O <sub>3</sub> Fe <sub>2</sub> O <sub>3</sub> FeO MnO MgO CaO BaO Na <sub>2</sub> O total cations(apfu) Si Ti Al Cr Fe <sup>3+</sup> Fe <sup>2+</sup> Mn Mg Ca Ba Na K tot. cat. tot. oxy.	0.40  Ik/14/2  6 / 1.  52.82  0.02  29.34  0.00  0.12  0.00  0.00  12.06  0.00  4.91  0.09  99.36  8 (O)  2.40  0.00  1.57  0.00  0.00  0.00  0.00  0.00  0.00  0.00  0.00  0.00  0.00  0.00  0.00  0.00  0.59  0.00  0.43  0.01  5.00  7.97	0.40  Ik/14/2  7 / 1.  56.19  0.03  27.18  0.00  0.25  0.00  0.00  9.29  0.00  6.25  0.08  99.27  8 (O)  2.54  0.00  1.45  0.00  0.01  0.00  0.00  0.00  0.00  0.00  0.00  0.00  5.00  7.99	0.28  Ik/14/2  12 / 1.  55.60 0.03 27.69 0.00 0.29 0.00 0.00 0.03 9.64 0.00 6.20 0.04 99.52 8 (O) 2.51 0.00 1.47 0.00 0.01 0.00 0.00 0.00 0.00 0.00 0.0	0.23  Ik/14/2  13 / 1 .  51.74  0.02  29.88  0.00  0.30  0.00  0.01  12.84  0.00  4.44  0.05  99.28  8 (O)  2.36  0.00  1.61  0.00  0.01  0.00  0.01  0.00  0.01  0.00  0.01  0.00  0.01  0.00  0.01  0.00  0.01  0.00  0.01  0.00  0.01  0.00  0.01  0.00  0.01  0.00  0.00  0.00  0.00  0.00  0.00  0.797	0.06  Ik/14/2  16 / 1.  53.95  0.05  27.89  0.00  0.11  0.00  10.59  0.00  5.51  0.06  98.17  8 (O)  2.47  0.00  1.51  0.00  0.00  0.00  0.00  0.00  0.00  0.00  0.00  0.00  0.52  0.00  0.49  0.00  5.00  7.98	0.06  Ik/14/2  18 / 1.  53.70  0.00  28.62  0.02  0.22  0.00  0.00  11.53  0.00  5.18  0.05  99.32  8 (O)  2.44  0.00  1.53  0.00  0.01  0.00  0.00  0.00  0.00  0.00  0.00  0.00  0.00  0.00  5.00  7.98	0.11  Ik/14/2  22 / 1.  53.43  0.00  28.62  0.00  0.16  0.00  0.05  0.00  11.38  0.00  5.06  0.07  98.77  8 (O)  2.44  0.00  1.54  0.00  0.01  0.00  0.00  0.00  0.00  0.00  0.00  0.56  0.00  0.45  0.00  5.00  7.99	0.23  Ik/14/2  23 / 1 .  55.33  0.00  27.75  0.00  0.01  0.00  0.02  0.00  9.90  0.00  5.99  0.07  99.07  8 (O)  2.51  0.00  1.48  0.00  0.00  0.00  0.00  0.00  0.00  0.00  0.00  0.00  0.00  0.00  0.53  0.00  5.00  7.98	0.34  Ik/14/2  24 / 1 .  55.67  0.01  27.63  0.00  0.11  0.00  0.02  0.00  9.97  0.00  6.21  0.05  99.67  8 (O)  2.50  0.00  1.47  0.00  0.00  0.00  0.00  0.00  0.00  0.00  0.00  0.00  0.48  0.00  0.54  0.00  5.00  7.97

Table 4.4 continued....

Sample No.	Ik/14/2	Ik/14/2	BG/3	BG/3	BG/3	BG/3	BG/3	BG/3	BG/3
Ref.Point	27 / 1 .	28 / 1 .	4/1.	5 / 1 .	7/1.	11 / 1 .	12 / 1 .	26 / 1 .	6/1.
SiO <sub>2</sub>	53.17	53.10	59.37	57.13	63.80	55.15	52.64	38.10	53.87
$TiO_2$	0.02	0.00	0.01	0.00	0.02	0.00	0.02	0.07	0.02
$Al_2O_3$	28.97	28.69	24.88	26.49	21.63	27.73	28.08	28.33	28.43
$Cr_2O_3$	0.00	0.00	0.00	0.00	0.00	0.00	0.00	0.00	0.00
$Fe_2O_3$	0.03	0.00	0.55	0.03	0.18	0.26	0.32	6.78	0.15
FeO	0.00	0.00	0.00	0.00	0.00	0.00	0.00	0.00	0.00
MnO	0.03	0.00	0.03	0.00	0.00	0.02	0.03	0.11	0.03
MgO	0.00	0.00	0.12	0.02	0.03	0.02	0.10	0.01	0.02
CaO	11.66	11.38	2.16	7.72	2.57	10.37	8.29	23.85	11.19
BaO	0.00	0.00	0.00	0.00	0.00	0.00	0.00	0.00	0.00
Na <sub>2</sub> O	5.09	5.14	8.04	7.06	10.06	6.00	5.32	0.00	5.56
$K_2O$	0.05	0.09	2.70	0.35	0.26	0.09	1.28	0.02	0.12
total	99.02	98.40	97.86	98.80	98.55	99.64	96.08	97.27	99.39
cations(apfu)	8 (O)	8 (O)	8 (O)	8 (O)	8 (O)	8 (O)	8 (O)	8 (O)	8 (O)
Si	2.42	2.43	2.68	2.58	2.85	2.49	2.46	1.86	2.44
Ti	0.00	0.00	0.00	0.00	0.00	0.00	0.00	0.00	0.00
Al	1.55	1.55	1.32	1.41	1.14	1.47	1.55	1.63	1.52
Cr	0.00	0.00	0.00	0.00	0.00	0.00	0.00	0.00	0.00
Fe <sup>3+</sup>	0.00	0.00	0.02	0.00	0.01	0.01	0.01	0.26	0.01
Fe <sup>2+</sup>	0.00	0.00	0.00	0.00	0.00	0.00	0.00	0.00	0.00
Mn	0.00	0.00	0.00	0.00	0.00	0.00	0.00	0.00	0.00
Mg	0.00	0.00	0.01	0.00	0.00	0.00	0.01	0.00	0.00
Ca	0.57	0.56	0.10	0.37	0.12	0.50	0.42	1.25	0.54
Ba	0.00	0.00	0.00	0.00	0.00	0.00	0.00	0.00	0.00
Na	0.45	0.46	0.70	0.62	0.87	0.52	0.48	0.00	0.49
K	0.00	0.01	0.16	0.02	0.01	0.01	0.08	0.00	0.01
tot. cat.	5.00	5.00	5.00	5.00	5.00	5.00	5.00	5.00	5.00
tot. oxy.	7.97	7.98	7.92	7.96	7.98	7.96	7.96	7.80	7.95
An	55.71	54.74	10.84	36.92	12.19	48.61	42.64	99.90	52.30
Ab	44.01	44.74	73.02	61.09	86.34	50.89	49.52	0.00	47.03
Or	0.28	0.52	16.14	1.99	1.47	0.50	7.84	0.10	0.67

Table 4.5 Representative electron microprobe (EPMA) analysis of chrome spinels (chromites) from the ultramafic rocks of MUC.

Chrome-spinel (Chromite) composition of the ultramafic of MUC Table 4.5

Table 4.5				ultramafic of M		M/16/OD	M/16/OD	M/16/OD	M/17/OD	M/0D/D
Sample Mineral	M/16/OP Al-Chr	M/8R/P Al-Chr								
Ref Point	1/1.	2/1.	4/1.	5/1.	7 / 1 .	8/1.	17 / 1 .	27 / 1 .	17 / 1 .	2/1.
SiO <sub>2</sub>	0.15	0.06	0.03	0.05	0.05	0.05	0.03	0.03	0.03	0.05
$TiO_2$	0.41	0.45	0.47	0.39	0.40	0.40	0.67	0.52	0.67	0.46
$Al_2O_3$	13.81	13.81	13.51	13.67	13.46	13.75	12.89	15.88	12.89	14.68
$Cr_2O_3$ $FeO^T$	46.47 33.62	46.24 34.07	45.87 33.31	46.29 34.21	48.30 33.06	46.70 34.06	38.16 42.32	45.46 33.02	38.16 42.32	43.30 32.20
MnO	0.47	0.41	0.37	0.37	0.47	0.17	0.33	0.28	0.33	1.62
MgO	2.75	2.50	2.69	2.56	2.86	2.52	2.04	3.13	2.04	4.34
CaO	0.01	0.05	0.00	0.07	0.04	0.06	0.01	0.00	0.01	0.00
Na <sub>2</sub> O	0.04	0.04	0.06	0.05	0.06	0.05	0.04	0.04	0.04	0.04
K <sub>2</sub> O	0.01	0.00	0.01	0.01	0.00	0.00	0.00	0.00	0.00	0.01
NiO ZnO	0.00 1.69	0.00 1.88	0.00 1.58	0.00 1.82	0.00 1.76	0.00 1.82	0.00 1.32	0.00 1.54	0.00 1.32	0.00 0.98
Total	99.44	99.50	97.88	99.48	100.46	99.57	97.80	99.90	97.80	97.67
Fe <sub>2</sub> O <sub>3</sub>	6.19	6.51	6.26	6.82	5.77	6.30	14.51	5.26	14.51	8.26
FeO	28.05	28.21	27.67	28.07	27.86	28.40	29.26	28.29	29.26	24.77
Total	100.06	100.15	98.51	100.17	101.03	100.20	99.26	100.43	99.26	98.50
Cations : Si	4(O) 0.01	4(O) 0.00	4(O) 0.00							
Ti	0.01	0.00	0.00	0.00	0.00	0.00	0.00	0.00	0.00	0.00
Al	0.56	0.56	0.55	0.55	0.54	0.55	0.53	0.63	0.53	0.59
Cr	1.26	1.25	1.26	1.25	1.29	1.26	1.05	1.21	1.05	1.17
Fe <sup>+3</sup>	0.16	0.17	0.16	0.18	0.15	0.16	0.38	0.13	0.38	0.21
Fe <sup>+2</sup>	0.80	0.81	0.80 0.01	0.80	0.79	0.81 0.00	0.85 0.01	0.80	0.85	0.71 0.05
Mn Mg	0.01 0.14	0.01 0.13	0.14	0.01 0.13	0.01 0.14	0.00	0.01	0.01 0.16	0.01 0.11	0.03
Ca	0.00	0.00	0.00	0.00	0.00	0.00	0.00	0.00	0.00	0.00
Na	0.00	0.00	0.00	0.00	0.00	0.00	0.00	0.00	0.00	0.00
K	0.00	0.00	0.00	0.00	0.00	0.00	0.00	0.00	0.00	0.00
Ni	0.00	0.00	0.00	0.00	0.00	0.00	0.00	0.00	0.00	0.00
Zn Total	0.05 3.00	0.06 3.00	0.05 3.00	0.06 3.00	0.05 3.00	0.06 3.00	0.04 3.00	0.05 3.00	0.04 3.00	0.03 3.00
Cr#	69.30	69.20	69.49	69.44	70.66	69.50	66.51	65.76	66.51	66.43
Mg#	14.89	13.66	14.75	14.00	15.45	13.65	11.07	16.47	11.07	23.78
Fe#	85.11	86.34	85.25	86.00	84.55	86.35	88.93	83.53	88.93	76.22
Fe <sup>3+</sup> #	0.17	0.17	0.17	0.18	0.16	0.17	0.31	0.14	0.31	0.23
YFe <sup>3+</sup> # Sample	0.08 M/8/P	0.08 M/16/OP	0.08 M/16/OP	0.09 M/16/OP	0.07 M/16/OP	0.08 M/8R/P	0.19 M/8R/P	0.07 M/8/P	0.19 IK/3/P	0.11 IK/3/P
Mineral	Al-Chr	Al-Chr								
Ref Point	3 / 1 .	19 / 1 .	21 / 1 .	29 / 1 .	23 / 1 .	21 / 1 .	26 / 1 .	21 / 1 .	12 / 1 C	26 / 1 C
SiO <sub>2</sub>	0.01	0.00	0.04	0.04	0.02	0.02	0.04	0.03	0.00	0.00
TiO <sub>2</sub>	0.43	0.44 19.35	0.25 21.19	0.48 19.28	0.28 21.87	0.23	0.26	0.27	0.30	0.32 10.63
$Al_2O_3$ $Cr_2O_3$	15.03 43.08	42.69	41.74	43.09	41.42	19.14 38.84	21.60 39.54	18.91 39.50	12.96 46.32	51.52
FeO <sup>T</sup>	32.68	31.85	29.88	31.32	30.47	31.98	29.35	31.67	34.96	32.49
MnO	1.60	0.44	0.34	0.29	0.21	1.62	1.34	1.69	1.26	1.18
MgO	3.88	3.50	3.69	3.39	3.70	4.61	4.92	4.48	1.74	1.86
CaO No. O	0.00 0.03	0.00 0.07	0.00 0.07	0.00 0.03	0.00 0.05	0.00 0.03	0.02 0.05	0.00	0.02 0.05	0.03 0.03
Na <sub>2</sub> O K <sub>2</sub> O	0.00	0.07	0.07	0.03	0.03	0.03	0.03	0.00	0.00	0.00
NiO	0.00	0.00	0.00	0.00	0.00	0.00	0.00	0.00	0.12	0.23
ZnO	1.00	2.06	2.12	2.19	2.41	0.78	1.41	0.99	0.00	0.00
Total	97.75	100.41	99.32	100.09	100.43	97.24	98.56	97.54	97.73	98.29
Fe <sub>2</sub> O <sub>3</sub>	7.94 25.54	4.92	3.22	3.94	3.50	7.83	5.19	7.33	6.08	3.71
FeO Total	98.54	27.43 100.90	26.98 99.65	27.77 100.49	27.32 100.78	24.93 98.03	24.68 99.08	25.07 98.27	29.49 98.34	29.15 98.66
Cations :	4(O)	4(O)								
Si	0.00	0.00	0.00	0.00	0.00	0.00	0.00	0.00	0.00	0.00
Ti	0.01	0.01	0.01	0.01	0.01	0.01	0.01	0.01	0.01	0.01
Al	0.61	0.75	0.82	0.75	0.84	0.76	0.84	0.75	0.54	0.44
Cr Fe <sup>+3</sup>	1.17 0.20	1.11 0.12	1.09 0.08	1.13 0.10	1.07 0.09	1.03 0.20	1.03 0.13	1.05 0.19	1.29 0.16	1.44 0.10
Fe <sup>+2</sup>	0.73	0.75	0.74	0.77	0.74	0.70	0.68	0.70	0.87	0.86
Mn	0.05	0.01	0.01	0.01	0.01	0.05	0.04	0.05	0.04	0.04
Mg	0.20	0.17	0.18	0.17	0.18	0.23	0.24	0.22	0.09	0.10
Ca	0.00	0.00	0.00	0.00	0.00	0.00	0.00	0.00	0.00	0.00
Na K	0.00	0.00	0.00	0.00 0.00	0.00 0.00	0.00	0.00	0.00	0.00	0.00 0.00
K Ni	0.00	0.00	0.00	0.00	0.00	0.00	0.00	0.00	0.00	0.00
Zn	0.03	0.06	0.06	0.07	0.07	0.02	0.04	0.03	0.00	0.00
Total	3.00	3.00	3.00	3.00	3.00	3.00	3.00	3.00	3.00	3.00
Cr#	65.79	59.68	56.92	59.99	55.96	57.65	55.12	58.35	70.57	76.48
Mg#	21.32	18.53	19.61 80.39	17.87	19.45	24.77	26.22 73.78	24.16	9.52	10.21 89.79
Fe# Fe <sup>3+</sup> #	78.68 0.22	81.47 0.14	0.10	82.13 0.11	80.55 0.10	75.23 0.22	0.16	75.84 0.21	90.48 0.16	0.10
YFe <sup>3+</sup> #	0.10	0.06	0.04	0.05	0.04	0.10	0.06	0.09	0.08	0.05
	r Al Chromito C	I CI ' E	CL F . C	T C M	CI M	D D				

 $\begin{array}{c} Fe^{+\#} = 0.10 & 0.00 & 0.04 & 0.05 \\ \text{Notes: Al-Chr, Al-Chromite; Ch. Chromite; Fe-Chr, Ferrian Chromite; Cr-Mag, Chrome Magnetite; R-Rim Mag, Magnetite;. Cr# = <math>100^{\circ}$  Cr/(Cr+Al); Mg # =  $100^{\circ}$  Mg/(Mg+Fe); Fe # =  $100^{\circ}$  Fe/(Fe+Mg);  ${}^{Y}Fe^{3+\#} = Fe^{3+}/(Fe^{3+} + Cr + Al)$ : Fe $^{3+} \# = Fe^{3+}/(Fe^{3+} + Fe^{2+})$ .

Table 4.5 conti Sample	IK/3/P	IK/3/P	IK/3/P	IK/3/P	IK/3/P	IK/3/P	IK/3/P	M/16/OP	M/16/OP	M/10/P
Mineral	Al-Chr	Al-Chr	Chr	Chr	Chr	Chr	Chr	Fe-Chr	Fe-Chr	Fe-Chr
Ref Point SiO <sub>2</sub>	37 / 1C 0.03	73 / 1 C 0.01	11 / 1 C 0.00	23 / 1 C 0.02	29 / 1 C 0.02	45 / 1 C 0.00	51 / 1 C 0.00	18 / 1 0.034	22 / 1 0.004	66 / 1 0.03
SiO <sub>2</sub> ΓiO <sub>2</sub>	0.03	0.01	0.00	0.02	0.65	0.47	0.00	1.782	1.940	1.27
$Al_2O_3$	12.41	12.57	2.60	3.52	2.57	2.91	2.41	1.511	1.526	0.16
Cr <sub>2</sub> O <sub>3</sub>	48.83	46.09	41.05	44.25	46.59	46.55	45.84	37.034	37.899	31.40
$FeO^T$	33.56	35.82	47.97	44.38	43.72	43.91	44.81	53.928	54.317	58.88
MnO	1.27	1.21	1.56	1.65	1.70	1.83	1.70	0.334	0.367	0.89
MgO	1.81	1.71	0.72	0.59	0.57	0.52	0.56	0.799	0.790	0.44
CaO N= O	0.03 0.03	0.01 0.02	0.03 0.03	0.01 0.05	0.02 0.04	0.00 0.04	0.03 0.04	0.028 0.045	0.027 0.000	0.02 0.06
Na <sub>2</sub> O K <sub>2</sub> O	0.00	0.02	0.03	0.00	0.00	0.04	0.00	0.043	0.000	0.00
NiO	0.05	0.00	0.10	0.11	0.24	0.04	0.07	0.00	0.00	0.07
ZnO	0.00	0.00	0.00	0.00	0.00	0.00	0.00	0.628	0.761	0.00
Total	98.31	97.66	95.03	95.30	96.12	96.29	96.21	96.133	97.631	94.92
Fe <sub>2</sub> O <sub>3</sub>	4.38	6.78	20.86	16.87	16.22	16.40	17.15	25.826	25.544	33.37
FeO	29.62	29.71	29.20	29.20	29.12	29.15	29.38	30.689	31.331	28.85
Total Cations :	98.75 4(O)	98.34 4(O)	97.12 4(O)	96.99 4(O)	97.74 4(O)	97.93 4(O)	97.93 4(O)	98.720 4(O)	100.189 4(O)	98.26 4(O)
Si	0.00	0.00	0.00	0.00	0.00	0.00	0.00	0.001	0.000	0.00
Ti	0.01	0.01	0.03	0.02	0.02	0.01	0.02	0.050	0.054	0.04
Al	0.51	0.52	0.12	0.16	0.11	0.13	0.11	0.067	0.067	0.01
Cr	1.36	1.29	1.23	1.32	1.39	1.38	1.37	1.102	1.112	0.96
Fe <sup>+3</sup>	0.12	0.18	0.60	0.48	0.46	0.46	0.49	0.731	0.713	0.97
Fe <sup>+2</sup>	0.87	0.88	0.93	0.92	0.92	0.92	0.93	0.966	0.972	0.93
Mn Mg	0.04 0.09	0.04 0.09	0.05 0.04	0.05 0.03	0.05 0.03	0.06 0.03	0.05 0.03	0.011 0.045	0.012 0.044	0.03 0.03
Ca	0.09	0.09	0.04	0.03	0.03	0.03	0.00	0.043	0.001	0.03
Na Na	0.00	0.00	0.00	0.00	0.00	0.00	0.00	0.003	0.000	0.00
K	0.00	0.00	0.00	0.00	0.00	0.00	0.00	0.000	0.000	0.00
Ni	0.00	0.00	0.00	0.00	0.01	0.00	0.00	0.000	0.000	0.00
Zn	0.00	0.00	0.00	0.00	0.00	0.00	0.00	0.022	0.026	0.00
Total	3.00	3.00	3.00	3.00	3.00	3.00	3.00	3.000	3.000	3.00
Cr# Mg#	72.52 9.82	71.09 9.30	91.37 4.21	89.40 3.48	92.40 3.37	91.48 3.08	92.73 3.29	94.27 4.43	94.34 4.30	99.23 2.63
Fe#	90.18	90.70	95.79	96.52	96.63	96.92	96.71	95.57	95.70	97.37
Fe <sup>3+</sup> #	0.12	0.17	0.39	0.34	0.33	0.34	0.34	0.43	0.42	0.51
YFe <sup>3+</sup> #	0.06	0.09	0.31	0.24	0.23	0.23	0.25	0.38	0.38	0.50
Sample	M/10/P	HG/10/H	HG/10/H	HG/10/H	HG/10/H	HG/10/H	HG/10/H	HG/10/H	HG/10/H	IK/3/P
Mineral	Fe-Chr	Fe-Chr**	Fe-Chr**	Fe-Chr**	Fe-Chr**	Fe-Chr**	Fe-Chr**	Fe-Chr**	Fe-Chr	Cr-Mag
Ref Point SiO <sub>2</sub>	83 / 1 . 0.01	116 / 1 0.01	118 / 1 0.00	121 / 1 0.01	127 / 1 0.01	133 / 1 0.00	147 / 1 0.00	175 / 1 0.01	181 / 1 0.02	16 / 1 R 0.00
TiO <sub>2</sub>	0.17	1.02	1.31	1.01	1.26	1.25	1.19	1.50	1.24	0.34
$Al_2O_3$	0.06	0.19	0.26	0.21	0.18	0.21	0.27	0.32	0.25	0.00
$Cr_2O_3$	19.56	36.83	34.77	34.30	36.88	35.70	35.80	36.88	36.05	13.50
FeO <sup>T</sup>	71.90	53.93	56.14	56.64	54.73	57.02	55.10	53.79	54.90	77.91
MnO	0.21	0.85	0.76	0.38	0.70	0.50	0.52	0.34	0.35	0.51
MgO CaO	0.15 0.04	0.26	0.43	0.18	0.41	0.31				
Na <sub>2</sub> O	0.04				0.00		0.46	0.60	0.41	0.08
	0.07	0.00	0.00	0.01	0.00	0.00	0.02	0.02	0.02	0.05
K <sub>2</sub> O	0.07	0.00	0.00 0.03	0.01 0.00	0.05	0.00 0.09	0.02 0.07	0.02 0.03	0.02 0.01	0.05 0.01
	0.07 0.02 0.23		0.00	0.01		0.00	0.02	0.02	0.02	0.05
NiO ZnO	0.02 0.23 0.00	0.00 0.04 0.19 0.00	0.00 0.03 0.00 0.22 0.00	0.01 0.00 0.01 0.27 0.00	0.05 0.02 0.31 0.00	0.00 0.09 0.00 0.28 0.00	0.02 0.07 0.01 0.31 0.00	0.02 0.03 0.02 0.30 0.00	0.02 0.01 0.01 0.16 0.00	0.05 0.01 0.00 0.34 0.00
NiO ZnO Total	0.02 0.23 0.00 93.33	0.00 0.04 0.19 0.00 95.22	0.00 0.03 0.00 0.22 0.00 95.68	0.01 0.00 0.01 0.27 0.00 94.97	0.05 0.02 0.31 0.00 96.38	0.00 0.09 0.00 0.28 0.00 97.10	0.02 0.07 0.01 0.31 0.00 95.62	0.02 0.03 0.02 0.30 0.00 95.60	0.02 0.01 0.01 0.16 0.00 95.17	0.05 0.01 0.00 0.34 0.00 92.74
NiO ZnO Total Fe <sub>2</sub> O <sub>3</sub>	0.02 0.23 0.00 93.33 47.60	0.00 0.04 0.19 0.00 95.22 27.94	0.00 0.03 0.00 0.22 0.00 95.68 30.02	0.01 0.00 0.01 0.27 0.00 94.97 30.38	0.05 0.02 0.31 0.00 96.38 28.49	0.00 0.09 0.00 0.28 0.00 97.10 30.35	0.02 0.07 0.01 0.31 0.00 95.62 29.20	0.02 0.03 0.02 0.30 0.00 95.60 27.27	0.02 0.01 0.01 0.16 0.00 95.17 28.31	0.05 0.01 0.00 0.34 0.00 92.74 53.36
NiO ZnO Total Fe <sub>2</sub> O <sub>3</sub> FeO	0.02 0.23 0.00 93.33 47.60 29.06	0.00 0.04 0.19 0.00 95.22 27.94 28.79	0.00 0.03 0.00 0.22 0.00 95.68 30.02 29.12	0.01 0.00 0.01 0.27 0.00 94.97 30.38 29.30	0.05 0.02 0.31 0.00 96.38 28.49 29.10	0.00 0.09 0.00 0.28 0.00 97.10 30.35 29.71	0.02 0.07 0.01 0.31 0.00 95.62 29.20 28.83	0.02 0.03 0.02 0.30 0.00 95.60 27.27 29.25	0.02 0.01 0.01 0.16 0.00 95.17 28.31 29.43	0.05 0.01 0.00 0.34 0.00 92.74 53.36 29.89
NiO ZnO Total Fe <sub>2</sub> O <sub>3</sub> FeO Total	0.02 0.23 0.00 93.33 47.60 29.06 98.09	0.00 0.04 0.19 0.00 95.22 27.94 28.79 98.02	0.00 0.03 0.00 0.22 0.00 95.68 30.02 29.12 98.69	0.01 0.00 0.01 0.27 0.00 94.97 30.38 29.30 98.01	0.05 0.02 0.31 0.00 96.38 28.49 29.10 99.23	0.00 0.09 0.00 0.28 0.00 97.10 30.35 29.71 100.14	0.02 0.07 0.01 0.31 0.00 95.62 29.20 28.83 98.54	0.02 0.03 0.02 0.30 0.00 95.60 27.27 29.25 98.33	0.02 0.01 0.01 0.16 0.00 95.17 28.31 29.43 98.00	0.05 0.01 0.00 0.34 0.00 92.74 53.36 29.89 98.08
NiO ZnO Total Fe <sub>2</sub> O <sub>3</sub> FeO Total Cations:	0.02 0.23 0.00 93.33 47.60 29.06	0.00 0.04 0.19 0.00 95.22 27.94 28.79	0.00 0.03 0.00 0.22 0.00 95.68 30.02 29.12	0.01 0.00 0.01 0.27 0.00 94.97 30.38 29.30	0.05 0.02 0.31 0.00 96.38 28.49 29.10	0.00 0.09 0.00 0.28 0.00 97.10 30.35 29.71	0.02 0.07 0.01 0.31 0.00 95.62 29.20 28.83	0.02 0.03 0.02 0.30 0.00 95.60 27.27 29.25	0.02 0.01 0.01 0.16 0.00 95.17 28.31 29.43 98.00 4(O) 0.00	0.05 0.01 0.00 0.34 0.00 92.74 53.36 29.89
NiO ZnO Total Fe <sub>2</sub> O <sub>3</sub> FeO Total Cations:	0.02 0.23 0.00 93.33 47.60 29.06 98.09 4(O) 0.00 0.00	0.00 0.04 0.19 0.00 95.22 27.94 28.79 98.02 4(O) 0.00 0.03	0.00 0.03 0.00 0.22 0.00 95.68 30.02 29.12 98.69 4(O) 0.00 0.04	0.01 0.00 0.01 0.27 0.00 94.97 30.38 29.30 98.01 4(O) 0.00 0.03	0.05 0.02 0.31 0.00 96.38 28.49 29.10 99.23 4(O) 0.00 0.04	0.00 0.09 0.00 0.28 0.00 97.10 30.35 29.71 100.14 4(O) 0.00	0.02 0.07 0.01 0.31 0.00 95.62 29.20 28.83 98.54 4(O) 0.00 0.03	0.02 0.03 0.02 0.30 0.00 95.60 27.27 29.25 98.33 4(O)	0.02 0.01 0.01 0.16 0.00 95.17 28.31 29.43 98.00 4(O) 0.00	0.05 0.01 0.00 0.34 0.00 92.74 53.36 29.89 98.08 4(O) 0.00 0.01
NiO ZnO Total Fe <sub>2</sub> O <sub>3</sub> FeO Total Cations: Si Ti Al	0.02 0.23 0.00 93.33 47.60 29.06 98.09 4(O) 0.00 0.00	0.00 0.04 0.19 0.00 95.22 27.94 28.79 98.02 4(O) 0.00 0.03 0.01	0.00 0.03 0.00 0.22 0.00 95.68 30.02 29.12 98.69 4(O) 0.00 0.04	0.01 0.00 0.01 0.27 0.00 94.97 30.38 29.30 98.01 4(O) 0.00 0.03 0.01	0.05 0.02 0.31 0.00 96.38 28.49 29.10 99.23 4(O) 0.00 0.04	0.00 0.09 0.00 0.28 0.00 97.10 30.35 29.71 100.14 4(O) 0.00 0.04	0.02 0.07 0.01 0.31 0.00 95.62 29.20 28.83 98.54 4(O) 0.00 0.03	0.02 0.03 0.02 0.30 0.00 95.60 27.27 29.25 98.33 4(O) 0.00 0.04	0.02 0.01 0.01 0.16 0.00 95.17 28.31 29.43 98.00 4(O) 0.00 0.04	0.05 0.01 0.00 0.34 0.00 92.74 53.36 29.89 98.08 4(O) 0.00 0.01
NiO ZnO Total Fe <sub>2</sub> O <sub>3</sub> FeO Total Cations: Si Ti Al Cr	0.02 0.23 0.00 93.33 47.60 29.06 98.09 4(0) 0.00 0.00 0.00	0.00 0.04 0.19 0.00 95.22 27.94 28.79 98.02 4(O) 0.00 0.03 0.01 1.12	0.00 0.03 0.00 0.22 0.00 95.68 30.02 29.12 98.69 4(O) 0.00 0.04 0.01	0.01 0.00 0.01 0.27 0.00 94.97 30.38 29.30 98.01 4(O) 0.00 0.03 0.01 1.05	0.05 0.02 0.31 0.00 96.38 28.49 29.10 99.23 4(O) 0.00 0.04 0.01 1.11	0.00 0.09 0.00 0.28 0.00 97.10 30.35 29.71 100.14 4(O) 0.00 0.04 0.01	0.02 0.07 0.01 0.31 0.00 95.62 29.20 28.83 98.54 4(O) 0.00 0.03 0.01	0.02 0.03 0.02 0.30 0.00 95.60 27.27 29.25 98.33 4(O) 0.00 0.04 0.01	0.02 0.01 0.01 0.16 0.00 95.17 28.31 29.43 98.00 4(O) 0.00 0.04 0.01	0.05 0.01 0.00 0.34 0.00 92.74 53.36 29.89 98.08 4(O) 0.00 0.01 0.00 0.42
NiO ZnO ZnO ZnO ZnO Znol Znol Znol Znol Znol Znol Znol Znol	0.02 0.23 0.00 93.33 47.60 29.06 98.09 4(O) 0.00 0.00 0.00 0.60 1.39	0.00 0.04 0.19 0.00 95.22 27.94 28.79 98.02 4(O) 0.00 0.03 0.01 1.12 0.81	0.00 0.03 0.00 0.22 0.00 95.68 30.02 29.12 98.69 4(O) 0.00 0.04 0.01 1.05 0.86	0.01 0.00 0.01 0.27 0.00 94.97 30.38 29.30 98.01 4(O) 0.00 0.03 0.01 1.05 0.88	0.05 0.02 0.31 0.00 96.38 28.49 29.10 99.23 4(O) 0.00 0.04 0.01 1.11 0.81	0.00 0.09 0.00 0.28 0.00 97.10 30.35 29.71 100.14 4(O) 0.00 0.04 0.01 1.06 0.86	0.02 0.07 0.01 0.31 0.00 95.62 29.20 28.83 98.54 4(O) 0.00 0.03 0.01 1.08	0.02 0.03 0.02 0.30 0.00 95.60 27.27 29.25 98.33 4(O) 0.00 0.04 0.01 1.12 0.79	0.02 0.01 0.01 0.16 0.00 95.17 28.31 29.43 98.00 4(O) 0.00 0.04 0.01 1.10 0.82	0.05 0.01 0.00 0.34 0.00 92.74 53.36 29.89 98.08 4(O) 0.00 0.01 0.00 0.42 1.56
NiO ZnO ZnO Total Fe <sub>2</sub> O <sub>3</sub> FeO Total Cations: Si Ti Al Cr Fe <sup>+3</sup> Fe <sup>+3</sup> Fe <sup>+2</sup>	0.02 0.23 0.00 93.33 47.60 29.06 98.09 4(O) 0.00 0.00 0.00 0.60 1.39 0.94	0.00 0.04 0.19 0.00 95.22 27.94 28.79 98.02 4(O) 0.03 0.01 1.12 0.81 0.93	0.00 0.03 0.00 0.22 0.00 95.68 30.02 29.12 98.69 4(O) 0.04 0.01 1.05 0.86 0.93	0.01 0.00 0.01 0.27 0.00 94.97 30.38 29.30 98.01 4(O) 0.00 0.03 0.01 1.05 0.88 0.95	0.05 0.02 0.31 0.00 96.38 28.49 29.10 99.23 4(O) 0.00 0.04 0.01 1.11 0.81 0.93	0.00 0.09 0.00 0.28 0.00 97.10 30.35 29.71 100.14 4(O) 0.04 0.01 1.06 0.86 0.94	0.02 0.07 0.01 0.31 0.00 95.62 29.20 28.83 98.54 4(O) 0.03 0.01 1.08 0.84 0.92	0.02 0.03 0.02 0.30 0.00 95.60 27.27 29.25 98.33 4(O) 0.04 0.04 0.01 1.12 0.79 0.94	0.02 0.01 0.01 0.16 0.00 95.17 28.31 29.43 98.00 4(O) 0.04 0.01 1.10 0.82 0.95	0.05 0.01 0.00 0.34 0.00 92.74 53.36 29.89 98.08 4(O) 0.01 0.00 0.42 1.56 0.97
NiO ZnO Total Fe <sub>2</sub> O <sub>3</sub> FeO Total Cations: Si Ti Al Cr Fe <sup>+3</sup> Fe <sup>+2</sup> Wn Mn	0.02 0.23 0.00 93.33 47.60 29.06 98.09 4(O) 0.00 0.00 0.00 0.60 1.39 0.94	0.00 0.04 0.19 0.00 95.22 27.94 28.79 98.02 4(O) 0.03 0.01 1.12 0.81 0.93 0.03	0.00 0.03 0.00 0.22 0.00 95.68 30.02 29.12 98.69 4(O) 0.00 0.04 0.01 1.05 0.86 0.93 0.02	0.01 0.00 0.01 0.27 0.00 94.97 30.38 29.30 98.01 4(O) 0.00 0.03 0.01 1.05 0.88 0.95 0.01	0.05 0.02 0.31 0.00 96.38 28.49 29.10 99.23 4(O) 0.00 0.04 0.01 1.11 0.81 0.93 0.02	0.00 0.09 0.00 0.28 0.00 97.10 30.35 29.71 100.14 4(O) 0.00 0.04 0.04 0.86 0.86 0.94	0.02 0.07 0.01 0.31 0.00 95.62 29.20 28.83 98.54 4(O) 0.00 0.03 0.01 1.08 0.84 0.92	0.02 0.03 0.02 0.30 0.00 95.60 27.27 29.25 98.33 4(O) 0.00 0.04 0.01 1.12 0.79 0.94	0.02 0.01 0.01 0.16 0.00 95.17 28.31 29.43 98.00 4(O) 0.00 0.04 0.01 1.10 0.82 0.95	0.05 0.01 0.00 0.34 0.00 92.74 53.36 29.89 98.08 4(O) 0.00 0.01 0.00 0.42 1.56 0.97
NiO ZnO ZnO Total Fe <sub>2</sub> O <sub>3</sub> FeO Total Cations: Si Ti Al Cr Fe <sup>+3</sup> Fe <sup>+2</sup> Mn Mg	0.02 0.23 0.00 93.33 47.60 29.06 98.09 4(O) 0.00 0.00 0.00 0.60 1.39 0.94	0.00 0.04 0.19 0.00 95.22 27.94 28.79 98.02 4(O) 0.00 0.03 0.01 1.12 0.81 0.93 0.03 0.03	0.00 0.03 0.00 0.22 0.00 95.68 30.02 29.12 98.69 4(O) 0.00 0.04 0.01 1.05 0.86 0.93 0.02	0.01 0.00 0.01 0.27 0.00 94.97 30.38 29.30 98.01 4(O) 0.00 0.03 0.01 1.05 0.88 0.95	0.05 0.02 0.31 0.00 96.38 28.49 29.10 99.23 4(O) 0.00 0.04 0.01 1.11 0.81 0.93 0.02 0.02	0.00 0.09 0.00 0.28 0.00 97.10 30.35 29.71 100.14 4(O) 0.00 0.04 0.01 1.06 0.86 0.94 0.02	0.02 0.07 0.01 0.31 0.00 95.62 29.20 28.83 98.54 4(O) 0.03 0.01 1.08 0.84 0.92	0.02 0.03 0.02 0.30 0.00 95.60 27.27 29.25 98.33 4(O) 0.04 0.04 0.01 1.12 0.79 0.94	0.02 0.01 0.01 0.16 0.00 95.17 28.31 29.43 98.00 4(O) 0.00 0.04 0.01 1.10 0.82 0.95 0.01 0.02	0.05 0.01 0.00 0.34 0.00 92.74 53.36 29.89 98.08 4(O) 0.01 0.00 0.42 1.56 0.97
NiO ZnO ZnO ZnO ZnO Total Fe <sub>2</sub> O <sub>3</sub> FeO Total Cations: Si Ti Al Cr Fe <sup>+3</sup> Fe <sup>+2</sup> Mn Mg Ca	0.02 0.23 0.00 93.33 47.60 29.06 98.09 4(O) 0.00 0.00 0.00 0.60 1.39 0.94 0.01	0.00 0.04 0.19 0.00 95.22 27.94 28.79 98.02 4(O) 0.03 0.01 1.12 0.81 0.93 0.03	0.00 0.03 0.00 0.22 0.00 95.68 30.02 29.12 98.69 4(O) 0.00 0.04 0.01 1.05 0.86 0.93 0.02 0.02	0.01 0.00 0.01 0.27 0.00 94.97 30.38 29.30 98.01 4(O) 0.00 0.03 0.01 1.05 0.88 0.95 0.01	0.05 0.02 0.31 0.00 96.38 28.49 29.10 99.23 4(O) 0.00 0.04 0.01 1.11 0.81 0.93 0.02	0.00 0.09 0.00 0.28 0.00 97.10 30.35 29.71 100.14 4(O) 0.00 0.04 0.04 0.01 1.06 0.86 0.94 0.02 0.02	0.02 0.07 0.01 0.31 0.00 95.62 29.20 28.83 98.54 4(O) 0.00 0.03 0.01 1.08 0.84 0.92 0.03	0.02 0.03 0.02 0.30 0.00 95.60 27.27 29.25 98.33 4(O) 0.00 0.04 0.01 1.12 0.79 0.94 0.01	0.02 0.01 0.01 0.16 0.00 95.17 28.31 29.43 98.00 4(O) 0.00 0.04 0.01 1.10 0.82 0.95	0.05 0.01 0.00 0.34 0.00 92.74 53.36 29.89 98.08 4(O) 0.00 0.01 0.00 0.42 1.56 0.97 0.02
NiO ZnO Total Fe <sub>2</sub> O <sub>3</sub> FeO Total Cations: Si Ti Al Cr Fe <sup>+3</sup> Fe <sup>+2</sup> Mn Mg Ca Na K	0.02 0.23 0.00 93.33 47.60 29.06 98.09 4(O) 0.00 0.00 0.60 1.39 0.94 0.01 0.01 0.00	0.00 0.04 0.19 0.00 95.22 27.94 28.79 98.02 4(O) 0.00 0.03 0.01 1.12 0.81 0.93 0.03 0.02 0.00 0.00 0.00	0.00 0.03 0.00 0.22 0.00 95.68 30.02 29.12 98.69 4(O) 0.00 0.04 0.01 1.05 0.86 0.93 0.02 0.02 0.00 0.00	0.01 0.00 0.01 0.27 0.00 94.97 30.38 29.30 98.01 4(O) 0.00 0.03 0.01 1.05 0.88 0.95 0.01 0.00 0.00 0.00	0.05 0.02 0.31 0.00 96.38 28.49 29.10 99.23 4(O) 0.00 0.04 0.01 1.11 0.81 0.93 0.02 0.02 0.00 0.00 0.00	0.00 0.09 0.00 0.28 0.00 97.10 30.35 29.71 100.14 4(O) 0.00 0.04 0.04 0.01 1.06 0.86 0.94 0.02 0.02 0.00 0.01	0.02 0.07 0.01 0.31 0.00 95.62 29.20 28.83 98.54 4(O) 0.00 0.03 0.01 1.08 0.84 0.92 0.02 0.03 0.00	0.02 0.03 0.02 0.30 0.00 95.60 27.27 29.25 98.33 4(O) 0.00 0.04 0.01 1.12 0.79 0.94 0.01 0.03 0.00 0.00	0.02 0.01 0.01 0.01 0.16 0.00 95.17 28.31 29.43 98.00 4(O) 0.00 0.04 0.01 1.10 0.82 0.95 0.01 0.02 0.00 0.00	0.05 0.01 0.00 0.34 0.00 92.74 53.36 29.89 98.08 4(O) 0.00 0.01 0.00 0.42 1.56 0.97 0.02 0.00 0.00 0.00 0.00 0.00
NiO ZnO ZnO ZnO ZnO Total Fe <sub>2</sub> O <sub>3</sub> FeO Total Cations: Si Ti Al Cr Fe <sup>*3</sup> Fe* <sup>2</sup> Mn Mg Ca Na Na K Ni	0.02 0.23 0.00 93.33 47.60 29.06 98.09 4(O) 0.00 0.00 0.60 1.39 0.94 0.01 0.01 0.00	0.00 0.04 0.19 0.00 95.22 27.94 28.79 98.02 4(O) 0.00 0.03 0.01 1.12 0.81 0.93 0.03 0.02 0.00 0.00 0.00 0.00	0.00 0.03 0.00 0.22 0.00 95.68 30.02 29.12 98.69 4(O) 0.00 0.04 0.01 1.05 0.86 0.93 0.02 0.02 0.02 0.00 0.00	0.01 0.00 0.01 0.27 0.00 94.97 30.38 29.30 98.01 4(O) 0.00 0.03 0.01 1.05 0.88 0.95 0.01 0.00 0.00 0.00	0.05 0.02 0.31 0.00 96.38 28.49 29.10 99.23 4(O) 0.00 0.04 0.01 1.11 0.81 0.93 0.02 0.02 0.00 0.00 0.00	0.00 0.09 0.00 0.28 0.00 97.10 30.35 29.71 100.14 4(O) 0.00 0.04 0.01 1.06 0.86 0.94 0.02 0.02 0.02	0.02 0.07 0.01 0.31 0.00 95.62 29.20 28.83 98.54 4(O) 0.00 0.03 0.01 1.08 0.84 0.92 0.02 0.03 0.00 0.03	0.02 0.03 0.02 0.30 0.00 95.60 27.27 29.25 98.33 4(O) 0.00 0.04 0.01 1.12 0.79 0.94 0.03 0.00 0.00 0.00	0.02 0.01 0.01 0.16 0.00 95.17 28.31 29.43 98.00 4(O) 0.00 0.04 0.01 1.10 0.82 0.95 0.01 0.02 0.00 0.00	0.05 0.01 0.00 0.34 0.00 92.74 53.36 29.89 98.08 4(O) 0.00 0.01 0.00 0.42 1.56 0.97 0.02 0.00 0.00 0.00 0.00 0.00
NiO ZnO ZnO ZnO ZnO Total Fe <sub>2</sub> O <sub>3</sub> FeO Total Cations: Si Ti Al Cr Fe <sup>+3</sup> Fe <sup>+2</sup> Mn Mg Ca Na K K Ni Zn	0.02 0.23 0.00 93.33 47.60 29.06 98.09 4(O) 0.00 0.00 0.00 0.60 1.39 0.94 0.01 0.00 0.01	0.00 0.04 0.19 0.00 95.22 27.94 28.79 98.02 4(O) 0.03 0.01 1.12 0.81 0.93 0.03 0.02 0.00 0.00 0.00 0.00	0.00 0.03 0.00 0.22 0.00 95.68 30.02 29.12 98.69 4(O) 0.00 0.04 0.01 1.05 0.86 0.93 0.02 0.02 0.00 0.00 0.00	0.01 0.00 0.01 0.27 0.00 94,97 30.38 29.30 98.01 4(O) 0.00 0.03 0.01 1.05 0.88 0.95 0.01 0.00 0.00 0.00 0.01 0.00 0.00	0.05 0.02 0.31 0.00 96.38 28.49 29.10 99.23 4(O) 0.04 0.01 1.11 0.81 0.93 0.02 0.02 0.00 0.00 0.00 0.00 0.00 0.0	0.00 0.09 0.09 0.00 0.28 0.00 97.10 30.35 29.71 100.14 4(O) 0.00 0.04 0.01 1.06 0.86 0.94 0.02 0.02 0.00 0.01 0.00	0.02 0.07 0.01 0.31 0.00 95.62 29.20 28.83 98.54 4(O) 0.00 0.03 0.01 1.08 0.84 0.92 0.02 0.03 0.00 0.00 0.00 0.00 0.00	0.02 0.03 0.02 0.30 0.00 95.60 27.27 29.25 98.33 4(O) 0.00 0.04 0.01 1.12 0.79 0.94 0.01 0.03 0.00 0.00 0.00 0.00 0.01	0.02 0.01 0.01 0.16 0.00 95.17 28.31 29.43 98.00 4(O) 0.00 0.04 0.01 1.10 0.82 0.95 0.01 0.02 0.00 0.00 0.00 0.00	0.05 0.01 0.00 0.34 0.00 92.74 53.36 29.89 98.08 4(O) 0.00 0.01 0.00 0.42 1.56 0.97 0.02 0.00 0.00 0.00 0.00 0.00 0.00 0.01
NiO ZnO ZnO ZnO ZnO Total Fe₂O₃ FeO Cations: Si Ti Al Cr Fe² Mn Mg Ca K Ni X Ni Zn Total	0.02 0.23 0.00 93.33 47.60 29.06 98.09 4(O) 0.00 0.00 0.00 0.60 1.39 0.94 0.01 0.01 0.00 0.01	0.00 0.04 0.19 0.00 95.22 27.94 28.79 98.02 4(O) 0.00 0.03 0.01 1.12 0.81 0.93 0.03 0.02 0.00 0.00 0.03	0.00 0.03 0.00 0.22 0.00 95.68 30.02 29.12 98.69 4(O) 0.00 0.04 0.01 1.05 0.86 0.93 0.02 0.02 0.00 0.00 0.01 1.05 0.00 0.01 1.05 0.00 0.00 0.00 0.01 1.05 0.00 0.00 0.00 0.00 0.00 0.00 0.01 0.00 0.00 0.00 0.00 0.00 0.00 0.00 0.00 0.00 0.00 0.00 0.00 0.00 0.00 0.00 0.00 0.00 0.00 0.00 0.00 0.00 0.00 0.00 0.00 0.00 0.00 0.00 0.00 0.00 0.00 0.00 0.00 0.00 0.00 0.00 0.00 0.00 0.00 0.00 0.00 0.00 0.00 0.00 0.00 0.00 0.00 0.00 0.00 0.00 0.00 0.00 0.00 0.00 0.00 0.00 0.00 0.00 0.00 0.00 0.00 0.00 0.00 0.00 0.00 0.00 0.00 0.00 0.00 0.00 0.00 0.00 0.00 0.00 0.00 0.00 0.00 0.00 0.00 0.00 0.00 0.00 0.00 0.00 0.00 0.00 0.00 0.00 0.00 0.00 0.00 0.00 0.00 0.00 0.00 0.00 0.00 0.00 0.00 0.00 0.00 0.00 0.00 0.00 0.00 0.00 0.00 0.00 0.00 0.00 0.00 0.00 0.00 0.00 0.00 0.00 0.00 0.00 0.00 0.00 0.00 0.00 0.00 0.00 0.00 0.00 0.00 0.00 0.00 0.00 0.00 0.00 0.00 0.00 0.00 0.00 0.00 0.00 0.00 0.00 0.00 0.00 0.00 0.00 0.00 0.00 0.00 0.00 0.00 0.00 0.00 0.00 0.00 0.00 0.00 0.00 0.00 0.00 0.00 0.00 0.00 0.00 0.00 0.00 0.00 0.00 0.00 0.00 0.00 0.00 0.00 0.00 0.00 0.00 0.00 0.00 0.00 0.00 0.00 0.00 0.00 0.00 0.00 0.00 0.00 0.00 0.00 0.00 0.00 0.00 0.00 0.00 0.00 0.00 0.00 0.00 0.00 0.00 0.00 0.00 0.00 0.00 0.00 0.00 0.00 0.00 0.00 0.00 0.00 0.00 0.00 0.00 0.00 0.00 0.00 0.00 0.00 0.00 0.00 0.00 0.00 0.00 0.00 0.00 0.00 0.00 0.00 0.00 0.00 0.00 0.00 0.00 0.00 0.00 0.00 0.00 0.00 0.00 0.00 0.00 0.00 0.00 0.00 0.00 0.00 0.00 0.00 0.00 0.00 0.00 0.00 0.00 0.00 0.00 0.00 0.00 0.00 0.00 0.00 0.00 0.00 0.00 0.00 0.00 0.00 0.00 0.00 0.00 0.00 0.00 0.00 0.00 0.00 0.00 0.00 0.00 0.00 0.00 0.00 0.00 0.00 0.00 0.00 0.00 0.00 0.00 0.00 0.00 0.00 0.00 0.00 0.00 0.00 0.00 0.00 0.00 0.00 0.00 0.00 0.00 0.00 0.00 0.00 0.00 0.	0.01 0.00 0.01 0.27 0.00 94.97 30.38 29.30 98.01 4(O) 0.00 0.03 0.01 1.05 0.88 0.95 0.01 0.00 0.00 0.00 0.00 0.01 0.00 0.00 0.01 0.00 0.00 0.01 0.00 0.00 0.00 0.00 0.00 0.00 0.00 0.00 0.00 0.00 0.00 0.00 0.00 0.00 0.00 0.00 0.00 0.00 0.00 0.00 0.00 0.00 0.00 0.00 0.00 0.00 0.00 0.00 0.00 0.00 0.00 0.00 0.00 0.00 0.00 0.00 0.00 0.00 0.00 0.00 0.00 0.00 0.00 0.00 0.00 0.00 0.00 0.00 0.00 0.00 0.00 0.00 0.00 0.00 0.00 0.00 0.00 0.00 0.00 0.00 0.00 0.00 0.00 0.00 0.00 0.00 0.00 0.00 0.00 0.00 0.00 0.00 0.00 0.00 0.00 0.00 0.00 0.00 0.00 0.00 0.00 0.00 0.00 0.00 0.00 0.00 0.00 0.00 0.00 0.00 0.00 0.00 0.00 0.00 0.00 0.00 0.00 0.00 0.00 0.00 0.00 0.00 0.00 0.00 0.00 0.00 0.00 0.00 0.00 0.00 0.00 0.00 0.00 0.00 0.00 0.00 0.00 0.00 0.00 0.00 0.00 0.00 0.00 0.00 0.00 0.00 0.00 0.00 0.00 0.00 0.00 0.00 0.00 0.00 0.00 0.00 0.00 0.00 0.00 0.00 0.00 0.00 0.00 0.00 0.00 0.00 0.00 0.00 0.00 0.00 0.00 0.00 0.00 0.00 0.00 0.00 0.00 0.00 0.00 0.00 0.00 0.00 0.00 0.00 0.00 0.00 0.00 0.00 0.00 0.00 0.00 0.00 0.00 0.00 0.00 0.00 0.00 0.00 0.00 0.00 0.00 0.00 0.00 0.00 0.00 0.00 0.00 0.00 0.00 0.00 0.00 0.00 0.00 0.00 0.00 0.00 0.00 0.00 0.00 0.00 0.00 0.00 0.00 0.00 0.00 0.00 0.00 0.00 0.00 0.00 0.00 0.00 0.00 0.00 0.00 0.00 0.00 0.00 0.00 0.00 0.00 0.00 0.00 0.00 0.00 0.00 0.00 0.00 0.00 0.00 0.00 0.00 0.00 0.00 0.00 0.00 0.00 0.00 0.00 0.00 0.00 0.00 0.00 0.00 0.00 0.00 0.00 0.00 0.00 0.00 0.00 0.00 0.00 0.00 0.00 0.00 0.00 0.00 0.00 0.00 0.00 0.00 0.00 0.00 0.00 0.00 0.00 0.00 0.00 0.00 0.00 0.00 0.00 0.00 0.00 0.00 0.00 0.00 0.00 0.00 0.00 0.00 0.00 0.00 0.00 0.00 0.00 0.00 0.00 0.00 0.00 0.00 0.00 0.00 0.00 0.00 0.00 0.00 0.00 0.00 0.00 0.00 0.00 0.00 0.00 0.00 0.00 0.00 0.00 0.00 0.00 0.00 0.	0.05 0.02 0.31 0.00 96.38 28.49 29.10 99.23 4(O) 0.00 0.04 0.01 1.11 0.81 0.93 0.02 0.02 0.00 0.00 0.00 0.00 0.00 0.0	0.00 0.09 0.00 0.28 0.00 97.10 30.35 29.71 100.14 4(O) 0.00 0.04 0.01 1.06 0.86 0.94 0.02 0.02 0.00 0.01 0.00 0.01 0.00 0.01	0.02 0.07 0.01 0.31 0.00 95.62 29.20 28.83 98.54 4(O) 0.00 0.03 0.01 1.08 0.84 0.92 0.02 0.03 0.00 0.00 0.00 0.00 0.00 0.0	0.02 0.03 0.02 0.30 0.00 95.60 27.27 29.25 98.33 4(O) 0.00 0.04 0.01 1.12 0.79 0.94 0.01 0.03 0.00 0.00 0.00 0.00 0.01 0.01 0.03 0.00 0.00 0.00 0.00 0.00 0.00 0.00 0.00 0.00 0.00 0.00 0.00 0.00 0.00 0.00 0.00 0.00 0.00 0.00 0.00 0.00 0.00 0.00 0.00 0.00 0.00 0.00 0.00 0.00 0.00 0.00 0.00 0.00 0.00 0.00 0.00 0.00 0.00 0.00 0.00 0.00 0.00 0.00 0.00 0.00 0.00 0.00 0.00 0.00 0.00 0.00 0.00 0.00 0.00 0.00 0.00 0.00 0.00 0.00 0.00 0.00 0.00 0.00 0.00 0.00 0.00 0.00 0.00 0.00 0.00 0.00 0.00 0.00 0.00 0.00 0.00 0.00 0.00 0.00 0.00 0.00 0.00 0.00 0.00 0.00 0.00 0.00 0.00 0.00 0.00 0.00 0.00 0.00 0.00 0.00 0.00 0.00 0.00 0.00 0.00 0.00 0.00 0.00 0.00 0.00 0.00 0.00 0.00 0.00 0.00 0.00 0.00 0.00 0.00 0.00 0.00 0.00 0.00 0.00 0.00 0.00 0.00 0.00 0.00 0.00 0.00 0.00 0.00 0.00 0.00 0.00 0.00 0.00 0.00 0.00 0.00 0.00 0.00 0.00 0.00 0.00 0.00 0.00 0.00 0.00 0.00 0.00 0.00 0.00 0.00 0.00 0.00 0.00 0.00 0.00 0.00 0.00 0.00 0.00 0.00 0.00 0.00 0.00 0.00 0.00 0.00 0.00 0.00 0.00 0.00 0.00 0.00 0.00 0.00 0.00 0.00 0.00 0.00 0.00 0.00 0.00 0.00 0.00 0.00 0.00 0.00 0.00 0.00 0.00 0.00 0.00 0.00 0.00 0.00 0.00 0.00 0.00 0.00 0.00 0.00 0.00 0.00 0.00 0.00 0.00 0.00 0.00 0.00 0.00 0.00 0.00 0.00 0.00 0.00 0.00 0.00 0.00 0.00 0.00 0.00 0.00 0.00 0.00 0.00 0.00 0.00 0.00 0.00 0.00 0.00 0.00 0.00 0.00 0.00 0.00 0.00 0.00 0.00 0.00 0.00 0.00 0.00 0.00 0.00 0.00 0.00 0.00 0.00 0.00 0.00 0.00 0.00 0.00 0.00 0.00 0.00 0.00 0.00 0.00 0.00 0.00 0.00 0.00 0.00 0.00 0.00 0.00 0.00 0.00 0.00 0.00 0.00 0.00 0.00 0.00 0.00 0.00 0.00 0.00 0.00 0.00 0.00 0.00 0.00 0.00 0.00 0.00 0.00 0.00 0.00 0.00 0.00 0.00 0.00 0.00 0.00 0.00 0.00 0.00 0.00 0.00 0.00 0.00 0.00 0.00 0.00 0.00 0.00 0.00 0.00 0.00 0.00 0.00 0.00 0.00 0.	0.02 0.01 0.01 0.01 0.00 95.17 28.31 29.43 98.00 4(O) 0.00 0.04 0.01 1.10 0.82 0.95 0.01 0.02 0.00 0.00 0.00 0.00 0.00 0.00 0.00 0.00 0.00 0.00 0.00 0.00 0.00 0.00 0.00 0.00 0.00 0.00 0.00 0.00 0.00 0.00 0.00 0.00 0.00 0.00 0.00 0.00 0.00 0.00 0.00 0.00 0.00 0.00 0.00 0.00 0.00 0.00 0.00 0.00 0.00 0.00 0.00 0.00 0.00 0.00 0.00 0.00 0.00 0.00 0.00 0.00 0.00 0.00 0.00 0.00 0.00 0.00 0.00 0.00 0.00 0.00 0.00 0.00 0.00 0.00 0.00 0.00 0.00 0.00 0.00 0.00 0.00 0.00 0.00 0.00 0.00 0.00 0.00 0.00 0.00 0.00 0.00 0.00 0.00 0.00 0.00 0.00 0.00 0.00 0.00 0.00 0.00 0.00 0.00 0.00 0.00 0.00 0.00 0.00 0.00 0.00 0.00 0.00 0.00 0.00 0.00 0.00 0.00 0.00 0.00 0.00 0.00 0.00 0.00 0.00 0.00 0.00 0.00 0.00 0.00 0.00 0.00 0.00 0.00 0.00 0.00 0.00 0.00 0.00 0.00 0.00 0.00 0.00 0.00 0.00 0.00 0.00 0.00 0.00 0.00 0.00 0.00 0.00 0.00 0.00 0.00 0.00 0.00 0.00 0.00 0.00 0.00 0.00 0.00 0.00 0.00 0.00 0.00 0.00 0.00 0.00 0.00 0.00 0.00 0.00 0.00 0.00 0.00 0.00 0.00 0.00 0.00 0.00 0.00 0.00 0.00 0.00 0.00 0.00 0.00 0.00 0.00 0.00 0.00 0.00 0.00 0.00 0.00 0.00 0.00 0.00 0.00 0.00 0.00 0.00 0.00 0.00 0.00 0.00 0.00 0.00 0.00 0.00 0.00 0.00 0.00 0.00 0.00 0.00 0.00 0.00 0.00 0.00 0.00 0.00 0.00 0.00 0.00 0.00 0.00 0.00 0.00 0.00 0.00 0.00 0.00 0.00 0.00 0.00 0.00 0.00 0.00 0.00 0.00 0.00 0.00 0.00 0.00 0.00 0.00 0.00 0.00 0.00 0.00 0.00 0.00 0.00 0.00 0.00 0.00 0.00 0.00 0.00 0.00 0.00 0.00 0.00 0.00 0.00 0.00 0.00 0.00 0.00 0.00 0.00 0.00 0.00 0.00 0.00 0.00 0.00 0.00 0.00 0.00 0.00 0.00 0.00 0.00 0.00 0.00 0.00 0.00 0.00 0.00 0.00 0.00 0.00 0.00 0.00 0.00 0.00 0.00 0.00 0.00 0.00 0.00 0.00 0.00 0.00 0.00 0.00 0.00 0.00 0.00 0.00 0.00 0.00 0.00 0.00 0.00 0.00 0.00 0.00 0.00 0.00 0.00 0.00 0.00 0.00 0.00 0.00 0.	0.05 0.01 0.00 0.34 0.00 92.74 53.36 29.89 98.08 4(O) 0.00 0.01 0.00 0.42 1.56 0.97 0.02 0.00 0.00 0.00 0.00 0.00 0.00 0.00 0.00 0.00 0.00 0.00 0.00 0.00 0.00 0.00 0.00 0.00 0.00 0.00 0.00 0.00 0.00 0.00 0.00 0.00 0.00 0.00 0.00 0.00 0.00 0.00 0.00 0.00 0.00 0.00 0.00 0.00 0.00 0.00 0.00 0.00 0.00 0.00 0.00 0.00 0.00 0.00 0.00 0.00 0.00 0.00 0.00 0.00 0.00 0.00 0.00 0.00 0.00 0.00 0.00 0.00 0.00 0.00 0.00 0.00 0.00 0.00 0.00 0.00 0.00 0.00 0.00 0.00 0.00 0.00 0.00 0.00 0.00 0.00 0.00 0.00 0.00 0.00 0.00 0.00 0.00 0.00 0.00 0.00 0.00 0.00 0.00 0.00 0.00 0.00 0.00 0.00 0.00 0.00 0.00 0.00 0.00 0.00 0.00 0.00 0.00 0.00 0.00 0.00 0.00 0.00 0.00 0.00 0.00 0.00 0.00 0.00 0.00 0.00 0.00 0.00 0.00 0.00 0.00 0.00 0.00 0.00 0.00 0.00 0.00 0.00 0.00 0.00 0.00 0.00 0.00 0.00 0.00 0.00 0.00 0.00 0.00 0.00 0.00 0.00 0.00 0.00 0.00 0.00 0.00 0.00 0.00 0.00 0.00 0.00 0.00 0.00 0.00 0.00 0.00 0.00 0.00 0.00 0.00 0.00 0.00 0.00 0.00 0.00 0.00 0.00 0.00 0.00 0.00 0.00 0.00 0.00 0.00 0.00 0.00 0.00 0.00 0.00 0.00 0.00 0.00 0.00 0.00 0.00 0.00 0.00 0.00 0.00 0.00 0.00 0.00 0.00 0.00 0.00 0.00 0.00 0.00 0.00 0.00 0.00 0.00 0.00 0.00 0.00 0.00 0.00 0.00 0.00 0.00 0.00 0.00 0.00 0.00 0.00 0.00 0.00 0.00 0.00 0.00 0.00 0.00 0.00 0.00 0.00 0.00 0.00 0.00 0.00 0.00 0.00 0.00 0.00 0.00 0.00 0.00 0.00 0.00 0.00 0.00 0.00 0.00 0.00 0.00 0.00 0.00 0.00 0.00 0.00 0.00 0.00 0.00 0.00 0.00 0.00 0.00 0.00 0.00 0.00 0.00 0.00 0.00 0.00 0.00 0.00 0.00 0.00 0.00 0.00 0.00 0.00 0.00 0.00 0.00 0.00 0.00 0.00 0.00 0.00 0.00 0.00 0.00 0.00 0.00 0.00 0.00 0.00 0.00 0.00 0.00 0.00 0.00 0.00 0.00 0.00 0.00 0.00 0.00 0.00 0.00 0.00 0.00 0.00 0.00 0.00 0.00 0.00 0.00 0.00 0.00 0.00 0.00 0.00 0.00 0.00 0.00 0.00 0.00 0.00 0.
NiO ZnO ZnO ZnO ZnO Total Fe <sub>2</sub> O <sub>3</sub> FeO Total Cations: Si Ti Al Cr Fe <sup>+3</sup> Fe <sup>+2</sup> Mn Mg Ca Na K Ni Zn Total Cr#	0.02 0.23 0.00 93.33 47.60 29.06 98.09 4(O) 0.00 0.00 0.00 0.60 1.39 0.94 0.01 0.01 0.00 0.01 0.00 0.01	0.00 0.04 0.19 0.00 95.22 27.94 28.79 98.02 4(O) 0.00 0.03 0.01 1.12 0.81 0.93 0.03 0.02 0.00 0.00 0.00 0.00 0.00 0.03	0.00 0.03 0.00 0.22 0.00 95.68 30.02 29.12 98.69 4(O) 0.00 0.04 0.01 1.05 0.86 0.93 0.02 0.02 0.00 0.02 0.00 0.00 0.00 0.01 1.05 0.00 0.00 0.00 0.00 0.00 0.00 0.00 0.00 0.00 0.00 0.00 0.00 0.00 0.00 0.00 0.00 0.00 0.00 0.00 0.00 0.00 0.00 0.00 0.00 0.00 0.00 0.00 0.00 0.00 0.00 0.00 0.00 0.00 0.00 0.00 0.00 0.00 0.00 0.00 0.00 0.00 0.00 0.00 0.00 0.00 0.00 0.00 0.00 0.00 0.00 0.00 0.00 0.00 0.00 0.00 0.00 0.00 0.00 0.00 0.00 0.00 0.00 0.00 0.00 0.00 0.00 0.00 0.00 0.00 0.00 0.00 0.00 0.00 0.00 0.00 0.00 0.00 0.00 0.00 0.00 0.00 0.00 0.00 0.00 0.00 0.00 0.00 0.00 0.00 0.00 0.00 0.00 0.00 0.00 0.00 0.00 0.00 0.00 0.00 0.00 0.00 0.00 0.00 0.00 0.00 0.00 0.00 0.00 0.00 0.00 0.00 0.00 0.00 0.00 0.00 0.00 0.00 0.00 0.00 0.00 0.00 0.00 0.00 0.00 0.00 0.00 0.00 0.00 0.00 0.00 0.00 0.00 0.00 0.00 0.00 0.00 0.00 0.00 0.00 0.00 0.00 0.00 0.00 0.00 0.00 0.00 0.00 0.00 0.00 0.00 0.00 0.00 0.00 0.00 0.00 0.00 0.00 0.00 0.00 0.00 0.00 0.00 0.00 0.00 0.00 0.00 0.00 0.00 0.00 0.00 0.00 0.00 0.00 0.00 0.00 0.00 0.00 0.00 0.00 0.00 0.00 0.00 0.00 0.00 0.00 0.00 0.00 0.00 0.00 0.00 0.00 0.00 0.00 0.00 0.00 0.00 0.00 0.00 0.00 0.00 0.00 0.00 0.00 0.00 0.00 0.00 0.00 0.00 0.00 0.00 0.00 0.00 0.00 0.00 0.00 0.00 0.00 0.00 0.00 0.00 0.00 0.00 0.00 0.00 0.00 0.00 0.00 0.00 0.00 0.00 0.00 0.00 0.00 0.00 0.00 0.00 0.00 0.00 0.00 0.00 0.00 0.00 0.00 0.00 0.00 0.00 0.00 0.00 0.00 0.00 0.00 0.00 0.00 0.00 0.00 0.00 0.00 0.00 0.00 0.00 0.00 0.00 0.00 0.00 0.00 0.00 0.00 0.00 0.00 0.00 0.00 0.00 0.00 0.00 0.00 0.00 0.00 0.00 0.00 0.00 0.00 0.00 0.00 0.00 0.00 0.00 0.00 0.00 0.00 0.00 0.00 0.00 0.00 0.00 0.00 0.00 0.00 0.00 0.00 0.00 0.00 0.00 0.00 0.00 0.00 0.00 0.00 0.00 0.00 0.00 0.00 0.00 0.00 0.00 0.00 0.	0.01 0.00 0.01 0.27 0.00 94.97 30.38 29.30 98.01 4(O) 0.00 0.03 0.01 1.05 0.88 0.95 0.01 0.00 0.00 0.00 0.01 0.00 0.00 0.00 0.01 0.00 0.00 0.01 0.00 0.00 0.00 0.00 0.00 0.00 0.00 0.00 0.00 0.00 0.00 0.00 0.00 0.00 0.00 0.00 0.00 0.00 0.00 0.00 0.00 0.00 0.00 0.00 0.00 0.00 0.00 0.00 0.00 0.00 0.00 0.00 0.00 0.00 0.00 0.00 0.00 0.00 0.00 0.00 0.00 0.00 0.00 0.00 0.00 0.00 0.00 0.00 0.00 0.00 0.00 0.00 0.00 0.00 0.00 0.00 0.00 0.00 0.00 0.00 0.00 0.00 0.00 0.00 0.00 0.00 0.00 0.00 0.00 0.00 0.00 0.00 0.00 0.00 0.00 0.00 0.00 0.00 0.00 0.00 0.00 0.00 0.00 0.00 0.00 0.00 0.00 0.00 0.00 0.00 0.00 0.00 0.00 0.00 0.00 0.00 0.00 0.00 0.00 0.00 0.00 0.00 0.00 0.00 0.00 0.00 0.00 0.00 0.00 0.00 0.00 0.00 0.00 0.00 0.00 0.00 0.00 0.00 0.00 0.00 0.00 0.00 0.00 0.00 0.00 0.00 0.00 0.00 0.00 0.00 0.00 0.00 0.00 0.00 0.00 0.00 0.00 0.00 0.00 0.00 0.00 0.00 0.00 0.00 0.00 0.00 0.00 0.00 0.00 0.00 0.00 0.00 0.00 0.00 0.00 0.00 0.00 0.00 0.00 0.00 0.00 0.00 0.00 0.00 0.00 0.00 0.00 0.00 0.00 0.00 0.00 0.00 0.00 0.00 0.00 0.00 0.00 0.00 0.00 0.00 0.00 0.00 0.00 0.00 0.00 0.00 0.00 0.00 0.00 0.00 0.00 0.00 0.00 0.00 0.00 0.00 0.00 0.00 0.00 0.00 0.00 0.00 0.00 0.00 0.00 0.00 0.00 0.00 0.00 0.00 0.00 0.00 0.00 0.00 0.00 0.00 0.00 0.00 0.00 0.00 0.00 0.00 0.00 0.00 0.00 0.00 0.00 0.00 0.00 0.00 0.00 0.00 0.00 0.00 0.00 0.00 0.00 0.00 0.00 0.00 0.00 0.00 0.00 0.00 0.00 0.00 0.00 0.00 0.00 0.00 0.00 0.00 0.00 0.00 0.00 0.00 0.00 0.00 0.00 0.00 0.00 0.00 0.00 0.00 0.00 0.00 0.00 0.00 0.00 0.00 0.00 0.00 0.00 0.00 0.00 0.00 0.00 0.00 0.00 0.00 0.00 0.00 0.00 0.00 0.00 0.00 0.00 0.00 0.00 0.00 0.00 0.00 0.00 0.00 0.00 0.00 0.00 0.00 0.00 0.00 0.00 0.00 0.00 0.00 0.00 0.00 0.00 0.00 0.00 0.00 0.00 0.00 0.	0.05 0.02 0.31 0.00 96.38 28.49 29.10 99.23 4(O) 0.00 0.04 0.01 1.11 0.81 0.93 0.02 0.02 0.00 0.00 0.00 0.00 0.00 0.01 0.00 0.00 0.00 0.00 0.00 0.00 0.00 0.00 0.00 0.00 0.00 0.00 0.00 0.00 0.00 0.00 0.00 0.00 0.00 0.00 0.00 0.00 0.00 0.00 0.00 0.00 0.00 0.00 0.00 0.00 0.00 0.00 0.00 0.00 0.00 0.00 0.00 0.00 0.00 0.00 0.00 0.00 0.00 0.00 0.00 0.00 0.00 0.00 0.00 0.00 0.00 0.00 0.00 0.00 0.00 0.00 0.00 0.00 0.00 0.00 0.00 0.00 0.00 0.00 0.00 0.00 0.00 0.00 0.00 0.00 0.00 0.00 0.00 0.00 0.00 0.00 0.00 0.00 0.00 0.00 0.00 0.00 0.00 0.00 0.00 0.00 0.00 0.00 0.00 0.00 0.00 0.00 0.00 0.00 0.00 0.00 0.00 0.00 0.00 0.00 0.00 0.00 0.00 0.00 0.00 0.00 0.00 0.00 0.00 0.00 0.00 0.00 0.00 0.00 0.00 0.00 0.00 0.00 0.00 0.00 0.00 0.00 0.00 0.00 0.00 0.00 0.00 0.00 0.00 0.00 0.00 0.00 0.00 0.00 0.00 0.00 0.00 0.00 0.00 0.00 0.00 0.00 0.00 0.00 0.00 0.00 0.00 0.00 0.00 0.00 0.00 0.00 0.00 0.00 0.00 0.00 0.00 0.00 0.00 0.00 0.00 0.00 0.00 0.00 0.00 0.00 0.00 0.00 0.00 0.00 0.00 0.00 0.00 0.00 0.00 0.00 0.00 0.00 0.00 0.00 0.00 0.00 0.00 0.00 0.00 0.00 0.00 0.00 0.00 0.00 0.00 0.00 0.00 0.00 0.00 0.00 0.00 0.00 0.00 0.00 0.00 0.00 0.00 0.00 0.00 0.00 0.00 0.00 0.00 0.00 0.00 0.00 0.00 0.00 0.00 0.00 0.00 0.00 0.00 0.00 0.00 0.00 0.00 0.00 0.00 0.00 0.00 0.00 0.00 0.00 0.00 0.00 0.00 0.00 0.00 0.00 0.00 0.00 0.00 0.00 0.00 0.00 0.00 0.00 0.00 0.00 0.00 0.00 0.00 0.00 0.00 0.00 0.00 0.00 0.00 0.00 0.00 0.00 0.00 0.00 0.00 0.00 0.00 0.00 0.00 0.00 0.00 0.00 0.00 0.00 0.00 0.00 0.00 0.00 0.00 0.00 0.00 0.00 0.00 0.00 0.00 0.00 0.00 0.00 0.00 0.00 0.00 0.00 0.00 0.00 0.00 0.00 0.00 0.00 0.00 0.00 0.00 0.00 0.00 0.00 0.00 0.00 0.00 0.00 0.00 0.00 0.00 0.00 0.00 0.00 0.00 0.00 0.00 0.00 0.00 0.00 0.00 0.	0.00 0.09 0.00 0.28 0.00 97.10 30.35 29.71 100.14 4(O) 0.00 0.04 0.01 1.06 0.86 0.94 0.02 0.02 0.02 0.00 0.01 0.00 0.01 0.00 0.01 0.00 0.01 0.00 0.00 0.00 0.00 0.00 0.00 0.00 0.00 0.00 0.00 0.00 0.00 0.00 0.00 0.00 0.00 0.00 0.00 0.00 0.00 0.00 0.00 0.00 0.00 0.00 0.00 0.00 0.00 0.00 0.00 0.00 0.00 0.00 0.00 0.00 0.00 0.00 0.00 0.00 0.00 0.00 0.00 0.00 0.00 0.00 0.00 0.00 0.00 0.00 0.00 0.00 0.00 0.00 0.00 0.00 0.00 0.00 0.00 0.00 0.00 0.00 0.00 0.00 0.00 0.00 0.00 0.00 0.00 0.00 0.00 0.00 0.00 0.00 0.00 0.00 0.00 0.00 0.00 0.00 0.00 0.00 0.00 0.00 0.00 0.00 0.00 0.00 0.00 0.00 0.00 0.00 0.00 0.00 0.00 0.00 0.00 0.00 0.00 0.00 0.00 0.00 0.00 0.00 0.00 0.00 0.00 0.00 0.00 0.00 0.00 0.00 0.00 0.00 0.00 0.00 0.00 0.00 0.00 0.00 0.00 0.00 0.00 0.00 0.00 0.00 0.00 0.00 0.00 0.00 0.00 0.00 0.00 0.00 0.00 0.00 0.00 0.00 0.00 0.00 0.00 0.00 0.00 0.00 0.00 0.00 0.00 0.00 0.00 0.00 0.00 0.00 0.00 0.00 0.00 0.00 0.00 0.00 0.00 0.00 0.00 0.00 0.00 0.00 0.00 0.00 0.00 0.00 0.00 0.00 0.00 0.00 0.00 0.00 0.00 0.00 0.00 0.00 0.00 0.00 0.00 0.00 0.00 0.00 0.00 0.00 0.00 0.00 0.00 0.00 0.00 0.00 0.00 0.00 0.00 0.00 0.00 0.00 0.00 0.00 0.00 0.00 0.00 0.00 0.00 0.00 0.00 0.00 0.00 0.00 0.00 0.00 0.00 0.00 0.00 0.00 0.00 0.00 0.00 0.00 0.00 0.00 0.00 0.00 0.00 0.00 0.00 0.00 0.00 0.00 0.00 0.00 0.00 0.00 0.00 0.00 0.00 0.00 0.00 0.00 0.00 0.00 0.00 0.00 0.00 0.00 0.00 0.00 0.00 0.00 0.00 0.00 0.00 0.00 0.00 0.00 0.00 0.00 0.00 0.00 0.00 0.00 0.00 0.00 0.00 0.00 0.00 0.00 0.00 0.00 0.00 0.00 0.00 0.00 0.00 0.00 0.00 0.00 0.00 0.00 0.00 0.00 0.00 0.00 0.00 0.00 0.00 0.00 0.00 0.00 0.00 0.00 0.00 0.00 0.00 0.00 0.00 0.00 0.00 0.00 0.00 0.00 0.00 0.00 0.00 0.00 0.00 0.00 0.00 0.00 0.00 0.00 0.00 0.00 0.00 0.00 0.00 0.00 0.00 0.00 0.00 0.00 0.00 0.00 0.00 0.00 0.00 0.00 0.00 0.00 0.00 0.00 0.00 0.00 0.00 0.00 0.00 0.00 0.00 0.00 0.00 0.00 0.00 0.00 0.00 0.00 0.00 0.00 0.00 0.00 0.00 0.00 0.00 0.00 0.00 0.00 0.00 0.00 0.00 0.00 0.00 0.00 0.00 0.00 0.00 0.00 0.00 0.00 0.00 0.00 0.00 0.00 0.00 0.00 0.00 0.00 0.00 0.00 0.00 0.00 0.00 0.00 0	0.02 0.07 0.01 0.31 0.00 95.62 29.20 28.83 98.54 4(O) 0.00 0.03 0.01 1.08 0.84 0.92 0.03 0.00 0.03 0.01 0.00 0.00 0.00 0.00	0.02 0.03 0.02 0.30 0.00 95.60 27.27 29.25 98.33 4(O) 0.00 0.04 0.01 1.12 0.79 0.94 0.01 0.03 0.00 0.00 0.00 0.00 0.01 0.01 0.00 0.00 0.00 0.00 0.00 0.00 0.00 0.00 0.00 0.00 0.00 0.00 0.00 0.00 0.00 0.00 0.00 0.00 0.00 0.00 0.00 0.00 0.00 0.00 0.00 0.00 0.00 0.00 0.00 0.00 0.00 0.00 0.00 0.00 0.00 0.00 0.00 0.00 0.00 0.00 0.00 0.00 0.00 0.00 0.00 0.00 0.00 0.00 0.00 0.00 0.00 0.00 0.00 0.00 0.00 0.00 0.00 0.00 0.00 0.00 0.00 0.00 0.00 0.00 0.00 0.00 0.00 0.00 0.00 0.00 0.00 0.00 0.00 0.00 0.00 0.00 0.00 0.00 0.00 0.00 0.00 0.00 0.00 0.00 0.00 0.00 0.00 0.00 0.00 0.00 0.00 0.00 0.00 0.00 0.00 0.00 0.00 0.00 0.00 0.00 0.00 0.00 0.00 0.00 0.00 0.00 0.00 0.00 0.00 0.00 0.00 0.00 0.00 0.00 0.00 0.00 0.00 0.00 0.00 0.00 0.00 0.00 0.00 0.00 0.00 0.00 0.00 0.00 0.00 0.00 0.00 0.00 0.00 0.00 0.00 0.00 0.00 0.00 0.00 0.00 0.00 0.00 0.00 0.00 0.00 0.00 0.00 0.00 0.00 0.00 0.00 0.00 0.00 0.00 0.00 0.00 0.00 0.00 0.00 0.00 0.00 0.00 0.00 0.00 0.00 0.00 0.00 0.00 0.00 0.00 0.00 0.00 0.00 0.00 0.00 0.00 0.00 0.00 0.00 0.00 0.00 0.00 0.00 0.00 0.00 0.00 0.00 0.00 0.00 0.00 0.00 0.00 0.00 0.00 0.00 0.00 0.00 0.00 0.00 0.00 0.00 0.00 0.00 0.00 0.00 0.00 0.00 0.00 0.00 0.00 0.00 0.00 0.00 0.00 0.00 0.00 0.00 0.00 0.00 0.00 0.00 0.00 0.00 0.00 0.00 0.00 0.00 0.00 0.00 0.00 0.00 0.00 0.00 0.00 0.00 0.00 0.00 0.00 0.00 0.00 0.00 0.00 0.00 0.00 0.00 0.00 0.00 0.00 0.00 0.00 0.00 0.00 0.00 0.00 0.00 0.00 0.00 0.00 0.00 0.00 0.00 0.00 0.00 0.00 0.00 0.00 0.00 0.00 0.00 0.00 0.00 0.00 0.00 0.00 0.00 0.00 0.00 0.00 0.00 0.00 0.00 0.00 0.00 0.00 0.00 0.00 0.00 0.00 0.00 0.00 0.00 0.00 0.00 0.00 0.00 0.00 0.00 0.00 0.00 0.00 0.00 0.00 0.00 0.00 0.00 0.00 0.00 0.00 0.00 0.00 0.00 0.00 0.00 0.00 0.00 0.00 0.	0.02 0.01 0.01 0.01 0.16 0.00 95.17 28.31 29.43 98.00 4(O) 0.00 0.04 0.01 1.10 0.82 0.95 0.01 0.02 0.00 0.00 0.00 0.00 0.00 0.00 0.00 0.00 0.00 0.00 0.00 0.00 0.00 0.00 0.00 0.00 0.00 0.00 0.00 0.00 0.00 0.00 0.00 0.00 0.00 0.00 0.00 0.00 0.00 0.00 0.00 0.00 0.00 0.00 0.00 0.00 0.00 0.00 0.00 0.00 0.00 0.00 0.00 0.00 0.00 0.00 0.00 0.00 0.00 0.00 0.00 0.00 0.00 0.00 0.00 0.00 0.00 0.00 0.00 0.00 0.00 0.00 0.00 0.00 0.00 0.00 0.00 0.00 0.00 0.00 0.00 0.00 0.00 0.00 0.00 0.00 0.00 0.00 0.00 0.00 0.00 0.00 0.00 0.00 0.00 0.00 0.00 0.00 0.00 0.00 0.00 0.00 0.00 0.00 0.00 0.00 0.00 0.00 0.00 0.00 0.00 0.00 0.00 0.00 0.00 0.00 0.00 0.00 0.00 0.00 0.00 0.00 0.00 0.00 0.00 0.00 0.00 0.00 0.00 0.00 0.00 0.00 0.00 0.00 0.00 0.00 0.00 0.00 0.00 0.00 0.00 0.00 0.00 0.00 0.00 0.00 0.00 0.00 0.00 0.00 0.00 0.00 0.00 0.00 0.00 0.00 0.00 0.00 0.00 0.00 0.00 0.00 0.00 0.00 0.00 0.00 0.00 0.00 0.00 0.00 0.00 0.00 0.00 0.00 0.00 0.00 0.00 0.00 0.00 0.00 0.00 0.00 0.00 0.00 0.00 0.00 0.00 0.00 0.00 0.00 0.00 0.00 0.00 0.00 0.00 0.00 0.00 0.00 0.00 0.00 0.00 0.00 0.00 0.00 0.00 0.00 0.00 0.00 0.00 0.00 0.00 0.00 0.00 0.00 0.00 0.00 0.00 0.00 0.00 0.00 0.00 0.00 0.00 0.00 0.00 0.00 0.00 0.00 0.00 0.00 0.00 0.00 0.00 0.00 0.00 0.00 0.00 0.00 0.00 0.00 0.00 0.00 0.00 0.00 0.00 0.00 0.00 0.00 0.00 0.00 0.00 0.00 0.00 0.00 0.00 0.00 0.00 0.00 0.00 0.00 0.00 0.00 0.00 0.00 0.00 0.00 0.00 0.00 0.00 0.00 0.00 0.00 0.00 0.00 0.00 0.00 0.00 0.00 0.00 0.00 0.00 0.00 0.00 0.00 0.00 0.00 0.00 0.00 0.00 0.00 0.00 0.00 0.00 0.00 0.00 0.00 0.00 0.00 0.00 0.00 0.00 0.00 0.00 0.00 0.00 0.00 0.00 0.00 0.00 0.00 0.00 0.00 0.00 0.00 0.00 0.00 0.00 0.00 0.00 0.00 0.00 0.00 0.00 0.00 0.00 0.00 0.00 0.00 0.00 0.00 0.00 0.	0.05 0.01 0.00 0.34 0.00 92.74 53.36 29.89 98.08 4(O) 0.00 0.01 0.00 0.42 1.56 0.97 0.02 0.00 0.00 0.00 0.00 0.00 0.00 0.00 0.00 0.00 0.00 0.00 0.00 0.00 0.00 0.00 0.00 0.00 0.00 0.00 0.00 0.00 0.00 0.00 0.00 0.00 0.00 0.00 0.00 0.00 0.00 0.00 0.00 0.00 0.00 0.00 0.00 0.00 0.00 0.00 0.00 0.00 0.00 0.00 0.00 0.00 0.00 0.00 0.00 0.00 0.00 0.00 0.00 0.00 0.00 0.00 0.00 0.00 0.00 0.00 0.00 0.00 0.00 0.00 0.00 0.00 0.00 0.00 0.00 0.00 0.00 0.00 0.00 0.00 0.00 0.00 0.00 0.00 0.00 0.00 0.00 0.00 0.00 0.00 0.00 0.00 0.00 0.00 0.00 0.00 0.00 0.00 0.00 0.00 0.00 0.00 0.00 0.00 0.00 0.00 0.00 0.00 0.00 0.00 0.00 0.00 0.00 0.00 0.00 0.00 0.00 0.00 0.00 0.00 0.00 0.00 0.00 0.00 0.00 0.00 0.00 0.00 0.00 0.00 0.00 0.00 0.00 0.00 0.00 0.00 0.00 0.00 0.00 0.00 0.00 0.00 0.00 0.00 0.00 0.00 0.00 0.00 0.00 0.00 0.00 0.00 0.00 0.00 0.00 0.00 0.00 0.00 0.00 0.00 0.00 0.00 0.00 0.00 0.00 0.00 0.00 0.00 0.00 0.00 0.00 0.00 0.00 0.00 0.00 0.00 0.00 0.00 0.00 0.00 0.00 0.00 0.00 0.00 0.00 0.00 0.00 0.00 0.00 0.00 0.00 0.00 0.00 0.00 0.00 0.00 0.00 0.00 0.00 0.00 0.00 0.00 0.00 0.00 0.00 0.00 0.00 0.00 0.00 0.00 0.00 0.00 0.00 0.00 0.00 0.00 0.00 0.00 0.00 0.00 0.00 0.00 0.00 0.00 0.00 0.00 0.00 0.00 0.00 0.00 0.00 0.00 0.00 0.00 0.00 0.00 0.00 0.00 0.00 0.00 0.00 0.00 0.00 0.00 0.00 0.00 0.00 0.00 0.00 0.00 0.00 0.00 0.00 0.00 0.00 0.00 0.00 0.00 0.00 0.00 0.00 0.00 0.00 0.00 0.00 0.00 0.00 0.00 0.00 0.00 0.00 0.00 0.00 0.00 0.00 0.00 0.00 0.00 0.00 0.00 0.00 0.00 0.00 0.00 0.00 0.00 0.00 0.00 0.00 0.00 0.00 0.00 0.00 0.00 0.00 0.00 0.00 0.00 0.00 0.00 0.00 0.00 0.00 0.00 0.00 0.00 0.00 0.00 0.00 0.00 0.00 0.00 0.00 0.00 0.00 0.00 0.00 0.00 0.00 0.00 0.00 0.00 0.00 0.00 0.00 0.00 0.00 0.00 0.00 0.00 0.
K,O NiO ZnO Total Fe <sub>2</sub> O <sub>3</sub> FecO Total Cations: Si Ti Al Cr Fe <sup>+3</sup> Ca Mn Mg K Ni X T Total Cr# Mg# Fe#	0.02 0.23 0.00 93.33 47.60 29.06 98.09 4(O) 0.00 0.00 0.60 1.39 0.94 0.01 0.00 0.01 0.00 0.01	0.00 0.04 0.19 0.00 95.22 27.94 28.79 98.02 4(O) 0.03 0.01 1.12 0.81 0.93 0.03 0.02 0.00 0.00 0.00 0.00 1.12 0.81 0.93 1.00 1.00 1.00 1.00 1.00 1.00 1.00 1.00 1.00 1.00 1.00 1.00 1.00 1.00 1.00 1.00 1.00 1.00 1.00 1.00 1.00 1.00 1.00 1.00 1.00 1.00 1.00 1.00 1.00 1.00 1.00 1.00 1.00 1.00 1.00 1.00 1.00 1.00 1.00 1.00 1.00 1.00 1.00 1.00 1.00 1.00 1.00 1.00 1.00 1.00 1.00 1.00 1.00 1.00 1.00 1.00 1.00 1.00 1.00 1.00 1.00 1.00 1.00 1.00 1.00 1.00 1.00 1.00 1.00 1.00 1.00 1.00 1.00 1.00 1.00 1.00 1.00 1.00 1.00 1.00 1.00 1.00 1.00 1.00 1.00 1.00 1.00 1.00 1.00 1.00 1.00 1.00 1.00 1.00 1.00 1.00 1.00 1.00 1.00 1.00 1.00 1.00 1.00 1.00 1.00 1.00 1.00 1.00 1.00 1.00 1.00 1.00 1.00 1.00 1.00 1.00 1.00 1.00 1.00 1.00 1.00 1.00 1.00 1.00 1.00 1.00 1.00 1.00 1.00 1.00 1.00 1.00 1.00 1.00 1.00 1.00 1.00 1.00 1.00 1.00 1.00 1.00 1.00 1.00 1.00 1.00 1.00 1.00 1.00 1.00 1.00 1.00 1.00 1.00 1.00 1.00 1.00 1.00 1.00 1.00 1.00 1.00 1.00 1.00 1.00 1.00 1.00 1.00 1.00 1.00 1.00 1.00 1.00 1.00 1.00 1.00 1.00 1.00 1.00 1.00 1.00 1.00 1.00 1.00 1.00 1.00 1.00 1.00 1.00 1.00 1.00 1.00 1.00 1.00 1.00 1.00 1.00 1.00 1.00 1.00 1.00 1.00 1.00 1.00 1.00 1.00 1.00 1.00 1.00 1.00 1.00 1.00 1.00 1.00 1.00 1.00 1.00 1.00 1.00 1.00 1.00 1.00 1.00 1.00 1.00 1.00 1.00 1.00 1.00 1.00 1.00 1.00 1.00 1.00 1.00 1.00 1.00 1.00 1.00 1.00 1.00 1.00 1.00 1.00 1.00 1.00 1.00 1.00 1.00 1.00 1.00 1.00 1.00 1.00 1.00 1.00 1.00 1.00 1.00 1.00 1.00 1.00 1.00 1.00 1.00 1.00 1.00 1.00 1.00 1.00 1.00 1.00 1.00 1.00 1.00 1.00 1.00 1.00 1.00 1.00 1.00 1.00 1.00 1.00 1.00 1.00 1.00 1.00 1.00 1.00 1.00 1.00 1.00 1.00 1.00 1.00 1.00 1.00 1.00 1.00 1.00 1.00 1.00 1.00 1.00 1.00 1.00 1.00 1.00 1.00 1.00 1.00 1.00 1.00 1.00 1.00 1.00 1.	0.00 0.03 0.00 0.22 0.00 95.68 30.02 29.12 98.69 4(O) 0.00 0.04 0.01 1.05 0.86 0.93 0.02 0.02 0.00 0.00 0.00 0.01 1.05 0.86 0.93 0.02 0.00 0.00 0.00 0.00 0.00 0.01 1.05 0.86 0.93 0.02 0.00 0.00 0.00 0.00 0.00 0.00 0.00 0.00 0.01 0.00 0.00 0.00 0.00 0.00 0.00 0.00 0.00 0.00 0.00 0.00 0.00 0.00 0.00 0.00 0.00 0.00 0.00 0.00 0.00 0.00 0.00 0.00 0.00 0.00 0.00 0.00 0.00 0.00 0.00 0.00 0.00 0.00 0.00 0.00 0.00 0.00 0.00 0.00 0.00 0.00 0.00 0.00 0.00 0.00 0.00 0.00 0.00 0.00 0.00 0.00 0.00 0.00 0.00 0.00 0.00 0.00 0.00 0.00 0.00 0.00 0.00 0.00 0.00 0.00 0.00 0.00 0.00 0.00 0.00 0.00 0.00 0.00 0.00 0.00 0.00 0.00 0.00 0.00 0.00 0.00 0.00 0.00 0.00 0.00 0.00 0.00 0.00 0.00 0.00 0.00 0.00 0.00 0.00 0.00 0.00 0.00 0.00 0.00 0.00 0.00 0.00 0.00 0.00 0.00 0.00 0.00 0.00 0.00 0.00 0.00 0.00 0.00 0.00 0.00 0.00 0.00 0.00 0.00 0.00 0.00 0.00 0.00 0.00 0.00 0.00 0.00 0.00 0.00 0.00 0.00 0.00 0.00 0.00 0.00 0.00 0.00 0.00 0.00 0.00 0.00 0.00 0.00 0.00 0.00 0.00 0.00 0.00 0.00 0.00 0.00 0.00 0.00 0.00 0.00 0.00 0.00 0.00 0.00 0.00 0.00 0.00 0.00 0.00 0.00 0.00 0.00 0.00 0.00 0.00 0.00 0.00 0.00 0.00 0.00 0.00 0.00 0.00 0.00 0.00 0.00 0.00 0.00 0.00 0.00 0.00 0.00 0.00 0.00 0.00 0.00 0.00 0.00 0.00 0.00 0.00 0.00 0.00 0.00 0.00 0.00 0.00 0.00 0.00 0.00 0.00 0.00 0.00 0.00 0.00 0.00 0.00 0.00 0.00 0.00 0.00 0.00 0.00 0.00 0.00 0.00 0.00 0.00 0.00 0.00 0.00 0.00 0.00 0.00 0.00 0.00 0.00 0.00 0.00 0.00 0.00 0.00 0.00 0.00 0.00 0.00 0.00 0.00 0.00 0.00 0.00 0.00 0.00 0.00 0.00 0.00 0.00 0.00 0.00 0.00 0.00 0.00 0.00 0.00 0.00 0.00 0.00 0.00 0.00 0.00 0.00 0.00 0.00 0.00 0.00 0.00 0.00 0.00 0.00 0.00 0.00 0.00 0.00 0.00 0.00 0.00 0.00 0.00 0.00 0.00 0.00 0.00 0.00 0.00 0.00 0.00 0.00 0.00 0.00 0.00 0.	0.01 0.00 0.01 0.27 0.00 94.97 30.38 29.30 98.01 4(O) 0.00 0.03 0.01 1.05 0.88 0.95 0.01 0.00 0.00 0.00 0.00 0.01 1.05 0.00 0.00 0.01 1.05	0.05 0.02 0.31 0.00 96.38 28.49 29.10 99.23 4(O) 0.00 0.04 0.01 1.11 0.81 0.93 0.02 0.02 0.00 0.00 0.00 0.00 0.00 0.0	0.00 0.09 0.00 0.28 0.00 97.10 30.35 29.71 100.14 4(O) 0.00 0.04 0.01 1.06 0.86 0.94 0.02 0.02 0.02 0.00 0.01 0.00 0.01 0.00 0.01 1.06 0.86 0.94 1.06 1.06 1.06 1.06 1.06 1.06 1.06 1.06 1.06 1.06 1.06 1.06 1.06 1.06 1.06 1.06 1.06 1.06 1.06 1.06 1.06 1.06 1.06 1.06 1.06 1.06 1.06 1.06 1.06 1.06 1.06 1.06 1.06 1.06 1.06 1.06 1.06 1.06 1.06 1.06 1.06 1.06 1.06 1.06 1.06 1.06 1.06 1.06 1.06 1.06 1.06 1.06 1.06 1.06 1.06 1.06 1.06 1.06 1.06 1.06 1.06 1.06 1.06 1.06 1.06 1.06 1.06 1.06 1.06 1.06 1.06 1.06 1.06 1.06 1.06 1.06 1.06 1.06 1.06 1.06 1.06 1.06 1.06 1.06 1.06 1.06 1.06 1.06 1.06 1.06 1.06 1.06 1.06 1.06 1.06 1.06 1.06 1.06 1.06 1.06 1.06 1.06 1.06 1.06 1.06 1.06 1.06 1.06 1.06 1.06 1.06 1.06 1.06 1.06 1.06 1.06 1.06 1.06 1.06 1.06 1.06 1.06 1.06 1.06 1.06 1.06 1.06 1.06 1.06 1.06 1.06 1.06 1.06 1.06 1.06 1.06 1.06 1.06 1.06 1.06 1.06 1.06 1.06 1.06 1.06 1.06 1.06 1.06 1.06 1.06 1.06 1.06 1.06 1.06 1.06 1.06 1.06 1.06 1.06 1.06 1.06 1.06 1.06 1.06 1.06 1.06 1.06 1.06 1.06 1.06 1.06 1.06 1.06 1.06 1.06 1.06 1.06 1.06 1.06 1.06 1.06 1.06 1.06 1.06 1.06 1.06 1.06 1.06 1.06 1.06 1.06 1.06 1.06 1.06 1.06 1.06 1.06 1.06 1.06 1.06 1.06 1.06 1.06 1.06 1.06 1.06 1.06 1.06 1.06 1.06 1.06 1.06 1.06 1.06 1.06 1.06 1.06 1.06 1.06 1.06 1.06 1.06 1.06 1.06 1.06 1.06 1.06 1.06 1.06 1.06 1.06 1.06 1.06 1.06 1.06 1.06 1.06 1.06 1.06 1.06 1.06 1.06 1.06 1.06 1.06 1.06 1.06 1.06 1.06 1.06 1.06 1.06 1.06 1.06 1.06 1.06 1.06 1.06 1.06 1.06 1.06 1.06 1.06 1.06 1.06 1.06 1.06 1.06 1.06 1.06 1.06 1.06 1.06 1.06 1.06 1.06 1.06 1.06 1.06 1.06 1.06 1.06 1.06 1.06 1.06 1.06 1.06 1.06 1.06 1.06 1.06 1.06 1.06 1.06 1.06 1.06 1.06 1.06 1.06 1.06 1.06 1.06 1.06 1.06 1.06 1.06 1.06 1.06 1.06 1.06 1.06 1.06 1	0.02 0.07 0.01 0.31 0.00 95.62 29.20 28.83 98.54 4(O) 0.00 0.03 0.01 1.08 0.84 0.92 0.02 0.03 0.00 0.00 0.00 0.00 0.03 0.01 1.08 0.94 0.95 0.00 0.00 0.00 0.00 0.00 0.00 0.00 0.01 1.08 0.09 0.00 0.00 0.00 0.00 0.00 0.00 0.00 0.00 0.00 0.00 0.00 0.00 0.00 0.00 0.00 0.00 0.00 0.00 0.00 0.00 0.00 0.00 0.00 0.00 0.00 0.00 0.00 0.00 0.00 0.00 0.00 0.00 0.00 0.00 0.00 0.00 0.00 0.00 0.00 0.00 0.00 0.00 0.00 0.00 0.00 0.00 0.00 0.00 0.00 0.00 0.00 0.00 0.00 0.00 0.00 0.00 0.00 0.00 0.00 0.00 0.00 0.00 0.00 0.00 0.00 0.00 0.00 0.00 0.00 0.00 0.00 0.00 0.00 0.00 0.00 0.00 0.00 0.00 0.00 0.00 0.00 0.00 0.00 0.00 0.00 0.00 0.00 0.00 0.00 0.00 0.00 0.00 0.00 0.00 0.00 0.00 0.00 0.00 0.00 0.00 0.00 0.00 0.00 0.00 0.00 0.00 0.00 0.00 0.00 0.00 0.00 0.00 0.00 0.00 0.00 0.00 0.00 0.00 0.00 0.00 0.00 0.00 0.00 0.00 0.00 0.00 0.00 0.00 0.00 0.00 0.00 0.00 0.00 0.00 0.00 0.00 0.00 0.00 0.00 0.00 0.00 0.00 0.00 0.00 0.00 0.00 0.00 0.00 0.00 0.00 0.00 0.00 0.00 0.00 0.00 0.00 0.00 0.00 0.00 0.00 0.00 0.00 0.00 0.00 0.00 0.00 0.00 0.00 0.00 0.00 0.00 0.00 0.00 0.00 0.00 0.00 0.00 0.00 0.00 0.00 0.00 0.00 0.00 0.00 0.00 0.00 0.00 0.00 0.00 0.00 0.00 0.00 0.00 0.00 0.00 0.00 0.00 0.00 0.00 0.00 0.00 0.00 0.00 0.00 0.00 0.00 0.00 0.00 0.00 0.00 0.00 0.00 0.00 0.00 0.00 0.00 0.00 0.00 0.00 0.00 0.00 0.00 0.00 0.00 0.00 0.00 0.00 0.00 0.00 0.00 0.00 0.00 0.00 0.00 0.00 0.00 0.00 0.00 0.00 0.00 0.00 0.00 0.00 0.00 0.00 0.00 0.00 0.00 0.00 0.00 0.00 0.00 0.00 0.00 0.00 0.00 0.00 0.00 0.00 0.00 0.00 0.00 0.00 0.00 0.00 0.00 0.00 0.00 0.00 0.00 0.00 0.00 0.00 0.00 0.00 0.00 0.00 0.00 0.00 0.00 0.00 0.00 0.00 0.00 0.00 0.00 0.00 0.00 0.00 0.00 0.00 0.00 0.00 0.00 0.00 0.00 0.00 0.00 0.00 0.00 0.00 0.00 0.00 0.	0.02 0.03 0.02 0.30 0.00 95.60 27.27 29.25 98.33 4(O) 0.00 0.04 0.01 1.12 0.79 0.94 0.01 0.03 0.00 0.00 0.00 0.03 0.00 0.00 0.00 0.01 1.00 0.00 0.00 0.00 0.01 0.01 0.03 0.00 0.00 0.00 0.00 0.00 0.00 0.01 0.01 0.01 0.02 0.03 0.00 0.00 0.00 0.00 0.00 0.01 0.01 0.01 0.00 0.00 0.00 0.00 0.00 0.00 0.01 0.01 0.01 0.00 0.00 0.00 0.00 0.00 0.00 0.00 0.00 0.00 0.00 0.00 0.00 0.00 0.00 0.00 0.00 0.00 0.00 0.00 0.00 0.00 0.00 0.00 0.00 0.00 0.00 0.00 0.00 0.00 0.00 0.00 0.00 0.00 0.00 0.00 0.00 0.00 0.00 0.00 0.00 0.00 0.00 0.00 0.00 0.00 0.00 0.00 0.00 0.00 0.00 0.00 0.00 0.00 0.00 0.00 0.00 0.00 0.00 0.00 0.00 0.00 0.00 0.00 0.00 0.00 0.00 0.00 0.00 0.00 0.00 0.00 0.00 0.00 0.00 0.00 0.00 0.00 0.00 0.00 0.00 0.00 0.00 0.00 0.00 0.00 0.00 0.00 0.00 0.00 0.00 0.00 0.00 0.00 0.00 0.00 0.00 0.00 0.00 0.00 0.00 0.00 0.00 0.00 0.00 0.00 0.00 0.00 0.00 0.00 0.00 0.00 0.00 0.00 0.00 0.00 0.00 0.00 0.00 0.00 0.00 0.00 0.00 0.00 0.00 0.00 0.00 0.00 0.00 0.00 0.00 0.00 0.00 0.00 0.00 0.00 0.00 0.00 0.00 0.00 0.00 0.00 0.00 0.00 0.00 0.00 0.00 0.00 0.00 0.00 0.00 0.00 0.00 0.00 0.00 0.00 0.00 0.00 0.00 0.00 0.00 0.00 0.00 0.00 0.00 0.00 0.00 0.00 0.00 0.00 0.00 0.00 0.00 0.00 0.00 0.00 0.00 0.00 0.00 0.00 0.00 0.00 0.00 0.00 0.00 0.00 0.00 0.00 0.00 0.00 0.00 0.00 0.00 0.00 0.00 0.00 0.00 0.00 0.00 0.00 0.00 0.00 0.00 0.00 0.00 0.00 0.00 0.00 0.00 0.00 0.00 0.00 0.00 0.00 0.00 0.00 0.00 0.00 0.00 0.00 0.00 0.00 0.00 0.00 0.00 0.00 0.00 0.00 0.00 0.00 0.00 0.00 0.00 0.00 0.00 0.00 0.00 0.00 0.00 0.00 0.00 0.00 0.00 0.00 0.00 0.00 0.00 0.00 0.00 0.00 0.00 0.00 0.00 0.00 0.00 0.00 0.00 0.00 0.00 0.00 0.00 0.00 0.00 0.00 0.00 0.00 0.00 0.00 0.00 0.00 0.00 0.00 0.00 0.00 0.00 0.00 0.00 0.00 0.00 0.00 0.	0.02 0.01 0.01 0.16 0.00 95.17 28.31 29.43 98.00 4(O) 0.00 0.04 0.01 1.10 0.82 0.95 0.01 0.02 0.00 0.00 0.00 0.00 0.00 0.00 0.01	0.05 0.01 0.00 0.34 0.00 92.74 53.36 29.89 98.08 4(O) 0.00 0.01 0.00 0.42 1.56 0.97 0.02 0.00 0.00 0.00 0.00 0.00 0.00 0.00 0.01
NiO ZnO ZnO ZnO ZnO Total Fe <sub>2</sub> O <sub>3</sub> FeO Total Cations: Si Ti Al Cr Fe <sup>+3</sup> Fe <sup>+2</sup> Mn Mg Ca Na K Ni Zn Total Cr#	0.02 0.23 0.00 93.33 47.60 29.06 98.09 4(O) 0.00 0.00 0.00 0.60 1.39 0.94 0.01 0.01 0.00 0.01 0.00 0.01	0.00 0.04 0.19 0.00 95.22 27.94 28.79 98.02 4(O) 0.00 0.03 0.01 1.12 0.81 0.93 0.03 0.02 0.00 0.00 0.00 0.00 0.00 0.03	0.00 0.03 0.00 0.22 0.00 95.68 30.02 29.12 98.69 4(O) 0.00 0.04 0.01 1.05 0.86 0.93 0.02 0.02 0.00 0.02 0.00 0.00 0.00 0.01 1.05 0.00 0.00 0.00 0.00 0.00 0.00 0.00 0.00 0.00 0.00 0.00 0.00 0.00 0.00 0.00 0.00 0.00 0.00 0.00 0.00 0.00 0.00 0.00 0.00 0.00 0.00 0.00 0.00 0.00 0.00 0.00 0.00 0.00 0.00 0.00 0.00 0.00 0.00 0.00 0.00 0.00 0.00 0.00 0.00 0.00 0.00 0.00 0.00 0.00 0.00 0.00 0.00 0.00 0.00 0.00 0.00 0.00 0.00 0.00 0.00 0.00 0.00 0.00 0.00 0.00 0.00 0.00 0.00 0.00 0.00 0.00 0.00 0.00 0.00 0.00 0.00 0.00 0.00 0.00 0.00 0.00 0.00 0.00 0.00 0.00 0.00 0.00 0.00 0.00 0.00 0.00 0.00 0.00 0.00 0.00 0.00 0.00 0.00 0.00 0.00 0.00 0.00 0.00 0.00 0.00 0.00 0.00 0.00 0.00 0.00 0.00 0.00 0.00 0.00 0.00 0.00 0.00 0.00 0.00 0.00 0.00 0.00 0.00 0.00 0.00 0.00 0.00 0.00 0.00 0.00 0.00 0.00 0.00 0.00 0.00 0.00 0.00 0.00 0.00 0.00 0.00 0.00 0.00 0.00 0.00 0.00 0.00 0.00 0.00 0.00 0.00 0.00 0.00 0.00 0.00 0.00 0.00 0.00 0.00 0.00 0.00 0.00 0.00 0.00 0.00 0.00 0.00 0.00 0.00 0.00 0.00 0.00 0.00 0.00 0.00 0.00 0.00 0.00 0.00 0.00 0.00 0.00 0.00 0.00 0.00 0.00 0.00 0.00 0.00 0.00 0.00 0.00 0.00 0.00 0.00 0.00 0.00 0.00 0.00 0.00 0.00 0.00 0.00 0.00 0.00 0.00 0.00 0.00 0.00 0.00 0.00 0.00 0.00 0.00 0.00 0.00 0.00 0.00 0.00 0.00 0.00 0.00 0.00 0.00 0.00 0.00 0.00 0.00 0.00 0.00 0.00 0.00 0.00 0.00 0.00 0.00 0.00 0.00 0.00 0.00 0.00 0.00 0.00 0.00 0.00 0.00 0.00 0.00 0.00 0.00 0.00 0.00 0.00 0.00 0.00 0.00 0.00 0.00 0.00 0.00 0.00 0.00 0.00 0.00 0.00 0.00 0.00 0.00 0.00 0.00 0.00 0.00 0.00 0.00 0.00 0.00 0.00 0.00 0.00 0.00 0.00 0.00 0.00 0.00 0.00 0.00 0.00 0.00 0.00 0.00 0.00 0.00 0.00 0.00 0.00 0.00 0.00 0.00 0.00 0.00 0.00 0.00 0.00 0.00 0.00 0.00 0.00 0.00 0.00 0.00 0.00 0.00 0.00 0.00 0.00 0.	0.01 0.00 0.01 0.27 0.00 94.97 30.38 29.30 98.01 4(O) 0.00 0.03 0.01 1.05 0.88 0.95 0.01 0.00 0.00 0.00 0.01 0.00 0.00 0.00 0.01 0.00 0.00 0.01 0.00 0.00 0.00 0.00 0.00 0.00 0.00 0.00 0.00 0.00 0.00 0.00 0.00 0.00 0.00 0.00 0.00 0.00 0.00 0.00 0.00 0.00 0.00 0.00 0.00 0.00 0.00 0.00 0.00 0.00 0.00 0.00 0.00 0.00 0.00 0.00 0.00 0.00 0.00 0.00 0.00 0.00 0.00 0.00 0.00 0.00 0.00 0.00 0.00 0.00 0.00 0.00 0.00 0.00 0.00 0.00 0.00 0.00 0.00 0.00 0.00 0.00 0.00 0.00 0.00 0.00 0.00 0.00 0.00 0.00 0.00 0.00 0.00 0.00 0.00 0.00 0.00 0.00 0.00 0.00 0.00 0.00 0.00 0.00 0.00 0.00 0.00 0.00 0.00 0.00 0.00 0.00 0.00 0.00 0.00 0.00 0.00 0.00 0.00 0.00 0.00 0.00 0.00 0.00 0.00 0.00 0.00 0.00 0.00 0.00 0.00 0.00 0.00 0.00 0.00 0.00 0.00 0.00 0.00 0.00 0.00 0.00 0.00 0.00 0.00 0.00 0.00 0.00 0.00 0.00 0.00 0.00 0.00 0.00 0.00 0.00 0.00 0.00 0.00 0.00 0.00 0.00 0.00 0.00 0.00 0.00 0.00 0.00 0.00 0.00 0.00 0.00 0.00 0.00 0.00 0.00 0.00 0.00 0.00 0.00 0.00 0.00 0.00 0.00 0.00 0.00 0.00 0.00 0.00 0.00 0.00 0.00 0.00 0.00 0.00 0.00 0.00 0.00 0.00 0.00 0.00 0.00 0.00 0.00 0.00 0.00 0.00 0.00 0.00 0.00 0.00 0.00 0.00 0.00 0.00 0.00 0.00 0.00 0.00 0.00 0.00 0.00 0.00 0.00 0.00 0.00 0.00 0.00 0.00 0.00 0.00 0.00 0.00 0.00 0.00 0.00 0.00 0.00 0.00 0.00 0.00 0.00 0.00 0.00 0.00 0.00 0.00 0.00 0.00 0.00 0.00 0.00 0.00 0.00 0.00 0.00 0.00 0.00 0.00 0.00 0.00 0.00 0.00 0.00 0.00 0.00 0.00 0.00 0.00 0.00 0.00 0.00 0.00 0.00 0.00 0.00 0.00 0.00 0.00 0.00 0.00 0.00 0.00 0.00 0.00 0.00 0.00 0.00 0.00 0.00 0.00 0.00 0.00 0.00 0.00 0.00 0.00 0.00 0.00 0.00 0.00 0.00 0.00 0.00 0.00 0.00 0.00 0.00 0.00 0.00 0.00 0.00 0.00 0.00 0.00 0.00 0.00 0.00 0.00 0.00 0.00 0.00 0.00 0.00 0.00 0.00 0.00 0.00 0.00 0.00 0.00 0.00 0.	0.05 0.02 0.31 0.00 96.38 28.49 29.10 99.23 4(O) 0.00 0.04 0.01 1.11 0.81 0.93 0.02 0.02 0.00 0.00 0.00 0.00 0.00 0.01 0.00 0.00 0.00 0.00 0.00 0.00 0.00 0.00 0.00 0.00 0.00 0.00 0.00 0.00 0.00 0.00 0.00 0.00 0.00 0.00 0.00 0.00 0.00 0.00 0.00 0.00 0.00 0.00 0.00 0.00 0.00 0.00 0.00 0.00 0.00 0.00 0.00 0.00 0.00 0.00 0.00 0.00 0.00 0.00 0.00 0.00 0.00 0.00 0.00 0.00 0.00 0.00 0.00 0.00 0.00 0.00 0.00 0.00 0.00 0.00 0.00 0.00 0.00 0.00 0.00 0.00 0.00 0.00 0.00 0.00 0.00 0.00 0.00 0.00 0.00 0.00 0.00 0.00 0.00 0.00 0.00 0.00 0.00 0.00 0.00 0.00 0.00 0.00 0.00 0.00 0.00 0.00 0.00 0.00 0.00 0.00 0.00 0.00 0.00 0.00 0.00 0.00 0.00 0.00 0.00 0.00 0.00 0.00 0.00 0.00 0.00 0.00 0.00 0.00 0.00 0.00 0.00 0.00 0.00 0.00 0.00 0.00 0.00 0.00 0.00 0.00 0.00 0.00 0.00 0.00 0.00 0.00 0.00 0.00 0.00 0.00 0.00 0.00 0.00 0.00 0.00 0.00 0.00 0.00 0.00 0.00 0.00 0.00 0.00 0.00 0.00 0.00 0.00 0.00 0.00 0.00 0.00 0.00 0.00 0.00 0.00 0.00 0.00 0.00 0.00 0.00 0.00 0.00 0.00 0.00 0.00 0.00 0.00 0.00 0.00 0.00 0.00 0.00 0.00 0.00 0.00 0.00 0.00 0.00 0.00 0.00 0.00 0.00 0.00 0.00 0.00 0.00 0.00 0.00 0.00 0.00 0.00 0.00 0.00 0.00 0.00 0.00 0.00 0.00 0.00 0.00 0.00 0.00 0.00 0.00 0.00 0.00 0.00 0.00 0.00 0.00 0.00 0.00 0.00 0.00 0.00 0.00 0.00 0.00 0.00 0.00 0.00 0.00 0.00 0.00 0.00 0.00 0.00 0.00 0.00 0.00 0.00 0.00 0.00 0.00 0.00 0.00 0.00 0.00 0.00 0.00 0.00 0.00 0.00 0.00 0.00 0.00 0.00 0.00 0.00 0.00 0.00 0.00 0.00 0.00 0.00 0.00 0.00 0.00 0.00 0.00 0.00 0.00 0.00 0.00 0.00 0.00 0.00 0.00 0.00 0.00 0.00 0.00 0.00 0.00 0.00 0.00 0.00 0.00 0.00 0.00 0.00 0.00 0.00 0.00 0.00 0.00 0.00 0.00 0.00 0.00 0.00 0.00 0.00 0.00 0.00 0.00 0.00 0.00 0.00 0.00 0.00 0.00 0.00 0.00 0.00 0.00 0.00 0.00 0.00 0.00 0.00 0.	0.00 0.09 0.00 0.28 0.00 97.10 30.35 29.71 100.14 4(O) 0.00 0.04 0.01 1.06 0.86 0.94 0.02 0.02 0.02 0.00 0.01 0.00 0.01 0.00 0.01 0.00 0.01 0.00 0.00 0.00 0.00 0.00 0.00 0.00 0.00 0.00 0.00 0.00 0.00 0.00 0.00 0.00 0.00 0.00 0.00 0.00 0.00 0.00 0.00 0.00 0.00 0.00 0.00 0.00 0.00 0.00 0.00 0.00 0.00 0.00 0.00 0.00 0.00 0.00 0.00 0.00 0.00 0.00 0.00 0.00 0.00 0.00 0.00 0.00 0.00 0.00 0.00 0.00 0.00 0.00 0.00 0.00 0.00 0.00 0.00 0.00 0.00 0.00 0.00 0.00 0.00 0.00 0.00 0.00 0.00 0.00 0.00 0.00 0.00 0.00 0.00 0.00 0.00 0.00 0.00 0.00 0.00 0.00 0.00 0.00 0.00 0.00 0.00 0.00 0.00 0.00 0.00 0.00 0.00 0.00 0.00 0.00 0.00 0.00 0.00 0.00 0.00 0.00 0.00 0.00 0.00 0.00 0.00 0.00 0.00 0.00 0.00 0.00 0.00 0.00 0.00 0.00 0.00 0.00 0.00 0.00 0.00 0.00 0.00 0.00 0.00 0.00 0.00 0.00 0.00 0.00 0.00 0.00 0.00 0.00 0.00 0.00 0.00 0.00 0.00 0.00 0.00 0.00 0.00 0.00 0.00 0.00 0.00 0.00 0.00 0.00 0.00 0.00 0.00 0.00 0.00 0.00 0.00 0.00 0.00 0.00 0.00 0.00 0.00 0.00 0.00 0.00 0.00 0.00 0.00 0.00 0.00 0.00 0.00 0.00 0.00 0.00 0.00 0.00 0.00 0.00 0.00 0.00 0.00 0.00 0.00 0.00 0.00 0.00 0.00 0.00 0.00 0.00 0.00 0.00 0.00 0.00 0.00 0.00 0.00 0.00 0.00 0.00 0.00 0.00 0.00 0.00 0.00 0.00 0.00 0.00 0.00 0.00 0.00 0.00 0.00 0.00 0.00 0.00 0.00 0.00 0.00 0.00 0.00 0.00 0.00 0.00 0.00 0.00 0.00 0.00 0.00 0.00 0.00 0.00 0.00 0.00 0.00 0.00 0.00 0.00 0.00 0.00 0.00 0.00 0.00 0.00 0.00 0.00 0.00 0.00 0.00 0.00 0.00 0.00 0.00 0.00 0.00 0.00 0.00 0.00 0.00 0.00 0.00 0.00 0.00 0.00 0.00 0.00 0.00 0.00 0.00 0.00 0.00 0.00 0.00 0.00 0.00 0.00 0.00 0.00 0.00 0.00 0.00 0.00 0.00 0.00 0.00 0.00 0.00 0.00 0.00 0.00 0.00 0.00 0.00 0.00 0.00 0.00 0.00 0.00 0.00 0.00 0.00 0.00 0.00 0.00 0.00 0.00 0.00 0.00 0.00 0.00 0.00 0.00 0.00 0.00 0.00 0.00 0.00 0.00 0.00 0.00 0.00 0.00 0.00 0.00 0.00 0.00 0.00 0.00 0.00 0.00 0.00 0.00 0.00 0.00 0.00 0.00 0.00 0.00 0.00 0.00 0.00 0.00 0.00 0.00 0.00 0.00 0.00 0.00 0.00 0.00 0.00 0.00 0.00 0.00 0.00 0.00 0.00 0.00 0.00 0.00 0.00 0.00 0.00 0.00 0.00 0.00 0.00 0.00 0.00 0.00 0.00 0.00 0.00 0.00 0.00 0.00 0.00 0.00 0.00 0.00 0	0.02 0.07 0.01 0.31 0.00 95.62 29.20 28.83 98.54 4(O) 0.00 0.03 0.01 1.08 0.84 0.92 0.03 0.00 0.03 0.01 0.00 0.00 0.00 0.00	0.02 0.03 0.02 0.30 0.00 95.60 27.27 29.25 98.33 4(O) 0.00 0.04 0.01 1.12 0.79 0.94 0.01 0.03 0.00 0.00 0.00 0.00 0.01 0.01 0.00 0.00 0.00 0.00 0.00 0.00 0.00 0.00 0.00 0.00 0.00 0.00 0.00 0.00 0.00 0.00 0.00 0.00 0.00 0.00 0.00 0.00 0.00 0.00 0.00 0.00 0.00 0.00 0.00 0.00 0.00 0.00 0.00 0.00 0.00 0.00 0.00 0.00 0.00 0.00 0.00 0.00 0.00 0.00 0.00 0.00 0.00 0.00 0.00 0.00 0.00 0.00 0.00 0.00 0.00 0.00 0.00 0.00 0.00 0.00 0.00 0.00 0.00 0.00 0.00 0.00 0.00 0.00 0.00 0.00 0.00 0.00 0.00 0.00 0.00 0.00 0.00 0.00 0.00 0.00 0.00 0.00 0.00 0.00 0.00 0.00 0.00 0.00 0.00 0.00 0.00 0.00 0.00 0.00 0.00 0.00 0.00 0.00 0.00 0.00 0.00 0.00 0.00 0.00 0.00 0.00 0.00 0.00 0.00 0.00 0.00 0.00 0.00 0.00 0.00 0.00 0.00 0.00 0.00 0.00 0.00 0.00 0.00 0.00 0.00 0.00 0.00 0.00 0.00 0.00 0.00 0.00 0.00 0.00 0.00 0.00 0.00 0.00 0.00 0.00 0.00 0.00 0.00 0.00 0.00 0.00 0.00 0.00 0.00 0.00 0.00 0.00 0.00 0.00 0.00 0.00 0.00 0.00 0.00 0.00 0.00 0.00 0.00 0.00 0.00 0.00 0.00 0.00 0.00 0.00 0.00 0.00 0.00 0.00 0.00 0.00 0.00 0.00 0.00 0.00 0.00 0.00 0.00 0.00 0.00 0.00 0.00 0.00 0.00 0.00 0.00 0.00 0.00 0.00 0.00 0.00 0.00 0.00 0.00 0.00 0.00 0.00 0.00 0.00 0.00 0.00 0.00 0.00 0.00 0.00 0.00 0.00 0.00 0.00 0.00 0.00 0.00 0.00 0.00 0.00 0.00 0.00 0.00 0.00 0.00 0.00 0.00 0.00 0.00 0.00 0.00 0.00 0.00 0.00 0.00 0.00 0.00 0.00 0.00 0.00 0.00 0.00 0.00 0.00 0.00 0.00 0.00 0.00 0.00 0.00 0.00 0.00 0.00 0.00 0.00 0.00 0.00 0.00 0.00 0.00 0.00 0.00 0.00 0.00 0.00 0.00 0.00 0.00 0.00 0.00 0.00 0.00 0.00 0.00 0.00 0.00 0.00 0.00 0.00 0.00 0.00 0.00 0.00 0.00 0.00 0.00 0.00 0.00 0.00 0.00 0.00 0.00 0.00 0.00 0.00 0.00 0.00 0.00 0.00 0.00 0.00 0.00 0.00 0.00 0.00 0.00 0.00 0.00 0.00 0.00 0.00 0.00 0.00 0.00 0.00 0.00 0.	0.02 0.01 0.01 0.01 0.16 0.00 95.17 28.31 29.43 98.00 4(O) 0.00 0.04 0.01 1.10 0.82 0.95 0.01 0.02 0.00 0.00 0.00 0.00 0.00 0.00 0.00 0.00 0.00 0.00 0.00 0.00 0.00 0.00 0.00 0.00 0.00 0.00 0.00 0.00 0.00 0.00 0.00 0.00 0.00 0.00 0.00 0.00 0.00 0.00 0.00 0.00 0.00 0.00 0.00 0.00 0.00 0.00 0.00 0.00 0.00 0.00 0.00 0.00 0.00 0.00 0.00 0.00 0.00 0.00 0.00 0.00 0.00 0.00 0.00 0.00 0.00 0.00 0.00 0.00 0.00 0.00 0.00 0.00 0.00 0.00 0.00 0.00 0.00 0.00 0.00 0.00 0.00 0.00 0.00 0.00 0.00 0.00 0.00 0.00 0.00 0.00 0.00 0.00 0.00 0.00 0.00 0.00 0.00 0.00 0.00 0.00 0.00 0.00 0.00 0.00 0.00 0.00 0.00 0.00 0.00 0.00 0.00 0.00 0.00 0.00 0.00 0.00 0.00 0.00 0.00 0.00 0.00 0.00 0.00 0.00 0.00 0.00 0.00 0.00 0.00 0.00 0.00 0.00 0.00 0.00 0.00 0.00 0.00 0.00 0.00 0.00 0.00 0.00 0.00 0.00 0.00 0.00 0.00 0.00 0.00 0.00 0.00 0.00 0.00 0.00 0.00 0.00 0.00 0.00 0.00 0.00 0.00 0.00 0.00 0.00 0.00 0.00 0.00 0.00 0.00 0.00 0.00 0.00 0.00 0.00 0.00 0.00 0.00 0.00 0.00 0.00 0.00 0.00 0.00 0.00 0.00 0.00 0.00 0.00 0.00 0.00 0.00 0.00 0.00 0.00 0.00 0.00 0.00 0.00 0.00 0.00 0.00 0.00 0.00 0.00 0.00 0.00 0.00 0.00 0.00 0.00 0.00 0.00 0.00 0.00 0.00 0.00 0.00 0.00 0.00 0.00 0.00 0.00 0.00 0.00 0.00 0.00 0.00 0.00 0.00 0.00 0.00 0.00 0.00 0.00 0.00 0.00 0.00 0.00 0.00 0.00 0.00 0.00 0.00 0.00 0.00 0.00 0.00 0.00 0.00 0.00 0.00 0.00 0.00 0.00 0.00 0.00 0.00 0.00 0.00 0.00 0.00 0.00 0.00 0.00 0.00 0.00 0.00 0.00 0.00 0.00 0.00 0.00 0.00 0.00 0.00 0.00 0.00 0.00 0.00 0.00 0.00 0.00 0.00 0.00 0.00 0.00 0.00 0.00 0.00 0.00 0.00 0.00 0.00 0.00 0.00 0.00 0.00 0.00 0.00 0.00 0.00 0.00 0.00 0.00 0.00 0.00 0.00 0.00 0.00 0.00 0.00 0.00 0.00 0.00 0.00 0.00 0.00 0.00 0.00 0.00 0.00 0.00 0.00 0.00 0.00 0.00 0.00 0.00 0.00 0.	0.05 0.01 0.00 0.34 0.00 92.74 53.36 29.89 98.08 4(O) 0.00 0.01 0.00 0.42 1.56 0.97 0.02 0.00 0.00 0.00 0.00 0.00 0.00 0.00 0.00 0.00 0.00 0.00 0.00 0.00 0.00 0.00 0.00 0.00 0.00 0.00 0.00 0.00 0.00 0.00 0.00 0.00 0.00 0.00 0.00 0.00 0.00 0.00 0.00 0.00 0.00 0.00 0.00 0.00 0.00 0.00 0.00 0.00 0.00 0.00 0.00 0.00 0.00 0.00 0.00 0.00 0.00 0.00 0.00 0.00 0.00 0.00 0.00 0.00 0.00 0.00 0.00 0.00 0.00 0.00 0.00 0.00 0.00 0.00 0.00 0.00 0.00 0.00 0.00 0.00 0.00 0.00 0.00 0.00 0.00 0.00 0.00 0.00 0.00 0.00 0.00 0.00 0.00 0.00 0.00 0.00 0.00 0.00 0.00 0.00 0.00 0.00 0.00 0.00 0.00 0.00 0.00 0.00 0.00 0.00 0.00 0.00 0.00 0.00 0.00 0.00 0.00 0.00 0.00 0.00 0.00 0.00 0.00 0.00 0.00 0.00 0.00 0.00 0.00 0.00 0.00 0.00 0.00 0.00 0.00 0.00 0.00 0.00 0.00 0.00 0.00 0.00 0.00 0.00 0.00 0.00 0.00 0.00 0.00 0.00 0.00 0.00 0.00 0.00 0.00 0.00 0.00 0.00 0.00 0.00 0.00 0.00 0.00 0.00 0.00 0.00 0.00 0.00 0.00 0.00 0.00 0.00 0.00 0.00 0.00 0.00 0.00 0.00 0.00 0.00 0.00 0.00 0.00 0.00 0.00 0.00 0.00 0.00 0.00 0.00 0.00 0.00 0.00 0.00 0.00 0.00 0.00 0.00 0.00 0.00 0.00 0.00 0.00 0.00 0.00 0.00 0.00 0.00 0.00 0.00 0.00 0.00 0.00 0.00 0.00 0.00 0.00 0.00 0.00 0.00 0.00 0.00 0.00 0.00 0.00 0.00 0.00 0.00 0.00 0.00 0.00 0.00 0.00 0.00 0.00 0.00 0.00 0.00 0.00 0.00 0.00 0.00 0.00 0.00 0.00 0.00 0.00 0.00 0.00 0.00 0.00 0.00 0.00 0.00 0.00 0.00 0.00 0.00 0.00 0.00 0.00 0.00 0.00 0.00 0.00 0.00 0.00 0.00 0.00 0.00 0.00 0.00 0.00 0.00 0.00 0.00 0.00 0.00 0.00 0.00 0.00 0.00 0.00 0.00 0.00 0.00 0.00 0.00 0.00 0.00 0.00 0.00 0.00 0.00 0.00 0.00 0.00 0.00 0.00 0.00 0.00 0.00 0.00 0.00 0.00 0.00 0.00 0.00 0.00 0.00 0.00 0.00 0.00 0.00 0.00 0.00 0.00 0.00 0.00 0.00 0.00 0.00 0.00 0.00 0.00 0.00 0.00 0.00 0.00 0.00 0.

Table 4.5 continued....

Sample	IK/3/P	IK/3/P	IK/3/P	IK/3/P	IK/3/P	IK/3/P	IK/3/P	IK/3/P
Mineral	Mag	Mag	Mag	Mag	Mag	Mag	Mag	Mag
Ref Point	15 / 1 R	17 / 1 R	22 / 1 R	4 / 1 R	30 / 1 R	52 / 1 R	62 / 1 R	66 / 1 R
SiO <sub>2</sub>	0.00	0.00	0.06	0.14	0.00	0.60	0.02	0.09
$TiO_2$	0.12	0.14	0.07	0.11	0.04	0.09	0.24	0.14
$Al_2O_3$	0.03	0.02	0.02	0.00	0.00	0.06	0.00	0.00
$Cr_2O_3$	7.96	4.62	9.65	4.57	5.10	4.66	9.14	2.55
FeO <sup>T</sup>	83.43	86.62	81.76	87.30	87.11	86.34	82.87	88.72
MnO	0.21	0.04	0.35	0.01	0.12	0.08	0.29	0.00
MgO	0.06	0.07	0.11	0.08	0.03	0.93	0.04	0.05
CaO	0.03	0.01	0.00	0.05	0.01	0.00	0.03	0.03
Na <sub>2</sub> O	0.01	0.02	0.00	0.01	0.00	0.02	0.01	0.02
$K_2O$	0.00	0.00	0.02	0.00	0.00	0.00	0.01	0.00
NiO	0.18	0.26	0.19	0.27	0.31	0.42	0.32	0.28
ZnO	0.00	0.00	0.00	0.00	0.00	0.00	0.00	0.00
Total	92.03	91.80	92.23	92.54	92.72	93.20	92.97	91.88
Fe <sub>2</sub> O <sub>3</sub>	59.28	62.76	57.58	63.08	63.06	62.79	58.44	64.87
FeO	30.08	30.14	29.94	30.54	30.37	29.84	30.29	30.35
Total	97.97	98.09	98.00	98.86	99.04	99.49	98.82	98.38
Cations :	4(O)	4(O)	4(O)	4(O)	4(O)	4(O)	4(O)	4(O)
Si	0.00	0.00	0.00	0.01	0.00	0.02	0.00	0.00
Ti	0.00	0.00	0.00	0.00	0.00	0.00	0.01	0.00
Al	0.00	0.00	0.00	0.00	0.00	0.00	0.00	0.00
Cr	0.25	0.14	0.30	0.14	0.16	0.14	0.28	0.08
Fe <sup>+3</sup>	1.75	1.85	1.69	1.84	1.84	1.81	1.71	1.91
Fe <sup>+2</sup>	0.98	0.99	0.98	0.99	0.99	0.95	0.98	0.99
Mn	0.01	0.00	0.01	0.00	0.00	0.00	0.01	0.00
Mg	0.00	0.00	0.01	0.00	0.00	0.05	0.00	0.00
Ca	0.00	0.00	0.00	0.00	0.00	0.00	0.00	0.00
Na	0.00	0.00	0.00	0.00	0.00	0.00	0.00	0.00
K	0.00	0.00	0.00	0.00	0.00	0.00	0.00	0.00
Ni	0.01	0.01	0.01	0.01	0.01	0.01	0.01	0.01
Zn	0.00	0.00	0.00	0.00	0.00	0.00	0.00	0.00
Total	3.00	3.00	3.00	3.00	3.00	3.00	3.00	3.00
Cr#	99.44	99.36	99.69	100.00	100.00	98.12	100.00	100.00
Mg#	0.35	0.41	0.65	0.46	0.18	5.26	0.23	0.29
Fe#	99.65	99.59	99.35	99.54	99.82	94.74	99.77	99.71
Fe <sup>3+</sup> #	0.64	0.65	0.63	0.65	0.65	0.65	0.63	0.66
YFe <sup>3+</sup> #	0.88	0.93	0.85	0.93	0.92	0.93	0.86	0.96

re # 0.50 0.52 0.53 Notes: Al-Chr, Al-Chromite; Chr, Chromite; Fe-Chr, Ferrian Chromite; Cr-Mag, Chrome Magnetite; R-Rim Mag, Magnetite;. Cr# =  $100^{\circ}$  Cr/(Cr+Al); Mg # =  $100^{\circ}$  Mg/(Mg+Fe); Fe # =  $100^{\circ}$  Fe/(Fe+Mg);  ${}^{Y}Fe^{3*}\# = Fe^{3*}/(Fe^{3*}+Cr+Al): Fe^{3*}\# = Fe^{3*}/(Fe^{2*}+Fe^{2*}).$ 

Table 4.6 Representative Laser Ablation (LA-ICPMS) analysis of chrome spinels (chromites) from the ultramafic rocks of MUC.

Table 4.6	LA-HR-ICP-MS data of chrome spinel from the ultramafic rock of MUC									
Ref. Point	Spl-2	Spl-5	Spl-6	Spl-7	Spl-8	Spl-9	Spl-10	Spl-11	Spl-12	Spl-13
Sc	4.70	5.11	4.20	5.06	4.16	5.01	4.12	5.30	4.52	4.81
Y	5.87	4.21	6.01	4.17	5.95	4.13	5.89	0.47	3.61	4.82
La	2.70	2.53	3.30	2.82	1.73	2.00	1.96	2.71	2.55	1.75
Ce	4.27	4.89	3.20	2.61	2.16	2.89	2.06	4.30	4.91	2.21
Pr	0.99	0.93	1.11	0.54	0.42	0.40	0.48	0.99	0.93	0.43
Nd	4.58	3.70	5.29	2.09	1.95	1.85	2.26	4.58	3.72	1.98
Sm	1.34	1.17	1.75	0.47	0.58	0.69	0.72	1.34	1.17	0.58
Eu	0.54	0.43	0.62	0.17	0.18	0.23	0.27	0.54	0.43	0.18
Gd	1.61	1.57	2.08	0.58	0.50	0.67	0.86	1.61	1.57	0.51
Tb	0.24	0.26	0.36	0.10	0.08	0.11	0.13	0.24	0.26	0.08
Dy	1.22	1.94	1.82	0.64	0.63	0.72	0.77	1.23	1.94	0.64
Но	0.30	0.43	0.28	0.12	0.13	0.15	0.17	0.30	0.43	0.13
Er	0.92	1.00	0.56	0.25	0.32	0.41	0.39	0.93	1.00	0.33
Tm	0.14	0.16	0.05	0.04	0.05	0.06	0.05	0.14	0.16	0.05
Yb	0.97	0.98	0.33	0.30	0.27	0.40	0.31	0.97	0.99	0.27
Lu	0.14	0.14	0.05	0.04	0.03	0.05	0.04	0.14	0.14	0.03
Th	0.23	0.12	0.29	0.06	0.16	NA	NA	0.23	0.12	0.16
U	1.02	1.05	0.99	0.41	0.41	0.48	0.45	1.03	1.05	0.42
∑REE	19.96	20.13	20.81	10.77	9.02	10.63	10.46	20.04	20.21	9.17
$\sum$ LREE	16.02	15.21	17.36	9.28	7.52	8.72	8.61	16.09	15.28	7.64
$\Sigma$ HREE	3.94	4.92	3.46	1.49	1.51	1.91	1.85	3.95	4.93	1.53
∑LREE/∑HRE	I 4.07	3.09	5.02	6.24	4.99	4.57	4.64	4.07	3.10	4.98
Ce*	0.63	0.76	0.40	0.51	0.61	0.78	0.51	0.63	0.76	0.61

Note: All values are in ppm

Table 4.7: Estimated maximum, minimum, and average value of Al<sub>2</sub>O<sub>3</sub>, FeO/MgO, and TiO<sub>2</sub> of parental melts in ultramafic rocks from the study area in comparison with parental melt of different tectonic setting

	Al <sub>2</sub> O <sub>3</sub> (melt-	TiO <sub>2</sub> (melt-	(FeO/MgO)(melt-		Toc(Ol-	
	spinel)	spinel)	Ol)	$\Delta \log (fo_2)$	Spinel)	References
Madawara Ultramafic complex						This study
Peridotite	9.22-14.22					-
	(11.74)	0.32-0.69 (0.49)				
Olivine Pyroxenite	11.49-14.30	0.34-0.80		"+0.26:	929-	
	(12.53)	(0.56)	1.72-1.92 (1.78)	+2.14"	1095	
Alaskan Type compl	ex					Habtoor et.al (2016)
Peridotite	11.21-15.56	0.82-2.85		"-0.18:	671-	
Peridonte	(13.79)	(1.62)	0.92-0.99 (0.95)	+4.13"	981	
Dunite	11.82-15.12	0.97-2.77		"+1.88:		
Dunite	(13.68)	(1.83)	0.58-1.4 (0.90)	+3.01"	614-864	
MORB	~15	0.32-2.20	1.2-1.6			Wilson (1989)
BABB	~17	0.45-1.45				Kamenetsky et.al (2001)
Boninites (SSZ)	10.6-14.4	0.10-0.52	0.7-1.4			Wilson (1989), Hicky and Frey (1981)
Layered Intrusion						Mondal et.al (2006)
Bushveld complex	11.5	0.74				
Great dyke	11.1	0.61				
Archean low Ti Siliceous High Mg Basalt						Mondal et.al (2006)
Barberton	12.7-13.4	0.74				
Pilbara	10.1-11.7	0.58-0.75				

Table 4.8: Comparison between worldwide Alaskan-type intrusion and Madawara

	Alaskan-type complexes	Madawara ultramafic complexe
Age	Mostly in Phanerozoic and	Archean
	Proterozoic, Rarely in Archean	
Geological setting	Close to end of subduction, prior to	Subduction
	accretion-collision	
Size	Most are small in size, ranging	Mostly small size (3 km <sup>2</sup> ),
	from 12 to 40 km <sup>2</sup>	Madawara intrusion is biggest (6
		km <sup>2</sup> )
Morphology and zoning	Crude concentric zoning of	Crude concentric zoning of
	lithologies grading from olivine-	different lithology grading from
	rich ultramafic core to mafic rim:	peridotite core to gabbro; lack of
	lack of chilled margins	chilled margins, margins
C	California and disable made as late	are commonly sheared
Sequence of intrusion	Gabbroic and dioritic rocks as late intrusion	Late intrusion of gabbro rock
Lithology		followed by diorite
Lithology	Dunite, hornblendite,	Peridotite, olivine-pyroxenite,
	clinopyroxenite, gabbro, minor diorite, and syenite rocks	pyroxenite, Hbl-pyroxenite, Hornblendite, Gabbro, Diorite,
	diorite, and syemic rocks	and Qtz-diorite. Syenite is
		not recorded
Texture	Accumulated texture with minor or	The ultramafic rocks shows
Texture	no trapped liquid	cumulate to adcumulate texture
Mineralogy	Abundant clinopyroxene, primary	Abundant olivine, Cpx, (Cpx >>
1/111101111015)	hornblende, magnetite, lack of	Opx) subordinate amount of
	orthppyroxene, and plagioclase in	primary hornblende, magnetite,
	ultramafic rock.	Opx is present but not much, and
		plagioclase is absent in
		ultramafic rocks.
Chromite	Common occurrences of chromite	Common occurrences of
	in dunite.	chromite in peridotite, olivine
		pyroxenite, and pyroxenite
Mineral chemistry	High Mg-olivine, diopsidic	Moderate Mg-olivine, diopsidic
	clinopyroxene, phlogopite mica,	clinopyroxene, and hornblende
	and hornblende are calcic with wide	are calcic.
G : 1.1 : :	range of composition.	W. I. D. G. I
Cr-spinel chemistry	High Fe-Cr, and low Al-chromite,	High Fe-Cr chromite, low MgO
	magnetite, and ilmenite are frequent	and low Al-chromite. The YFe <sup>3+</sup> #
	in the late stage	is variable. Magnetite and
		ilmenite are frequent in the late
Bulk rock geochemistry	Low incompatible elements,	stage.  Low incompatible elements,
Durk fock geochemistry	relatively high LILE and	relatively high LILE, Th and low
	low HFSE, no EU anomalies	HFSE, no Eu anomalies recorded
Mineralization	PGE mineralization associated with	PGE mineralization associated
T.IIICI WIIZWIICII	chromite, some Cu–Ni	with chromite, some
	mineralization.	Cu–Ni mineralization.
	SSE: high field strength elements: I II E	1

Note. Hbl: Hornblende; HFSE: high-field strength elements; LILE: large-ion lithophile elements; PGE: platinum group elements; REE: rare earth element. The features of Alaskan-type complex are after Johan (2002), Helmy and El Mahallawi (2003), Pettigrew and Hattori (2006), Thakurta et al. (2008), and Su et al. (2013).

## **CHAPTER-V**

# Geochemistry and Radiogenic isotopes

In this chapter, an attempt has been made to present the whole rock geochemistry (major, trace and PGE elements), as well as Nd isotope data for the Madawara ultramafic complex (MUC) covering Madawara, Ikauna, Girar and the Hanumathgarh regions. The principal aim is to address their petrogenetic processes such as magmatic differentiation, composition of potential mantle reservoirs, degree of melting and depth of magma generation. Major and trace element data for 49 samples of MUC including (Madawara, Ikauna and Hanumathgarh) is presented. Among 49 samples analyzed, 18 ultramafic samples from Madawara, 5 ultramafic samples from Ikauna, 10 ultramafic rocks from Hanumathgarh, 5 mafic rock samples from the Madawara, 4 samples of mafic rocks from the Ikauna and 7 intermediated rocks from the Ikauna analyzed for the full range of major and trace elements present in Table 5.1 and Table 5.2.

#### 5.1 Madawara section

The studied ultramafic rocks have been divided into three groups (Group-I, Group II, Group III) on the basis of modal mineralogy, major element geochemistry and their REE patterns. The group I samples display a narrow range of SiO<sub>2</sub> (36.41-41.02 wt.%), high in MgO contents (31.43-37.57 wt.%), moderate Fe<sub>2</sub>O<sub>3</sub> (8.07-11.92 wt.%), very low Al<sub>2</sub>O<sub>3</sub> (2.47-3.51 wt.%), and low to high CaO contents (1.60-3.49 wt.%). On the other hand, the rocks of group II display higher SiO<sub>2</sub> (41.63-50.77 wt.%), lower MgO contents (25.11-29.07 wt.%), moderate to high Fe<sub>2</sub>O<sub>3</sub> (7.86-12.10 wt.%), low to moderate Al<sub>2</sub>O<sub>3</sub> (2.80-5.03 wt.%) and high CaO contents (3.10-8.96 wt.%) compared to the ultramafic rocks of the group I. The studied group-I ultramafic

possibly corresponds to early differentiates in view of very high MgO contents (> 30 wt.% MgO) whereas group-II ultramafic samples (<30 wt.% MgO) could possibly represent flows or evolved melts through magmatic differentiation. These ultramafic rocks (MgO > 18 wt.%) show komatiite affinity. Globally, komatiites have been divided into two varieties based on elemental characteristics; Al-depleted and Al-undepleted (Arndt, 2003). Furthermore, (Arndt, 2003) proposes that Al-depleted komatiites are characterized by low alumina content with "high CaO/Al<sub>2</sub>O<sub>3</sub> >1 and low Al<sub>2</sub>O<sub>3</sub>/ TiO<sub>2</sub> <18, whilst Al-undepleted komatiites are characterized by lower CaO/Al<sub>2</sub>O<sub>3</sub> <1 and higher Al<sub>2</sub>O<sub>3</sub>/TiO<sub>2</sub> >18". All the studied ultramafic samples from the Madawara are showing dominantly Al- depleted but a few samples exhibit Al- undepleted character as reflected in their wide range of CaO/Al<sub>2</sub>O<sub>3</sub> (0.52-2.48) and Al<sub>2</sub>O<sub>3</sub>/TiO<sub>2</sub> (11.76 to 19.47) values, showing affinity mainly towards the Al-depleted komatiites (See figure 5 a-b). In the ternary diagrams of AFM (Irvine and Baragar, 1971); CaO-MgO-Al<sub>2</sub>O<sub>3</sub> (after Jenson 1976, modified by Viljoen et al., 1982); Al<sub>2</sub>O<sub>3</sub>- (FeO+TiO<sub>2</sub>)-MgO triangular diagram (Jenson, 1976 modified by Viljoen et al., 1982) the studied samples plot in the komatiite field (See Figure 5.1 ab), Further, on the AFM (Na<sub>2</sub>O+K<sub>2</sub>O-FeO-MgO) diagram (Beard, 1986) the group-I and group-II ultramafic rocks plot in the arc-related ultramafic cumulate field (See Figure 5.1c). Ultramafic rocks of komatiite affinity are characterized by very low content of incompatible elements (U, Th, Zr, Rb, Ba, Sr with chondritic to sub-chondritic REE contents) with complimentary high contents of compatible elements such as Cr, Ni, Co and V. The Madawara rock samples (group I and group II) exhibit high to very high content Cr (3272-6262 ppm), Ni (768-1961ppm), and Co (76-134 ppm). The rocks of group-II samples also show high content of Sc (18-24 ppm), and V (74-115 ppm) whilst group-I samples show low content of Sc (4-15 ppm), and V (70-94 ppm) contents. The observed high contents of Sc, V in group II could be possibly linked to the accumulation of

more pyroxene whilst their low contents in group I possibly controlled by olivine and spinel. The mafic rocks of the studied Madawara sample show a considerable variation in their major and trace element chemistry. The group III ultramafic rocks shows low content of MgO, Ni, Cr and high content of SiO<sub>2</sub> in comparison to the ultramafic of "group-I and group-II" ultramafic rocks. In the ternary diagrams of AFM (after Irvine and Baragar, 1971); CaO-MgO-Al<sub>2</sub>O<sub>3</sub> after (Jenson, 1976), modified by (Viljoen et al., 1982); Al<sub>2</sub>O<sub>3</sub>- (FeO+TiO<sub>2</sub>)-MgO triangular diagram (Jenson, 1976 modified by Viljoen et al., 1982), the studied samples plot in the komatiite to basaltic komatiitic field (See Figure 5.1 a-b), Further, on the AFM (Na<sub>2</sub>O+K<sub>2</sub>O-FeO-MgO) diagram (Beard, 1986) the group-III ultramafic rocks plot in the "arc-related ultramafic-mafic cumulate field" (See Figure 5.1c). However, the mafic rocks of the Madawara (group-IV) low MgO, low to moderate SiO<sub>2</sub> contents high CaO and Al<sub>2</sub>O<sub>3</sub> contents in comparison to the all the ultramafics of Madawara.

The group-III samples are characterized by a slight variation in SiO<sub>2</sub> (48-51.53 wt.%), low to moderate Al<sub>2</sub>O<sub>3</sub> contents (3.89-5.41 wt.%), moderate to high Fe<sub>2</sub>O<sub>3</sub> (6.24-11.73 wt.%), moderate to high MgO (15.75-27.18 wt.%), moderate to high CaO (10.76-13.11 wt.%) with low content of MnO, Na<sub>2</sub>O and K<sub>2</sub>O. On the other hand, the group-IV samples (mafic rocks) are characterized by the very narrow range of SiO<sub>2</sub> (50.04-50.81 wt.%), high Al<sub>2</sub>O<sub>3</sub> contents (14.99-16.59 wt.%), moderate to low Fe<sub>2</sub>O<sub>3</sub> (5.70-6.78 wt.%) with moderate MgO contents (8.99-9.46 wt.%), high CaO contents (12.60-13.14 wt.%) and low contents of MnO, Na<sub>2</sub>O and K<sub>2</sub>O. The group-III rocks have shown high Cr (900-1256 ppm), Sc (33-54 ppm), V (119-247 ppm) whilst group-IV rocks have low contents Cr (372-527 ppm), Sc (27-32 ppm) and V (119-146 ppm). Although the group-III rocks have high Cr, contents, they have low Ni content (32-53 ppm) in comparison with the group-IV rocks showing high Ni contents (219-244 ppm) of the studied area. The studied group-III and group-IV rock samples projected on the ternary classification diagrams of AFM (after Irvine and

Baragar, 1971); CaO-MgO-Al<sub>2</sub>O<sub>3</sub> after ("Jenson (1976"), modified by (Viljoen et.al., 1982), and Al<sub>2</sub>O<sub>3</sub>-(Fe<sub>2</sub>O<sub>3</sub>+TiO<sub>2</sub>)-MgO (Jenson, modified by Viljoen et.al., 1982), where all the rock samples plot on the komatiitic-basalt to tholeiitic field. (See figure 5.2a-b). Further, on the AFM (Na<sub>2</sub>O+K<sub>2</sub>O-FeO-MgO) diagram (Beard, 1986) the group-III and group-IV rocks plot in the arcrelated mafic cumulate field (See Figure 5.2 c). They are characterized by the large variation in the incompatible element contents like Ba (38-163 ppm), Sr (59-224 ppm), Zr (29-219 ppm), and moderate to high compatible elements like Cr (525-1256 ppm) and Ni (0-244 ppm).

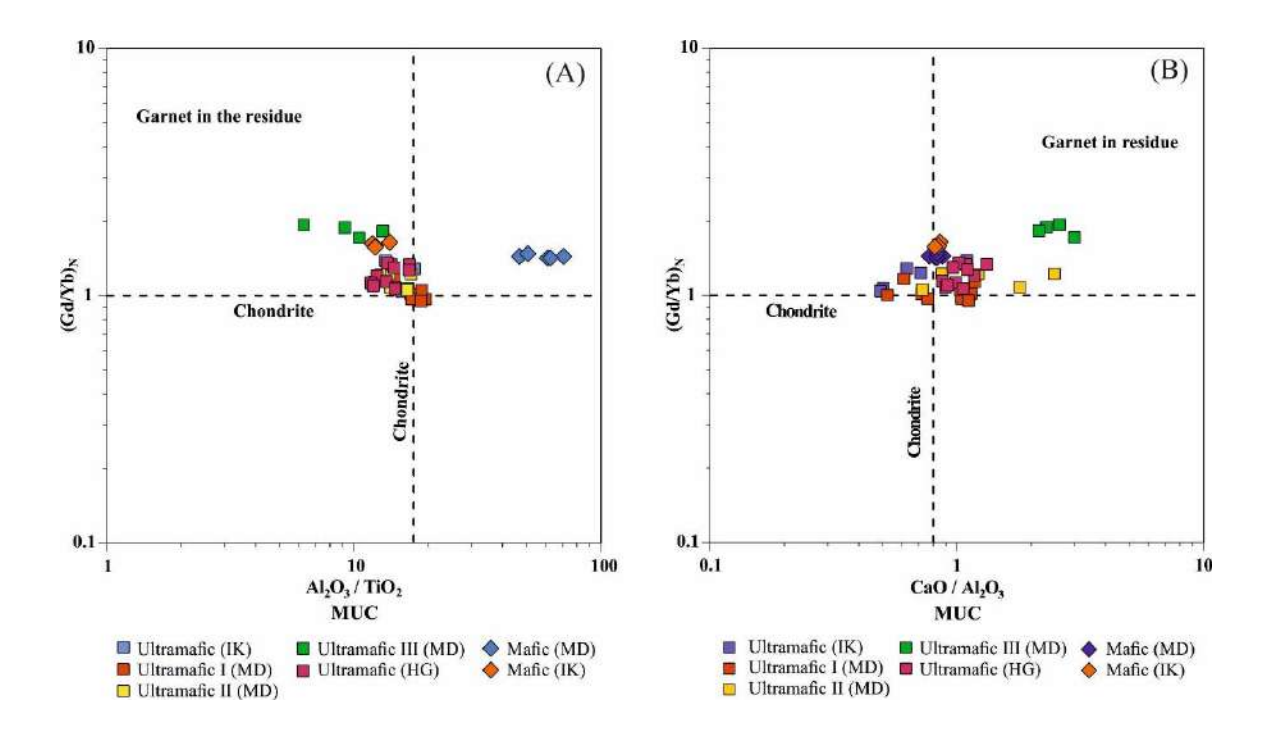


**Figure 5.1** (a)  $(Gd/Yb)_N$  versus  $Al_2O_3/TiO_2$  (after Arndt 2003) indicates residual garnet's role in most studied samples. (b)  $(Gd/Yb)_N$  versus  $CaO/Al_2O_3$  (after Jahn et.al., 2003) shows the role in most studied samples.

On Harker's binary plots, the major element oxides of the studied ultramafic and mafic rocks (group-I group-II, group-III) together with mafic rocks (group-IV) of the Madawara ultramafic-mafic complex, define a moderate to strong negative correlation against the MgO except Fe<sub>2</sub>O<sub>3</sub> and Na<sub>2</sub>O+K<sub>2</sub>O which do not show any systematic correlation. The negative trends

of SiO<sub>2</sub>, CaO and Al<sub>2</sub>O<sub>3</sub> against MgO can be attributed to the removal of olivine, garnet and pyroxene either fractionation or their retention in the residual source (See figure 5.2).

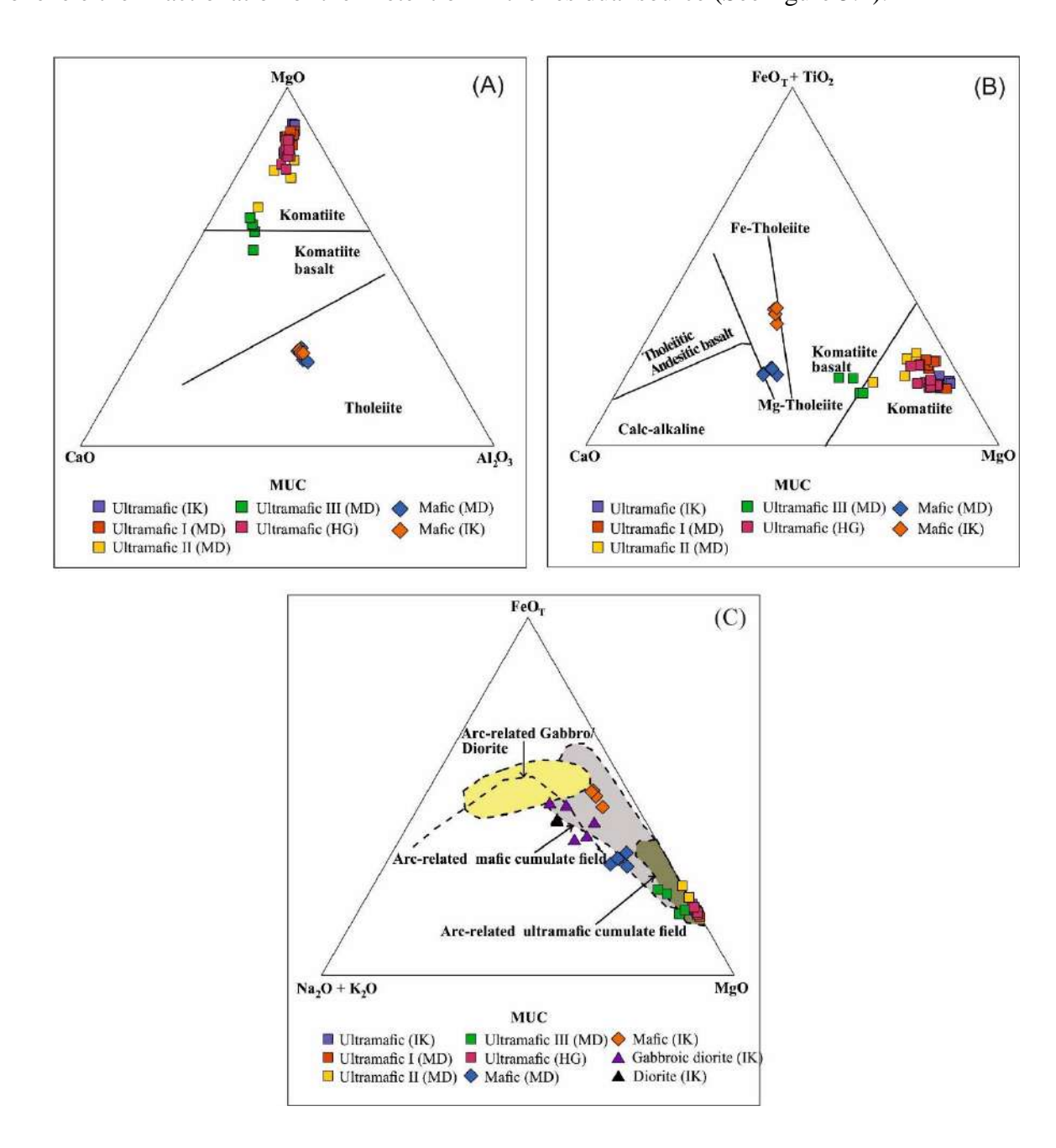


**Figure 5.2** (a) AFM diagrams after (Irvine and Baragar, 1971) (a) CaO-MgO-Al<sub>2</sub>O<sub>3</sub> diagram after Jenson (1976), Modified by Viljoen et al., (1982). (b) Al<sub>2</sub>O<sub>3</sub>-(Fe<sub>2</sub>O<sub>3</sub>+TiO<sub>2</sub>)-MgO triangular diagram (Jenson, 1976; modified by Viljoen et al., (1982). (c) (Na<sub>2</sub>O+K<sub>2</sub>O)-FeO<sub>t</sub>-MgO discrimination ternary diagram for the ultramafic-mafic rocks of MUC. Fields of both cumulate and non-cumulate rocks are from Beard (1986).

On the Harker's binary plot the trace elements define a moderate to strong positive correlation against MgO where compatible elements (Ni, Cr, Co) which could be related to the fractionation of olivine and pyroxene (See figure 5.3). On the contrary, the weak negative trends of Sc, V against MgO can be attributed to the control of clinopyroxene whilst Rb, Ba, don't display any correlation possibly related to their mobility during secondary processes (See figure 5.4). The rocks of group-I of Madawara show low total REE content (6.21-12.0 ppm, few samples with subchondritic total REE) whilst the group-II samples show slightly higher total REE contents (12.22-20.07 ppm) but resembling chondritic REE pattern. Chondrite normalized REE patterns of all the samples of group-I display slightly fractionated REE patterns whilst three samples show nearly flat REE patterns (MD-3, MW-8, MW-10) with variable moderate to weak negative to positive Eu anomalies (Eu/Eu\*=0.56-1.20). All the studied samples of group-I show (Gd/Yb)<sub>N</sub> ratios ranging between 0.95-1.16 (See figure 5. 5a). It is possible that the mobility of the Eu<sup>2+</sup> during secondary processes, such as "hydrothermal alteration or low-grade metamorphism," is responsible for the observed negative Eu anomalies (Sun and Nesbitt, 1978; Arndt 1994). On the primitive mantle normalized multi-element diagram, (Sun and McDonough, 1989), the group-I ultramafic rocks of Madawara complex show variable contents in large ion lithophile elements but show depletion in high field strength elements (HFSE) with strong negative Nb-Ta and variable negative Zr-Hf anomalies (See figure 5. 5 b). On the other hand, the group-II ultramafic samples from the MUC display slightly "fractionated REE patterns" [(Gd/Yb)<sub>N</sub>=1.06-1.29] with very weak negative Eu anomalies (Eu/Eu\*=0.75-0.99). On the "primitive mantle normalized multi-element diagram," (Sun and McDonough, 1989) the group-II ultramafic rocks of Madawara complex show weak negative Nb-Ta and Sr anomalies coupled with very weak negative Zr-Hf anomaly, but variable Y anomalies (See figure 5.5 c-d).

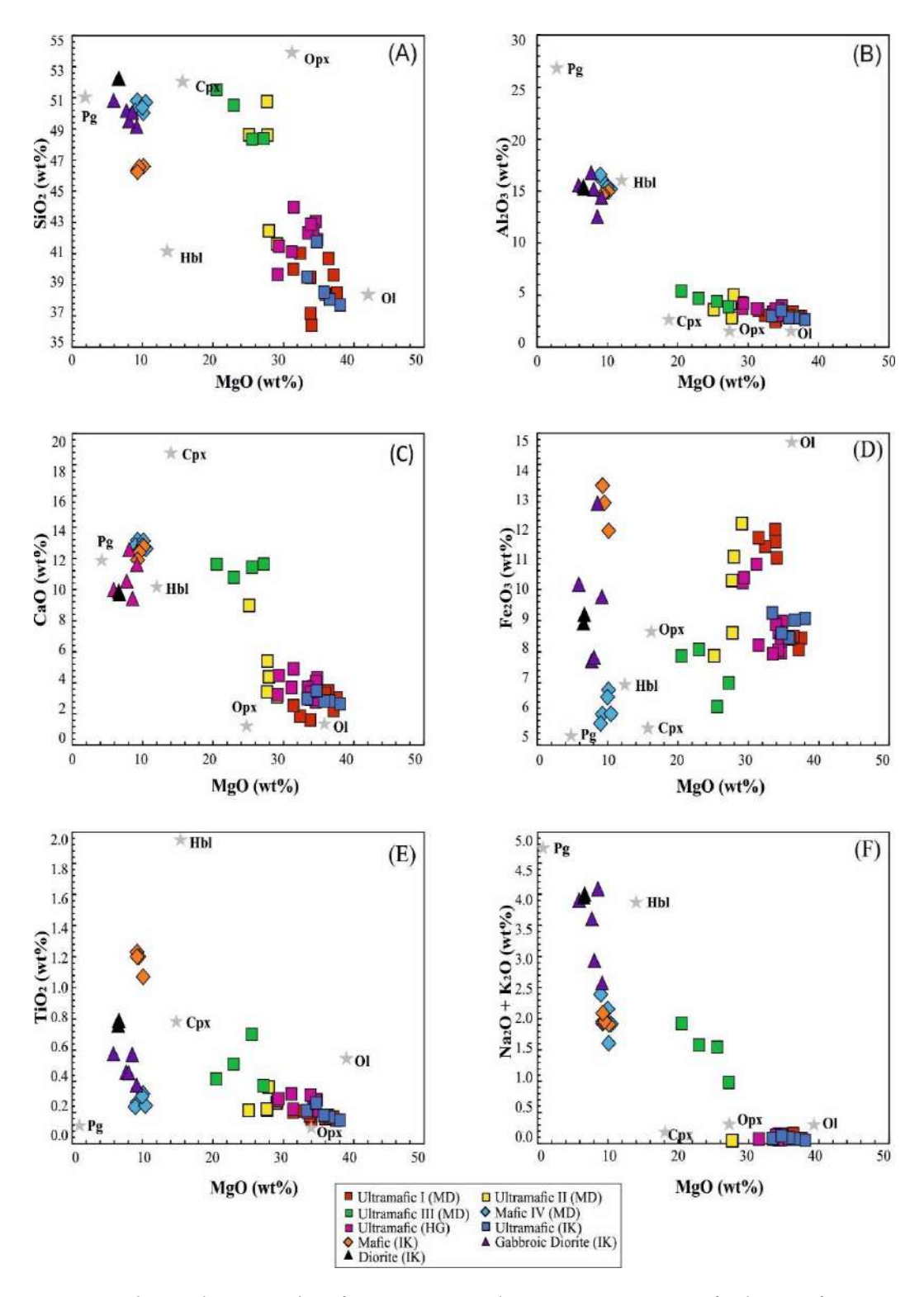
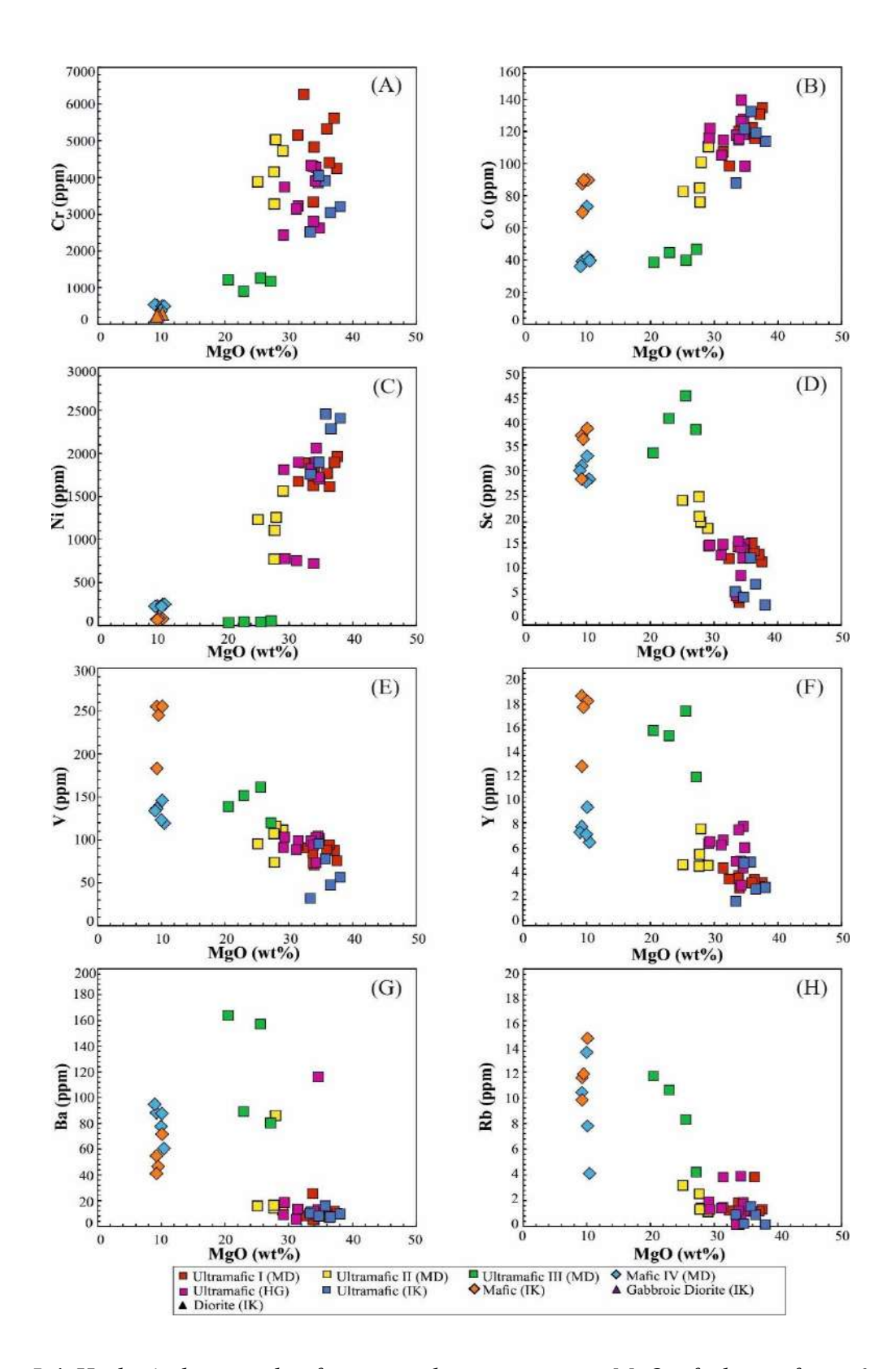


Figure 5.3 Harker's binary plot for major oxides against MgO of ultramafic-mafic of the Madawara ultramafic complex.



**Figure 5.4** Harker's binary plot for trace elements against MgO of ultramafic-mafic of the Madawara ultramafic complex

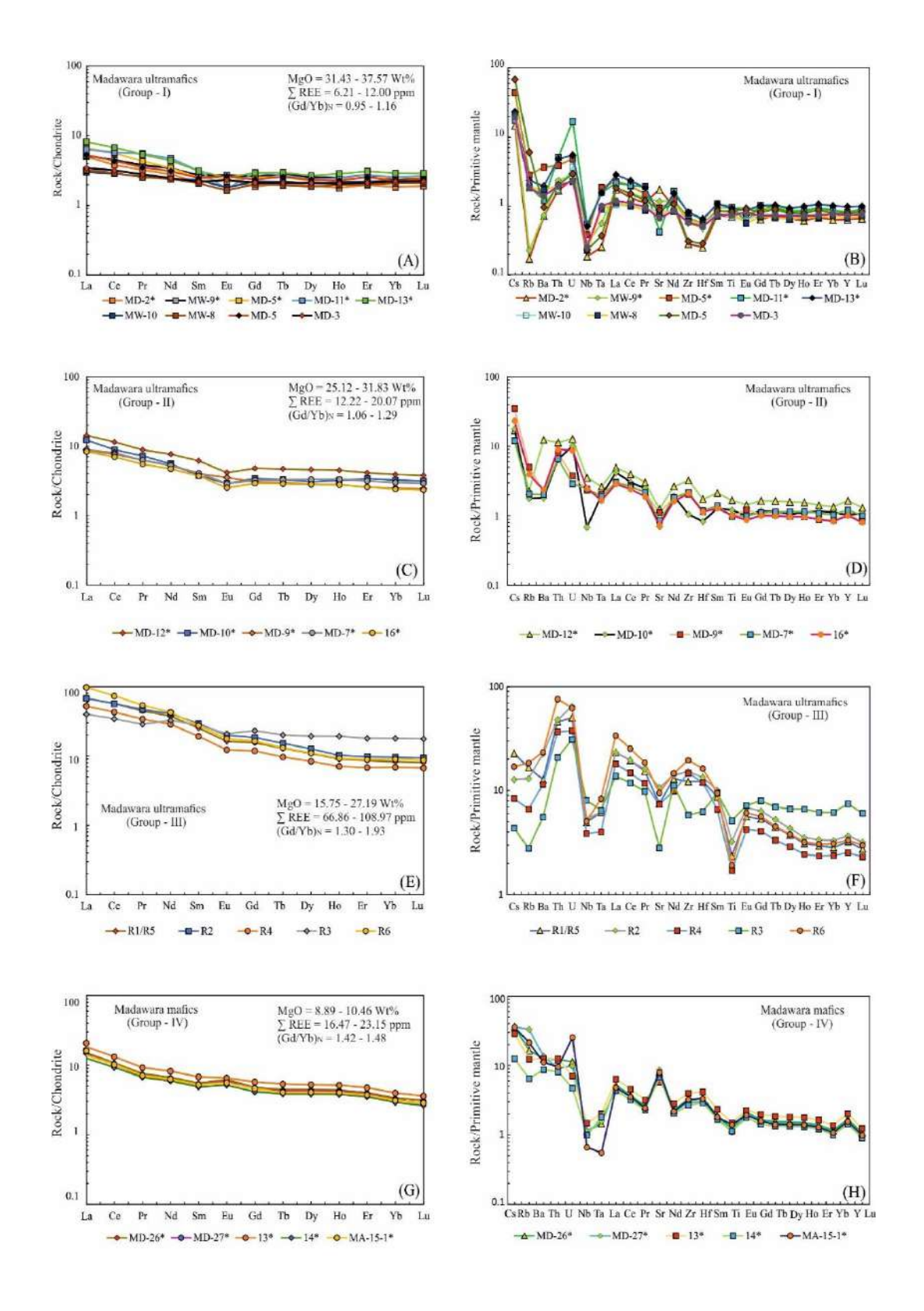


Figure 5.5 (a-h) Chondrite-normalized REE patterns and primitive normalized multi-element spider diagrams of the ultramafic-mafic of the Madawara region

The rocks of group-III ultramafic characterized by moderately high REE contents (66.86-108.97 ppm), whilst the group-IV mafic rock samples display low REE contents (16.47-23.15 ppm). Chondrite normalized REE patterns of group-III display slightly flat HREE patterns with slight negative Eu anomaly (Eu/Eu\*=0.79-0.83 ppm) (See figure 5.5 e). All the studied group-III samples show "fractionated REE patterns" with (Gd/Yb)<sub>N</sub> ranging from 1.29-1.93 with slight LREE enrichment. On the primitive mantle normalized multi-element diagram, (Sun and McDonough, 1989) all the samples of group-III rocks display strong negative Nb-Ta-Ti anomalies coupled with slightly positive Zr-Hf-Y anomalies except on sample (R-3) which shows strong negative Nb-Ta as well as negative Zr-Hf-Ti anomalies but positive Y anomalies (see figure 5.5 f). On the other hand, the mafic rocks of group-IV show low REE content ranging from 16.47 ppm-23.15 ppm displaying slightly fractionated LREE with flat HREE pattern with positive Eu anomalies (Eu/Eu\*=1.04-1.20 ppm) could be related to an accumulation of plagioclase (see figure 5.5 g). On the primitive mantle normalized multi-element diagram (Sun and McDonough, 1989) all the group IV mafic rocks exhibit strong negative Nb-Ta-Ti anomalies with positive Sr-Zr-Hf-Y anomalies (See figure 5.5 h).

#### **5.2 Ikauna Section**

The ultramafic rocks of the Ikauna section have a narrow range of low SiO<sub>2</sub> (37.01-43.05 wt.%), high MgO contents (33.39-38.05 wt.%), moderate Fe<sub>2</sub>O<sub>3</sub> (7.93-8.59 wt.%), low Al<sub>2</sub>O<sub>3</sub> (2.64-3.49 wt.%), and low to moderate CaO contents (1.38-3.82 wt.%). Majority of the studied ultramafic samples are cumulate in nature (> 35 wt.% MgO). They exhibit both Al-depleted to undepleted characters [CaO/Al<sub>2</sub>O<sub>3</sub> (0.48-1.10) and Al<sub>2</sub>O<sub>3</sub>/TiO<sub>2</sub> (13.42 to 17.60)]. In the ternary diagrams of AFM (after Irvine and Baragar, 1971); CaO-MgO-Al<sub>2</sub>O<sub>3</sub> after (Jenson, 1976) modified by (Viljoen et al., 1982); and Al<sub>2</sub>O<sub>3</sub>- (FeO+TiO<sub>2</sub>)-MgO (Jenson, 1976 modified by

Viljoen et al., (1982) the studied samples display the komatiite field (See figure 5.2 a-b). Further, on the AFM (Na<sub>2</sub>O+K<sub>2</sub>O-FeO-MgO) diagram (Beard, 1986) the studied samples display arcrelated ultramafic cumulate field (See Figure 5.2 c). The ultramafic of the Ikauna samples showing very high content Cr (2509-4316 ppm), Ni (1759-2455ppm) and Co (87-132 ppm). The ultramafic samples of Ikauna show low content of Sc (3-15 ppm) and V (31-104 ppm) but Ni and Cr contents are higher compared to the ultramafic rocks of Madawara.

The ultramafic rocks of the Ikauna show chondritic to sub-chondritic total REE content (6.67-12.60 ppm). Chondrite normalized REE patterns display slightly "fractionated REE patterns" [ $(Gd/Yb)_N = 1.04-1.38$ ] with variable (moderate to weak negative to positive Eu anomalies (Eu/Eu\*=0.84-1.12) (see figure 5. 6a). The observed negative Eu anomalies "could be related to the mobility of the Eu<sup>2+</sup> during the secondary process such as either through hydrothermal alteration or low-grade metamorphism," (Sun and Nesbitt, 1978; Arndt 1994). On the "primitive mantle normalized" (Sun and McDonough, 1989), the ultramafic rocks of Ikauna show strong negative Nb-Ta but weak negative Zr-Hf anomalies (See figure 5.6 b). Four samples of mafic rocks and seven intermediate rocks of Ikauna were analyzed for major and trace elements. The mafic rocks display a narrow range of SiO<sub>2</sub> (46.24-46.60 wt.%) and are characterized by higher Al<sub>2</sub>O<sub>3</sub> (14.61-14.95 wt.%), Fe<sub>2</sub>O<sub>3</sub> (11.88-13.33 wt.%), high CaO (11.89-12.73 wt.%) but moderate MgO (9.27-10.14 wt.%). These rocks have low contents of Na<sub>2</sub>O, K<sub>2</sub>O, P<sub>2</sub>O<sub>5</sub> but high TiO<sub>2</sub> (1.07-1.23 wt.%). On the triangular diagrams of AFM (after Irvine and Baragar, 1971); CaO-MgO-Al<sub>2</sub>O<sub>3</sub> after (Jenson (1976) modified by (Viljoen et al., 1982) and Al<sub>2</sub>O<sub>3</sub>- (Fe<sub>2</sub>O<sub>3</sub>+TiO<sub>2</sub>)-MgO (Jenson, 1976 modified by Viljoen et al., 1982) these samples define clear tholeitic field (See figure 5.2 a-b).

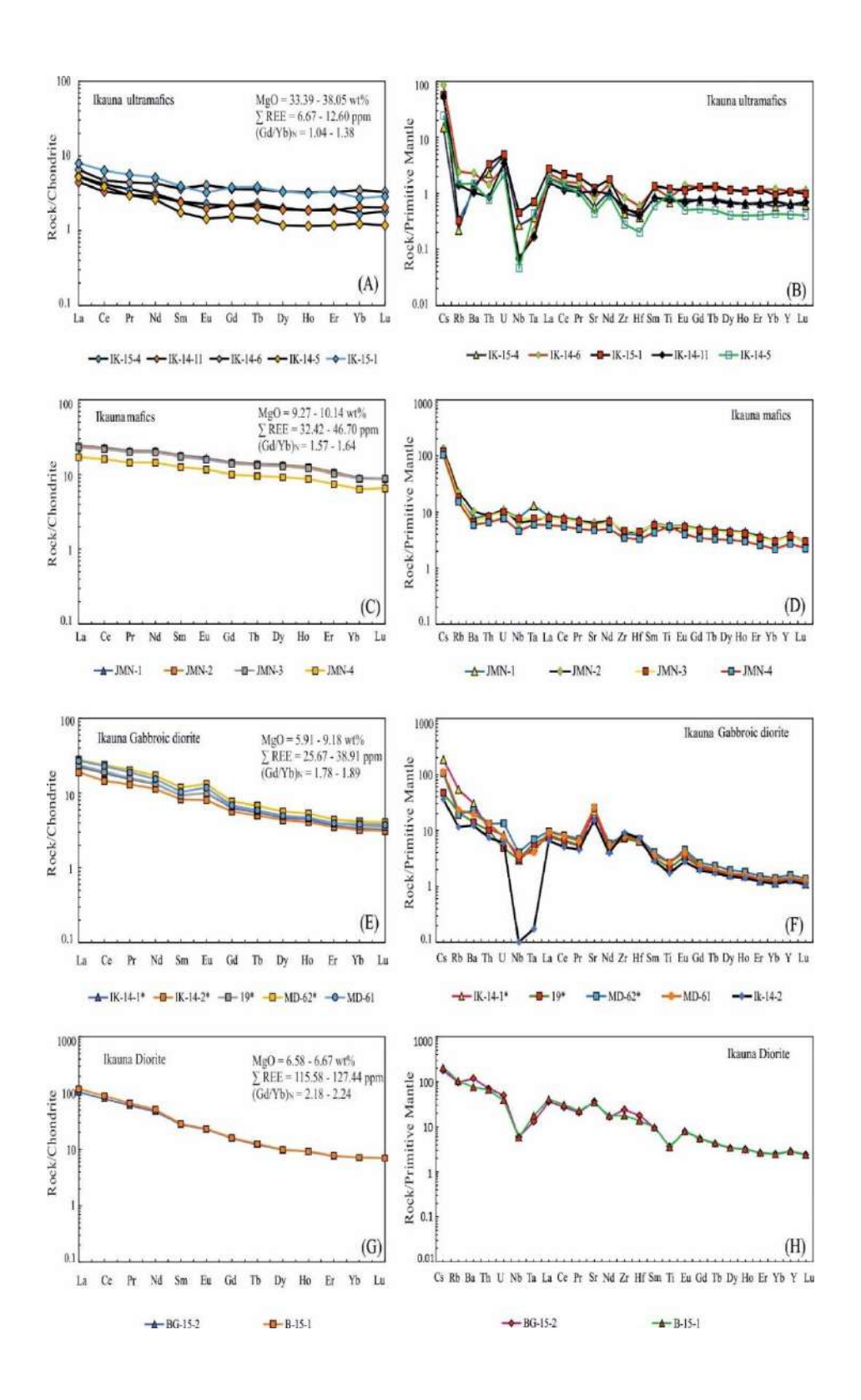


Figure 5.6 (a-h) Chondrite-normalized REE patterns and primitive normalized multi-element spider diagrams of the ultramafic-mafic of the Ikauna region.

Further, on the "AFM (Na<sub>2</sub>O+K<sub>2</sub>O-FeO-MgO) diagram (Beard, 1986), the mafic rocks plot close to the arc-related gabbro field (See Figure 5.2 c). The mafic rocks show low incompatible elements [(Ba (41-71 ppm), Rb (9-14), Sr (98-137), Zr (38-51), Y (12-17 ppm)] and low to moderate compatible elements [V (183-255 ppm), Ni (64-78 ppm), and Cr (225-287 ppm)]. These mafic rocks contain moderate total REE contents (32.42-46.70 ppm). The chondrite normalized REE patterns show slightly fractionated REE patterns with (Gd/Yb)<sub>N</sub> ratio ranging (1.57-1.64) (see figure 5.6 c). On the primitive mantle normalized multi-element diagram (Sun and McDonough, 1989), these samples exhibit weak negative Nb-Zr-Hf anomaly but positive Y anomalies. (See figure 5.6 d).

The intermediate rocks in the Ikauna have two varieties with one group gabbroic diorite diorite) dominated by amphibole with minor plagioclase. The gabbroic diorites show SiO<sub>2</sub> ranging from 49.16-50.83 wt.%, as well as MgO ranging from 5.90-9.18 wt.%. They are characterized by moderate to high content of CaO (9.40-12.54 wt.%), Al<sub>2</sub>O<sub>3</sub> (12.54-16.79 wt.%), and Fe<sub>2</sub>O<sub>3</sub> (7.71-12.76 wt.%). Their N<sub>2</sub>O+K<sub>2</sub>O contents are low (2.57-4.08 wt.%). The other diorites display higher SiO<sub>2</sub> contents [52.40-52.46 wt.%,] when compared with amphibole-rich counterpart] and with low MgO (6.62-6.58 wt.%). They are characterized by high CaO (9.69-9.87 wt.%), Al<sub>2</sub>O<sub>3</sub> (15.29-15.49 wt.%), Fe<sub>2</sub>O<sub>3</sub> (8.92-9.20 wt.%) and Na<sub>2</sub>O+K<sub>2</sub>O (3.95-4.0 wt.%). On the AFM (Na<sub>2</sub>O+K<sub>2</sub>O-FeO-MgO) diagram, (Beard, 1986) both the gabbroic diorite and diorite rocks plot close to the arcrelated gabbro-diorite field (See Figure 5.2c).

On Harker's binary plots, the major element oxides of the studied ultramafic, mafic to intermediate rocks of Ikauna, form two clusters against the MgO. The cluster nature of SiO<sub>2</sub>, CaO and Al<sub>2</sub>O<sub>3</sub> against MgO can be attributed to the origin of magmas by various degree of melting

from different depths in the mantle source reservoirs (see figure 5.3) and the similar scenario can be seen with Harker's trace element plot especially the compatible elements (Ni, Cr, Co) as well (See figure 5.4). The intermediate rocks of gabbroic diorite samples contain low to moderate REE (25.67 to 38.91 ppm). The chondrite normalized REE patterns shows a slightly fractionated REE pattern with (Gd/Yb)<sub>N</sub> ratios ranging (1.78-1.89) and positive Eu anomalies (Eu/Eu\*=1.15-1.37). On the primitive mantle normalized multi-element plot, (Sun and McDonagh, 1989), those samples exhibit weak negative Nb anomalies (except on sample IK-14-2 show strong negative Nb-Ta anomaly), but positive Zr-Hf, Sr, Y anomalies. (Figure 5.6 e-f).

The diorite samples contain high total REE (115.58-127.44 pm). The chondrite normalized REE patterns are fractionated with (Gd/Yb)<sub>N</sub> ratios ranging from 2.18-2.24. On the primitive mantle normalized multi-element diagram, (Sun and McDonagh, 1989), they exhibit strong negative Nb-Ta-Ti but positive Zr-Hf-Sr-Y anomalies. (See figure 5.6 g-h).

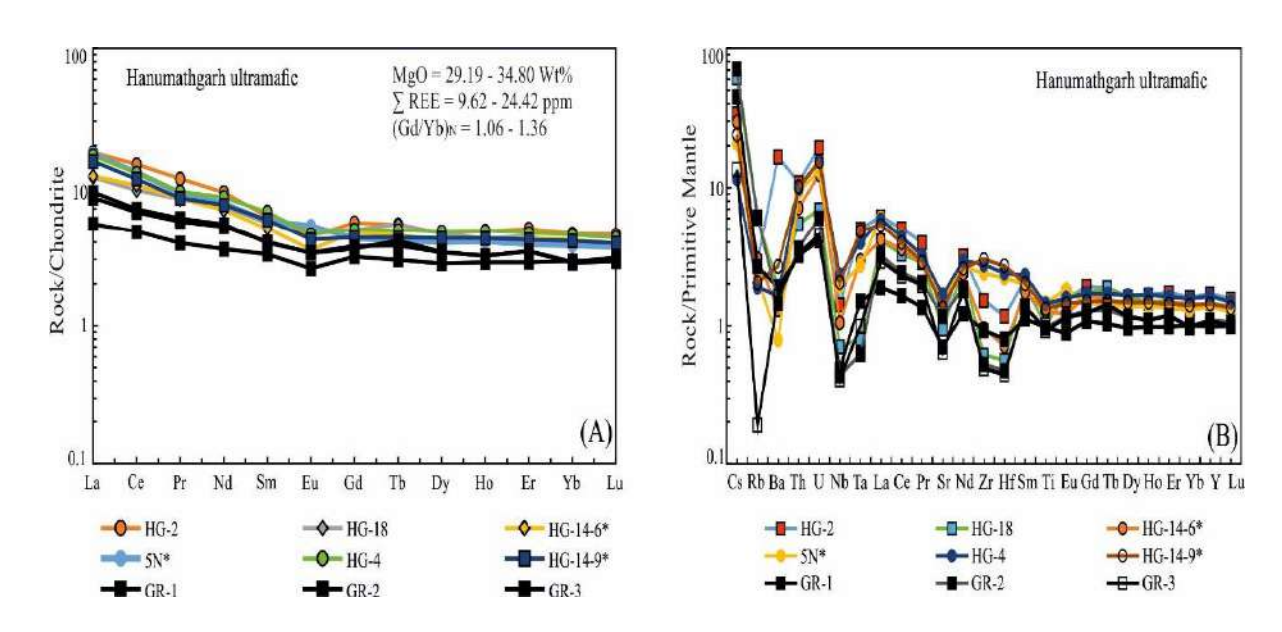


**Figure 5.7** (a-b) Chondrite-normalized REE patterns and primitive normalized multi-element spider diagrams of the ultramafic-mafic of the Hanumathgarh region.

### 5.3 Hanumathgarh Section

The ultramafic rocks of the Hanumathgarh section have a very narrow range of low SiO<sub>2</sub> (39.66-42.09 wt.%), high in MgO contents (29.18-34.80 wt.%), moderate Fe<sub>2</sub>O<sub>3</sub> (7.93-10.87 wt.%), low to moderate Al<sub>2</sub>O<sub>3</sub> (3.05-4.21 wt.%), and high CaO contents (2.78-4.89 wt.%). Most of the studied ultramafic samples from the Hanumathgarh generally show CaO/Al<sub>2</sub>O<sub>3</sub> (0.87-1.32) and Al<sub>2</sub>O<sub>3</sub>/TiO<sub>2</sub> (11.73 to 16.81), showing affinity towards the Barberton-type komatiites. Further, on the AFM (after Irvine and Baragar, 1971); CaO-MgO-Al<sub>2</sub>O<sub>3</sub> after ("Jenson, 1976"), modified by ("Viljoen et al., 1982"); and Al<sub>2</sub>O<sub>3</sub>-(FeO+TiO<sub>2</sub>)-MgO ("Jenson, 1976 modified by Viljoen et al., (1982" the studied ultramafic samples plot in the komatiite field (See figure 5.2a-b). Further, on the "AFM (Na<sub>2</sub>O+K<sub>2</sub>O-FeO-MgO) diagram," (Beard, 1986) the ultramafic rocks plot in the "arc-related ultramafic cumulate field." (See Figure 5.2c). The ultramafic rocks of the Hanumathgarh showing very high contents of Cr (2426-4268 ppm), Ni (718-2057 ppm) and Co (98-139 ppm). The ultramafic samples showing low content of Sc (9-16 ppm), and V (73-103 ppm). The compatible elements (Ni, Cr) of the Hanumathgarh ultramafic rocks are lower in abundances compared to the ultramafic of Madawara and Ikauna regions.

The Hanumathgarh ultramafic rocks also contain "low to moderate total REE" (10.35-24.41 ppm). They display slightly fractionated REE patterns with Gd/Yb)<sub>N</sub> ratio ranging (1.06-1.21). On the primitive mantle normalized multi element diagram (Sun and McDonagh, 1989), the samples exhibit distinct negative Nb-Ta- anomaly with variable Zr-Hf anomalies (see figure 5.7 a-b) and crossings of LIL elements (Rb, Ba).

## 5.4. Whole rock Sr-Nd Isotopes

The whole rock Sr-Nd isotopic data for the MUC including (Madawara, Hanumathgarh, Ikauna and Girar) are presented in the Table 5.3. The total 18 samples analyzed, out of which 7 ultramafic-mafic samples from the Madawara section, 3 ultramafic to intermediate rocks from Ikauna-Girar section and 8 ultramafic samples from the Girar-Hanumathgarh section. The studied

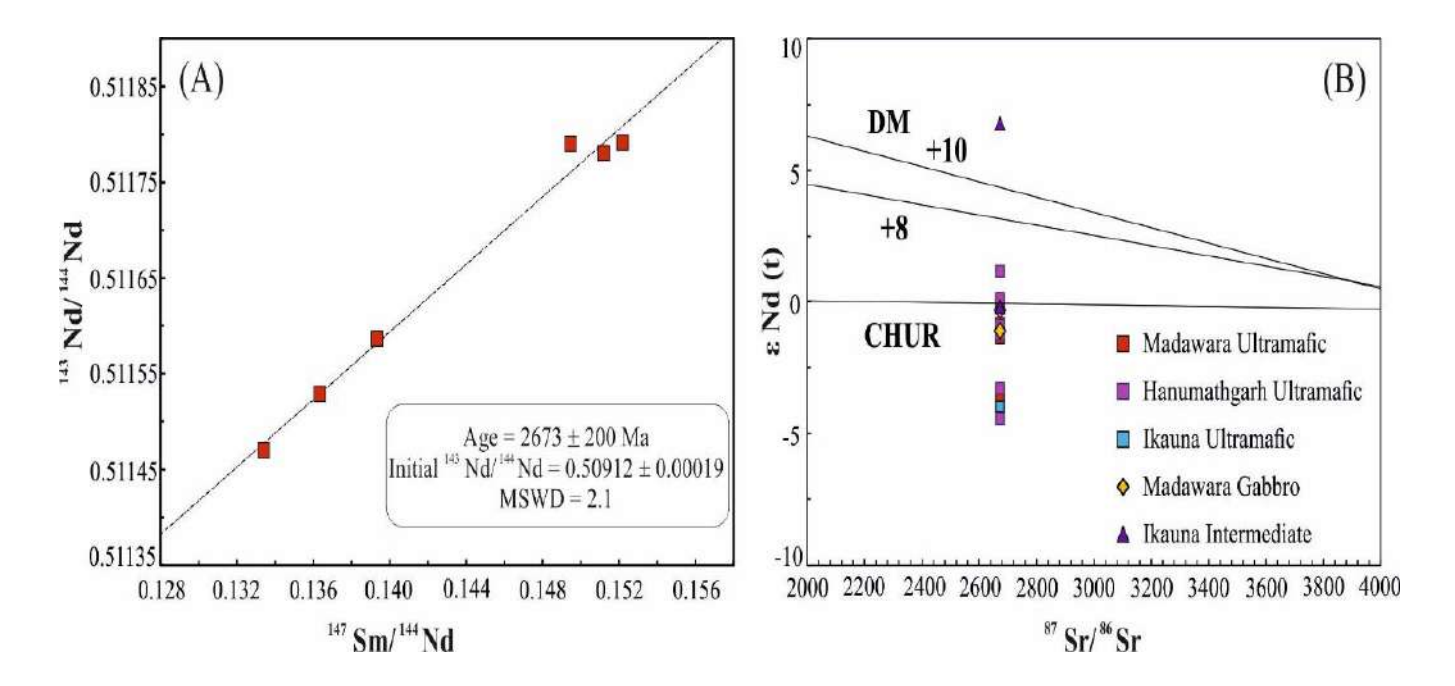


Figure 5.8 (a) Sm-Nd whole rock isochron for the ultramafic-mafic of Madawara ultramafic complex. (b)  $\varepsilon$ Nd versus time evolution diagram showing the involvement of depleted to slightly enriched mantle source.

rocks from the MUC show the large spread in <sup>147</sup>Sm/<sup>144</sup>Nd range (0.1145-0.1866) but limited range of <sup>143</sup>Nd/<sup>144</sup>Nd (0.511003-0.511989) values. On the other hand, the rocks form the MUC show large spread in <sup>87</sup>Sr/<sup>86</sup>Sr with range (0.7028-0.7933) and <sup>87</sup>Rb/<sup>86</sup>Sr range (0.0331-0.5117). It appears that Rb/Sr ratios were affected by secondary processes as Rb is mobile and disturbed. The anomalous Rb/Sr ratios in turn affected the initial Sr isotope ratios. Consequently, Sr isotopes are not very useful for constraining the composition of mantle source reservoirs. Therefore, Sr isotopes

are not used to constrain the mantle sources of the studied ultramafic-mafic-intermediate rocks of Madawara ultramafic-mafic complex.

The Sm-Nd isotope data used primarily in defining whole rock isochron for "constraining the timing of ultramafic-mafic magmatism and also to identify potential mantle source reservoirs as well as spatial link between mantle evolution and crustal growth." Sm-Nd whole rock isochrons are useful to date the Archean rocks because of long half-life period. Furthermore, Sm and Nd are relatively immobile. The <sup>143</sup>Nd/<sup>144</sup>Nd and <sup>147</sup>sm/<sup>144</sup>Nd are used to define whole rock isochron, where <sup>144</sup>Nd is used for ratioing isotope value it is not possible to measure absolute concentration of parent and daughter product of <sup>147</sup>Sm and <sup>143</sup>Nd. The isochron is calculated using the following equation.

$$\left(\frac{143_{Nd}}{144_{Nd}}\right)_{Present} = \left(\frac{143_{Nd}}{144_{Nd}}\right)_{Intial} + \left(\frac{147_{Sm}}{143_{Nd}}\right)_{Present} + (e^{\lambda t} - 1)$$

Where, t= age of the rock.  $\lambda$  is the decay constant of  $^{147}$ Sm=6.64X10 $^{-12}$ y-1 (Lugmair and Marti, 1978) corresponding to a half-life of 1.06X10 $^{11}$  Year. ( $e^{\lambda t}$ -1) is the slope of isochron, which defines age of the system.

Again, the isotopic evolution of Nd in the planet Earth is described in terms of CHUR (Chondritic Uniform Reservoir: (DePaolo, 1988) and depleted mantle models. The CHUR model is defined to have initial <sup>143</sup>Nd/<sup>144</sup>Nd and <sup>147</sup>Sm/<sup>144</sup>Nd ratios equal to those of chondrites. The CHUR is widely used for comparison of initial isotopic compositions of studied rocks with that of primitive mantle at the time of their generation. The εNd(t) values can be calculated by using the following equation by (DePaolo and Wasserberg, 1976) given below with the εNd notation:

$$\varepsilon N d_{(t)i} = \left[ \frac{143_{Nd}/144_{Nd})_{Sample}^{t}}{143_{Nd}/144_{Nd})_{CHUR}^{t}} - 1 \right] \times 10^{4}$$

Where t is the intrusive age/Present time, i= initial isotopic ratio, CHUR=chondrite Uniform Reservoir. The present-day composition of CHUR is (Jacobsen and Wasserburg, 1980, Faure, 1986) has used for the calculation. ( $^{147}$ Sm/ $^{144}$ Nd = 0.1967,  $^{143}$ Nd/ $^{144}$ Nd = 0.51263).

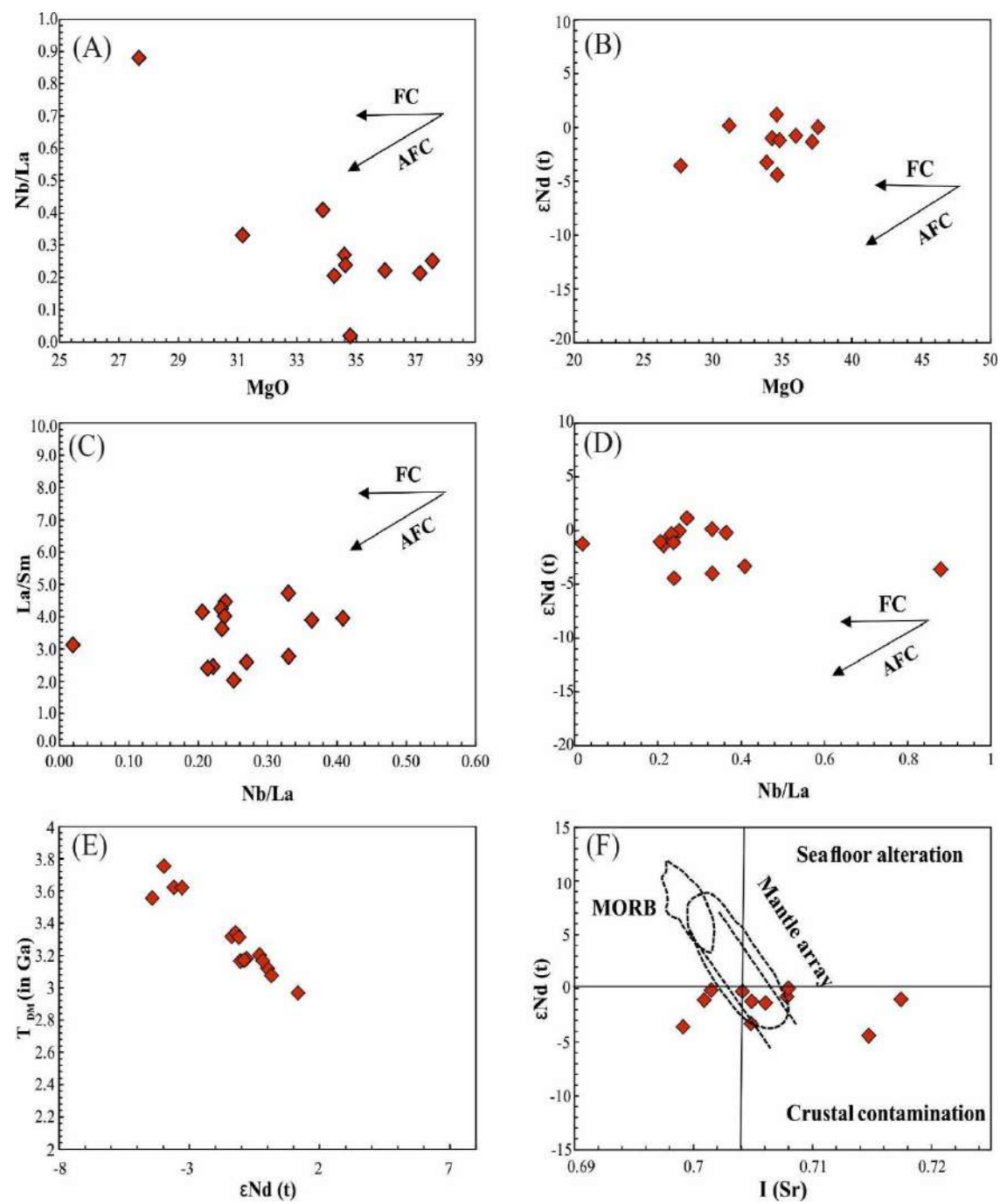


Figure 5.9 (a-b) Plot of Nb/La and  $\varepsilon Nd(t)$  versus MgO (c-d) Plots of La/Sm and  $\varepsilon Nd(t)$  versus Nb/La (e) Ti/Y versus  $\varepsilon Nd(t)$  diagram after shellnutt et al., (2015) (f)  $I_{sr}$  versus  $\varepsilon Nd(t)$  diagram to

examine the fractionation crystallization (FC) and assimilation fractionation crystallization (AFC) processes.

The mantle peridotite's partial melting would result in melts with lower Sm/Nd ratios than the source because Nd is more incompatible than Sm. On the other hand, the source's residue would be significantly richer in Sm, resulting in a greater Sm/Nd ratio. This implies that older crustal rocks should currently have <sup>143</sup>Nd/<sup>144</sup>Nd ratios that are usually lower than CHUR (negative Nd), and older mantle domains depleted in melt should eventually acquire <sup>143</sup>Nd/<sup>144</sup>Nd ratios that are higher than CHUR (positive Nd). The Nd model ages have also calculated for the studied samples, as it provides important information to decipher the time of crust separation from the mantle reservoirs, which will give implication on the time framework for separation of ultramafic magmas from their mantle source. Neodymium model age is a time at which analyzed geological material separated from mantle reservoirs (CHUR or Depleted Mantle, DM (DePaolo, 1988) and form part of the crust with a different Sm/Nd ratio. Here in the present study, "the depleted mantle (DM) model" is used in the calculation for this model ages are denoted as T<sub>DM</sub> Model age can be written as

$$T_{DM} = \frac{1}{\lambda} ln \left[ 1 + \frac{(143_{Nd}/144_{Nd})_{Sample} - (143_{Nd}/144_{Nd})_{DM}}{(147_{Sm}/144_{Nd})_{Sample} - (147_{Sm}/144_{Nd})_{DM}} \right]$$

The present-day composition of the "DM is used as  $^{147}$ Sm/ $^{144}$ Nd = 0.222 and  $^{143}$ Nd/ $^{144}$ Nd = 0.513114." (Michard et al., 1985).

The seven samples of the MUC define an imprecise Sm-Nd whole rock isochron ( $r^2$ =0.97) age of 2673±200 Ma with an initial <sup>143</sup>Nd/<sup>144</sup>Nd values of 0.50912±0.00019 and MSWD value of 2.1 (see figure 5.8 a). Their  $\varepsilon$ Nd values (T=2673 Ma) values ranging -4.43 to +1.15 except three

anomalous samples (MW-7, MA-15-1 and BG-2) show anomalous values [(high negative to high positive values (-9.0 <and >+5.0)]. A model age ( $T_{DM}$ ) has obtained for the ultramafic-mafic of the Madawara section with range 3.12-3.32 Ga except one sample (16) showing 3.62 Ga Ikauna section with a range 2.97-3.17 Ga except one sample (Ik-15-3) 3.75 Ga and Hanumathgarh section with a range 3.08-3.62 Ga (See table 5.3). The  $T_{DM}$  calculated with respect to obtained isochron age is nearly synchronous with metabasalt of the Girar greenstone belt (2.98 Ga) and the granitegneiss of the southern Bundelkhand craton (3.2-3.4 Ga) as well as younger U-Pb age of the detrital zircon of the felsic rock (3.2 Ga) of the Girar greenstone belt.

The Ultramafic-mafic samples of the MUC show a good negative correlation in the bivariant diagram of  $\epsilon Nd(t)$  versus  $T_{DM}$  (see figure 5.9 e). In addition, there is no obvious correlation between MgO versus  $\epsilon Nd(t)$  and Nb/La versus  $\epsilon Nd(t)$  (see figure 5.9 b-d). On the  ${}^{87}Sr/{}^{86}Sr$  ( $I_{Sr}$ ) versus  $\epsilon Nd(t)$  diagram, the samples plot within or near to the mantle array except few samples plot away from the mantle array as well as upper crust due to affected the initial Sr isotope ratios (see figure 5.9 f).

# 5.5. PGE geochemistry

The platinum group element consists of Ru, Rh, Pd, Os, Ir, and Pt with atomic numbers 44 to 46 and 77 to 78 respectively. PGEs are considered to be refractory elements and are used as tracers for mantle petrogenesis. The PGEs are divided on the basis of their physical and chemical characteristics into two sub-groups such as the Ir-group (IPGE-Os, Ir, Ru) and the Pd-group (PPGEs-Rh, Pt, Pd). The PGEs are both siderophiles as well as chalcophile in nature. The IPGEs are more compatible and occur as refractory phases whilst PPGEs are corresponding to relatively incompatible in nature.

## 5.5.1. PGE in Madawara region

The PGE compositions of the ultramafics of Madawara ultramafic complex (MUC) have variable PGE contents (see table 5.2). The PGE concentration of the Madawara ultramafic of group I is marked by 1.32-9.22 ppb Os, 0.72-15.01 ppb Ir, 4.66-89.66 ppb Ru among IPGE, and 9.08-111.50 ppb Pd, 17.13-234.17 ppb Pt, 0.77-36.98 ppb Rh among PPGE. The ultramafic of the Madawara has moderate to a high concentration of  $\Sigma$ PGE in the range of 30.92-372.13 ppb. The samples show a higher concentration of  $\Sigma PPGE$  in the range of 28.88-349.22 ppb than the  $\Sigma IPGE$ which varies between 6.70-112.58 ppb. The samples are characterized by high  $\Sigma PPGE/\Sigma IPGE$ (>1) varies between 2.80 to 4.69. The samples show a higher concentration of Ni (1612.48-1961.53 ppm) and a lower concentration of Cu (16.50-24.12 ppm) which reflects the Ni/Cu ratio (66.86-118.91) displaying nearly higher than the primitive mantle value (Ni/Cu=71.4). The Pd/Pt ratio of the samples shows (Pd/Pt: 0.27-0.77) which is comparable to the primitive mantle ratio of 0.55. (Sun and McDonough, 1995). The Pd/Ir ratio shows variation from 3.36-18.76 and is distinctly higher than Pt/Pd (1.31-3.68). The chondrite normalized PGE patterns of Madawara exhibit a variable degree of fractionation and shows negative Ir, Rh, and positive Pt anomalies (see figure 5.9 c & d). The Pt anomaly  $(Pt/Pt *) = Pt_N/\sqrt{Rh_N \times Pd_N}$  of the studied samples show in the range of 1.01-2.28 which is more than the primitive mantle values. The samples show lower value of Cu and high value of Pd, which reflects the low Cu/Pd ratio (171-2196) (Cu/Pd=6300 for PM) and high Cu/Zr ratio (2.35-6.99).

The ultramafic of group II shows 0.40-4.21 ppb Os, 1.00-3.20 ppb Ir, 1.60-6.40 ppb Ru among IPGE, and 6.80-69.26 ppb Pd, 8.80-28.60 ppb Pt, 0.50-5.08 ppb Rh among PPGE. The ultramafic of Group II of the Madawara has a low to moderate concentration of  $\Sigma$ PGE in the range of 29.70-101.24 ppb, which is lower in comparison to the group I ultramafics. The samples show a higher

concentration of  $\Sigma$ PPGE in the range of 25.00-95.88 ppb than the  $\Sigma$ IPGE which varies between 3.60-12.40 ppb. The samples are characterized by high  $\Sigma$ PPGE/ $\Sigma$ IPGE (>1) varies between 2.02 to 13.72. The samples show low to moderate concentrations of Ni (768.91-1530.40 ppm) and a low to moderate concentration of Cu (9.66-64.55 ppm) which reflects the Ni/Cu ratio (20.45-79.58) displaying nearly lower than the primitive mantle value (Ni/Cu=71.4). The Pd/Pt ratio of the samples shows (Pd/Pt: 0.39-3.22) which is lower than the primitive mantle ratio of 0.55. (Sun and McDonough, 1995). The Pd/Ir ratio shows a wide variation from 2.13-59.82 and is distinctly higher than Pt/Pd (0.31-2.59). The chondrite normalized PGE patterns of Madawara ultramafics group II exhibit a variable degree of fractionation and shows slightly negative Ir, and variable Rh, Pt anomalies (see figure 5.9 e & f). The Pt anomaly  $(Pt/Pt*) = Pt_N/\sqrt{Rh_N \times Pd_N}$  of the studied samples show in the range between 0.37-2.79, which shows variable in comparison to the primitive mantle values (Pt/Pt\*=1). The samples show low to moderate value of Cu and low value of Pd, which reflects the low to moderate Cu/Pd ratio (139-5280) (Cu/Pd=6300 for PM) and high Cu/Zr ratio (1.91-6.08) except one sample have low value.

The mafic rocks show 1.67-2.17 ppb Os, 0.59-1.12 ppb Ir, 1.13-1.29 ppb Ru among IPGE, and 38.10-43.62 ppb Pd, 16.76-42.69 ppb Pt, 1.77-2.35 ppb Rh among PPGE. The mafic samples have a low to moderate concentration of ∑PGE in the range of 64.93-85.96 ppb, which is lower in comparison to the ultramafics. The samples show a higher concentration of ∑PPGE in the range of 62.16-83.16 ppb than the ∑IPGE which varies between 3.90 to 4.09 ppb. The samples are characterized by high ∑PPGE/∑IPGE (>1) varies in between 15.92 to 20.33. The samples show the low concentration of Ni (121.71-236.07 ppm) and a moderate concentration of Cu (168.25-218.45 ppm) which reflects the Ni/Cu ratio (0.55-1.40) displaying nearly lower than the primitive mantle value (Ni/Cu=71.4). The Pd/Pt ratio of the samples shows (Pd/Pt: 0.89-2.60) which is

higher than the primitive mantle ratio of 0.55 (Sun and McDonough, 1995). The Pd/Ir ratio shows a wide variation from 33.80-73.59 and is distinctly higher than Pt/Pd (0.38-1.12). The chondrite normalized PGE patterns of Madawara mafic rocks exhibit a variable degree of fractionation and shows slightly negative Ir and positive Rh anomalies (see figure 5.9 e & f). The Pt anomaly  $(Pt/Pt*) = Pt_N/\sqrt{Rh_N \times Pd_N}$  of the studied samples show in the range between 0.60-1.44, which shows variable in comparison to the primitive mantle values (Pt/Pt\*=1). The samples show low to moderate value of Cu and moderate value of Pd, which reflects the moderate to high Cu/Pd ratio (4415-5007) (Cu/Pd=6300 for PM) and high Cu/Zr ratio (7.41-8.76).

#### 5.5.2. PGE in Ikauna region

The PGE concentration of the Ikauna ultramafic is marked by 12.26-100.69 ppb Os, 3.57-18.16 ppb Ir, 9.14-15.49 ppb Ru among IPGE, and 5.84-30.57 ppb Pd, 8.68-28.97 ppb Pt, 1.67-6.14 ppb Rh among PPGE. The ultramafic of the Ikauna has moderate to a high concentration of  $\Sigma$ PGE in the range of 46.66-200.02 ppb except for one sample (IK-14-1) which shows a very high anomalous value (401.27 ppb). The samples show a lower concentration of  $\Sigma$ PPGE in the range of 16.19-65.67 ppb than the  $\Sigma$ IPGE which varies between 25.42-134.34 ppb. The samples are characterized by low  $\Sigma$ PPGE/ $\Sigma$ IPGE (<1) varies in between 0.49 to 0.92. The samples show a higher concentration of Ni (1759.12-2455.82 ppm) and a lower concentration of Cu (12.81-19.35 ppm) which reflects the Ni/Cu ratio (116.47-187.89) displaying higher than the primitive mantle value (Ni/Cu=71.4). The Pd/Pt ratio of the samples shows (Pd/Pt: 0.55-0.1.06) which is comparable to the primitive mantle ratio of 0.55 (Sun and McDonough, 1995). The Pd/Ir ratio shows variation from 1.64-1.89 and is slightly comparable with Pt/Pd (0.95-1.81). The chondrite normalized PGE patterns of Ikauna ultramafic exhibit a variable degree of fractionation and shows negative Ir and positive Ru anomalies (see figure 5.9a). The Pt anomaly (Pt/Pt\*) =

 $Pt_N/\sqrt{Rh_N \times Pd_N}$  of the studied samples show in the range between 0.68-1.11, which is also lower than the primitive mantle values. The samples show lower value of Cu and high value of Pd, which reflects the low Cu/Pd ratio (494-2553) (Cu/Pd=6300 for PM) and high Cu/Zr ratio (2.01-4.85).

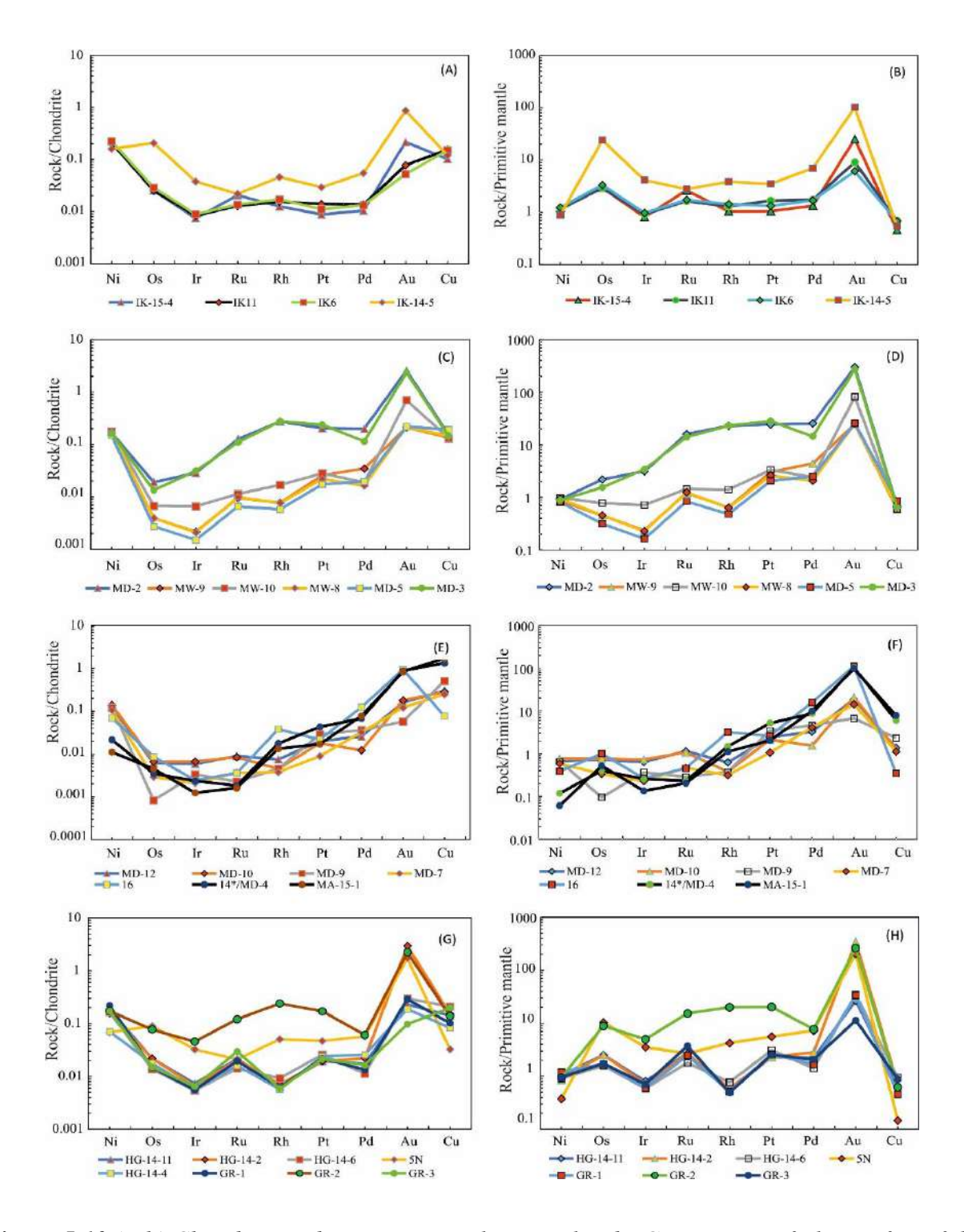


Figure 5.10 (a-h) Chondrite and primitive mantle normalized PGE patterns of ultramafics of the MUC

## 5.5.3. PGE in Hanumathgarh region

The PGE concentration of the Hanumathgarh ultramafic is marked by 6.66-43.55 ppb Os, 2.58-21.91 ppb Ir, 2.58-21.91 ppb Ru among IPGE, and 6.28-33.98 ppb Pd, 19.13-168.35 ppb Pt, 0.76-32.00 ppb Rh among PPGE. The ultramafic of the Hanumathgarh has moderate to a high concentration of  $\Sigma$ PGE in the range of 39.60-293.53 ppb. The samples show a higher concentration of  $\Sigma$ PPGE in the range of 29.74-234.33 ppb than the  $\Sigma$ IPGE which varies between 19.29-144.91 ppb. The samples are characterized by high  $\Sigma PPGE/\Sigma IPGE$  ( $\ge 1$ ) varies in between 0.99 to 1.71. The samples show wide variation of concentration of Ni (751.52-2407.79 ppm) and a lower concentration of Cu (4.10-26.24 ppm) which reflects the Ni/Cu ratio (68.93-187.89) displaying slightly higher than the primitive mantle value (Ni/Cu=71.4). The Pd/Pt ratio of the samples shows (Pd/Pt: 0.20-0.69) which is comparable to the primitive mantle ratio of 0.55 (Sun and McDonough, 1995). The Pd/Ir ratio shows variation from 1.55-5.28 and is comparable with Pt/Pd (1.45-4.95). The chondrite normalized PGE patterns of Hanumathgarh exhibit a variable degree of fractionation and shows negative Ir, Rh, and positive Pt, Ru anomalies (See figure 5.9 g & h). The Pt anomaly  $(Pt/Pt *) = Pt_N/\sqrt{Rh_N \times Pd_N}$  of the studied samples show in the range in between 1.01-2.93, which is also higher than the primitive mantle values. The samples show lower value of Cu and high value of Pd, which reflects the low Cu/Pd ratio (128-4176) (Cu/Pd=6300 for PM) and low to high Cu/Zr ratio (0.15-4.49).

Sample	IK-15-4	IK-14-11	IK-14-6	termediate rocks IK-14-5	IK-15-1	JMN-1	JMN-2	JMN-3	JMN-4	IK-14-1
Location	Ikauna	Ikauna	Ikauna	Ikauna	Ikauna	Ikauna	Ikauna	Ikauna	Ikauna	Ikauna
Rock type	Ultramafic	Ultramafic	Ultramafic	Ultramafic	Ultramafic	Mafic	Mafic	Mafic	Mafic	Gab diorite
SiO <sub>2</sub>	37.71	38.06	38.52	39.49	41.76	46.37	46.60	46.55	46.24	50.19
$Al_2O_3$	2.64	2.83	2.82	2.98	3.49	14.61	14.95	14.70	14.64	16.80
$e_2O_3$	9.07	9.01	8.46	9.25	8.60	13.33	11.88	12.77	13.32	7.72
ΛnO	0.11	0.17	0.15	0.12	0.13	0.14	0.13	0.13	0.14	0.12
ИgO	38.05	36.55	35.77	33.39	34.71	9.27	10.14	9.52	9.28	7.72
CaO	1.65	1.42	1.38	2.12	3.82	12.32	12.73	12.37	11.89	10.52
√a <sub>2</sub> O	0.04	0.05	0.06	0.06	0.09	1.48	1.51	1.52	1.57	2.79
$K_2O$	0.01	0.02	0.03	0.02	0.03	0.47	0.40	0.44	0.52	0.82
$\Gamma iO_2$	0.15	0.17	0.18	0.21	0.26	1.23	1.07	1.20	1.20	0.46
$P_2O_5$	0.03	0.03	0.04	0.03	0.04	0.12	0.10	0.11	0.11	0.03
LOI	9.98	NA	NA	NA	6.95	0.00	0.00	0.00	0.00	1.28
lum	99.44	88.31	87.41	87.67	99.88	99.34	99.51	99.31	98.91	98.44
Sc	3.86	7.94	12.97	6.44	5.39	36.80	38.14	36.08	28.33	19.83
V	56.35	47.66	77.75	31.99	95.60	255.29	255.45	245.01	183.31	123.85
Cr	3206.21	3038.99	3905.94	2509.24	4043.52	231.32	287.45	264.31	226.00	401.63
Co	113.88	119.07	132.38	87.93	121.39	87.53	89.78	89.73	69.79	44.29
Ni	2407.79	2283.77	2455.82	1759.12	1892.59	70.05	73.91	78.17	64.90	48.01
Cu	12.81	19.35	18.92	15.10	19.19	116.62	114.46	112.76	98.35	34.38
Zn	41.26	78.08	79.36	61.10	42.56	96.78	87.46	92.02	72.48	114.63
Ga	2.90	3.79	4.94	3.19	4.65	14.59	14.24	14.20	10.74	12.94
Rb	0.14	0.89	1.55	0.92	0.21	11.54	14.60	11.85	9.82	34.47
Sr	11.95	22.54	17.30	9.23	26.11	124.97	137.81	120.35	98.76	464.49
Y	2.95	2.82	4.94	1.88	4.87	17.84	17.44	16.96	12.37	6.03
Zr	4.87	6.11	9.37	3.12	5.74	45.88	50.60	51.86	38.72	86.10
Nb	0.19	0.05	0.05	0.03	0.33	5.64	4.54	5.41	3.28	2.12
Cs	0.12	0.43	0.68	0.19	0.45	0.86	1.08	0.97	0.83	1.46
Ba	9.77	7.27	16.03	10.34	7.95	54.80	71.58	46.61	41.15	209.26
_a	1.28	1.05	1.55	1.24	1.88	5.79	5.65	5.43	4.03	5.28
Ce	2.54	2.04	2.87	2.38	3.88	14.11	13.75	13.33	9.81	11.34
Pr	0.34	0.29	0.42	0.28	0.54	1.97	1.92	1.88	1.37	1.46
Nd	1.46	1.35	1.99	1.22	2.40	9.67	9.44	9.19	6.74	6.17
Sm	0.37	0.37	0.55	0.27	0.60	2.75	2.69	2.63	1.92	1.43
Eu	0.13	0.11	0.23	0.08	0.19	0.96	0.92	0.92	0.68	0.58
Gd	0.44	0.45	0.74	0.31	0.78	3.01	2.94	2.86	2.05	1.30
Гb	0.09	0.08	0.13	0.05	0.14	0.52	0.51	0.49	0.36	0.21
Dy	0.51	0.49	0.85	0.30	0.84	3.42	3.35	3.24	2.34	1.18
Но	0.11	0.11	0.18	0.07	0.18	0.72	0.71	0.68	0.49	0.25
Er	0.32	0.31	0.54	0.19	0.55	1.77	1.75	1.68	1.22	0.60
Гт	0.06	0.05	0.09	0.03	0.09	0.24	0.24	0.23	0.17	0.09
Yb	0.28	0.35	0.59	0.21	0.46	1.53	1.48	1.49	1.08	0.57
Lu	0.05	0.05	0.08	0.03	0.07	0.22	0.22	0.22	0.17	0.08
Hf	0.12	0.12	0.18	0.06	0.14	1.22	1.37	1.37	1.02	2.02
Га	0.02	0.01	0.01	0.02	0.03	0.53	0.29	0.32	0.24	0.20
Pb	3.50	9.44	32.81	6.69	2.57	1.68	1.99	1.64	1.22	18.11
Th	0.19	0.07	0.12	0.07	0.28	0.72	0.73	0.72	0.56	0.91
U	0.10	0.07	0.06	0.05	0.10	0.22	0.23	0.21	0.16	0.17
REET	7.98	7.10	10.84	6.67	12.60	46.70	45.56	44.27	32.42	30.53
Al <sub>2</sub> O <sub>3</sub> /TiO <sub>2</sub>	17.60	16.65	15.67	14.19	13.42	11.88	13.97	12.25	12.20	36.59
CaO/Al <sub>2</sub> O <sub>3</sub>	0.63	0.50	0.49	0.71	1.09	0.84	0.85	0.84	0.81	0.63
Gd/Yb) <sub>N</sub>	1.28	1.07	1.04	1.23	1.38	1.62	1.64	1.58	1.57	1.89
Eu/Eu) <sub>N</sub>	0.99	0.86	1.12	0.88	0.85	1.02	0.99	1.02	1.03	1.28
Zr/Y	1.65	2.17	1.90	1.66	1.18	2.57	2.90	3.06	3.13	14.28
Nb/Y	0.07	0.02	0.01	0.02	0.07	0.32	0.26	0.32	0.27	0.35
Nb/Th	0.99	0.69	0.38	0.51	1.16	7.81	6.25	7.57	5.89	2.32
Nb/La	0.15	0.05	0.03	0.03	0.17	0.97	0.80	1.00	0.82	0.40
.a/Nb	6.65	20.93	33.45	37.15	5.77	1.03	1.24	1.00	1.23	2.50
.a/Ba	0.13	0.14	0.10	0.12	0.24	0.11	0.08	0.12	0.10	0.03
Th/Zr	0.04	0.01	0.01	0.02	0.05	0.02	0.01	0.01	0.01	0.01
Nb/Zr	0.04	0.01	0.00	0.02	0.06	0.12	0.09	0.10	0.08	0.02
Zr/Nb	25.36	121.73	202.42	93.24	17.57	8.13	11.14	9.58	11.79	40.68
Nb/Yb	0.68	0.14	0.08	0.16	0.70	3.68	3.07	3.62	3.05	3.73
Nb/ 1 b Γh/Yb	0.68	0.14	0.08	0.10	0.70	0.47	0.49	0.48	0.52	1.61
Nb/U	1.93	0.21	0.21	0.74	3.14	25.15	19.53	25.58	20.23	12.29
Nb/Yb) <sub>PM</sub>	0.47	0.10	0.74	0.74	0.49	2.55	2.12	2.51	2.11	2.58
Th/Yb) <sub>PM</sub>	3.95	1.20	1.21	1.81	3.52	2.33	2.12	2.78	3.00	9.33
		0.49		0.34	0.34	0.64		0.75	0.76	
Hf/Sm) <sub>PM</sub>	0.45		0.47				0.73			2.03

Table 5.1 Continues....

Sample	IK-14-2	19	MD-62	MD-61	BG-15-2	B-15-1	MD-2	MW-9	MD-5	MD-11
Location	Ikauna	Ikauna	Ikauna	Ikauna	Ikauna	Ikauna	Madawara	Madawara	Madawara	Madawara
Rock type	Gab diorite	Gab diorite	Gab diorite	Gab diorite	Diorite	Diorite	Ultramafic	Ultramafic	Ultramafic	Ultramafic
$SiO_2$	49.16	49.52	50.84	50.07	52.24	52.24	36.41	37.16	39.48	41.02
$Al_2O_3$	14.41	15.23	15.56	12.54	15.29	15.49	2.58	2.47	3.07	3.04
$Fe_2O_3$	9.77	7.82	10.16	12.76	9.20	8.92	11.01	11.52	11.92	11.38
MnO	0.14	0.12	0.15	0.16	0.11	0.10	0.15	0.14	0.16	0.12
MgO	9.18	8.08	5.91	8.57	6.67	6.58	34.00	33.84	33.80	32.38
CaO	11.59	12.54	9.98	9.40	9.69	9.87	2.95	2.92	1.60	1.85
Na <sub>2</sub> O	2.25	2.51	3.44	3.59	2.24	2.09	bdl	bdl	-0.21	-0.21
K <sub>2</sub> O	0.33	0.43	0.46	0.49	1.76	1.86	bdl	bdl	0.00	0.00
TiO <sub>2</sub>	0.38	0.45	0.58	0.57	0.79	0.76	0.15	0.20	0.18	0.21
P <sub>2</sub> O <sub>5</sub>	0.03	0.04	0.04	0.06	0.38	0.43	0.03	0.03	0.02	0.02
LOI	0.74	1.29	0.76	0.84	1.71	1.97	12.09	11.20	10.08	9.78
Sum	97.96	98.01	97.87	99.05	100.08	100.31	99.16	99.31	100.10	99.60
Sc	20.37	22.02	16.68	14.42	15.25	15.01	4.32	5.25	15.21	12.87
V	120.07	134.35	141.47	121.74	207.04	215.43	70.69	72.84	84.82	90.90
Cr	376.76	521.77	46.90	40.72	53.50	53.57	4825.07	3325.64	4305.10	6262.36
Co	54.65	41.27	48.77	54.62	59.91	68.66	120.13 1823.31	120.03 1730.40	114.67	98.61 1889.35
Ni	55.53	41.52	28.40	29.46	13.92	14.39			1621.02	
Cu 7-	37.22	87.38	344.85	279.69	25.39	37.55	19.13	16.99	14.60	51.97
Zn	131.18	135.25	105.49	69.86	96.38	222.49	40.44	46.21	198.89	100.33
Ga Rb	13.94 7.33	13.09 13.23	15.07 11.98	15.10 14.79	20.83 61.02	21.40 65.34	3.35 0.11	3.32 0.14	4.51 1.81	6.46 1.22
Sr	325.80	311.14	526.11	550.62	764.15	723.59	36.78	24.83	1.81	8.93
Y	5.70	6.40	7.29	6.37	12.86	13.15	2.91	3.86	3.68	3.60
Zr	101.37	80.03	92.18	89.58	268.86	196.44	3.18	6.33	7.52	8.94
Nb	0.07	2.19	2.89	2.61	4.23	4.13	0.13	0.33	0.28	0.39
Cs	0.28	0.37	0.83	0.88	1.39	1.62	0.13	0.14	0.25	0.14
Ba	85.47	97.02	163.58	136.27	826.95	526.11	5.01	5.14	25.50	8.46
La	4.48	5.60	6.62	6.39	24.57	27.71	1.20	1.25	1.58	1.49
Ce	8.92	11.90	14.55	14.04	48.30	54.48	2.33	2.73	3.47	3.54
Pr	1.24	1.52	1.93	1.79	5.71	6.22	0.31	0.36	0.41	0.53
Nd	5.33	6.30	8.02	7.20	21.98	23.72	1.31	1.60	1.62	2.23
Sm	1.25	1.42	1.81	1.59	4.22	4.34	0.33	0.41	0.38	0.48
Eu	0.47	0.58	0.77	0.69	1.31	1.34	0.14	0.16	0.13	0.10
Gd	1.17	1.37	1.58	1.41	3.21	3.29	0.38	0.53	0.52	0.61
Tb	0.19	0.22	0.25	0.22	0.45	0.47	0.08	0.11	0.10	0.10
Dy	1.10	1.24	1.44	1.26	2.47	2.50	0.48	0.64	0.57	0.60
Но	0.23	0.26	0.30	0.26	0.51	0.52	0.10	0.14	0.14	0.14
Er	0.58	0.65	0.73	0.65	1.25	1.27	0.33	0.46	0.41	0.45
Tm	0.09	0.10	0.11	0.10	0.19	0.19	0.05	0.08	0.06	0.07
Yb	0.54	0.62	0.70	0.65	1.22	1.22	0.31	0.39	0.43	0.43
Lu	0.08	0.09	0.10	0.10	0.18	0.18	0.05	0.06	0.06	0.07
Hf	2.25	1.92	2.17	2.00	5.43	4.19	0.08	0.15	0.17	0.19
Ta	0.01	0.24	0.28	0.17	0.53	0.72	0.01	0.02	0.08	0.06
Pb	13.66	14.56	13.80	11.38	24.82	18.61	2.40	7.86	6.93	5.96
Th	0.63	0.86	1.11	1.13	5.99	5.55	0.14	0.20	0.33	0.43
U	0.13	0.10	0.28	0.16	1.05	0.80	0.05	0.06	0.10	0.35
$REE_T$	25.67	31.87	38.91	36.34	115.58	127.44	7.40	8.93	9.88	10.84
Al <sub>2</sub> O <sub>3</sub> /TiO <sub>2</sub>	38.43	33.54	27.02	22.00	19.35	20.38	16.99	12.13	17.45	14.56
CaO/Al <sub>2</sub> O <sub>3</sub>	0.80	0.82	0.64	0.75	0.63	0.64	1.14	1.18	0.52	0.61
(Gd/Yb) <sub>N</sub>	1.78	1.84	1.85	1.79	2.18	2.24	1.01	1.14	1.00	1.16
(Eu/Eu) <sub>N</sub>	1.16	1.26	1.35	1.37	1.05	1.04	1.21	1.03	0.89	0.56
Zr/Y	17.79	12.51	12.65	14.06	20.91	14.93	1.09	1.64	2.04	2.48
Nb/Y	0.01	0.34	0.40	0.41	0.33	0.31	0.05	0.05	0.08	0.11
Nb/Th	0.11	2.56	2.60	2.30	0.71	0.74	0.93	1.03	0.84	0.91
Nb/La	0.02	0.39	0.44	0.41	0.17	0.15	0.11	0.17	0.17	0.26
La/Nb	61.96	2.56	2.29	2.45	5.81	6.70	9.04	6.06	5.72	3.80
La/Ba	0.05	0.06	0.04	0.05	0.03	0.05	0.24	0.24	0.06	0.18
Th/Zr	0.01	0.01	0.01	0.01	0.02	0.03	0.05	0.03	0.04	0.05
Nb/Zr	0.00	0.03	0.03	0.03	0.02	0.02	0.04	0.03	0.04	0.04
Zr/Nb	1400.87	36.59	31.92	34.30	63.56	47.52	23.96	30.70	27.24	22.81
Nb/Yb	0.13	3.55	4.10	4.00	3.47	3.40	0.42	0.53	0.64	0.90
Th/Yb	1.17	1.39	1.58	1.74	4.91	4.56	0.46	0.52	0.77	1.00
Nb/U	0.57	21.71	10.22	16.39	4.04	5.16	2.58	3.49	2.73	1.11
(Nb/Yb) <sub>PM</sub>	0.09	2.45	2.83	2.76	2.40	2.35	0.29	0.37	0.44	0.63
(Th/Yb) <sub>PM</sub>	6.79	8.04	9.16	10.06	28.49	26.46	2.66	3.00	4.45	5.79
(Hf/Sm) <sub>PM</sub>	2.58	1.94	1.72	1.81	1.85	1.39	0.34	0.51	0.65	0.58
(Ta/La) <sub>PM</sub>	0.03	0.71	0.72	0.44	0.36	0.43	0.15	0.31	0.82	0.72

Table 5.1 Continues....

Table 5.1 Conti	MD-13	MW-10	MW-8	MD-5	MD-3	MD-12	MD-10	MD-9	MD-7	16
Location	Madawara									
Rock type	Ultramafic									
SiO <sub>2</sub>	40.00	38.49	39.64	40.69	38.39	42.47	41.63	48.62	48.61	50.77
$Al_2O_3$	3.51	2.92	2.92	3.38	2.99	5.03	4.30	3.62	3.00	2.81
$Fe_2O_3$	11.66	8.43	8.07	8.49	8.41	11.04	12.10	7.86	8.61	10.29
MnO	0.16	0.12	0.12	0.11	0.13	0.17	0.15	0.17	0.18	0.18
MgO	31.43	37.57	37.15	36.37	35.97	27.95	29.07	25.12	27.74	27.68
CaO	2.53	3.04	2.22	3.49	3.33	4.38	3.10	8.96	5.38	3.41
Na <sub>2</sub> O	-0.14	0.06	0.06	0.12	0.05	bdl o.oo	-0.05	bdl	0.03	0.01
K <sub>2</sub> O	0.01	0.02	0.02	0.04	0.02	0.02	0.01	0.03	0.02	0.03 0.22
TiO <sub>2</sub>	0.20	0.15 0.04	0.17 0.04	0.18 0.04	0.16 0.03	0.36 0.04	0.26 0.03	0.21 0.02	0.21 0.02	0.22
P <sub>2</sub> O <sub>5</sub> LOI	9.84	7.58	8.53	5.87	9.50	7.37	8.51	4.45	5.98	3.82
Sum	99.22	98.42	98.94	98.78	98.98	98.82	99.12	99.03	99.77	99.24
Sc	15.68	12.24	13.73	14.36	15.89	19.99	18.76	24.18	21.08	24.89
V	93.42	75.77	87.89	94.51	87.97	115.58	111.59	95.48	74.09	107.35
Cr	5149.44	4243.17	5607.48	4398.58	5321.56	5026.53	4717.44	3876.23	3272.78	4144.88
Co	107.19	134.67	130.61	115.72	122.43	100.71	110.50	82.66	76.01	84.92
Ni	1670.26	1961.53	1891.82	1612.48	1765.63	1255.29	1563.00	1228.85	1102.62	768.91
Cu	23.75	16.50	17.95	24.12	18.04	25.17	23.61	46.24	18.17	9.66
Zn	146.96	40.94	68.46	53.13	39.12	103.34	158.67	131.73	80.07	99.57
Ga	5.84	3.93	3.99	4.16	4.17	7.16	6.81	5.06	4.08	4.74
Rb	1.49	1.32	1.17	3.82	1.17	1.43	1.13	3.17	1.31	2.51
Sr	15.61	17.88	16.14	18.52	14.00	26.42	14.80	23.49	17.94	15.36
Y	4.46	3.32	3.03	3.57	3.31	7.51	4.66	4.72	5.52	4.59
Zr	9.11	7.03	6.74	3.45	6.44	36.11	11.71	22.89	24.23	23.27
Nb	0.36	0.18	0.16	0.17	0.18	2.53	0.49	1.67	1.74	1.74
Cs	0.18	0.14	0.17	0.54	0.15	0.13	0.14	0.28	0.09	0.18
Ba	13.57	10.09	12.05	6.74	9.81	86.25	12.55	15.82	14.09	16.45
La	1.95	0.72	0.76	1.26	0.82	3.38	2.89	2.09	2.07	1.98
Ce	4.13	1.76	1.80	2.67	1.95	7.00	5.40	4.88	4.63	4.27
Pr	0.51	0.25	0.24	0.33	0.27	0.84	0.68	0.59	0.60	0.52
Nd	2.06	1.12	1.12	1.46	1.15	3.57	2.58	2.44	2.47	2.20
Sm	0.48	0.35	0.32	0.38	0.33	0.94	0.57	0.61	0.62	0.57
Eu	0.15	0.11	0.10	0.15	0.13	0.24	0.17	0.20	0.17	0.15
Gd	0.61	0.45	0.42	0.48	0.43	0.98	0.70	0.63	0.66	0.60
Tb	0.11 0.68	0.08	0.07 0.48	0.10 0.59	0.08	0.18	0.12	0.11	0.12 0.84	0.11 0.71
Dy Ho	0.16	0.53	0.48	0.39	0.53	1.16 0.25	0.78 0.18	0.73	0.84	0.71
Er	0.10	0.12 0.36	0.11	0.13	0.12 0.35	0.23	0.18	0.16 0.43	0.19	0.43
Tm	0.08	0.06	0.05	0.42	0.05	0.08	0.08	0.45	0.08	0.43
Yb	0.50	0.39	0.36	0.38	0.38	0.66	0.55	0.42	0.51	0.41
Lu	0.07	0.06	0.05	0.06	0.06	0.10	0.08	0.06	0.07	0.06
Hf	0.20	0.17	0.16	0.09	0.16	0.53	0.26	0.35	0.37	0.35
Ta	0.06	0.04	0.04	0.02	0.04	0.11	0.08	0.08	0.08	0.07
Pb	7.68	3.08	9.42	2.74	2.84	1.77	7.80	1.46	1.31	1.64
Th	0.41	0.15	0.17	0.17	0.17	0.96	0.55	0.67	0.56	0.76
U	0.11	0.08	0.05	0.06	0.05	0.27	0.21	0.08	0.06	0.18
$REE_T$	12.00	6.36	6.21	8.48	6.66	20.07	15.36	13.42	13.55	12.22
Al <sub>2</sub> O <sub>3</sub> /TiO <sub>2</sub>	17.48	19.47	17.18	18.78	18.69	13.91	16.46	17.07	14.08	12.81
CaO/Al <sub>2</sub> O <sub>3</sub>	0.72	1.04	0.76	1.03	1.11	0.87	0.72	2.48	1.79	1.22
$(Gd/Yb)_N$	1.01	0.97	0.97	1.05	0.95	1.23	1.06	1.22	1.08	1.22
(Eu/Eu) <sub>N</sub>	0.83	0.80	0.80	1.09	1.07	0.76	0.81	1.00	0.79	0.76
Zr/Y	2.04	2.12	2.23	0.97	1.95	4.81	2.51	4.85	4.39	5.07
Nb/Y	0.08	0.05	0.05	0.05	0.05	0.34	0.10	0.35	0.31	0.38
Nb/Th	0.88	1.23	0.98	0.97	1.09	2.63	0.89	2.49	3.11	2.27
Nb/La	0.19	0.25	0.21	0.13	0.22	0.75	0.17	0.80	0.84	0.88
La/Nb	5.39	3.98	4.68	7.57	4.52	1.33	5.93	1.25	1.19	1.14
La/Ba	0.14	0.07	0.06	0.19	0.08	0.04	0.23	0.13	0.15	0.12
Th/Zr	0.05	0.02	0.02	0.05	0.03	0.03	0.05	0.03	0.02	0.03
Nb/Zr	0.04	0.03	0.02	0.05	0.03	0.07	0.04	0.07	0.07	0.07
Zr/Nb	25.21	38.91	41.29	20.69	35.49	14.27	24.02	13.72	13.94	13.39
Nb/Yb	0.73	0.46	0.46	0.44	0.48	3.82	0.89	3.93	3.42	4.26
Th/Yb	0.83	0.38	0.47	0.45	0.44	1.45	1.00	1.58	1.10	1.88
Nb/U	3.14	2.35	3.41	2.70	3.76	9.45	2.30	21.16	28.58	9.47
(Nb/Yb) <sub>PM</sub>	0.50	0.32	0.32	0.30	0.33	2.64	0.61	2.72	2.36	2.95
(Th/Yb) <sub>PM</sub>	4.79	2.19	2.71	2.61	2.56	8.43	5.77	9.17	6.38	10.89
(Hf/Sm) <sub>PM</sub>	0.60	0.68	0.74	0.34	0.67	0.82	0.64	0.83	0.84	0.88
(Ta/La) <sub>PM</sub>	0.55	0.93	0.81	0.20	0.84	0.53	0.48	0.67	0.62	0.58

Table 5.1 Continues....

Location  Rock type  SiO <sub>2</sub> Al <sub>2</sub> O <sub>3</sub> Fe <sub>2</sub> O <sub>3</sub> MnO  MgO  CaO	Madawara Ultramafic 50.53 4.68	Madawara Ultramafic 48.35	Madawara Ultramafic 48.38	Madawara Ultramafic	Madawara Mafic	Madawara Mafic	Madawara Mafic	Madawara	Madawara	Hanumath Ultramafic
SiO <sub>2</sub> Al <sub>2</sub> O <sub>3</sub> Fe <sub>2</sub> O <sub>3</sub> MnO MgO	50.53 4.68	48.35		Ultramafic	Mafic	Mafic	Mafic	M-6:-	3.4 C	I II
Al <sub>2</sub> O <sub>3</sub> Fe <sub>2</sub> O <sub>3</sub> MnO MgO	4.68		40.20			wanc	ivianc	Mafic	Mafic	Ultramane
Fe <sub>2</sub> O <sub>3</sub> MnO MgO			48.38	51.53	50.82	50.17	50.04	50.72	50.39	43.05
MnO MgO	0.07	4.39	3.90	5.41	16.07	16.60	14.99	15.20	15.39	3.10
MgO	8.07	6.25	7.00	7.86	6.00	5.70	6.79	6.02	6.55	8.35
	0.24	0.22	0.28	0.25	0.11	0.10	0.12	0.12	0.12	0.13
CaO	22.96	25.56	27.19	20.51	9.26	8.99	10.12	10.46	9.99	34.60
	10.76	11.41	11.63	11.60	13.14	12.82	13.11	12.60	12.82	2.78
Na <sub>2</sub> O	1.21	1.13	0.78	1.52	1.63	1.55	1.35	1.79	1.83	0.04
K <sub>2</sub> O	0.36	0.42	0.20	0.41	0.30	0.84	0.26	0.13	0.32	0.02
TiO <sub>2</sub>	0.51	0.70	0.37	0.41	0.26	0.24	0.32	0.24	0.30	0.21
$P_2O_5$	0.18	0.17	0.13	0.24	0.02	0.02	0.03	0.02	0.03	0.04
LOI	1.40	1.30	1.30	2.20	0.81	1.89	2.28	1.00	1.00	5.87
Sum	100.90	99.89	101.16	101.94	98.43	98.92	99.41	98.29	98.74	98.19
Sc	40.10	44.50	37.95	33.41	30.90	29.98	32.78	28.31	27.78	12.99
V	151.89	161.43	119.88	138.91	136.62	133.86	146.15	119.39	123.17	104.43
Cr	900.89	1256.83	1165.20	1207.25	516.70	527.96	492.91	488.59	372.20	3858.40
Co	44.67	40.01	46.72	38.68	39.17	36.12	41.75	39.67	73.28	127.58
Ni	42.60	37.87	53.38	32.31	225.80	219.94	241.32	244.86	219.53	1898.43
Cu	25.66	27.56	59.11	26.12	137.19	139.83	120.28	97.83	134.17	17.43
Zn	181.36	252.65	185.63	235.69	131.74	104.06	61.36	205.72	222.11	61.40
Ga	13.33	13.53	11.82	15.04	12.63	12.67	11.73	11.21	12.85	5.52
Rb	10.57	8.28	4.20	11.68	10.41	20.89	7.80	4.10	13.51	1.69
Sr	157.46	224.92	156.07	200.84	169.68	181.29	120.33	143.04	166.84	14.92
Y	14.75	16.67	11.53	15.15	7.69	7.24	9.18	6.47	7.07	4.49
Zr	136.76	170.30	164.84	219.16	36.28	33.14	44.52	29.80	35.87	10.32
Nb	3.54	3.81	2.76	3.62	0.81	0.80	1.05	0.71	0.47	0.35
Cs	0.18	0.10	0.07	0.13	0.28	0.28	0.23	0.10	0.28	0.35
Ba	89.31	157.19	80.27	163.85	88.17	94.81	87.72	60.58	77.62	13.12
La	15.99	16.03	12.39	23.18	3.57	3.38	4.33	2.98	3.29	1.29
Ce	34.75	34.68	26.24	44.97	6.59	6.23	8.07	5.66	6.26	2.92
Pr	4.24	4.43	3.24	5.12	0.72	0.66	0.88	0.63	0.67	0.37
Nd	17.55	19.04	13.39	19.88	3.11	2.92	3.81	2.75	2.93	1.66
Sm	3.87	4.48	2.93	4.20	0.84	0.80	1.04	0.74	0.80	0.50
Eu	0.94	1.15	0.71	1.03	0.36	0.34	0.38	0.30	0.32	0.15
Gd	3.18	3.79	2.43	3.36	0.98	0.93	1.18	0.85	0.94	0.64
Tb	0.48	0.57	0.36	0.49	0.17	0.16	0.20	0.14	0.15	0.11
Dy	2.76	3.21	2.12	2.80	1.13	1.07	1.32	0.98	1.04	0.71
Но	0.51	0.58	0.40	0.52	0.25	0.24	0.29	0.21	0.23	0.16
Er	1.42	1.62	1.13	1.47	0.66	0.64	0.78	0.58	0.62	0.47
Tm	0.21	0.24	0.17	0.22	0.09	0.08	0.11	0.08	0.08	0.07
Yb	1.40	1.62	1.17	1.52	0.57	0.54	0.68	0.49	0.53	0.49
Lu	0.20	0.24	0.17	0.22	0.08	0.07	0.09	0.07	0.07	0.07
Hf	3.78	4.13	3.70	5.02	1.04	0.91	1.28	0.90	1.02	0.25
Ta	0.25	0.26	0.16	0.34	0.06	0.06	0.08	0.07	0.02	0.06
Pb	10.36	30.25	39.06	14.01	12.23	12.73	8.22	9.26	6.26	10.51
Th	3.90	4.08	3.11	6.45	1.03	0.78	1.06	0.69	0.81	0.27
U	1.05	1.35	0.79	1.31	0.24	0.21	0.15	0.10	0.53	0.09
REET	87.50	91.66	66.86	108.97	19.09	18.06	23.15	16.47	17.93	9.62
Al <sub>2</sub> O <sub>3</sub> /TiO <sub>2</sub>	9.17	6.26	10.51	13.07	60.87	70.63	46.86	62.54	50.63	14.76
CaO/Al <sub>2</sub> O <sub>3</sub>	2.30	2.60	2.98	2.14	0.82	0.77	0.87	0.83	0.83	0.90
(Gd/Yb) <sub>N</sub>	1.88	1.93	1.72	1.82	1.42	1.44	1.44	1.42	1.48	1.08
(Eu/Eu) <sub>N</sub>	0.80		0.79	0.81		1.19	1.04	1.14		0.80
		0.83			1.20				1.14	
Zr/Y	9.27	10.22	14.30	14.47	4.72	4.58	4.85	4.61	5.08	2.30
Nb/Y	0.24	0.23	0.24	0.24	0.11	0.11	0.11	0.11	0.07	0.08
Nb/Th	0.91	0.93	0.89	0.56	0.79	1.02	0.99	1.03	0.58	1.28
Nb/La	0.22	0.24	0.22	0.16	0.23	0.24	0.24	0.24	0.14	0.27
La/Nb	4.52	4.20	4.49	6.40	4.42	4.22	4.14	4.20	6.99	3.71
La/Ba	0.18	0.10	0.15	0.14	0.04	0.04	0.05	0.05	0.04	0.10
Th/Zr	0.03	0.02	0.02	0.03	0.03	0.02	0.02	0.02	0.02	0.03
Nb/Zr	0.03	0.02	0.02	0.02	0.02	0.02	0.02	0.02	0.01	0.03
Zr/Nb	38.63	44.67	59.76	60.53	44.90	41.45	42.53	41.98	76.23	29.67
Nb/Yb	2.54	2.35	2.35	2.38	1.42	1.49	1.55	1.44	0.89	0.70
Th/Yb	2.79	2.51	2.65	4.24	1.80	1.45	1.57	1.39	1.53	0.55
Nb/U	3.37	2.82	3.48	2.77	3.39	3.90	7.07	7.21	0.89	4.04
(Nb/Yb) <sub>PM</sub>	1.75	1.62	1.63	1.64	0.98	1.03	1.07	0.99	0.62	0.49
(Th/Yb) <sub>PM</sub>	16.19	14.57	15.40	24.58	10.44	8.43	9.12	8.06	8.90	3.19
	1.40	1.33	1.82	1.72	1.78	1.64	1.78	1.74	1.84	0.72
(Hf/Sm) <sub>PM</sub>			-			-			-	

Table 5.1 Continues....

Sample	GR-2	GR-3	HG-8	HG-11	HG-2	HG-18	HG-14-6	5N	HG-4	HG-14-9
Location	Hanumath	Hanumath	Hanumath	Hanumath	Hanumath	Hanumath	Hanumath	Hanumath	Hanumath	Hanumath
Rock type	Ultramafic	Ultramafic	Ultramafic	Ultramafic	Ultramafic	Ultramafic	Ultramafic	Ultramafic	Ultramafic	Ultramafic
$SiO_2$	42.49	42.33	41.91	42.64	43.07	43.98	39.67	41.12	42.89	41.47
$Al_2O_3$	3.05	3.35	3.97	3.69	3.47	3.70	3.72	3.72	3.72	4.21
$Fe_2O_3$	8.05	7.93	8.97	8.62	7.97	8.21	10.22	10.81	8.88	10.38
MnO	0.12	0.12	0.12	0.12	0.12	0.12	0.13	0.15	0.12	0.15
MgO	34.21	33.49	34.80	34.26	34.64	31.45	29.19	31.17	33.88	29.33
CaO	2.93	3.69	4.32	3.75	4.08	4.89	3.24	3.68	3.40	4.46
Na <sub>2</sub> O	0.04	0.05	0.12	0.11	0.11	0.04	-0.08	-0.10	0.10	-0.03
$K_2O$	0.02	0.02	0.03	0.04	0.04	0.03	0.01	0.01	0.03	0.02
$TiO_2$	0.21	0.20	0.28	0.27	0.28	0.22	0.28	0.32	0.31	0.29
$P_2O_5$	0.04	0.04	0.04	0.05	0.05	0.05	0.03	0.03	0.05	0.04
LOI	7.70	7.23	4.10	4.48	5.52	6.83	8.31	8.78	5.23	8.31
Sum	98.86	98.45	98.66	98.03	99.35	99.52	94.73	99.70	98.61	98.61
Sc	15.08	5.67	15.69	9.61	14.63	15.64	15.29	13.54	16.22	15.51
V	102.93	98.70	101.94	73.71	99.24	98.78	91.08	88.75	93.99	103.24
Cr	3902.01	4316.89	2619.76	4268.69	4067.35	3221.27	2426.43	3142.64	2799.23	3737.94
Co	126.39	117.74	98.47	139.48	118.06	114.67	116.03	105.24	115.32	122.01
Ni	1893.54	1823.06	1695.79	2057.88	1722.44	1895.90	1808.89	751.52	718.43	774.32
Cu	24.72	15.38	26.94	17.70	19.00	27.90	26.24	4.10	13.43	10.44
Zn	55.67	49.26	57.54	56.41	129.57	49.36	235.75	23.99	45.77	49.22
Ga	4.86	5.02	6.30	3.85	7.10	6.08	6.18	5.32	5.70	5.82
Rb	3.90	0.12	1.15	0.80	1.85	3.80	1.92	1.40	1.20	1.29
Sr	24.55	13.57	28.09	13.10	22.86	19.96	31.47	33.75	35.06	28.24
Y	4.99	4.97	6.04	3.11	7.69	6.64	6.36	6.23	7.42	6.51
Zr	5.91	5.50	10.62	6.63	17.01	6.88	10.69	26.63	30.68	33.36
Nb	0.31	0.29	0.05	0.36	1.01	0.50	0.75	1.37	1.64	1.46
Cs	0.56	0.11	0.10	0.13	0.27	0.49	0.23	0.16	0.09	0.19
Ba	10.14	11.33	12.75	9.24	116.10	13.43	9.12	5.50	11.40	18.66
La	2.19	2.00	2.33	1.77	4.22	2.80	2.86	4.14	4.02	3.65
Ce	4.26	4.04	5.22	3.81	8.96	5.83	6.34	7.82	7.76	7.05
Pr	0.57	0.54	0.66	0.45	1.10	0.78	0.79	0.86	0.89	0.79
Nd	2.52	2.42	2.88	1.84	4.30	3.39	3.20	3.59	3.96	3.49
Sm	0.60	0.61	0.75	0.43	0.95	0.85	0.77	0.88	1.02	0.89
Eu	0.19	0.19	0.22	0.12	0.26	0.28	0.20	0.31	0.26	0.24
Gd	0.76	0.73	0.96	0.52	1.14	1.01	0.97	0.87	1.02	0.89
Tb	0.14	0.15	0.16	0.08	0.20	0.20	0.17	0.15	0.18	0.16
Dy	0.85	0.86	1.00	0.49	1.18	1.18	1.01	1.01	1.21	1.08
Но	0.18	0.18	0.22	0.11	0.27	0.24	0.23	0.23	0.27	0.24
Er	0.57	0.57	0.63	0.31	0.83	0.73	0.71	0.64	0.77	0.69
Tm	0.09	0.09	0.09	0.05	0.12	0.12	0.11	0.09	0.12	0.10
Yb	0.49	0.48	0.60	0.32	0.78	0.62	0.70	0.64	0.77	0.69
Lu	0.08	0.07	0.09	0.05	0.12	0.10	0.10	0.09	0.11	0.10
Hf	0.15	0.14	0.26	0.15	0.36	0.17	0.22	0.68	0.74	0.83
Ta	0.03	0.04	0.00	0.07	0.21	0.03	0.12	0.11	0.16	0.20
Pb	4.89	2.87	6.83	4.48	10.82	4.24	18.14	1.26	2.04	2.41
Th	0.31	0.28	0.39	0.18	0.93	0.46	0.60	0.79	0.84	0.86
U	0.13	0.09	0.20	0.14	0.41	0.15	0.26	0.28	0.32	0.32
REE <sub>T</sub>	13.50	12.93	15.81	10.35	24.42	18.13	18.16	21.31	22.36	20.07
Al <sub>2</sub> O <sub>3</sub> /TiO <sub>2</sub>	14.52	16.75	14.18	13.67	12.39	16.82	13.52	11.74	12.00	14.67
CaO/Al <sub>2</sub> O <sub>3</sub>	0.96	1.10	1.09	1.02	1.18	1.32	0.87	0.99	0.91	1.06
(Gd/Yb) <sub>N</sub>	1.30	1.27	1.34 0.79	1.36	1.20	1.34	1.14	1.13	1.10	1.06
(Eu/Eu) <sub>N</sub>	0.87	0.88		0.77	0.75	0.93	0.72	1.06	0.79	0.82
Zr/Y	1.18	1.11	1.76	2.13	2.21	1.04	1.68	4.27	4.14	5.13
Nb/Y	0.06	0.06	0.01	0.12	0.13	0.08	0.12	0.22	0.22	0.22
Nb/Th	1.01	1.05	0.12	2.07	1.09	1.09	1.24	1.74	1.96	1.69
Nb/La	0.14	0.15	0.02	0.21	0.24	0.18	0.26	0.33	0.41	0.40
La/Nb	7.03	6.84	51.75	4.86	4.19	5.55	3.81	3.03	2.45	2.51
La/Ba	0.22	0.18	0.18	0.19	0.04	0.21	0.31	0.75	0.35	0.20
Th/Zr	0.05	0.05	0.04	0.03	0.05	0.07	0.06	0.03	0.03	0.03
Nb/Zr	0.05	0.05	0.00	0.06	0.06	0.07	0.07	0.05	0.05	0.04
Zr/Nb	18.95	18.87	235.78	18.17	16.88	13.63	14.28	19.50	18.67	22.90
Nb/Yb	0.64	0.61	0.08	1.15	1.28	0.81	1.06	2.14	2.15	2.11
Th/Yb	0.63	0.58	0.65	0.56	1.18	0.74	0.86	1.23	1.10	1.24
Nb/U	2.47	3.08	0.22	2.52	2.47	3.47	2.87	4.89	5.09	4.50
(Nb/Yb) <sub>PM</sub>	0.44	0.42	0.05	0.80	0.89	0.56	0.73	1.48	1.48	1.46
(Th/Yb) <sub>PM</sub>	3.68	3.39	3.77	3.24	6.84	4.29	4.96	7.14	6.36	7.21
(Hf/Sm) <sub>PM</sub>	0.35	0.32	0.51	0.50	0.55	0.30	0.41	1.11	1.04	1.34
(Ta/La) <sub>PM</sub>	0.20	0.34	0.01	0.65	0.82	0.20	0.71	0.45	0.68	0.91

Table 5.2	Selected trace and PGE concentration of ultramafic -mafic rocks of MUC.

Sample	IK-15-1	IK-15-4	IK-14-11	IK-14-6	IK-14-5	MD-2	MW-9	MW-10	MW-8
Location	Ikauna	Ikauna	Ikauna	Ikauna	Ikauna	Madawara	Madawara	Madawara	Madawara
Rock type	Ultramafic								
Ni	1892.59	2407.79	2283.77	2455.82	1759.12	1823.31	1730.40	1961.53	1891.82
Ru	95.05	14.61	9.14	9.66	15.49	89.66	6.77	8.05	6.98
Rh	31.90	1.67	2.07	2.29	6.14	36.53	1.02	2.25	1.01
Pd	42.57	5.84	7.61	7.41	30.57	111.50	19.32	10.58	9.08
Os	38.72	12.29	12.26	13.94	100.69	9.22	1.90	3.25	1.90
Ir	23.67	3.57	4.02	4.26	18.16	13.70	1.03	3.15	1.00
Pt	169.37	8.68	13.80	10.96	28.97	201.19	25.23	27.67	21.65
Au	289.20	30.15	10.82	7.31	121.68	360.95	29.71	97.51	30.43
∑PGE	401.28	46.66	48.89	48.51	200.02	372.13	48.50	46.90	34.64
∑PPGE	243.84	16.19	23.47	20.66	65.67	349.22	45.57	40.50	31.74
∑IPGE	157.44	30.47	25.42	27.86	134.34	112.58	9.71	14.45	9.88
∑PPGE/∑IPGE	1.55	0.53	0.92	0.74	0.49	3.10	4.69	2.80	3.21
Pd/Ir	1.80	1.64	1.89	1.74	1.68	8.14	18.67	3.36	9.09
Pt/Pt*	1.47	0.89	1.11	0.85	0.68	1.01	1.81	1.81	2.28
Ni/Cu	98.65	187.89	118.03	129.77	116.47	95.32	101.86	118.91	105.42
$(Cu/Pd)*10^3$	450.67	2192.56	2543.03	2553.66	494.13	171.57	879.54	1559.59	1976.93
Cu/Zr	3.34	2.63	3.17	2.02	4.85	6.02	2.68	2.35	2.66
Pd/Cu	0.00222	0.00046	0.00039	0.00039	0.00202	0.00583	0.00114	0.00064	0.00051
$(Ni/Pd)*10^3$	44457.99	411962.79	300162.25	331396.46	57551.07	16353.30	89587.59	185455.83	208401.16
$(Cu/Ir)*10^3$	810.48	3591.49	4807.58	4446.94	831.75	1396.55	16422.19	5235.06	17970.11
Pd/Os	1.10	0.48	0.62	0.53	0.30	12.09	10.18	3.26	4.78
Cu/Pd	450.67	2192.56	2543.03	2553.66	494.13	171.57	879.54	1559.59	1976.93
Pd/Pt	0.25	0.67	0.55	0.68	1.06	0.55	0.77	0.38	0.42
Pt/Pd	3.98	1.48	1.81	1.48	0.95	1.80	1.31	2.62	2.38

Table 5.2 Continues.....

Sample	MD-5	MD-3	MD-12	MD-10	MD-9	MD-7	16.00	14.00	MA-15-1
Location	Madawara	Madawara	Madawara						
Rock type	Ultramafic	Mafic	Mafic						
Ni	1612.48	1765.63	1357.92	1533.40	1319.79	1172.96	768.91	236.07	121.71
Ru	4.66	78.07	6.40	6.00	1.60	2.60	2.54	1.29	1.14
Rh	0.77	36.98	1.00	0.60	0.60	0.50	5.08	2.35	1.77
Pd	10.98	63.67	14.40	6.80	20.20	18.00	69.26	38.11	43.63
Os	1.32	6.51	3.00	3.20	0.40	1.40	4.21	1.68	2.17
Ir	0.72	15.01	2.80	3.20	1.60	1.00	1.16	1.12	0.59
Pt	17.13	234.17	19.80	17.60	28.60	8.80	21.54	42.70	16.76
Au	30.67	328.01	22.40	25.00	8.00	17.00	133.41	122.67	117.57
∑PGE	30.92	356.33	41.00	31.40	51.40	29.70	101.24	85.96	64.93
∑PPGE	28.88	334.82	35.20	25.00	49.40	27.30	95.88	83.16	62.17
∑IPGE	6.70	99.58	12.20	12.40	3.60	5.00	7.91	4.09	3.90
∑PPGE/∑IPGE	4.31	3.36	2.89	2.02	13.72	5.46	12.13	20.33	15.93
Pd/Ir	15.32	4.24	5.14	2.13	12.63	18.00	59.82	33.88	73.59
Pt/Pt*	1.88	1.54	1.67	2.79	2.63	0.94	0.37	1.44	0.61
Ni/Cu	66.86	97.90	35.66	42.70	20.45	37.39	79.58	1.40	0.56
$(Cu/Pd)*10^3$	2196.35	283.29	2644.31	5280.44	3195.64	1742.83	139.52	4415.00	5007.07
Cu/Zr	6.99	2.80	1.91	2.49	6.08	2.58	0.42	7.42	8.76
Pd/Cu	0.00046	0.00353	0.00038	0.00019	0.00031	0.00057	0.00717	0.00023	0.00020
$(Ni/Pd)*10^3$	146850.84	27732.82	94299.72	225499.41	65336.09	65164.22	11102.49	6194.67	2789.73
$(Cu/Ir)*10^3$	33639.72	1201.79	13599.29	11220.94	40345.00	31371.00	8346.76	149580.78	368494.73
Pd/Os	8.31	9.78	4.80	2.13	50.50	12.86	16.46	22.74	20.09
Cu/Pd	2196.35	283.29	2644.31	5280.44	3195.64	1742.83	139.52	4415.00	5007.07
Pd/Pt	0.64	0.27	0.73	0.39	0.71	2.05	3.22	0.89	2.60
Pt/Pd	1.56	3.68	1.38	2.59	1.42	0.49	0.31	1.12	0.38

Sample	HG-11	HG-2	HG-14-6*	5N*	HG-4	GR-1	GR-2	GR-3
Location	Hanumath							
Rock type	Ultramafic							
Ni	2057.88	1722.44	1808.89	751.52	774.32	2407.79	1898.43	1893.54
Ru	15.13	14.68	10.04	14.98	11.36	13.88	85.70	20.92
Rh	0.88	0.94	1.23	6.76	0.76	0.83	32.00	0.79
Pd	9.73	12.39	6.28	31.90	14.39	7.46	33.98	9.13
Os	10.56	10.64	6.66	43.55	8.60	7.12	37.30	7.31
Ir	3.53	3.11	2.58	15.56	2.73	2.65	21.91	3.10
Pt	19.13	19.15	25.52	46.30	23.66	21.53	168.35	21.06
Au	32.12	412.07	41.72	243.43	26.21	40.38	313.27	13.60
∑PGE	43.83	46.24	42.29	144.07	50.14	39.60	293.53	41.39
∑PPGE	29.74	32.49	33.04	84.96	38.81	29.82	234.33	30.98
∑IPGE	29.22	28.44	19.29	74.09	22.69	23.65	144.91	31.33
∑PPGE/∑IPGE	1.02	1.14	1.71	1.15	1.71	1.26	1.62	0.99
Pd/Ir	2.76	3.98	2.43	2.05	5.28	2.82	1.55	2.94
Pt/Pt*	2.09	1.79	2.93	1.01	2.29	2.77	1.63	2.51
Ni/Cu	116.26	90.64	68.93	183.21	74.18	187.89	108.92	76.59
$(Cu/Pd)*10^3$	1818.65	1533.83	4176.84	128.60	725.28	1717.50	512.98	2707.82
Cu/Zr	2.67	1.12	2.45	0.15	0.31	1.24	2.95	4.49
Pd/Cu	0.00055	0.00065	0.00024	0.00778	0.00138	0.00058	0.00195	0.00037
$(Ni/Pd)*10^3$	211436.92	139019.07	287920.48	23560.24	53799.96	322702.38	55874.46	207385.94
$(Cu/Ir)*10^3$	5015.77	6103.58	10155.04	263.60	3827.35	4835.20	795.64	7974.29
Pd/Os	0.92	1.16	0.94	0.73	1.67	1.05	0.91	1.25
Cu/Pd	1818.65	1533.83	4176.84	128.60	725.28	1717.50	512.98	2707.82
Pd/Pt	0.51	0.65	0.25	0.69	0.61	0.35	0.20	0.43
Pt/Pd	1.97	1.55	4.06	1.45	1.64	2.89	4.95	2.31

Table 5.3 Sm-Nd and Rb-Sr isotope data for the ultramafic mafic of MUC.

Sample No.	Rock type	[Sm] ppm	[Nd] ppm	<sup>147</sup> Sm/ <sup>144</sup> Nd	<sup>143</sup> Nd/ <sup>144</sup> Nd	±2 sm	e Nd (0)	T <sub>DM</sub> (Ma)	Epsilon value (eNdT)	Age (Ma)	[Rb] ppm	[Sr] ppm	<sup>87</sup> Rb/ <sup>86</sup> Sr	<sup>87</sup> Sr/ <sup>86</sup> Sr	±2 sm	I (Sr)
Madawara	ultramafic-n	nafic region	(epsilon at 2	2.67Ga)												
MD-15-3	Ultramafic	0.33	1.15	0.1393	0.51159	12	-0.80	3181	-0.80	2673	1.17	14.00	0.083	0.71104	12	0.70785
MW-8	Ultramafic	0.32	1.12	0.1484	0.51172	7	-1.37	3318	-1.37	2673	1.17	16.14	0.139	0.71142	12	0.70606
MW-10	Ultramafic	0.35	1.12	0.1430	0.51169	29	-0.01	3122	-0.01	2673	1.32	17.88	0.067	0.71058	11	0.70797
MD-4	Mafic	0.70	2.54	0.1495	0.51179	30	-0.31	3203	-0.31	2673	5.47	142.77	0.110	0.70838	15	0.70411
16	Ultramafic	0.57	2.20	0.1516	0.51166	20	-3.59	3623	-3.59	2673	2.51	15.36	0.518	0.71913	16	0.69913
T-14	Mafic	0.74	2.75	0.1512	0.51178	8	-1.10	3314	-1.10	2673	4.10	143.04	0.083	0.70412	14	0.70090
Ikauna ultr	amafic-mafic	e region (eps	silon at 2.67	Ga)												
IK-15-3	Ultramafic	0.46	1.74	0.1564	0.51172	7	-3.98	3754	-3.98	2673	0.66	12.40	0.151	0.73128	12	0.72545
IK-14-4	Intermediat	1.34	5.20	0.1468	0.51175	14	-0.19	3168	-0.19	2673	5.62	408.27	0.033	0.70278	12	0.70149
Hanumath	garh ultramat	fic-mafic reg	gion (epsilor	n at 2.67Ga)												
HG-14-2	Ultramafic	0.95	4.30	0.1397	0.51141	5	-4.43	3557	-4.43	2673	1.85	22.86	0.224	0.72338	12	0.71472
5-N	Ultramafic	0.88	3.59	0.1380	0.51161	4	0.15	3077	0.15	2673	1.40	33.75	0.156	0.73360	12	0.72759
HG-14-11	Ultramafic	0.43	1.84	0.1334	0.51147	5	-1.04	3166	-1.04	2673	0.80	13.10	0.158	0.72354	7	0.71744
HG-14-4	Ultramafic	1.02	3.96	0.1539	0.51172	5	-3.29	3621	-3.29	2673	1.20	35.06	0.165	0.71122	14	0.70484
HG-14-10	Ultramafic	0.95	3.93	0.1363	0.51153	8	-0.90	3171	-0.90	2673	1.69	26.35	0.183	0.79334	16	0.78625
HG-14-8	Ultramafic	0.75	2.88	0.1522	0.51179	4	-1.23	3341	-1.23	2673	1.15	28.09	0.116	0.70938	8	0.70489
GR-15-1	Ultramafic	0.50	1.66	0.1368	0.51164	5	1.17	2969	1.17	2673	1.69	14.92	0.223	0.76881	11	0.76020

# **Chapter-VI**

# Petrogenesis and sources

In this chapter an attempt has been made to integrate field, petrographic characteristics, mineral chemistry, whole rock geochemistry, and Nd isotope data of the Madawara Ultramafic Complex to unravel the effect of secondary processes on the "elemental mobility, crustal contamination, magmatic differentiation processes, nature, and composition of the potential mantle reservoirs as well as depth and degree of melting of mantle sources."

#### **6.1.** Effect of secondary processes on elemental mobility:

It is necessary to evaluate the elemental mobility as the studied ultramafic mafic rocks affected by post-magmatic secondary processes such as fluid flow hydrothermal alteration and low-grade metamorphism prior to the use of data sets to decipher the petrogenetic process. (Arndt et.al.,2008 Gruau et al., 1992; Chavagnac, 2004; Jayananda et al., 2008, 2016). The metamorphism and hydrothermal alteration of Archean ultramafic-mafic rocks are commonly associated with late-stage fluid flow and metamorphism (Anhaeusser, 2015; Johnson et al., 2016; Guice et al., 2018; 2019). Therefore, it's crucial to determine whether the chemistry of analysed samples retains its original chemistry or is impacted by a later process. The mobility of the large ion lithophile element (LILE) and other incompatible elements, such as REE, has been shown that they are controlled by fluid movement, hydrothermal alteration, and metamorphism in accordance to geochemical and isotopic investigations on the ultramafic of various cratons of the world. (Bau, 1981) has shown the mobility of "REE and other incompatible elements" ability to form complexes with fluorine and CO<sub>2</sub>-rich fluid phases. Further, the geochemical and isotopic study from the ultramafic

greenstone component of southern Africa reveals that the REE patterns are not disturbed by fluids except Eu and Ce (Lecuyer et al., 1994). In summary, the elements which are affected, together with their depletion or enrichment in different lithologies of interest depend upon the product of several factors which include the protolith mineralogy, fluid characteristics. composition/mineralogy of proximal lithologies, and pre-existing structures (Barton and Ilchik, 1991; Putnis and Austrheim, 2010). The relative mobility of trace elements including REE in highly altered rocks can be checked by plotting individual elements against the most immobile elements (e.g., Zr, Y, and Yb) and determining the R<sup>2</sup> value ("Guice, 2019 and references therein"). The studied samples must be cogenetic and the reliability of these tests is greatest for large, wellcharacterized datasets ("Guice et al., 2018, 2019"). Therefore, it is crucial to determine how the secondary alteration process affects the ultramafic-mafic samples from the study location.

The petrographic study of the studied MUC reveals that the primary mineralogy of ultramafic samples has been affected by the hydrothermal alteration process (LOI>4.0 wt.%), however, they still preserve their remnant cumulate textures. The primary mineralogy has been altered to secondary minerals including serpentine, tremolite, chlorite and actinolite, however, few relict olivine grains are still preserved in very few samples. On the other hand, the mafic and intermediate rocks are not affected by the secondary hydrothermal alteration process (LOI<2.0 wt.%) and preserve the primary mineralogy (See table 5.1). The petrographic study inferred that the presence of tiny carbonate veins in a few ultramafic samples indicates fluid flow-assisted alteration which slightly changed the major and traces element abundances such as K, Rb, and Ba, which is also reflected by non-linearity on Harker's binary diagrams (See figure 6.1). The HFSEs (Yb, Y, Zr) are immobile during post-magmatic hydrothermal alteration and low-grade metamorphism as

documented in many Precambrian greenstone terrains (Guice et al., 2018, 2019; Jayananda et al., 2008, 2016, 2022).

Therefore, here in the present study, Yb is preferred as a reference immobile element to monitor the mobility of other trace elements (Guice et al. 2018). All the analyzed ultramafic samples of MUC show Sm, Y, Nb, Hf, Zr, U, and Th linear trend against Yb, attesting their immobility during fluid-induced hydrothermal alteration except a few samples from Madawara and Hanumathgarh. On the contrary, mobile elements like (Rb, and Ba,) show no obvious correlation with Yb, reflecting their post-magmatic mobility characteristics (see figure 6.1). However, the majority of the samples that have been studied show a consistent Al<sub>2</sub>O<sub>3</sub>/TiO<sub>2</sub> ratio and smooth REE patterns in the ultramafic, with the exception of a few samples that have either positive or negative Eu anomalies. It suggests that the alteration process has not affected/significant influence on the elemental mobility of REE except Eu (see figure 5.5-5.7). In addition, the studied samples show no significant Ce (Ce/Ce\*=0.86-1.02) anomalies, suggesting a negligible effect on rare earth elements and HFSE from fluid-induced alteration processes and low-grade metamorphism except for Eu (Polat and Hofmann, 2003) (see figure 5.5-5.7). Further, despite the high MgO contents of the ultramafic samples of the MUC (25.11-38.05 wt.%), they display negative Eu (Eu/Eu\*=0.56-0.95) anomaly, which points out that these rocks are highly susceptible for the secondary alteration process ("Jayananda et.al., 2008, 2016, 2023; Tushipokla and Jayananda, 2013"). (Sun and Nesbitt, 1978), showed that seawater hydrothermal alteration can contribute to the Eu anomalies. The mobility of Eu is probably caused by circulating fluids associated with hydrothermal plumbing systems in the oceanic domain.

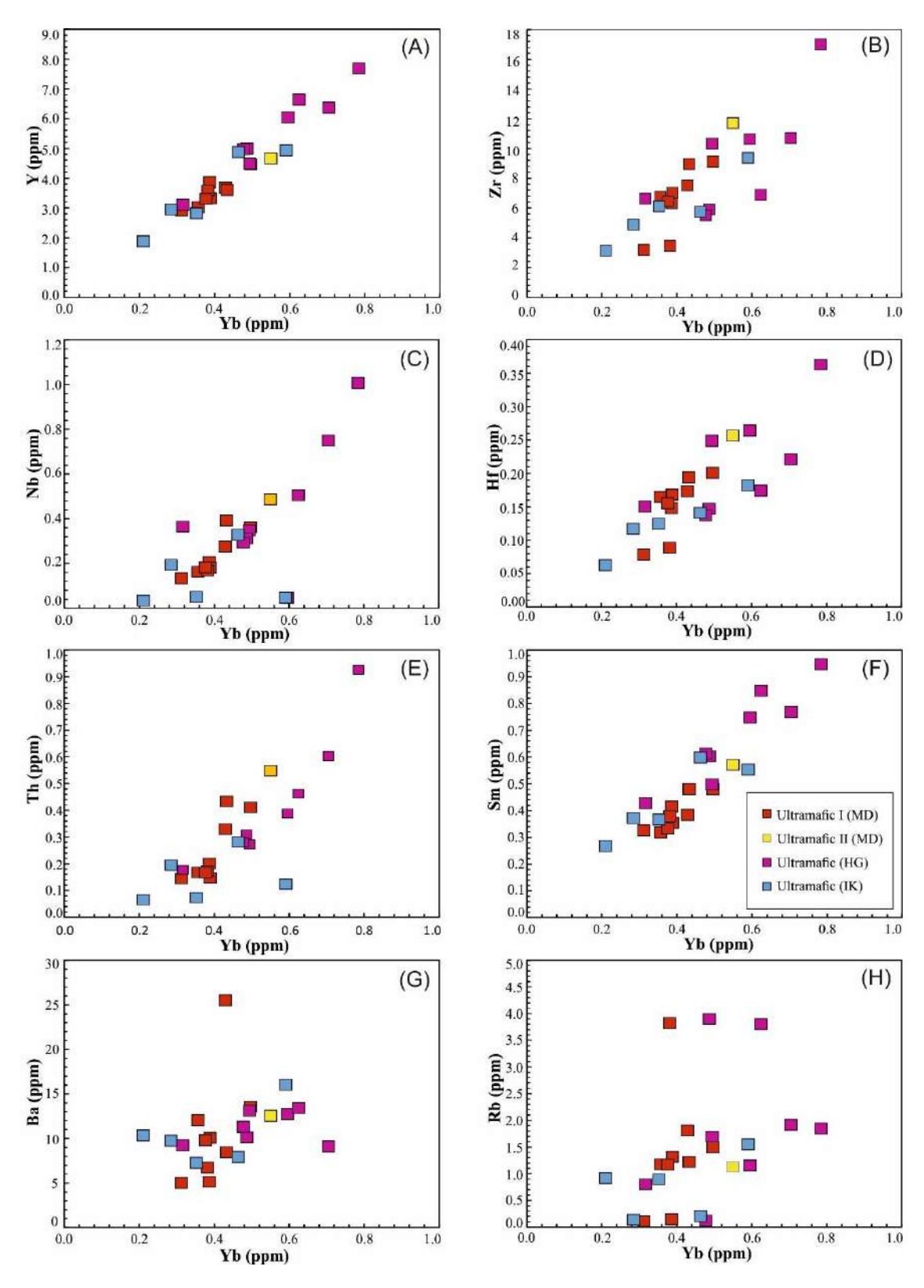


Figure 6.1 Bivariant diagrams of Yb versus selected trace elements of the ultramafic-mafic of MUC.

The super chondritic value observed in a few samples is attributed to carbonatitic metasomatism processes or may be due to the presence of amphibole or rutile in the source region (Foley et.al, 2002; Green et.al, 1995). The coherent variations of the chondrite normalized REE (expect Eu), and primitive mantle normalized trace element patterns except few samples from Hanumathgarh indicate the relative immobility of REE and high field strength elements (HFSE) like Nb, Ta, Zr, Hf, Y, consistent with the robustness of these elements during alteration and metamorphism indicating their primary igneous signatures (Middelburg et.al., 1998). In conclusion, with the exception of LILE and Eu contents, the lateral processes had little effect on the incompatible components of the sample under study. Finally, the immobile elements like REE, Nb, Th, Zr, and Y as well as their ratio can be used to constrain the magmatic differentiation histories and mantle sources.

#### **6.2.** Crustal contamination:

Crustal contamination occurs when hot, mantle-derived ultramafic to mafic magma migrates upward through the more felsic continental crust and becomes enriched in incompatible elements when it melts the surrounding continental crust and combines with magma. The material exchange between the melts and crustal rocks is very common, as hot magma migrates upward from their mantle sources ("Hawksworth et. al., 1984; Mahoney, 1989; Carlson, 1991; Hergt et.al., 1991"). In addition, studies have shown that, generally, Crustal materials can be assimilated by mantle-derived magmas both during ascents to the surface and/or protracted residence in the crustal magma chamber as well as the modification within the mantle reservoirs before magma ascent or separation from the sources. (Mohr, 1987). Studies also have shown that mantle-derived magmas

could be contaminated by crustal material either along their ascending conduit through the crust or within their mantle sources (Su et al., 2012). In order to describe the contamination of ultramafic magmas, "geological, elemental, and isotopic parameters have been employed" (Kerrich and Xie, 2002). It is possible to assess the degree of crustal contamination by looking at certain trace element ratios and their fractionation patterns. For instance, the crustal contamination or subduction component in the mantle sources may be associated to the presence of negative Nb and Ta anomalies. (Arnd et al., 1998, Zhu et al., 2009).

The elemental ratios similar distribution/partition coefficients of incompatible elements such as Nb/La and Nb/Th are used to constrain the possible crustal contamination and source metasomatism. Therefore, the trace element ratios with a similar partition coefficient (e.g., Nb/La, Ta/La, Nb/Th) have been used for mafic to ultramafic rocks as well as for cumulate rocks for evaluation of crustal contamination because such ratios are less sensitive to both fractionations, and melting process (Zou and Zindler 1996; Zou, 2007). The crustal contaminated sample could decrease the "Nb/La, Ta/La, and Nb/Th ratios" and increase the Th/Yb ratio. The ratio of Nb/La is used for cumulate rocks as it is a highly incompatible trace element and prefers to concentrate in the inter cumulus liquid. The ratio of these element pairs (Nb/Ta, Ta/La, Nb/Th) also represents the source magma from which it has been crystallized. Therefore, it is useful as an indicator for both contamination and source metasomatism.

The field observation indicates that the studied ultramafic intrusive into the older continental land mass and has sheared relationship with the country rock. The crustal contamination can be identified using primitive mantle normalized trace element contents such (Nb/Th) <sub>PM</sub> and (Ta/Th)<sub>PM</sub> are indicators of the extent of Ta and Nb anomalies, whereas (Th/Yb)<sub>PM</sub> is a sensitive indicator of crustal contamination. ("Wang and Zhou, 2006; Zhang et al., 2009").

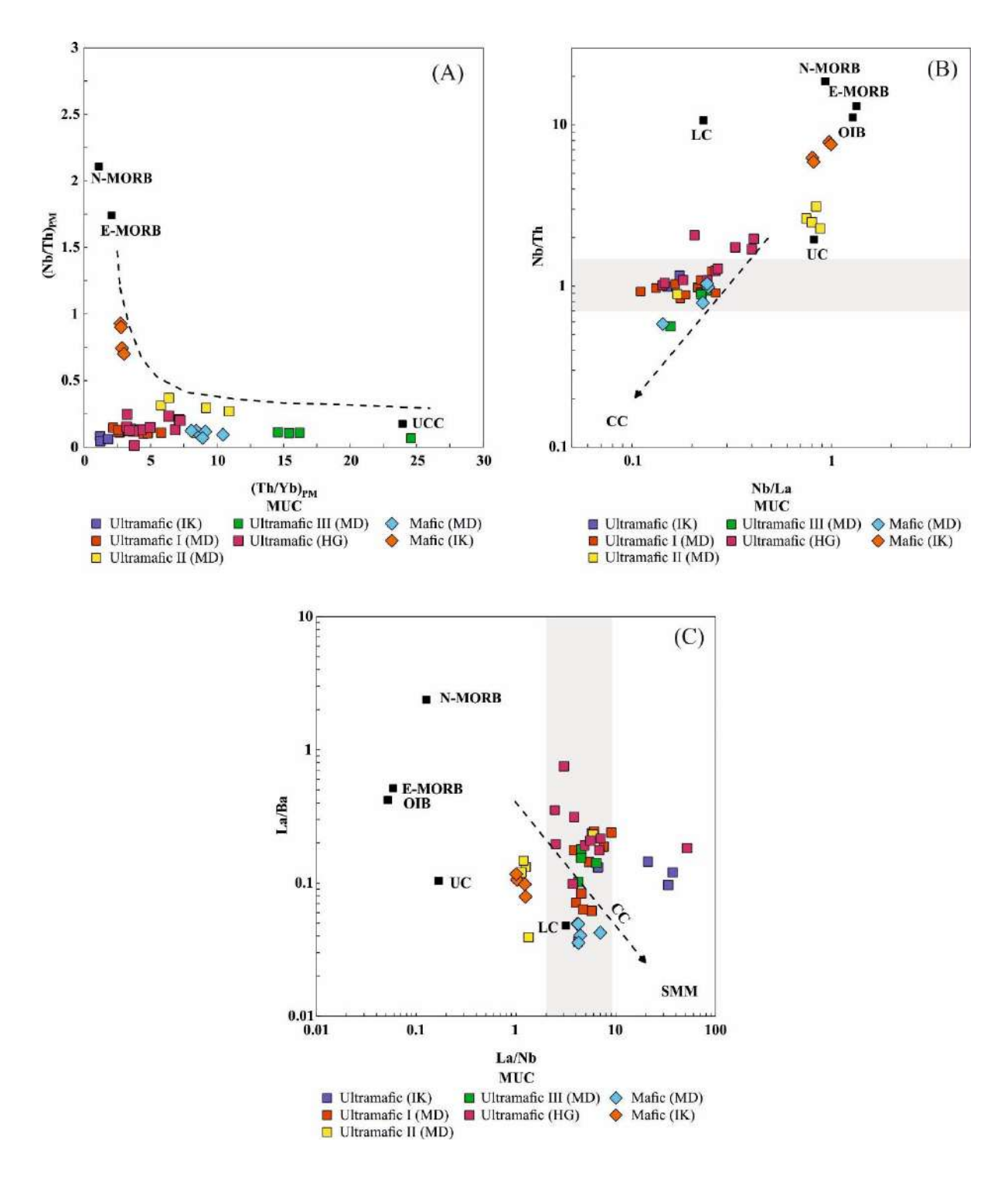


**Figure 6.2** (a-c) Correlation diagrams of trace elemental ratios of MUC in the southern Bundelkhand craton.  $(Th/Yb)_{PM}$ ,  $(Nb/Th)_{PM}$  are the primitive mantle normalized values. Data sources of the primitive mantle (PM), Normal mid-oceanic ridge basalt (N-MORB), Enriched mid-oceanic ridge basalt (E-MORB), Oceanic Island basalt (OIB), Lower crust and Upper crust values are from Sun and McDonough (1989).

Further, magmas derived from the primitive mantle "(N-MORB, E-MORB) have high (Nb/Th)<sub>PM</sub> and low (Th/Yb)<sub>PM</sub> values." (Hofmann, 1988). Whereas, the "upper continental crust (UCC) has low (Nb/Th)<sub>PM</sub> (0.14) and high (Th/Yb)<sub>PM</sub> (24.89) values." (Taylor and McLennan, 1985). Therefore, the crustal contamination can be drawn by using "between (Nb/Th)<sub>PM</sub> versus (Th/Yb)<sub>PM</sub> diagram." (Taylor and McLennan, 1985) (see figure 6.2 a). A curved mixing trend line between these two compositions has been used to indicate increasing degrees of crustal contamination of mantle-derived magmas ("Ihlenfeld and Keays, 2011, Jowitt and Ernst, 2013, Keays and Lightfoot, 2010"). A good fit curve between (Nb/Th)<sub>PM</sub> versus (Th/Yb)<sub>PM</sub> has been reflected as mixing line between two end-member components as "mid-oceanic ridge basalt (MORB) and upper continental crust (UCC)" implies the presence of a high-energy system that allowed the more complete mixing and homogenization of the mantle-derived magma with crust contamination during its ascent. Compared to N-MORB (normal mid-oceanic ridge basalt), and Ocean Island basalt (OIB), the ultramafic-mafic rocks of the studied area have very low (Nb/Th)<sub>PM</sub>, and low to moderate (Th/Yb)<sub>PM</sub> ratios, with lie below the mixing line between "MORB and UCC" indicating low degrees of crustal contamination (except the few mafic samples from Madawara) (see figure 6.2 a). However, the crustal contamination trends (except very few samples) seem to have no chemical affinity with upper and lower crust as displayed in the (Nb/Th)<sub>PM</sub> versus (Th/Yb)<sub>PM</sub> and Nb/La versus Nb/Th diagrams (see figure 6.2 b). Additionally, "the ultramafic mafic rocks' high La/Nb and low La/Ba ratios suggest that they may have come via source metasomatism or subduction-modified mantle sources (see figure 6.2 c). (Jolly et al., 1992), also discussed about mantle-derived melts are inevitably affected by crustal contamination during their ascent through the continental crust. "The crustal rocks usually have low Nb contents and high Zr, Hf contents. Therefore, crustal contamination will lead to depletion in Nb and Ta and be enriched in Pb, Zr,

and Hf." For example, the presence of negative Nb and Ta anomalies could be related to crustal assimilation or subduction-linked arc sources. (Arndt et al., 1998; Zhou et al., 2009). In this study, the ultramafic samples display negative Nb, and Ta anomalies as well as negative Zr-Hf anomalies (except a few samples from Hanumathgarh) precluding the significant crustal contamination of the mantle derived magma. Further, there is no trend of increasing SiO<sub>2</sub> or LREE with increasing MgO precludes any large-scale crustal contamination with an older crustal component which is supported by the features of the trace elements, such as the absence of positive Zr-Hf anomalies in the majority of the samples on the primitive mantle normalized trace element diagrams (Polat et al., 2005; Zhao et al., 2007; Deng et al., 2013).

In addition, the crustally contaminated samples show slight enrichment of "large ion lithophile elements (LILE; e.g. Rb, Ba)" and depleted in "high field strength elements (HFSE) (e.g. Nb, Ta)." That led to the lower value Nb/Th, Ta/La than the primitive mantle (Nb/Th=8.75, Ta/La=0.06) and higher than the average continental crust value (Nb/Th=1.20, Ta/La=0.02). ("Taylor, 1985, Rudnick and Gao et al., 2003; Barth et al., 2000"). In this study, most of the ultramafic-mafic samples display very low Nb/Th (0.38-1.28) which is lower than the primitive mantle values indicating either traces of crustal contamination or arc source (Condie, 2003). Few ultramafic mafic samples show lower than the primitive mantle values and higher in comparison to continental crust (Nb/Th=2.07-7.81) signifies the traces of crustal contamination. Further, all the samples display a lower value of Ta/La (0.01-0.06) which is lower than the primitive mantle and higher than the crustal values, implying possible traces of older preexisting crustal source due to slightly higher La content (wood et al., 1993). These characteristics suggest that the studied rocks were possibly affected by a low degree of contamination of pre-existing continental sources. However, all the ultramafic mafic samples contain very low content of Th (0.07 to 1.067). In the

other hand, the few ultramafic/mafic samples of Madawara precluding the significant input from the "upper and middle crust as the crust is rich in Th (Th = 6.5 for the middle crust, and Th = 10.5 for the upper crust)," (Rudnick and Gao, 2003) suggests against the significant crustal contribution. Scholars like, (Fan and Kerrich, 1997) pointed out that continental crust displays "lower Ti/Zr ratio values (Ti/Zr=54) compared to primitive mantle values of 116." The ultramafic samples exhibit higher Ti/Zr values (52-404) whereas the mafic samples exhibit low Ti/Zr values (11-50). In the continental crust, the Ti phase acts as a compatible element in the form of Ti-bearing phases like rutile and titanite, and Zr is considered an incompatible element. The melting and assimilation of the continental crust will decrease the Ti/Zr ratio (Ti/Zr<20) (Rudnick and Gao, 2003, Khanna and Sai, 2020). In the present study, the ultramafic mafic samples show a high value of Ti/Zr (>42.51) which precludes crustal contamination except for the samples of Madawara ultramafic-mafic rocks (Group III variety) are in the range of 11-24 are considered to be affected by traces of the old crust contamination (See table 5.1).

This observation is also further substantiated by an isotope study of ultramafic mafic rocks. (Kerrich and Xie, 2002) in their work used isotopic ratios to interpret the contamination of ultramafic magma. In the present study majority of the ultramafic mafic samples exhibit  $\varepsilon$ Nd values [ $\varepsilon$ Nd(T)=-1.37 to +1.17] are calculated for the respective time of their formation. Few samples display high negative [ $\varepsilon$ Nd(T) = -3.29 to -4.43] values, which may be related to the contamination of the preexisting crustal material either during their ascent which are further supported by their slightly increase in LREE on chondrite normalized REE patterns (see figure 5.5-5.7). The relatively constant  $\varepsilon$ Nd(T) values (-1.37 to 1.17) except a few samples further indicate "depleted to primitive mantle sources" with possible little traces of contamination of older continental crust. Furthermore, crustal assimilation can lead to a positive correlation between

εNd(t) versus MgO, and Nb/La (Su et al., 2021). The absence of correlation between these values suggests insignificant crustal contamination (Vervoort and Blichert-Toft, 1999) (see figure 5.9 a-d). In conclusion, the secondary process had a negligible to no impact on the incompatible elements of the examined samples, with the exception of LILE and Eu concentrations. Because of this, their petrogenesis, including magmatic differentiation processes and potential mantle source reservoirs, are constrained by the REE, other immobile elements, and their elemental ratios (HFSE), together with transition elements (Sc, Y, Ni, Cr, and Co).

## **6.3. Fractional crystallization:**

The analyzed samples are mainly ultramafic - mafic to intermediate in composition. The ultramafic rocks define fractionation trends on the binary diagrams and they demonstrate moderate to strong linear trends for both major and trace elements. It indicates that the magmas were produced by the differentiation of a single parental magma. The negative correlation of SiO<sub>2</sub>, Al<sub>2</sub>O<sub>3</sub>, CaO, and TiO<sub>2</sub>, against MgO suggests that the parental magmas evolved through a fractional crystallization process with the removal of olivine and pyroxene (see fig 5.3) as fractionating phases. Further, the strong negative correlation with Sc, V, and positive correlation with Cr, Ni, and Co against MgO can be attributed to the fractionation or accumulation of olivine and clinopyroxene. On the other hand, the mafic to intermediate rocks (gabbro, gabbroic diorite, and diorite) show distinct trends and/or clusters defined by the moderate negative correlation of SiO<sub>2</sub>, Al<sub>2</sub>O<sub>3</sub>, Na<sub>2</sub>O+K<sub>2</sub>O against MgO, while CaO, Cr, Ni and Sc correlate positively, which probably controlled by fractionation of plagioclase, clinopyroxene and amphibole. These two trends on the Harker's binary diagrams signify that their parental magmas originated by different degrees of partial melting at variable depths in the mantle. Both the magmas evolved independently with a point of inflection at MgO

at ~12 wt%. This differentiation trend is also observed by the progressive increase in the contents of Zr, total REE with the decrease of MgO in both ultramafic rocks as well as gabbro to diorite.

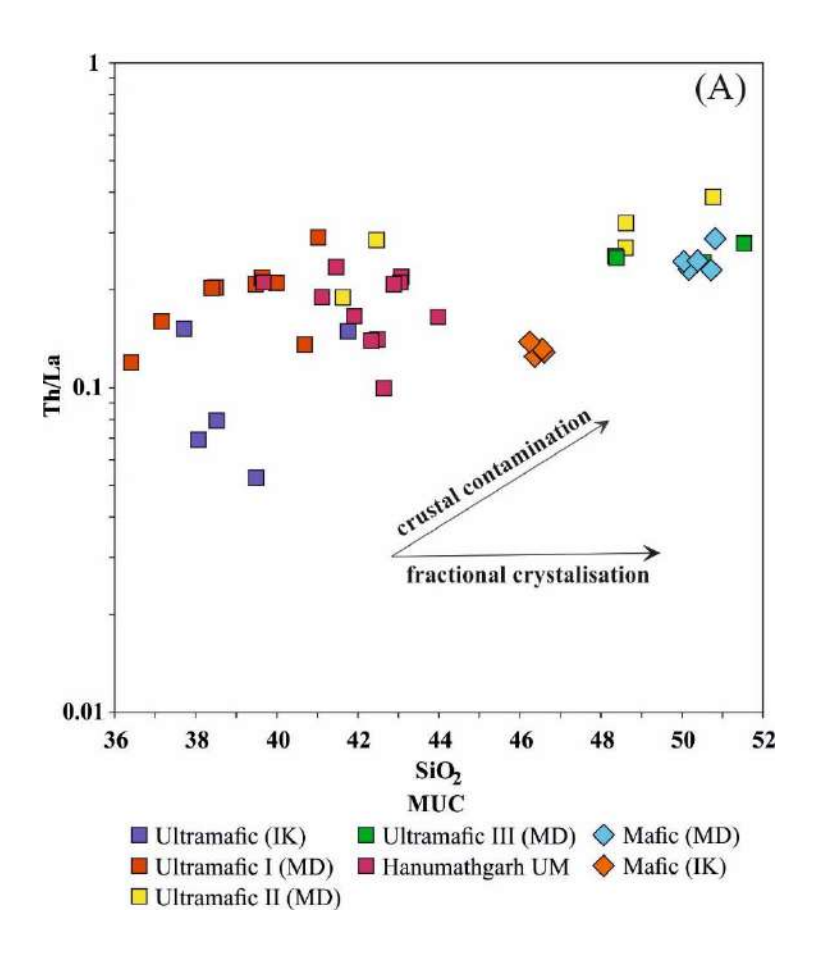


**Figure 6.3** SiO<sub>2</sub> versus Th/La indicating fractional crystallization of the ultramafic mafic of the MUC.

The "chondrite normalized REE patterns" show variable trends but all display flat to slight "light rare earth element (LREE)" enrichment with nearly flat "heavy rare earth element (HREE)" pattern (See figure 5.4-5.7.). The value of ∑REE [6.67 to 127.44 ppm] increases as MgO decreases in the sequence peridotite, olivine pyroxenite, pyroxenite as well as hornblende gabbro, gabbroic diorite, and diorite rocks. The peridotite (group-I) bears the lowest REE content (<10 ppm). The olivine pyroxenite and pyroxenite (group-II) have REE concentrations that range from 12-20 ppm with

flat HREE patterns. Such an increase in total REE content suggests the fractionation of REE into residual liquids during the course of fractional crystallization. The slight increase of REE from (16.27 to 127.44 ppm) in gabbro, gabbroic diorite, and diorite have similar REE patterns with subparallel nature suggesting they evolved through single parental magma which possibly derived from a single source. In addition, in the  $\varepsilon$ Nd (T) versus MgO, Nb/La (see figs. 5.7 c-d), and SiO<sub>2</sub> versus Th/La (see figure 6.1g), of the ultramafic mafic rock studied show more affinity towards the fractionation trends rather than the combined assimilation and fractional crystallization process (AFC). To summarize, the ultramafic-mafic rocks and gabbro-diorite are evolved independently by magmatic differentiation processes mainly through fractional crystallization of parental magmas originated by a variable degree of melting at different depths in the mantle.

## 6.4. Composition of sources and melting processes

Globally the ultramafic magmas (particularly komatiites) are classified into two types depending upon the Al<sub>2</sub>O<sub>3</sub> content such as Aluminum depleted (Barberton type) and Aluminum un-depleted (Munro type) magma (Arndt 2003). The Al-depleted (Barberton type) komatiites are the most common oldest Archean greenstone belts (>3.3 Ga), whereas the Al- un-depleted (Munro type) komatiites commonly found in the Neoarchean greenstone belts (~2.7 Ga) and extending into Proterozoic or even younger ages. The "anhydrous melting of hot mantle sources at various depths is thought to have created both Al-depleted and Al-undepleted komatiites." The deeper mantle melting, which left garnet as a residual phase, is thought to be the cause of the Al-depleted komatiites. At relatively low pressures in shallower mantle, the garnet melts near peridotite solidus and is removed from the residues before melts acquired the ultramafic (komatiites) composition which results in the formation of Al-undepleted komatiites (Arndt, 2003). "Experimental studies have found that, the Al-depleted komatiite magma generated by partial melting of mantle peridotite

at very high pressure (8-14 Gpa) with corresponding depths of about 300-400 km." (Ohtani et al., 1989; Herzberg, 1999). On the other hand, the Al-undepleted komatiites are formed through the high degree of partial melting of peridotitic source at shallower depth of 150-200 km (5-6.5 Gpa), and the younger komatiite formed at low pressure (3-4 Gpa) with depth 100-130 km. The "(CaO/Al<sub>2</sub>O<sub>3</sub>) and (Al<sub>2</sub>O<sub>3</sub>/TiO<sub>2</sub>)" ratios, together with (Gd/Yb)<sub>N</sub> values, have been widely employed by researchers to describe the involvement of the residual or melting phase and to constrain the depth of melting in source mantle reservoirs (Jahn et.al., 1982, Gruau et al., 1992 Alvaro et al., 2014). The high "CaO/Al<sub>2</sub>O<sub>3</sub> (>1.0) and (Gd/Yb)<sub>N</sub> (>1.0) are the indications of garnet involvement as a residual phase, whereas, low CaO/Al<sub>2</sub>O<sub>3</sub> (<1.0) and (Gd/Yb)<sub>N</sub> (<1.0) are the indication of garnet entering into a melt phase." The studied samples show rocks showing the "CaO/Al<sub>2</sub>O<sub>3</sub> ratio (0.5-2.98) and (Gd/Yb)<sub>N</sub> values" (>1, with some samples near one or even less) are explained by different levels of garnet participation in the residual phases and/or garnet involve in the melt phase.

# 6.4.1 Depth of magma generation and temperature of eruption.

The observed geochemical characteristics such as: high MgO (>30%), Ni (2509 to 5321 ppm), Cr (718 to 2455 ppm), and [(Gd/Yb)<sub>N</sub> >1] of the studied ultramafic rocks found that, "magma generation at great depths with retention of garnet in the residue of mantle source during melting process implying a derivation of these ultramafic magmas at depths around 250-300 km." The mafic rocks with intermediate MgO (7-11%), and lower Ni (225-528 ppm, except four sample show anomalously high content of nickel), and Cr (28-244 ppm) suggest that these rocks generated at a shallower depth. A similar study from Dharwar craton ("Jayananda et al., 2008") found that those rocks with low CaO/Al<sub>2</sub>O<sub>3</sub> (<1.0) and high Al<sub>2</sub>O<sub>3</sub>/TiO<sub>2</sub> (>16) ratios and higher content of Zr, Hf, and Y compared to primitive mantle might suggest that these magmas generated at lesser

depth (<250 km) without garnet present in residue. The same interpretation can be drawn from the (La/Sm)n versus (Sm/Yb)n diagram (see figure 6.4 a).

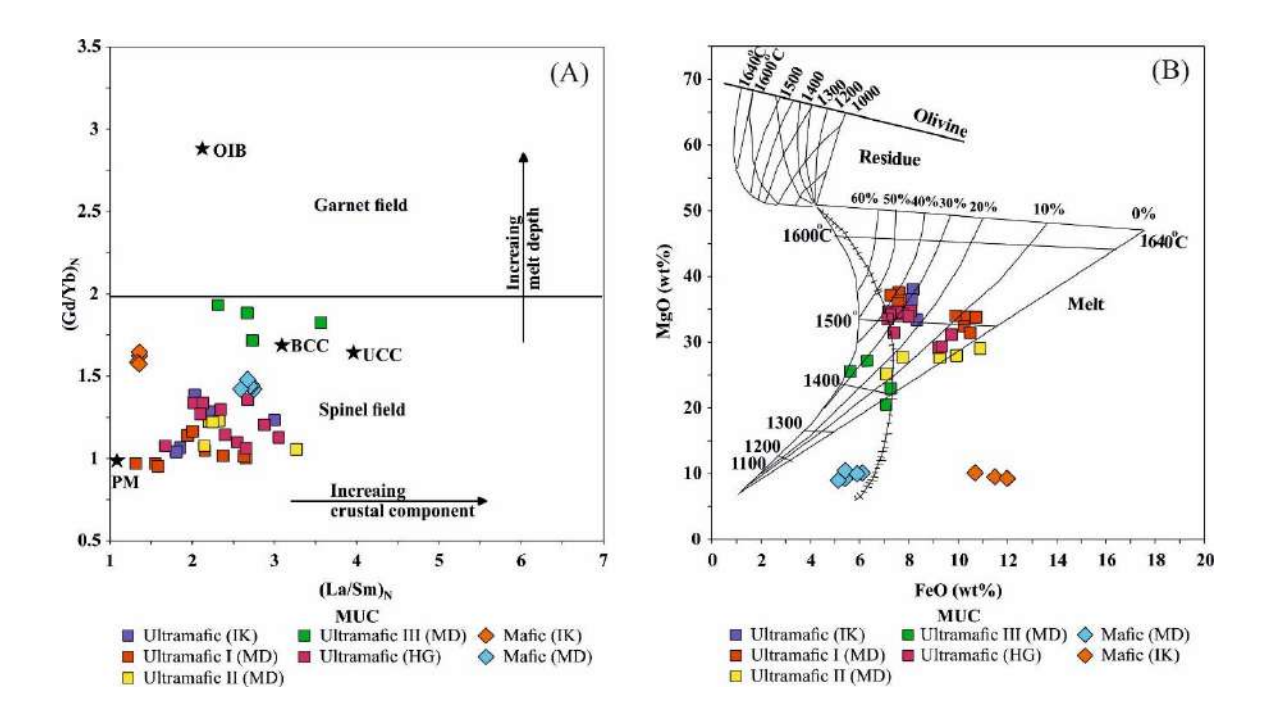


Figure 6.4 (a) (La/Sm)<sub>CN</sub> vs (Gd/Yb)<sub>CN</sub> diagram as a proxy for lithospheric contribution and/or degree of partial melting vs depth of melting. The diagram shows that the melt has generated in both spinel and garnet stability zones with a considerable crustal input. The garnet-spinel stability fields are taken from 'Alvaro et al. (2014). CN, chondrite normalized; PM, primitive mantle; OIB, ocean island basalt (McDonough & Sun, 1989); UC, upper crust; BCC, bulk continental crust (Rudnick & Gao, 2003). (b) MgO (wt.%) versus FeO (wt.%). Fields of partial melts and residue (after Hanson and Langmuir, 1978) of MUC, Bundelkhand Craton.

Using (Roeder and Ernslie, 1970) equations, (Hanson and Langmuir, 1978) simulated partial melting of the mantle, which depends on the "partitioning behaviors of magnesium and iron between olivine and melt and determined the abundance of MgO and FeO in the residual solids and melts. The findings are displayed in the MgO-FeO diagram, which displays a field of melts and residual solids that are both contoured for the amount of partial melting and temperatures." This bivariate figure is used to examine the relationship between the ultramafic and related mafic

rocks as well as to constrain the liquidus temperature and degree of melting. The rocks from the present study projected on the MgO versus FeO bivariate plot (See fig 6.4b), the "ultramafic rocks fall in the liquidus field indicate that these rocks could have been in equilibrium with the surrounding peridotitic upper mantle" while the mafic rocks falling outside the liquidus field and not in equilibrium with peridotitic upper mantle. In addition, the ultramafic rocks show moderate to high degrees of melting (30-50 %) and the temperature ranges from 1440-1550°C, whilst the studied mafic rocks show low degrees of partial melting (10-20 %) with a temperature around 1300°C. Thus, it is more likely the ultramafic and mafic rocks of this study revealed at different depths with varying degrees of partial melting.

#### **6.4.1.1.** Constraints from trace elements

In the present study, the ultramafic rocks show the total REE content ranging from subchondritic (6.67 to 9.89 ppm) to chondritic (10.84 to 15.81 ppm) except a few rock samples show slightly higher total REE (18 to 24 ppm) suggesting their derivation from heterogeneous mantle source reservoirs ranging in composition from highly depleted to primitive mantle compositions. On the other hand, the mafic rocks from this study show a wide range of total REE contents (16.47 to 127.44 ppm), which also implies heterogeneous mantle sources. The anomalies of incompatible elements (Y, Hf and Zr) from primitive mantle normalized (Sun and McDonough, 1989) multi-element diagram gives information about mantle source as well as residual mineralogy ("Jayananda et al., 2016 and references are therein"). The strong negative anomalies of Y, Hf, and Zr from the oldest Archean ultramafic rocks of Barberton, Superior Province, and Western Dharwar have been linked to the magma formation at a large depth (almost 400 km), with garnet (majorite?) in the residues. ("Lahaye et al., 1995; Polat et al., 1999; Jayananda et al., 2008, 2016"). The stability range of "majorite garnet in the mantle peridotite suggests pressure from 12-14 Gpa,

corresponding depths of magma generation below 400 km." ("Miller et al., 1991; Herzberg, 1992; Xie et al., 1993; Fan and Kerrich, 1997"). Consequently, the retention of majorite garnet in residue results in strong negative anomalies of Y, Hf and Zr. The studied ultramafic-mafic rocks from Madawara Ultramafic Complex exhibit negative to flat Hf and Zr anomalies with flat to positive Y anomalies preclude the presence of considerable majorite garnets in the residues. Therefore, it shows that melt may originate from shallower depths (between 300 and 200 km). Further, Niobium (Nb) anomaly from primitive mantle normalized, (Sun and McDonough, 1989) multi-element diagram is used to effectively characterize mantle sources, particularly in distinguishing between plume and arc sources. ("Jochum et al., 1991; Puchtel et al., 1997"). The negative Nb anomaly has been interpreted as either magma generated in shallow depth in an arc setting or it could be crustal contamination ("Polat and Kerrich, 2000") while positive Nb anomaly attributed to the melting of plume source in the deep mantle or it could be related to recycled slab component at great depth ("Kerrich and Xie, 2002). The studied rocks of the Madawara Ultramafic Complex invariably show strong negative Nb-Ta anomalies and negative Zr-Hf anomalies in primitive normalized ("Sun and McDonough, 1989") multi-element diagram attributes to the magma generation relatively deeper depths in arc settings or it could be likely to contributions from recycled subduction derived crust whist few ultramafic samples shows negative Nb-Ta anomalies and positive Y anomalies with variable Zr-Hf anomalies reveals their derivation from shallower sources.

Incompatible element ratios, "such as Nb/Th and Nb/U, are thought to be useful in determining the mantle sources of Archaean ultramafic and mafic rock." ("Condie 2003"). In the Nb/Th and Nb/U diagram, all the ultramafic-mafic shows the fields defined for the primitive mantle to continental crust and subduction-derived component. The low value of Nb/Th may

probably be related to contamination as the studied ultramafic rocks are spatially associated with "older granitoid basement rocks." ("Barth et.al., 2000 Rudnick and Gao, 2003") or arc source (Condie 2003). However, the crustal contamination trend does not seem the only process to account for the observed trends as demonstrated in the plots of (Th/Yb)<sub>PM</sub> versus (Nb/Th)<sub>PM</sub> and Nb/La versus Nb/Th (see figure 6.2 a-b). The LILE (Rb, Th) is mobile in aqueous fluid whilst the HFSE (Nb, Zr) are relatively immobile in aqueous fluid (Turner et al.,1997). The Nb/Zr and Nb/Y elemental ratio will change as a function of source composition whilst the lower Th/Zr and Rb/Y signifies the mantle source will be modified by slab melts and higher Th/Zr and Rb/Y ratio indicate that the magma derived from hydrous fluids that alter mantle sources (Zhou and Zhou 2007). The Nb/Zr versus Th/Zr diagram, suggests that their mantle source is modified by slab melt rather than aqueous fluids (see figure 6.6 b).

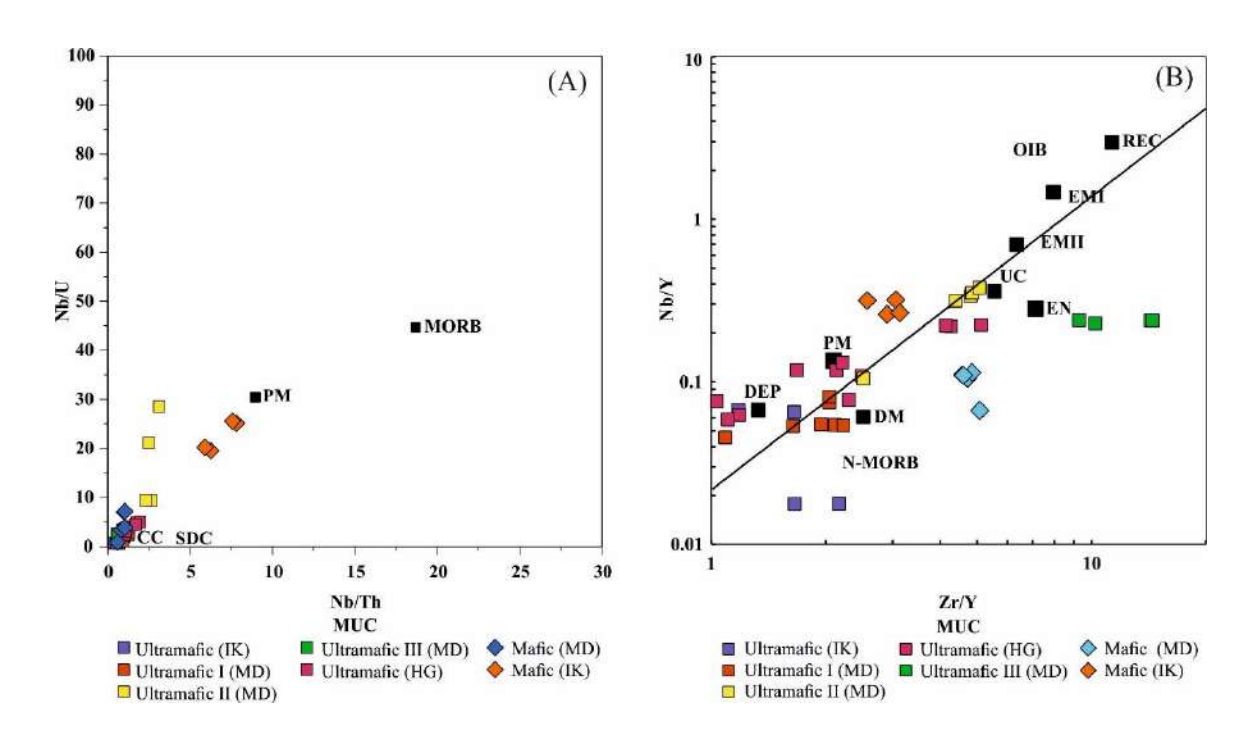


**Figure 6.5** (a) Nb/U versus Nb/Th plot (after Saunders et al., 1988) shows primitive mantle reservoirs with minor crustal contamination for the ultramafic-mafic of MUC. (b) Nb/Y versus Zr/Y (Condie, 2003) plot indicating depleted to primitive mantle source reservoirs for the ultramafic-mafic rocks of MUC.

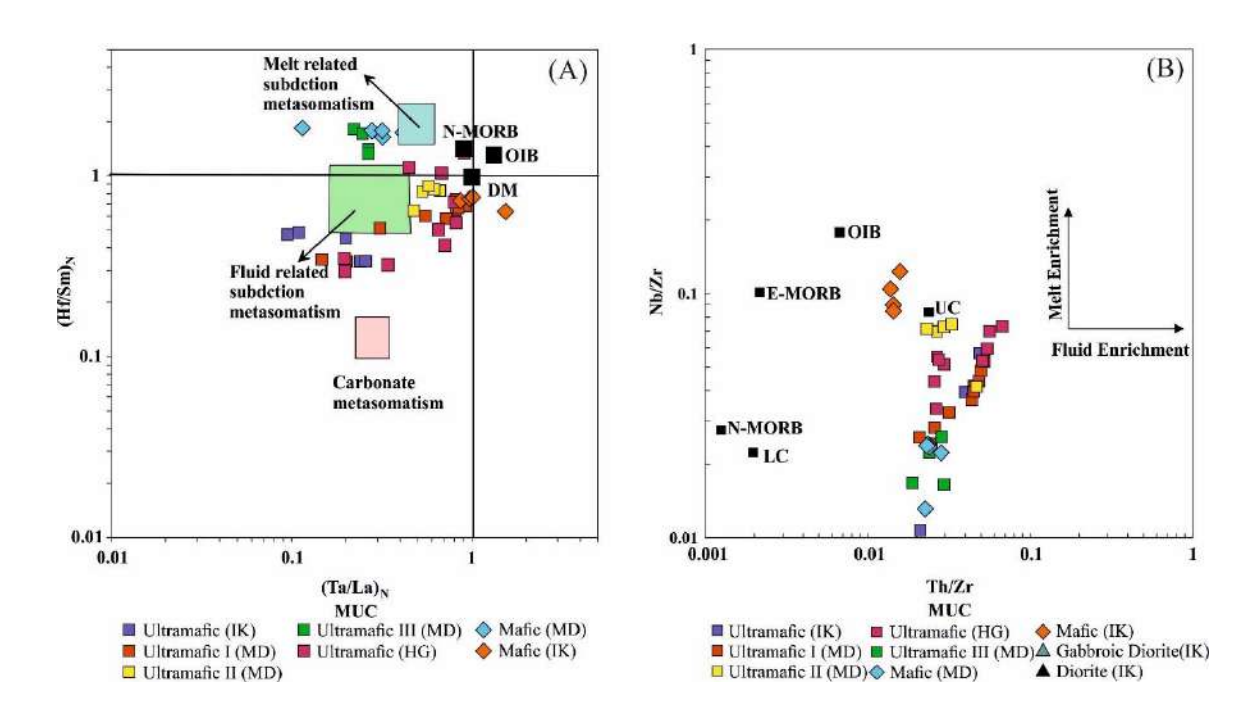


**Figure 6.6** (a) (Ta/La) <sub>PM</sub> versus (Hf/Sm) <sub>PM</sub> (after Laflèche et al., 1998) (b) Th/Zr and Nb/Zr plot for the ultramafic-mafic of MUC.

The Nb/Y and Zr/Y ratios can be employed to differentiate between different mantle source reservoirs and can establish significant constraints on the mantle source as well as tectonic settings, particularly in the discriminating plume and non-plume sources. (Fitton et al. 1997; Baksi 2001). By analysing the Nb/Y and Zr/Y ratios (Chavagnac, 2004.) demonstrated that the ultramafic rocks are generated from a plume-like mantle source and utilised this evidence to refute subduction-related processes and/or crustal contamination as the origin of komatiites. All of the ultramafic-mafic samples that were examined for this study mostly display plume-arc sources on the "Nb/Y and Zr/Y" diagram, with compositions ranging from depleted mantle to primitive mantle (see figure 6.1 b). The Zr/Nb and Nb/Th ratios of oceanic basalts and komatiites of various ages have been utilised for tracing mantle sources ("Condie, 2003"). The majority of the ultramafic-mafic samples in the present study of the MUC display "arc field with a few mafic samples extending PM to the OIB field." (See figure 6.7 b).

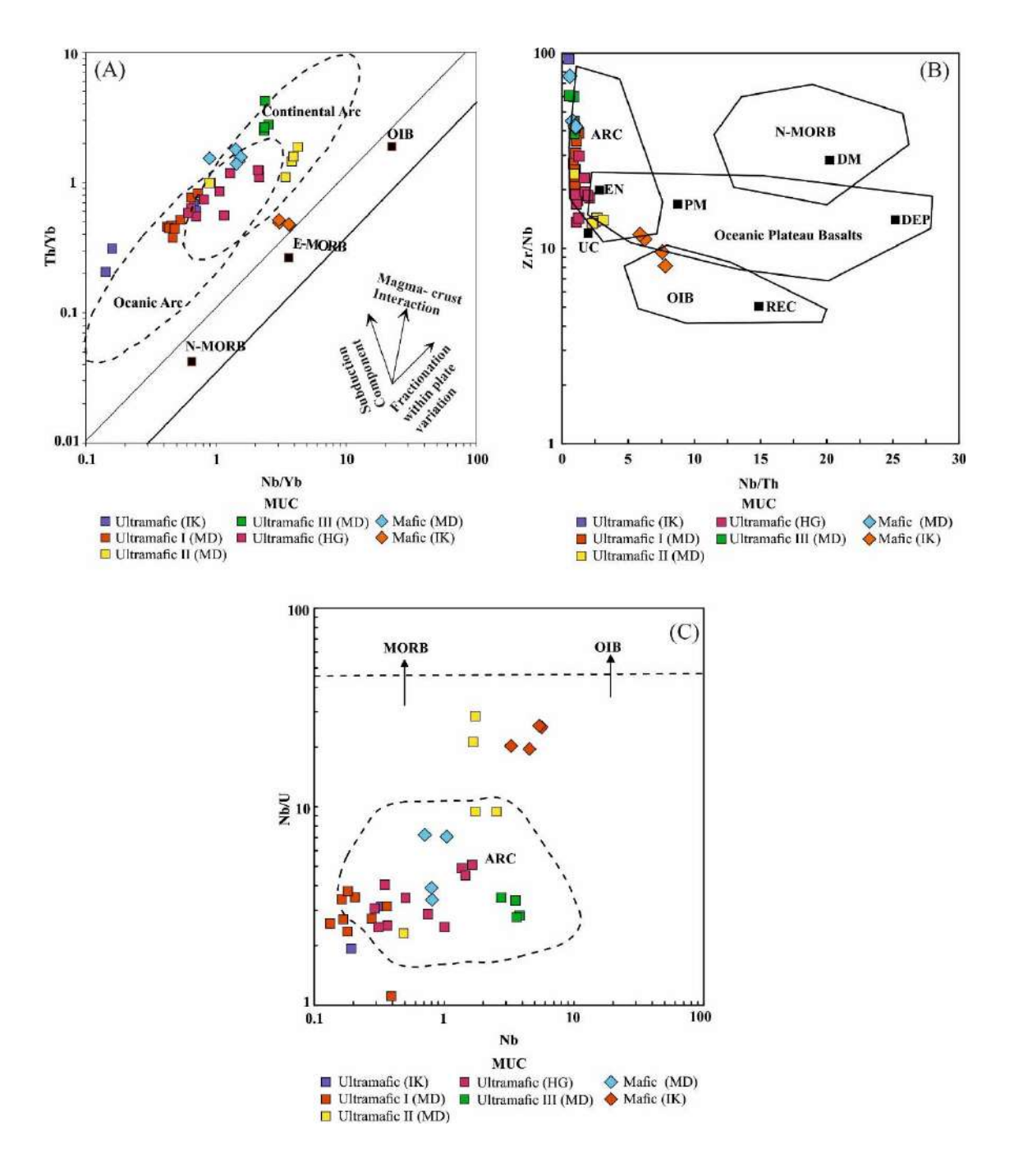


Figure 6.7 (a) Th/Yb versus Nb/Yb binary plot (Pearce, 2008) indicating depleted mantle with arc source reservoirs for the ultramafic-mafic rocks. (b) Zr/Nb versus Nb/Th plot (Condie, 2003) showing arc to the primitive mantle for the ultramafic-mafic rocks of MUC. Abbreviations used: subduction (SUB); PM, primitive mantle; DM, depleted mantle; ARC, arc-related sources; N-MORB, normal ocean ridge basalt; OIB, oceanic island basalt; DEP, deep depleted mantle; EN, enriched component. (c) Plot Nb/U versus Nb showing arc affinity for the ultramafic-mafic of MUC. Data for the primitive mantle and normal mid-oceanic ridge basalt (N-MORB) are from Sun and McDonough (1989); oceanic island basalt (OIB) and island arc basalt (IAB) are from Niu and O'Hara (2003).

Hoffman (1988), suggested that the Nb/U ratio will not change during partial melting and magmatic differentiation and their distribution coefficient remains constant, implying the origin of the sources. The "Nb/U ratio of MORB and OIB is nearly 47 and 50 respectively. The Nb/U ratio of arc volcanic (0.3-9) and net continental crust is ~9.7." (Chung et al., 2001; Rudnick and fountain, 1995, Campbell 2002). If mantle rock is contaminated with crustal material, the Nb/U will be in the range between ~9 and ~50. In the present study, most of the ultramafic of the study area has a lower ratio (0.22-9.47) except a few ultramafic samples from Madawara suggested they are formed in arc sources (see figure 6.7 c).

In summary, incompatible element ratios of ultramafic-mafic rocks shows that "their origin from heterogeneous mantle reservoirs with depleted to primitive mantle signatures with arc source." This is consistent with Nd isotope measurements showing Nd values [ $ENd_{(T)} = -1.37$  to +1.17] indicating depleted to primitive mantle source reservoirs with possible minor crustal contamination.

## 6.5. Origin of Madawara ultramafic-mafic rocks

On Harker's binary diagrams the ultramafic-mafic rocks from Madawara region exhibit moderate to strong correlations with MgO. The moderate to strong correlations are observed in the studied samples between MgO with Al<sub>2</sub>O<sub>3</sub> and CaO, suggesting the removal of olivine and pyroxene as fractionating phases. On the other hand, the positive correlation between MgO with Ni and Cr suggests fractionation of olivine, spinel, and clinopyroxene (see figure 5.1).

The studied ultramafic-mafic rock samples display variations in REE contents ranging from 6.21 to 108.97 ppm, where ultramafic samples display sub-chondritic to chondritic (6.21 to 22.07 ppm) total REE contents, whereas the mafic samples display moderate to high total REE

(16.47 to 108.97 ppm) contents, indicating that they originated from heterogenous mantle sources with compositions "ranging from very depleted to primitive mantle."

The  $(Al_2O_3/TiO_2)$ ,  $(CaO/Al_2O_3)$  ratios, together with  $(Gd/Yb)_N$  (see figure 5.1 a-b) values have been used to decipher the "depth of melting and assess the mineralogy of the residue of the mantle." (Jahn et.al., 1982; Alvaro et al., 2014). The studied ultramafic show low to high values of  $(Gd/Yb)_N$  (0.9-2.0), with low values of  $Al_2O_3/TiO_2$  (12.12-19.46) coupled with low to intermediate values  $CaO/Al_2O_3$  (0.52-2.47) implying that the "absence of garnet in the residue." This is corroborated with flat HREEs patterns in the chondrite normalized diagrams "precluding major garnet influence in the mantle source residue" (see figure 5.5-5.7). The presence of garnet (majorite?) in the residual mineralogy that the ultramafic magma generation at a greater depth in the mantle (> 350 km), whereas the absence of garnet suggests that ultramafic magma generation at a shallow depth (<350km). This is also in agreement with all the ultramafic samples displayed in the spinel peridotite field of the shallow depth in nature.

The studied ultramafic samples of the Madawara regions show negative Nb-Ta and negative Zr-Hf anomalies indicating a shallower to deeper mantle (200-250 km) whilst the mafic samples show negative Nb-Ta with positive Y anomalies, and variable Zr-Hf anomalies suggesting either melt generated at shallow mantle in arc environments or possible contamination by the crustal source during their emplacement (see figure 5.4).

Primitive mantle-normalized trace element concentration ratios, such as (Ta/Th)<sub>PM</sub>, and (Nb/Th)<sub>PM</sub> provide information on the extent of Nb and Ta anomalies, while (Th/Yb)<sub>PM</sub> provides information about crustal contamination. (Wang and Zhou, 2006; Zhang et al., 2009). The ultramafic-mafic rocks from the present study revealed extremely low (Ta/Th)<sub>PM</sub> and (Nb/Th)<sub>PM</sub> values but moderate to substantial (Th/Yb)<sub>PM</sub> values suggest minor degrees of crustal

contamination in comparison to Normal Mid-oceanic Ridge Basal (N-MORB) and Ocean Island Basalt (OIB)(see figure 6.2 a). The crustal contamination trend, however, does not appear to have any chemical affinity with either the upper or the lower continental crustal sources, according to the graphs of (Th/Yb)<sub>PM</sub> versus (Nb/Th)<sub>PM</sub> and Nb/La versus Nb/Th (see figure 6.2 a-b). The ultramafic-mafic rocks' high La/Nb, Ba/Nb, and low La/Ba ratios indicate that they may be linked to materials transported to the subduction zone, which eventually affected the mantle reservoirs, which probably interacted with ascending ultramafic magmas (see figure 6.2 c).

The Nb/U ratios of MORB and OIB, according to Hoffman (1988), are 47±10. According to Sun and McDonough (1995), the MORB and OIB have Nb/U ratios of about 50, whereas the upper continental crust has a ratio of 9. (Rudnick and Fountain, 1995). On the other hand, the arc volcanic rock has a lower ratio of (0.3-9) in comparison to MORB and OIB (Chung et.al. 2001). The Nb/U ratio should be between 9 and 50; if ultramafic rocks are derived from the mantle and subsequently affected by contamination of crustal minerals. Few ultramafic samples (group II) show greater values (>10) attributable to either crustal contamination, however, the majority of the samples from the Madawara ultramafic-mafic rocks show the Nb/U ratio range from 0.88 to 9.47 indicating either an arc source or stemmed from metasomatic mantle. The Zr/Nb and Nb/Th ratios of ultramafic mafic magmas (komatiites and oceanic basalts) of different ages have been used to characterize mantle sources. ("Condie, 2003"). The studied samples plot in the arc sources and extend into primitive mantle (see figure 6.7b). To summarize, the ratios of the incompatible elements reveal that their derivation from shallower arc with moderate to deeper source. This is consistent with the Nd isotopic composition of the present study. The εNd (T=2673 Ma) values varies from [-1.37 to -0.01] except one anomalous value (-3.59) indicate that "their origin from the

depleted mantle source with possible minor older crustal contribution or metasomatized mantle through subduction mechanism."

## 6.6. Origin of Ikauna ultramafic-mafic rocks.

The ultramafic-mafic rocks of the Ikauna region show low CaO/Al<sub>2</sub>O<sub>3</sub> (0.48-1.10), low  $Al_2O_3/TiO_2$  (11.87-17.60) values coupled with low values of [(Gd/Yb)<sub>N</sub> =1.04-1.38] signifies garnet (presence of minor garnet in the residue) and suggest that their derivation from different depths in mantle source whilst the high-Mg intermediate rocks show high values of Al<sub>2</sub>O<sub>3</sub>/TiO<sub>2</sub> (19.35-38.42), low values of CaO/Al<sub>2</sub>O<sub>3</sub> (0.62-0.82) coupled with medium values of (Gd/Yb)<sub>N</sub> (1.57-2.2), precludes significant garnet in the residue and suggest also their derivation from the shallower mantle source (see figure 5.1) The ultramafic-mafic exhibit low to moderate REE contents (6.67-13.50 ppm), (32.40-46.70 ppm) respectively suggesting depleted mantle reservoirs. In contrast, the gabbroic diorite to diorite to rocks show higher REE contents, (Gabbroic diorite=25.67-38.91 ppm, and diorite = 115.58=127.44 ppm) (see figure 5.6). All the ultramaficmafic to intermediate rocks display nearly flat HREE patterns suggesting their derivation from a homogeneous source of primitive to the depleted mantle and evolved through the fractional crystallization process. The strong Nb-Ta anomalies and flat to positive Y anomalies of ultramafic-mafic to intermediate rocks on the primitive mantle normalized multi-element diagrams (Sun and McDonough, 1989) suggest the magma generation at shallower mantle reservoirs with possible contamination of old continental crust. This observation was also substantiated by the Nd isotopic composition of the present study [ENd (T=2673 Ma) values of -3.98 to +1.17, excluding one intermediate sample (+6.78) reveals they are derived from the depleted mantle with possible lesser old crustal contamination. On the Nb/Th vs. Nb/U as well as Nb/Y vs. Zr/Y diagrams, samples are displaying from primitive to depleted mantle signature with arc source and possibly

traces of old continental crust input. Further, on the Zr/Nb versus Nb/Th diagrams, the samples plotted in the arc sources extend into the primitive mantle with three samples plotted in the IOB source. In summary, both incompatible elemental ratio and isotopic ratios of ultramafic-mafic rocks and intermediate rocks of the Ikauna sector indicate their derivation from heterogeneous reservoirs including shallow arc mantle to slightly deeper mantle with variable input through subduction mechanism.

## 6.7 Origin of Hanumathgarh ultramafic rocks:

The ultramafic rocks of the Hanumathgarh show low to high CaO/Al<sub>2</sub>O<sub>3</sub> (0.87-1.32), low values of Al<sub>2</sub>O<sub>3</sub>/TiO<sub>2</sub> (11.73-16.81) coupled with low to high values of (Gd/Yb)<sub>N</sub> (1.06-1.36) suggesting the variable role of garnet (minor residual garnet or absence of garnet in the residue) and suggests that their derivation from relatively shallower to deeper mantle source. The ultramafic rocks exhibit low REE contents (10.35-24.57 ppm) with a nearly flat HREE pattern precluding major garnet influence in the mantle residues. This is also consistent with all ultramafic-mafic samples displayed in the spinel peridotite field of the shallow depth in nature.

On the "primitive mantle normalized multi-element diagram" these ultramafic rocks display negative Nb-Ta with slight positive Y anomalies and variable Zr-Hf anomalies suggesting either melt generated at shallow mantle in arc environments or possible contamination by the crustal source during their emplacement. This observation also substantiated by Nd isotopic composition of the present study [ $\epsilon$ Nd (T=2673 Ma) values of -1.23 to +0.15, reveals their derivation from the depleted mantle with possible minor old crustal contamination. The majority of the samples from the Hanumathgarh ultramafic rocks show the Nb/U ratio range from 0.22 to 5.09 indicating either an arc source or stemmed from metasomatic mantle. On the "Nb/Th versus Nb/U as well as Nb/Y

versus Zr/Y diagrams," samples are falling in between the fields defined for the primitive mantle and arc source. Further, Zr/Nb versus Nb/Th diagrams, the samples plot in the arc sources. In summary, both incompatible elemental ratios and isotopic data of ultramafic rocks of the Hanumathgarh region "suggest that their derivation from shallow depleted arc mantle" with variable input through subduction showing primitive mantle characteristics.

## 6.8. Implication for PGE mineralization

The PGEs are considered potentially useful indicators of partial melting, magmatic differentiation, and sulfide saturation of the parental melt. PGEs occur mainly in ppb to ppm levels in the ultramafic rocks and they are mostly found in the layered intrusion associated with chromites in the form of alloys or sulfides in the peridotites. The IPGEs are more compatible and occur as refractory phases whilst PPGEs are corresponding to relatively incompatible in nature. The IPGEs are frequently associated with chromite as alloys, but the PPGEs are primarily related with sulphides of Fe, Ni, and Cu and are typically occurred in gabbro, norite, and peridotites ("Barnes et al, 1988") The PGEs are both siderophiles as well as chalcophile in nature and their behavior as well as abundance is controlled by several parameters such as partial melting of the mantle, crystal fractionation, mantle heterogeneity, melt percolation and enrichment and depletion process in the mantle (Zhang et al., 2005; Naldrett et al., 2010; Huang et al., 2019; Li et al., 2020). Therefore, PGE geochemistry has been used as an effective tool for mantle-derived ultramafic magine magmas to serve as a geochemical tracer to understand mantle evolution, core-mantle differentiation, and petrogenesis. In addition to their economic importance, the lower concentration of PGE also uses as tectono- magmatic evolution in ultramafic mafic systems (e.g., Basalt, komatiite). Several researchers have reported PGE abundances in rocks generated from the mantle. Understanding the PGE compositions in the mantle using low degree partial melts, such as basalts, is challenging

because these rocks are rich in sulphides that keep PGE in the source and fractionate them during magma ascent and eruption.

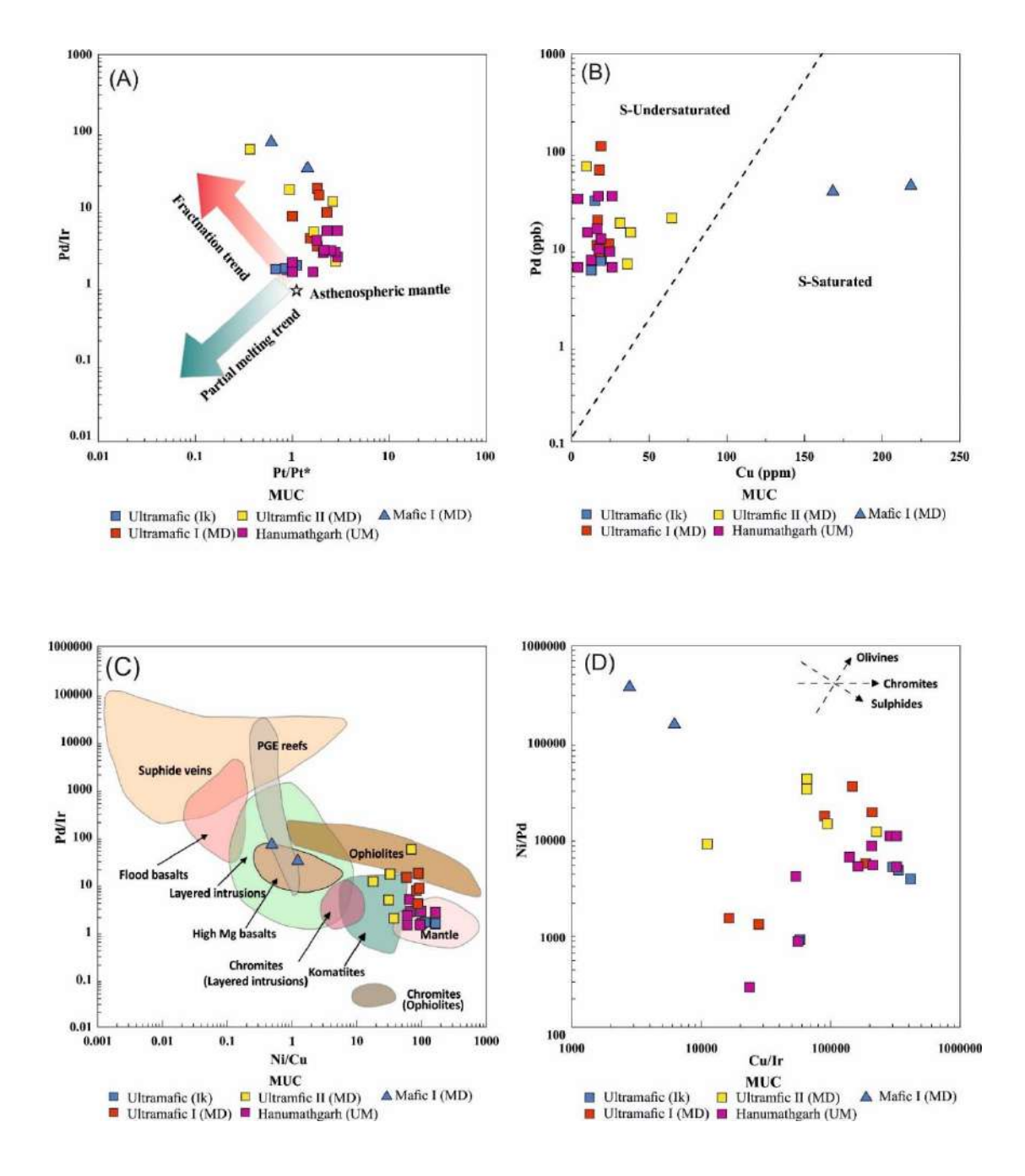


Figure 6.8 (a)  $Pt/Pt*[Pt_N/(Rh_N*Pd_N)1/2]$  versus Pd/Ir of the studied samples showing the role of fractional crystallization. Fractionation and partial melting trends are from Garuti et al. (1997). (b) Cu versus Pd plot indicating sulphur under-saturated nature of the studied samples (after Hoatson & Keays, 1989); (c) Pd/Ir versus Ni/Cu diagram (after Barnes, 1990) in which the studied samples occupying the field of near komatitic field indicating moderate to high degree of partial

melting. (d) Cu/Ir vs. Ni/Pd variation diagram in which the ultramafics showing the olivine and sulphide fractionation trend (after Barnes et al., 1985).

However, the conditions that lead to the formation of komatiites, such as "high partial melting temperatures of hot, dry peridotite, sulphur undersaturation, rapid ascent, minimal differentiation, and contamination before eruption," make it possible to extract significant amounts of compatible elements from the mantle. (Arndt et al., 2003; Barnes et al., 1985). Thus, the siderophile element is trapped by ultramafic magma, which also offers information on the quantity of PGE in the mantle.

The Archean geodynamics preserves a variety of geochemical signatures, including the evolution of the mantle, ancient subduction histories, plume-arc interactions, including various episodes of crustal growth and accretionary histories, hydrothermal activity, mineralization, and precious metal mobilization. The many Archean greenstone belts, as well as several ultramafic mafic intrusive complexes with various geodynamic settings, were formed by the high-temperature differentiation and fractionation process. (e.g., Layered ultramafic-mafic complex, ophiolitic complex, Alaskan type ultramafic complex, post-orogenic extensional complex). These mafic and ultramafic bodies significantly contribute to the generation of orthomagamatic deposits including chromite, titanium vanadiferous magnetite, gold, Ni-Cu sulfides, and PGE deposit. The PGE along with the trace element geochemistry of the ultramafic mafic provide important information on thermal evolution and metallogenic characteristics in the Archean earth.

The ultramafic of the MUC display variable in PGE concentration together with their elemental ration in Madawara, Ikauna and Hanumathgarh region. The observed variations in PGE distribution pattern could be related with the different magmatic processes such as the degree of partial melting, crystal fractionation and sulphide segregation and mantle heterogeneity (Zhang et al., 2005; Naldrett et al., 2010; Saha et al., 2015). The Ir group PGE and Pd group PGE behave

differently due to having different solubilities in the silicate magma. According to Barnes and Picard (1993), the PGE's distribution coefficients during partial melting are "Pd (0.21) < Pt (0.68) < Rh (2.1) < Ru-Os-Ir (6.3) and decrease with a rise in oxygen fugacity." The better compatibility with high melting levels shows that Ir-group PGE is preferable to remain in the refractory phase, like olivine and chrome spinel. As a result of different behavior, the Pd/Ir is used as an index of fractionation of PGE in different magmatic processes. The Pd/Ir ratio increases with the fractionation of the magma. The Pd/Ir (~1) signifies relatively unfractionated material and the ratio increase with the magmatic differentiation/fractionation process, whereas the residual mantle have Pd/Ir(<1) and the ratio decreases with an increase in the degree of partial melting. In the present study, the Index of fractionation Pd/Ir shows varies from relatively unfractionated in Ikauna ultramafic (1.64-1.89) to mildly and slightly fractionated in both Hanumathgarh and Madawara ultramafic (1.55-18.76). The Pd/Ir of group II ultramafics (2.13-59.82) and mafic (33.80-73.59) show high fractionated values suggests the ultramafic -mafic rocks are formed through the magmatic differentiation process. The Pt anomaly (Pt/Pt\*) gives a measure of deviation in reference to the primitive asthenosphere (Pt/Pt\*=1). It significantly varies from positive (Pt/Pt\*>1) to negative (Pt/Pt\*<1) anomaly attributed to different petrological processes. The distinct behavior between the residual mantle and crystal fractionation can be drawn by the Pt/Pt\* versus Pd/Ir diagram. (Garuti et al., 1997). The mantle residues in the form of lherzolite harzburgite and dunite massive define increasing negative Pt-anomalies with decreasing Pd/Ir values in most of the ophiolitic rock. However, mantle rocks formed through crystal fractionation have positive Ptanomalies with respect to the primitive mantle values and define a clear negative trend of Pt/Pt\* with increase in Pd/Ir (See figure 6.8 a). This trend is mostly observed in the Ural-Alaskan type magmatic complex formed due to magmatic fractionation. In the present study, the Pt/Pt\* versus Pd/Ir diagram, the ultramafics mafic shows a magmatic fractionation trend (see figure 5.8 a)

In comparison to Pt and Pd, the Os-Ir-Ru (IPGE) have higher melting points, larger bulk partition coefficients, and exhibit more compatible behaviour during partial melting. According to Mitchell and Keays (1981), PPGE are generally incompatible and preferentially enter the melt phase while IPGE are more likely to be concentrated in the mantle residue. As a result, with low degrees of partial melting, the magma becomes enriched with Pd and Pt, while IPGE concentration rises during high degrees of partial melting. Due to the continuous melting of olivine and PGE alloys, the magma created by a high degree of partial melting has high abundances of Ni and IPGE while the magma formed by a low degree of partial melting contains a relatively higher abundance of Cu and PPGE. Most of the studied ultramafic samples of Ikauna have "high relatively high in Ni and IPGE contents and moderate Cu and PPGE contents, consistent with their generation by the high degree of partial melting devoid of sulphides in the source." On the other hand, the PGE geochemistry of Madawara and Hanumathgarh samples have moderately high PPGE contents and low IPGE contents suggest that, their origin by a relatively low degree of mantle melting in comparison to Ikauna ultramafic rocks. In the present study, the Cu versus Pd diagram, all the ultramafic samples display sulpher undersaturated character (see figure 6.8 b), suggest the mantle melt by the high degree of partial melting. Further, the relatively lower Pd/Ir ratio observed in the ultramafic of Madawara, Ikauna and Hanumathgarh suggest a high degree of partial melting, However, only a few Madawara ultramafic and mafic samples show high Pd/Ir ratios, which point to low partial melting rates that result in the incorporation of interstitial sulphides into the melt phase, yielding PPGE-rich melt (Barnes and Lightfoot, 2005.) Whereas, (Barnes and Fiorentini 2008), demonstrated that the distribution of Ru, Rh and Ir in the form of either PGM or Os-Ir alloy in the olivine and chromite is the responsible concentration of IPGE. (Alard et .al 2000), also suggested that the presence of sulphide included in the silicate phase is marked by high concentrations of Os and Ir which results in the lowering of Pd/Ir ratio. So, silicate hosted in the sulphides is marked by the high degree of partial melting. On the other hand, in a low degree of partial melting, sulphide-bearing melts produce interstitial sulphides through fractional crystallization. As partial melting increases, it is likely that IPGE alloys and silicate-hosted sulphides may melt, resulting in a decreased Pd/Ir ratio (Barnes et al., 1985). In the summary, this observation is consistent with the low Pd/Ir ratio of the majority of the ultramafic samples suggests higher degree of partial melting and few ultramafic and mafic samples have a higher Pd/Ir ratios suggesting a comparatively low degree of partial melting. A high to the low degree of partial melting for the generation of ultramafic mafic magma is corroborated with sulpher undersaturation to saturation of the parental magma. This is also observed in Ni/Cu versus Pd/Ir diagram (See figure, where all the ultramafic samples show high Ni/Cu and Low Pd/Ir ratio displayed near the mantle field (See figure 6.8c). In the Cu/Ir and Ni/Pd diagram showing olivine fractionation trend. (See figure 6.8 d)

The PGE concentration in the "primitive upper mantle is characterized by 3.9±0.5 Os, 3.5±0.4 ppb Ir, 7.0±0.9 ppb Ru, 7.6±1.3 ppb Pt, 7.1±1.3 ppb Pd (Becker et al., 2006). The samples with higher IPGE and lower PPGE correspond to the high degree of partial melting while the samples with high PPGE and low IPGE signify the low degree of partial melting. In the present study, the ultramafic shows variable enrichment with respect to the primitive mantle values suggest mantle heterogeneity with high to moderate degree of partial melting of the mantle.

In this chapter I found that, the ultramafic rocks show moderate to high content PGE content while the mafic rocks have low PGE content. Further, the low Pd/Ir ratio with a high degree of parental melting of the Ikauna ultramafics suggest the presence of PGE in the form of alloys within the olivine or chromite. However, the ultramafic of the Madawara showed relatively higher Pd/Ir ratio with lower degree partial melting attributed to the PPGE enrichment melt phase in the form of interstitial sulphides which is corroborated with the petrographic studies.

## **CHAPTER-VII**

# **Discussion and Conclusion**

In this chapter, an attempt has been made to integrate the results of field, petrographic, elemental, and isotope data along with the published data to address the ultramafic-mafic magmatism and its spatial relation with the adjoining basement/greenstone belt and tectonic context of the ultramafic-mafic magmatism.

# 7.1. Time relationship of Ultramafic-mafic magmatism with an adjoining basement

The Bundelkhand craton has episodic accretion and crustal growth, according to published U-Pb zircon dates, in combination with Nd and Hf isotope studies of basement TTG granitoids, and greenstone sequences. The U-Pb zircon ages indicate that the "first accretion event took place at around 3.5 Ga TTG in the central block of the Bundelkhand craton." However, the oldest xenocryst zircon indicates 3.59 Ga and 3.95 Ga TTG according to the Zr-Hf two-stage model ages, showing that the crust formation goes back to Eoarchean. (Saha et al., 2011; Kaur et al., 2016; Joshi et al., 2016). The zircon & Hf(t) value indicates near chondritic to slightly negative, which suggests that 3.55Ga TTG was likely created by the melting of oceanic crust that came from a depleted mantle source at around 3.95Ga (Kaur et al., 2016). The crustal accretion episodes reported from the central and southern cratonic blocks of the Bundelkhand craton connected to the considerably younger age of 3.4-3.2 Ga TTG. ("Mondal et al., 2002; Saha et al., 2011; Kaur et al., 2016; Singh et.al., 2019"). The 3.4-3.2 Ga TTG formed by melting of the depleted mantle source in conjunction with plume-related tectonic settings shows the &Nd(t) value between 0.53 to

1.96 [near chondritic to positive] (Joshi et al., 2022). However, the majority of researchers reported that this "Paleoarchean TTGs (3.4–3.2 Ga) origin may have been generated by the melting of mafic crust at varying depths in subduction zone tectonic settings" (Chauhan et al., 2018; Singh et al., 2021). It is further substantiated by the presence of both low and high HREE TTG leads to the possibility that it was generated by melting at different depths of the sources. According to Kaur et al. (2016), "rather than juvenile sources, the Paleoarchean TTG is the product of the reworking of an older Eoarchean mafic crust." According to Verma et al., (2016), a more recent episode of TTG-type granitoid formation was recorded at 2669±7.4 Ma in the central sector of the Bundelkhand craton. This suggests that the Bundelkhand craton experienced Neoarchean TTG accretion.

The greenstone of the central block contains earlier ultramafic-mafic-felsic assemblages along with metasediments (BIF) and late felsic assemblages (Singh and Slabunov 2016). However, the greenstone belt of the southern block contains metavolcanic along with BIF-dominated rocks (Sing and Slabunov, 2018, Hiloidari et al., 2021). Early ultramafic-mafic volcanism in the (CBGB) produced an Sm-Nd isochron age of around 3.4 Ga and \(\epsilon\) Nd(T) shows values close to chondrite to highly positive. It reveals that the genesis of ultramafic mafic rocks is from a depleted mantle reservoir ("Malviya et al., 2006; Singh et al., 2019"). The geochemical signature of these ultramafic mafic volcanic shows island arc settings for their formation (Malviya et al., 2006). In summary, the ultramafic mafic magmatism of the (CBGB) is contemporaneous with the accreted Paleoarchean TTG. It endorses that the Paleoarchean ultramafic mafic volcanism and felsic plutonism are coeval in nature. From the above discussion, it is pointed out that, the 3.4-3.2 Ga could be a major outburst of crust accretion both in the central part as well as the southern Bundelkhand craton (Kaur et al, 2014; 2016). Early felsic assemblages of the (CBGB) yielded U-

Pb zircon ages of 2.81 Ga, while late felsic assemblages yielded 2.56 Ga. It supports two episodes of felsic volcanism that took place between the Mesoarchean and Neoarchean periods (Singh and Slabunov, 2016). According to geochemical and isotopic analyses of felsic volcanism, "central Bundelkhand may have undergone two subduction-accretion events, one in the Mesoarchean (2.81-2.71 Ga) and the other in the Neoarchean (2.56-2.53 Ga) age." (Singh and Slabunov et al., 2015b; Slabunov and Singh et al., 2019; 2021). The initiation of the subduction processes may have been reflected in the earlier felsic volcanic phase, which dates back to 2.8 Ga, and the closure of the subduction process may have been reflected in the later felsic volcanic phase, which dates back to 2.56 Ga. ("Singh and Slabunov, 2018"). The Mesoarchean event is indicated by the presence of BIF of the central block of the Bundelkhand, which is thought to have formed after early ultramafic mafic volcanism is considered to have been deposited at around 2.8 Ga. (Singh and Slabunov 2013;2015).

The (SBGB) comprises of mainly quartzite, BIF along with metavolcanic rock. The Sm-Nd isotopic study of the BIF reveals both mantle and crustal sources displayed by quartz and Fe-rich bands respectively (Alfmova et al., 2019). These metavolcanic rocks are well-exposed in Khurrat, Badwar, and Girar areas. In a recent study, Sm-Nd whole rock isochron for the metavolcanic of SBGB yielded 2986±190 Ma (MSWD=2.0) (Hiloidari et al., 2021). The geochemistry and isotopic study of meta basalts reveal that they formed from depleted mantle sources with signatures of back-arc basin basalt (BABB). (Hiloidari et al., 2021). The presence of the detrital zircon in the quartzite provides U-Pb zircon ages close to 3.2 to 3.4 Ga suggests the existence of older TTG-type granitoid in the southern Bundelkhand. ("Singh and Slabunov 2016").

In the present study, the (MUC) shows an intrusive relationship with TTG type granitoid and Sm-Nd whole rock isochron on ultramafic rocks define an imprecise age 2673±200 Ma

(MSWD=1.5). The obtained age is much younger than the nearby metavolcanic rocks of greenstone assemblages (2986±190 Ma) in the SBGB. Therefore, it appears the studied Madawara ultramafic-mafic complex is not part of the greenstone sequences in the southern Bundelkhand craton and they probably originated by independent petrogenetic processes through mantle differentiation.

## 7.2 Implications for mantle evolution and crustal growth

The ultramafic-mafic magmatism during Archean contributes significantly to our understanding of integrated mantle evolution and crustal growth through time ("Polat and Kerrich, 2000; Singh et al., 2019; Jayananda et al., 2008, 2016, 2023"). The incompatible elements and "Nd-Hf isotope data of Archean ultramafic-mafic magmatism in the greenstone belts indicate that the mantle reservoirs from which these magmas originated were already depleted." Such depleted mantle reservoirs were created as a result of the earlier extraction of magma from the deep mantle, which led to an early crust-forming event that may have occurred in the Eoarchean or may have been connected to the worldwide differentiation of silicate earth around 4.5 Ga. (Blichert-Toft and Arndt, 1999; Polat et al., 2000; Kerrich and Xie, 2002; Condie, 2003; Chavagnac; Mole; 2015; Singh; 2019; Jayananda et al., 2023). The long-term depletion of the mantle reservoir and complimentary accretion with the growth of the continental crust is determined by using Nb/U and Th/U elemental ratio. The ratio of Th/U and Nb/U with reference to the primitive mantle is 4.05 and 34 respectively. The separation of the continental crust from the mantle reveals a major change in the Nb/U ratio without affecting the Nb/Th ratio, whereas the removal of the N-MORB (depleted mantle) caused a change in the Th/U ratio without affecting the Nb/U ratio (Campbell 2002) As a result, this ratio can be utilised to interpret mantle evolution beneath both the oceanic as well as continental crusts. The ultramafic-mafic rocks from the CBGB have Nd isotope data [εNd(T=3435)=0.24to9.09] that range from primitive to dominantly depleted mantle sources, whereas the SBGB have Nd isotope data [εNd(T=2986)=-0.37 to7.58] that show depleted mantle signatures with possible trace amounts of contamination. (Singh et al., 2019; Hiloidari et al., 2021). Such depleted mantle reservoirs indicate that the mantle has differentiated into an earlier crust formation event in the form of oceanic plateaus. As a result, the elemental composition and isotopic ratio of the ultramafic mafic in Bundelkhand demonstrate the depletion of both shallow and deep mantle sources.

The incompatible elemental ratios in the present investigation "(Nb/U, Nb/Th, Zr/Nb, Nb/Yb, and Th/Yb)" combined with "sub chondritic to moderate REE concentrations" [6-12 ppm (ultramafic) to 38-127 ppm (mafic rocks)] reveal that these magmas originated from the dominantly depleted mantle reservoirs with minor involvement of primitive mantle reservoirs. This is consistent with the observed Nd isotope data (indicate  $\varepsilon$ Nd (T=2673Ma) =-1.17 to +1.37) of ultramafic- mafic rocks. The prevalence of such dominant depleted mantle reservoirs (ca. 2700 Ma) implies an earlier phase of extraction of the ultramafic magmas possibly during 3300-3000 Ma.

The Bundelkhand craton exhibits five episodes of felsic crust formation and crustal growth that took place during approximately "3.55 Ga, 3.44Ga, 3.3Ga, 3.2Ga, and 2.71-2.68 Ga." (Joshi et al., 2022). The TTGs and transitional TTG ages in the central Dharwar craton are comparable to these ages (Jayananda et al., 2018, 2019b). This implies major episodes of felsic magmatism of the TTG type, which indicate the rapid rates of continental growth during Archean. This is supported by Nd isotopic data  $[\varepsilon Nd(T) = 0.53$  to 1.96] for Paleoarchean TTG-type granitoids, which suggests the presence of a depleted upper mantle with or without minimal inputs from the pre-existing crust. Conversely, Nd isotope data  $[\varepsilon Nd(T) = 0.36$  to -2.61] for Neoarchean TTG-type

granitoids indicate the depleted mantle with a minor crustal input signature (Joshi et al., 2022). In Paleoarchean TTG-type granitoids, (Singh et al., 2021) have reported that Hf isotopic evidence [EHf(T) =4.3 to -4.6] that reveals the existence of a "depleted upper mantle with minimal inputs from the pre-existing crust." In conclusion, the aforementioned justifications imply that the Paleoarchean mantle was "heterogeneous but generally variably depleted". The central and southern greenstone belts, as well as the surrounding TTG-type granitoid basement and the ultramafic and mafic of the MUC are invaded by the 2.57–2.52 Ga high K–granitoids (sanukitoids and anatectic granites), which most likely represent the culmination of major accretion and stabilization of the Bundelkhand craton. Sanukitoids (2.57-2.55 Ga) are abundant both in incompatible and compatible elements and their  $\varepsilon Nd$  (T)=-1.0 to -3.0 indicates they may have formed from the metasomatized mantle through fluid flux derived from the crust (Singh et al., 2021; Joshi et al., 2022). These mantle reservoirs could have developed by prolonged depletion and subsequent enrichment, either through sedimentation or fluid flux derived from the crust in the subduction zone (Joshi et al., 2017, 2022). The "high-K anatectic granites (2.57-2.52)," which were created by the melting of intermediate to felsic crust indicates that they were created through partial melting or reworking of an earlier TTG source in a collision setting ("Joshi et al., 2017, 2022"). The U-Pb zircon ages show that sanukitoids and high-K anatectic granites were formed simultaneously ("Joshi et al., 2022"). The cratonisation of the Bundelkhand craton marked by the emplacement of hot juvenile sanukitoids magmas, which reworked the pre-existing continental crust and produced the high-K anatectic granites.

The above line of arguments based on Nd isotope data of TTGs, greenstone volcanics, sanukitoids, and present studied Madawara ultramafic-mafic complex reveal "long-term depletion of mantle reservoirs suggesting large-scale differentiation of mantle and continental growth during

ca. 3.5-2.7 Ga in the Bundelkhand craton." The Dharwar craton has been shown to have similarly depleted mantle reservoirs and rapid continental growth (Jayananda et al., 2008, 2020, and 2023).

## 7.3 Tectonic context of ultramafic-mafic magmatism

"Although numerous studies have addressed the tectonic context of the formation of the Archean crust, it still remains the subject of much discussion and debated topic in solid earth sciences ("Polat et al., 2002; Bedard, 2018; Wyman, 2018; Kusky et al., 2018, 2021; Nutman et al., 2021; Windley et al., 2021; Jayananda et al., 2023"). The "thermal and dynamic state of the mantle" in particular convection patterns, controlled the tectonics in the Archean Earth to a large extent (Monteux et al., 2020; Jayananda et al., 2023). Most commonly, the Archean cratons are distinguished from the post-archean collisional orogens by the presence of distinctive lithological assemblages that include ultramafic-mafic rocks with komatiite-komatiitic basalt affinity and associated TTG-type granitoids, which point to the particular tectonic processes operated during the Archean. To explain the formation of ultramafic magmas, in the Archean cratons elsewhere in the globe has been explained by two end-member models that predominantly include vertical or horizontal tectonics. Many studies have postulated a mantle plume model ("Ohtani et al., 1989; Arndt 2003") in which ultramafic magma with komatiite affinity erupted in either a plume-related intraplate environment ("Lahaye et al., 1995; Herzberg, 1999") or plume-derived oceanic basalt in the form of plateaus. ("Condie and Abbott 1999; Kerr et al., 2000; Polat and Kerrich 2000; Chavagnac 2004; Jayananda et al., 2008, 2013, 2016, 2023"). However, few workers suggested the formation and emplacement of komatiite magmas Barberton greenstone belt formed in an arc tectonic setting (Grove et al.,1999 Parman et al., 2001). On the other hand, De Wit et al. 1987 linked the formation and eruption of komatiite magma to the "divergent setting of an oceanic spreading centre." A very similar type of tectonic setting also operated in the Bundelkhand craton.

Likewise, the formation of the greenstone belt of the central and southern Bundelkhand craton is also related to subduction-related tectonic settings (Singh et al., 2019; Hiloidari et al., 2021).

The tectonic context of the magma generation can be strongly inferred from elemental and isotopic data. The elemental composition of magmas produced in subduction-related arc settings differs from that of magmas produced in plume settings. To distinguish between plume and arc-related sources, (Campbell (2002) and Condie, 2003) used elemental abundances like Nb, Ta, Hf, Zr, Y, and Ti as well as their ratios like Nb/Y, Zr/Y, Nb/U and Nb/Th. Magmas produced in arc environments exhibit distinctive depletion of Nb, Ta, and Ti with enrichment in Th, U, Ba, Rb, and Sr, whereas magmas produced in plume environments exhibit severe depletion of Hf, Zr, and Y". In the current study, "low to moderate CaO/Al<sub>2</sub>O<sub>3</sub>, moderate Al<sub>2</sub>O<sub>3</sub>/TiO<sub>2</sub> ratios, strong negative Nb-Ta anomalies, and flat to variable Zr-Hf-Y anomalies on multi-element spider diagrams indicate that the studied ultramafic, mafic, and intermediate rocks originated from an arc mantle source at various depths." (see figure 5.5-5.7). Nb/Y versus Zr/Y and Zr/Nb versus Nb/Th diagrams, which show that all of the examined ultramafic-mafic to intermediate rocks exhibit arcrelated tectonic settings, provide additional support for this claim (see figure 6.7b). Even though elemental abundances and ratios of incompatible trace elements point out towards arc settings, the observed high MgO content (20.05 to 38.05 wt%), compatible elements like Ni (1102 to 2456 ppm), Cr (2509 to 6262 ppm) of these ultramafic rocks require different tectonic scenario to be explained. These ultramafic magmas exhibit sub-chondritic to chondritic total REE content (6.27 to 12.60 ppm) which corresponds to melting at the deeper level of the mantle with a high degree of partial melting (20-50%) with initial temperature ranging from 1400-1500°C (see fig 6.4b). The noted geochemical traits (high MgO, high Ni, high Cr, and sub-chondritic to chondritic total REE) and moderate Pd/Ir ratio combined with strong negative Nb-Ta anomalies could correspond to

abducted mantle material due to back thrusting of the subducting slab under the oceanic lithosphere. Upon the upward movement, decompression melting is initiated due to the sudden lowering of pressure which could give raise to the observed high contents of MgO, Ni, Cr, and very low total REE in the arc-related tectonic settings. Furthermore, the emplacement of abducted mantle component melting the surrounding upper part of the lower crust gives raise to the gabbro, gabbroic-diorite, and diorite in the studied area of Madawara ultramafic-mafic to intermediate complex.

The TTG-type granitoid in the Bundelkhand craton exhibit major four distinct episodes at ca. ~3.55 Ga, ~3.44 Ga, ~3.3 Ga, and ~3.2 Ga which pre-date the formation of the Madawara ultramafic-mafic complex. However, within the analytical error, the occurrence of younger granitoids (2.71-2.68 Ga) corresponds with the genesis of the MUC. Considering the subcontemporaneous nature of the Madawara Ultramafic Complex and surrounding younger TTGs implies their link to a major tectonic event. The younger Neoarchean (2.71-2.68Ga) TTG-type granitoids attributed to the shallow melting of subduction-related island arcs (Verma et al., 2016; Singh et al., 2021; Joshi et al., 2022). In addition, the sanukitoids of the Bundelkhand craton are identified as these rocks formed from an enriched source since they have \( \varepsilon \) Values (-1.6 to -3.6) and EHf(t) values (-15.7 to -3.9) (Halla et al., 2009; Jayananda et al., 2018, 2020; Singh et al., 2021; Joshi et al., 2017, 2022). The εNd(t) values (-3.6 to -8.7) and εHf(t) values (-3.6 to -8.1) of the anatectic granites of the Bundelkhand craton support an origin by partial melting of an earlier continental crust. (Joshi et al., 2017, 2022; Singh et al., 2019b, 2021). In the present study, the age obtained for the MUC is an imprecise whole-rock Sm-Nd (2673±200 Ma, MSWD=2.1) isotope data which is actually post-dating the adjacent southern greenstone belt of southern Bundelkhand craton dated at 2986±190 Ma, MSWD=2.0; (Hiloidari et al., 2021). This greenstone belt is

attributed to having developed in the back-arc setting. On the other hand, the greenstone belt in the central Bundelkhand craton with older "whole rock Sm-Nd isotope age of 3435±161 Ma." (Singh et al., 2019) represents the remnant of oceanic crust possibly accreted in an oceanic convergence setting. The present studied ultramafic unit most likely corresponds to the portion of oceanic crust that has been preserved in an arc setting next to the oldest (ca 3.4-3.2 Ga.) TTG-type crust.

The absence of pillow structure and spinifex textures in the studied ultramafic-mafic rocks together with the absence of sedimentary assemblages preclude that these rocks originated as greenstone assemblages erupted in a marine environment. Also, elemental ratios point against their origin in hotspot environments associated with plumes. Further, their occurrence as massive discontinued large elongated outcrops and association with relatively younger TTGs imply their genetic link to the accretion of younger TTGs and following emplacement of calc-alkaline high K- granitoids. Such rock association in the Neoarchean probably formed in the oceanic arc environments. The above-mentioned time relationships of younger 2.71-2.68 Ga TTGs and ca. 2.67 Ga Madawara Ultramafic complex imply that they are spatially linked to a tectonic setting. The elemental ratios of studied rocks suggest ultramafic-mafic magma generation in the deeper mantle probably related to slab breakoff and fluid input. Alternatively, these ultramafic-mafic magmas may be related to tectonically abducted mantle material through back thrusting in an oceanic arc setting wherein upward moving mantle could be melted through decompression leading to the origin of ultramafic-mafic magmas at different levels. Although with the data presented in this thesis, it is not possible to precisely differentiate between the two mechanisms.

The proposed model involves the subduction of oceanic crust at shallow levels under high geothermal gradients to produce magmas which upon eruption built oceanic island arc crust. The continuation of subduction triggered the melting at a slightly deeper level (about 100 km) followed by the slab break off can yield hot magma which is generally basaltic in nature. Because of their tendency to travel upward and the ponding that results at the island arc crust's base, triggers the arc crust melts at various depths, which in turn generates the parental magmas of the TTG-type granitoids ("Jayananda et al., 2015, 2018, 2023; Singh et al., 2021; Joshi et al., 2022"). Continued subduction may cause back thrusting and abduction of deeper mantle fragments to higher levels, which might have caused decompression melting leading to the formation of ultramafic-mafic magmas and continued down going oceanic slab and eventual break off at great depths (200 Km?) may cause mantle upwelling leading to enrichment of shallow sub-arc mantle and its eventual melt generated "calc-alkaline high-K magmas (sanukitoids) between 2.57-2.52 Ga." ("Singh et al., 2019, Joshi et al., 2022"). Finally, the ""heat flux and fluid associated with the emplacement of hot sanukitoids magmas cause remelting of deeper ancient and newly formed juvenile TTG crust close to 2.5 Ga generated anatectic melts."" ("Slabunov and Singh, 2019; Singh et al., 2019, 2021; Joshi et al., 2017, 2022").

#### 7.4 Conclusions

The findings, which are based on a combination of field, elemental, whole rock geochemistry, including PGE geochemistry, and Nd isotope data of the MUC, are summed up as follows:

- Field relationships reveal that ultramafic-mafic rocks of southern Bundelkhand craton suggests that ultramafic-mafic rocks do not represent eruptions but products of tectonically emplaced materials in oceanic arc settings.
- 2. Textural relationships and elemental chemistry of Cr-spinel (chromite) from the Madawara ultramafic complex reveal their origin from deeper mantle associated with arc environments.

- 3. The whole rocks Sm-Nd isochron define an age of 2673±200 Ma (MSWD=2.1) which is sub-contemporaneous with ca. 2700 Ma TTGs. The Nd isotopic data (εNd = +1.17 to -1.37) indicate that "their origin is from heterogeneous mantle reservoirs (depleted to primitive mantle) with minor crustal contamination."
- 4. Whole rock geochemistry particularly negative Nb-Ta, Zr-Hf anomalies in ultramafic rocks and negative Nb-Ta, coupled positive Y and variable Zr-Hf anomalies in mafic rocks are consistent with their origin from different depths in the mantle and their origin is possibly linked to melting of mantle associated tectonics oceanic arc setting (abduction of mantle fragments following decompression melting and melting of deeper mantle linked to slab breakoff).
- 5. PGE geochemistry in the complex of ultramafic rocks reveals magmatic fractionation processes with increasing Pd/Ir ratios with decreasing Pt anomalies, indicating that their parent magmas originated from high degree partial melting at various mantle depths (100-200 km).

## 7.5 Future scopes

The future work will be mainly focused on the adjoining granitoids of TTG affinity along with least studied volcano sedimentary sequences of greenstone belt of the southern Bundelkhand craton. The integration of surrounding TTG type granitoids, volcano sedimentary unit along with separate phases of ultramafic-mafic intrusive called MUC will help to reconstruct the complete geotectonic evolution of the southern Bundelkhand craton.

#### References

Abbott, D., Drury, R., & Smith, W. H. (1994). Flat to steep transition in subduction style. Geology, 22(10), 937-940.

Adam, J., Rushmer, T., O'Neil, J., & Francis, D. (2012). Hadean greenstones from the Nuvvuagittuq fold belt and the origin of the Earth's early continental crust. Geology, 40(4), 363-366.

Albarède, F. (1998). The growth of continental crust. Tectonophysics, 296(1-2), 1-14.

Alfimova, N., Raza, M. B., Felitsyn, S., Matrenichev, V., Bogomolov, E., Nasipuri, P., ... & Kumar, V. (2019). Isotopic Sm-Nd signatures of Precambrian banded iron formation from the Fennoscandian shield, East-European Platform, and Bundelkhand craton, India. Precambrian Research, 328, 1-8.

Althoff, F., Barbey, P., & Boullier, A. M. (2000). 2.8–3.0 Ga plutonism and deformation in the SE Amazonian craton: the Archaean granitoids of Marajoara (Carajás Mineral Province, Brazil). Precambrian Research, 104(3-4), 187-206.

Anhaeusser, C. R. (2015). Metasomatized and hybrid rocks associated with a Palaeoarchaean layered ultramafic intrusion on the Johannesburg Dome, South Africa. Journal of African Earth Sciences, 102, 203-217.

Arculus, R. J., Lapierre, H., & Jaillard, E. (1999). Geochemical window into subduction and accretion processes: Raspas metamorphic complex, Ecuador. Geology, 27(6), 547-550.

Arndt, N. (2003). Komatiites, kimberlites, and boninites. Journal of Geophysical Research: Solid Earth, 108(B6).

Arndt, N. (2003). Komatiites, kimberlites, and boninites. Journal of Geophysical Research: Solid Earth, 108(B6).

Arndt, N. T. (1994). Archean komatiites. In Developments in Precambrian geology (Vol. 11, pp. 11-44). Elsevier.

Arth, J. G., & Hanson, G. N. (1975). Geochemistry and origin of the early Precambrian crust of northeastern Minnesota. Geochimica et Cosmochimica Acta, 39(3), 325-362.

Bagai, Z., Armstrong, R., & Kampunzu, A. B. (2002). U–Pb single zircon geochronology of granitoids in the Vumba granite–greenstone terrain (NE Botswana):: Implications for the evolution of the Archaean Zimbabwe craton. Precambrian Research, 118(3-4), 149-168.

Balakrishnan, S., & Rajamani, V. (1987). Geochemistry and petrogenesis of granitoids around the Kolar Schist Belt, south India: constraints for the evolution of the crust in the Kolar area. The Journal of Geology, 95(2), 219-240.

Balaram, V., Singh, S. P., Satyanarayanan, M., & Anjaiah, K. V. (2013). Platinum group elements geochemistry of ultramafic and associated rocks from Pindar in Madawara Igneous Complex, Bundelkhand massif, central India. Journal of earth system science, 122(1), 79-91.

Ballhaus, C., Berry, R. F., & Green, D. H. (1990). Oxygen fugacity controls in the Earth's upper mantle. Nature, 348(6300), 437-440.

Barker, F. (1979). Trondhjemite: definition, environment and hypotheses of origin. In Developments in petrology (Vol. 6, pp. 1-12). Elsevier.

Barnes, S. J., & Roeder, P. L. (2001). The range of spinel compositions in terrestrial mafic and ultramafic rocks. Journal of petrology, 42(12), 2279-2302.

Barton, M. D., Ilchik, R. P., & Marikos, M. A. (1991). Metasomatism. Reviews in Mineralogy and Geochemistry, 26(1), 321-349.

Basu, A. K. (2007). Role of the Bundelkhand Granite Massif and the Son-Narmada megafault in Precambrian crustal evolution and tectonism in Central and Western India. Journal-Geological Society of India, 70(5), 745.

Beard, J. S. (1986). Characteristic mineralogy of arc-related cumulate gabbros: implications for the tectonic setting of gabbroic plutons and for andesite genesis. Geology, 14(10), 848-851.

Bédard, J. H. (2018). Stagnant lids and mantle overturns: Implications for Archaean tectonics, magmagenesis, crustal growth, mantle evolution, and the start of plate tectonics. Geoscience Frontiers, 9(1), 19-49.

Bhatt, S. C., Singh, V. K., & Hussain, A. (2011). Implications of shear indicators for tectonic evolution of Mauranipur shear zone, Bundelkhand craton, central India. Singh and Chandra) 2nd Proc. of Precambrian Continental Growth and Tectonism, Angel Publiation, New Delhi, 36-49.

Bhattacharya, A. R., & Singh, S. P. (2013). Proterozoic crustal scale shearing in the Bundelkhand massif with special reference to quartz reefs. Journal of the Geological Society of India, 82(5), 474-484.

Bowring, S. A., Williams, I. S., & Compston, W. (1989). 3.96 Ga gneisses from the slave province, Northwest Territories, Canada. Geology, 17(11), 971-975.

Cawood, P. A., Kröner, A., Collins, W. J., Kusky, T. M., Mooney, W. D., & Windley, B. F. (2009). Accretionary orogens through Earth history. Geological Society, London, Special Publications, 318(1), 1-36.

Chaudhuri, T., Wan, Y., Mazumder, R., Ma, M., & Liu, D. (2018). Evidence of enriched, Hadean mantle reservoir from 4.2-4.0 Ga zircon xenocrysts from Paleoarchean TTGs of the Singhbhum Craton, Eastern India. Scientific reports, 8(1), 1-12.

Chavagnac, V. (2004). A geochemical and Nd isotopic study of Barberton komatiites (South Africa): implication for the Archean mantle. Lithos, 75(3-4), 253-281.

Chavagnac, V. (2004). A geochemical and Nd isotopic study of Barberton komatiites (South Africa): implication for the Archean mantle. Lithos, 75(3-4), 253-281.

Chen, B., Suzuki, K., Tian, W., Jahn, B. M., & Ireland, T. (2009). Geochemistry and Os–Nd–Sr isotopes of the Gaositai Alaskan-type ultramafic complex from the northern North China craton: implications for mantle–crust interaction. Contributions to Mineralogy and Petrology, 158(5), 683-702.

Choukroune, P., Ludden, J. N., Chardon, D., Calvert, A. J., & Bouhallier, H. (1997). Archaean crustal growth and tectonic processes: a comparison of the Superior Province, Canada and the Dharwar Craton, India. Geological Society, London, Special Publications, 121(1), 63-98.

Condie, K. C. (1981). Archean greenstone belts. Elsevier.

Condie, K. C., Viljoen, M. J., & Kable, E. J. D. (1977). Effects of alteration on element distributions in Archean tholeites from the Barberton greenstone belt, South Africa. Contributions to Mineralogy and Petrology, 64(1), 75-89.

Dale, J., Holland, T., & Powell, R. (2000). Hornblende–garnet–plagioclase thermobarometry: a natural assemblage calibration of the thermodynamics of hornblende. Contributions to Mineralogy and Petrology, 140(3), 353-362.

Dare, S. A., Pearce, J. A., McDonald, I., & Styles, M. T. (2009). Tectonic discrimination of peridotites using fO2–Cr# and Ga–Ti–FeIII systematics in chrome–spinel. Chemical Geology, 261(3-4), 199-216.

De Wit, M. J., de Ronde, C. E., Tredoux, M., Roering, C., Hart, R. J., Armstrong, R. A., ... & Hart, R. A. (1992). Formation of an Archaean continent. Nature, 357(6379), 553-562.

Deb, T., & Bhattacharyya, T. (2022). The evolution of the fracture systems under progressive sinistral shear in the Bundelkhand Craton, Central India: A review and new insights. Earth-Science Reviews, 104238.

DeBari, S. M., & Coleman, R. G. (1989). Examination of the deep levels of an island arc: Evidence from the Tonsina ultramafic-mafic assemblage, Tonsina, Alaska. Journal of Geophysical Research: Solid Earth, 94(B4), 4373-4391.

DePaolo, D. J. (1988). Age dependence of the composition of continental crust: evidence from Nd isotopic variations in granitic rocks. Earth and Planetary Science Letters, 90(3), 263-271.

DePaolo, D. J., & Wasserburg, G. J. (1976). Nd isotopic variations and petrogenetic models. Geophysical Research Letters, 3(5), 249-252.

Dhuime, B., Hawkesworth, C. J., Cawood, P. A., & Storey, C. D. (2012). A change in the geodynamics of continental growth 3 billion years ago. Science, 335(6074), 1334-1336.

Dick, H. J., & Bullen, T. (1984). Chromian spinel as a petrogenetic indicator in abyssal and alpine-type peridotites and spatially associated lavas. Contributions to mineralogy and petrology, 86(1), 54-76.

Eyuboglu, Y., Dilek, Y., Bozkurt, E., Bektas, O., Rojay, B., & Sen, C. (2010). Structure and geochemistry of an Alaskan-type ultramafic—mafic complex in the Eastern Pontides, NE Turkey. Gondwana Research, 18(1), 230-252.

Farooqui, S. A., & Singh, P. K. (2010). PGE mineralisation in ultramafic/mafic enclaves of Ikauna area, Bundelkhand craton, India. In Advances in Geosciences: Volume 20: Solid Earth (SE) (pp. 111-120).

Faure, G. (2013). Origin of igneous rocks: the isotopic evidence. Springer Science & Business Media.

Fleet, M. E., & Barnett, R. L. (1978). Al iv/Al vi partitioning in calciferous amphiboles from the Frood Mine, Sudbury, Ontario. The Canadian Mineralogist, 16(4), 527-532.

Foley, S., Tiepolo, M., & Vannucci, R. (2002). Growth of early continental crust controlled by melting of amphibolite in subduction zones. Nature, 417(6891), 837-840.

Gervilla, F., Padrón-Navarta, J. A., Kerestedjian, T., Sergeeva, I., González-Jiménez, J. M., & Fanlo, I. (2012). Formation of ferrian chromite in podiform chromitites from the Golyamo Kamenyane serpentinite, Eastern Rhodopes, SE Bulgaria: a two-stage process. Contributions to Mineralogy and Petrology, 164(4), 643-657.

Gerya, T. (2014). Precambrian geodynamics: concepts and models. Gondwana Research, 25(2), 442-463.

Giret, A., Bonin, B., & Leger, J. M. (1980). Amphibole compositional trends in oversaturated and undersaturated alkaline plutonic ring-composition. The Canadian Mineralogist, 18(4), 481-495.

Glikson, A. Y. (1979). Early Precambrian tonalite-trondhjemite sialic nuclei. Earth-Science Reviews, 15(1), 1-73.

Gokarn et al. 2013

Groves, D. I., & Santosh, M. (2021). Craton and thick lithosphere margins: The sites of giant mineral deposits and mineral provinces. Gondwana Research, 100, 195-222.

Gruau, G., Tourpin, S., Fourcade, S., & Blais, S. (1992). Loss of isotopic (Nd, O) and chemical (REE) memory during metamorphism of komatiites: new evidence from eastern Finland. Contributions to Mineralogy and Petrology, 112(1), 66-82.

Guice, G. (2019). Origin and geodynamic significance of ultramafic-mafic complexes in the North Atlantic and Kaapvaal Cratons (Doctoral dissertation, Cardiff University).

Guice, G. L., McDonald, I., Hughes, H. S., MacDonald, J. M., Blenkinsop, T. G., Goodenough, K. M., ... & Gooday, R. J. (2018). Re-evaluating ambiguous age relationships in Archean cratons: Implications for the origin of ultramafic-mafic complexes in the Lewisian Gneiss Complex. Precambrian Research, 311, 136-156.

Guitreau, M., Mukasa, S. B., Loudin, L., & Krishnan, S. (2017). New constraints on the early formation of the Western Dharwar Craton (India) from igneous zircon U-Pb and Lu-Hf isotopes. Precambrian Research, 302, 33-49.

Habtoor, A., Ahmed, A. H., & Harbi, H. (2016). Petrogenesis of the Alaskan-type maficultramafic complex in the Makkah quadrangle, western Arabian Shield, Saudi Arabia. Lithos, 263, 33-51.

Halla, J. (2005). Late Archean high-Mg granitoids (sanukitoids) in the southern Karelian domain, eastern Finland: Pb and Nd isotopic constraints on crust— mantle interactions. Lithos, 79(1-2), 161-178.

Helmy, H. M., & El Mahallawi, M. M. (2003). Gabbro Akarem mafic-ultramafic complex, Eastern Desert, Egypt: a Late Precambrian analogue of Alaskan-type complexes. Mineralogy and Petrology, 77(1), 85-108.

- Helmy, H. M., Abd El-Rahman, Y. M., Yoshikawa, M., Shibata, T., Arai, S., Tamura, A., & Kagami, H. (2014). Petrology and Sm–Nd dating of the Genina Gharbia Alaskan-type complex (Egypt): insights into deep levels of Neoproterozoic island arcs. Lithos, 198, 263-280.
- Hey, M. H. (1954). A new review of the chlorites. Mineralogical magazine and journal of the Mineralogical Society, 30(224), 277-292.
- Hiloidari, S., Satyanarayanan, M., Singh, S. P., Bhutani, R., Subramanyam, K. S. V., & Sarma, D. S. (2021). Evidence for Mesoarchean subduction in Southern Bundelkhand Craton, India: Geochemical fingerprints from metavolcanics of Kurrat-Girar-Badwar Greenstone Belt. Geochemistry, 81(3), 125787.
- Himmelberg, G. R., & Loney, R. A. (1995). Characteristics and petrogenesis of Alaskan-type ultramafic-mafic intrusions, southeastern Alaska. US Government Printing Office.
- Huang, X. L., Wilde, S. A., & Zhong, J. W. (2013). Episodic crustal growth in the southern segment of the Trans-North China Orogen across the Archean-Proterozoic boundary. Precambrian Research, 233, 337-357.
- Hurley, P. M., & Rand, J. R. (1969). Pre-Drift Continental Nuclei: Two ancient nuclei appear to have had a peripheral growth and no pre-drift fragmentation and dispersal. Science, 164(3885), 1229-1242.
- Irvine, T. N. (1974). Petrology of the Duke Island ultramafic complex southeastern Alaska.
- Irvine, T. N., & Baragar, W. R. A. (1971). A guide to the chemical classification of the common volcanic rocks. Canadian journal of earth sciences, 8(5), 523-548.
- Isozaki, Y., Aoki, K., Nakama, T., & Yanai, S. (2010). New insight into a subduction-related orogen: A reappraisal of the geotectonic framework and evolution of the Japanese Islands. Gondwana Research, 18(1), 82-105.
- Jacobsen, S. B., & Wasserburg, G. J. (1980). Sm-Nd isotopic evolution of chondrites. Earth and Planetary Science Letters, 50(1), 139-155.
- Jahn, B. M., & Zhang, Z. Q. (1984). Archean granulite gneisses from eastern Hebei Province, China: rare earth geochemistry and tectonic implications. Contributions to Mineralogy and Petrology, 85(3), 224-243.
- Jahn, B. M., Glikson, A. Y., Peucat, J. J., & Hickman, A. H. (1981). REE geochemistry and isotopic data of Archean silicic volcanics and granitoids from the Pilbara Block, Western Australia: implications for the early crustal evolution. Geochimica et Cosmochimica Acta, 45(9), 1633-1652.
- Jayananda, M., Aadhiseshan, K. R., Kusiak, M. A., Wilde, S. A., Sekhamo, K. U., Guitreau, M., ... & Gireesh, R. V. (2020). Multi-stage crustal growth and Neoarchean geodynamics in the Eastern Dharwar Craton, southern India. Gondwana Research, 78, 228-260.
- Jayananda, M., Chardon, D., Peucat, J. J., & Fanning, C. M. (2015). Paleo-to Mesoarchean TTG accretion and continental growth in the western Dharwar craton, Southern India: constraints from SHRIMP U–Pb zircon geochronology, whole-rock geochemistry and Nd–Sr isotopes. Precambrian Research, 268, 295-322.

Jayananda, M., Duraiswami, R. A., Aadhiseshan, K. R., Gireesh, R. V., Prabhakar, B. C., Kafo, K. U., ... & Namratha, R. (2016). Physical volcanology and geochemistry of Palaeoarchaean komatiite lava flows from the western Dharwar craton, southern India: implications for Archaean mantle evolution and crustal growth. International Geology Review, 58(13), 1569-1595.

Jayananda, M., Guitreau, M., Aadhiseshan, K. R., Miyazaki, T., & Chung, S. L. (2022). Origin of the oldest (3600–3200 Ma) cratonic core in the Western Dharwar Craton, Southern India: Implications for evolving tectonics of the Archean Earth. Earth-Science Reviews, 104278.

Jayananda, M., Kano, T., Peucat, J. J., & Channabasappa, S. (2008). 3.35 Ga komatiite volcanism in the western Dharwar craton, southern India: constraints from Nd isotopes and whole-rock geochemistry. Precambrian Research, 162(1-2), 160-179.

Jayananda, M., Martin, H., Peucat, J. J., & Mahabaleswar, B. (1995). Late Archaean crust-mantle interactions: geochemistry of LREE-enriched mantle derived magmas. Example of the Closepet batholith, southern India. Contributions to Mineralogy and Petrology, 119(2), 314-329.

Jayananda, M., Moyen, J. F., Martin, H., Peucat, J. J., Auvray, B., & Mahabaleswar, B. (2000). Late Archaean (2550–2520 Ma) juvenile magmatism in the Eastern Dharwar craton, southern India: constraints from geochronology, Nd–Sr isotopes and whole rock geochemistry. Precambrian Research, 99(3-4), 225-254.

Jayananda, M., Santosh, M., & Aadhiseshan, K. R. (2018). Formation of Archean (3600–2500 Ma) continental crust in the Dharwar Craton, southern India. Earth-Science Reviews, 181, 12-42.

Kamenetsky, V. S., & Kamenetsky, M. B. (2010). Magmatic fluids immiscible with silicate melts: examples from inclusions in phenocrysts and glasses, and implications for magma evolution and metal transport. Geofluids, 10(1-2), 293-311.

Kampunzu, A. B., Tombale, A. R., Zhai, M., Bagai, Z., Majaule, T., & Modisi, M. P. (2003). Major and trace element geochemistry of plutonic rocks from Francistown, NE Botswana: evidence for a Neoarchaean continental active margin in the Zimbabwe craton. Lithos, 71(2-4), 431-460.

Kaur, P., Zeh, A., & Chaudhri, N. (2014). Characterisation and U–Pb–Hf isotope record of the 3.55 Ga felsic crust from the Bundelkhand Craton, northern India. Precambrian Research, 255, 236-244.

Kemp, A. I. S., Hawkesworth, C. J., Paterson, B. A., & Kinny, P. D. (2006). Episodic growth of the Gondwana supercontinent from hafnium and oxygen isotopes in zircon. Nature, 439(7076), 580-583.

Kinny, P. D. (1986). 3820 Ma zircons from a tonalitic Armîsoq gneiss in the Godthåb district of Southern West Greenland. Earth and Planetary Science Letters, 79(3-4), 337-347.

Kraskovski, S. A. (1961). On the thermal field in old shields. Izv Akad Nauk Arm SSR, Geol Geogr Nauki, Engl Transl, 247250.

- Krause, J., Brügmann, G. E., & Pushkarev, E. V. (2011). Chemical composition of spinel from Uralian-Alaskan-type Mafic-Ultramafic complexes and its petrogenetic significance. Contributions to Mineralogy and Petrology, 161(2), 255-273.\
- Kroner, A., Compston, W., Guo-Wei, Z., An-Lin, G., & Todt, W. (1988). Age and tectonic setting of Late Archean greenstone-gneiss terrain in Henan Province, China, as revealed by single-grain zircon dating. Geology, 16(3), 211-215.
- Laurent, O., Martin, H., Moyen, J. F., & Doucelance, R. (2014). The diversity and evolution of late-Archean granitoids: Evidence for the onset of "modern-style" plate tectonics between 3.0 and 2.5 Ga. Lithos, 205, 208-235.
- Leake, B. E., Woolley, A. R., Arps, C. E., Birch, W. D., Gilbert, M. C., Grice, J. D., ... & Youzhi, G. (1997). Nomenclature of amphiboles; report of the Subcommittee on Amphiboles of the International Mineralogical Association Commission on new minerals and mineral names. Mineralogical magazine, 61(405), 295-310.
- Lesnov, F. (2013). Consistent patterns of rare earth element distribution in accessory minerals from rocks of mafic-ultramafic complexes. Open Geosciences, 5(1), 112-173.
- Li, X., Mo, X., Bader, T., Scheltens, M., Yu, X., Dong, G., & Huang, X. (2014). Petrology, geochemistry and geochronology of the magmatic suite from the Jianzha Complex, central China: petrogenesis and geodynamic implications. Journal of Asian Earth Sciences, 95, 164-181.
- Lugmair, G. W., & Marti, K. (1978). Lunar initial 143Nd/144Nd: differential evolution of the lunar crust and mantle. Earth and Planetary Science Letters, 39(3), 349-357.
- Malviya, V. P., Arima, M., Pati, J. K., & Kaneko, Y. (2006). Petrology and geochemistry of metamorphosed basaltic pillow lava and basaltic komatiite in the Mauranipur area: subduction related volcanism in the Archean Bundelkhand craton, Central India. Journal of Mineralogical and Petrological Sciences, 101(4), 199-217.
- Martin, H. (1986). Effect of steeper Archean geothermal gradient on geochemistry of subduction-zone magmas. Geology, 14(9), 753-756.
- Martin, H. (1993). The mechanisms of petrogenesis of the Archaean continental crust—comparison with modern processes. Lithos, 30(3-4), 373-388.
- Martin, H., Smithies, R. H., Rapp, R., Moyen, J. F., & Champion, D. (2005). An overview of adakite, tonalite–trondhjemite–granodiorite (TTG), and sanukitoid: relationships and some implications for crustal evolution. Lithos, 79(1-2), 1-24.
- McCulloch, M. T., & Bennett, V. C. (1994). Progressive growth of the Earth's continental crust and depleted mantle: geochemical constraints. Geochimica et Cosmochimica Acta, 58(21), 4717-4738.
- Michard, A., Gurriet, P., Soudant, M., & Albarede, F. (1985). Nd isotopes in French Phanerozoic shales: external vs. internal aspects of crustal evolution. Geochimica et Cosmochimica Acta, 49(2), 601-610.

- Mole, D. R., Thurston, P. C., Marsh, J. H., Stern, R. A., Ayer, J. A., Martin, L. A. J., & Lu, Y. J. (2021). The formation of Neoarchean continental crust in the south-east Superior Craton by two distinct geodynamic processes. Precambrian Research, 356, 106104.
- Mondal, M. E. A., Goswami, J. N., Deomurari, M. P., & Sharma, K. K. (2002). Ion microprobe 207Pb/206Pb ages of zircons from the Bundelkhand massif, northern India: implications for crustal evolution of the Bundelkhand–Aravalli protocontinent. Precambrian Research, 117(1-2), 85-100.
- Moorbath, S., Taylor, P. N., & Goodwin, R. (1981). Origin of granitic magma by crustal remobilisation: Rb-Sr and Pb/Pb geochronology and isotope geochemistry of the late Archaean Qôrqut Granite Complex of southern West Greenland. Geochimica et Cosmochimica Acta, 45(7), 1051-1060.
- Moyen, J. F., & Martin, H. (2012). Forty years of TTG research. Lithos, 148, 312-336.
- Nisbet, E. G., Cheadle, M. J., Arndt, N. T., & Bickle, M. J. (1993). Constraining the potential temperature of the Archaean mantle: a review of the evidence from komatiites. Lithos, 30(3-4), 291-307.
- Nisbet, E. G., Cheadle, M. J., Arndt, N. T., & Bickle, M. J. (1993). Constraining the potential temperature of the Archaean mantle: a review of the evidence from komatiites. Lithos, 30(3-4), 291-307.
- Nisbet, E. G., Cheadle, M. J., Arndt, N. T., & Bickle, M. J. (1993). Constraining the potential temperature of the Archaean mantle: a review of the evidence from komatiites. Lithos, 30(3-4), 291-307.ence from komatiites. Lithos, 30(3-4), 291-307.
- Nutman, A. P., & Collerson, K. D. (1991). Very early Archean crustal-accretion complexes preserved in the North Atlantic craton. Geology, 19(8), 791-794.
- Nutman, A. P., Wan, Y., Du, L., Friend, C. R., Dong, C., Xie, H., ... & Liu, D. (2011). Multistage late Neoarchaean crustal evolution of the North China Craton, eastern Hebei. Precambrian Research, 189(1-2), 43-65.
- Nyblade, A. A., & Pollack, H. N. (1993). A global analysis of heat flow from Precambrian terrains: implications for the thermal structure of Archean and Proterozoic lithosphere. Journal of Geophysical Research: Solid Earth, 98(B7), 12207-12218.
- Oliveira, F. B. D., Molina, E. C., & Marroig, G. (2009). Paleogeography of the South Atlantic: a route for primates and rodents into the New World?. In South American primates (pp. 55-68). Springer, New York, NY.
- Parkinson, I. J., & Pearce, J. A. (1998). Peridotites from the Izu–Bonin–Mariana forearc (ODP Leg 125): evidence for mantle melting and melt–mantle interaction in a supra-subduction zone setting. Journal of Petrology, 39(9), 1577-1618.
- Pati, J. K. (2020). Evolution of Bundelkhand craton. Episodes Journal of International Geoscience, 43(1), 69-87.

- Pati, J. K., Reimold, W. U., Koeberl, C., & Pati, P. (2008). The Dhala structure, Bundelkhand craton, Central India—eroded remnant of a large Paleoproterozoic impact structure. Meteoritics & Planetary Science, 43(8), 1383-1398.
- Paton, C., Woodhead, J. D., Hellstrom, J. C., Hergt, J. M., Greig, A., & Maas, R. (2010). Improved laser ablation U-Pb zircon geochronology through robust downhole fractionation correction. Geochemistry, Geophysics, Geosystems, 11(3).
- Pettigrew, N. T., & Hattori, K. H. (2006). The Quetico intrusions of western Superior Province: Neo-Archean examples of Alaskan/Ural-type mafic—ultramafic intrusions. Precambrian Research, 149(1-2), 21-42.
- Polat, A. (2012). Growth of Archean continental crust in oceanic island arcs. Geology, 40(4), 383.
- Polat, A., & Hofmann, A. W. (2003). Alteration and geochemical patterns in the 3.7–3.8 Ga Isua greenstone belt, West Greenland. Precambrian Research, 126(3-4), 197-218.
- Polat, A., Kerrich, R., & Wyman, D. A. (1999). Geochemical diversity in oceanic komatiites and basalts from the late Archean Wawa greenstone belts, Superior Province, Canada: trace element and Nd isotope evidence for a heterogeneous mantle. Precambrian Research, 94(3-4), 139-173.
- Potrel, A. (1994). Evolution tectono-métamorphique d'un segment de croûte continentale archéenne. Exemple de l'Amsaga (RI Mauritanie), Dorsale Réguibat (Craton Ouest Africain) (Doctoral dissertation, Université Rennes 1).
- Pradhan, V. R., Meert, J. G., Pandit, M. K., Kamenov, G., & Mondal, M. E. A. (2012). Paleomagnetic and geochronological studies of the mafic dyke swarms of Bundelkhand craton, central India: implications for the tectonic evolution and paleogeographic reconstructions. Precambrian Research, 198, 51-76.
- Putnis, A., & Austrheim, H. (2010). Fluid-induced processes: metasomatism and metamorphism. Geofluids, 10(1-2), 254-269.
- Raczek, I., Stoll, B., Hofmann, A. W., & Peter Jochum, K. (2001). High-Precision Trace Element Data for the USGS Reference Materials BCR-1, BCR-2, BHVO-1, BHVO-2, AGV-1, AGV-2, DTS-1, DTS-2, GSP-1 and GSP-2 by ID-TIMS and MIC-SSMS. Geostandards Newsletter, 25(1), 77-86.
- Radhakrishna, T., Tomson, J. K., Chandra, R., & Ramakrishna, C. (2020). Geochemistry of NW-SE trending Palaeoproterozoic mafic dyke intrusions in the Bundelkhand Craton, India and subcontinental lithospheric mantle processes. Precambrian Research, 351, 105956.
- Ramiz, M. M., Ahmad, I., Mondal, M. E. A., & Rahaman, W. (2022). Multistage Neoarchean magma genesis in the Bundelkhand Craton, India: Evidence from whole-rock elemental and Nd isotopic study of mafic magmatic enclaves and granitoids. Geosystems and Geoenvironment, 100085.
- Rao, J. M. (2004). The wide spread 2 Ga dyke activity in the Indian shield-evidences from Bundelkhand mafic dyke swarm, central India and their tectonic implications. Gondwana Research, 7(4), 1219-1228.

- Reymer, A., & Schubert, G. (1984). Phanerozoic addition rates to the continental crust and crustal growth. Tectonics, 3(1), 63-77.
- Roeder, P. L., & Emslie, R. (1970). Olivine-liquid equilibrium. Contributions to mineralogy and petrology, 29(4), 275-289.
- Ruan, B., Yu, Y., Lv, X., Feng, J., Wei, W., Wu, C., & Wang, H. (2017). Occurrence and mineral chemistry of chromite and related silicates from the Hongshishan mafic-ultramafic complex, NW China with petrogenetic implications. Mineralogy and Petrology, 111(5), 693-708.
- Saha, L., Frei, D., Gerdes, A., Pati, J. K., Sarkar, S., Patole, V., ... & Nasipuri, P. (2016). Crustal geodynamics from the Archaean Bundelkhand Craton, India: constraints from zircon U–Pb–Hf isotope studies. Geological Magazine, 153(1), 179-192.
- Sarvothaman, H. (2001). Archaean high-Mg granitoids of mantle origin in the Eastern Dharwar Craton of Andhra Pradesh. Geological Society of India, 58(3), 261-268.
- Sato, H. (1977). Nickel content of basaltic magmas: identification of primary magmas and a measure of the degree of olivine fractionation. Lithos, 10(2), 113-120.
- Shields, G. A., & Webb, G. E. (2004). Has the REE composition of seawater changed over geological time?.
- Shirey, S. B., & Hanson, G. N. (1984). Mantle-derived Archaean monozodiorites and trachyandesites. Nature, 310(5974), 222-224.
- Singh, P. K., Verma, S. K., Moreno, J. A., Singh, V. K., Malviya, V. P., Oliveira, E. P., ... & Arima, M. (2019). Geochemistry and SmNd isotope systematics of mafic-ultramafic rocks from the Babina and Mauranipur greenstone belts, Bundelkhand Craton, India: Implications for tectonic setting and Paleoarchean mantle evolution. Lithos, 330, 90-107.
- Singh, S. P., Subramanyam, K. S. V., Manikyamba, C., Santosh, M., Singh, M. R., & Kumar, B. C. (2018). Geochemical systematics of the Mauranipur-Babina greenstone belt, Bundelkhand Craton, Central India: insights on Neoarchean mantle plume-arc accretion and crustal evolution. Geoscience Frontiers, 9(3), 769-788.
- Singh, V. K., Slabunov, A. I., Nesterova, N. S., Singh, M. M., & Bhatt, S. C. (2021). Tectonostratigraphic terranes of the Bundelkhand Craton (Indian shield). In Geological and Geo-environmental processes on earth (pp. 155-164). Springer, Singapore.
- Singh, V. K., Verma, S. K., Singh, P. K., Slabunov, A. I., Mishra, S., & Chaudhary, N. (2020). Archean crustal evolution of the Bundelkhand Craton: evidence from granitoid magmatism. Geological Society, London, Special Publications, 489(1), 235-259.
- Slabunov, A. I., & Singh, V. K. (2019). The new tectonic division of the Bundelkhand Craton, Indian Shield. Труды Ферсмановской научной сессии ГИ КНЦ РАН, (16), 521-524.
- Smithies, R. H., Ivanic, T. J., Lowrey, J. R., Morris, P. A., Barnes, S. J., Wyche, S., & Lu, Y. J. (2018). Two distinct origins for Archean greenstone belts. Earth and Planetary Science Letters, 487, 106-116.

- Souza, A. F. (2007). Ecological interpretation of multiple population size structures in trees: the case of Araucaria angustifolia in South America. Austral Ecology, 32(5), 524-533.
- Steenfelt, A., Garde, A. A., & Moyen, J. F. (2005). Mantle wedge involvement in the petrogenesis of Archaean grey gneisses in West Greenland. Lithos, 79(1-2), 207-228.
- Stein, M., & Hofmann, A. W. (1994). Mantle plumes and episodic crustal growth. Nature, 372(6501), 63-68.
- STERN, R. A., & HANSON, G. N. (1991). Archean high-Mg granodiorite: a derivative of light rare earth element-enriched monzodiorite of mantle origin. Journal of Petrology, 32(1), 201-238.
- STERN, R. A., & HANSON, G. N. (1991). Archean high-Mg granodiorite: a derivative of light rare earth element-enriched monzodiorite of mantle origin. Journal of Petrology, 32(1), 201-238.
- Stevenson, R., Henry, P., & Gariépy, C. (1999). Assimilation–fractional crystallization origin of Archean sanukitoid suites: western Superior Province, Canada. Precambrian Research, 96(1-2), 83-99.
- Su, B. X., Qin, K. Z., Sakyi, P. A., Malaviarachchi, S. P., Liu, P. P., Tang, D. M., ... & Mao, Q. (2012). Occurrence of an Alaskan-type complex in the Middle Tianshan Massif, Central Asian Orogenic Belt: inferences from petrological and mineralogical studies. International Geology Review, 54(3), 249-269.
- Sun, S. S., & McDonough, W. F. (1989). Chemical and isotopic systematics of oceanic basalts: implications for mantle composition and processes. Geological Society, London, Special Publications, 42(1), 313-345.
- Sun, S. S., & Nesbitt, R. W. (1978). Petrogenesis of Archaean ultrabasic and basic volcanics: evidence from rare earth elements. Contributions to Mineralogy and Petrology, 65(3), 301-325.
- Sun, S. S., & Nesbitt, R. W. (1978). Petrogenesis of Archaean ultrabasic and basic volcanics: evidence from rare earth elements. Contributions to Mineralogy and Petrology, 65(3), 301-325.
- Sun, S. S., & Nesbitt, R. W. (1978). Petrogenesis of Archaean ultrabasic and basic volcanics: evidence from rare earth elements. Contributions to Mineralogy and Petrology, 65(3), 301-325.
- Tanaka, T., Togashi, S., Kamioka, H., Amakawa, H., Kagami, H., Hamamoto, T., ... & Dragusanu, C. (2000). JNdi-1: a neodymium isotopic reference in consistency with LaJolla neodymium. Chemical Geology, 168(3-4), 279-281.
- Tanner, S. D., Cousins, L. M., & Douglas, D. J. (1994). Reduction of space charge effects using a three-aperture gas dynamic vacuum interface for inductively coupled plasma-mass spectrometry. Applied spectroscopy, 48(11), 1367-1372.
- Tassara, S., Reich, M., Konecke, B. A., González-Jiménez, J. M., Simon, A. C., Morata, D., ... & Corgne, A. (2020). Unraveling the Effects of Melt–Mantle Interactions on the Gold Fertility of Magmas. Frontiers in Earth Science, 8, 29.

Thakurta, J., Ripley, E. M., & Li, C. (2008). Geochemical constraints on the origin of sulfide mineralization in the Duke Island Complex, southeastern Alaska. Geochemistry, Geophysics, Geosystems, 9(7).

Uysal, I., Zaccarini, F., Sadiklar, M. B., Bernhardt, H. J., Bigi, S., & Garuti, G. (2009). Occurrence of rare Ru–Fe–Os–Ir–oxide and associated Platinum-group minerals (PGM) in the chromitite of Mugla ophiolite, SW-Turkey. Neues Jahrbuch für Mineralogie (Abhandlungen), 185, 323-333.

Verma et.al, 2016

Viljoen, M. J. (1969). An introduction to the geology of the Barberton granite-greenstone terrain. Spec. Publ. Geol. Soc. S. Afr., 2, 9-28.

Wan, Y. S., Liu, S. J., Xie, H. Q., Dong, C. Y., Li, Y., Bai, W. Q., & Liu, D. Y. (2018). Formation and evolution of the Archean continental crust of China: A review. China Geology, 1(1), 109-136.

Weis, D., Kieffer, B., Maerschalk, C., Barling, J., De Jong, J., Williams, G. A., ... & Mahoney, J. B. (2006). High-precision isotopic characterization of USGS reference materials by TIMS and MC-ICP-MS. Geochemistry, Geophysics, Geosystems, 7(8).

Wilson, M. (Ed.). (1989). Igneous petrogenesis. Dordrecht: Springer Netherlands.

Woodhead, J. D., Hellstrom, J., Hergt, J. M., Greig, A., & Maas, R. (2007). Isotopic and elemental imaging of geological materials by laser ablation inductively coupled plasma-mass spectrometry. Geostandards and Geoanalytical Research, 31(4), 331-343.

Wyman, D. A. (2019). 2.8 Ga Subduction-related magmatism in the Youanmi Terrane and a revised geodynamic model for the Yilgarn Craton. Precambrian Research, 327, 14-33.

Yaxley, G. M., Berry, A. J., Kamenetsky, V. S., Woodland, A. B., & Golovin, A. V. (2012). An oxygen fugacity profile through the Siberian Craton—Fe K-edge XANES determinations of Fe3+/ $\sum$  Fe in garnets in peridotite xenoliths from the Udachnaya East kimberlite. Lithos, 140, 142-151.

Zhai, M. (2014). Multi-stage crustal growth and cratonization of the North China Craton. Geoscience Frontiers, 5(4), 457-469.

Research Article Open Access

Satyanarayanan Manavalan\*, Surya Prakash Singh, Vysetti Balaram, and Mohanty Niranjan

# Geochemistry of the Madawara Igneous Complex, Bundelkhand Craton, Central India: Implications for PGE Metallogeny

DOI 10.1515/geo-2015-0016

Received March 25, 2014; accepted September 10, 2014

Abstract: The southern part of the Bundelkhand craton contains a series of a E-W trending mafic and ultramafic rocks, about 40 km in length and 2-4 km wide, that occur as intrusions within the Bundelkhand Gneissic Complex (BnGC). They are confined between the Madawara-Karitoran and Sonrai-Girar shear zones. Dunite, harzburgite, lherzolite and websterite are the commonly occurring ultramafic rocks that have high MgO, Ni, Cr, PGE and low Al<sub>2</sub>O<sub>3</sub>, CaO, K<sub>2</sub>O, TiO<sub>2</sub> and V contents, and shows peridotitic affinity. A distinct trend of crystallization from peridotite to komatiitic basalt has been inferred from geochemical plots, which also indicates the occurrence of at least two varieties among the ultramafic suite of the Madawara ultramafic complex, namely, Group I comprising dunite, spinel peridotite, harzburgite and lherzolite, and Group II consisting of pyroxenite, websterite and olivine websterite. In several places, the rocks of Group II have an intrusive relationship with Group I, and are relatively enriched in total platinum group elements (PGE  $\sim$ 300 ppb). The discrimination diagrams suggest that the PGE are enriched in low sulphur-fugacity source magma at moderate to deeper depths by high degree of partial melting of the mantle.

**Keywords:** PGE mineralization; Madawara; Bundelkhand Craton; Central India

## 1 Introduction

Mafic/ultramafic intrusions related to intracratonic magmatism occur in several shield areas [1]. Mineral systems associated with these events include Ni-Cu-PGE miner-

\*Corresponding Author: Satyanarayanan Manavalan: CSIR-National Geophysical Research Institute, Hyderabad-500007, India, E-mail: msnarayanan@ngri.res.in

**Surya Prakash Singh:** Department of Geology, Bundelkhand University, Jhansi 284001, India

**Vysetti Balaram, Mohanty Niranjan:** CSIR-National Geophysical Research Institute, Hyderabad-500007, India

alization in mafic-ultramafic rocks and base metals in metavolcanic rocks (VHMS type) in the Kaapvaal craton, Barberton greenschist belt and Superior Province [2]. Hence these lithologies have attracted attention in recent years for their potential to host viable metallic mineral deposits. The genesis of these metal associations within the host lithologies have now been established, apart from understanding the mantle evolution and its contribution to crustal growth [1–3]. The Bundelkhand craton preserves the different phases of Archean magmatism, metamorphism and deformation events [4] which were followed by emplacement of Bundelkhand granitoids (BG), quartz reef [5] and mafic dykes during the Paleoproterozoic [6-8]. The Meso to Neoarchean Bundelkhand gneissic complex (BnGC) comprises high grade rocks reaching up to granulite facies followed by low grade metamorphic rocks of greenschist facies of Bundelkhand Metasediments and Metavolcanics (BnMM) rocks [9, 10] and the mafic-ultramafic intrusions occuring along the E-W trending Mauranipur-Mohar-Babina shear zone in the central part [11] and Madawara-Karitoran shear in southern parts of the craton [12]. The Madawara Igneous Complex (Figure 1) occurs as giant lensoidal intrusion into the BnGC and is nearly undeformed and unmetamorphosed [12-14]. The occurrences of PGE within the Madawara Igneous Complex (MIC) of the Bundelkhand craton were first reported by Farooqui and Singh (2006) [15]. The identification of sperrylite and other important PGMs in these rocks based on the SEM-EDX data [16–20] suggest that MIC could be a new potential prospect for PGE deposits in the Indian shield. Hence the detailed geochemical study of ultramafic and associated rocks are presented here.

# 2 Geological framework

The Bundelkhand craton is considered as one of the oldest nuclei in the northern part of the Indian shield. It is delineated by the E-W trending Son-Narmada lineament/faults from the Mahakoshal group of rocks in the south, the WNW-ESE trending Yamuna fault in the north from the foreland basin of Himalaya and the NE-SW trending Great Boundary Fault (GBF) from the Aravalli belt [4].

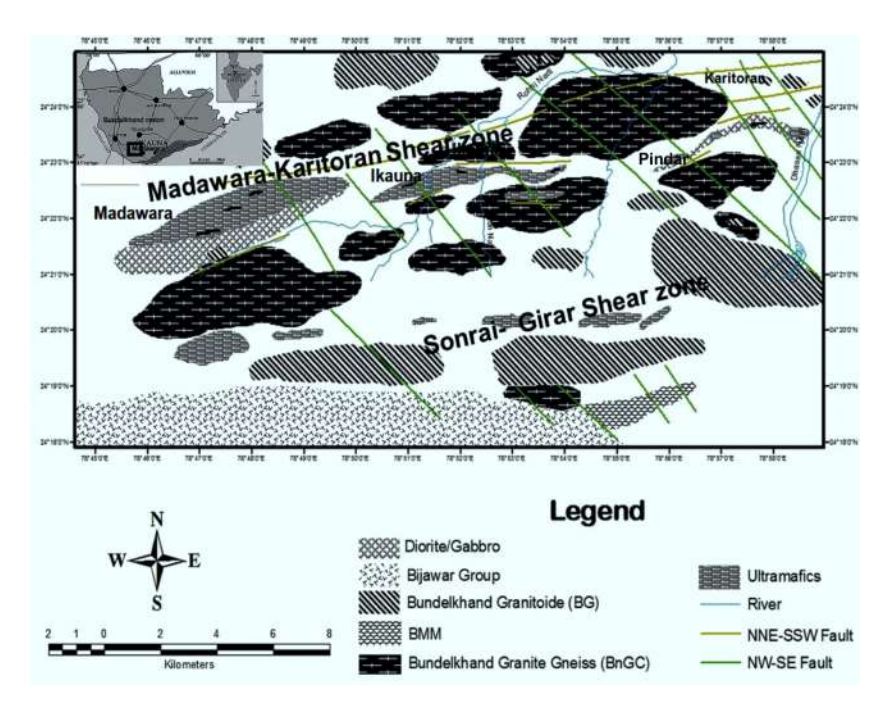


Figure 1: Geological map of Madawara Igneous Complex (inset showing study area in Bundelkhand craton) (After Singh et al. [16]).

A detailed stratigraphy of the area modified after Singh et al. (2010) [16] is given in Table 1. Geological studies around the southern part of the craton revealed occurrences of E-W trending, high grade metamorphosed rocks of BnGC (gneisses, migmatites, granite-gneisses, amphibolites, hornblende-biotite gneisses) around Rajola and north of Madawara, followed by less deformed and low grade metamorphosed rocks of Bundelkhand metasedimentary rocks and metavolcanic rocks (banded magnetitequartzite, quartzite, mica schist) [7] that are exposed at Girar and Baraitha. The ultramafic rocks of Madawara trending E-W and ENE-WSW and associated with peridotite, pyroxenite and diorite/gabbro occur as scattered lensoidal bodies in the area covering more than 400 km<sup>2</sup> and have been reported from the southern part of the Bundelkhand craton (Figure 1) [5, 12, 14, 21, 22]. These ultramafic bodies are subparallel and are confined between the Madawara - Karitoran shear zone in the north and Sonrai -Girar shear zone in the south. The sheared relationship between ultramafic rocks of the MIC and BnGC has been recorded at several places, where the ultramafic rocks are mylonitised and recrystallised, and in places altered to serpentine-talc-chlorite schists [7]. The presence of pegmatites and thick zones of mylonites and phyllonites indicate hydrothermal activity in the area that may be responsible for alteration of ultramafic rocks at several places.

*Madawara Ultramafites*: The ultramafic rocks at Madawara town represent the largest exposure. It is about 3 km wide and 4-5 km long, comprising dunite, peridotite,

spinel- bearing peridotite, pyroxenite and websterite followed by gabbro and diorite in subsequent stages. The rocks are relatively hard and compact, dark bluish gray and are medium to coarse grained. Chromespinel occurs as disseminated crystals while granular crystals of olivine, magnetite and pyroxenes are common. Porphyritic texture is rare. Sulphides are visible at many places. Globular aggregates of altered olivine in pyroxenites (2-10 cm in diametre) are common in the southern part of the Madawara ultramafic rocks. The gabbro/diorites intrude into these ultramafic rocks in the southern part of Madawara.

**Pindar Ultramafites:** These ultramafic rocks are medium to coarse grained and consist of peridotite, Crspinel bearing peridotite, harzburgite, lherzolite, dunite and pyroxenite. However, the area is dominated by peridotite and dunite. The olivine websterite is very dark bluish gray coloured, hard and compact, characterized by coarse grained cumulates of olivine (Figure 2a). They occur as small to large size lenses (up to 8-10 metres in length and 4-5 metres in width) and close to peridotite and websterite in composition. The contact of these lenses with BnGC is normally crushed, altered and at some places, they are sheared and mylonitised. Talc-chlorite schist occurs along the sheared contact, while websterites are scattered bodies within the ultramafic rocks and their orientation is also parallel to the main ultramafic complex.

**Ikauna Ultramafites**: The PGE bearing Ikauna ultramafic body is 3500 m long and 90-180 m wide [15]. It strikes E-W and dips 50° to 70° to the north. The high grade meta-

Table 1: Stratigraphy of Bundelkhand Craton (After Singh et al. [15]).

Vindhyan Supergroup (1400-700 Ma)	Lower Vindhyan limestone and dolomite, quartzite, Kaimure sandstone, Rewa sandstone and shale, Bhan- der carbonate
Bijawar/Gwalior Group (1800-1600Ma)	Sandstone, quartzite, mica quartzite, meta-basalts, fer- ruginous shale and sandstone, limestone and dolomite
Mafic emplacement (2000-1800Ma)	Dolerite, gabbro, lamproites, quartz veins and reefs, granites
Late phase granitic emplacement (2300-2000Ma)	Quartz reef, Granitoids, Pegmatites, diaspore and pyrophyllites
Bundelkhand Granitoids (BG) (2600-2500 Ma)	Leucogranite, biotite granite, hornblende granite, hornblende-biotite granite
Madawara Ultramafic Complex	Peridotite, dunite, harzburgite, spinel bearing peridotite, pyroxenite, gabbro, diorite, granite, talc chlorite schist
Bundelkhand meta sedimentaries and metavolcanics (BMM) (3300-2600 Ma)	BMQ, rhyolite, andesite, rhyodacite, quartzite, micaceous quartzite, chlorite schist, talc schist, pyroxenite, gabbro, peridotite and calc-schist
Bundelkhand Gneissic Complex (>3300 Ma)	Granite-gneisses, calc silicate gneisses, quartzites, garnetiferous gneiss, sillimanite-cordierite gneiss, amphibolite, TTG

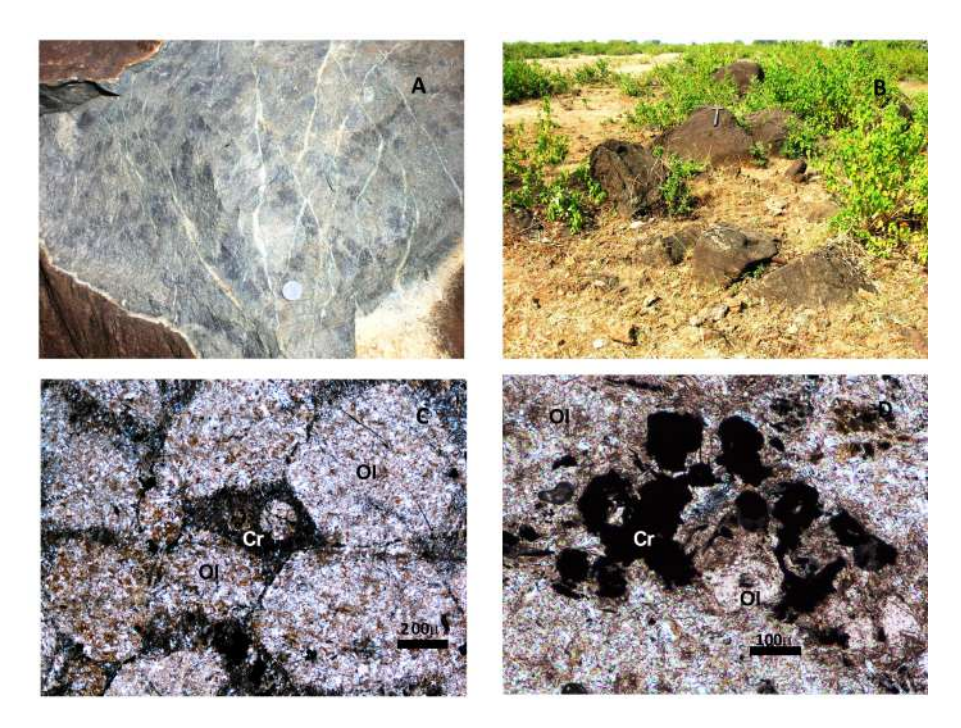


Figure 2: (A) Peridotite showing serpentine veins, (B) Outcrop of ultramafic rock in Ikauna, (C) Photomicrograph under crossed nicols of olivine (OI) cumulates, (D) Chromite (Cr) within altered olivine.

morphic rock, which hosts these ultramafic rocks, contain several E-W trending subvertical shear zones, dipping to the north. The ultramafic body of Ikauna is almost flat with small hillocks of nodular lenses of pyroxenite. These lensoidal dark coloured pyroxenites are strongly crushed at their margin, in places crenulated and are few metres (10-50 m) wide and 15-100 m length. The contact is altered, in places shows rotation signatures, and is partially enveloped by chlorite + talc-actinolite schists. The chromespinel -bearing ultramafic rock has also been traced for more than 1 km along the strike length. The contact of the intrusive body with gneisses or diorites is marked by mylonite. The Ikauna ultramafic body is also cut by NW- SE trending faults in several places. Most of the ultramafic rocks are commonly altered to serpentine, talc and chlorite schists along the shear zone (Figure 2b).

# 3 Petrography

The ultramafic rocks of the Madawara Igneous Complex (MIC) are medium to coarse grained, more or less uniform in texture and ranges from peridotite to pyroxenite. Detailed petrographic and geochemical analyzes indicate that the peridotites are represented by lherzolite and harzburgite, while the pyroxenites are mostly olivine-rich orthopyroxenites (websterite). The lherzolite and harzburgite consist of olivine cumulates where interstices are filled with chromite, magnetite and sulfides. Olivine grains are cumulus and are medium to coarse grained (Figure 2c). The interstitial space is either occupied by orthopyroxene or clinopyroxene with fine grained chromite and magnetite (Figure 2d). SEM-EDS (Hitachi®, Japan) studies have indicated presence of sulfide phases, for example, pentlandite, pyrrhotite, chalcopyrite, with inclusions of chromite and platinum group minerals (PGM) like sperrylite, wolframite and an Ir-tungstate alloy occur as disseminated grains in the inter-spaces of olivine or along the cleavage in pyroxenes (Figure 3a-b) [16, 17]. The fine- to medium- grained chromites, magnetite, titanomagnetite and granular aggregates of pentlandite occur in olivine-rich orthopyroxenites, where these minerals are also present along the cleavages of pyroxene and intra-granular spaces of olivine. The alteration of olivine, pseudomorphic texture, and appearance of talc, chlorite and serpentine as secondary minerals were also recorded in few thin sections, indicating very low-grade metamorphism at the marginal area of deformed zones.

#### 3.1 Methodology

Major oxides, minor and trace elements (including REE and PGE) were determined in fifteen representative samples representing rocks from Madawara, Pindar and Ikauna, Major elements were analyzed at the National Geophysical Research Institute (NGRI), India by XRF (Phillips® 234 MAGIX PRO Model 2440), with a relative standard deviation of < 3% [23]. For trace elements, the sample powders were dissolved in reagent grade HF: HNO<sub>3</sub> mixture in Savillex screw top vessels and heated at 140°-146°C. Solutions were analyzed by ICP-MS (Perkin Elmer SCIEX ELAN DRC II) at NGRI. 103Rh was used as an internal standard [24]. External drift was corrected by repeated analyzes of a 1: 5000 solution of UB-N (certified reference material obtained from ANRT, France), which was also used as a calibration standard. Instrument response was corroborated relative to two independent digestions of the JP-1 (certified reference material obtained from GSJ, Japan). Precision and accuracy are better than 5% (1 $\sigma$ ) for the majority of trace elements, but varied up to 10% ( $1\sigma$ ) in the case of HREE. Mg# is calculated as Mg/(Mg+Fe<sub>total</sub>). Chondrite and primitive mantle normalisation values are taken from Sun and McDonough [25]. Analysis of PGE and Au was carried out by following the NiS-fire assay method with Te co-precipitation and ICP-MS described in Balaram et al. [26]. The certified reference material WPR-1 was used as calibration standard and WMG-1 was analyzed as an unknown to check accuracy. The overall precision of PGE analysis was better than 10% (1 $\sigma$ ) at ppb levels. Most abundant and recommended isotopes relatively free from isobaric interferences were used for all elements and were selected based on their abundance levels and the lack of interferences from other elements normally present in rock samples.

#### 4 Results

The whole rock analyzes of representative ultramafic rock samples from the MIP are presented in Table 2 and are characterized by high MgO, Ni, Cr, and PGE, and extremely low Al<sub>2</sub>O<sub>3</sub>, CaO, K<sub>2</sub>O, TiO<sub>2</sub> and V contents. The geochemical characteristics of the ultramafic rocks exposed around Madawara shows variation from high MgO ( $\sim$ 47 wt %; picritic) to moderate MgO (~32 wt %; gabbroic). A Jenson cation plot (Figure 4) shows that these rocks were derived from melt which is peridotitic in nature. The norm mineral classification and petrographic study reveal that these ultramafites are lherzolite, olivine websterite, orthopyroxen-

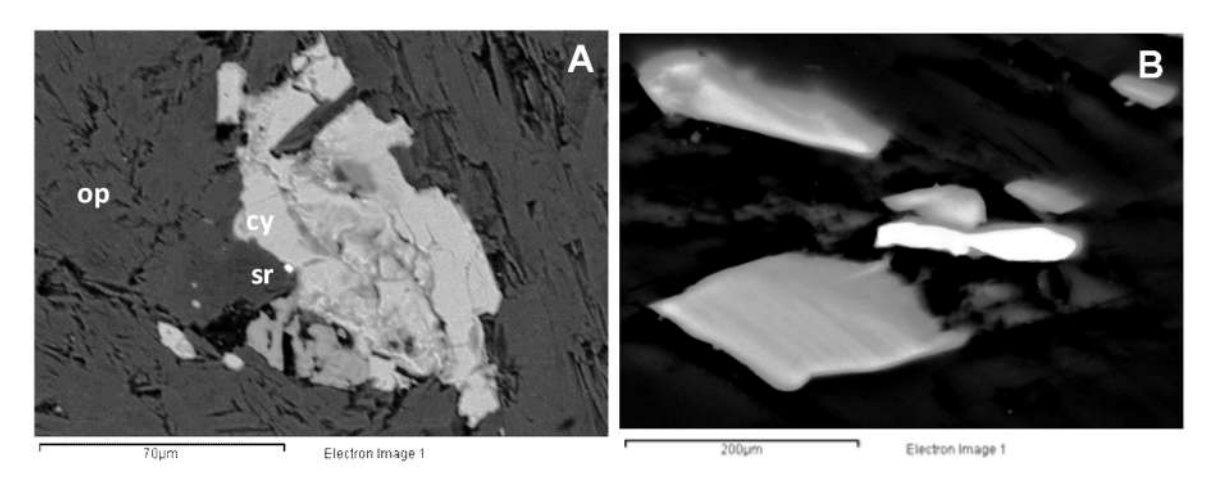


Figure 3: SEM-EDS image showing (A) Sperrylite [sr] associated with the chalcopyrite [cy] in the matrix of pyroxene [cy], (B) Dumble shaped Iridium-Tunsgten alloy.

ite, harzburgite in composition. The relatively clear to partial linear regression relationship between MgO and SiO<sub>2</sub>, TiO<sub>2</sub>, CaO, Cr, Ni and total PGE (Figure 5a-f) indicate crystallization trend from peridotite composition of primitive magma to Mg-olivine fractionation followed by differentiated Fe-rich olivine, spinel/magnetite and sulfide crystallization. There is a broad range of Ni and Cr concentration in the ultramafic rocks and their associated rocks from Madawara. Maximum concentration of Ni (up to 2655 ppb) and Cr (up to 5538 ppb) are recorded in dunite while the lowest value of Ni and Cr is in diorite. A decrease in the Mg# in these ultramafites leads to their corresponding gradual decrease in Ni and Cr concentrations. A strong linear correlation of SiO<sub>2</sub> vs. Zr, Al<sub>2</sub>O<sub>3</sub> vs. Y, TiO<sub>2</sub> vs. Zr and Y vs. Zr (Figure 6a-d) shows that these rocks has undergone high degree of partial melting at shallow to moderate depths.

The REE plots and spider diagram show at least two types of trend (Figure 7a-b) for ultramafites and associated rocks from Madawara, Ikauna and Pindar. The REE patterns of dunite, spinel peridotite, harzburgite and lherzolite shows essentially a strong Eu negative anomaly (termed here as Group I) (Figure 7a). These rocks display a relatively uniform and unfractionated REE trend, and are characterized by low MgO, high CaO, SiO<sub>2</sub>, Ni, Cu and relatively high PGE. The flat LREE pattern, with mild positive Eu anomaly pattern (Figure 7b) is recorded in differentiated variety of ultramafic rocks representing pyroxenite and peridotites II (termed here as Group II) and are inevitably associated with Group I type of MIP representing the last intrusive phase. Besides REE patterns, the spider diagrams of these two categories (Figure 8a-b), show distinct trend for each group, although they both display slight LILE enrichment, especially for pyroxenites, with values ranging in between those of N-MORB and E-MORB.

The mantle normalized spider diagram of Group I and Group II shows negative and positive anomalies for Ti respectively. A strong Nb negative anomaly is also present in Group I when compared to Group II suggesting partial melting of primary melt component associated with crustal inputs. This is also supported by the overall high positive anomalies of Rb, K, La, Sr and Sm values and strong depletion in U, Nb, Hf.

#### 4.1 PGE geochemistry

The PGE and Au values of ultramafic rocks from Madawara listed in Table 1 indicate a narrow range of Ir and Ru contents varying from 7.2 to 17.6 ppb and 41.8 to 100.2 ppb respectively. Rhodium contents are fairly constant with a range from 1.4 to 11.2 ppb, whereas Pt contents vary from 6.8 to 131.6 ppb and Pd from 6.8 to 77.2 ppb. Gold also displays a wide variation, ranging from 21.8 to 1426.8 ppb. Both Group I and II of ultramafic rocks have a similar primitive mantle normalized siderophile element pattern (Figure 9a-b) and are enriched in PPGE (Rh, Pt, Pd) and Cu relative to IPGE (Ir and Ru) and Ni. MgO displays a relatively good correlation with PGE. Thus it is inferred that the fractionation of olivine, pyroxene and spinel has significantly influenced the PGE distributions in these rocks. The geochemical studies indicate that olivine, chrome-spinel and/or sulfides are the most compatible mineral phases for PGE-enrichment [3, 27, 28]. The Pd/Ir and Pd/Rh ranges from 0.6 to 5.0 (average 1.7) and 1.3 to 20.3 (average 5.6) respectively. The strong positive Au and Pt anomalies, corroborated with REE and multi-element diagram, indicate the presence of chloride and carbonate enriched fluid components in the system during magmatism [29].

Table 2: Geochemical data representing ultramafic rocks from Madawara (MD), Pindar (P) and Ikauna (I) localities in Madawara Igneous Complex (\* Data from Balaram *et al.*, 2013 [18]). H-Harzburgite, L-Lherzolite, W-Wehrlite, O-Orthopvroxenite.

						<b>+</b>	+	,	+	+					
Analyte	MD24	<b>MD25</b>	MD29	WD-8	MD19	P-64°	P-65 <sup>°</sup>	P-66°	P-67	P-68°	I-37	I-38	I-39	I-40	I-41
Rock type	Н	Н	0	0	0	M	8	8	8	×	Т	Т	Т	Т	Н
Group	п	1	1	п	I	П	П	п	1	<b>-</b>	п	ı	Ι	I	Ι
Major oxides (in wt %)	des (in w	t %)													
Si0 <sub>2</sub>	43.7	43.1	50.9	44.5	44.7	41.7	41	40.1	41.8	42.8	42	41.4	41.7	40.1	40.2
$Al_2O_3$	0.87	0.87	0.88	0.73	0.85	2.06	2.69	2.35	2.67	2.02	2.57	2.72	3.88	5.16	1.86
Fe0	8.8	8.8	10.3	10.7	10.4	4.6	4.8	4.9	4.5	4.7	5.4	4.7	4.9	8.7	4.9
$Fe_2O_3T$	11.5	11.6	13.4	14.1	13.5	9	6.2	6.4	5.8	6.2	7.1	6.1	6.5	11.4	6.4
MnO	0.14	0.14	0.13	0.1	0.14	0.12	0.14	0.12	0.11	0.11	0.15	0.12	0.15	0.2	90.0
MgO	35.4	35.6	29.5	34.5	34.2	94	45.3	45.2	45.1	45.8	41.3	42.2	41.1	31.6	47.3
Ca0	2.31	1.72	1.61	0.08	0.07	99.0	1.41	1.63	1.34	0.44	3.53	3.67	2.55	2.18	0.64
$Na_2O$	0.02	0.01	0.01	0.02	0.02	90.0	0.11	0.04	90.0	0.03	0.05	90.0	0.04	0.02	0.04
$K_2O$	0.01	0.01	0.01	0.01	0.01	0.03	0.03	0.03	0.04	0.02	0.03	0.03	0.04	0.03	0.03
TiO <sub>2</sub>	0.53	0.46	0.27	0.1	0.45	0.17	0.21	0.18	0.19	0.16	0.18	0.17	0.24	1.71	0.16
$P_2O_5$	0.03	0.03	0.05	0.01	0.01	0.02	0.02	0.02	0.2	0.02	0.07	0.02	0.02	0.08	0.02
lo1	9.6	7.23	2.2	6.87	6.55	4.06	3.65	4.68	3.22	2.95	3.47	4.08	4.24	8.27	3.76
Sum	100.1	100.7	66	100.9	100.5	100.9	100.8	100.7	100.5	100.5	100.3	100.6	100.4	100.8	100.5

Analyte	MD24	MD25	MD29	MD-8	MD19	P-64*	P-65*	P-66*	P-67*	P-68*	I-37	I-38	I-39	I-40	I-41
Rock type	Н	Н	0	0	0	×	M	8	M	×	1	Т	Г	Г	Н
Group	II	Ι	Ι	П	Ι	П	II	П	Ι	Ι	П	Ι	Ι	Ι	Ι
Trace elements (ppm)	nents (p	(md													
Sc	13.8	12.5	7.2	7.1	11.4	10	12.3	10.7	11.7	10.9	14.3	12.5	13.4	44.3	9.4
>	9.88	83	33.2	27.8	81.4	47.4	62.4	52.3	57.1	50.1	63.8	55.5	63.5	363.5	44.1
Cr	4810	5538	955	2540	5280	2703	3150	2297	2890	2721	2547	3021	3248	1922	3840
Co	116	116	61.5	168	6.06	137	133	131	127	119	132	124	133	149	121
ï	1728	1740	1483	2064	1738	2655	2616	2434	2581	2466	2260	2259	2278	915	2606
Cu	23.7	20.2	18	62.7	18.1	11.2	16	24.9	11.4	63	44.5	28.2	15.3	18.8	16.7
Zn	37.1	40.5	39.3	52.4	52.8	111.4	476.7	253.5	84.1	611.8	540.5	153.8	73.8	331.5	142.8
Ga	4.5	4.3	6.7	1.3	4.1	3.9	5.2	4.4	4.8	4.7	5.2	6.2	6.7	25.4	9.6
Rb	0.88	0.64	0.44	0.7	9.0	0.81	1.11	1.15	1.65	2.12	1.03	0.97	1.93	0.72	0.69
Sr	21.3	9.5	6.3	8.5	9.4	4.8	18.5	5.1	5.2	9.4	13.6	11.8	9	2.7	3.7
>	3.5	3.1	3.7	1	2.7	2.8	4.2	3.6	3.8	4.3	4.2	3.8	3.8	3.7	2.9
Zr	6	∞	18	1.5	8.1	4.7	11.2	4	2	6.1	6.9	2.7	9.6	64.9	5.3
Nb	0.28	0.22	0.37	0.12	0.28	0.08	0.09	0.04	0.1	0.08	0.09	0.09	0.13	1.28	0.07
Cs	0.13	0.07	0.05	90.0	0.09	0.37	0.41	0.52	0.44	0.45	0.23	0.35	0.57	90.0	0.15
Ва	11.2	16.5	12.3	17.1	13.1	1.7	3.2	2.7	4.6	7.8	6.2	2	5.1	2.5	1.4
La	0.94	0.77	0.73	0.5	0.55	1.59	2.29	2.12	2.01	3.87	2.28	2.27	2.65	8.8	1.24
Ce	2.8	2.3	2.3	1.4	1.9	3.3	4.4	3.9	4	8.2	4.7	4.4	5.8	18.1	5.6
Pr	0.36	0.31	0.33	0.18	0.28	0.27	0.37	0.32	0.32	0.58	0.37	0.35	0.44	1.43	0.22
ΡN	1.6	1.4	1.6	8.0	1.2	1.3	1.9	1.5	1.7	2.8	1.9	1.8	2.1	7.1	1.1
Sm	0.44	0.38	0.49	0.17	0.35	0.34	0.48	0.4	0.43	0.64	0.5	0.44	0.53	1.62	0.32
Eu	0.14	0.12	0.09	0.08	0.08	0.11	0.15	0.12	0.11	0.13	0.14	0.12	0.13	0.18	0.09
P9	0.58	0.5	0.57	0.22	0.42	0.42	9.0	0.48	0.53	0.75	0.59	0.55	0.59	1.58	0.38
ТЪ	0.1	0.08	0.1	0.03	0.07	0.08	0.12	0.1	0.1	0.13	0.11	0.11	0.12	0.23	0.08
Dy	0.59	0.53	0.61	0.16	0.43	0.47	0.69	0.58	0.61	0.75	0.7	0.64	0.67	0.94	0.49
Ю	0.14	0.12	0.13	0.03	0.1	0.1	0.15	0.13	0.14	0.16	0.15	0.14	0.15	0.16	0.11
丘	0.41	0.35	0.41	0.09	0.31	0.32	0.45	0.4	0.42	0.47	0.47	0.41	0.45	0.47	0.32
Tm	0.07	90.0	0.07	0.02	0.05	90.0	0.07	0.07	0.07	0.07	0.08	0.07	0.07	0.07	0.05
Υb	0.38	0.37	0.4	0.09	0.31	0.31	0.41	0.37	0.38	0.43	0.42	0.39	0.43	0.45	0.3
Lu	0.07	90.0	0.07	0.01	0.05	0.05	90.0	0.05	90.0	0.07	90.0	90.0	0.07	0.09	0.05
Ŧ	0.19	0.16	0.36	0.04	0.17	0.1	0.29	0.1	0.12	0.13	0.15	0.14	0.14	1.29	0.13
Та	0.03	0.02	0.04	0.03	0.02	0.02	0.02	0	0.05	0.03	0.07	0.04	0.03	0.27	0.03
Pb	10.4	9.5	12.3	10.6	14.2	12.3	12.4	11.2	8.2	23	13.2	11.4	2.6	12.6	11.7
무	0.17	0.14	0.31	90.0	0.16	0.07	0.1	0.09	0.09	0.18	0.13	0.13	0.13	0.27	0.07
n	0.09	0.1	0.19	0.18	0.11	90.0	0.1	0.21	0.09	0.22	0.11	0.14	0.08	0.16	90.0

Analyte MD24 MD25 MD29	MD24	MD25	MD29	MD-8	MD19	P-64*	P-65*	P-66*	P-67*	P-68 <sup>*</sup>	I-37	I-38	I-39	I-40	I-41
Rock type	Н	Н	0	0	0	×	M	M	×	M	Г	Т	Г	П	Н
Group	Ш	Ι	Ι	П	Ι	П	Ш	II	Ι	Ι	П	Ι	Ι	Ι	Ι
Precious 6	lements	(qdd)													
Ru	81.4	83.4	72.6	100.2	74.6	41.8	48.6	59.4	8.99	52.4	65.6	54.2	53.6	44.4	59.6
Rh	11.2	3.8	1.4	2.4	5.4	2.8	3.4	٣	4.2	8.2	5.4	4.6	5.6	2.4	3.8
Pd	48.8	77.2	13.4	17	26.8	13.6	10.8	9.8	15.2	14.4	99	10.8	12.4	8.2	12.2
Ag 784.6 57	784.6	27	58.6	79.4	226.6	26.6	62	41.4	9.99	9.69	165.4	84.2	148.4	130.4	129.6
Re	355.8	44.8	77.4	210.2	290.2	10.4	11.6	12	14	9.4	36.4	164.2	93	172.2	233.8
0s	9.9	4	2.2	9.7	9	65.2	24.2	54.8	28	63.8	46.4	22	38.6	6	59.8
<u>_</u>	17.6	15.4	7.2	9.4	13.8	10	11.8	12.6	14.6	12.6	17.2	13.6	15.2	4.4	16.8
Pt	49.6	86.4	8.9	131.6	35	24.6	29	27	28.6	30.4	47	33.8	23.4	31.8	29.4
Au	59.4	9.99	52.8	42.2	1426.8	29.8	29.6	21.8	38.6	35.6	49.2	28.6	39.8	26.2	27.8

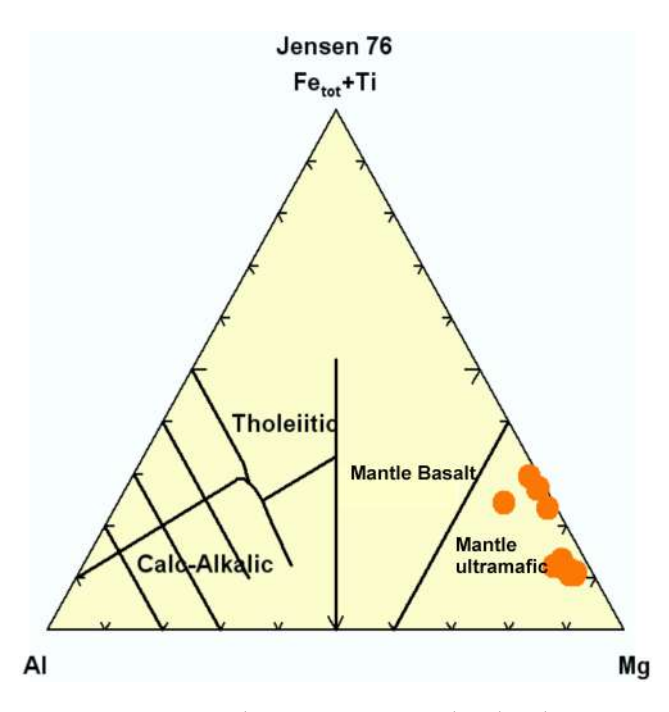


Figure 4: Jenson cation plot from the ultramafic rock of MIC. (Modified after Jenson (1976) [52]).

#### 5 Discussion

The geochemical data from the ultramafic rocks presented here reflect their mineralogy and allows them to be distinguished into two main groups of ultramafic rocks: (1) harzburgites, spinel peridotites and dunites and (2) pyroxenites and peridoties II. There are linear correlation between certain elements (like Cr, Co, Ni) in the ultramafic rocks which suggest that they basically represent a melt that was extracted from the peridotite and subsequently contaminated by crustal components and fractionated at several stages as shown in Figure 5d-e. The pyroxenite has high PGE, LREE and LILE, and hence differs from the other ultramafic rocks and associated diorites. The presence of high Ir-low Pd (Figure 10a), high MgO and HREE suggests partial melting for these ultramafites at relatively high temperature. The partial melting of the primitive mantle may lead to the formation of either S-saturated or Sundersaturated melts [3, 30]. It is advocated that where Sundersaturated magma is formed by high degrees of partial melting, the PGE remain in the primary melt, leading to enrichment of PGE, especially PPGE [28]. The Pd/Rh vs. Ni/Cu and Pd/Ir vs. Ni/Cu variation diagrams (Figure 10bc), proposed by Barnes [31], display that most of the ultramafic rocks show peridotitic affinity. The negative correlation between Pd/Ir and Ni/Cu ( $r^2 = -0.4$ ) (Figure 10c) suggests that Pd may have behaved like Cu and was removed, whereas Ir associated with Ni and was retained

during melt-rock interaction. The range of Ni/Cu and Pd/Ir (0.83 to 31.9) ratios for the ultramafic rocks from Madawara suggests sulfide under saturated conditions.

REE contents normalized to chondrite values show variable enrichments in LREE [(La/Sm)N between 1.45 and 2.0] with mild positive Eu anomalies (Eu/Eu\* from 1.08 to 2.26) and nearly flat HREE patterns [(Gd/La)<sub>n</sub> 0.94-1.49] for the pyroxenites. The  $(Gd/La)_N$  is similar to those of pyroxenites analyzed from elsewhere [32–34, 34]. The pyroxenites in ultramafic massifs are normally considered as depleted in LREE and highly enriched in HREE contents [32]. In contrast to this, LREE enrichment and higher contents of Zr, Nb and U and very low HREE have been reported from a few locations, for example, Hungary and the French Massif Central [32, 33], Herbeira massif [34] and harzburgite of Herbeira [35]. Hence, the trace element concentrations including PGE appear unique and differ from those of other pyroxenites in ultramafic massifs reported elsewhere, for example, Ronda, Ortegal, Horoman, Cabo-Ortegal, Alpine, Ronda massifs, Beni Boussera, the Alps, massive pyroxenites from Herbeira.

The mafic rocks and pyroxenites from orogenic peridotites show a characteristic depletion in incompatible elements [36, 37]. The absence of such depletion from the Group II rocks suggests that the source area of pyroxenite parental melts should originally be either enriched in incompatible elements or had received LILE enrichment by reaction with carbonic fluids or by metasomatism of carbonatite related fluids. The last hypothesis is preferred

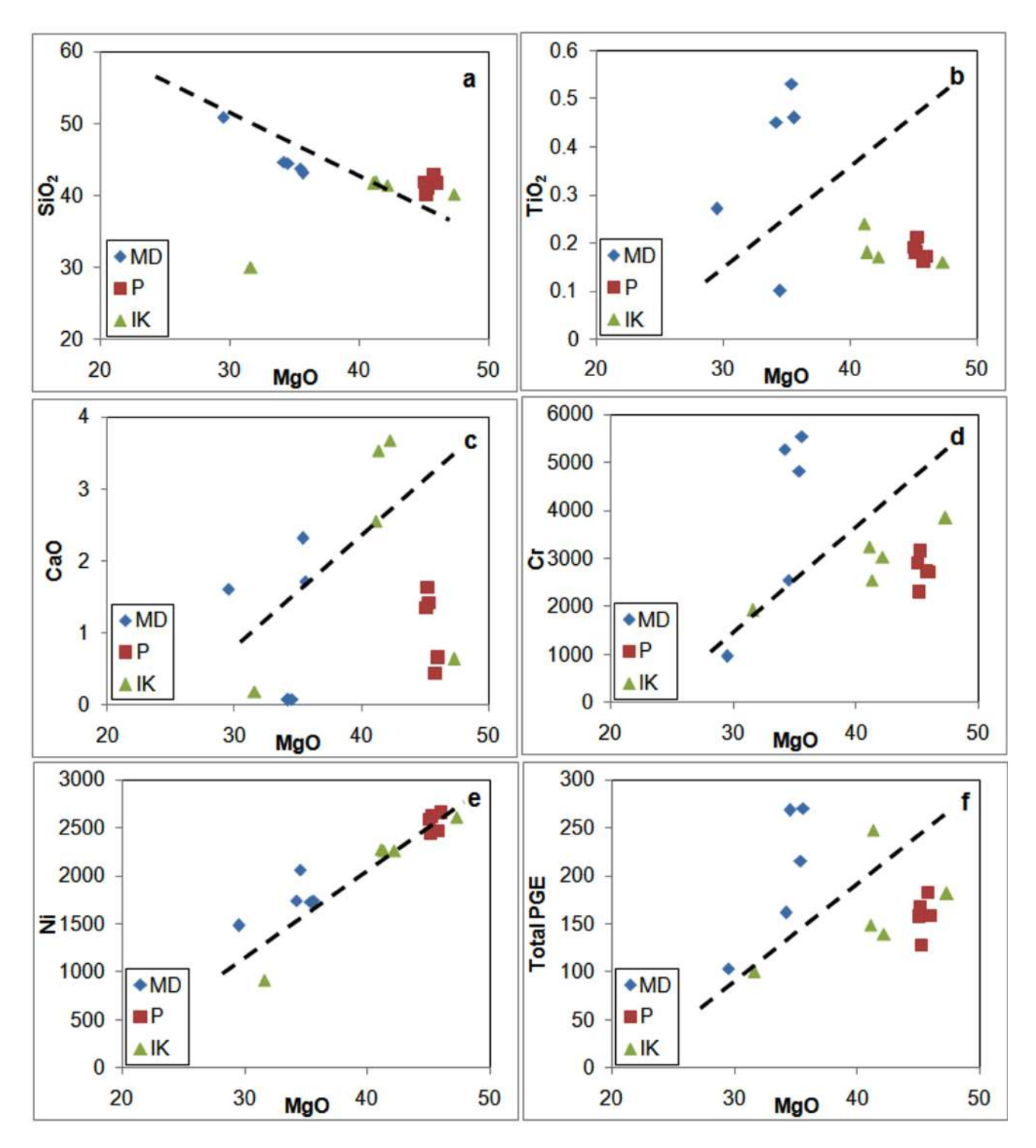
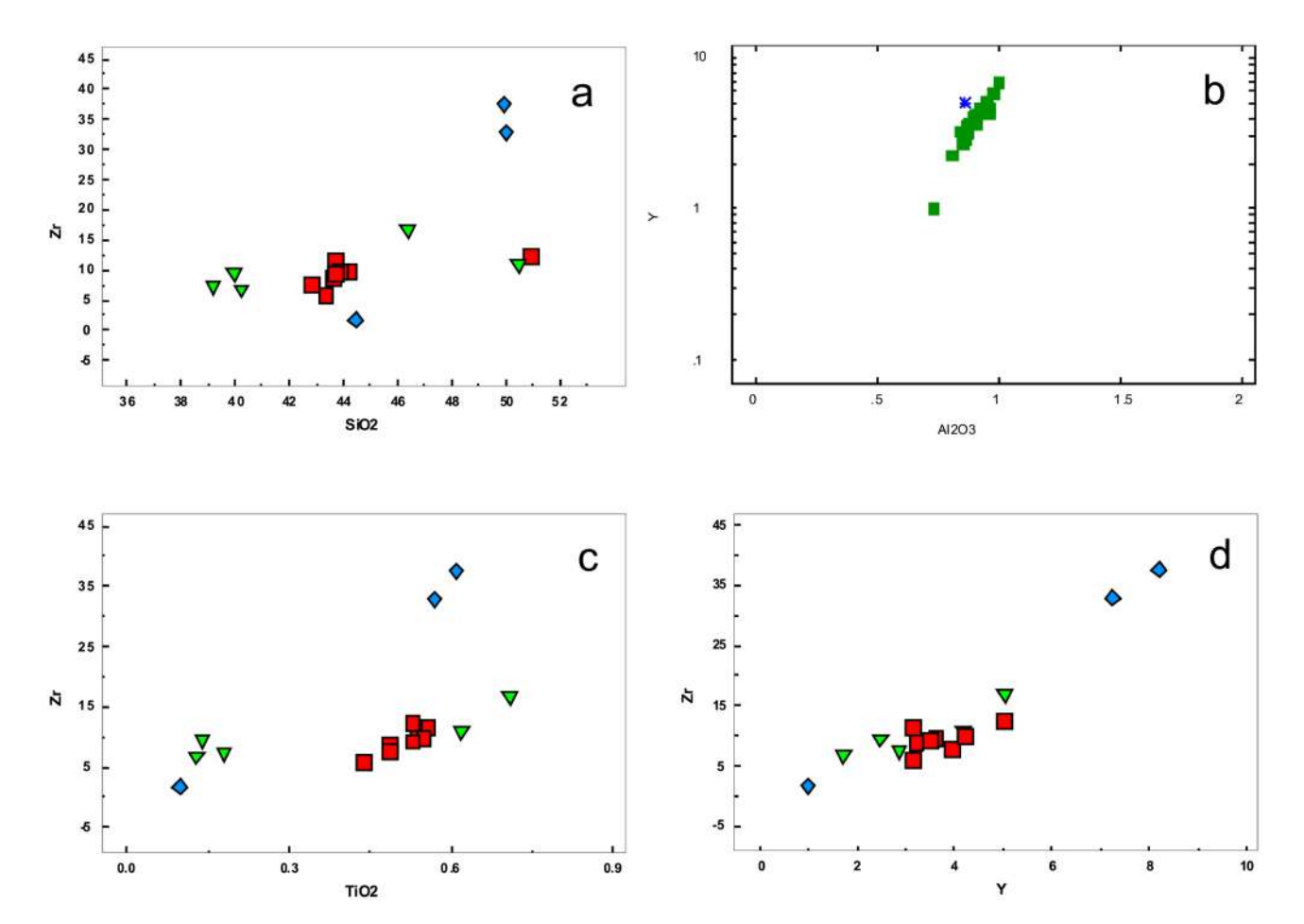


Figure 5: Variation diagrams showing plots between MgO and (a) SiO<sub>2</sub>, (b) TiO<sub>2</sub>, (c) CaO, (d) Cr, (e) Ni and (f) Total PGE. (MD-Madawara; P-Pindar; IK-Ikauna).



 $\textbf{Figure 6:} \ \ \text{Bivariate plots showing strong linear correlation between (a) SiO}_2 \ \text{vs.Zr, (b)} \ \ \text{Al}_2 O_3 \ \text{vs.Y, (c)} \ \ \text{TiO}_2 \ \text{vs.Zr} \ \text{and (d)} \ \text{Y vs. Zr.}$ 

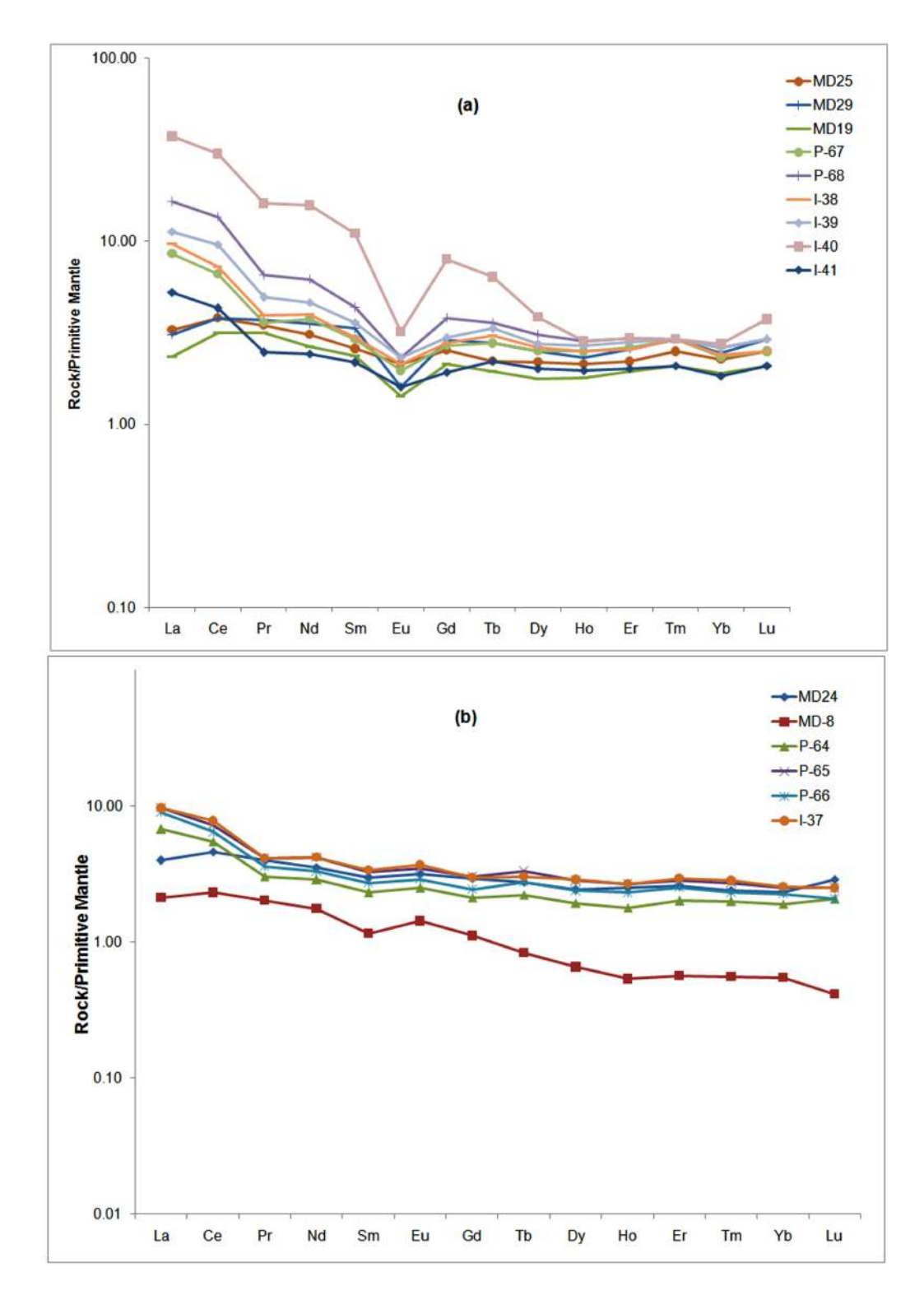


Figure 7: Chondrite-normalized REE patterns of ultramafic rocks representing (a) Group I and (b) Group II. Normalization values are from Sun and McDonough [25].

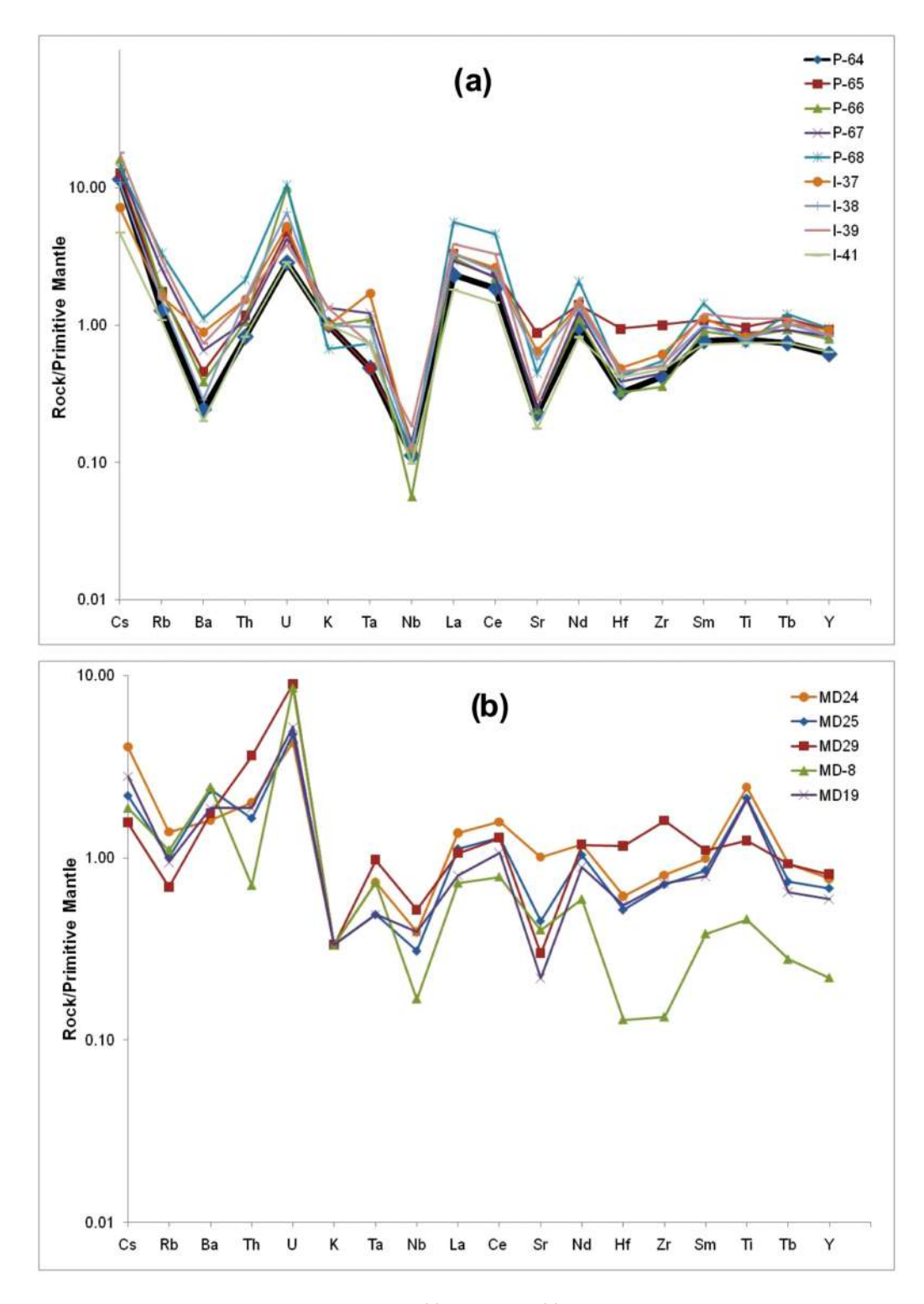


Figure 8: Primitive-mantle normalized spidergram representing (a) Group I and (b) Group II. Normalization values are from Sun and Mc-Donough [25].

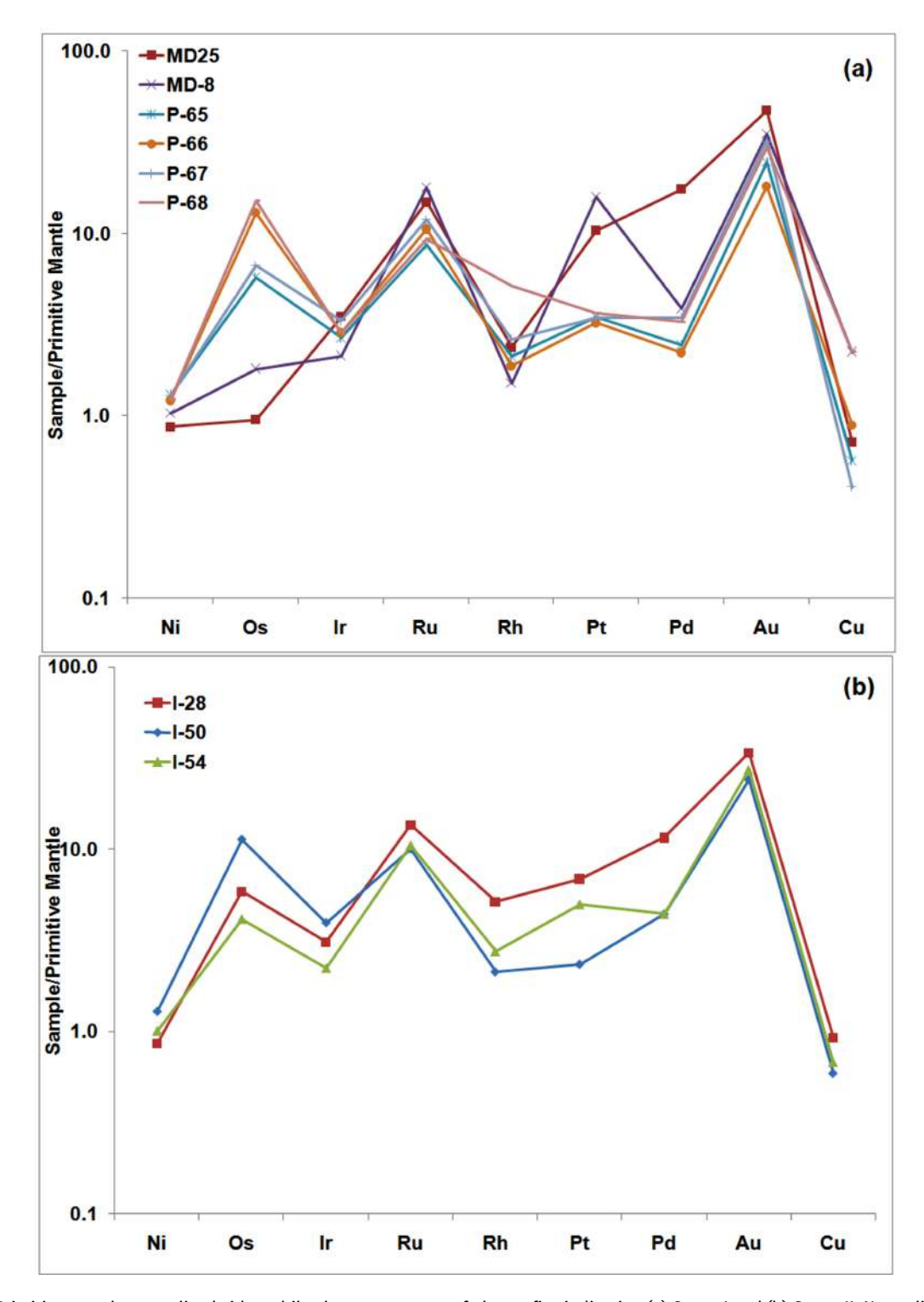


Figure 9: Primitive-mantle normalized siderophile element patterns of ultramafics indicating (a) Group I and (b) Group II. Normalization values are from Sun and McDonough [25].

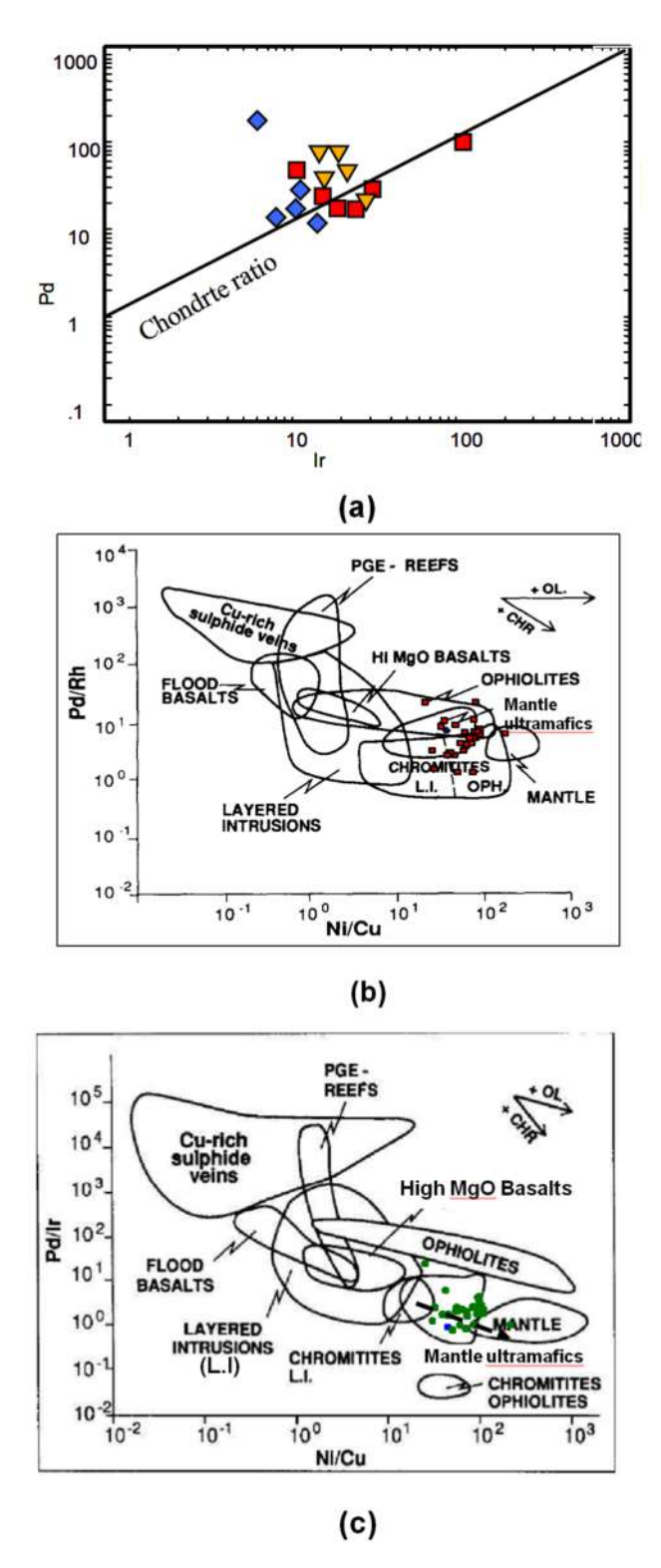


Figure 10: PGE variation diagrams showing (a) Ir vs. Pd (Chondrite ratio from Sun and McDonough [25]), (b) (Ni/Cu) vs. (Pd/Rh), and (c) Ni/Cu vs. Pd/Ir. (Fields for 10 b-c are from modified after Barnes and Maier [2]).

here, as it would also account for the depletion of LILE in peridotites. The melt percolation into interstitial space of harzburgite due to partial melting of asthenoshpere proposed by Zhou et al. [38] and Chen et al. [39] may also be considered for the genesis of pyroxenite. The enrichment in LILE associated with a generalised, although variable LREE enrichment from peridotites and pyroxenites have been reported from other places, and hence the enrichment of LREE is considered as possibly due to metasomatism of carbonatite related fluid or crustal contamination [34, 35]. Therefore, such variation in LREE enrichment of rocks from Madawara is noteworthy. LREE-enriched rocks with flat patterns have also been described from the Horoman, Cabo Ortegal, Alpine and Ronda massifs [36, 37, 40]. The presence of such occurrences are limited and their origin is not well constrained. The origin of pyroxenites enriched with crustal elements, has also been caused by thinning and upwelling of asthenosphere and late melt percolation into the harzburgite. Recently, Gruau et al. [41] have proposed various mechanisms for selective LREE enrichment in peridotites. In the present case, and by comparison with the models proposed by Gruau et al. [41], the REE trend points to high-temperature contamination of the ultramafic rocks through interaction with LREE-rich melts.

#### 5.1 Magma evolution

The physical and chemical changes recorded across the harzburgite-dunite-pyroxenite suite in the Madawara complex could have been theoretically generated by increasing degrees of partial melting [42–44]. Different types of REE pattern have been described for the evolution of ultrabasic magma. The U-shaped REE patterns of peridotites reported from Oman ophiolite has been explained as the product of interaction of peridotites with LREE-enriched melts [45, 46]. The processes that include a mantle origin involving disequilibrium mechanisms [47], the effect of melt transportation [48] and the entrapment of small melt fractions [49] are important points during the course of crystallisation of ultrabasic magma. The variation in REE patterns of peridotites has been interpreted in terms of the contamination by assimilated continental crustal material [41]. The positive correlations between Zr vs. SiO<sub>2</sub>, Y vs. Al<sub>2</sub>O<sub>3</sub>, TiO<sub>2</sub> vs Zr and Zr vs Y (Figure 6a-d), in Madawara ultramafic rocks are similar to those recorded globally in anhydrous peridotites [50] and indicate a similar source for evolution of the magma. The decrease in Pd/Ir ratios close to chondrite (Figure 10a) suggests that early/initial phase of magma was perhaps developed from fertile mantle under sulphur under-saturated conditions, whereas the pyroxenites and Group II type magma, which are presumably enriched in sulphides, are developed in the subsequent stages. The range of Pd/Ir (0.7 to 5.0) and Pt/Au (0.03 to 3.1) ratios indicate that sulphur and chloride rich fluid activity causes the mobilisation of the Pt and Au from the magma. The LREE depleted pattern is characteristic of late Archean ultramafites and is generally believed to indicate that these magma originated by a high degree of partial melting of the mantle. The strong negative Eu anomaly reflects plagioclase fractionation in the melt. The Pd/Rh vs. Ni/Cu and Pd/Ir vs. Ni/Cu variation diagrams (Figure 10c-d) proposed by Barnes et al. [51] and HREE fractionation trend support the view that Group I ultramafic rocks of Madawara are close to mantle composition and are less fractionated, whereas Group II type of rocks are more evolved and are enriched with dissolved sulphur

# 6 Concluding remarks

The ultramafic rocks of the Madawara Igneous Complex are enriched in Ir, Pt, Au, Ni, Cr and depleted in Cu, Al, Ca and V. The field relationship and geochemical study suggest two distinct categories. The geochemical and petrological data show that they are derived from variable degrees of partial melting of a primitive mantle composition. Based on major and trace- element systematics, and published experimental melting studies, it is inferred that these ultramafites represent high degree of partial melt equivalent to those that represent a batch melt extracted from a primitive fertile mantle composition at pressures between 1 and 3 GPa [1]. Different suites of magma were developed due to the variations in the degree of partial melting that are not easily related to a simple lithospheric column generated during a single upwelling event. The relatively high Ir and low Pd/Ir ratio are usually considered as signatures for high degree of partial melting of fertile mantle at moderate to greater depth. The high degree of partial melt would promote HREE enrichment in the melt, leaving a strongly LREE- depleted source. The high values of IPGE in a few samples and flat to slightly enriched LREE may be considered as having formed due to the dissolved sulphur and chloride fluid phases and carbonatite metasomatism.

**Acknowledgement:** The authors (MS and VB) are grateful to the Director, CSIR-National Geophysical Research Institute (NGRI), Hyderabad, for his support and permission to publish this paper. Profs. L.G. Gwalani and D.I. Groves are profusely thanked for critical evaluation

and providing useful suggestion for improving the final manuscript. This work forms part of the Ministry of Earth Sciences, Government of India funded project vide letter no. MoES/PO(Geosci)/4/2013.

### References

- [1] Walter M.J., Melting residues of fertile peridotite and the origin of cratonic lithosphere. In: Fei Y., Bertka M., Mysen B.O. (Eds.), Mantle Petrology: Field Observations and High-Pressure Experimentation. A Tribute to France R. (Joe) Boyd. Spec. Publ. No. 6 -Geochemical Society, St.Louis MO, USA, 1999, 22-240.
- [2] Barnes S.J., Maier W.D., The fractionation of Ni, Cu and the noble metals in silicate and sulphide liquids. In: Keays R.R., Lesher C.M., Lightfoot P.C., Farrow C.E.G. (Eds). Dynamic processes in Magmatic Ore Deposits and their Applications to Mineral Exploitation - Short Course Notes, vol. 13 Geol. Ass. Can., St.John's NL, 1999, 69-106.
- [3] Naldrett A.J., Wilson A., Kinnaird J., Chunnett G., PGE tenor and metal ratios within and below the Merensky Reef, Bushveld Complex: Implications for its genesis. J. Petrology, 2009, 50, 625-659.
- [4] Singh S.P., Singh M.M., Srivastava G.S., Basu A.K., Crustal evolution in Bundelkhand area, Central India. Jour. Himalayan Geol., 2007, 28, 79-101.
- [5] Pati J.K., Bhusan R., Prakash K., PGEs concentration in metamorphosed mafic-ultramafic rocks of southern Bundelkhand craton, Central India. Proc. MSI-2007 & Nat Sem on Exploration for PGE, Gold & Diamond in India, NGRI, Hyderabad, 2007, 46.
- [6] Mondal M.E.A., Goswami J.N., Deomurari M.P., Sharma K.K., Ion microprobe 207Pb/206Pb ages of Zircons from the Bundelkhand massif, northern India, implications for crustal evolution of the Bundelkhand-Aravalli Proto Continent. Precambrian Res., 2002, 117, 85-110.
- [7] Singh S.P., Archaean Geology of Bundelkhand craton, Central India: An overview. Gondwana Geological Magazine, 2012, Special Vol.13, 125-140.
- [8] Mohan M.R., Singh S.P., Santosh M., Siddique M.A., Balaram V., TTG suite form the Bundelkhand Craton, Central India: Geochemistry, petrogenesis and implications for Archaean crustal evolution. J. Asian Earth Sci., 2012, 58, 38-50.
- [9] Saha L., Pant N.C., Pati J.K., Upadhyay D., Berndt J., Bhattacharya A., Satynarayanan M., Neoarchean high-pressure margarite-phengitic muscovite-chlorite corona mantled corundum in quartz-free high-Mg, Al phlogopite-chlorite schists from the Bundelkhand craton, north central India. Contrib. Mineral. Petr., 2011, 161, 511-530.
- [10] Singh S.P., Dwivedi S.B., Garnet-sillimanite-cordierite-quartz bearing assemblages from early Archean supracrustal rocks of Bundelkhand Massif, Central India. Curr. Sci., 2009, 97, 103-107.
- [11] Malviya P., Arima M., Pati J.K., Kaneko Y., Petrology and geochemistry of metamorphosed basaltic pillow lava and basaltic komatiite in the Mauranipur area: subduction related volcanism in the Archaean Bundelkhand craton, Central India. J. Miner.

- Petrol. Sci., 2006, 101, 199-217.
- [12] Basu A.K., Geology of parts of the Bundelkhand Granite Massif. Rec. Geol. Surv. India, 1986, 117, 61-124.
- [13] Prakash R., Swarup P., Srivastava R.N., Geology and mineralization in the southern parts of Bundelkhand in Lalitpur district, Uttar Pradesh. Jour. Geol. Soc. India, 1975, 16, 143-156.
- [14] Sharma R.P., Lithostratigraphy, structure and petrology of the Bundelkhand group. In: Valdia K.S., Bhatia S.B., Gaur V.K. (Eds). Geology of Vindhyanchal, Hindustan Publishing Corporation, New Delhi, 1982, 30-46.
- [15] Farooqui S.A., Singh A.K., Platinum mineralization in Ikauna Area, Lalitpur district, Uttar Pradesh. Jour. Geol. Soc. India, 2006, 68, 582-584.
- [16] Singh S.P., Balaram V., Satyanarayanan M., Anjaiah K.V., Kharia A., Platinum group elements in basic and ultrabasic rocks around Madawara, Bundelkhand Massif, Central India. Current Science, 2010, 99(3), 375-383.
- [17] Singh S.P., Balaram V., Satyanarayanan M., Sarma D.S., Subramanyam K.S.V., Anjaiah K.V., Kharia A., Platinum Group Minerals from the Madawara Ultramafic-mafic Complex, Bundelkhand Massif, Central India: A Preliminary Note. Jour. Geol. Soc. India, 2011, 78, 281-283.
- [18] Balaram V., Singh S.P., Satyanarayanan M., Anjaiah K.V., Platinum group elements geochemistry of ultramafic and associated rocks from Pindar in Madawara Igneous Complex, Bundelkhand massif, Central India. J. Earth Syst. Sci., 2013, 122, 79-91.
- [19] Satyanarayanan M., Balaram V., Singh S.P., Sarma D.S., Anjaiah K.V., Kharia A., Platinum group elements in Madawara Igneous Complex, Bundelkhand massif, Central India: Some exciting results. DCS-DST Newsletter, 2011, 21(1), 19-24.
- [20] Singh S.P., Balaram V., Satyanarayanan M., Anjaiah K.V., Kharya A., Madawara ultramafic complex in Bundelkhand Craton: A new PGE repository for exploration in Central India. Journal of Economic Geology and Georesource Management, 2010, 7(1-2), 54-71.
- [21] Singh S.P., Singh M.M., Geochemistry of Archean Mafic and Ultramafics Rocs from central part of Bundelkhand craton: Implication in the Archean crustal Evolution. Journal of Economic Geology and Georesource Management, 2008, 8, 1-15.
- [22] Satyanarayanan M., Singh S.P., Balaram V., Anjaiah K.V., Trace, Rare Earth Element (REE) and Platinum Group Element (PGE) Geochemistry of the mafic and ultramafic rocks from Bundelk-hand Craton, Central India. Adv. Geosci., 2010, 20, 57-79.
- [23] Krishna A.K., Murthy N.N., Govil P.K., Multielement analysis of soils by wavelength-dispersive X-ray fluorescence spectrometry. Atomic Spectroscopy, 2007, 28, 202-214.
- [24] Balaram V., Rao T.G., Rapid determination of REEs and other trace elements in geological samples by microwave acid digestion and ICP-MS. Atomic Spectroscopy, 2003, 24, 206-212.
- [25] Sun S.S., McDonough W. F., Chemical and isotopic systematics of oceanic basalts: implications for mantle composition and processes. In: Saunders, A.D., Norry M.J. (Eds.) Magmatism in Ocean Basins. Geol. Soc. London Spec. Publ., 1989, 42, 313-345.
- [26] Balaram V., Mathur R., Banakar V.K., Hein J.R., Rao C.R.M., Rao T.G., Dasaram B., Determination of the platinum group elements (PGE) and gold (Au) in manganese nodule reference samples by nickel sulfide fire-assay and Te coprecipitation with ICP-MS. Indian J. Mar. Sci., 2006, 35, 7-16.

- [27] Zhou M.F., PGE distribution in 2.7 Ga layered komatiite flows from the Belingwe greenstone belt, Zimbabwe. Chem. Geol., 1994, 118, 155-172.
- [28] Barnes S.J, Naldrett A.J., Gorton M.P., The origin of the fractionation of the platinum-group elements in terrestrial magmas. Chem. Geol., 1995, 53, 303-323.
- [29] Zangana N.A., Downes H., Thirlwall M.F., Hegner E., Relationship between deformation, equilibration temperatures, REE and radiogenic isotopes in mantle xenoliths (Ray Pic, Massif Central, France): an example of plume-lithosphere interaction? Contrib. Mineral. Petr., 1997, 127, 187-203.
- [30] Sproule R.A., Lesher C.M., Ayer J.A., Thurston P.C., Komatiites and komatiitic basalts of the Abitibi greenstone belt: A proposed model for their formation; Precamb. Res., 2002, 115, 153-186.
- [31] Barnes S.J., The use of metal ratios in prospecting for platinum group element deposits in mafic and ultramafic intrusions. J. Geochem. Exploration, 1990, 37, 91-99.
- [32] Downes H., Embey-Isztin A., Thirlwall M.F., Petrology and geochemistry of spinel peridotite xenoliths from the western Pannonian Basin (Hungary): evidence for an association between enrichment and texture in the upper mantle, Contrib. Min. Petr., 1992, 107, 340-354.
- [33] Downes H., Dupuy C., Textural, isotopic and REE variations in spinel peridotite xenoliths, Massif Central, France. Ear. Planet. Sci. Letts., 1987, 82, 121-135.
- [34] Gravestock P.J., The chemical causes of uppermost mantle heterogeneities. Unpublished PhD thesis, Milton Keynes, United Kingdom, Open University, 1992, 1-299.
- [35] Peucat J.J., Bernard-Griffiths J., Gil Ibarguchi J.I., Dallmeyer R.D., Menot P., Cornichet J., Iglesias Ponce de León M., Geochemical and geochronological cross-section of the deep Variscan crust: the Cabo Ortegal high-pressure nappe (Northwestern Spain). Tectonophysics, 1990, 177, 263-292.
- [36] Takazawa E., Frey F.A., Shimizu N., Obata M., Bodinier J.L., Geochemical evidence for melt migration and reaction in the upper mantle. Nature, 1992, 359, 55-58.
- [37] Garrido C.J., Bodinier J.L., Diversity of mafic rocks in the Ronda peridotite: Evidence for pervasive melt-rock reaction during heating of subcontinental lithosphere by upwelling asthenosphere, J. Petrology, 1999, 40, 729-754.
- [38] Zhou M.-F., Robinson P.T., Malpas J., Edwards S.J., Liang Q., REE and PGE Geochemical Constraints on the Formation of Dunites in the Luobusa ophiolite, Southern Tibet. J. Petrology, 2004, 3, 1-25.

- [39] Chen G., Xia B., Platinum-group elemental geochemistry of mafic and ultramafic rocks from the Xigaze ophiolite, southern Tibet, J. Asian Earth Sci., 2008, 32, 406-422.
- [40] Zanetti A., Mazzucchelli M., Rivalenti G., Vannucci R., The Finero phlogopite-peridotite massif: an example of subductionrelated metasomatism, Contrib. Mineral. Petr., 1999, 134, 107-122.
- [41] Gruau G., Bernard-Griffiths J., Lecuyer C., The origin of U-shaped rare earth patterns in ophiolite peridotites: assessing the role of secondary alteration and melt/rock reaction. Geochim. Cosmochim. Acta, 1998, 62, 3545-3560.
- [42] Mysen, B., Kushiro, I., Compositional variations of coexisting phases with degree of melting of peridotite in the upper mantle. Am. Mineral., 1997, 62, 843-865.
- [43] Dick H.J.B., Bullen T., Chromian spinel as a petrogenetic indicator in abyssal and alpine-type peridotites and spatially associated lavas. Contrib. Mineral. Petr., 1984, 86, 54-76.
- [44] Nicolas A., Structures of Ophiolites and Dynamics of Oceanic Lithosphere. Kluwer Academic, Dordrecht, 1989, 367.
- [45] Godard, M., Jousselin D., Bodinier J.-L., Relationships between geochemistry and structure beneath a palaeo-spreading centre: a study of the mantle section in the Oman ophiolite. Earth Planet. Sci. Lett., 2000, 180, 133-148.
- [46] Takazawa E., Okayasu T., Satoh K., Geochemistry and origin of the basal lherzolites from the northern Oman ophiolite (northern Fizh block). Geochem. Geophys., 2003, 4, 1021.
- [47] Prinzhofer A., Allegre C.J., Residual peridotites and the mechanisms of partial melting. Earth Planet. Sci. Lett., 1985, 74, 251-265.
- [48] Navon O., Stolper E., Geochemical consequences of melt percolation: the upper mantle as a chromatographic column. J. Geology, 1987, 95, 285-307.
- [49] Song Y., Frey F.A., Geochemistry of peridotite xenoliths in basalt from Hannuoba, Eastern China: implications for subcontinental mantle heterogeneity. Geochem. Cosmochim. Acta, 1989, 53, 97-113.
- [50] McDonough W.F., Frey F.A., Rare-earth elements in upper mantle rocks. In: Lipin, B.R., McKay G.A. (Eds.) Geochemistry and Mineralogy of Rare Earth Elements. Mineralogical Society of America, Rev. Mineral., 1989, 21, 99-145.
- [51] Barnes S.J., Lesher C.M., Keays R.R., Geochemistry of mineralised and barren komatiites from thePerseverance nickel deposit, Western Australia. Lithos, 1995, 34, 209-234.
- [52] Jensen L.S., A New Cation Plot for Classifying Subalkalic Volcanic Rocks. Ontario Div. Mines, Misc. Paper, 1976, 66, 1-22.

#### RESEARCH ARTICLE

WILEY

# Chromian spinel compositions from Madawara ultramafics. Bundelkhand Craton: Implications on petrogenesis and tectonic evolution of the southern part of Bundelkhand Craton, **Central India**

Niranian Mohanty<sup>1</sup> | Surva Pratap Singh<sup>2</sup> | Manavalan Satyanarayanan<sup>1</sup> | Mudlappa Jayananda<sup>3</sup> | Madiwalappa Mallappa Korakoppa<sup>4</sup> | Sikha Hiloidari<sup>1</sup>

#### Correspondence

Manavalan Satvanaravanan, CSIR-National Geophysical Research Institute, Hyderabad

Email: icpmsnarayanan@gmail.com

#### **Funding information**

Ministry of Earth Sciences, Grant/Award Number: MoES/P.O.(Geosciences)/4/2013

Handling Editor: N.V. Chalapathi Rao

Madawara ultramafic complex (MUC) in the southern part of Bundelkhand Craton, Central India comprises peridotite, olivine pyroxenite, pyroxenite, gabbro, and diorite. Coarse-grained olivine, clinopyroxene (Cpx), amphibole (Amp), Al-chromite, Fechromite, and magnetite with rare orthopyroxene (Opx) are common minerals in peridotite. Chromites are usually coarse-grained euhedral found as disseminated crystals in the olivine matrix showing both homogeneous and zoned texture. Al-chromite, primarily characterizes Cr-spinels and its subsequent fluid activity and alteration can result in the formation of Fe-chromite, chrome magnetite, and magnetite. Mineral chemistry data suggest that Al-chromite is characterized by moderately high Cr<sub>2</sub>O<sub>3</sub> (38.16-51.52 wt.%) and  $Fe_2O_3$  (3.22-14.51 wt.%) and  $Iow Al_2O_3$  (10.63-1.52 wt.%)21.87 wt.%), MgO (1.71-4.92 wt.%), and TiO<sub>2</sub> (0.22-0.67 wt.%), whereas the homogeneous Fe-chromite type is characterized by high Fe<sub>2</sub>O<sub>3</sub> (25.54-47.60 wt.%), moderately low  $Cr_2O_3$  (19.56-37.90 wt.%), and very low  $Al_2O_3$  (0.06-1.53 wt.%). Subsequent alteration of Al-chromite and Fe-chromite leads to formation of Cr-magnetite and magnetite. The Cr# of Al-chromite varies from 55.12 to 76.48 and YFe<sup>3+</sup># from 8 to 19, whereas the ferrian chromite has high Cr# varying from 94.27 to 99.53 while its <sup>Y</sup>Fe<sup>3+</sup># varies from 38 to 70. As a whole, the primary Al-chromite shows low Al<sub>2</sub>O<sub>3</sub>, TiO<sub>2</sub> contents, and high Fe#, Cr# values. Olivines have forsterite ranging from 75.96% to 77.59%. The bulk-rock geochemistry shows continental arc geochemical affinities indicated by the high concentration of large-ion lithophile elements and U, Th relative to the low concentration of high-field strength elements. These petrological and mineralogical as well as primary Al-chromite compositions plotted in different discrimination diagrams suggest an arc environment that is similar to Alaskan-type intrusion.

#### **KEYWORDS**

Alaskan-type intrusion, Bundelkhand Craton, Cr-spinel, parental melt, petrogenesis

<sup>&</sup>lt;sup>1</sup>CSIR-National Geophysical Research Institute, Hyderahad, India

<sup>&</sup>lt;sup>2</sup>Department of Geology, Bundelkhand University, Jhansi, India

<sup>&</sup>lt;sup>3</sup>Centre for Earth, Ocean and Atmospheric Sciences, University of Hyderabad, Hyderabad, India

<sup>&</sup>lt;sup>4</sup>Geological Survey of India, SR, Hyderabad, India

.0991034, 2019, 4, Downloaded from https://onlinelibrary.wiley.com/doi/10.1002/gj.3286 by University Of Hyderabad, Wiley Online Library on [30/01/2023]. See

articles are governed by the applicable Creative Commons License

#### 1 | INTRODUCTION

Chromian spinel (Cr-spinel) (Mg $^{+2}$ , Fe $^{+2}$ ) (Cr $^{+3}$ , Al $^{+3}$ , Fe $^{+3}$ )<sub>2</sub> O<sub>4</sub> is the common ubiquitous accessory phase in many ultramafic-mafic rocks of different tectonic settings (Barnes & Roeder, 2001; Dick & Bullen, 1984; Hamlyn & Keays, 1979; Irvine, 1965, 1967), and their chemistry

is very sensitive to melt composition, melt-rock interaction process, crystallization sequence, oxygen fugacity, pressure-temperature conditions, and degree of partial melting of the source region (Arai, 1980; Barnes & Roeder, 2001; González-Jiménez et al., 2011; Proenza, Gervilla, Melgarejo, & Bodinier, 1999; Sack & Ghiorso, 1991). Cr-spinel is one of the first mineral to crystallize from

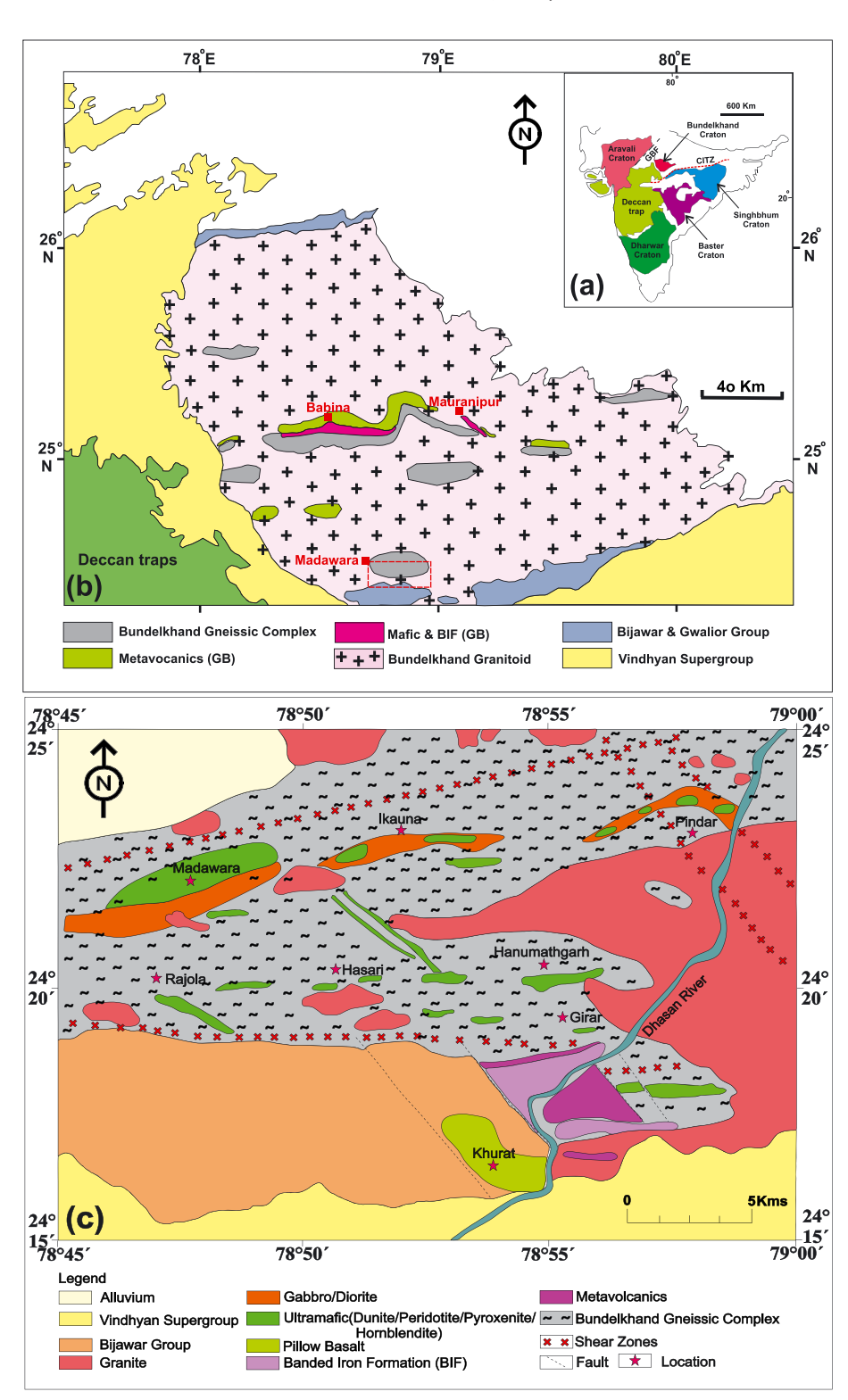


**FIGURE 1** (a) Tectonic framework of the Indian Shield showing Bundelkhand Craton in the north of Central India Tectonic Zone (CITZ). (b) Simplified geological map of Bundelkhand Craton showing the study area in dotted red rectangle near Madawara (modified after Singh et al., 2017). (c) Geological map of MUC showing distribution of ultramafic-mafic rocks along with other lithological units and their relationship (modified after Singh et al., 2011) [Colour figure can be viewed at wileyonlinelibrary.com]

MOHANTY ET AL. 2101

ultramafic-mafic magmas and is the only primary mineral that is highly stable even in completely serpentinized peridotites (Ahmed, Helmy, Arai, & Yoshikawa, 2008; Arai, Kadoshima, & Morishita, 2006; Dick & Bullen, 1984; Dong et al., 2017; Karipi, Tsikouras, Hatzipanagiotou, & Grammatikopoulos, 2007). Cr-spinel is a strong refractory mineral and thought to be resistant to post-magmatic processes such as alteration and regional metamorphism (Burkhard, 1993; Mellini, Rumori, & Viti, 2005), and therefore, it is very useful in evaluating the tectonic provenance of even strongly hydrated mantle peridotites (Saumur & Hattori, 2013) and highly metamorphosed rocks (Arai et al., 2011; Kamenetsky, Crawford, & Meffre, 2001; Rollinson, 2008; Uysal et al.,

2009). The chemical composition of Cr-spinel depends on the degree of depletion of the mantle and the type of melt formed at different tectonic settings, namely, MORB, IAT, OIB, and boninite (Arai et al., 2011; Zaccarini et al., 2011). Therefore, chromite is an important petrogenetic indicator to discriminate the tectonic setting in which the host rocks were emplaced (Arai et al., 2006; Dönmez et al., 2014; González-Jiménez et al., 2011; Pal, 2011; Rollinson, 2008).

Cr-spinels are classified into three categories according to their dominant trivalent ions, such as spinel series (Al<sup>3+</sup>—dominant), magnetite series (Fe<sup>3+</sup>—dominant), and chromite series (Cr<sup>3+</sup>—dominant). Significant solid solution and compositional variations occur between

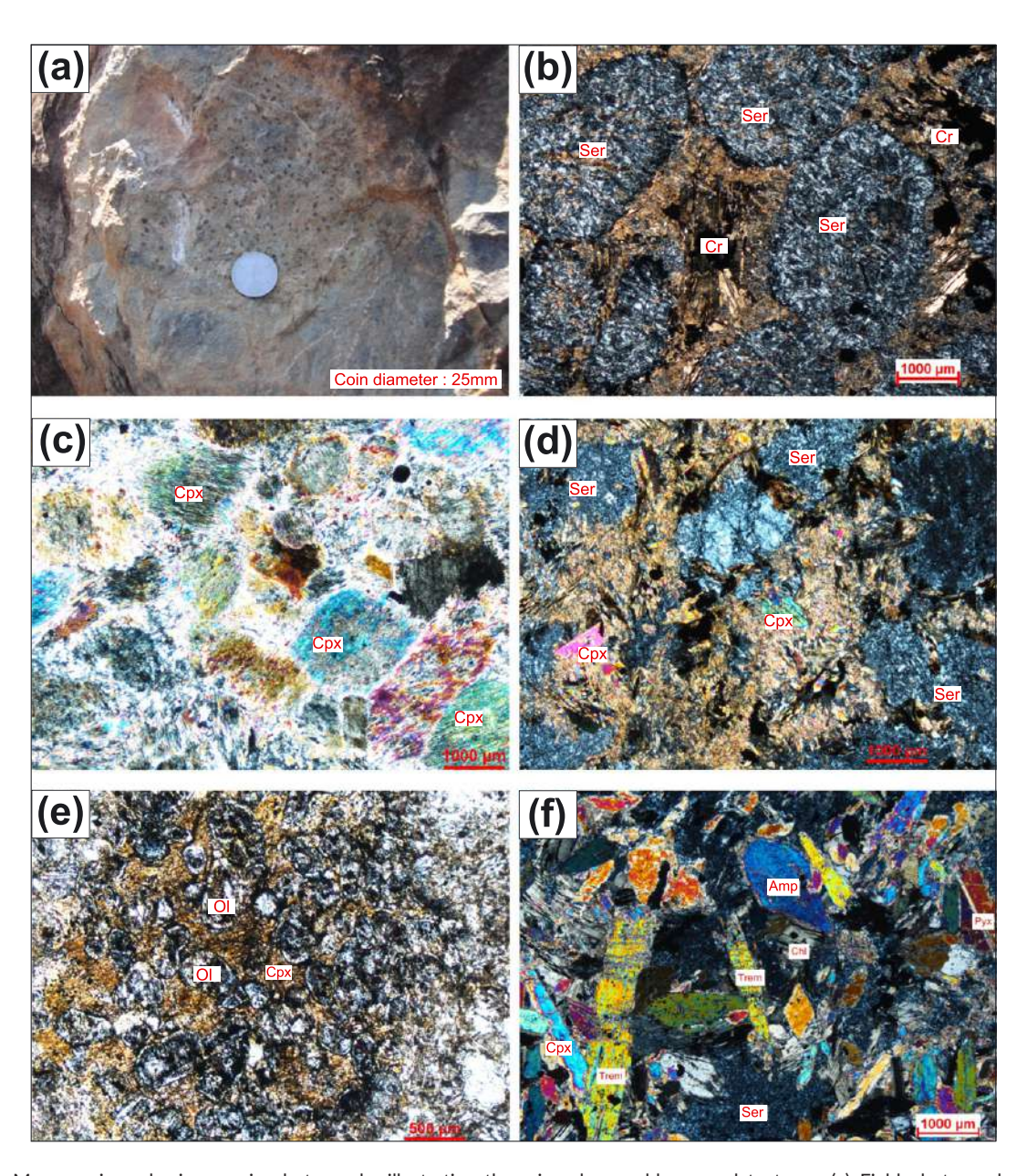


FIGURE 2 Megascopic and microscopic photographs illustrating the mineral assemblages and textures. (a) Field photograph of peridotite showing large number of embedded Cr-spinel crystals at Madawara. (b) Microphotograph of peridotite showing cumulate texture sieved by inclusions of euhedral to subhedral chromite grains in the olivine pseudomorph as well as its grain boundary. (c) Cumulate pyroxenite with inclusion of chromite grains and serpentine particularly in left bottom corner. (d) Cumulate peridotite showing olivine pseudomorph along with presence of pyroxenes in the intercumulus space, which are altered to serpentine (olivine) and tremolite-chlorite (clinopyroxene). (e) Poikilitic texture in olivine pyroxenite showing rounded crystals of olivine and euhedral spinel. (f) Hornblende mantled by tremolite with chlorite in hornblende-pyroxene rich ultramafic rock. Abbreviations: Amp - amphibole, ChI - chlorite, Cpx - clinopyoxene, OI - olivine, Pyx - pyroxene, Ser - Serpentine, Trem - tremolite [Colour figure can be viewed at wileyonlinelibrary.com]

0991034, 2019, 4, Downloaded from https onlinelibrary.wiley.com/doi/10.1002/gj 3286 by University Of Hyderabad, Wiley Online Library on [30/01/2023]. See the Terms/ and Conditions on Wiley Online Library for rules of use; OA articles are governed by the applicable Creative Commons License

them. The Cr# [100Cr/(Cr + Al) atomic ratio] and the Mg# [100Mg/ (Mg + Fe $^{2+}$ ) atomic ratio] of Cr-spinel and many other bivariant ratios are also considered as good discriminators for estimating partial melting of the source and to decipher the tectonic settings of ultramafic-mafic rocks (Kamenetsky et al., 2001; Rollinson, 2005).

The ultramafic-mafic rocks occur as scattered lensoidal bodies in the southern part of Bundelkhand Craton near Madawara, Ikauna, Pindar, Hanumathgarh, Bhikampur, Ramgarh, and Hansra villages and are collectively known as Madawara ultramafic complex (MUC), that comprises dunite, peridotite, hornblende-rich peridotite, olivine pyroxenite, pyroxenite, gabbro, and diorite (Figure 1B-C). Recently, this complex has acquired the status of being considered as a potential source for platinum group elements (PGE) (Balaram, Singh, Satyanarayanan, & Anjaiah, 2013; Faroogui & Singh, 2006, 2010; Satyanarayanan, Balaram, Roy, Anjaiah, & Singh, 2010; Satyanarayanan, Singh, Balaram, & Niranjan, 2015; Singh & Dwivedi, 2009). The ultramafic rocks around Madawara are distributed in about 400-km<sup>2</sup> area as linear bodies (Figure 1c), nearly unmetamorphosed, less deformed, and highly serpentinized (Farooqui & Singh, 2006; Singh et al., 2011). The Cr-spinels are medium- to coarse-grained, occur as inclusions in peridotites, olivine pyroxenites (Figure 2a-c), and sometimes in pyroxenites in different proportions, which are characterized by relatively high PGE values (ranging between 400 to 1,200 ppb; Balaram et al., 2013; Farooqui & Singh, 2010; Satyanarayanan et al., 2015). A detailed mineralogical studies including the composition of Cr-spinel has not been carried out so far. The primary objective of the present work is to study the genesis of Cr-spinel through the analysis of its current mineralogical and compositional data. Further, an attempt is made to evaluate the petrogenesis and possible tectonic setting for the mafic-ultramafic magmatism through mineral chemistry of Cr-spinels in peridotites and the bulk-rock geochemistry of MUC.

#### 2 | GEOLOGY

The Bundelkhand Craton lies to the north of Son-Narmada lineament (SONA) in the Indian Shield (Basu, 1986), occupying an area of around 26,000 km<sup>2</sup>. The gneisses, volcano-sedimentary units and intrusive granites are major lithologies of this craton. It comprises of E-W trending Mesoarchaean gneisses known as Bundelkhand gneissic complex (BnGC) and the Babina-Mauranipur greenstone belt in the central part (Figure 1b; Singh et al., 2017). Various granites were emplaced during the Neoarchean (Mondal, Goswami, Deomurari, & Sharma, 2002). All these lithologies are intruded by NE-SW trending quartz reefs and NW-SE trending dolerite dike swarms during the crustal-scale shearing (Basu, 1986; Basu, 2010; Bhattacharya & Singh, 2013; Mondal et al., 2002; Singh, Singh, Srivastava, & Basu, 2007). Geochronological studies carried out by several workers in the Bundelkhand Craton (Joshi et al., 2017; Kaur, Zeh, Chaudhri, & Eliyas, 2016; Kumar, Raju, Pathak, & Pandey, 2010; Mondal et al., 2002; Mondal, Sharma, Rahman, & Goswami, 1998; Saha et al., 2016; Sarkar, 1996; Verma, Verma, Oliveira, Singh, & Moreno, 2016) suggest that accretion of tonalite-trondhjemite-granodiorite (TTG) occurred in three phases from 3,500 to 3,200 Ma (Kaur et al., 2016). Ultramaficmafic and basalt-andesite-rhyolite-dacite magmatism (plume-arc type) in the Mauranipur–Babina greenstone belt accreted at approximately 2,700 to 2,545 Ma (Singh et al., 2017). The cratonization is marked by emplacement of Bundelkhand granitoids that occurred subsequent to the greenstone volcanism from 2,552 to 2,525 Ma (Joshi et al., 2017; Kaur et al., 2016; Mondal et al., 2002; Saha et al., 2016). NE–SW trending quartz reefs probably corresponding to the late stage fluid-rich residual liquid of granite magmatism, yield ages between 2,300 and 2,400 Ma (Li et al., 2017; Pati et al., 2007). The <sup>40</sup>Ar/<sup>39</sup>Ar age estimates of the dolerite dike swarms emplacements are in between 2,150 and 2,000 Ma (Rao, Rao, Widdowson, & Kelley, 2005).

The southern part of the Bundelkhand Craton also preserves high-grade basement rocks such as granitic gneisses, gneisses, migmatite, amphibolites, and hornblende-biotite gneisses. These rocks are exposed around Rajola and north of Madawara (Figure 1c). The low-grade metamorphosed volcano-sedimentary rocks such as banded haematite-magnetite quartzite, quartzite, mica-schists, and amphibolites are exposed around Girar, Baraitha, and Badwar villages. These rock units may be part of a separate greenstone belt in the southern Bundelkhand Craton.

The MUC lies at the southern fringe of the Bundelkhand Craton where two distinct intrusions trending E-W to ENE-WSW have been mapped (Singh et al., 2011). The largest ultramafic body is exposed at the SE part of Madawara village and is in the form of a low lying ridge that is ~400 m wide and extends laterally up to 5 km. These lensoidal ultramafic-mafic units consist of dunite, peridotite, pyroxenite, olivine pyroxenite, hornblendite, gabbro, and diorite, which are exposed at Madawara, Ikauna, Pindar, Hanumathgarh, and at many other places (Satyanarayanan et al., 2015; Figure 1c). These ultramafic-mafic bodies are nearly subparallel and are confined between the Madawara-Karitoran shear zone in the north and Sonrai-Girar shear zone in the south. Both MUC and BnGC have been affected by shearing and fluid flow, demonstrating a fluid-induced alteration of the ultramafic rocks into serpentine-talc-chlorite schists and talctremolite-actinolite schists. These ultramafic units are further traversed by Bundelkhand granitoids and NE-SW trending quartz reefs. At Madawara, the intrusion is asymmetric with ultramafic rocks in the centre comprising of dunite, peridotite, olivine pyroxenite, pyroxenite, and hornblende-rich peridotite, and hornblendite. The outer rim consists of gabbro and diorite. The peridotite occurs as elliptical masses trending ENE-WSW, parallel to the elongation of intrusions as well as Madawara-Karitoran shear zone.

#### 3 | PETROGRAPHY

Peridotite consists essentially of olivine (70–80%), clinopyroxene (10–20%), and accessory Cr-spinel (5–10%). Olivines occur as euhedral to subhedral cumulate crystals and have been altered to serpentine, while the clinopyroxenes have been altered to tremolite and chlorite. Euhedral to subhedral Cr-spinel grains are enclosed in olivine as well as in the interspaces. Magnetites are crystallized along the fracture surface of the olivine. Sparse amount of orthopyroxenes are also seen in some of the sections. Sulphide phases such as chalcopyrite, pentaldite, and millerite crystallize in the interstitial spaces of olivine (Figure 2b and 2d).

FIGURE 3 Back-scattered electron (BSE) images showing (a) cumulate peridotite with large grain olivine pseudomorph altered to serpentine and intercumulus phase containing clinopyroxene altered to tremolite and in some part to chlorite, (b) homogeneous Cr-spinel (Al-chromite) in serpentinised peridotite, (c) zoned chromite with Al-chromite core rimmed by Cr-magnetite, (d) partly altered zoned Cr-spinel crystals present as inclusion in the pyroxene with very thin rim of ferritchromite in the olivine pyroxenite, (e) euhedral zoned Cr-spinel in peridotite with core-rim compositional variation and presence of magnetite and ilmenite in the intercumulus space, (f) zoned Cr-spinel in amphibole-rich peridotite, (g) homogeneous Fe-chromite present in the matrix of olivine in peridotite rock, and (h) alteration of Cr-magnetite and magnetite in peridotite Abbrevations: Al-chr: Al-chromite; Fe-chr: ferrian chromite; Cr-mag: Chrome magnetite; mag: Magnetite; Ol: Olivine; Ser: Serpentine; Amp: Amphibole; Chl: Chlorite [Colour figure can be viewed at wileyonlinelibrary.com]

Pyroxenite contains clinopyroxene (60-70%), olivine (5-10%), Crspinel (5%), magnetite (10-15%), and amphiboles (5-10%). Olivine is altered to serpentine, the relicts of which are observed within the olivine pyroxenite body. Pyroxenes are altered to tremolite, actinolite, and chlorite. In some cases, primary hornblendes are also altered to chlorite. Cr-spinel grains are invariably small and mostly occur as inclusions both in olivine and pyroxene (Figure 2c and 2e). The olivine pyroxenite contains clinopyroxene and primary hornblende as well as relict olivines, in which the large clinopyroxene oikocrysts poikilitically enclose small subrounded relict olivine chadacrysts (Figure 2e). In hornblende peridotite, the primary hornblendes are found in interspaces of pyroxenes and are altered to actinolite along their margins. Most of the pyroxenes are also altered to tremolite actinolite. Magnetite and chromite occur as accessory phases while magnetite and titano-magnetite are more abundant than chromite in this rock (Figure 2f). Cr-spinel in the peridotite, olivine pyroxenite, and pyroxenites of the present studied rocks are mainly grouped into two textural varieties such as homogeneous and zoned type (Figure 3b-c). They mainly occur as both intercumulus and intragranular spaces of olivine minerals.

The gabbro contains essentially plagioclase and clinopyroxene (40–60% each) with accessory magnetite. Diorite contains equal amount of plagioclase and hornblende but most of the plagioclase are altered to epidote. Cr-spinel are absent while magnetite, illmenite, and titano-magnetite are present (Figures not shown here).

#### 4 | ANALYTICAL TECHNIQUES

#### 4.1 | Whole-rock geochemistry

Major elements were determined by wavelength-dispersive X-ray fluorescence (XRF) spectrometry (Philips PW-2440 Magic-PRO®) at National Geophysical Research Institute (NGRI), Hyderabad, following

**TABLE 1** Olivine composition of the Madawara ultramafic intrusion

TABLE 1	Olivine comp	osition of th	ie Madawar	a uitramatic	intrusion						
Sample mineral Ref. point	M/16/OP Olivine 8/1.	M/16/OP Olivine 9/1.	M/16/OP Olivine 10/1.	M/16/OP Olivine 11/1.	M/16/OP Olivine 13/1.	M/16/OP Olivine 21/1.	M/16/OP Olivine 22/1.	M/16/OP Olivine 23/1.	M/16/OP Olivine 24/1.	M/16/OP Olivine 25/1.	M/16/OP Olivine 11/1.
SiO <sub>2</sub>	39.46	39.49	39.04	39.46	39.24	38.45	38.66	38.80	38.76	39.29	37.81
TiO <sub>2</sub>	0.02	0.01	0.00	0.02	0.01	0.03	0.01	0.00	0.03	0.00	0.09
$Al_2O_3$	0.00	0.04	0.00	0.02	0.01	0.02	0.03	0.01	0.00	0.01	0.06
Cr <sub>2</sub> O <sub>3</sub>	0.02	0.17	0.00	0.00	0.12	0.70	0.07	0.08	0.00	0.00	1.29
$FeO^T$	21.39	21.50	21.09	21.19	21.40	22.05	20.96	21.78	21.61	20.61	22.13
MnO	0.29	0.25	0.26	0.21	0.23	0.23	0.29	0.20	0.29	0.21	0.33
MgO	40.41	40.26	40.17	40.37	40.26	39.08	39.55	40.06	40.02	40.03	38.87
CaO	0.00	0.00	0.00	0.04	0.03	0.02	0.03	0.02	0.00	0.00	0.00
Na <sub>2</sub> O	0.02	0.00	0.02	0.02	0.03	0.00	0.01	0.01	0.03	0.00	0.01
K <sub>2</sub> O	0.02	0.01	0.00	0.01	0.00	0.01	0.00	0.00	0.01	0.01	0.01
NiO	0.00	0.00	0.00	0.00	0.00	0.00	0.00	0.00	0.00	0.00	0.00
Total	101.63	101.72	100.57	101.34	101.32	100.58	99.61	100.97	100.75	100.17	100.60
Fe <sub>2</sub> O <sub>3</sub>	0.00	0.00	0.00	0.00	0.00	0.00	0.00	0.46	0.54	0.00	0.45
FeO	21.39	21.50	21.09	21.19	21.40	22.05	20.96	21.36	21.13	20.61	21.72
Total	101.63	101.72	100.57	101.34	101.32	100.58	99.61	101.01	100.80	100.17	100.65
Cations	4(O)	4(O)	4(O)	4(O)	4(O)	4(O)	4(O)	4(O)	4(O)	4(O)	4(O)
Si	1.00	1.00	1.00	1.00	1.00	0.99	1.00	0.99	1.00	1.01	0.98
Ti	0.00	0.00	0.00	0.00	0.00	0.00	0.00	0.00	0.00	0.00	0.00
Al	0.00	0.00	0.00	0.00	0.00	0.00	0.00	0.00	0.00	0.00	0.00
Cr	0.00	0.00	0.00	0.00	0.00	0.01	0.00	0.00	0.00	0.00	0.03
Fe <sup>+3</sup>	0.00	0.00	0.00	0.00	0.00	0.00	0.00	0.01	0.01	0.00	0.01
Fe <sup>+2</sup>	0.45	0.46	0.45	0.45	0.46	0.48	0.45	0.46	0.45	0.44	0.47
Mn	0.01	0.01	0.01	0.00	0.00	0.01	0.01	0.00	0.01	0.00	0.01
Mg	1.53	1.52	1.54	1.53	1.53	1.51	1.53	1.53	1.53	1.53	1.50
Ca	0.00	0.00	0.00	0.00	0.00	0.00	0.00	0.00	0.00	0.00	0.00
Na	0.00	0.00	0.00	0.00	0.00	0.00	0.00	0.00	0.00	0.00	0.00
K	0.00	0.00	0.00	0.00	0.00	0.00	0.00	0.00	0.00	0.00	0.00
Ni	0.00	0.00	0.00	0.00	0.00	0.00	0.00	0.00	0.00	0.00	0.00
Total	3.00	2.99	3.00	3.00	3.00	3.00	3.00	3.00	3.00	2.99	3.00
Olivine (Fo)	77.11	76.95	77.25	77.25	77.03	75.96	77.08	76.97	77.15	77.59	76.13
Olivine (Fa)	22.89	23.05	22.75	22.75	22.97	24.04	22.92	23.03	22.85	22.41	23.87

10991034, 2019, 4, Downloaded from https://onlinelibrary.wiley.com/doi/10.1002/gj.3286 by University Of Hyderabad, Wiley Online Library on [30.01/2023]. See the Terms and Conditions (https://onlinelibrary.wiley.com/doi/10.1002/gj.3286 by University Of Hyderabad, Wiley Online Library on [30.01/2023]. See the Terms and Conditions (https://onlinelibrary.wiley.com/doi/10.1002/gj.3286 by University Of Hyderabad, Wiley Online Library on [30.01/2023]. See the Terms and Conditions (https://onlinelibrary.wiley.com/doi/10.1002/gj.3286 by University Of Hyderabad, Wiley Online Library on [30.01/2023]. See the Terms and Conditions (https://onlinelibrary.wiley.com/doi/10.1002/gj.3286 by University Of Hyderabad, Wiley Online Library on [30.01/2023]. See the Terms and Conditions (https://onlinelibrary.wiley.com/doi/10.1002/gj.3286 by University Of Hyderabad, Wiley Online Library on [30.01/2023]. See the Terms and Conditions (https://onlinelibrary.wiley.com/doi/10.1002/gj.3286 by University Of Hyderabad, Wiley Online Library on [30.01/2023]. See the Terms and Conditions (https://onlinelibrary.wiley.com/doi/10.1002/gj.3286 by University Of Hyderabad, Wiley Online Library on [30.01/2023]. See the Terms and Conditions (https://onlinelibrary.wiley.com/doi/10.1002/gj.3286 by University Of Hyderabad, Wiley Online Library on [30.01/2023]. See the Terms and Conditions (https://onlinelibrary.wiley.com/doi/10.1002/gj.3286 by University Of Hyderabad, Wiley Online Library on [30.01/2023]. See the Terms and Conditions (https://onlinelibrary.wiley.com/doi/10.1002/gj.3286 by University Of Hyderabad, Wiley Online Library on [30.01/2023]. See the Terms and Conditions (https://onlinelibrary.wiley.com/doi/10.1002/gj.3286 by University Of Hyderabad, Wiley Online Library on [30.01/2023]. See the Terms and Conditions (https://onlinelibrary.wiley.com/doi/10.1002/gj.3286 by University Of Hyderabad, Wiley Online Library.wiley.com/doi/10.1002/gj.3286 by University Of Hyderabad, Wiley Online Library.wiley.wiley. -and-conditions) on Wiley Online Library for rules of use; OA articles are governed by the applicable Creative Commons License

 TABLE 2
 Cr-spinel composition of the Madawara ultramafic intrusion

IADLE 2	Ci-spirier com	position of the	z Mauawara (	aitiainane inti	351011					
Sample mineral Ref. point	M/16/OP Al-Chr* 1/1.	M/16/OP Al-Chr* 2/1.	M/16/OP Al-Chr* 4/1.	M/16/OP Al-Chr* 5/1.	M/16/OP Al-Chr* 7/1.	M/16/OP Al-Chr* 8/1.	M/16/OP Al-Chr* 17/1.	M/16/OP Al-Chr* 27/1.	M/16/OP Al-Chr* 17/1.	M/8R/P Al-Chr* 2/1.
SiO <sub>2</sub>	0.15	0.06	0.03	0.05	0.05	0.05	0.03	0.03	0.03	0.05
TiO <sub>2</sub>	0.41	0.45	0.47	0.39	0.40	0.40	0.67	0.52	0.67	0.46
$Al_2O_3$	13.81	13.81	13.51	13.67	13.46	13.75	12.89	15.88	12.89	14.68
Cr <sub>2</sub> O <sub>3</sub>	46.47	46.24	45.87	46.29	48.30	46.70	38.16	45.46	38.16	43.30
$FeO^T$	33.62	34.07	33.31	34.21	33.06	34.06	42.32	33.02	42.32	32.20
MnO	0.47	0.41	0.37	0.37	0.47	0.17	0.33	0.28	0.33	1.62
MgO	2.75	2.50	2.69	2.56	2.86	2.52	2.04	3.13	2.04	4.34
CaO	0.01	0.05	0.00	0.07	0.04	0.06	0.01	0.00	0.01	0.00
Na <sub>2</sub> O	0.04	0.04	0.06	0.05	0.06	0.05	0.04	0.04	0.04	0.04
K <sub>2</sub> O	0.01	0.00	0.01	0.01	0.00	0.00	0.00	0.00	0.00	0.01
NiO	0.00	0.00	0.00	0.00	0.00	0.00	0.00	0.00	0.00	0.00
ZnO	1.69	1.88	1.58	1.82	1.76	1.82	1.32	1.54	1.32	0.98
Total	99.44	99.50	97.88	99.48	100.46	99.57	97.80	99.90	97.80	97.67
Fe <sub>2</sub> O <sub>3</sub>	6.19	6.51	6.26	6.82	5.77	6.30	14.51	5.26	14.51	8.26
FeO	28.05	28.21	27.67	28.07	27.86	28.40	29.26	28.29	29.26	24.77
Total	100.06	100.15	98.51	100.17	101.03	100.20	99.26	100.43	99.26	98.50
Cations:	4(O)	4(O)	4(O)	4(O)	4(O)	4(O)	4(O)	4(O)	4(O)	4(O)
Si	0.01	0.00	0.00	0.00	0.00	0.00	0.00	0.00	0.00	0.00
Ti	0.01	0.01	0.01	0.01	0.01	0.01	0.02	0.01	0.02	0.01
Al	0.56	0.56	0.55	0.55	0.54	0.55	0.53	0.63	0.53	0.59
Cr	1.26	1.25	1.26	1.25	1.29	1.26	1.05	1.21	1.05	1.17
Fe <sup>+3</sup>	0.16	0.17	0.16	0.18	0.15	0.16	0.38	0.13	0.38	0.21
Fe <sup>+2</sup>	0.80	0.81	0.80	0.80	0.79	0.81	0.85	0.80	0.85	0.71
Mn	0.01	0.01	0.01	0.01	0.01	0.00	0.01	0.01	0.01	0.05
Mg	0.14	0.13	0.14	0.13	0.14	0.13	0.11	0.16	0.11	0.22
Ca	0.00	0.00	0.00	0.00	0.00	0.00	0.00	0.00	0.00	0.00
Na	0.00	0.00	0.00	0.00	0.00	0.00	0.00	0.00	0.00	0.00
K	0.00	0.00	0.00	0.00	0.00	0.00	0.00	0.00	0.00	0.00
Ni	0.00	0.00	0.00	0.00	0.00	0.00	0.00	0.00	0.00	0.00
Zn	0.05	0.06	0.05	0.06	0.05	0.06	0.04	0.05	0.04	0.03
Total	3.00	3.00	3.00	3.00	3.00	3.00	3.00	3.00	3.00	3.00
Cr#	69.30	69.20	69.49	69.44	70.66	69.50	66.51	65.76	66.51	66.43
Mg#	14.89	13.66	14.75	14.00	15.45	13.65	11.07	16.47	11.07	23.78
Fe#	85.11	86.34	85.25	86.00	84.55	86.35	88.93	83.53	88.93	76.22
Fe <sup>3+</sup> #	0.17	0.17	0.17	0.18	0.16	0.17	0.31	0.14	0.31	0.23
<sup>γ</sup> Fe <sup>3+</sup> #	0.08	0.08	0.08	0.09	0.07	0.08	0.19	0.07	0.19	0.11
Sample mineral Ref. point	M/8/P Al-Chr* 3/1.	M/16/OP Al-Chr* 19/1.	M/16/OP Al-Chr* 21/1.	M/16/OP Al-Chr* 29/1.	M/16/OP Al-Chr* 23/1.			M/8/P Al-Chr* 21/1.	IK/3/P Al-Chr* 12/1 C	IK/3/P Al-Chr* 26/1 C
SiO <sub>2</sub>	0.01	0.00	0.04	0.04	0.02	0.02	0.04	0.03	0.00	0.00
TiO <sub>2</sub>	0.43	0.44	0.25	0.48	0.28	0.23	0.26	0.27	0.30	0.32
$Al_2O_3$	15.03	19.35	21.19	19.28	21.87	19.14	21.60	18.91	12.96	10.63
Cr <sub>2</sub> O <sub>3</sub>	43.08	42.69	41.74	43.09	41.42	38.84	39.54	39.50	46.32	51.52
FeO <sup>T</sup>	32.68	31.85	29.88	31.32	30.47	31.98	29.35	31.67	34.96	32.49
MnO	1.60	0.44	0.34	0.29	0.21	1.62	1.34	1.69	1.26	1.18
MgO	3.88	3.50	3.69	3.39	3.70	4.61	4.92	4.48	1.74	1.86
CaO	0.00	0.00	0.00	0.00	0.00	0.00	0.02	0.00	0.02	0.03
Na <sub>2</sub> O	0.03	0.07	0.07	0.03	0.05	0.03	0.02	0.00	0.05	0.03
K <sub>2</sub> O	0.00	0.01	0.01	0.00	0.03	0.00	0.03	0.00	0.00	0.00
NiO	0.00	0.00	0.00	0.00	0.00	0.00	0.00	0.00	0.12	0.00
INIO	0.00	0.00	0.00	0.00	0.00	0.00	0.00	0.00	0.12	0.23



TABLE 2 (Continued)

Semple   May	TABLE 2 (Co	Hilliueu)									
February   Februar	mineral	Al-Chr*	Al-Chr*	Al-Chr*	Al-Chr*	Al-Chr*	Al-Ch	r* Al-Chı	r* Al-Chr*	Al-Chr*	Al-Chr*
FeyOrs   7.94   4.92   3.22   3.94   3.50   7.83   5.19   7.33   6.08   3.71   7.10   7.01   7.01   7.01   7.01   7.01   7.01   7.01   7.01   7.01   7.01   7.01   7.01   7.01   7.01   7.01   7.01   7.01   7.01   7.01   7.01   7.01   7.01   7.01   7.01   7.01   7.01   7.01   7.01   7.01   7.01   7.01   7.01   7.01   7.01   7.01   7.01   7.01   7.01   7.01   7.01   7.01   7.01   7.01   7.01   7.01   7.01   7.01   7.01   7.01   7.01   7.01   7.01   7.01   7.01   7.01   7.01   7.01   7.01   7.01   7.01   7.01   7.01   7.01   7.01   7.01   7.01   7.01   7.01   7.01   7.01   7.01   7.01   7.01   7.01   7.01   7.01   7.01   7.01   7.01   7.01   7.01   7.01   7.01   7.01   7.01   7.01   7.01   7.01   7.01   7.01   7.01   7.01   7.01   7.01   7.01   7.01   7.01   7.01   7.01   7.01   7.01   7.01   7.01   7.01   7.01   7.01   7.01   7.01   7.01   7.01   7.01   7.01   7.01   7.01   7.01   7.01   7.01   7.01   7.01   7.01   7.01   7.01   7.01   7.01   7.01   7.01   7.01   7.01   7.01   7.01   7.01   7.01   7.01   7.01   7.01   7.01   7.01   7.01   7.01   7.01   7.01   7.01   7.01   7.01   7.01   7.01   7.01   7.01   7.01   7.01   7.01   7.01   7.01   7.01   7.01   7.01   7.01   7.01   7.01   7.01   7.01   7.01   7.01   7.01   7.01   7.01   7.01   7.01   7.01   7.01   7.01   7.01   7.01   7.01   7.01   7.01   7.01   7.01   7.01   7.01   7.01   7.01   7.01   7.01   7.01   7.01   7.01   7.01   7.01   7.01   7.01   7.01   7.01   7.01   7.01   7.01   7.01   7.01   7.01   7.01   7.01   7.01   7.01   7.01   7.01   7.01   7.01   7.01   7.01   7.01   7.01   7.01   7.01   7.01   7.01   7.01   7.01   7.01   7.01   7.01   7.01   7.01   7.01   7.01   7.01   7.01   7.01   7.01   7.01   7.01   7.01   7.01   7.01   7.01   7.01   7.01   7.01   7.01   7.01   7.01   7.01   7.01   7.01   7.01   7.01   7.01   7.01   7.01   7.01   7.01   7.01   7.01   7.01   7.01   7.01   7.01   7.01   7.01   7.01   7.01   7.01   7.01   7.01   7.01   7.01   7.01   7.01   7.01   7.01   7.01   7.01   7.01   7.01   7.01   7.01   7.01   7.01   7.01   7.01   7.01	ZnO	1.00	2.06	2.12	2.19	2.41	0.78	1.41	0.99	0.00	0.00
Fe	Total	97.75	100.41	99.32	100.09	100.43	97.24	98.56	97.54	97.73	98.29
Total	Fe <sub>2</sub> O <sub>3</sub>	7.94	4.92	3.22	3.94	3.50	7.83	5.19	7.33	6.08	3.71
Cations:         4(O)	FeO	25.54	27.43	26.98	27.77	27.32	24.93	24.68	25.07	29.49	29.15
Si         0.00         0.00         0.00         0.00         0.00         0.00         0.00         0.00         0.00         0.00         0.00         0.00         0.00         0.00         0.00         0.00         0.00         0.00         0.00         0.00         0.00         0.00         0.00         0.00         0.00         0.00         0.00         0.00         0.00         0.00         0.00         0.00         0.00         0.00         0.00         0.00         0.00         0.00         0.00         0.00         0.00         0.00         0.00         0.00         0.00         0.00         0.00         0.00         0.00         0.00         0.00         0.00         0.00         0.00         0.00         0.00         0.00         0.00         0.00         0.00         0.00         0.00         0.00         0.00         0.00         0.00         0.00         0.00         0.00         0.00         0.00         0.00         0.00         0.00         0.00         0.00         0.00         0.00         0.00         0.00         0.00         0.00         0.00         0.00         0.00         0.00         0.00         0.00         0.00         0.00         0.00 <th< td=""><td>Total</td><td>98.54</td><td>100.90</td><td>99.65</td><td>100.49</td><td>100.78</td><td>98.03</td><td>99.08</td><td>98.27</td><td>98.34</td><td>98.66</td></th<>	Total	98.54	100.90	99.65	100.49	100.78	98.03	99.08	98.27	98.34	98.66
Ti	Cations:	4(O)	4(O)	4(O)	4(O)	4(O)	4(O)	4(0)	4(O)	4(O)	4(O)
AI         0.61         0.75         0.82         0.75         0.84         0.76         0.84         0.75         0.54         0.44           Cr         1.17         1.11         1.09         1.13         1.07         1.03         1.03         1.05         1.29         1.44           Fe³2         0.20         0.12         0.08         0.10         0.07         0.74         0.70         0.88         0.70         0.87         0.86           Mn         0.05         0.01         0.01         0.01         0.01         0.05         0.04         0.05         0.04         0.06           Ca         0.00         0.00         0.00         0.00         0.00         0.00         0.00         0.00         0.00         0.00         0.00         0.00         0.00         0.00         0.00         0.00         0.00         0.00         0.00         0.00         0.00         0.00         0.00         0.00         0.00         0.00         0.00         0.00         0.00         0.00         0.00         0.00         0.00         0.00         0.00         0.00         0.00         0.00         0.00         0.00         0.00         0.00         0.00	Si	0.00	0.00	0.00	0.00	0.00	0.00	0.00	0.00	0.00	0.00
Cr         1.17         1.11         1.09         1.13         1.03         1.03         1.03         1.09         1.29         1.44           Fe¹³         0.20         0.12         0.08         0.10         0.09         0.20         0.13         0.19         0.16         0.08           Mn         0.05         0.01         0.01         0.01         0.01         0.01         0.05         0.04         0.05         0.04         0.06           Mn         0.05         0.01         0.01         0.01         0.01         0.05         0.04         0.05         0.04         0.00         0.00         0.00         0.00         0.00         0.00         0.00         0.00         0.00         0.00         0.00         0.00         0.00         0.00         0.00         0.00         0.00         0.00         0.00         0.00         0.00         0.00         0.00         0.00         0.00         0.00         0.00         0.00         0.00         0.00         0.00         0.00         0.00         0.00         0.00         0.00         0.00         0.00         0.00         0.00         0.00         0.00         0.00         0.00         0.00         0.00	Ti	0.01	0.01	0.01	0.01	0.01	0.01	0.01	0.01	0.01	0.01
Fe <sup>20</sup> 0.20         0.12         0.08         0.10         0.09         0.20         0.13         0.19         0.16         0.10           Fe <sup>22</sup> 0.73         0.75         0.74         0.77         0.74         0.70         0.88         0.70         0.81         0.04           Mn         0.05         0.01         0.01         0.01         0.01         0.05         0.04         0.05         0.04         0.05         0.01           Ma         0.00         0.00         0.00         0.00         0.00         0.00         0.00         0.00         0.00         0.00         0.00         0.00         0.00         0.00         0.00         0.00         0.00         0.00         0.00         0.00         0.00         0.00         0.00         0.00         0.00         0.00         0.00         0.00         0.00         0.00         0.00         0.00         0.00         0.00         0.00         0.00         0.00         0.00         0.00         0.00         0.00         0.00         0.00         0.00         0.00         0.00         0.00         0.00         0.00         0.00         0.00         0.00         0.00         0.00         0.00 </td <td>Al</td> <td>0.61</td> <td>0.75</td> <td>0.82</td> <td>0.75</td> <td>0.84</td> <td>0.76</td> <td>0.84</td> <td>0.75</td> <td>0.54</td> <td>0.44</td>	Al	0.61	0.75	0.82	0.75	0.84	0.76	0.84	0.75	0.54	0.44
Fe <sup>2</sup> 0.73         0.75         0.74         0.77         0.74         0.70         0.68         0.70         0.87         0.86           Mn         0.05         0.01         0.01         0.01         0.01         0.05         0.04         0.04         0.04           Mg         0.20         0.17         0.18         0.17         0.18         0.23         0.24         0.22         0.09         0.00           Ca         0.00         0.00         0.00         0.00         0.00         0.00         0.00         0.00         0.00         0.00         0.00         0.00         0.00         0.00         0.00         0.00         0.00         0.00         0.00         0.00         0.00         0.00         0.00         0.00         0.00         0.00         0.00         0.00         0.00         0.00         0.00         0.00         0.00         0.00         0.00         0.00         0.00         0.00         0.00         0.00         0.00         0.00         0.00         0.00         0.00         0.00         0.00         0.00         0.00         0.00         0.00         0.00         0.00         0.00         0.00         0.00         0.00		1.17	1.11	1.09	1.13	1.07	1.03	1.03	1.05	1.29	1.44
Mn         0.05         0.01         0.01         0.01         0.01         0.01         0.02         0.04         0.05         0.04         0.05         0.04         0.05         0.04         0.05         0.04         0.05         0.00         0.00         0.00         0.00         0.00         0.00         0.00         0.00         0.00         0.00         0.00         0.00         0.00         0.00         0.00         0.00         0.00         0.00         0.00         0.00         0.00         0.00         0.00         0.00         0.00         0.00         0.00         0.00         0.00         0.00         0.00         0.00         0.00         0.00         0.00         0.00         0.00         0.00         0.00         0.00         0.00         0.00         0.00         0.00         0.00         0.00         0.00         0.00         0.00         0.00         0.00         0.00         0.00         0.00         0.00         0.00         0.00         0.00         0.00         0.00         0.00         0.00         0.00         0.00         0.00         0.00         0.00         0.00         0.00         0.00         0.00         0.00         0.00         0.00 <th< td=""><td>Fe<sup>+3</sup></td><td>0.20</td><td>0.12</td><td>0.08</td><td>0.10</td><td>0.09</td><td>0.20</td><td>0.13</td><td>0.19</td><td>0.16</td><td>0.10</td></th<>	Fe <sup>+3</sup>	0.20	0.12	0.08	0.10	0.09	0.20	0.13	0.19	0.16	0.10
Mg	Fe <sup>+2</sup>	0.73	0.75	0.74	0.77	0.74	0.70	0.68	0.70	0.87	0.86
Ca         0.00         0.00         0.00         0.00         0.00         0.00         0.00         0.00         0.00         0.00         0.00         0.00         0.00         0.00         0.00         0.00         0.00         0.00         0.00         0.00         0.00         0.00         0.00         0.00         0.00         0.00         0.00         0.00         0.00         0.00         0.00         0.00         0.00         0.00         0.00         0.00         0.00         0.00         0.00         0.00         0.00         0.00         0.00         0.00         0.00         0.00         0.00         0.00         0.00         0.00         0.00         0.00         0.00         0.00         0.00         0.00         0.00         0.00         0.00         0.00         0.00         0.00         0.00         0.00         0.00         0.00         0.00         0.00         0.00         0.00         0.00         0.00         0.00         0.00         0.00         0.00         0.00         0.00         0.00         0.00         0.00         0.00         0.00         0.00         0.00         0.00         0.00         0.00         0.00         0.00         0.00 <th< td=""><td>Mn</td><td>0.05</td><td>0.01</td><td>0.01</td><td>0.01</td><td>0.01</td><td>0.05</td><td>0.04</td><td>0.05</td><td>0.04</td><td>0.04</td></th<>	Mn	0.05	0.01	0.01	0.01	0.01	0.05	0.04	0.05	0.04	0.04
Na         0.00         0.00         0.00         0.00         0.00         0.00         0.00         0.00         0.00         0.00         0.00         0.00         0.00         0.00         0.00         0.00         0.00         0.00         0.00         0.00         0.00         0.00         0.00         0.00         0.00         0.00         0.00         0.00         0.00         0.00         0.00         0.00         0.00         0.00         0.00         0.00         0.00         0.00         0.00         0.00         0.00         0.00         0.00         0.00         0.00         0.00         0.00         0.00         0.00         0.00         0.00         0.00         0.00         0.00         0.00         0.00         0.00         0.00         0.00         0.00         0.00         0.00         0.00         0.00         0.00         0.00         0.00         0.00         0.00         0.00         0.00         0.00         0.00         0.00         0.00         0.00         0.00         0.00         0.00         0.00         0.00         0.00         0.00         0.00         0.00         0.00         0.00         0.00         0.00         0.00         0.00 <th< td=""><td>Mg</td><td>0.20</td><td>0.17</td><td>0.18</td><td>0.17</td><td>0.18</td><td>0.23</td><td>0.24</td><td>0.22</td><td>0.09</td><td>0.10</td></th<>	Mg	0.20	0.17	0.18	0.17	0.18	0.23	0.24	0.22	0.09	0.10
K         0.00         0.00         0.00         0.00         0.00         0.00         0.00         0.00         0.00         0.00         0.00         0.00         0.00         0.00         0.00         0.00         0.00         0.00         0.00         0.00         0.00         0.00         0.00         0.00         0.00         0.00         0.00         0.00         0.00         0.00         0.00         0.00         0.00         0.00         0.00         0.00         0.00         0.00         0.00         0.00         0.00         0.00         0.00         0.00         0.00         0.00         0.00         0.00         0.00         0.00         0.00         0.00         0.00         0.00         0.00         0.00         0.00         0.00         0.00         0.00         0.00         0.00         0.00         0.00         0.00         0.00         0.00         0.00         0.00         0.00         0.00         0.00         0.00         0.00         0.00         0.00         0.00         0.00         0.00         0.00         0.00         0.00         0.00         0.00         0.00         0.00         0.00         0.00         0.00         0.00         0.00	Ca	0.00	0.00	0.00	0.00	0.00	0.00	0.00	0.00	0.00	0.00
Ni         0.00         0.00         0.00         0.00         0.00         0.00         0.00         0.00         0.00         0.00         0.00         0.00         0.00         0.00         0.00         0.00         0.00         0.00         0.00         0.00         0.00         0.00         0.00         0.00         0.00         0.00         0.00         0.00         0.00         0.00         0.00         0.00         0.00         0.00         0.00         0.00         0.00         0.00         0.00         0.00         0.00         0.00         0.00         0.00         0.00         0.00         0.00         0.00         0.00         0.00         0.00         0.00         0.00         0.00         0.00         0.00         0.00         0.00         0.00         0.00         0.00         0.00         0.00         0.00         0.00         0.00         0.00         0.00         0.00         0.00         0.00         0.00         0.00         0.00         0.00         0.00         0.00         0.00         0.00         0.00         0.00         0.00         0.00         0.00         0.00         0.00         0.00         0.00         0.00         0.00         0.00	Na	0.00	0.00	0.00	0.00	0.00	0.00	0.00	0.00	0.00	0.00
Zh         0.03         0.06         0.06         0.07         0.07         0.02         0.04         0.03         0.00         0.00           Total         3.00         3.00         3.00         3.00         3.00         3.00         3.00         3.00         3.00         3.00         3.00         3.00         3.00         3.00         3.00         3.00         3.00         3.00         3.00         3.00         3.00         3.00         3.00         3.00         3.00         3.00         3.00         3.00         3.00         3.00         3.00         3.00         3.00         3.00         3.00         3.00         3.00         3.00         3.00         3.00         3.00         3.00         3.00         3.00         3.00         3.00         3.00         3.00         3.00         3.00         7.64         8         8         4.7         86.92         10.21         10.21         10.21         10.21         10.21         10.21         10.21         10.21         10.21         10.21         10.21         10.21         10.21         10.21         10.21         10.21         10.21         10.21         10.21         10.21         10.21         10.21         10.21         10.21<									0.00	0.00	
Total         3.00         3.00         3.00         3.00         3.00         3.00         3.00         3.00         3.00         3.00         3.00         3.00         3.00         3.00         3.00         3.00         3.00         3.00         3.00         3.00         3.00         3.00         3.00         3.00         3.00         3.00         3.00         3.00         3.00         3.00         3.00         3.00         3.00         3.00         3.00         3.00         3.00         3.00         3.00         3.00         3.00         3.00         3.00         3.00         3.00         3.00         3.00         4.00         4.00         4.00         2.2         2.41         9.52         10.21         10.16         0.10         10.10         0.02         0.01         0.06         0.04         0.05         0.04         0.01         0.06         0.09         0.08         0.05           Sample mineral mi										0.00	
Cr#         65.79         59.68         56.92         59.99         55.96         57.65         55.12         58.35         70.57         76.48           Mg#         21.32         18.53         19.61         17.87         19.45         24.77         26.22         24.16         9.52         10.21           Fe#         78.68         81.47         80.39         82.13         80.55         75.23         73.78         75.84         90.48         89.79           Fe##         0.22         0.14         0.10         0.01         0.02         0.16         0.21         0.16         0.10           Yee <sup>3+</sup> #         0.10         0.06         0.04         0.05         0.04         0.01         0.06         0.09         0.08         0.05           Sample mineral Al-Crb**         IK/3/P Al-Crb**         IK/3/P Chr**         IK/3/P Chr**         IK/3/P Chr**         IK/3/P Fe-Chr**         M/16/OP Fe-Chr**         Solution         M/16/OP Fe-Chr**         Fe-Chr**         Fe-Chr**         Solution         IK/3/P Chr**         IK/3/P Chr**											
Mg#         21.32         18.53         19.61         17.87         19.45         24.77         26.22         24.16         9.52         10.21           Fe#         78.68         81.47         80.39         82.13         80.55         75.23         73.78         75.84         90.48         89.79           Fe*#         0.22         0.14         0.10         0.01         0.01         0.06         0.09         0.08         0.05           Sample MIK/3/P coll of N/3/P mineral Al-Chr*         IK/3/P Al-Chr*         IK/3/P Chr*											
Fe#         78.68         81.47         80.39         82.13         80.55         75.23         73.78         75.84         90.48         89.79           Fe³*#         0.22         0.14         0.10         0.01         0.02         0.16         0.21         0.16         0.10           YFe³*#         0.10         0.06         0.04         0.05         0.04         0.10         0.06         0.09         0.08         0.05           Sample nineral Rkf3/P sinter         Ik/3/P Al-Chr*         Ik/3/P Chr*         Ik/3/P EFe-Chr*         M/16/OP Fe-Chr*         M/10/OP Fe-Chr*         M/10/OP M/10/OP Fe-Chr*         M/10/OP Fe-Chr*         M/10/OP											
Fe³*#         0.22         0.14         0.10         0.11         0.10         0.02         0.16         0.21         0.16         0.10           YFe³*#         0.10         0.06         0.04         0.05         0.04         0.10         0.06         0.09         0.08         0.05           Sample mineral R4l-Chr*         IK/3/P Al-Chr*         IK/3/P Chr*         IK/3/P Chr*         IK/3/P Fe-Chr*         Fe-Chr* </td <td>-</td> <td></td>	-										
YFe <sup>3+</sup> #         0.10         0.06         0.04         0.05         0.04         0.10         0.06         0.09         0.08         0.05           Sample mineral and Parker         IK/3/P Al-Chr* Al-Chr* Al-Chr* Al-Chr* Chr* Chr* Chr* Chr* Chr* Chr* Chr*											
Sample mineral metal mineral mineral Ref. point         IK/3/P Al-Chr* Al-Chr* Chr* Chr* Chr* Chr* Chr* Chr* Chr*											
mineral Ref. point         Al-Chr* Ref. point         Al-Chr* 73/1 C         Chr* 11/1 C         Chr* 23/1 C         Chr* 45/1 C         Chr* 51/1 C         Fe-Chr* 86/1         Fe-Chr* 66/1           SiO₂         0.03         0.01         0.00         0.02         0.00         0.00         0.034         0.004         0.03           TiO₂         0.29         0.22         0.97         0.72         0.65         0.47         0.75         1.782         1.940         1.27           Al₂O₃         12.41         12.57         2.60         3.52         2.57         2.91         2.41         1.511         1.526         0.16           Cr₂O₃         48.83         46.09         41.05         44.25         46.59         46.55         45.84         37.034         37.899         31.40           FeO¹         33.56         35.82         47.97         44.38         43.72         43.91         44.81         53.928         54.317         58.88           MmO         1.27         1.21         1.56         1.65         1.70         1.83         1.70         0.334         0.367         0.89           MgO         1.81         1.71         0.72         0.59         0.57         0.52											
$\begin{array}{c ccccccccccccccccccccccccccccccccccc$	mineral	Al-Chr*	Al-Chr*	Chr*	Chr*	Chr*	Chr*	Chr*	Fe-Chr*	Fe-Chr*	Fe-Chr*
$\begin{array}{c ccccccccccccccccccccccccccccccccccc$	SiO <sub>2</sub>	0.03	0.01	0.00	0.02	0.02	0.00	0.00	0.034	0.004	0.03
$ \begin{array}{c} \text{Cr}_2 \text{O}_3 & 48.83 & 46.09 & 41.05 & 44.25 & 46.59 & 46.55 & 45.84 & 37.034 & 37.899 & 31.40 \\ \text{FeO}^{T} & 33.56 & 35.82 & 47.97 & 44.38 & 43.72 & 43.91 & 44.81 & 53.928 & 54.317 & 58.88 \\ \text{MnO} & 1.27 & 1.21 & 1.56 & 1.65 & 1.70 & 1.83 & 1.70 & 0.334 & 0.367 & 0.89 \\ \text{MgO} & 1.81 & 1.71 & 0.72 & 0.59 & 0.57 & 0.52 & 0.56 & 0.799 & 0.790 & 0.44 \\ \text{CaO} & 0.03 & 0.01 & 0.03 & 0.01 & 0.02 & 0.00 & 0.03 & 0.028 & 0.027 & 0.02 \\ \text{Na}_2 \text{O} & 0.03 & 0.02 & 0.03 & 0.05 & 0.04 & 0.04 & 0.04 & 0.045 & 0.000 & 0.06 \\ \text{K}_2 \text{O} & 0.00 & 0.00 & 0.00 & 0.00 & 0.00 & 0.02 & 0.00 & 0.010 & 0.000 & 0.00 \\ \text{NiO} & 0.05 & 0.00 & 0.10 & 0.11 & 0.24 & 0.04 & 0.07 & 0.00 & 0.00 & 0.07 \\ \text{ZnO} & 0.00 & 0.00 & 0.00 & 0.00 & 0.00 & 0.00 & 0.00 & 0.628 & 0.761 & 0.00 \\ \text{Total} & 98.31 & 97.66 & 95.03 & 95.30 & 96.12 & 96.29 & 96.21 & 96.133 & 97.631 & 94.92 \\ \text{Fe}_2 \text{O}_3 & 4.38 & 6.78 & 20.86 & 16.87 & 16.22 & 16.40 & 17.15 & 25.826 & 25.544 & 33.37 \\ \text{FeO} & 29.62 & 29.71 & 29.20 & 29.20 & 29.12 & 29.15 & 29.38 & 30.689 & 31.331 & 28.85 \\ \text{Total} & 98.75 & 98.34 & 97.12 & 96.99 & 97.74 & 97.93 & 97.93 & 98.720 & 100.189 & 98.26 \\ \textbf{Cations:} & \textbf{4(O)} \\ \text{Al} & 0.51 & 0.52 & 0.12 & 0.16 & 0.11 & 0.13 & 0.11 & 0.067 & 0.067 & 0.01 \\ \text{Cr} & 1.36 & 1.29 & 1.23 & 1.32 & 1.39 & 1.38 & 1.37 & 1.102 & 1.112 & 0.96 \\ \end{array}$	TiO <sub>2</sub>	0.29	0.22	0.97	0.72	0.65	0.47	0.75	1.782	1.940	1.27
FeO <sup>T</sup> 33.56         35.82         47.97         44.38         43.72         43.91         44.81         53.928         54.317         58.88           MnO         1.27         1.21         1.56         1.65         1.70         1.83         1.70         0.334         0.367         0.89           MgO         1.81         1.71         0.72         0.59         0.57         0.52         0.56         0.799         0.790         0.44           CaO         0.03         0.01         0.03         0.01         0.02         0.00         0.03         0.028         0.027         0.02           Na <sub>2</sub> O         0.03         0.02         0.03         0.05         0.04         0.04         0.04         0.045         0.000         0.06           K <sub>2</sub> O         0.00         0.00         0.00         0.00         0.00         0.00         0.00         0.00         0.00         0.00         0.00         0.00         0.00         0.00         0.00         0.00         0.00         0.00         0.00         0.00         0.00         0.00         0.00         0.00         0.00         0.00         0.00         0.00         0.00         0.00         0.00	$Al_2O_3$	12.41	12.57	2.60	3.52	2.57	2.91	2.41	1.511	1.526	0.16
MnO         1.27         1.21         1.56         1.65         1.70         1.83         1.70         0.334         0.367         0.89           MgO         1.81         1.71         0.72         0.59         0.57         0.52         0.56         0.799         0.790         0.44           CaO         0.03         0.01         0.02         0.00         0.03         0.028         0.027         0.02           Na <sub>2</sub> O         0.03         0.01         0.02         0.00         0.03         0.028         0.027         0.02           Na <sub>2</sub> O         0.03         0.02         0.03         0.05         0.04         0.04         0.04         0.045         0.000         0.00           NiO         0.05         0.00         0.00         0.00         0.00         0.00         0.00         0.00         0.00         0.00         0.00         0.00         0.00         0.00         0.00         0.00         0.00         0.00         0.00         0.00         0.00         0.00         0.00         0.00         0.00         0.00         0.00         0.00         0.00         0.00         0.00         0.00         0.00         0.00         0.00         0.00	Cr <sub>2</sub> O <sub>3</sub>	48.83	46.09	41.05	44.25	46.59	46.55	45.84	37.034	37.899	31.40
$\begin{array}{c ccccccccccccccccccccccccccccccccccc$	FeO <sup>T</sup>	33.56	35.82	47.97	44.38	43.72	43.91	44.81	53.928	54.317	58.88
$ \begin{array}{c ccccccccccccccccccccccccccccccccccc$	MnO	1.27	1.21	1.56	1.65	1.70	1.83	1.70	0.334	0.367	0.89
$\begin{array}{c ccccccccccccccccccccccccccccccccccc$	MgO	1.81	1.71	0.72	0.59	0.57	0.52	0.56	0.799	0.790	0.44
K <sub>2</sub> O         0.00         0.00         0.00         0.00         0.00         0.00         0.00         0.00         0.00         0.00         0.00         0.00         0.00         0.00         0.00         0.00         0.00         0.00         0.00         0.00         0.00         0.00         0.00         0.00         0.00         0.00         0.00         0.00         0.00         0.00         0.00         0.00         0.00         0.00         0.00         0.00         0.00         0.00         0.00         0.00         0.00         0.00         0.00         0.00         0.00         0.00         0.00         0.00         0.00         0.00         0.00         0.00         0.00         0.00         0.00         0.00         0.00         0.00         0.00         0.00         0.00         0.00         0.00         0.00         0.00         0.00         0.00         0.00         0.00         0.00         0.00         0.00         0.00         0.00         0.00         0.00         0.00         0.00         0.00         0.00         0.00         0.00         0.00         0.00         0.00         0.00         0.00         0.00         0.00         0.00         0.00 <t< td=""><td>CaO</td><td>0.03</td><td>0.01</td><td>0.03</td><td>0.01</td><td>0.02</td><td>0.00</td><td>0.03</td><td>0.028</td><td>0.027</td><td>0.02</td></t<>	CaO	0.03	0.01	0.03	0.01	0.02	0.00	0.03	0.028	0.027	0.02
NiO         0.05         0.00         0.10         0.11         0.24         0.04         0.07         0.00         0.00         0.07           ZnO         0.00         0.00         0.00         0.00         0.00         0.00         0.00         0.00         0.00         0.00         0.00         0.00         0.00         0.00         0.00         0.00         0.00         0.00         0.00         0.00         0.00         0.00         0.00         0.00         0.00         0.00         0.00         0.00         0.00         0.00         0.00         0.00         0.00         0.00         0.00         0.00         0.00         0.00         0.00         0.00         0.00         0.00         0.00         0.00         0.00         0.00         0.00         0.00         0.00         0.00         0.00         0.00         0.00         0.00         0.00         0.00         0.00         0.00         0.00         0.00         0.00         0.00         0.00         0.00         0.00         0.00         0.00         0.00         0.00         0.00         0.00         0.00         0.00         0.00         0.00         0.00         0.00         0.00         0.00         0.00	Na <sub>2</sub> O	0.03	0.02	0.03	0.05	0.04	0.04	0.04	0.045	0.000	0.06
$ \begin{array}{c ccccccccccccccccccccccccccccccccccc$	K <sub>2</sub> O	0.00	0.00	0.00	0.00	0.00	0.02	0.00	0.010	0.000	0.00
$ \begin{array}{c ccccccccccccccccccccccccccccccccccc$	NiO			0.10				0.07			0.07
$ \begin{array}{c ccccccccccccccccccccccccccccccccccc$											
FeO         29.62         29.71         29.20         29.20         29.12         29.15         29.38         30.689         31.331         28.85           Total         98.75         98.34         97.12         96.99         97.74         97.93         97.93         98.720         100.189         98.26           Cations:         4(O)         4(O) <t< td=""><td></td><td></td><td></td><td></td><td></td><td></td><td></td><td></td><td></td><td></td><td></td></t<>											
Total         98.75         98.34         97.12         96.99         97.74         97.93         97.93         98.720         100.189         98.26           Cations:         4(O)         4(O) </td <td></td>											
Cations:         4(O)											
Si     0.00     0.00     0.00     0.00     0.00     0.00     0.00     0.00     0.001     0.000     0.00       Ti     0.01     0.01     0.03     0.02     0.02     0.01     0.02     0.050     0.054     0.04       Al     0.51     0.52     0.12     0.16     0.11     0.13     0.11     0.067     0.067     0.01       Cr     1.36     1.29     1.23     1.32     1.39     1.38     1.37     1.102     1.112     0.96											
Ti     0.01     0.01     0.03     0.02     0.02     0.01     0.02     0.050     0.054     0.04       Al     0.51     0.52     0.12     0.16     0.11     0.13     0.11     0.067     0.067     0.01       Cr     1.36     1.29     1.23     1.32     1.39     1.38     1.37     1.102     1.112     0.96	Cations:	4(O)	4(O)	4(O)		4(O)	4(O)	4(O)		4(O)	
Al 0.51 0.52 0.12 0.16 0.11 0.13 0.11 0.067 0.067 0.01 Cr 1.36 1.29 1.23 1.32 1.39 1.38 1.37 1.102 1.112 0.96											
Cr 1.36 1.29 1.23 1.32 1.39 1.38 1.37 1.102 1.112 0.96											
Fe <sup>+3</sup> 0.12 0.18 0.60 0.48 0.46 0.46 0.49 0.731 0.713 0.97											
	Fe <sup>+3</sup>	0.12	0.18	0.60	0.48	0.46	0.46	0.49	0.731	0.713	0.97

_			
7			
s)			
•			

10991034, 2019, 4, Downloaded from https://onlinelibrary.wiley.com/doi/10.1002/gj.3286 by University Of Hyderabad, Wiley Online Library on [30/01/2023]. See the Terms and Conditions (https://onlinelibrary.wiley.com/emms-and-conditions) on Wiley Online Library for rules of use; OA articles are governed by the applicable Creative Commons License

Sample mineral Ref. point	IK/3/P Al-Chr* 37/1C	IK/3/P Al-Chr* 73/1 C	IK/3/P Chr* 11/1 C	IK/3/P Chr* 23/1 C	IK/3/P Chr* 29/1 C	IK/3/P Chr* 45/1 C	IK/3/P Chr* 51/1 C	M/16/OP Fe-Chr* 18/1	M/16/OP Fe-Chr* 22/1	M/10/I Fe-Chr <sup>a</sup> 66/1
Fe <sup>+2</sup>	0.87	0.88	0.93	0.92	0.92	0.92	0.93	0.966	0.972	0.93
Mn	0.04	0.04	0.05	0.05	0.05	0.06	0.05	0.011	0.012	0.03
Mg	0.09	0.09	0.04	0.03	0.03	0.03	0.03	0.045	0.044	0.03
Ca	0.00	0.00	0.00	0.00	0.00	0.00	0.00	0.001	0.001	0.00
Na	0.00	0.00	0.00	0.00	0.00	0.00	0.00	0.003	0.000	0.00
K	0.00	0.00	0.00	0.00	0.00	0.00	0.00	0.000	0.000	0.00
Ni	0.00	0.00	0.00	0.00	0.01	0.00	0.00	0.000	0.000	0.00
Zn	0.00	0.00	0.00	0.00	0.00	0.00	0.00	0.022	0.026	0.00
Total	3.00	3.00	3.00	3.00	3.00	3.00	3.00	3.000	3.000	3.00
Cr#	72.52	71.09	91.37	89.40	92.40	91.48	92.73	94.27	94.34	99.23
Mg#	9.82	9.30	4.21	3.48	3.37	3.08	3.29	4.43	4.30	2.63
Fe#	90.18	90.70	95.79	96.52	96.63	96.92	96.71	95.57	95.70	97.37
Fe <sup>3+</sup> #	0.12	0.17	0.39	0.34	0.33	0.34	0.34	0.43	0.42	0.51
YFe <sup>3+</sup> #	0.06	0.09	0.31	0.24	0.23	0.23	0.25	0.38	0.38	0.50
Sample mineral Ref. point	M/10/P Fe-Chr* 83/1.	HG/10/H Fe-Chr** 116/1	HG/10/H Fe-Chr** 118/1	HG/10/H Fe-Chr** 121/1	HG/10/H Fe-Chr** 127/1	HG/10/H Fe-Chr** 133/1	HG/10/H Fe-Chr** 147/1	HG/10/H Fe-Chr** 175/1	HG/10/H Fe-Chr** 181/1	IK/3/P Cr-Mag 16/1 R
SiO <sub>2</sub>	0.01	0.01	0.00	0.01	0.01	0.00	0.00	0.01	0.02	0.00
ΓiO <sub>2</sub>	0.17	1.02	1.31	1.01	1.26	1.25	1.19	1.50	1.24	0.34
Al <sub>2</sub> O <sub>3</sub>	0.06	0.19	0.26	0.21	0.18	0.21	0.27	0.32	0.25	0.00
Cr <sub>2</sub> O <sub>3</sub>	19.56	36.83	34.77	34.30	36.88	35.70	35.80	36.88	36.05	13.50
eO <sup>T</sup>	71.90	53.93	56.14	56.64	54.73	57.02	55.10	53.79	54.90	77.91
MnO	0.21	0.85	0.76	0.38	0.70	0.50	0.52	0.34	0.35	0.51
MgO	0.15	0.26	0.43	0.18	0.41	0.31	0.46	0.60	0.41	0.08
CaO	0.04	0.00	0.00	0.01	0.00	0.00	0.02	0.02	0.02	0.05
Na <sub>2</sub> O	0.07	0.00	0.03	0.00	0.05	0.09	0.07	0.03	0.01	0.01
K <sub>2</sub> O	0.02	0.04	0.00	0.01	0.02	0.00	0.01	0.02	0.01	0.00
NiO	0.23	0.19	0.22	0.27	0.31	0.28	0.31	0.30	0.16	0.34
ZnO	0.00	0.00	0.00	0.00	0.00	0.00	0.00	0.00	0.00	0.00
Total	93.33	95.22	95.68	94.97	96.38	97.10	95.62	95.60	95.17	92.74
Fe <sub>2</sub> O <sub>3</sub>	47.60	27.94	30.02	30.38	28.49	30.35	29.20	27.27	28.31	53.36
FeO	29.06	28.79	29.12	29.30	29.10	29.71	28.83	29.25	29.43	29.89
Total	98.09	98.02	98.69	98.01	99.23	100.14	98.54	98.33	98.00	98.08
Cations:	4(O)	4(O)	4(O)	4(O)	4(O)	4(O)	4(O)	4(O)	4(O)	4(0)
Si	0.00	0.00	0.00	0.00	0.00	0.00	0.00	0.00	0.00	0.00
Γi Al	0.00	0.03	0.04	0.03	0.04	0.04	0.03	0.04	0.04	0.01
Cr Fe <sup>+3</sup>	0.60	1.12	1.05	1.05	1.11	1.06	1.08	1.12	1.10	0.42
Fe <sup>+2</sup>	1.39	0.81	0.86	0.88	0.81	0.86	0.84	0.79	0.82	1.56
	0.94	0.93	0.93	0.95	0.93	0.94	0.92	0.94	0.95	0.97
Mn	0.01	0.03	0.02	0.01	0.02	0.02	0.02	0.01	0.01	0.02
Mg	0.01	0.02	0.02	0.01	0.02	0.02	0.03	0.03	0.02	0.00
Ca	0.00	0.00	0.00	0.00	0.00	0.00	0.00	0.00	0.00	0.00
Na	0.01	0.00	0.00	0.00	0.00	0.01	0.00	0.00	0.00	0.00
Κ	0.00	0.00	0.00	0.00	0.00	0.00	0.00	0.00	0.00	0.00
Ni	0.01	0.01	0.01	0.01	0.01	0.01	0.01	0.01	0.00	0.01
Zn	0.00	0.00	0.00	0.00	0.00	0.00	0.00	0.00	0.00	0.00
Total	3.00	3.00	3.00	3.00	3.00	3.00	3.00	3.00	3.00	3.00
Cr#	99.53	99.23	98.90	99.11	99.26	99.13	98.89	98.70	98.99	100.00
Mg#	0.90	1.61	2.59	1.11	2.44	1.82	2.74	3.50	2.42	0.47

TABLE 2 (Continued)

·	ontinued)									
Sample mineral Ref. point	M/10/P Fe-Chr* 83/1.	HG/10/H Fe-Chr** 116/1	HG/10/H Fe-Chr** 118/1	HG/10/H Fe-Chr** 121/1	HG/10/H Fe-Chr** 127/1	HG/10/H Fe-Chr** 133/1	HG/10/H Fe-Chr** 147/1	HG/10/H Fe-Chr** 175/1	HG/10/H Fe-Chr** 181/1	IK/3/P Cr-Mag* 16/1 R
Fe#	99.10	98.39	97.41	98.89	97.56	98.18	97.26	96.50	97.58	99.53
Fe <sup>3+</sup> #	0.60	0.47	0.48	0.48	0.47	0.48	0.48	0.46	0.46	0.62
<sup>γ</sup> Fe <sup>3+</sup> #	0.70	0.42	0.45	0.46	0.42	0.45	0.43	0.41	0.43	0.79
Sample mineral Ref. point	IK/3/P Mag* 15/1 R	IK/3/P Mag* 17/1 R	IK/3/P Mag* 22/1 R	IK/3/P Mag* 4/1 R	IK/3/P Mag* 30/1 R	IK/3/P Mag* 52/1 R	IK/3/P Mag* 62/1 R	IK/3/P Mag* 66/1 R		
SiO <sub>2</sub>	0.00	0.00	0.06	0.14	0.00	0.60	0.02	0.09		
TiO <sub>2</sub>	0.12	0.14	0.07	0.11	0.04	0.09	0.24	0.14		
$Al_2O_3$	0.03	0.02	0.02	0.00	0.00	0.06	0.00	0.00		
Cr <sub>2</sub> O <sub>3</sub>	7.96	4.62	9.65	4.57	5.10	4.66	9.14	2.55		
$FeO^T$	83.43	86.62	81.76	87.30	87.11	86.34	82.87	88.72		
MnO	0.21	0.04	0.35	0.01	0.12	0.08	0.29	0.00		
MgO	0.06	0.07	0.11	0.08	0.03	0.93	0.04	0.05		
CaO	0.03	0.01	0.00	0.05	0.01	0.00	0.03	0.03		
Na <sub>2</sub> O	0.01	0.02	0.00	0.01	0.00	0.02	0.01	0.02		
K <sub>2</sub> O	0.00	0.00	0.02	0.00	0.00	0.00	0.01	0.00		
NiO	0.18	0.26	0.19	0.27	0.31	0.42	0.32	0.28		
ZnO	0.00	0.00	0.00	0.00	0.00	0.00	0.00	0.00		
Total	92.03	91.80	92.23	92.54	92.72	93.20	92.97	91.88		
Fe <sub>2</sub> O <sub>3</sub>	59.28	62.76	57.58	63.08	63.06	62.79	58.44	64.87		
FeO	30.08	30.14	29.94	30.54	30.37	29.84	30.29	30.35		
Total	97.97	98.09	98.00	98.86	99.04	99.49	98.82	98.38		
Cations:	4(O)	4(O)	4(O)	4(O)	4(O)	4(O)	4(O)	4(O)		
Si	0.00	0.00	0.00	0.01	0.00	0.02	0.00	0.00		
Ti	0.00	0.00	0.00	0.00	0.00	0.00	0.01	0.00		
Al	0.00	0.00	0.00	0.00	0.00	0.00	0.00	0.00		
Cr	0.25	0.14	0.30	0.14	0.16	0.14	0.28	0.08		
Fe <sup>+3</sup>	1.75	1.85	1.69	1.84	1.84	1.81	1.71	1.91		
Fe <sup>+2</sup>	0.98	0.99	0.98	0.99	0.99	0.95	0.98	0.99		
Mn	0.01	0.00	0.01	0.00	0.00	0.00	0.01	0.00		
Mg	0.00	0.00	0.01	0.00	0.00	0.05	0.00	0.00		
Ca	0.00	0.00	0.00	0.00	0.00	0.00	0.00	0.00		
Na	0.00	0.00	0.00	0.00	0.00	0.00	0.00	0.00		
K	0.00	0.00	0.00	0.00	0.00	0.00	0.00	0.00		
Ni	0.01	0.01	0.01	0.01	0.01	0.01	0.01	0.01		
Zn	0.00	0.00	0.00	0.00	0.00	0.00	0.00	0.00		
Total	3.00	3.00	3.00	3.00	3.00	3.00	3.00	3.00		
Cr#	99.44	99.36	99.69	100.00	100.00	98.12	100.00	100.00		
Mg#	0.35	0.41	0.65	0.46	0.18	5.26	0.23	0.29		
Fe#	99.65	99.59	99.35	99.54	99.82	94.74	99.77	99.71		
Fe <sup>3+</sup> #	0.64	0.65	0.63	0.65	0.65	0.65	0.63	0.66		
<sup>γ</sup> Fe <sup>3+</sup> #	0.88	0.93	0.85	0.93	0.92	0.93	0.86	0.96		

Abbrevations:. Al-Chr: Al-Chromite; Chr: Chromite; Fe-Chr: Ferrian Chromite; Cr-Mag: Chrome Magnetite; Mag: Magnetite. Cr# =  $100^*$  Cr/(Cr + Al); Mg# =  $100^*$  Mg/(Mg + Fe); Fe# =  $100^*$  Fe/(Fe + Mg);  $^{7}$ Fe $^{3+}$ # =  $^{2+}$ /(Fe $^{3+}$ + Cr + Al); Fe $^{3+}$ # =  $^{2+}$ /(Fe $^{3+}$ +Fe $^{2+}$ ). Analysed at \*GSI-Banglore and \*\*BHU.

routine method in which pressed pellets are prepared and analysed. Briefly, ~2.5 g of boric acid is taken in collapsible aluminium cups and ~2 g of finely powdered sample is spread on top and pressed with 25 tons of hydraulic pressure for preparing pressed pellets. The instrumental set-up and other parameters are described in detail elsewhere (Krishna & Govil, 2007). International rock reference materials

from the US Geological Survey (PCC-1, BHVO-1, BCR-1, and BIR-1), Geological Survey of Japan (JB-1, JB-1a, JB-2, JB-3, and JP-1), and Chinese reference material (GSR-3) were used to prepare the calibration curves of major elements and to check the accuracy of analytical data. The precision obtained for most of the major oxides were less than 2% RSD.

Trace and rare earth elements (REE) were analysed using solutions prepared from homogenized sample powder dissolved in reagent grade HF:HNO<sub>3</sub> acid mixture in Savillex® screwtop vessels. A test portion (0.05 g) of sample was weighed in 25 ml Savillex Teflon pressure decomposition vessels. To each sample, 10 ml of an acid mixture (containing 7:3 HF-HNO<sub>3</sub>) was added. Subsequently, 5 ml of 1 ng/ml <sup>103</sup>Rh solution was added as an internal standard to each Savillex vessel. After thorough swirling, the vessels were tightly closed and kept on a hot plate at ~140 °C for 48 hr. Following this, the vessels were opened, and the contents evaporated at 200 °C to near dryness with a few drops of HCIO<sub>4</sub> to ensure complete removal of HF from the mixture. It was further dissolved by adding 10 ml of 1:1 HNO<sub>3</sub>. Then the volume was made to 250 ml by adding Milli Q® de-ionized water (18 MΩ). Finally, the solution was stored in HDPE bottles. Matrix matching certified reference materials BHVO-1, BCR-1, PCC-1 (USGS), MRG-1 (CCRMP, Canada), DR-N, UB-N (ANRT, France), JGb-2, JB-2, and JP-1 (GSJ, Japan) along with couple of procedural blanks were also prepared with the sample batch by adopting the same protocol described above to negate errors due to reagent and handling (Satyanarayanan et al., 2018). In the present investigation, very clear solutions were obtained for all the samples and calibration standards. Solutions were analysed at NGRI, Hyderabad, by high resolution inductively coupled mass spectrometer (HR-ICP-MS; Nu Instruments Attom®, UK) in jump-wiggle mode at moderate resolution of 300, which permits all the analytes of interest to be measured accurately. Precision and accuracy are better than RSD 3% for most of the measured elements.

TABLE 3 Amphibale composition of the Madawara ultramatic intrusion

Sample mineral Ref. point	IK-13/P Mg-Hbl 1	IK-13/P Mg-Hbl 2	IK-13/P Mg-Hbl 10	IK-13/P Tr 3	IK-13/P Tr 4	IK-13/P Tr 5	IK-13/P Tr 6	IK-13/P Tr 7	IK-13/P Tr 8	IK-13/P Tr 9
SiO <sub>2</sub>	53.05	53.17	51.36	56.64	57.47	56.62	58.44	57.12	58.34	57.38
TiO <sub>2</sub>	0.25	0.34	0.37	0.00	0.00	0.03	0.02	0.04	0.01	0.00
Al <sub>2</sub> O <sub>3</sub>	3.81	3.81	5.55	0.53	0.10	0.22	0.05	0.00	0.08	0.28
Cr <sub>2</sub> O <sub>3</sub>	0.55	0.77	0.64	0.00	0.00	0.03	0.00	0.00	0.06	0.03
Fe <sub>2</sub> O <sub>3</sub>	4.03	5.30	3.55	0.00	0.00	1.71	1.02	0.00	0.35	0.43
FeO	1.25	0.02	1.67	3.43	2.49	1.55	2.51	2.84	2.95	2.98
MnO	0.22	0.16	0.05	0.07	0.02	0.12	0.06	0.10	0.07	0.10
MgO	20.62	20.99	20.11	22.42	22.82	22.56	22.63	22.68	22.30	22.46
NiO	0.07	0.02	0.27	0.02	0.11	0.26	0.04	0.07	0.12	0.08
CaO	12.47	12.35	12.56	13.91	14.02	13.41	13.36	13.75	13.22	13.57
Na <sub>2</sub> O	1.08	1.04	1.56	0.11	0.05	0.06	0.03	0.02	0.07	0.09
K <sub>2</sub> O	0.13	0.12	0.10	0.16	0.06	0.05	0.03	0.05	0.00	0.15
BaO	0.00	0.00	0.00	0.00	0.00	0.00	0.00	0.00	0.00	0.02
H <sub>2</sub> O*	2.15	2.17	2.14	2.16	2.17	2.16	2.20	2.16	2.18	2.17
Total	99.67	100.26	99.93	99.45	99.31	98.78	100.39	98.83	99.75	99.75
Cations.	23(O)	23(O)	23(O)	23(O)	23(O)	23(O)	23(O)	23(O)	23(O)	23(O)
Si	7.40	7.36	7.18	7.86	7.94	7.88	7.98	7.94	8.02	7.92
Al iv	0.60	0.62	0.82	0.09	0.02	0.04	0.01	0.00	0.00	0.05
Al vi	0.02	0.00	0.09	0.00	0.00	0.00	0.00	0.00	0.01	0.00
Ti	0.03	0.04	0.04	0.00	0.00	0.00	0.00	0.00	0.00	0.00
Cr	0.06	0.08	0.07	0.00	0.00	0.00	0.00	0.00	0.01	0.00
Fe <sup>3+</sup>	0.42	0.55	0.37	0.00	0.00	0.18	0.11	0.00	0.04	0.04
Fe <sup>2+</sup>	0.15	0.00	0.20	0.40	0.29	0.18	0.29	0.33	0.34	0.34
Mn	0.03	0.02	0.01	0.01	0.00	0.01	0.01	0.01	0.01	0.01
Mg	4.29	4.33	4.19	4.64	4.70	4.68	4.61	4.70	4.57	4.62
Ni	0.01	0.00	0.03	0.00	0.01	0.03	0.00	0.01	0.01	0.01
Ca	1.86	1.83	1.88	2.07	2.08	2.00	1.95	2.05	1.95	2.01
Na	0.29	0.28	0.42	0.03	0.01	0.02	0.01	0.01	0.02	0.02
K	0.02	0.02	0.02	0.03	0.01	0.01	0.01	0.01	0.00	0.03
Ва	0.00	0.00	0.00	0.00	0.00	0.00	0.00	0.00	0.00	0.00
OH*	2.00	2.00	2.00	2.00	2.00	2.00	2.00	2.00	2.00	2.00
Total	17.18	17.13	17.32	17.12	17.06	17.02	16.97	17.06	16.96	17.06
(Na + K)(A)	0.18	0.13	0.32	0.06	0.02	0.02	0.01	0.01	0.00	0.05
$Mg/(Mg + Fe^{+2})$	0.97	1.00	0.96	0.92	0.94	0.96	0.94	0.93	0.93	0.93

Note. Mg-Hbl: Magnesio hornblende; Tr: Tremolite.



#### 4.2 | Mineral chemistry

Samples were studied by both transmitted and reflected ore microscopy as well as by scanning electron microscopy (SEM-EDS) at NGRI, Hyderabad, under back-scattered electron (BSE) mode prior to EPMA analysis. Some part of the analysis of Cr-spinel and associated silicate minerals were carried out quantitatively using CAMECA SX-100 instrument at Geological Survey of India (GSI), Bangalore. The analytical conditions for silicate and oxide phases were set-up using 15 kV acceleration voltage and 15 nA beam current with 1 µm beam size. The counting time for peak measurement was 10 s and with half of the peak measurement time allotted for background measurement. Few analyses were also obtained using CAMECA SX-5 instrument at Banaras Hindu University (BHU), Varanasi. The corresponding analytical conditions were kept 15 keV accelerating voltage, 10 nA probe current with beam size of 1 µm. The precisions of all analysed elements were better than 1%. Natural minerals and synthetic oxides were used as standards, and a program based on the ZAF online procedure was used for data correction. The amount of Fe<sup>2+</sup> and Fe<sup>3+</sup> in the Cr-spinels was calculated assuming spinel stochiometry

(AB<sub>2</sub>O<sub>4</sub>; Droop, 1987). Representative analyses of each of the analysed phases are given in Tables 1–5.

#### 5 | RESULTS

## 5.1 | Chromian spinel

Representative microprobe analysis of Cr-spinels from the different rock types are given in Table 2. The EPMA data have been plotted in the Fe-Al-Cr triangular diagram showing five varieties of Cr-spinel, namely, Al-chromite, ferrous chromite, ferrian chromite, chrome magnetite, and magnetite (Figure 5a and 5b). The EPMA data on the core of homogeneous Cr-spinels, which are considered to be primarily magmatic, shows low Al<sub>2</sub>O<sub>3</sub> (10.63–21.87 wt.%), low MgO (1.71–4.92 wt.%), moderately high  $Cr_2O_3$  (38.16–51.5 wt.%), with  $Fe_2O_3$  ranging between 3.2 and 14.51 wt.%. They are Al-chromite in composition and are characterized by low Mg# (9.30–26.22) and moderately high Cr# (55.12–76.48). Their  $^{\rm Y}Fe^{3+}$ #[100Fe $^{3+}$ /(Cr + Al + Fe $^{3+}$ )] range in between 8 and 19.

**TABLE 4** Serpentine composition of the Madawara ultramafic intrusion

Sample mineral Ref. point	IK/13/P Serp 1	IK/13/P Serp 2	IK/13/P Serp 3	IK/13/P Serp 4	IK/13/P Serp 5	IK/13/P Serp 6	IK/13/P Serp 7	IK/13/P Serp 8	IK/13/P Serp 9
SiO <sub>2</sub>	43.31	39.59	30.54	42.02	42.38	40.43	41.69	43.39	42.27
TiO <sub>2</sub>	0.05	0.00	0.01	0.01	0.03	0.09	0.01	0.00	0.00
$Al_2O_3$	2.37	0.96	1.17	2.38	1.74	2.62	2.45	0.56	1.42
Cr <sub>2</sub> O <sub>3</sub>	0.60	0.41	1.72	0.52	0.07	0.29	0.06	0.01	0.10
Fe <sub>2</sub> O <sub>3</sub>	0.00	1.13	4.90	0.00	0.00	0.00	0.00	0.00	0.00
FeO	8.53	7.17	20.93	8.45	7.68	7.62	8.13	7.37	7.37
MnO	0.07	0.10	0.09	0.15	0.06	0.09	0.07	0.07	0.11
MgO	33.06	35.93	19.74	34.42	34.42	32.54	34.38	35.63	35.02
CaO	0.03	0.02	0.03	0.03	0.06	0.04	0.02	0.00	0.00
Na <sub>2</sub> O	0.01	0.01	0.01	0.00	0.01	0.03	0.02	0.00	0.00
K <sub>2</sub> O	0.02	0.01	0.03	0.00	0.03	0.02	0.02	0.02	0.00
NiO	0.23	0.28	0.32	0.33	0.29	0.23	0.27	0.19	0.19
Total	88.28	85.50	79.00	88.31	86.77	84.00	87.12	87.24	86.66
Cations	7 (O)	7 (0)	7 (O)	7 (O)	7 (O)	7 (0)	7 (O)	7 (O)	7 (0)
Si	2.04	1.94	1.81	1.99	2.03	2.00	2.00	2.06	2.03
Ti	0.00	0.00	0.00	0.00	0.00	0.00	0.00	0.00	0.00
Al	0.13	0.06	0.08	0.13	0.10	0.15	0.14	0.03	0.08
Cr	0.02	0.02	0.08	0.02	0.00	0.01	0.00	0.00	0.00
Fe <sup>3+</sup>	0.00	0.04	0.22	0.00	0.00	0.00	0.00	0.00	0.00
Fe <sup>2+</sup>	0.34	0.29	1.04	0.33	0.31	0.32	0.33	0.29	0.30
Mn	0.00	0.00	0.00	0.01	0.00	0.00	0.00	0.00	0.00
Mg	2.33	2.63	1.74	2.43	2.46	2.40	2.45	2.52	2.50
Ca	0.00	0.00	0.00	0.00	0.00	0.00	0.00	0.00	0.00
Na	0.00	0.00	0.00	0.00	0.00	0.00	0.00	0.00	0.00
K	0.00	0.00	0.00	0.00	0.00	0.00	0.00	0.00	0.00
Ni	0.01	0.01	0.02	0.01	0.01	0.01	0.01	0.01	0.01
Total	4.88	5.00	5.00	4.93	4.92	4.91	4.93	4.92	4.93
Fe <sup>3+</sup> /Fe <sup>2+</sup>	0.00	0.14	0.21	0.00	0.00	0.00	0.00	0.00	0.00
Si/Mg	0.88	0.74	1.04	0.82	0.83	0.83	0.81	0.82	0.81

Note. Serp: Serpentine.

Sample mineral Ref. point         Ik/13/P Chl	TABLE 5	Chlorite composition of the Madawara ultramafic intrus							
$\begin{array}{c ccccccccccccccccccccccccccccccccccc$	mineral	Chl	Chl	Chl	Chl	Chl			
$\begin{array}{c ccccccccccccccccccccccccccccccccccc$	SiO <sub>2</sub>	29.93	33.13	32.20	31.86	32.42			
$\begin{array}{c} \text{Cr}_2 \text{O}_3 & 0.32 & 0.83 & 2.22 & 2.42 & 2.43 \\ \text{Fe}_2 \text{O}_3 & 0.00 & 0.65 & 0.00 & 0.55 & 0.52 \\ \text{FeO} & 7.97 & 6.79 & 7.29 & 6.79 & 6.86 \\ \text{MnO} & 0.01 & 0.01 & 0.00 & 0.06 & 0.09 \\ \text{MgO} & 29.17 & 30.53 & 30.96 & 29.48 & 30.00 \\ \text{NiO} & 0.19 & 0.33 & 0.29 & 0.35 & 0.20 \\ \text{CaO} & 0.03 & 0.04 & 0.10 & 0.10 & 0.13 \\ \text{Na}_2 \text{O} & 0.01 & 0.03 & 0.03 & 0.01 & 0.05 \\ \text{K}_2 \text{O} & 0.01 & 0.04 & 0.03 & 0.01 & 0.05 \\ \text{BaO} & 0.00 & 0.02 & 0.00 & 0.00 & 0.00 \\ \text{H}_2 \text{O}^* & 12.14 & 12.30 & 12.29 & 11.92 & 12.15 \\ \text{Total} & 97.41 & 98.42 & 98.86 & 96.05 & 97.84 \\ \textbf{Cations} & \textbf{28(O)} & \textbf{28(O)} & \textbf{28(O)} & \textbf{28(O)} \\ \text{Si} & 5.91 & 6.45 & 6.28 & 6.40 & 6.39 \\ \text{Al iv} & 2.09 & 1.55 & 1.72 & 1.60 & 1.61 \\ \text{Al vi} & 2.00 & 1.59 & 1.36 & 1.35 & 1.38 \\ \text{Ti} & 0.01 & 0.01 & 0.01 & 0.01 & 0.01 \\ \text{Cr} & 0.05 & 0.13 & 0.34 & 0.38 & 0.38 \\ \text{Fe}^{3+} & 0.00 & 0.09 & 0.00 & 0.08 & 0.08 \\ \text{Fe}^{2+} & 1.33 & 1.11 & 1.19 & 1.14 & 1.13 \\ \text{Mn} & 0.00 & 0.00 & 0.00 & 0.01 & 0.02 \\ \text{Mg} & 8.58 & 8.86 & 9.01 & 8.83 & 8.81 \\ \text{Ni} & 0.03 & 0.05 & 0.05 & 0.06 & 0.03 \\ \text{Ca} & 0.01 & 0.01 & 0.02 & 0.02 & 0.03 \\ \text{Na} & 0.01 & 0.02 & 0.02 & 0.01 & 0.04 \\ \text{K} & 0.01 & 0.02 & 0.02 & 0.01 & 0.04 \\ \text{K} & 0.01 & 0.02 & 0.02 & 0.01 & 0.04 \\ \text{K} & 0.01 & 0.02 & 0.02 & 0.01 & 0.04 \\ \text{K} & 0.01 & 0.02 & 0.02 & 0.01 & 0.04 \\ \text{K} & 0.01 & 0.02 & 0.02 & 0.01 & 0.04 \\ \text{K} & 0.01 & 0.02 & 0.02 & 0.01 & 0.04 \\ \text{K} & 0.01 & 0.02 & 0.00 & 0.00 & 0.00 & 0.00 \\ \text{OH*} & 16.00 & 16.00 & 16.00 & 16.00 & 16.00 \\ \text{Total} & 36.02 & 35.89 & 36.02 & 35.90 & 35.92 \\ \text{Al total} & 4.09 & 3.14 & 3.08 & 2.95 & 2.99 \\ \text{Si} & 5.91 & 6.45 & 6.28 & 6.40 & 6.39 \\ \end{array}$	TiO <sub>2</sub>	0.07	0.05	0.07	0.07	0.06			
Fe <sub>2</sub> O <sub>3</sub> 0.00 0.65 0.00 0.55 0.52 FeO 7.97 6.79 7.29 6.79 6.86 MnO 0.01 0.01 0.00 0.06 0.09 MgO 29.17 30.53 30.96 29.48 30.00 NiO 0.19 0.33 0.29 0.35 0.20 CaO 0.03 0.04 0.10 0.10 0.13 Na <sub>2</sub> O 0.01 0.03 0.03 0.01 0.05 K <sub>2</sub> O 0.01 0.04 0.03 0.01 0.05 BaO 0.00 0.02 0.00 0.00 0.00 H <sub>2</sub> O* 12.14 12.30 12.29 11.92 12.15 Total 97.41 98.42 98.86 96.05 97.84 Cations 28(O) 28(O) 28(O) 28(O) 28(O) Si 5.91 6.45 6.28 6.40 6.39 Al iv 2.09 1.55 1.72 1.60 1.61 Al vi 2.00 1.59 1.36 1.35 1.38 Ti 0.01 0.01 0.01 0.01 0.01 Cr 0.05 0.13 0.34 0.38 0.38 Fe <sup>3+</sup> 0.00 0.09 0.00 0.00 0.08 Fe <sup>2+</sup> 1.33 1.11 1.19 1.14 1.13 Mn 0.00 0.00 0.00 0.00 0.00 Mg 8.58 8.86 9.01 8.83 8.81 Ni 0.03 0.05 0.05 0.06 0.03 Ca 0.01 0.01 0.01 0.01 0.02 Mg 8.58 8.86 9.01 8.83 8.81 Ni 0.03 0.05 0.05 0.06 0.03 Ca 0.01 0.01 0.02 0.02 0.03 Na 0.01 0.02 0.02 0.01 0.04 K 0.01 0.02 0.00 0.00 0.00 OH* 16.00 16.00 16.00 16.00 Total 36.02 35.89 36.02 35.90 35.92 Al total 4.09 3.14 3.08 2.95 2.99 Si 5.91 6.45 6.28 6.40 6.39	$Al_2O_3$	17.56	13.68	13.38	12.42	12.87			
FeO 7.97 6.79 7.29 6.79 6.86 MnO 0.01 0.01 0.01 0.00 0.06 0.09 MgO 29.17 30.53 30.96 29.48 30.00 NiO 0.19 0.33 0.29 0.35 0.20 CaO 0.03 0.04 0.10 0.10 0.13 Na <sub>2</sub> O 0.01 0.03 0.03 0.01 0.05 K <sub>2</sub> O 0.01 0.04 0.03 0.01 0.05 BaO 0.00 0.00 0.00 0.00 0.00 0.00 0.00 H <sub>2</sub> O* 12.14 12.30 12.29 11.92 12.15 Total 97.41 98.42 98.86 96.05 97.84 Cations 28(O) 28(O) 28(O) 28(O) 28(O) 28(O) 5i 5.91 6.45 6.28 6.40 6.39 Al iv 2.09 1.55 1.72 1.60 1.61 Al vi 2.00 1.59 1.36 1.35 1.38 Ti 0.01 0.01 0.01 0.01 0.01 0.01 Cr 0.05 0.13 0.34 0.38 0.38 Fe <sup>3+</sup> 0.00 0.09 0.00 0.00 0.00 0.00 0.00 0.0	Cr <sub>2</sub> O <sub>3</sub>	0.32	0.83	2.22	2.42	2.43			
MnO         0.01         0.01         0.00         0.06         0.09           MgO         29.17         30.53         30.96         29.48         30.00           NiO         0.19         0.33         0.29         0.35         0.20           CaO         0.03         0.04         0.10         0.10         0.13           Na2O         0.01         0.03         0.03         0.01         0.05           BaO         0.00         0.02         0.00         0.00         0.00           H <sub>2</sub> O*         12.14         12.30         12.29         11.92         12.15           Total         97.41         98.42         98.86         96.05         97.84           Cations         28(O)         28(O)         28(O)         28(O)         28(O)           Si         5.91         6.45         6.28         6.40         6.39           Al iv         2.09         1.55         1.72         1.60         1.61           Al vi         2.00         1.59         1.36         1.35         1.38           Ti         0.01         0.01         0.01         0.01         0.01           Cr         0.05 <th< td=""><td>Fe<sub>2</sub>O<sub>3</sub></td><td>0.00</td><td>0.65</td><td>0.00</td><td>0.55</td><td>0.52</td></th<>	Fe <sub>2</sub> O <sub>3</sub>	0.00	0.65	0.00	0.55	0.52			
MgO         29.17         30.53         30.96         29.48         30.00           NiO         0.19         0.33         0.29         0.35         0.20           CaO         0.03         0.04         0.10         0.10         0.13           Na₂O         0.01         0.03         0.03         0.01         0.05           K₂O         0.01         0.04         0.03         0.01         0.05           BaO         0.00         0.02         0.00         0.00         0.00           H₂O*         12.14         12.30         12.29         11.92         12.15           Total         97.41         98.42         98.86         96.05         97.84           Cations         28(O)         28(O)         28(O)         28(O)         28(O)           Si         5.91         6.45         6.28         6.40         6.39           Al iv         2.09         1.55         1.72         1.60         1.61           Al vi         2.00         1.59         1.36         1.35         1.38           Ti         0.01         0.01         0.01         0.01         0.01           Cr         0.05	FeO	7.97	6.79	7.29	6.79	6.86			
NiO         0.19         0.33         0.29         0.35         0.20           CaO         0.03         0.04         0.10         0.10         0.13           Na₂O         0.01         0.03         0.03         0.01         0.05           K₂O         0.01         0.04         0.03         0.01         0.05           BaO         0.00         0.02         0.00         0.00         0.00           H₂O*         12.14         12.30         12.29         11.92         12.15           Total         97.41         98.42         98.86         96.05         97.84           Cations         28(O)         28(O)         28(O)         28(O)         28(O)           Si         5.91         6.45         6.28         6.40         6.39           Al iv         2.09         1.55         1.72         1.60         1.61           Al vi         2.00         1.59         1.36         1.35         1.38           Ti         0.01         0.01         0.01         0.01         0.01           Cr         0.05         0.13         0.34         0.38         0.38           Fe²+         1.33         1.11	MnO	0.01	0.01	0.00	0.06	0.09			
$\begin{array}{cccccccccccccccccccccccccccccccccccc$	MgO	29.17	30.53	30.96	29.48	30.00			
$\begin{array}{c ccccccccccccccccccccccccccccccccccc$	NiO	0.19	0.33	0.29	0.35	0.20			
K2O         0.01         0.04         0.03         0.01         0.05           BaO         0.00         0.02         0.00         0.00         0.00           H2O*         12.14         12.30         12.29         11.92         12.15           Total         97.41         98.42         98.86         96.05         97.84           Cations         28(O)         28(O)         28(O)         28(O)         28(O)           Si         5.91         6.45         6.28         6.40         6.39           Al iv         2.09         1.55         1.72         1.60         1.61           Al vi         2.00         1.59         1.36         1.35         1.38           Ti         0.01         0.01         0.01         0.01         0.01         0.01           Cr         0.05         0.13         0.34         0.38         0.38           Fe <sup>3+</sup> 0.00         0.09         0.00         0.08         0.08           Fe <sup>2+</sup> 1.33         1.11         1.19         1.14         1.13           Mn         0.00         0.00         0.00         0.01         0.02           Mg         8.5	CaO	0.03	0.04	0.10	0.10	0.13			
BaO         0.00         0.02         0.00         0.00         0.00           H <sub>2</sub> O*         12.14         12.30         12.29         11.92         12.15           Total         97.41         98.42         98.86         96.05         97.84           Cations         28(O)         28(O)         28(O)         28(O)         28(O)           Si         5.91         6.45         6.28         6.40         6.39           Al iv         2.09         1.55         1.72         1.60         1.61           Al vi         2.00         1.59         1.36         1.35         1.38           Ti         0.01         0.01         0.01         0.01         0.01         0.01           Cr         0.05         0.13         0.34         0.38         0.38           Fe <sup>3+</sup> 0.00         0.09         0.00         0.08         0.08           Fe <sup>2+</sup> 1.33         1.11         1.19         1.14         1.13           Mn         0.00         0.00         0.00         0.01         0.02           Mg         8.58         8.86         9.01         8.83         8.81           Ni         0.	Na <sub>2</sub> O	0.01	0.03	0.03	0.01	0.05			
$\begin{array}{c ccccccccccccccccccccccccccccccccccc$	K <sub>2</sub> O	0.01	0.04	0.03	0.01	0.05			
Total         97.41         98.42         98.86         96.05         97.84           Cations         28(O)         28(O)         28(O)         28(O)         28(O)           Si         5.91         6.45         6.28         6.40         6.39           Al iv         2.09         1.55         1.72         1.60         1.61           Al vi         2.00         1.59         1.36         1.35         1.38           Ti         0.01         0.01         0.01         0.01         0.01           Cr         0.05         0.13         0.34         0.38         0.38           Fe <sup>3+</sup> 0.00         0.09         0.00         0.08         0.08           Fe <sup>2+</sup> 1.33         1.11         1.19         1.14         1.13           Mn         0.00         0.00         0.00         0.01         0.02           Mg         8.58         8.86         9.01         8.83         8.81           Ni         0.03         0.05         0.05         0.06         0.03           Ca         0.01         0.01         0.02         0.02         0.01         0.04           K         0.01	BaO	0.00	0.02	0.00	0.00	0.00			
Cations         28(O)         28(O)         28(O)         28(O)         28(O)         28(O)           Si         5.91         6.45         6.28         6.40         6.39           Al iv         2.09         1.55         1.72         1.60         1.61           Al vi         2.00         1.59         1.36         1.35         1.38           Ti         0.01         0.01         0.01         0.01         0.01           Cr         0.05         0.13         0.34         0.38         0.38           Fe <sup>3+</sup> 0.00         0.09         0.00         0.08         0.08           Fe <sup>2+</sup> 1.33         1.11         1.19         1.14         1.13           Mn         0.00         0.00         0.00         0.01         0.02           Mg         8.58         8.86         9.01         8.83         8.81           Ni         0.03         0.05         0.05         0.06         0.03           Ca         0.01         0.01         0.02         0.02         0.03           Na         0.01         0.02         0.02         0.01         0.04           K         0.01 <t< td=""><td>H<sub>2</sub>O*</td><td>12.14</td><td>12.30</td><td>12.29</td><td>11.92</td><td>12.15</td></t<>	H <sub>2</sub> O*	12.14	12.30	12.29	11.92	12.15			
Si       5.91       6.45       6.28       6.40       6.39         Al iv       2.09       1.55       1.72       1.60       1.61         Al vi       2.00       1.59       1.36       1.35       1.38         Ti       0.01       0.01       0.01       0.01       0.01         Cr       0.05       0.13       0.34       0.38       0.38         Fe³+       0.00       0.09       0.00       0.08       0.08         Fe²+       1.33       1.11       1.19       1.14       1.13         Mn       0.00       0.00       0.00       0.01       0.02         Mg       8.58       8.86       9.01       8.83       8.81         Ni       0.03       0.05       0.05       0.06       0.03         Ca       0.01       0.01       0.02       0.02       0.01       0.04         K       0.01       0.02       0.01       0.01       0.03         Ba       0.00       0.00       0.00       0.00       0.00         OH*       16.00       16.00       16.00       16.00       16.00         Total       36.02       35.89 <td< td=""><td>Total</td><td>97.41</td><td>98.42</td><td>98.86</td><td>96.05</td><td>97.84</td></td<>	Total	97.41	98.42	98.86	96.05	97.84			
Al iv 2.09 1.55 1.72 1.60 1.61 Al vi 2.00 1.59 1.36 1.35 1.38 Ti 0.01 0.01 0.01 0.01 0.01 Cr 0.05 0.13 0.34 0.38 0.38 Fe <sup>3+</sup> 0.00 0.09 0.00 0.08 0.08 Fe <sup>2+</sup> 1.33 1.11 1.19 1.14 1.13 Mn 0.00 0.00 0.00 0.01 0.02 Mg 8.58 8.86 9.01 8.83 8.81 Ni 0.03 0.05 0.05 0.06 0.03 Ca 0.01 0.01 0.02 0.02 0.03 Na 0.01 0.02 0.02 0.01 0.04 K 0.01 0.02 0.02 0.01 0.04 K 0.01 0.02 0.00 0.00 0.00 OH* 16.00 16.00 16.00 16.00 Total 36.02 35.89 36.02 35.90 35.92 Al total 4.09 3.14 3.08 2.95 2.99 Si 5.91 6.45 6.28 6.40 6.39	Cations	28(O)	28(O)	28(O)	28(O)	28(O)			
Al vi 2.00 1.59 1.36 1.35 1.38  Ti 0.01 0.01 0.01 0.01 0.01 0.01  Cr 0.05 0.13 0.34 0.38 0.38  Fe <sup>3+</sup> 0.00 0.09 0.00 0.08 0.08  Fe <sup>2+</sup> 1.33 1.11 1.19 1.14 1.13  Mn 0.00 0.00 0.00 0.01 0.02  Mg 8.58 8.86 9.01 8.83 8.81  Ni 0.03 0.05 0.05 0.06 0.03  Ca 0.01 0.01 0.02 0.02 0.03  Na 0.01 0.02 0.02 0.01 0.04  K 0.01 0.02 0.02 0.01 0.04  K 0.01 0.02 0.01 0.01 0.03  Ba 0.00 0.00 0.00 0.00 0.00  OH* 16.00 16.00 16.00 16.00  Total 36.02 35.89 36.02 35.90 35.92  Al total 4.09 3.14 3.08 2.95 2.99  Si 5.91 6.45 6.28 6.40 6.39	Si	5.91	6.45	6.28	6.40	6.39			
Ti         0.01         0.01         0.01         0.01         0.01           Cr         0.05         0.13         0.34         0.38         0.38           Fe³+         0.00         0.09         0.00         0.08         0.08           Fe²+         1.33         1.11         1.19         1.14         1.13           Mn         0.00         0.00         0.01         0.02           Mg         8.58         8.86         9.01         8.83         8.81           Ni         0.03         0.05         0.05         0.06         0.03           Ca         0.01         0.01         0.02         0.02         0.01         0.04           K         0.01         0.02         0.02         0.01         0.04           K         0.01         0.02         0.01         0.01         0.03           Ba         0.00         0.00         0.00         0.00         0.00           OH*         16.00         16.00         16.00         16.00         16.00           Total         36.02         35.89         36.02         35.90         35.92           Al total         4.09         3.14	Al iv	2.09	1.55	1.72	1.60	1.61			
Cr         0.05         0.13         0.34         0.38         0.38           Fe³+         0.00         0.09         0.00         0.08         0.08           Fe²+         1.33         1.11         1.19         1.14         1.13           Mn         0.00         0.00         0.01         0.02           Mg         8.58         8.86         9.01         8.83         8.81           Ni         0.03         0.05         0.05         0.06         0.03           Ca         0.01         0.01         0.02         0.02         0.03           Na         0.01         0.02         0.02         0.01         0.04           K         0.01         0.02         0.02         0.01         0.03           Ba         0.00         0.00         0.00         0.00         0.00           OH*         16.00         16.00         16.00         16.00         16.00           Total         36.02         35.89         36.02         35.90         35.92           Al total         4.09         3.14         3.08         2.95         2.99           Si         5.91         6.45         6.28 <td< td=""><td>Al vi</td><td>2.00</td><td>1.59</td><td>1.36</td><td>1.35</td><td>1.38</td></td<>	Al vi	2.00	1.59	1.36	1.35	1.38			
Fe³+         0.00         0.09         0.00         0.08         0.08           Fe²+         1.33         1.11         1.19         1.14         1.13           Mn         0.00         0.00         0.00         0.01         0.02           Mg         8.58         8.86         9.01         8.83         8.81           Ni         0.03         0.05         0.05         0.06         0.03           Ca         0.01         0.01         0.02         0.02         0.03           Na         0.01         0.02         0.02         0.01         0.04           K         0.01         0.02         0.01         0.01         0.03           Ba         0.00         0.00         0.00         0.00         0.00           OH*         16.00         16.00         16.00         16.00         16.00           Total         36.02         35.89         36.02         35.90         35.92           Al total         4.09         3.14         3.08         2.95         2.99           Si         5.91         6.45         6.28         6.40         6.39	Ti	0.01	0.01	0.01	0.01	0.01			
Fe <sup>2+</sup> 1.33         1.11         1.19         1.14         1.13           Mn         0.00         0.00         0.00         0.01         0.02           Mg         8.58         8.86         9.01         8.83         8.81           Ni         0.03         0.05         0.05         0.06         0.03           Ca         0.01         0.01         0.02         0.02         0.01         0.04           K         0.01         0.02         0.01         0.01         0.03           Ba         0.00         0.00         0.00         0.00         0.00           OH*         16.00         16.00         16.00         16.00         16.00           Total         36.02         35.89         36.02         35.90         35.92           Al total         4.09         3.14         3.08         2.95         2.99           Si         5.91         6.45         6.28         6.40         6.39	Cr	0.05	0.13	0.34	0.38	0.38			
Mn         0.00         0.00         0.00         0.01         0.02           Mg         8.58         8.86         9.01         8.83         8.81           Ni         0.03         0.05         0.05         0.06         0.03           Ca         0.01         0.01         0.02         0.02         0.03           Na         0.01         0.02         0.02         0.01         0.04           K         0.01         0.02         0.01         0.01         0.03           Ba         0.00         0.00         0.00         0.00         0.00           OH*         16.00         16.00         16.00         16.00         16.00           Total         36.02         35.89         36.02         35.90         35.92           Al total         4.09         3.14         3.08         2.95         2.99           Si         5.91         6.45         6.28         6.40         6.39	Fe <sup>3+</sup>	0.00	0.09	0.00	0.08	0.08			
Mg       8.58       8.86       9.01       8.83       8.81         Ni       0.03       0.05       0.05       0.06       0.03         Ca       0.01       0.01       0.02       0.02       0.03         Na       0.01       0.02       0.02       0.01       0.04         K       0.01       0.02       0.01       0.01       0.03         Ba       0.00       0.00       0.00       0.00       0.00         OH*       16.00       16.00       16.00       16.00       16.00         Total       36.02       35.89       36.02       35.90       35.92         Al total       4.09       3.14       3.08       2.95       2.99         Si       5.91       6.45       6.28       6.40       6.39	Fe <sup>2+</sup>	1.33	1.11	1.19	1.14	1.13			
Ni         0.03         0.05         0.05         0.06         0.03           Ca         0.01         0.01         0.02         0.02         0.03           Na         0.01         0.02         0.02         0.01         0.04           K         0.01         0.02         0.01         0.01         0.03           Ba         0.00         0.00         0.00         0.00         0.00           OH*         16.00         16.00         16.00         16.00         16.00           Total         36.02         35.89         36.02         35.90         35.92           Al total         4.09         3.14         3.08         2.95         2.99           Si         5.91         6.45         6.28         6.40         6.39	Mn	0.00	0.00	0.00	0.01	0.02			
Ca         0.01         0.01         0.02         0.02         0.03           Na         0.01         0.02         0.02         0.01         0.04           K         0.01         0.02         0.01         0.01         0.03           Ba         0.00         0.00         0.00         0.00         0.00           OH*         16.00         16.00         16.00         16.00         16.00           Total         36.02         35.89         36.02         35.90         35.92           Al total         4.09         3.14         3.08         2.95         2.99           Si         5.91         6.45         6.28         6.40         6.39	Mg	8.58	8.86	9.01	8.83	8.81			
Na         0.01         0.02         0.02         0.01         0.04           K         0.01         0.02         0.01         0.01         0.03           Ba         0.00         0.00         0.00         0.00         0.00           OH*         16.00         16.00         16.00         16.00         16.00           Total         36.02         35.89         36.02         35.90         35.92           Al total         4.09         3.14         3.08         2.95         2.99           Si         5.91         6.45         6.28         6.40         6.39	Ni	0.03	0.05	0.05	0.06	0.03			
K     0.01     0.02     0.01     0.01     0.03       Ba     0.00     0.00     0.00     0.00     0.00       OH*     16.00     16.00     16.00     16.00     16.00       Total     36.02     35.89     36.02     35.90     35.92       Al total     4.09     3.14     3.08     2.95     2.99       Si     5.91     6.45     6.28     6.40     6.39	Ca	0.01	0.01	0.02	0.02	0.03			
Ba         0.00         0.00         0.00         0.00         0.00           OH*         16.00         16.00         16.00         16.00         16.00           Total         36.02         35.89         36.02         35.90         35.92           Al total         4.09         3.14         3.08         2.95         2.99           Si         5.91         6.45         6.28         6.40         6.39	Na	0.01	0.02	0.02	0.01	0.04			
OH*       16.00       16.00       16.00       16.00       16.00         Total       36.02       35.89       36.02       35.90       35.92         Al total       4.09       3.14       3.08       2.95       2.99         Si       5.91       6.45       6.28       6.40       6.39	K	0.01	0.02	0.01	0.01	0.03			
Total         36.02         35.89         36.02         35.90         35.92           Al total         4.09         3.14         3.08         2.95         2.99           Si         5.91         6.45         6.28         6.40         6.39	Ва	0.00	0.00	0.00	0.00	0.00			
Al total 4.09 3.14 3.08 2.95 2.99 Si 5.91 6.45 6.28 6.40 6.39	OH*	16.00	16.00	16.00	16.00	16.00			
Si 5.91 6.45 6.28 6.40 6.39	Total	36.02	35.89	36.02	35.90	35.92			
	Al total	4.09	3.14	3.08	2.95	2.99			
Fe/Fe + Mg 0.13 0.12 0.12 0.12 0.12	Si	5.91	6.45	6.28	6.40	6.39			
	Fe/Fe + M	g 0.13	0.12	0.12	0.12	0.12			

Note. Chl: Chlorite.

The ferrous chromite, when compared with Al-chromite, is characterized by low  $Al_2O_3$  (2.60–3.52 wt.%), low Mg# (3.08–4.21), high Cr# (89.40–91.37), and high Fe $_2O_3$  (16.22–20.86 wt.%). The compositions of the homogeneous ferrian chromite are relatively low in  $Al_2O_3$  (0.06–1.53 wt.%),  $Cr_2O_3$  (19.56–37.90 wt.%) and MgO (0.15–0.80 wt.%) with high Fe $_2O_3$  (25.54–47.60 wt.%). They are characterized by low Mg# which vary from 0.90–4.43 and high Cr# (94.27 to 99.54) with  $^{\text{Y}}\text{Fe}^{3\text{+}}\text{#}$  ranging from 38 to 70 (Table 2).

The rim part of zoned Cr-spinel is usually characterized by chrome magnetite and magnetite (Figure 3c and 3e). Cr-magnetites show very low contents of Al $_2$ O $_3$  (<0.1 wt.%), Cr $_2$ O $_3$  (10.23–16.0 wt.%), TiO $_2$  (0.28–0.37 wt.%), and MgO (0.03–0.93 wt.%). The MnO content is low, which ranges from 0.01 to 0.68 wt.%, and their Fe $_2$ O $_3$  content is high ranging from 50.1 to 58.7 wt.%.

The magnetite and titano-magnetite are medium- to coarse-grained, homogeneous in nature, and occur as disseminated grains. They are associated with chrome-magnetite in the partly altered Cr-spinels (Figure 3h). The magnetite contains high Fe $_2$ O $_3$  (57.58 to 64.87 wt.%) and FeO (29.5 to 30.5 wt.%) and low TiO $_2$  (0.03 to 0.24 wt.%) and very low Cr $_2$ O $_3$  (2.55–9.66 wt.%) while Al $_2$ O $_3$  is completely absent.

The ferrous chromites are coarse-grained and homogeneous in nature. However, in some cases, core of ferrous chromite is classified as Al-chromite due to the presence of Al<sub>2</sub>O<sub>3</sub> and MgO and low Fe<sup>3+</sup># [Fe<sup>3+</sup>/(Fe<sup>3+</sup>+Fe<sup>2+</sup>)] (0.33–0.39; Table 2). The homogeneous ferrian chromite contains much higher ratios of Fe<sup>3+</sup># (0.38–0.70) signifying changes in chemical composition from Al-chromite to ferrian chromite.

#### 5.2 | Silicates

Olivine grains observed in peridotite and olivine pyroxenite have forsterite (Fo) ranging from 75.96% to 77.59%, MnO from 0.29 to 0.33 wt.%, and extremely low CaO (<0.04 wt.%; Table 1). Most of the amphiboles in peridotite shows a compositional variation in  $SiO_2$  (51.4–58.4 wt.%),  $Al_2O_3$  (<5.5 wt.%), and FeO (0.02–3.43 wt.%; Table 3). The secondary amphiboles are generally rich in MgO, poor in alkalis (Na + K < 0.5 wt.%) forming tremolite and magnesium-hornblende variety (Leake et al., 1997). Serpentine grains show compositional variation in  $SiO_2$  ranging from 39.6–43.3 wt.%, and MgO varies from 32.5–35.9 wt.% while  $Al_2O_3$  varies from 0.56 to 2.4 wt.% (Table 4). Chlorites are characterized by high  $Cr_2O_3$  (0.3–2.4 wt.%), low  $Al_2O_3$  (12.4–17.6 wt.%) with trace amount of  $TiO_2$ , MnO, and NiO (Table 5). In addition, some chlorite has high MgO and low FeO (6.8–8.0 wt.%), trending towards Mg-Cr rich chlorite.

#### 5.3 | Major and trace elements

Rocks from the MUC show a wide variation in chemical composition. Major and trace element abundances are given in Table 6. The peridotites show high MgO (32.38-36.34 wt.%) and low SiO<sub>2</sub> (37.7-41.0 wt.%), while the olivine pyroxenite and pyroxenite (Table 6) show relatively high SiO<sub>2</sub> (48.61-51.82 wt.%) and low MgO (23.51-27.74 wt.%). The peridotites have low  $\Sigma$ REE (7.9-10.9 ppm) and nearly flat chondrite-normalized HREE pattern (Gd/Yb)<sub>n</sub> = 1.01-1.24 with mild LREE enrichment (La/Sm) $_n$  = 1.78-2.63; Figure 4a). The pyroxenite and olivine-pyroxenite have relatively high ΣREE (13.42-14.56 ppm) with mild LREE and HREE fractionation (La/Yb)<sub>n</sub> = 1.7-2.1; Figure 4c). In the multi-element spider diagram, the peridotite, olivine pyroxenite, and pyroxenite display similar trace element patterns and are characterized by enrichment of large-ion lithophile elements, depletion of high-field strength elements with negative Nb, Zr, and Hf anomalies (Figure 4b,d). All the samples plot in the arc related ultramafic cumulate field in the AFM triangular diagram of Beard (1986; Figure 12a). On the Th/Yb versus Ta/Yb diagram (Pearce, 1983; Figure 12b), the samples plot in the active continental margin showing continental arc geochemical affinities.

 TABLE 6
 Major and trace element abundances in the Madawara ultramafic intrusion

Rock type	Peridotite									Olivine pyro	exenite	
Sample	MW-7de	MW-8de	MD-1de	MD-5de	MW-9de	MD-2de	MD-3de	MD-10de	MD-13	MD-7-Opy	MD-9-Opy	15
Major oxide	es in wt.%											
SiO <sub>2</sub>	37.66	37.83	38.19	39.31	37.16	36.41	38.07	37.09	41.02	48.61	48.62	51.82
Al <sub>2</sub> O <sub>3</sub>	1.85	2.43	3.13	3.10	2.47	2.58	2.42	2.27	3.04	3.00	3.62	3.34
Fe <sub>2</sub> O <sub>3</sub>	11.49	11.19	8.53	11.46	11.52	11.01	10.99	12.55	11.38	8.61	7.86	10.51
MnO	0.13	0.15	0.13	0.12	0.14	0.15	0.14	0.15	0.12	0.18	0.17	0.20
MgO	36.34	35.42	35.93	32.77	33.84	34.00	34.40	34.28	32.38	27.74	25.12	23.51
CaO	1.30	1.77	4.35	2.81	2.92	2.95	2.59	2.38	1.85	5.38	8.96	5.02
Na <sub>2</sub> O	-0.26	-0.25	0.06	-0.11	-0.18	-0.21	-0.24	-0.25	-0.21	0.03	-0.04	0.12
K <sub>2</sub> O	0.00	0.00	0.02	0.01	0.00	0.00	0.00	0.00	0.00	0.02	0.03	0.01
TiO <sub>2</sub>	0.17	0.15	0.16	0.16	0.20	0.15	0.17	0.15	0.21	0.21	0.21	0.29
P <sub>2</sub> O <sub>5</sub>	0.02	0.03	0.03	0.03	0.03	0.03	0.02	0.03	0.02	0.02	0.02	0.03
LOI	10.97	10.91	10.38	10.44	11.20	12.09	11.01	11.41	9.78	5.98	4.45	3.76
Total	99.66	99.62	100.91	100.11	99.31	99.16	99.58	100.05	99.60	99.77	99.03	98.61
Trace elem	ents in ppm											
Sc	12.76	12.98	12.33	13.37	14.27	11.85	14.05	11.08	15.68	11.00	25.00	10.70
V	63.08	79.55	65.21	82.07	74.21	69.59	75.24	66.54	93.42	39.00	146.00	65.70
Cr	4012.88	5373.85	2738.91	5386.89	3285.77	4586.18	5120.34	4036.01	5149.44	320.00	2100.00	2001.00
Со	125.29	125.83	121.74	112.67	122.90	122.13	122.08	130.44	107.19	270.00	103.00	93.70
Ni	1844.65	1841.74	1740.47	1809.83	1757.27	1807.68	1819.13	1991.48	1670.26	1460.00	674.00	1041.00
Cu	6.66	16.68	23.22	27.81	17.36	41.07	15.55	20.23	23.75	1750.00	628.00	42.80
Zn	122.65	247.68	97.25	101.24	189.16	206.56	112.04	155.97	146.96	105.00	80.00	0.00
Ga	3.41	3.94	4.25	5.19	3.91	4.22	4.24	3.73	5.84	0.00	0.00	0.00
Rb	0.96	1.66	1.23	1.28	1.50	1.30	1.17	1.38	1.49	8.10	3.60	7.68
Sr	6.46	22.34	76.14	7.79	28.42	43.97	31.48	38.51	15.61	73.00	110.00	57.90
Υ	3.62	3.16	3.58	3.71	4.35	3.30	3.45	3.48	4.46	3.00	9.20	5.36
Zr	7.69	8.06	6.70	8.57	14.46	7.56	7.01	8.38	9.11	24.00	32.00	24.00
Nb	0.24	0.24	0.28	0.31	0.39	0.24	0.28	0.27	0.36	0.97	1.70	1.16
Cs	0.09	0.21	0.28	0.15	0.19	0.18	0.16	0.19	0.18	0.90	0.79	0.00
Ва	11.92	9.85	14.43	13.29	5.22	9.79	9.67	9.30	13.57	79.00	140.00	55.40
La	1.11	1.27	1.54	1.46	1.67	1.64	1.62	1.32	1.95	5.30	5.70	3.43
Ce	2.33	2.93	3.36	3.38	3.80	3.40	3.50	2.95	4.13	11.00	14.00	7.28
Pr	0.31	0.36	0.40	0.45	0.47	0.42	0.43	0.38	0.51	1.30	1.90	0.86
Nd	1.37	1.46	1.63	1.74	1.89	1.60	1.72	1.57	2.06	5.50	7.80	3.56
Sm	0.40	0.34	0.38	0.39	0.43	0.36	0.40	0.37	0.48	0.98	1.80	0.88
Eu	0.13	0.10	0.14	0.11	0.14	0.13	0.12	0.10	0.15	0.27	0.59	0.27
Gd	0.52	0.46	0.49	0.49	0.59	0.46	0.49	0.48	0.61	0.70	1.80	0.89
Tb	0.10	0.08	0.09	0.09	0.10	0.08	0.09	0.09	0.11	0.00	0.00	0.15
Dy	0.62	0.48	0.54	0.56	0.65	0.50	0.55	0.52	0.68	0.51	1.50	1.00
Но	0.14	0.11	0.13	0.12	0.15	0.12	0.12	0.12	0.16	0.09	0.32	0.20
Er	0.42	0.36	0.41	0.41	0.47	0.37	0.39	0.39	0.51	0.25	0.92	0.20
Tm	0.06	0.05	0.06	0.06	0.07	0.05	0.06	0.06	0.08	0.00	0.00	0.09
Yb	0.35	0.34	0.37	0.38	0.45	0.35	0.36	0.37	0.50	0.25	0.83	0.55
Lu	0.05	0.05	0.06	0.06	0.07	0.05	0.06	0.06	0.07	0.04	0.13	0.09
Hf	0.17	0.17	0.15	0.19	0.31	0.16	0.17	0.18	0.20	0.53	0.99	0.66
Та	0.06	0.08	0.07	0.05	0.10	0.06	0.09	0.07	0.06	0.06	0.11	0.10
Pb	5.13	8.37	8.69	6.93	5.37	8.98	9.67	7.37	7.68	0.00	0.00	7.06
Th	0.28	0.26	0.29	0.35	0.41	0.25	0.31	0.26	0.41	0.85	0.62	0.69
U	0.11	0.10	0.13	0.12	0.11	0.08	0.16	0.38	0.11	0.29	0.78	0.19
(Gd/Yb) <sub>N</sub>	1.24	1.12	1.09	1.08	1.09	1.10	1.13	1.07	1.01	1.08	1.22	1.22
(La/Sm) <sub>N</sub>	1.78	2.41	2.61	2.41	2.52	2.99	2.59	2.32	2.63	2.15	2.21	1.70

Rock type	Rock type Peridotite										Olivine pyroxenite		
Sample	MW-7de	MW-8de	MD-1de	MD-5de	MW-9de	MD-2de	MD-3de	MD-10de	MD-13	MD-7-Opy	MD-9-Opy	15	
Ta/Yb	0.18	0.23	0.19	0.14	0.22	0.17	0.25	0.19	0.13	0.15	0.20	0.32	
Th/Yb	0.81	0.76	0.76	0.94	0.90	0.73	0.86	0.71	0.83	1.10	1.58	1.63	

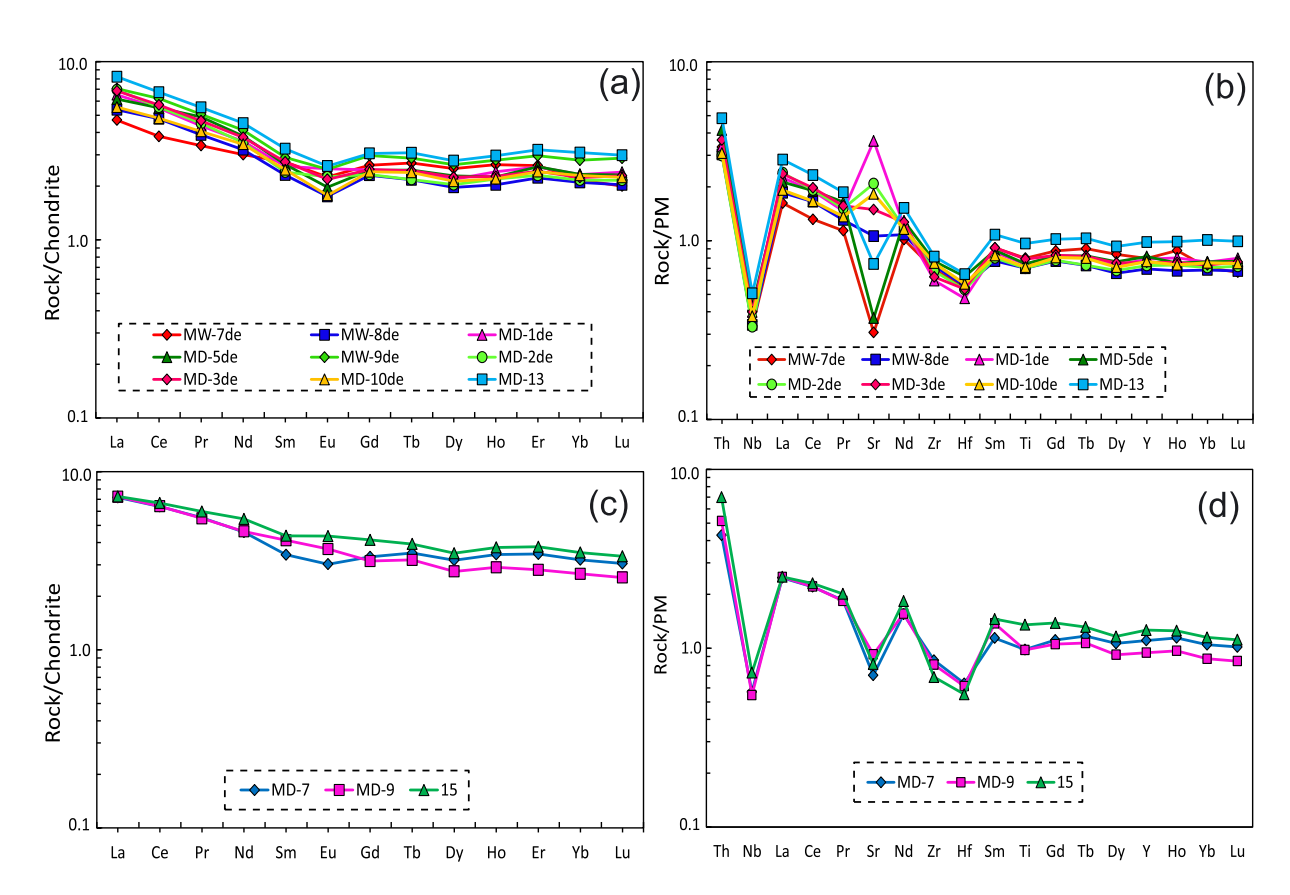


FIGURE 4 Chondrite-normalized REE pattern and primitive-mantle-normalized spider diagrams of (a-b) peridotite and (c-d) olivine pyroxenite, respectively from MUC. Normalization values are from McDonough and Sun (1995) [Colour figure can be viewed at wileyonlinelibrary.com]

## 5.4 | Oxygen fugacity

The oxygen fugacity ( $fO_2$ ) is an important parameter for physical and chemical processes that occur in the upper mantle. It provides an idea on the evolution of the magmatic systems controlled by different buffers and determines the crystallization of mineral assemblages during the process of fractional crystallization (Ballhaus, Berry, & Green, 1990, 1991). The temperature estimates based on equilibrium between olivine-spinel using the thermometry of Wan, Coogan, and Canil (2008) range from 929 to 1,095 °C. The textural evidences indicate the presence of magnetite, ulvospinel, ilemenite, and titanomagnetite phases in the peridotites that occur in the interstitial spaces of Cr-spinel, olivine, and pyroxene. Since these phases are very sensitive to oxidation, the empirical calibration of the oxygen fugacity barometer estimates based on the above phases would reflect the fluid behaviour that prevailed during the crystallization.

The empirical calibrations using the oxidation sensitive minerals with coexisting olivine and Cr-spinel in the peridotite and olivine pyroxenite point out that oxygen fugacity condition for ultramafics of Madawara prevailed between fayalite-magnetite-quartz (FMQ)

and magnetite-haematite (MH) buffers. The estimated results of -log fO2 obtained using thermodynamic data of Holland and Powell (2011) ranges from 14 to 17. The oxygen fugacity ( $\Delta \log (f O_2)^{FMQ}$ ) also ranges from 0.26 to 2.141 calculated based on Ballhaus et al. (1990, 1991) and Dare, Pearce, McDonald, and Styles (2009), which is lying above the FMQ buffer line (Figure 13). Thus oxidation state is observed to be much closer to the FMQ and above the wustitemagnetite (WM) as well as graphite buffers. The prevalence of high fugacity at the late cooling stage is also evident from the presence of spinel found commonly coexisting with magnetite, titanomagnetite, rutile, and ilmenite.

## Parental melt composition

The chemistry of Cr-spinel and olivine are sensitive to bulk composition of the melt, and their reaction with silicate liquid provides the best estimate of parental melt composition and the state of oxidation fugacity during cooling of magma (Barnes & Roeder, 2001; Dick & Bullen, 1984; González-Jiménez et al., 2011; Kamenetsky et al., 2001; Uysal et al., 2009). The mineral chemistry and textures of

0991034, 2019, 4, Downlo

aded from https://onlinelibrary.wiley.com/doi/10.1002/gj.3286 by University Of Hyderabad, Wiley Online Library on [30/01/2023]. See the Terms and Conditions (https://online

use; OA

articles are governed by the applicable Creative Commons

Al-chromite show that the core of Cr-spinels retain initial composition. In case of dunite and hornblende-rich ultramafic rock, most of the homogeneous Cr-spinels have changed its composition to ferrian chromite, chrome magnetite, and magnetite. This can be due to subsequent reaction with intercumulus liquid or subsolidus re-equilibration. The olivine in peridotite and olivine pyroxenite of MUC is less affected by post magmatic alteration and represents the early crystallization phases from the parental melt. The melt compositions involved in the formation of such Cr-spinel and olivine phases are used in the calculation to estimate the parental melt.

The  $Al_2O_3$  content of the parental melt equilibrium with Cr-spinel is calculated based on experimentally determined formula with the assumption that  $Al_2O_3$  content in spinel is the only function of  $Al_2O_3$  content in the melt (Kamenetsky et al., 2001; Maurel & Maurel, 1982) and is as follows:

$$\label{eq:Al2O3(Sp)} \text{Al}_2\text{O}_{3(\text{Sp})} = 0.035 \times (\text{Al}_2\text{O}_3)_{\text{Liq}}^{2.42} (\text{Al}_2\text{O}_3 \text{ in } \text{ wt.}\%).$$

The  $TiO_2$  content of the parental melt and Cr spinel is calculated by using the formula suggested by Kamenetsky et al. (2001) and Rollinson (2008) and is given as

$$\label{eq:TiO2} \text{TiO}_{2_{(\text{Meit})}} = 1.0963 \times \text{TiO}_{2_{(\text{Sp})}}^{~(0.7863)} \text{in wt.}\%.$$

The  $Al_2O_3$  content of the parental melt equilibrated with Cr-spinel ranges from 9.22 to 14.22 wt.% (average 11.74 wt.%) and 11.49 to 14.30 wt.% (average 12.53 wt.%) in peridotite and olivine pyroxenite, respectively. The  $TiO_2$  content of the parental melt ranges from 0.32 to 0.69 wt.% (average 0.49 wt.%) and 0.34 to 0.80 wt.% (average 0.56 wt.%) in peridotite and olivine pyroxenite, respectively (Table 7).

The (FeO/MgO) ratio of the parental melt is calculated using olivine composition from the olivine pyroxenite by using the equation of Roeder and Emslie (1970),

$$K_D = \frac{(FeO/MgO)_{Olv}}{(FeO/MgO)_{Liq}} \mbox{ where the coefficient} \\ K_D = 0.3 \mbox{ for olivine}.$$

The FeO/MgO ratio of the parental melt from which olivine is crystallized range from 1.72 to 1.92 wt.% (average 1.78 wt.%; Table 7).

#### 6 | DISCUSSION

#### 6.1 | Alteration and formation of zoned Cr-spinel

The alteration of Cr-spinel has been the subject of intense debate, and it is suggested that during alteration, Cr-spinel is gradually modified to ferrian chromite, chrome magnetite, and magnetite, leading to the formation of zoning within Cr-spinel (Barra et al., 2014; Gervilla et al., 2012; Ruan et al., 2017). The Cr-spinel from ultramafic rocks of MUC show zoning and distinct variation in mineral compositions during the alteration and physiochemical changes (Figure 3c–f). A detailed investigation of minerals was carried out under SEM-EDS at CSIR-NGRI Hyderabad. The BSE images show that most of Cr-spinels acquired zoning due to subsequent metasomatism and alteration where the core still preserve their original composition (Figure 3c and 3d). These crystals were crystallized along with olivine and some early formed sulphide.

In a few crystals, the appearance of a thin rim of Fe-chromite around Al-chromite (Figure 3d) is an indication of the beginning of physiochemical changes and replacement of  $Mg^{2+}$  and  $Al^{3+}$  from Crspinel with  $Fe^{2+}$  and minor amount of  $Fe^{3+}$ . Also, in some crystals, Fe-chromite and chrome magnetite grew at the rim of partly altered Al-chromites (Figure 3c). Such textural evidences indicate that ferrian chromite rim was involved first in the incorporation of  $Fe^{3+}$  from silicates followed by the formation of chrome magnetite. The SEM textural studies and EPMA data point out that ferrous chromite and ferrian chromite were formed successively at the rim of Al-chromite with varying  $Fe^{3+}/(Fe^{3+}+Fe^{2+})$  ratios during the advance stage of

**TABLE 7** Estimated maximum, minimum, and average value of  $Al_2O_3$ , FeO/MgO, and  $TiO_2$  of parental melts in ultramafic rocks from the study area in comparison with parental melt of different tectonic setting

	Al <sub>2</sub> O <sub>3(Melt)-Sp</sub>	TiO <sub>2(Melt)-Sp</sub>	(FeO/MgO) <sub>(Melt-OI)</sub>	$\Delta$ log (fo <sub>2</sub> )	$T^oc_{(OI\text{-}Sp)}$	References
Madawara ultramafic co	omplex					This study
Peridotite	9.22-14.22 (11.74)	0.32-0.69 (0.49)				
Olivine Pyroxennite	11.49-14.30 (12.53)	0.34-0.80 (0.56)	1.72-1.92 (1.78)	"+0.26: +2.14"	929-1095	
Alaskan-type complex						Habtoor, Ahmed, and Harbi (2016)
Peridotite	11.21-15.56 (13.79)	0.82-2.85 (1.62)	0.92-0.99 (0.95)	"-0.18: +4.13"	671-981	
Dunite	11.82-15.12 (13.68)	0.97-2.77 (1.83)	0.58-1.4 (0.90)	"+1.88: +3.01"	614-864	
MORB	~15	0.32-2.20	1.2-1.6			Wilson (1989)
BABB	~17	0.45-1.45				Kamenetsky et al. (2001)
Boninites (SSZ)	10.6-14.4	0.10-0.52	0.7-1.4			Wilson (1989), Hickey & Frey (1982)
Layered Intrusion						Mondal et al. (2006)
Bushveld complex	11.5	0.74				
Great dyke	11.1	0.61				
Archean low Ti Silicious	high Mg Basalt					Mondal et al. (2006)
Barberton	12.7-13.4	0.74				
Pilbara	10.1-11.7	0.58-0.75				

MOHANTY ET AL. 2115

physiochemical changes. Gervilla et al. (2012) suggested that the degree of oxidation state is a major factor for their stability. The ferrous chromites appear where  $Fe^{3+}/(Fe^{3+}+Fe^{2+})$  ratio is less than 0.4, while ferrian chromite formation begins with values greater than 0.4 (Gervilla et al., 2012). The core of some homogenous chromite (Figure 3g) showing high  $Fe^{3+}/(Fe^{3+}+Fe^{2+})$  ratio of 0.46 to 0.66 indicates its ferrian chromite nature.

The EPMA data of core of the Cr-spinel in the Cr-Al-Fe<sup>3+</sup> ternary diagram falls in the field of Al-chromite and few in the ferrian chromite region (Figure 5b). The rim composition of Cr-spinel lies towards the Fe<sup>3+</sup> enrichment and plots in the field of chrome magnetite (Cr-mag) and magnetite (mgt). The changes in chemical composition of core of the zoned Cr-spinels vary from Al-chromite to Fe-rich chromite indicating a Fe<sub>2</sub>O<sub>3</sub>-enrichment trend (Figure 7). The EPMA data of zoned crystals also suggests that Mg and Al decreased, whereas Fe increased significantly from aluminous-ferrous core to ferrian chromite rim and chrome magnetite (Table 2). The end of alteration is marked by the abundant presence of chlorite and magnetite minerals related to hydrothermal activities. Chlorite association with the ferrian chromite and magnetite rims are usually Cr-enriched (2.2-2.4 wt.%) and favours the formation from the alteration of Cr-spinels under the hydrous conditions (Gervilla et al., 2012; Grieco & Merlini, 2012; Mellini et al., 2005; Merlini, Grieco, & Diella, 2009). The high Mg and Cr content in chlorite may be due to the preferred partition from ferrian chromite.

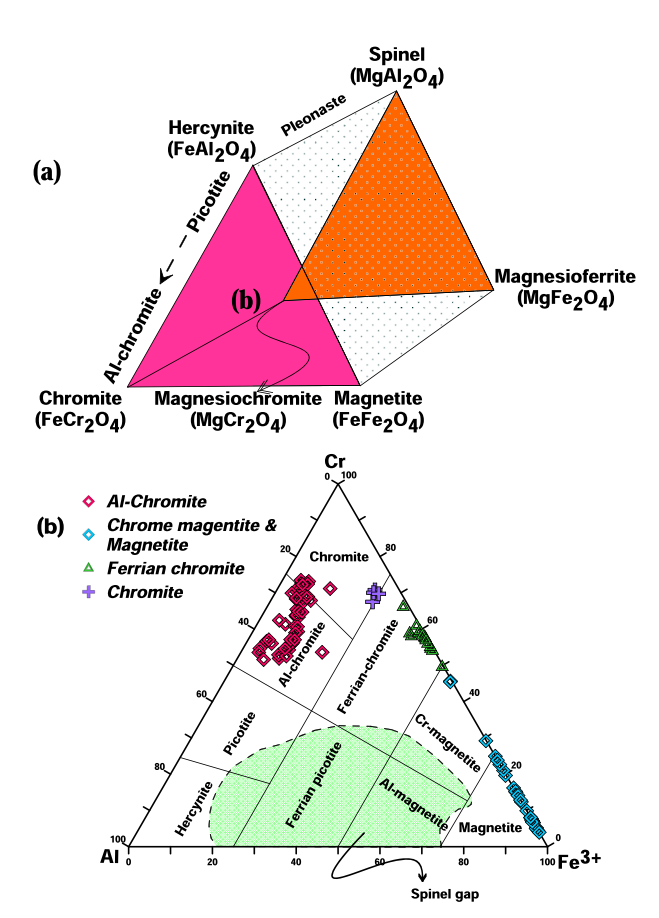


**FIGURE 5** (a) Spinel prism for the multicomponent systems of spinels for representation (after Deer, Howie, & Zussman, 1992). (b) Triangular classification diagram of spinel group of minerals in ultramafics of MUC (Field of "spinel gap" is from Barnes & Roeder, 2001) [Colour figure can be viewed at wileyonlinelibrary.com]

The primary Cr-spinel (Al-chromite) and olivine were crystallized from melts at high temperature, and during their cooling, they preserve geochemical signatures which can be used to track their involvement in fluid activities, alteration, and metasomatism. The interaction of FeO rich intercumulus magma with Cr-spinel under gradually decreasing temperature leads to the release of Fe $^{2+}$  from olivine that gets incorporated into the primary Al-chromite to form ferrous chromite (Figure 5b). The alteration of olivine and chromite under high H<sub>2</sub>O-saturated conditions with high silica activities (i.e., high fluid/rock ratios) promoted the formation of Fe-chromite and chlorite that has been envisaged by several workers (Barra et al., 2014; Gervilla et al., 2012; Mellini et al., 2005) and can be explained by the following reaction.

$$Cr$$
-spinel + Olivine + Silica + Water === > Fe-chromite + Chlorite

Gervilla et al. (2012) opined that ferrian chromites were formed under oxidizing and hydrothermal conditions with decrease in temperature and increase in  $fO_2$ . If the chromite/silicate and fluid/rock ratio is relatively high, then such conditions favour migration of  $Mg^{2+}$  and  $Al^{3+}$ , thereby leading to the formation of chrome magnetite, magnetite, and Mg-Cr-chlorite minerals. This is also indicated by the presence of serpentinization and high activity of hydrothermal fluids (Figure 3a and 3e).

## 6.2 | Petrogenesis

The data obtained from core of the primary Cr-spinel or chromite is considered to infer the primary magmatic characteristics and to decipher the petrogenesis of MUC. The plot between  $Cr_2O_3$  versus  $Fe_2O_3$  of primary Cr-spinel shows strong negative correlation as well as Fe-enrichment trend (Figure 6). In the Cr-Al-Fe<sup>3+</sup> triangular diagram, most of Cr-spinel plots near to the field of Alaskan-type

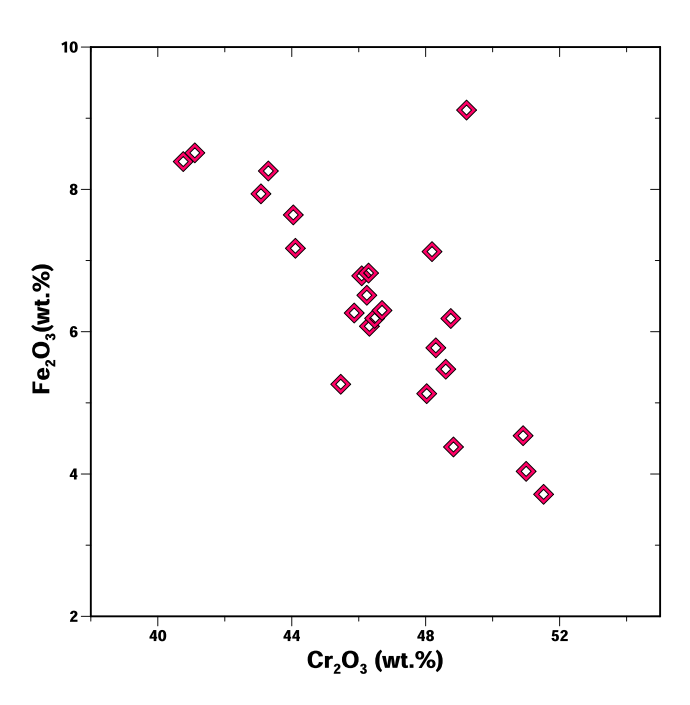


**FIGURE 6** Variation diagram between  $Cr_2O_3$  and  $Fe_2O_3$  showing a strong negative correlation of Al-chromite from MUC [Colour figure can be viewed at wileyonlinelibrary.com]

0991034, 2019, 4, Downloaded from https

elibrary.wiley.com/doi/10.1002/gj.3286 by University Of Hyderabad, Wiley Online Library on [30/01/2023]. See the Term

on Wiley Online Library for rules of use; OA articles are governed by the applicable Creative Commons

intrusion of island arc environment along with few data showing Fe enrichment trend (Figure 7a). Such Fe-enrichment trend in the Crspinel is mainly due to the replacement of Cr<sup>3+</sup> by Fe<sup>3+</sup>. It is formed either by reaction of spinel with intercumulus fluid over a considerable temperature, or it may be sub-solidus requilibriation with olivine. The Al-enrichment trend is very common in the case of layered intrusion due to the reaction of Cr-spinels with intercumulus liquid rich in plagioclase component, which is not the case in our present investigation. The chromite from the ophiolitic complex is characterized by constant Fe<sup>3+</sup> and substitutions of Cr<sup>3+</sup> by Al<sup>3+</sup> in the octahedral site of the chromite. This is also not the case of our analysed Cr-spinel (Barnes & Roeder, 2001; Bell & Claydon, 1992; Helmy & El Mahallawi, 2003; Krause, Brügmann, & Pushkarev, 2007; Nixon, Cabri, & Laflamme, 1990; Snoke, Quick, & Bowman, 1981). The changes in the composition from Al-chromite to Fe-chromite is related to intercumulus fluid activities at the island arc subduction zone and much close to Alaskan-type magmatism as has been recorded from elsewhere (Arai et al., 2011; Arai & Miura, 2016; Dönmez et al., 2014).

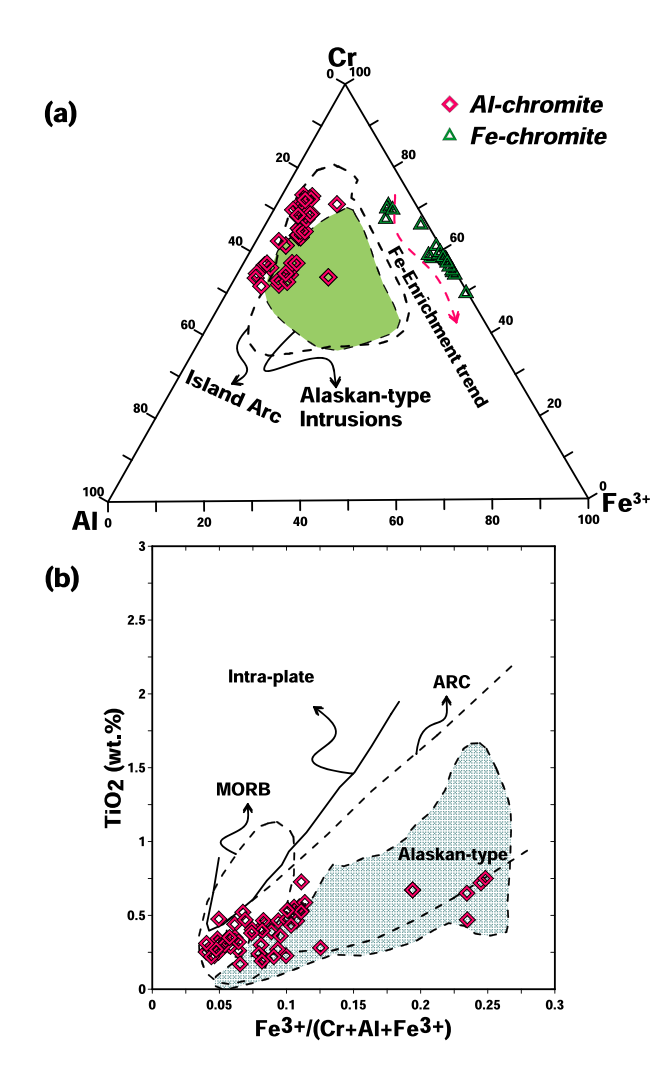


**FIGURE 7** (a) Cr-Al-Fe<sup>3+</sup> variation diagram of Al-chromite and Fechromite of the MUC showing an iron enrichment trend. The defined fields are from Barnes and Roeder (2001) and Wang, Wilde, and Wan (2010). (b)  ${\rm TiO_2}$  (wt.%) versus  ${\rm Fe^{3+}}/({\rm Cr+Al+Fe^{3+}})$  plot for Al-chromite in peridotite and olivine pyroxenite. The demarcated fields are from Arai (1992) and Barnes and Roeder (2001) [Colour figure can be viewed at wileyonlinelibrary.com]

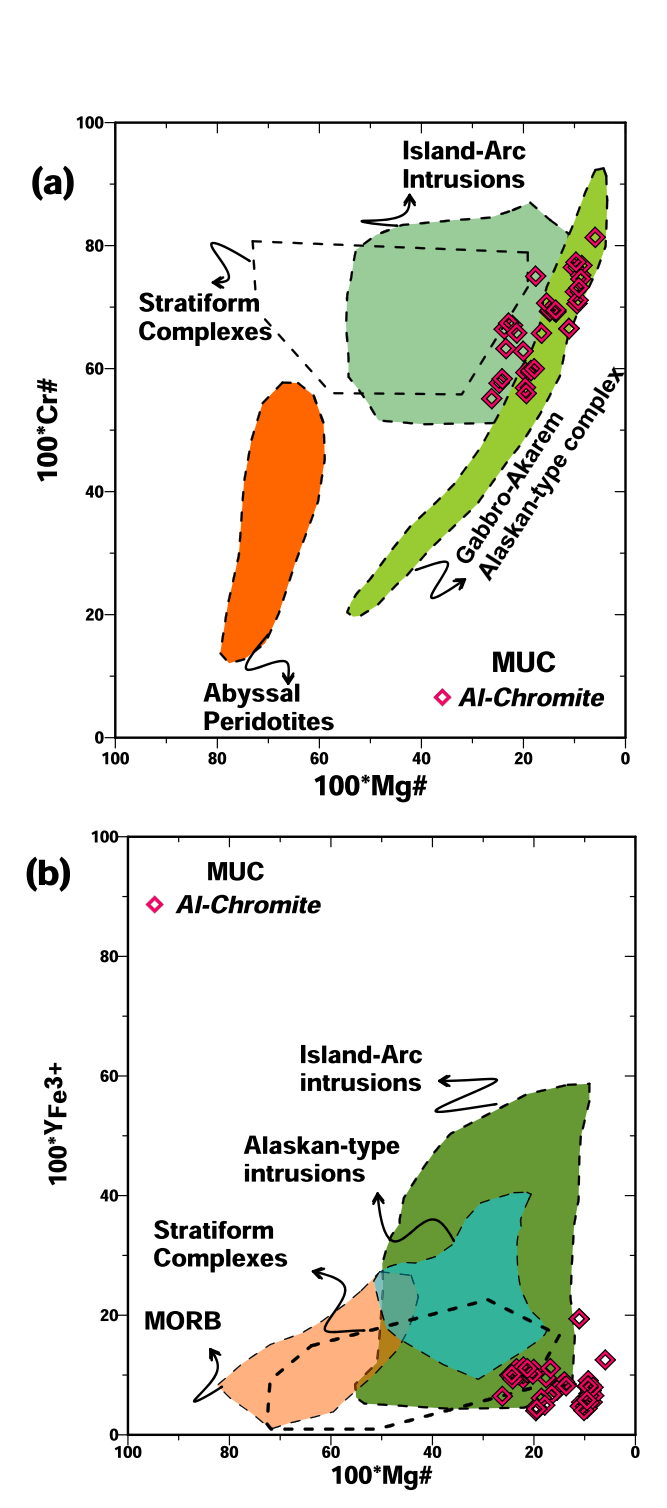


**FIGURE 8** (a) Bivariant diagram of 100\*Cr# versus 100\*Mg# of Alchromite showing distinct linear trend. Fields of stratiform complexes (Irvine, 1967, 1974), worldwide Alaskan-type intrusions (Barnes & Roeder, 2001; Farahat & Helmy, 2006; Helmy & El Mahallawi, 2003), island-arc intrusions (Spandler et al., 2003), and abyssal peridotites (Dick & Bullen, 1984) are shown here for comparison. Most of the Cr-spinel (Al-chromite) follows the trend of Alaskan-type complex. (b) Bivariant plot of 100\*γFe \*3 versus 100\*Mg# of Al-chromite. Field of Alaskan-type intrusions are obtained from (Himmelberg & Loney, 1995; Batanova et al., 2005) island-arc intrusions (Spandler et al., 2003), stratiform complexes (Irvine, 1967, 1974), and mid-oceanic Ridge basalt (MORB; Barnes & Roeder, 2001) are shown here in diagram for comparison [Colour figure can be viewed at wileyonlinelibrary.com]

0991034, 2019, 4, Downloaded from https://onlinelibrary.wiley.com/doi/10.1002/gj.3286 by University Of Hyderabad, Wiley Online Library on [30/01/2023]. See the Terms ons) on Wiley Online Library for rules of use; OA articles are governed by the applicable Creative Commons

The bivariant plots between  $TiO_2$  and  ${}^{V}Fe^{3+}$ # [Fe $^{3+}$ /(Fe $^{3+}$  +Cr + Al)] (Figure 7b) shows a linear relationship and most of the investigated Cr-spinels plot in the field of Alaskan-type complex (Barnes & Roeder, 2001). The high  $TiO_2$  content from the core of Cr-spinel (0.22–0.67 wt.%) are similar to those from Alaskan-type ultramaficmafic rocks at deeper level of island arc intrusion. Jan and Windley (1990) suggested that  $TiO_2$  wt.% level (0.3 wt.%) is the limiting factor

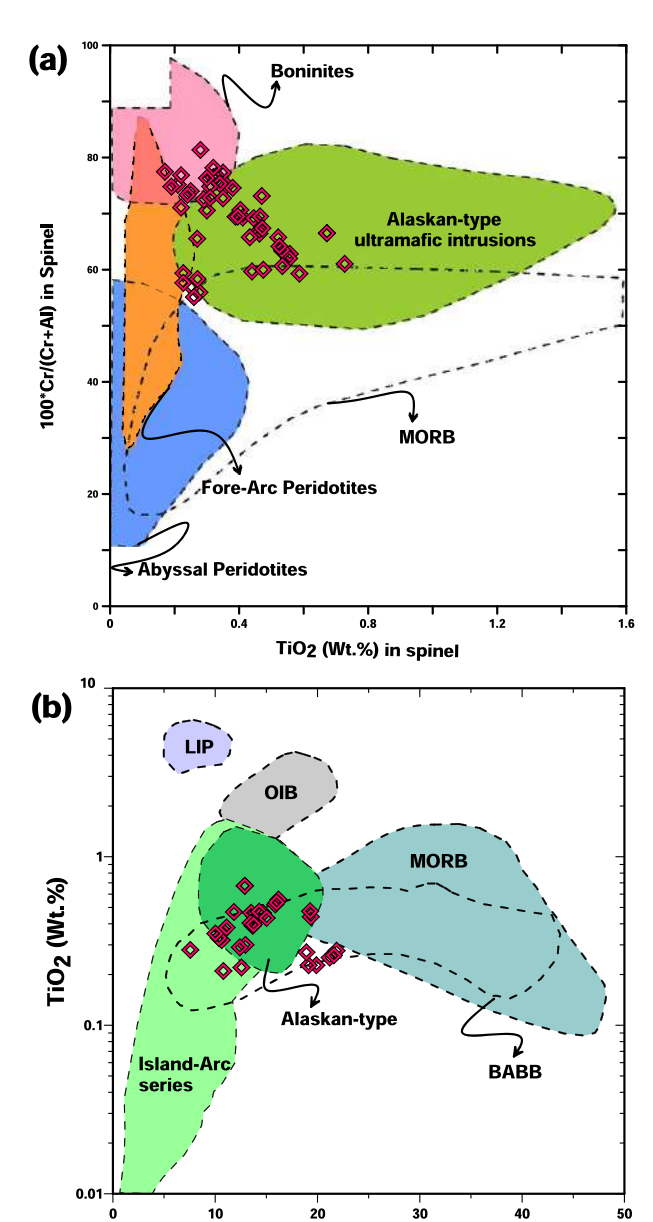


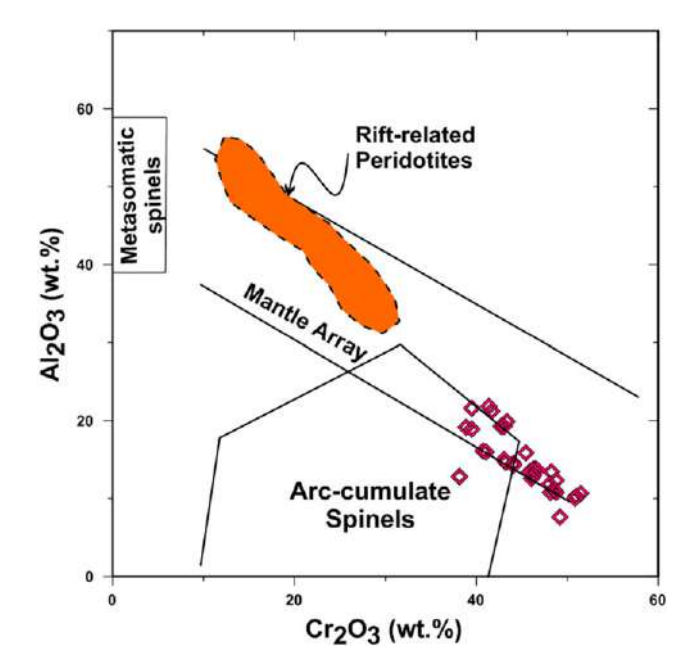
**FIGURE 9** (a) Plot of  $100^*$ Cr/(Cr + Al) versus  $TiO_2$  (wt.%) of Al-Chromite from the study area. Spinels from abyssal (Dick & Bullen, 1984) and fore arc (Ishii, Robinson, Maekawa, & Fiske, 1992) peridotites, MORB, boninites, (Arai, 1992; Barnes & Roeder, 2001), Aleutian xenoliths (Debari, Kay, & Kay, 1987) and Alaskan-type ultramafic intrusions (Himmelberg & Loney, 1995) are shown here for comparison. (b) Plot between  $Al_2O_3$  versus  $TiO_2$  in wt.% of Al chromite. Fields of LIP (large igneous province basalts), OIB (ocean-island basalts), MORB (mid-ocean ridge basalts), ARC, BABB (back-arc basin basalt) and MOR (mid-ocean ridge) peridotites are after Kamenetsky et al. (2001), and Alaskan-type complexes from Alaska were obtained from Himmelberg and Loney (1995) [Colour figure can be viewed at wileyonlinelibrary.com]

Al<sub>2</sub>O<sub>3</sub> (Wt.%)

between ophiolitic rocks from layered or stratiform complexes and in the Alaskan-type complex. The plot of Cr-spinel on the  ${}^{\gamma}\text{Fe}^{3+}\#$  versus  $\text{TiO}_2$  diagram shown in Figure 7b is a clear indication of Alaskan-type tectonic setting.

The analysed spinels are characterized by low Mg# (9.30-26.22), moderately high Cr# (55.15-81.35), and high Fe# [(100Fe<sup>2+</sup>/(Fe<sup>2+</sup> +Mg)] (73.78-88.93) values with very distinct linear trend similar to worldwide Alaskan-type intrusion (Figure 8a). In Figure 8b, Mg# versus YFe3+, the compositions of Cr-spinels plot outside the designated field but very close to the trend of Alaskan-type field. Further, the plot between Cr ratio and TiO<sub>2</sub> of the analysed Cr-spinel plots in the field of Alaskan-type intrusion (Figure 9a). The plots of spinel composition in the TiO<sub>2</sub> versus Al<sub>2</sub>O<sub>3</sub> diagram (Arai et al., 2011) is used to distinguish between the different tectonic settings such as mid-oceanic ridge, island arc including Alaskan-type environment and oceanic hotspot (Figure 9b). The core compositions of most of the Cr-spinels are in the range of  $Al_2O_3$  (10.63-21.87 wt.%) and  $TiO_2$  (0.22-0.67 wt.%) and lies in the field of island arc cumulates of Alaskan-type complex to back-arc basin basalt (BABB; Figure 9b). This mixed source of both island arc and BABB signifies that the subduction related geodynamic conditions with local extension due to the upwelling of anomalous high temperature convecting mantle is very similar to the origin of Alaskan-type ultramafic complex (Chen, Suzuki, Tian, Jahn, & Ireland, 2009; Ripley, 2009; Su, Qin, Santosh, Sun, & Tang, 2013; Tistl et al., 1994). This sometimes creates rifting and vertical uplifting of the Alaskan-type complex. Similarly the plots of Cr<sub>2</sub>O<sub>3</sub> versus Al<sub>2</sub>O<sub>3</sub> for the core composition lie towards the Arc-cumulate type tectonic setting for the Cr-spinels of MUC (Figure 10).

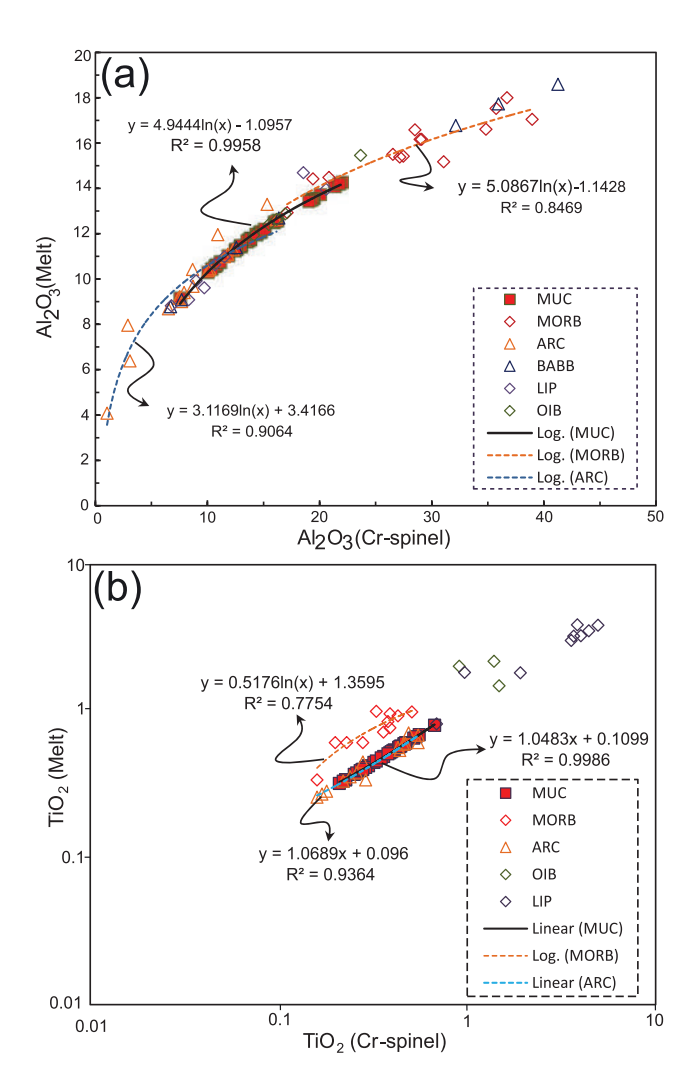
The parental melt is determined from the composition of primary Cr-spinel to address the composition of the melt involved in their formation. The calculated Al<sub>2</sub>O<sub>3</sub>, FeO/MgO, and TiO<sub>2</sub> ratios of the melts forming the Cr-spinel in Madawara ultramafics are listed in



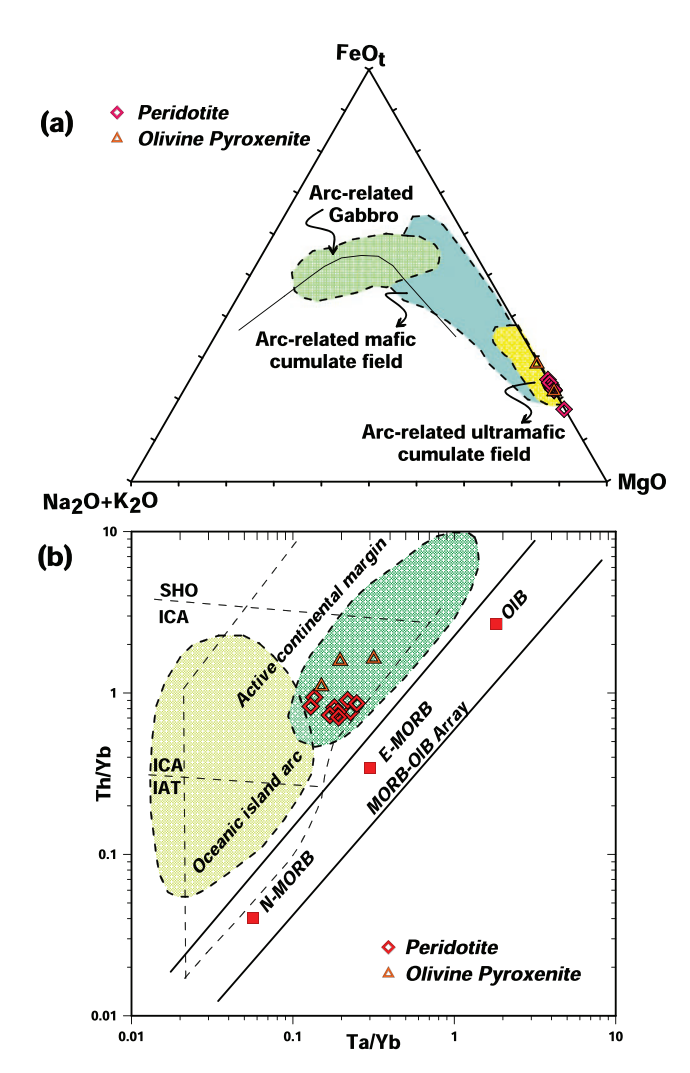
**FIGURE 10** Bivariate plot of  $Al_2O_3$  versus  $Cr_2O_3$  (wt.%) from Franz and Wirth (2000), modified after Seo, Oh, Choi, and Rajesh (2013), showing proximity to arc cumulate setting [Colour figure can be viewed at wileyonlinelibrary.com]

Table 7 and is also compared with parental melt composition estimates from different tectonic settings, namely, Taftafan Alaskan-type complex of western Arabian Shield (Habtoor et al., 2016), layered intrusions of Bushveld Complex (Mondal, Ripley, Li, & Frei, 2006), average BABB magma (Kamenetsky et al., 2001; Pearce, Barker, Edwards, Parkinson, & Leat, 2000), average worldwide boninites, and MORB magmas (Wilson, 1989). Using regression analyses, the estimated melt composition is compared with the melt composition from other tectonic settings. It is observed that the melt composition equilibrium with MUC resembles arc type of magma, which is similar to the magma involved during the formation of Alaskan-type complexes (Figure 11a,b). Apart from mineral chemistry data, the bulk-rock geochemistry suggests that they are slightly enriched in LILE with depletion in HFSE. They also display negative Nb, Zr, Hf anomalies, and positive U-Th anomalies (Figure 4), which further confirms their genesis from arc-related magma. The plots of Ta/Yb versus Th/Yb (Figure 12b) also show continental arc geochemical affinities for the ultramafics of Madawara.

The bivariant plots of oxygen fugacity against Cr# of spinel distinguishes the oxidation state for the ultramafic rocks crystallized from different tectonic settings (Ballhaus et al., 1991; Dare et al., 2009; Elburg & Kamenetsky, 2007; Habtoor et al., 2016). Cr-spinels in peridotites from arc magma are more oxidized than those from MORB magmas. The spinels formed from the hydrous arc magma are more oxidized in nature than the anhydrous conditions and shows higher  $fO_2$  values in comparison to the Cr-spinel formed in MORB setting (Ballhaus et al., 1991; Dare et al., 2009; Habtoor et al., 2016; Parkinson & Pearce, 1998; Pearce et al., 2000). The spinels from peridotite and pyroxenite from MUC plot in the arc peridotite region and show an increasing oxidation trend (Figure 13). Based on comparison of the parental melt estimation with worldwide tectonic settings, it is observed that the melt composition of MUC resemble arc



**FIGURE 11** Cr spinel-melt bivariate diagram for (a)  $Al_2O_3$  and (b)  $TiO_2$ . The estimated composition of parental melt that is in equilibrium with Cr-spinel from peridotite and olivine pyroxenite were calculated from EPMA data (in wt.%). Please see text for more details. The regression lines are derived from the experimental study of Maurel and Maurel (1982) and Cr spinel-melt inclusion studies in MORB, OIB, LIP, and ARC are from Kamenetsky et al. (2001). Only Alchromite data has been used for the calculation of the parental melt [Colour figure can be viewed at wileyonlinelibrary.com]



**FIGURE 12** (a) AFM tectonic discrimination diagram of whole-rock geochemistry of peridotite and olivine pyroxenite from MUC. The discriminating fields of both cumulate and non-cumulate ultramafic-mafic rocks are from Beard (1986). (b) Bivariate diagram of Th/Yb versus Ta/Yb (after Pearce, 1983; IAB: island arc basalt; IAT: island arc tholeiite; ICA: island arc calc-alkali; SHO: shoshonite; MORB: midoceanic ridge basalt; WPB: within-plate basalt; TH: tholeiite basalt; TR: transitional; ALK: alkali basalt) [Colour figure can be viewed at wileyonlinelibrary.com]

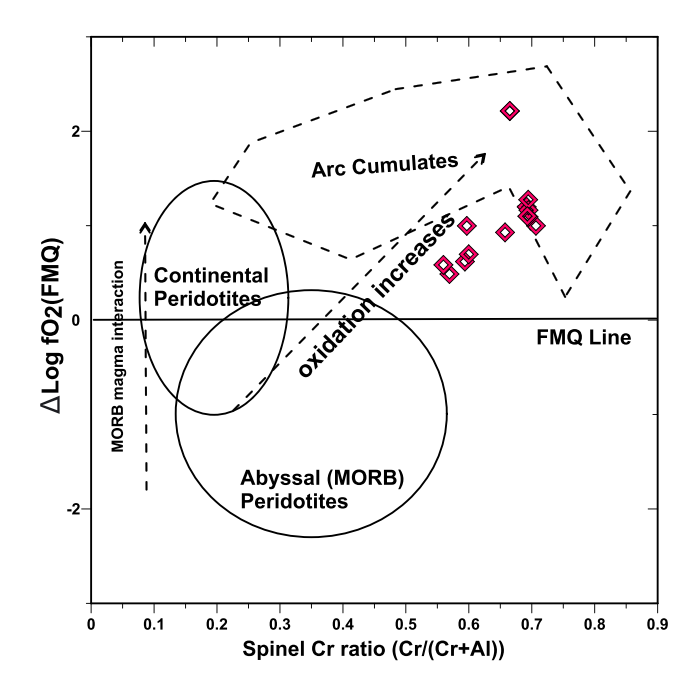


**FIGURE 13** Variation diagram for  $\Delta \log fO_2$  (FMQ) versus Cr# of Al-chromite from the study area. The field of Arc cumulates (Ballhaus, 1993) and Abyssal peridotites (Bryndzia & Wood, 1990) are shown here for comparison [Colour figure can be viewed at wileyonlinelibrary.com]

environment and is similar to Alaskan-type complex where  $fO_2$  increases with fractional crystallization under more oxidizing conditions.

# 6.3 | Relationship between subduction geodynamics and MUC magmatism

The mineral chemistry of Cr-spinel and bulk-rock geochemistry discussed in the preceding section provides significant information about conditions in the mantle during the emplacement and genesis of subduction-related magmatism in the southern part of Bundelkhand Craton. It indicates that the mafic and ultramafic intrusions of MUC in the area around 400 km<sup>2</sup> could be a part of the Archean orogeny. The peridotite and associated rock assemblages in the orogenic belts are usually classified as either Alpine-type (including ophiolite assemblages) or Alaskan-type intrusions (Irvine, 1974). The field relationship and geochemical data does not favour the former type. The Alaskantype ultramafic-mafic complex is thought to be island arc magmatism or shallow crustal level intrusion into continental basement (Dong et al., 2017; Irvine, 1974; Johan, 2002; Pettigrew & Hattori, 2006; Ripley, 2009; Su et al., 2013; Thakurta, Ripley, & Li, 2008). The origin of Alaskan-type complexes have been well documented and are considered to be formed in the subduction zones representing arc magmas or arc root complex (Chen et al., 2009; Debari & Coleman, 1989; Helmy et al., 2014; Helmy, Yoshikawa, Shibata, Arai, & Kagami, 2015; Irvine, 1974; Tistl et al., 1994). The morphology of Alaskan intrusions are very small compared to other types of ultramafic-mafic igneous complexes (Foley, Light, Nelson, & Harris, 1997). The Nizhni Tagil (70 km<sup>2</sup>) and Tulameen complexes (~80 km<sup>2</sup>) are considered to be exceptionally large intrusions (Johan, 2002). The correlation with the Alaskan-type magmatism has been made in Table 8.

**TABLE 8** Comparison between worldwide Alaskan-type intrusion and Madawara ultramafic complex

	Alaskan-type complex	Madawara ultramafic complex
Age	Mostly Phanerozoic	Archean
Geological setting	Close to end of subduction, prior to accretion-collision	Subduction
Size	Most are small in size, ranging from 12 to 40 $\mbox{km}^2$	Mostly small size (3 km²), Madawara intrusion is biggest (6 km²)
Morphology and zoning	Crude concentric zoning of lithologies grading from olivine-rich ultramafic core to mafic rim: lack of chilled margins	Crude concentric zoning of different lithology grading from peridotite core to gabbro; lack of chilled margins, margins are commonly sheared
Sequence of intrusion	Gabbroic and dioritic rocks as late intrusion	Late intrusion of gabbro rock followed by diorite
Lithology	Dunite, hornblendite, clinopyroxenite, gabbro, minor diorite, and syenite rocks	Peridotite, olivine-pyroxenite, pyroxenite, Hbl-pyroxenite, Hornblendite, Gabbro, Diorite, and Qtz-diorite. Syenite is not recorded
Texture	Accumulated texture with minor or no trapped liquid	The ultramafic rocks shows cumulate to adcumulate texture
Mineralogy	Abundant clinopyroxene, primary hornblende, magnetite, lack of Opx, and plagioclase in ultramafic rocks	Abundant olivine, Cpx, (Cpx > > Opx) subordinate amount of primary hornblende, magnetite, Opx is present but not much, and plagioclase is absent in ultramafic rocks
Chromite	Common occurrences of chromite in dunite	Common occurrences of chromite in peridotite, olivine pyroxenite, and pyroxenite
Mineral chemistry	High Mg-olivine, diopsidic clinopyroxene, phlogopite mica, and hornblende are calcic with wide range of composition	Moderate Mg-olivine, diopsidic clinopyroxene, and hornblende are calcic
Cr-spinel chemistry	High Fe-Cr, and low Al-chromite, magnetite, and ilmenite are frequent in the late stage	High Fe–Cr chromite, low MgO and low Al-chromite. The ${}^{\rm Y}{\rm Fe}^{3+}\#$ is variable. Magnetite and ilmenite are frequent in the late stage
Bulk rock geochemistry	Low incompatible elements, relatively high LILE and low HFSE, no EU anomalies	Low incompatible elements, relatively high LILE, Th and low HFSE, no EU anomalies recorded
Mineralization	PGE mineralization associated with chromite, some Cu–Ni mineralization	PGE mineralization associated with chromite, some Cu–Ni mineralization

Note. Hbl: Hornblende; HFSE: high-field strength elements; LILE: large-ion lithophile elements; PGE: platinum group elements; REE: rare earth element. The features of Alaskan-type complex are after Johan (2002), Helmy and El Mahallawi (2003), Pettigrew and Hattori (2006), Thakurta et al. (2008), and Su et al. (2013).

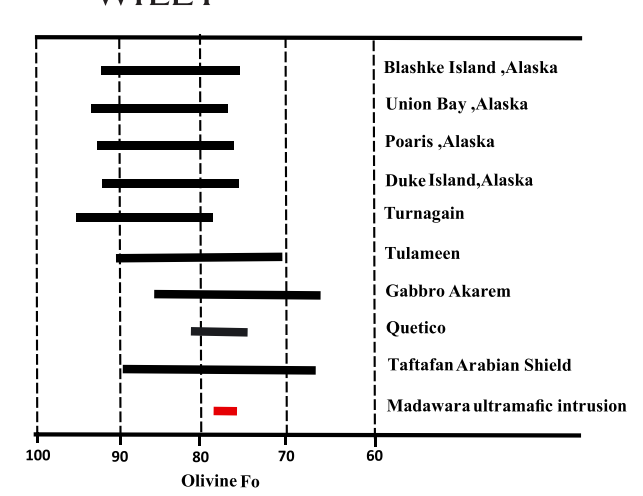


**FIGURE 14** Olivine (Fo) chemistry of peridotite and olivine pyroxenite from the study area and its comparison with olivine (Fo) content from worldwide Alaskan-type intrusions [Colour figure can be viewed at wileyonlinelibrary.com]

The Cr-spinel from Madawara ultramafics display a distinct negative correlation between  ${\rm Fe_2O_3}$  and  ${\rm Cr_2O_3}$  (Figure 6) and positive correlation between  ${\rm TiO_2}$  and  ${\rm Fe^{+3}\#}$  (Figure 7b). The mineral chemistry of Cr-spinel are characterized by low Mg# (9.30–26.22), variable  ${\rm Fe^{3+}\#}$  (4–19 wt.%), moderately high Cr# (55.12–76.48), and very high Fe# (73.78–88.93) relative to both stratiform and ophiolitic complexes (Figures 8 and 7a). All the analysed Cr-spinels when plotted in different discriminate diagrams differentiate a distinct subduction type geodynamics, which is similar to Alaskan-type tectonic model. The olivines of the MUC show forsterite contents in the range of 75.96–77.59. It coincides with forsterite range of the typical worldwide Alaskan-type complexes (Figure 14).

Geochemically, the peridotites show very low  $SiO_2$  and high MgO values and are characterized by enrichment of LILE and Th-U with negative Nb anomaly, thus, leading to high Th/Yb ratio. The bulk-rock geochemistry suggests that the ultramafic magma may have been generated by a high degree melting with probable melting of sub-arc mantle during slab break off. This could have triggered the mantle upwelling through the slab window and could be the mechanism for emplacement of MUC. Hence, the Cr-spinel chemistry and bulk-rock geochemistry displayed in different discrimination diagrams suggest that a subduction-related tectonic setting prevailed at the southern part of Bundelkhand Craton, which had resemblance towards the Alaskan-type magmatism.

#### 7 | CONCLUSIONS

 Cr-spinel (chromite) from the Madawara ultramafic complex can be classified mainly into three types on the basis of textural and mineral chemistry. Type I chromite shows homogeneous Al-chromite in composition which is more likely primary in nature. Type II chromites are zoned in nature showing core-rim compositional variation. Type III chromite shows homogeneous Fe-chromite in composition which is more likely modified in nature and is formed either by involvement of fluid in the

- subsequent stages of magmatic evolution or by alteration in the serpentinization process.
- 2. The primary type I Cr-spinel is characterized by low  $Al_2O_3$  (10.63–21.87 wt.%),  $TiO_2$  (0.2–0.6 wt.%), and Mg# (9.30–26.22) and high Cr# (55.12–76.48) and Fe# (73.78–90.70).
- The bulk geochemistry indicates mild LILE enrichment, HFSE depletion, negative Nb-Zr-Hf anomalies, and positive U-Th anomalies suggesting their accretion in arc-type geotectonic settings.
- 4. Parental melt calculation of type I Cr-spinel shows that low  $Al_2O_3$  (9.22 to 14.30 wt.%) and high oxygen fugacity (+0.26 to +2.14) could be related to magma generation in oxidizing environments of arc setting.
- 5. The plot of type I Cr-spinel in various discrimination diagrams suggests that MUC is formed in an arc environment, which is very similar to Alaskan-type magmatism.

#### **ACKNOWLEDGEMENTS**

The authors (N. M., M. S., and S. H.) are thankful to the Director, CSIR-NGRI, Hyderabad, for the permission to publish this work. N. M. is thankful to UGC, New Delhi, for the Research Fellowship. This work was sponsored by Ministry of Earth Sciences, New Delhi vide project MoES/P.O.(Geosciences)/4/2013. We are thankful to Geological Survey of India, Bangalore, and Banaras Hindu University, Varanasi for EPMA analysis. Drs. D. Srinivasa Sarma, A. Keshav Krishna, and S.S. Sawant are thanked for data acquisition through SEM-EDS, XRF, and HR-ICP-MS facilities at CSIR-NGRI.

#### ORCID

Manavalan Satyanarayanan http://orcid.org/0000-0002-7569-

## REFERENCES

- Ahmed, A. H., Helmy, H. M., Arai, S., & Yoshikawa, M. (2008). Magmatic unmixing in spinel from late Precambrian concentrically-zoned maficultramafic intrusions, Eastern Desert, Egypt. *Lithos*, 104(1), 85–98.
- Arai, S. (1980). Dunite-harzburgite-chromitite complexes as refractory residue in the Sangun-Yamaguchi zone, western Japan. *Journal of Petrology*, 21(1), 141–165.
- Arai, S. (1992). Chemistry of chromian spinel in volcanic rocks as a potential guide to magma chemistry. *Mineralogical Magazine*, 56, 173–184.
- Arai, S., Kadoshima, K., & Morishita, T. (2006). Widespread arc-related melting in the mantle section of the northern Oman ophiolite as inferred from detrital Cr-spinels. *Journal of the Geological Society*, 163(5), 869–879.
- Arai, S., & Miura, M. (2016). Formation and modification of chromitites in the mantle. Lithos, 264, 277-295.
- Arai, S., Okamura, H., Kadoshima, K., Tanaka, C., Suzuki, K., & Ishimaru, S. (2011). Chemical characteristics of chromian spinel in plutonic rocks: Implications for deep magma processes and discrimination of tectonic setting. *Island Arc*, 20(1), 125–137.
- Balaram, V., Singh, S. P., Satyanarayanan, M., & Anjaiah, K. V. (2013).
  Platinum group elements geochemistry of ultramafic and associated rocks from Pindar in Madawara Igneous Complex, Bundelkhand massif, Central India. *Journal of Earth System Science*, 122(1), 79–91.

MOHANTY ET AL. WILFY 2121

- Ballhaus, C. (1993). Redox states of lithospheric and asthenospheric upper mantle. *Contributions to Mineralogy and Petrology*, 114, 331–348.
- Ballhaus, C., Berry, R. F., & Green, D. H. (1990). Oxygen fugacity controls in the Earth's upper mantle. *Nature*, 348(6300), 437–440.
- Ballhaus, C., Berry, R. F., & Green, D. H. (1991). High pressure experimental calibration of the olivine-orthopyroxene-spinel oxygen geobarometer: Implications for the oxidation state of the upper mantle. *Contributions to Mineralogy and Petrology*, 107(1), 27–40.
- Barnes, S. J., & Roeder, P. L. (2001). The range of spinel compositions in terrestrial mafic and ultramafic rocks. *Journal of Petrology*, 42(12), 2279–2302.
- Barra, F., Gervilla, F., Hernández, E., Reich, M., Padrón-Navarta, J. A., & González-Jiménez, J. M. (2014). Alteration patterns of chromian spinels from La Cabaña peridotite, south-central Chile. *Mineralogy and Petrology*, 108(6), 819–836.
- Basu, A. K. (1986). Geology of parts of the Bundelkhand granite massif, Central India. Records of the Geological Survey of India, 117, 61–124.
- Basu, A. K. (2010). Precambrian geology of the Bundelkhand terrain, Central India and adjacent part of Western India. *Journal of Economic Geology and Georesource Management*, 7, 1–2.
- Batanova, V. G., Pertsev, A. N., Kamenetsky, V. S., Ariskin, A. A., Mochalov, A. G., & Sobolev, A. V. (2005). Crustal evolution of island-arc ultramafic magma: Galmoenan pyroxenite-dunite plutonic complex, Koryak Highland (Far East Russia). *Journal of Petrology*, 46(7), 1345–1366.
- Beard, J. S. (1986). Characteristic mineralogy of arc-related cumulate gabbros: Implications for the tectonic setting of gabbroic plutons and for andesite genesis. *Geology*, *14*(10), 848–851.
- Bell, B. R., & Claydon, R. V. (1992). The cumulus and post-cumulus evolution of chrome-spinels in ultrabasic layered intrusions: Evidence from the Cuillin Igneous Complex, Isle of Skye, Scotland. Contributions to Mineralogy and Petrology, 112(2), 242–253.
- Bhattacharya, A. R., & Singh, S. P. (2013). Proterozoic crustal scale shearing in the Bundelkhand massif with special reference to quartz reefs. Journal of the Geological Society of India, 82(5), 474–484.
- Bryndzia, L. T., & Wood, B. J. (1990). Oxygen thermobarometry of abyssal spinel peridotites: The redox state and C-O-H volatile composition of the Earth's sub-oceanic upper mantle. *American Journal of Science*, 290, 1093–1116.
- Burkhard, D. J. (1993). Accessory chromium spinels: Their coexistence and alteration in serpentinites. Geochemical et Cosmochimica Acta, 57(6), 1297–1306.
- Chen, B., Suzuki, K., Tian, W., Jahn, B. M., & Ireland, T. (2009). Geochemistry and Os-Nd-Sr isotopes of the Gaositai Alaskan-type ultramafic complex from the northern North China craton: Implications for mantle-crust interaction. *Contributions to Mineralogy and Petrology*, 158(5), 683-702.
- Dare, S. A., Pearce, J. A., McDonald, I., & Styles, M. T. (2009). Tectonic discrimination of peridotites using fO2–Cr# and Ga–Ti–FeIII systematics in chrome-spinel. *Chemical Geology*, 261(3–4), 199–216.
- Debari, S. M., Kay, S. M., & Kay, R. W. (1987). Ultramafic xenoliths from Adagdak Volcano, Adak, Aleutian Islands, Alaska: Deformed igneous cumulates from the Moho of an island arc. *Journal of Geology*, *95*, 329–341.
- Debari, S. M., & Coleman, R. G. (1989). Examination of the deep levels of an island arc: Evidence from the Tonsina Ultramafic-Mafic Assemblage, Tonsina, Alaska. *Journal of Geophysical Research. Solid Earth*, 94(B4), 4373–4391.
- Deer, W. A., Howie, R. A., & Zussman, J. (1992). An introduction to the rock-forming minerals (Vol. 2). (p. 558). Hong Kong: Longman Scientific & Technical.
- Dick, H. J., & Bullen, T. (1984). Chromian spinel as a petrogenetic indicator in abyssal and alpine-type peridotites and spatially associated lavas. Contributions to Mineralogy and Petrology, 86(1), 54-76.
- Dong, J., Song, S., Wang, M., Allen, M. B., Su, L., Wang, C., & Xu, B. (2017). Alaskan-type Kedanshan intrusion (Central Inner Mongolia, China):

- Superimposed subduction between the Mongol-Okhotsk and Paleo-Pacific oceans in the Jurassic. *Journal of Asian Earth Sciences*. https://doi.org/10.1016/j.jseaes.2017.11.010
- Dönmez, C., Keskin, S., Günay, K., Çolakoğlu, A. O., Çiftçi, Y., Uysal, İ., ... Yıldırım, N. (2014). Chromite and PGE geochemistry of the Elekdağ Ophiolite (Kastamonu, Northern Turkey): Implications for deep magmatic processes in a supra-subduction zone setting. *Ore Geology Reviews*, 57, 216–228.
- Droop, G. T. R. (1987). A general equation for estimating Fe3+ concentrations in ferromagnesian silicates and oxides from microprobe analyses, using stoichiometric criteria. *Mineralogical Magazine*, 51(361), 431–435.
- Elburg, M. A., & Kamenetsky, V. S. (2007). Dehydration processes determine fO2 of arc and intraplate magmas. Geochimica et Cosmochimica Acta, 71, A252.
- Farahat, E. S., & Helmy, H. M. (2006). Abu Hamamid Neoproterozoic Alaskan-type complex, south Eastern Desert, Egypt. *Journal of African Earth Sciences*, 45(2), 187–197.
- Farooqui, S. A., & Singh, A. K. (2006). Platinum mineralization in Ikauna Area, Lalitpur District, Uttar Pradesh. Geological Society of India, 68(4), 582–584.
- Farooqui, S. A., & Singh, P. K. (2010). PGE mineralisation in ultramafic/mafic enclaves of Ikauna area, Bundelkhand craton, India. In K. Satake (Ed.), Advances in geosciences Solid Earth, 20 (pp. 111–120). World Scientific Publishing Company. ISBN: 978-981-2838-18-6.
- Foley, J. P., Light, T. D., Nelson, S. W., & Harris, R. A. (1997). Mineral occurrences associated with mafic-ultramafic and related alkaline complexes in Alaska. *Economic Geology Monographs*, 9, 396–449.
- Franz, L., & Wirth, R. (2000). Spinel inclusions in olivine of peridotite xenoliths from TUBAF seamount (Bismarck Archipelago/Papua New Guinea): Evidence for the thermal and tectonic evolution of the oceanic lithosphere. Contributions to Mineralogy and Petrology, 140(3), 283–295.
- Gervilla, F., Padrón-Navarta, J. A., Kerestedjian, T., Sergeeva, I., González-Jiménez, J. M., & Fanlo, I. (2012). Formation of ferrian chromite in podiform chromitites from the Golyamo Kamenyane serpentinite, Eastern Rhodopes, SE Bulgaria: A two-stage process. Contributions to Mineralogy and Petrology, 164(4), 643–657.
- González-Jiménez, J. M., Proenza, J. A., Gervilla, F., Melgarejo, J. C., Blanco-Moreno, J. A., Ruiz-Sánchez, R., & Griffin, W. L. (2011). High-Cr and high-Al chromitites from the Sagua de Tánamo district, Mayarí-Cristal ophiolitic massif (eastern Cuba): Constraints on their origin from mineralogy and geochemistry of chromian spinel and platinum-group elements. Lithos, 125(1), 101–121.
- Grieco, G., & Merlini, A. (2012). Chromite alteration processes within Vourinos ophiolite. *International Journal of Earth Sciences*, 101(6), 1523–1533.
- Habtoor, A., Ahmed, A. H., & Harbi, H. (2016). Petrogenesis of the Alaskantype mafic-ultramafic complex in the Makkah quadrangle, western Arabian Shield, Saudi Arabia. *Lithos*, 263, 33–51.
- Hamlyn, P. R., & Keays, R. R. (1979). Origin of chromite compositional variation in the Panton Sill, Western Australia. Contributions to Mineralogy and Petrology, 69(1), 75–82.
- Helmy, H. M., & El Mahallawi, M. M. (2003). Gabbro Akarem maficultramafic complex, Eastern Desert, Egypt: A Late Precambrian analogue of Alaskan-type complexes. *Mineralogy and Petrology*, 77(1), 85–108.
- Helmy, H. M., El-Rahman, Y. M. A., Yoshikawa, M., Shibata, T., Arai, S., Tamura, A., & Kagami, H. (2014). Petrology and Sm-Nd dating of the Genina Gharbia Alaskan-type complex (Egypt): Insights into deep levels of Neoproterozoic island arcs. *Lithos*, 198, 263–280.
- Helmy, H. M., Yoshikawa, M., Shibata, T., Arai, S., & Kagami, H. (2015).
  Sm-Nd and Rb-Sr isotope geochemistry and petrology of Abu Hamamid intrusion, Eastern Desert, Egypt: An Alaskan-type complex in a backarc setting. Precambrian Research, 258, 234–246.

- Hickey, R. L., & Frey, F. A. (1982). Geochemical characteristics of boninite series volcanics: Implications for their source. Geochimica et Cosmochimica Acta, 46, 2099–2115.
- Himmelberg, G. R., & Loney, R. A. (1995). Characteristics and petrogenesis of Alaskan-type ultramafic-mafic intrusions, southeastern Alaska (Vol. 56). US Government Printing Office.
- Holland, T. J. B., & Powell, R. (2011). An improved and extended internally consistent thermodynamic dataset for phases of petrological interest, involving a new equation of state for solids. *Journal of Metamorphic Geology*, 29(3), 333–383.
- Irvine, T. N. (1965). Chromian spinel as a petrogenetic indicator: Part 1. Theory. Canadian Journal of Earth Sciences, 2(6), 648-672.
- Irvine, T. N. (1967). Chromian spinel as a petrogenetic indicator: Part 2. Petrologic applications. Canadian Journal of Earth Sciences, 4(1), 71–103
- Irvine, T. N. (1974). Petrology of the Duke Island ultramafic complex southeastern Alaska. *Geological Society of America Memoirs*, 138, 1–244.
- Ishii, T., Robinson, P. T., Maekawa, H., & Fiske, R. (1992). Petrological studies of peridotites from diapiric serpentinite seamounts in the Izu-Ogasawara-Mariana Forearc, Leg 125. In P. Fryer, J. A. Pearce, L. B. Stokking, et al. (Eds.), Proceedings of the ocean drilling program, scientific results (Vol. 125) (pp. 445–485). College Station, TX: Ocean Drilling Program.
- Jan, M. Q., & Windley, B. F. (1990). Chromian spinel-silicate chemistry in ultramafic rocks of the Jijal complex, Northwest Pakistan. *Journal of Petrology*, 31(3), 667–715.
- Johan, Z. (2002). Alaskan-type complexes and their platinum-group element mineralization. In L. J. Cabri (Ed.), *Geology, geochemistry, mineralogy and mineral beneficiation of platinum-group elements* (Vol. 54) (pp. 669–719). Ottawa Ontario: Can Inst Min Met Spec.
- Joshi, K. B., Bhattacharjee, J., Rai, G., Halla, J., Ahmad, T., Kurhila, M., ... Choudhary, A. K. (2017). The diversification of granitoids and plate tectonic implications at the Archaean-Proterozoic boundary in the Bundelkhand Craton, Central India. Geological Society, London, Special Publications, 449(1), 123–157.
- Kamenetsky, V. S., Crawford, A. J., & Meffre, S. (2001). Factors controlling chemistry of magmatic spinel: An empirical study of associated olivine, Cr-spinel and melt inclusions from primitive rocks. *Journal of Petrology*, 42(4), 655–671.
- Karipi, S., Tsikouras, B., Hatzipanagiotou, K., & Grammatikopoulos, T. A. (2007). Petrogenetic significance of spinel-group minerals from the ultramafic rocks of the Iti and Kallidromon ophiolites (Central Greece). *Lithos*, 99(1), 136–149.
- Kaur, P., Zeh, A., Chaudhri, N., & Eliyas, N. (2016). Unravelling the record of Archaean crustal evolution of the Bundelkhand Craton, northern India using U-Pb zircon-monazite ages, Lu-Hf isotope systematics, and whole-rock geochemistry of granitoids. *Precambrian Research*, 281, 384-413.
- Krause, J., Brügmann, G. E., & Pushkarev, E. V. (2007). Accessory and rock forming minerals monitoring the evolution of zoned mafic-ultramafic complexes in the Central Ural Mountains. *Lithos*, 95(1), 19–42.
- Krishna, A. K., & Govil, P. K. (2007). Soil contamination due to heavy metals from an industrial area of Surat, Gujarat, Western India. Environmental Monitoring and Assessment, 124(1-3), 263-275.
- Kumar, S., Raju, S., Pathak, M., & Pandey, A. (2010). Magnetic susceptibility mapping of felsic magmatic lithounits in the central part of Bundelkhand massif, Central India. *Journal of the Geological Society of India*, 75(3), 539–548.
- Leake, B. E., Woolley, A. R., Arps, C. E., Birch, W. D., Gilbert, M. C., Grice, J. D., ... Linthout, K. (1997). Report. Nomenclature of amphiboles: Report of the subcommittee on amphiboles of the international mineralogical association commission on new minerals and mineral names. *Mineralogical Magazine*, 61(2), 295–321.
- Li, S. S., Keerthy, S., Santosh, M., Singh, S. P., Deering, C., Satyanarayanan, M., ... Sajinkumar, K. S. (2017). Anatomy of impactites and shocked zircon grains from Dhala reveals Paleoproterozoic meteorite impact in

- the Archean basement rocks of Central India. *Gondwana Research*, 54, 81–101.
- Maurel, C., & Maurel, P. (1982). Étude expérimentale de la distribution de l'aluminium entre bain silicaté basique et spinelle chromifère. Implications pétrogénétiques: Teneur en chrome des spinelles. Bulletin de Mineralogie, 105, 197-202.
- McDonough, W. F., & Sun, S. S. (1995). The composition of the Earth. *Chemical Geology*, 120(3–4), 223–253.
- Mellini, M., Rumori, C., & Viti, C. (2005). Hydrothermally reset magmatic spinels in retrograde serpentinites: formation of "ferritchromit" rims and chlorite aureoles. Contributions to Mineralogy and Petrology, 149(3), 266–275.
- Merlini, A., Grieco, G., & Diella, V. (2009). Ferritchromite and chromianchlorite formation in mélange-hosted Kalkan chromitite (Southern Urals, Russia). American Mineralogist, 94(10), 1459–1467.
- Mondal, M. E. A., Goswami, J. N., Deomurari, M. P., & Sharma, K. K. (2002). Ion microprobe <sup>207</sup> Pb/<sup>206</sup> Pb ages of zircons from the Bundelkhand massif, northern India: Implications for crustal evolution of the Bundelkhand–Aravalli protocontinent. *Precambrian Research*, 117(1), 85–100.
- Mondal, M. E. A., Sharma, K. K., Rahman, A., & Goswami, J. N. (1998). Ion microprobe <sup>207</sup> Pb/<sup>206</sup> Pb zircon ages for gneiss-granitoid rocks from Bundelkhand massif: Evidence for Archaean components. *Current Science*, 70–75.
- Mondal, S. K., Ripley, E. M., Li, C., & Frei, R. (2006). The genesis of Archaean chromitites from the Nuasahi and Sukinda massifs in the Singhbhum Craton, India. *Precambrian Research*, 148(1–2), 45–66.
- Nixon, G. T., Cabri, L. J., & Laflamme, J. G. (1990). Platinum-group-element mineralization in lode and placer deposits associated with the Tulameen Alaskan-type complex, British Columbia. The Canadian Mineralogist, 28(3), 503–535.
- Pal, T. (2011). Petrology and geochemistry of the Andaman ophiolite: Melt-rock interaction in a suprasubduction-zone setting. *Journal of the Geological Society*, 168(4), 1031–1045.
- Parkinson, I. J., & Pearce, J. A. (1998). Peridotites from the Izu-Bonin– Mariana forearc (ODP Leg 125): Evidence for mantle melting and melt-mantle interaction in a supra-subduction zone setting. *Journal of Petrology*, 39(9), 1577–1618.
- Pati, J. K., Patel, S. C., Pruseth, K. L., Malviya, V. P., Arima, M., Raju, S., ... Prakash, K. (2007). Geology and geochemistry of giant quartz veins from the Bundelkhand Craton, Central India and their implications. *Journal of Earth System Science*, 116(6), 497–510.
- Pearce, J. A. (1983). Role of the sub-continental lithosphere in magma genesis at active continental margins. In C. J. Hawkesworth, & M. J. Norry (Eds.), *Continental basalts and mantle xenoliths* (pp. 230–249). Nantwich: Shiva.
- Pearce, J. A., Barker, P. F., Edwards, S. J., Parkinson, I. J., & Leat, P. T. (2000). Geochemistry and tectonic significance of peridotites from the South Sandwich arc-basin system, South Atlantic. Contributions to Mineralogy and Petrology, 139(1), 36-53.
- Pettigrew, N. T., & Hattori, K. H. (2006). The Quetico intrusions of western Superior Province: Neo-Archean examples of Alaskan/Ural-type maficultramafic intrusions. *Precambrian Research*, 149(1), 21–42.
- Proenza, J., Gervilla, F., Melgarejo, J., & Bodinier, J. L. (1999). Al- and Crrich chromitites from the Mayari-Baracoa ophiolitic belt (Eastern Cuba); consequence of interaction between volatile-rich melts and peridotites in suprasubduction mantle. *Economic Geology*, 94(4), 547–566.
- Rao, J. M., Rao, G. P., Widdowson, M., & Kelley, S. P. (2005). Evolution of Proterozoic mafic dyke swarms of the Bundelkhand granite massif, Central India. *Current Science*, 502–506.
- Ripley, E. M. (2009). Magmatic sulfide mineralization in Alaskan-type complexes. New developments in magmatic Ni-Cu and PGE deposits. (pp. 219-228). Beijing: Geological publishing house.
- Roeder, P. L., & Emslie, R. (1970). Olivine-liquid equilibrium. Contributions to Mineralogy and Petrology, 29(4), 275–289.

- Rollinson, H. (2008). The geochemistry of mantle chromitites from the northern part of the Oman ophiolite: Inferred parental melt compositions. Contributions to Mineralogy and Petrology, 156(3), 273-288.
- Ruan, B., Yu, Y., Lv, X., Feng, J., Wei, W., Wu, C., & Wang, H. (2017). Occurrence and mineral chemistry of chromite and related silicates from the Hongshishan mafic-ultramafic complex, NW China with petrogenetic implications. Mineralogy and Petrology, 111(5), 693-708.
- Sack, R. O., & Ghiorso, M. S. (1991). Chromite as a petrogenetic indicator. Reviews in Mineralogy and Geochemistry, 25(1), 323-354.
- Saha, L., Frei, D., Gerdes, A., Pati, J. K., Sarkar, S., Patole, V., ... Nasipuri, P. (2016). Crustal geodynamics from the Archaean Bundelkhand Craton, India: Constraints from zircon U-Pb-Hf isotope studies. Geological Magazine, 153(1), 179-192.
- Sarkar, A. (1996). Geochronology and geochemistry of mid Archaean Trondhjemitic gneisses from Bundelkhand craton, Central India. Recent Researches in Geology, 16, 76-92.
- Satyanarayanan, M., Balaram, V., Roy, P., Anjaiah, K. V., & Singh, S. P. (2010). Trace, rare earth element (REE) and platinum group element (PGE) geochemistry of the mafic and ultramafic rocks from Bundelkhand craton, Central India. In K. Satake (Ed.), Advances in geosciences, Volume 20: Solid Earth (pp. 57-79). World Scientific Publishing Company, ISBN. ISBN: 978-981-283-817-9.
- Satyanarayanan, M., Balaram, V., Sawant, S. S., Subramanyam, K. S. V., Vamsi Krishna, G., Dasaram, B., & Manikyamba, C. (2018). Rapid determination of REE, PGE, and other trace elements in geological and environmental materials by high resolution inductively coupled plasma mass spectrometry. Atomic Spectroscopy, 39(1), 1-15.
- Satyanarayanan, M., Singh, S. P., Balaram, V., & Niranjan, M. (2015). Geochemistry of the Madawara Igneous Complex. Bundelkhand craton. Central India: Implications for PGE metallogeny. Open Geosciences, 7(1), 836-853.
- Saumur, B. M., & Hattori, K. (2013). Zoned Cr-spinel and ferritchromite alteration in forearc mantle serpentinites of the Rio San Juan Complex, Dominican Republic. Mineralogical Magazine, 77(1), 117-136.
- Seo, J., Oh, C. W., Choi, S. G., & Rajesh, V. J. (2013). Two ultramafic rock types in the Hongseong area, South Korea: Tectonic significance for Northeast Asia. Lithos, 175, 30-39.
- Singh, S. P., Balaram, V., Satyanarayanan, M., Sarma, D. S., Subramanyam, K. S. V., Anjaiah, K. V., & Kharia, A. (2011). Platinum group minerals from the Madawara ultramafic-mafic complex, Bundelkhand massif, Central India: A preliminary note. Journal Geological Society of India, 78, 281-283.
- Singh, S. P., & Dwivedi, S. B. (2009). Garnet-sillimanite-cordierite-quartzbearing assemblages from early Archean supracrustal rocks of Bundelkhand massif, Central India. Current Science (00113891), 97(1), 103-107.
- Singh, S. P., Singh, M. M., Srivastava, G. S., & Basu, A. K. (2007). Crustal evolution in Bundelkhand area, Central India. Journal of Himalayan Geology, 28, 79-101.
- Singh, S. P., Subramanyam, K. S. V., Manikyamba, C., Santosh, M., Singh, M. R., & Kumar, B. C. (2017). Geochemical systematics of the Mauranipur-Babina greenstone belt, Bundelkhand craton, Central India: Insights on Neoarchean mantle plume-arc accretion and crustal evolution. Geoscience Frontiers. (available online). https://doi.org/10.1016/j. gsf.2017.08.008

- Snoke, A. W., Quick, J. E., & Bowman, H. R. (1981). Bear Mountain Igneous Complex, Klamath Mountains, California: An ultrabasic to silicic calealkaline suite. Journal of Petrology, 22(4), 501-552.
- Spandler, C. J., Arculus, R. J., Eggins, S. M., Mavrogenes, J. A., Price, R. C., & Reav. A. J. (2003). Petrogenesis of the Greenhills Complex. Southland. New Zealand: Magmatic differentiation and cumulate formation at the roots of a Permian island-arc volcano. Contributions to Mineralogy and Petrology, 144(6), 703-721.
- Su, B. X., Qin, K. Z., Santosh, M., Sun, H., & Tang, D. M. (2013). The Early Permian mafic-ultramafic complexes in the Beishan Terrane, NW China: Alaskan-type intrusive or rift cumulates? Journal of Asian Earth Sciences, 66, 175-187.
- Thakurta, J., Ripley, E. M., & Li, C. (2008). Geochemical constraints on the origin of sulfide mineralization in the Duke Island Complex, southeastern Alaska. Geochemistry, Geophysics, Geosystems, 9(7). https://doi.org/ 10.1029/2008GC001982
- Tistl, M., Burgath, K. P., Höhndorf, A., Kreuzer, H., Munoz, R., & Salinas, R. (1994). Origin and emplacement of Tertiary ultramafic complexes in northwest Colombia: Evidence from geochemistry and K-Ar, Sm-Nd and Rb-Sr isotopes. Earth and Planetary Science Letters, 126(1-3),
- Uvsal, I., Tarkian, M., Sadiklar, M. B., Zaccarini, F., Meisel, T., Garuti, G., & Heidrich, S. (2009). Petrology of Al-and Cr-rich ophiolitic chromitites from the Muğla, SW Turkey: Implications from composition of chromite, solid inclusions of platinum-group mineral, silicate, and basemetal mineral, and Os-isotope geochemistry. Contributions to Mineralogy and Petrology, 158(5), 659-674.
- Verma, S. K., Verma, S. P., Oliveira, E. P., Singh, V. K., & Moreno, J. A. (2016). LA-SF-ICP-MS zircon U-Pb geochronology of granitic rocks from the central Bundelkhand greenstone complex, Bundelkhand craton, India. Journal of Asian Earth Sciences, 118, 125-137.
- Wan, Z., Coogan, L. A., & Canil, D. (2008). Experimental calibration of aluminum partitioning between olivine and spinel as a geothermometer. American Mineralogist, 93(7), 1142-1147.
- Wang, Z., Wilde, S. A., & Wan, J. (2010). Tectonic setting and significance of 2.3-2.1 Ga magmatic events in the Trans-North China Orogen: New constraints from the Yanmenguan mafic-ultramafic intrusion in the Hengshan-Wutai-Fuping area. Precambrian Research, 178(1-4),
- Wilson, M. (1989). Igneous petrogenesis. (p. 446). London: Unwin Hyman.
- Zaccarini, F., Garuti, G., Proenza, J. A., Campos, L., Thalhammer, O. A., Aiglsperger, T., & Lewis, J. F. (2011). Chromite and platinum group elements mineralization in the Santa Elena Ultramafic Nappe (Costa Rica): Geodynamic implications. Geologica Acta, 9(3-4), 407-423.

How to cite this article: Mohanty N, Singh Satyanarayanan M, Jayananda M, Korakoppa MM, Hiloidari S. Chromian spinel compositions from Madawara ultramafics, Bundelkhand Craton: Implications on petrogenesis and tectonic evolution of the southern part of Bundelkhand Craton, Central India. Geological Journal. 2019;54:2099-2123. https:// doi.org/10.1002/gj.3286

Geochemistry and Nd isotope study of Ultramafic-Mafic rocks from southern Bundelkhand Craton, Central India: Implications for Archean Mantle Evolution, Crustal growth and PGE mineralisation.

by Niranjan Mohanty

Submission date: 30-Jan-2023 05:29PM (UTC+0530)

Submission ID: 2002439780

File name: Thesis\_Draft.pdf (2.54M)

Word count: 35998 Character count: 193370 Geochemistry and Nd isotope study of Ultramafic-Mafic rocks from southern Bundelkhand Craton, Central India: Implications for Archean Mantle Evolution, Crustal growth and PGE mineralisation.

**ORIGINALITY REPORT** 

7% SIMILARITY INDEX

12%

INTERNET SOURCES

16%

1%

STUDENT PAPERS

PRIMARY SOURCES

pericles.pericles-prod.literatumonline.com

6%

Niranjan Mohanty, Surya Pratap Singh,
Manavalan Satyanarayanan, Mudlappa
Jayananda et al. "Chromian spinel
compositions from Madawara ultramafics,
Bundelkhand Craton: Implications on
petrogenesis and tectonic evolution of the
southern part of Bundelkhand Craton, Central
India", Geological Journal, 2019

1%

Certified that

The similarity

arises from

research publica
tions in which

student is the

first author.

(Prof. M. Jayanando

M. S. thomas again

P. Choukroune, J. N. Ludden, D. Chardon, A. J. Calvert, H. Bouhallier. "Archaean crustal growth and tectonic processes: a comparison of the Superior Province, Canada and the Dharwar Craton, India", Geological Society, London, Special Publication, 1997

<1%

Dr. M. SATHYANARAYANAN डॉ. एम. सत्यनारायणन

वरिष्ट्र प्रधान वेसानक Senior Principal Scientist स्थान भूगोतिकीय अनुस्थान संस्थान सर्वाक्षण स्थान संस्थान संस्थान प्रशासन सरकार) स्थान कर Technology, Govt of India) सर्वात देशाबाद Hyderabad - 500007



Dr. M. Jayananda, FASc, FNASc, FNA Professor Centre for Earth, Ocean and Atmospheric Sciences University of Hyderabad Hyderabad-500 046, Telangana, India



## हैदराबाद विश्वविद्यालय University of Hyderabad पृथ्वी, महासागर और वायुमंडलीय विज्ञान केंद्र Centre for Earth, Ocean and Atmospheric Sciences

Prof. C. R. Rao Road, Gachibowli, Hyderabad – 500 046 (Telangana), India Tel: 91-40-23132669, Mobile: 91-8618421127

email: mjayan.geol@gmail.com

Dr. M. Jayananda FNA, FASc, FNASc Professor

To Date: 30/01/2023

The Librarian University of Hyderabad Hyderabad

## Madam/Sir,

I am herewith forwarding the PhD thesis entitled 'Geochemistry and Nd isotope study of ultramafic-mafic rocks of Bundelkhand craton, central India: Implications for mantle evolution, crustal growth and PGE mineralization' submitted by my student Mr Niranjan Mohanty bearing registration number 14ESPE05. The similarity index of the thesis is found to be 17% as checked from the Turnitin in the Department library. I am certifying that out of 17% similarity, 7% (serial No. 1 & 2 of the report) similarity arises from research publications in which the student is the first author. Therefore, I request you to kindly do the needful at your end.

Thanking you and kind regards

Sincerely yours

nee ?!

(M. Jayananda)